TECTONIC INTERPRETATION OF THE PAPUA NEW GUINEA REGION FROM REPEAT SATELLITE MEASUREMENTS

KIM MOBBS

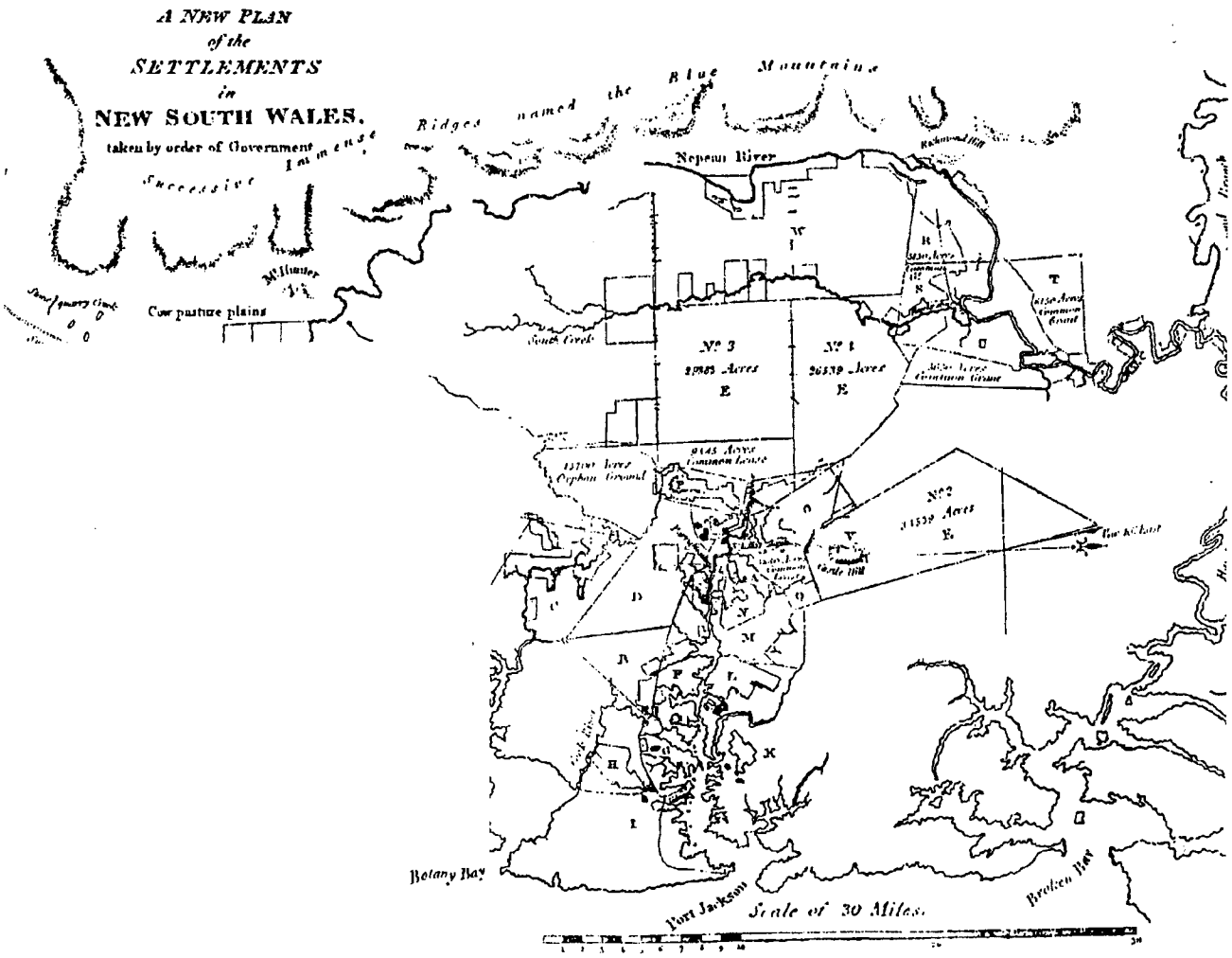

UNISURV S-48, 1997

Reports from

SCHOOL OF GEOMATIC ENGINEERING

THE UNIVERSITY OF NEW SOUTH WALES SYDNEY NSW 2052 AUSTRALIA

UNISURV REPORT S-48, 1997

TECTONIC INTERPRETATION OF THE PAPUA NEW GUINEA REGION FROM REPEAT SATELLITE MEASUREMENTS

KIM MOBBS

Received: September, 1996
Accepted: August, 1997

SCHOOL OF GEOMATIC ENGINEERING
UNIVERSITY OF NEW SOUTH WALES
SYDNEY NSW 2052
AUSTRALIA

National Library of Australia

Card No. and ISBN 0 85839 073 6

Abstract

The Australian and Pacific plates are in collision, with the Australian plate moving northeast at approximately 70 mm/y and the Pacific plate moving northwest at approximately 100 mm/y. The Papua New Guinea region forms a small part of this boundary.

The region has been studied since the late 1960's when the plate tectonic theory revolutionised geophysics. Several different models have been proposed to explain the complex array of geological features in terms of plate tectonic theory. These range from relatively simple models involving two microplates in a buffer zone between the major plates, to more complex models with up to four microplates proposed.

With the recent advances in the area of satellite geodesy, particularly the introduction of the GPS system, geodetic measurements are now sufficiently precise over long distances to allow these measurements to be used as another tool for understanding the complexities of plate tectonic motion.

A network of 11 survey sites was established in 1981 and observed with the Transit Doppler System. This network encompassed most of the major tectonic features in the region. Between August 1990 and July 1994, the Doppler network was re-observed and extended by a series of GPS surveys. The analysis of the Doppler data found to it be unreliable and unsuitable for geodetic analysis, which left only the GPS data. The GPS data were reduced in the GAMIT/GLOBK software. The results of this analysis and the interpretation of the results form the basis of this thesis.

Motion across the New Britain Trench has been found to be 130±5 mm/y which is in agreement with geological estimates of the motion. Towards the western end of the trench, motion decreases to 105±11 mm/y.

This analysis shows that the Bismarck Sea Seismic Lineation is spreading at a rate of 127±11 mm/y in the east and 116±11 mm/y further west. This is also in agreement with geological estimates.

Towards the western end of the Woodlark basin, the rate of opening was found to be 21±10 mm/y. This is statistically different to the geological estimates for the spreading rate, but supports the proposal that spreading decreases to the west.

The motion of Jacquinot Bay is clearly not representative of either the Australian plate or the Pacific plate, which supports the proposal for the existence of the South Bismarck plate.

Manus and Kavieng appear to be moving with the Pacific plate. This supports the models in which there is no North Bismarck plate.

A number of sites on the Papua New Guinea mainland and the Solomon Sea appear to be moving with the Australian plate. These sites are Port Moresby, Alotau, Misima, Morobe, Lae, Losuia and Guasopa. This has several implications. There appears to be no significant compression occurring along the Owen Stanley Ranges. There is no clearly defined boundary between the Australian plate and the proposed Solomon plate. The motions of Losuia and Guasopa are indicating that the Solomon Sea is moving as part of the Australian plate, which brings the existence of the Solomon plate into question. If this plate does not exist, the implication is that the New Britain Trench is accommodating the convergence between the Australian and Pacific plates.

Acknowledgments

This thesis could not have been completed without the help and support of many people.

My supervisor for this work was Art Stolz. Co-supervisors were Kurt Lambeck and Peter Morgan. I wish to thank Art for giving me the opportunity of participating in such an interesting project. Art has always encouraged me to pursue my own ideas and given me the freedom to approach the problem in a different way to that which he originally envisaged. All three of my supervisors have given advice on various aspects of this thesis, with the result that my ideas are presented much more clearly and logically.

Many thanks must be extended to Peter Morgan and his team at the University of Canberra. Peter was a valuable source of technical assistance for operating the GAMIT/GLOBK software. He generously made available his computing resources, GPS data and solutions from the Australasian region. Without additional data provided by Peter, many of my survey sites would have only single occupations, and this research would have been a first epoch determination rather an interpretation from geodetic results.

The staff and students in Peter's laboratory made me very welcome in the time I spent there. Although the working hours were long, the environment was very congenial which made the workload seem less daunting. Specific thanks must go to Barry McDowall for ploughing through the Doppler work, and confirming that I was not going mad; and to Russell Tiesler, whose practical advice on GAMIT/GLOBK was invaluable.

This research would not have been possible without the PNG surveys. There are many people who were involved with the surveys, and I would like to thank all of them for their contribution.The PNG National Mapping Bureau (NMB) contributed most significantly to these surveys, providing substantial funds, equipment and personnel. Special thanks are due to Doug Barsby and Wesley Loratung from this organization. Allan Graham of Newcastle TAFE, Simon McElroy, Roger Harvey, Simon McClusky and Art Stolz from the University of

New South Wales, organized and participated in the field campaigns. The other participants were: Mike Awai, Doug Barsby, Buddy Castillo, Rira Kizana, Wesley Loratung, Reva Mase, Loina Madanga, Wahun Nohu, John Oa, Peter Pako and Maipo Vaieke, NMB; David Paino and Nelson Welbourne, Department of Lands and Physical Planning, Rabaul; Francis Katiak, Mike Meuliners and Selam Pambui, Arman Larmer Surveys; John Gilliland and Vic Macolino, University of South Australia; Martin Hendy, University of New South Wales and; Grant Kilpatrick, Sydney TAFE. Arman Larmer Surveys, of Port Moresby, through Ian Sparks, provided GPS receivers, office space and hospitality. AUSLIG and the University of South Australia loaned instruments. The Volcanological Observatory in Rabaul and Department of Lands and Physical Planning there, provided assistance and operational support. We are particularly indebted to Nick Lauer, Adelbert Alois, Piten Nama and Tony Luben from these two organizations. Other significant support for the field campaigns was provided by the Australian Research Council, the Australian National University and the University of New South Wales. Additional thanks must also go to NMB for providing extra survey data at various sites between 1992-1994. This data was invaluable.

Paul Tregonning and Simon McClusky both offered a great deal of advice on running GAMIT/GLOBK, which was greatly appreciated. I would also like to thank Simon for his suggestions about reference frame problems.

I would also like to thank Merrin and Bruce Harvey for proof reading my thesis, and offering advice on presentation. Merrin deserves particular thanks for keeping me sane at critical points throughout my degree. His door was always open when I needed advice or moral support.

This research was completed whilst receiving an Australian Postgraduate Award and an Engineering Scholarship.

Finally, a very special thankyou must go to Jean-Francois and my family, Mum, Dad, and Becca for the love and support they have given me throughout this degree. They have seen me through depression when things were not going well, and elation when they were. I could not have finished without their support.

Table of Contents

Introduction 1
1.1 The Tectonic Setting 1
1.2 The Problem 2
1.3 The Geodetic Technique 2
1.4 The Aim of this Thesis 3
1.5 Overview of this Thesis 4

Tectonics of the Papua New Guinea Region 6
2.1 A Brief History of the Development of the Plate Tectonic Theory 6
2.2 Structure of the Earth 10
2.2.1 The Core 11
2.2.2 The Mantle 11
2.2.3 The Crust 11
2.2.4 Lithosphere, Asthenosphere and Mesosphere 12
Lithosphere/Asthenosphere Boundary 13
Interactions Between Lithosphere, Asthenosphere and Mesosphere 14
Properties of the Lithosphere and Asthenosphere 15
2.3 Plate Boundaries 18
2.3.1 Destructive Boundaries 18
Subduction Zones 18
Zones of Collision between Continents and Island Arcs 24
2.3.2 Constructive Plate Boundaries 25
Ocean Ridges 25
Backarc Spreading 26
2.3.3 Conservative Plate Boundaries 27
2.3.4 Source of Plate Motion 27
Convection 27
Plate Motion - Cause or Effect? 29
2.3.5 Forces acting on a Plate 31
Slab Pull 31
Subduction Suction 32
Ridge Push 32
Mantle Drag 32
Resistance 32
2.3.6 Life Cycle of a plate 33
2.4 Tectonics of the Papua New Guinea Region 34
2.4.1 Regional Setting and History 34
2.4.2 Motion of the Major Plates Surrounding the Papua New Guinea Region 36
2.4.3 Tectonic Features of the Papua New Guinea Region 36
Trenches 37

Accreted Terrains 47
Transform Faults and Spreading Centres 51
Triple Junctions 56
2.4.4 Tectonic Models of the Region 60
Johnson and Molnar (1972) 60
Curtis (1973) 61
Krause (1973) 63
Taylor (1975) 63
Hamilton (1979) 64
Davies *et al.* (1984) 65
McClusky *et al.* (1994) 66

Satellite Systems and their use in Geodesy 68
3.1 Introduction 68
3.1.1 History of Satellite Geodesy 68
Early Satellites Launched 69
3.1.2 Early Satellite Geodetic Techniques 70
Photogrammetric systems 70
Geodetic SECOR System 71
Laser Ranging Systems 74
Transit Doppler System 74
3.2 The Transit Doppler System 75
3.2.1 Basic Principles of Doppler Operation 76
3.2.2 Error sources 77
Ionospheric Delay 77
Tropospheric Refraction 78
Propagation Delay 79
Timing Errors 79
Interstation Timing Bias 80
Orbit Errors 81
General Relativistic Correction 81
3.2.3 Range Equations 81
3.2.4 Short Arc Geodetic Adjustment (SAGA) 83
3.3 Global Positioning System (GPS) 84
3.3.1 General Overview 84
3.3.2 Satellite Constellation 86
Degradation of Accuracy - Selective Availability 88
Restriction of Access - Anti-Spoofing 90
3.3.3 Signal Propagation 90
Propagation in the Ionosphere 91
Propagation in the Troposphere 98
3.3.4 Receivers and Antennas 99
C/A-code carrier receivers 99
P-code receivers 103
Y-code receivers 103
Antennas 103
Multipath 104

Doppler and GPS Surveys 105
4.1 Doppler Surveys 105

4.1.1 1975 Doppler Survey 105
4.1.2 1981 Doppler Survey 107
4.2 GPS Surveys 110
4.2.1 The 1990 Survey 110
4.2.2 The 1991 Survey 113
Urasi 114
Wari 116
Bunama 116
Alotau 116
Guasopa 116
Misima 117
4.2.3 The May 1992 Survey 118
4.2.4 The August 1992 Survey 120
4.2.5 The May-June 1993 Survey 122
4.2.6 The August-September 1993 Survey 123
4.2.7 The 1994 Survey 125

Stability Analysis of the 1981 Doppler Survey 126
5.1 Introduction 126
5.2 Origin of Data and Software 127
5.3 Input Data and Solution Controls 128
5.3.1. "a - cards" 128
Processing Switches 128
Reference Frame Constants 130
5.3.2. "b - cards" 131
5.3.3 "c - cards" 132
5.4 Results of the Stability Tests on the 1974 Test Data 132
5.4.1 Fixed Coordinate Constraints 133
5.4.2 Azimuth and Elevation Constraints 135
5.4.3 Orbit State Vector Constraints 136
5.4.4 Error Model Constraints 138
Initial Range Offset 139
Inter-station Timing Bias 139
Frequency Bias 140
Oscillator Offset and Drift 141
Residual Tropospheric Delay 141
5.4.5 Range-in-pass Constraint 142
5.4.6 Centre of Mass Constraint 142
5.4.7 Summary of 1974 Test Data Stability Analysis 143
5.5 1981 Stability Test 144
5.5.1 Coordinate Constraints 144
5.5.2 Azimuth and Elevation Constraints 149
5.5.3 Orbit State Vector Constraints 153
5.5.4 Error Model Constraints 161
5.5.5 Baseline Length Constraints 162
5.5.6 Centre of Mass Constraints 162
5.5.7 Range-in-pass Constraint 164
5.5.8 Summary of 1981 Data Stability Analysis 164
5.6 Errors in the Input File and Their Effects 165
5.7 Conclusions 165

GPS Analysis and Results 167
6.1 Raw Data 167
6.2 GAMIT Processing Strategy 168
6.2.1 Clocks 169
6.2.2 Orbits 173
6.2.3 Modelling 174
6.2.4 Data cleaning 174
6.2.5 Ionospheric Effects on the Data 178
6.2.6 GAMIT Quality Assurance 179
6.3 GLOBK Processing Strategy 183
6.3.1 A Consistent Reference Frame 183
6.3.2 Final Station Positions and Velocities with Formal Precisions 192
6.3.3 Precision Indicators of the Final Results 192
6.3.4 GLOBK/GLORG Quality Assurance 195
Confidence in the 1990 results 195
Confidence in the final results 202
6.3.5 Absolute Velocities and Velocity Residuals 214

Interpretation of the Results 216
7.1 Absolute Velocity Vectors and Velocity Residuals 216
7.2 Interpretation of the Results 222
7.2.1 Motion across the New Britain Trench 222
7.2.2 Motion across the Bismarck Sea Seismic Lineation 225
7.2.3 Motion across the Woodlark Spreading Centre 227
7.2.4 Sites on the Australian Plate. 229
7.3 Geodetic Results Applied to Unresolved Questions. 231
7.3.1 Is there a South Bismarck plate? 232
7.3.2 Is there a North Bismarck plate? 233
7.3.3 Is there a Solomon Sea plate? 234
Where is the south-western boundary between the Australian plate and proposed Solomon plate? 234
7.3.4 Is the Trobriand Trough Active? 236
7.3.5 Where is the south-western boundary between the Australian and South Bismarck plates? 237
7.3.6 Where is the boundary between the Australian and Caroline/Pacific plate to the north of New Guinea? 237
7.4 The Localised effect of the Woodlark Spreading Centre. 239
7.5 Eastward Motion of Aiambak 239

Conclusions and Recommendations 242
8.1 Summary of the Main Results 242
8.2 Suggested Future Research 245
8.2.1 The Bismarck Sea Region 246
8.2.2 The Solomon Sea Region 247
8.2.3 The Pacific Boundary Region 248
8.2.4 Northern and Western Papua New Guinea 248

List of Figures

Figure 2.1 The structure of the Earth....12
Figure 2.2 Lithosphere, asthenosphere and mesosphere....13
Figure 2.3 Curves of critical stress vs lithosphere heat flow for tensional stress (A) and compressional stress (B)....17
Figure 2.4 Convection patterns in the mantle....29
Figure 2.5 The forces acting on a lithospheric plate....32
Figure 2.6a Tectonic elements of the Papua New Guinea region....37
Figure 2.6b Proposed tectonic plates of the Papua New Guinea region....38
Figure 2.7 Seismicity of the Papua New Guinea region....41
Figure 2.8 Cross sections of seismicity across Papua New Guinea and the western end of the New Britain Trench....43
Figure 2.9 Deep seismicity associated with the New Britain Trench....44
Figure 2.10 Stability of triple junctions determined by vector analysis....57
Figure 2.11 Vector diagram of the relative motions of the Bismarck, Solomon and Australian plates....58
Figure 2.12 Vector diagram of the relative motions of the Australian, Pacific and Solomon plates....59
Figure 2.13. Vector diagram for the Solomon, Pacific, South Bismarck triple junction....60
Figure 2.14 Interpretations of the plate boundary configurations for the region....62
Figure 2.15 Rates of change of baseline lengths from the comparison between Dopper and GPS lengths....67

Figure 3.1 Illustration of the simultaneous and orbital modes of operation for the SECOR system....73
Figure 3.2 The layers of the Earth's atmosphere which affect the propagation of satellite signals....85

Figure 4.1 The 1975 and 1981 Doppler survey networks....108
Figure 4.2 The survey networks observed with GPS in 1990, 1991 and 1992....111
Figure 4.3 The networks surveyed with GPS in August 1992, May 1993 and August 1993....121
Figure 4.4 The location of the sites in the 1994 GPS survey....125

Figure 5.1 Effect on the final coordinates of changing the "fixed" coordinate constraint from ±0.3m to ±1m....133
Figure 5.2 Effect on the final coordinates of loosening the "fixed" coordinate constraint from ±0.3m to ±3m....134
Figure 5.3 The effect on the site coordinates of tightening the orbit constraints to the recommended values for broadcast ephemerides....136
Figure 5.4 Effect of applying the 1981 atomic oscillator constraint (1000 s) to the 1974 solution....139

Figure 5.5 The effect on site coordinates of using 1 x 10^{-6} as the frequency bias constraint.....140
Figure 5.6 Effect on the station coordinates of changing the Range-in-pass constraint from 0.10 m to 0.07 m. 142
Figure 5.7 Effects on baseline lengths of changing the fixed coordinate constraint from 3 cm to 1 cm 145
Figure 5.8 Oscillations in the z-coordinate for three iterations.....146
Figure 5.9 Plot of the X and Y coordinates of Losuia, Carteret and Kavieng projected onto the equatorial plane. 149
Figure 5.10 Equatorial azimuth and elevation of a line PQ.....151
Figure 5.11 Four iterations of the solution at Kavieng, clearly showing divergence. 154
Figure 5.12 (a) - (b) Corrections to coordinates in the first four iterations of the solution 155
Figure 5.12 (c) - (d) Corrections to coordinates in the first four iterations of the solution 156
Figure 5.13 The corrections to a priori coordinates at Kavieng with orbit constraints of 50m for X, Y, Z and velocity constraints on X, Y, Z of 0.5ms^{-1}.....157
Figure 5.14 The differences in site coordinates from two solutions with small differences in orbit constraints.....159
Figure 5.15 Differences in site coordinates from two solutions with small differences in orbital constraints. 160
Figure 5.16 The effect of applying the atomic oscillator constraints to the rubidium oscillators. 162
Figure 5.17 Shows the effect upon the coordinates of changing the constraints on the centre of mass from 5 m to 0.01 m. 163
Figure 5.18 The effect of changing the range-in-pass constraint from 0.075 m to 0.07 m.....164

Figure 6.1 (a) Between station difference for satellite PRN16, sites Morobe and Tasmania. Modelling included using the i-file. 172
Figure 6.1 (b) Between station difference for satellite PRN16, sites Morobe and Tasmania. Modelling did not include using the i-file. 172
Figure 6.2 (a) The effect on the GPS signal of ionospheric scintillations. 180
Figure 6.2 (b) The effect on the GPS signal of the long wavelength ionospheric fluctuations which occur at night. 181
Figure 6.3 (a-b) The global tracking network available for processing in 1990, 1991, 1992, 1993.....187
Figure 6.3 (c-d) The global tracking network available for processing in 1990, 1991, 1992, 1993.....188
Figure 6.4 The mean number of observations per day from the 1990 campaign to the present. 189
Figure 6.5 The availability of global tracking stations and satellites from 1990 to 1994.....190
Figure 6.6 Shows the comparison between baseline lengths from McClusky (1993) and the GLOBK on the 1990 campaign. 196
Figure 6.7 Graph showing the transformation parameters from GLORG for three solutions. 202
Figure 6.8 Repeatability of Port Moresby. 207

Figure 6.9 Repeatability of Morobe. 208
Figure 6.10 Repeatability of Losuia. 209
Figure 6.11 Baseline repeatability of Port Moresby to Losuia. 212
Figure 6.12 Baseline repeatability for Losuia to Jacquinot Bay. 213

Figure 7.1(a) Velocity residuals with respect to the Australian plate and the Pacific plate 217
Figure 7.1(b) Velocity residuals with respect to the Australian plate and the Pacific plate 218
Figure 7.2 Absolute velocities of the survey sites. 219
Figure 7.3 Rates of motion across the New Britain Trench along various baselines. 224
Figure 7.4 Rates of motion across the Bismarck Sea Seismic Lineation along various baselines. 226
Figure 7.5 Rates of motion across the Woodlark Spreading Centre along various baselines. 228
Figure 7.6 Rates of motion between four sites on the Australian plate. 230
Figure 7.7 Rates of motion across the Papuan Peninsula from Morobe and Port Moresby to Lae. 231
Figure 7.8 (a-b) The location of the survey sites relative to the zones of: (a) shallow seismicity, and (b) intermediate depth seismicity. 238
Figure 7.9 A cross section of seismicity at Vanimo. 240
Figure 7.10 NUVEL-1 estimates of plate velocities for random points on the Australian and Pacific plates in relation to the tectonic features and boundaries associated with intense seismic activity. 241

List of Tables

Table 4.1 - The number of passes observed at each site in the 1975 Doppler survey. 106
Table 4.2 Observation schedule for the 1981 Doppler survey 109
Table 4.3 The observation schedule of the 1990 GPS survey. 113
Table 4.4 Connections between 1990 GPS sites and 1981 Doppler sites 113
Table 4.5 The connection at Misima 116
Table 4.6 Data collected during the 1991 GPS survey. 117
Table 4.7 The 1992 GPS survey as executed. 118
Table 4.8 The data processed in the August 1992 survey. 119
Table 4.9 The observation schedule of the May 1993 survey. 122
Table 4.10 (a-b) The observation schedule for the period 18th August to 5th September, 1993. 123
Table 4.11 Observations in the 1994 GPS survey 125

Table 5.1 Summary of the tests performed on the "fixed" coordinate constraints. 135
Table 5.2 Summary of the tests performed on the orbital constraints. 137
Table 5.3 Error Model constraints used in the 1981 and 1974 Doppler solutions. 138
Table 5.4 Effects of altering the error model constraints. 141
Table 5.5 Shows the differences between a priori coordinates and the final coordinates of McClusky (1993) 147
Table 5.6 Summary of the tests performed on the orbit constraints. 161

Table 6.1 Quality Assurance: Comparison of daily corrections to a standard set of a priori coordinates from the constrained GAMIT solutions for 1990. 182
Table 6.2 The geodetic coordinates of all sites in the Papua New Guinea surveys. 193
Table 6.3 Final cartesian coordinates and formal uncertainties for the sites in the Papua New Guinea region. 194
Table 6.4 Constraints applied to the GLOBK solution of the 1990 data in both the loosely constrained solution and the tightly constrained solution. 197
Table 6.5(a) Coordinates of the global sites from the 1990-only GLOBK solution with loose constraints applied to the CIGNET sites 198
Table 6.5(b) Coordinates of the global sites from the 1990-only solution with tight constraints applied to the CIGNET sites. 199
Table 6.6 Coordinates of the Papua New Guinea and regional sites from the 1990-only solution with both loose and tight constraints applied to the CIGNET sites. 200
Table 6.7 Adjustments to the unconstrained IGS Core site positions and velocities. 203

Table 6.8 Coordinate adjustments to the seven sites constrained in GLORG.....204
Table 6.9 The horizontal velocity components for three sites from two solutions 205
Table 6.10 The transform parameters used to stabilise the reference frame in GLORG.....205
Table 6.11 Comparison between the rate for each site determined by the forward GLOBK solution, and the rate determined by the slope of the line of best fit determined by the GLOBK back-solution.....209

Table 7.1 Comparisons of the rate of baseline change. 221

Chapter 1

Introduction

1.1 The Tectonic Setting

The region surrounding Papua New Guinea is a very active seismic and volcanic area. It is the site of oblique collision between the Pacific and Australian plates. There are a number of significant tectonic features in the region, which are shown in Figure 2.6. Perhaps the most prominent is the San Cristobel Trench/ New Britain Trench system and the numerous associated volcanoes. The Australian and proposed Solomon plates are being rapidly subducted beneath the Pacific and proposed Bismarck plates along this trench system at a rate of 12 - 14 cm/y, decreasing to approximately 5 cm/y in the west, according to most current models.

The Bismarck Sea Seismic Lineation and Woodlark Basin Spreading Centre are regions in which oblique spreading is occurring. The Bismarck Sea Seismic Lineation is thought to be a back-arc spreading centre. It is opening at a rate of approximately 10-13 cm/y in the east. To the west, the motion is accommodated in a "leaky transform" fault, where left-lateral transform motion intermittently undergoes spreading. The Woodlark Basin Spreading Centre is opening at a greater rate in the East, and, according to current theories, is propagating into the Papuan Peninsula in the west. Estimates of motion are approximately 6 cm/y in the east, decreasing to the west.

The Trobriand Trough and Manus Trench are ocean trenches that may or may not be currently accommodating subduction. If they are active, the subduction rate on each is very slow. Opinion is divided on this issue.

The central and northern areas of Papua New Guinea are characterised by mountain ranges. These include the Papuan Fold Belt, and the New Guinea Highlands in central Papua New Guinea; the Adelbert and Finisterre Ranges, and the Bewani and Toricelli Mountains to the north; and the Owen Stanley Ranges along the Papuan Peninsula. The mountain ranges in the central

region are separated from those in the north by the Ramu Markham Fault Zone, a north dipping fault. Opinion is divided on the location of the northern boundary of the Australian plate in this broad area of tectonic activity.

1.2 The Problem

Although some of the tectonic features mentioned above are clearly active, others are not. Within this complex tectonic setting, researchers using a variety of techniques have proposed a number of microplates located between the Australian and Pacific plates. Interpretations range from simple two-microplate models to more complex scenarios in which there are up to 4 microplates. In all models, microplates are proposed for the Solomon Sea and the southern Bismarck Sea. Additional plates are proposed in some models, and include one or two of the following: a north Bismarck plate, a Trobriand plate and a Woodlark plate.

The discrepancies between the interpretations of different researchers indicate that there is scope for further work to resolve the remaining problems and arrive at a definitive model of the region.

1.3 The Geodetic Technique

Traditionally, fields such as geology and seismology have been involved in applying the theory of plate tectonics to the Earth, to understand the surface features and the underlying processes involved in their formation. Great advances in the accuracy and precision of satellite-based positioning techniques have been made in the last few decades. In addition, reductions of over an order of magnitude have occurred in the cost and the mass/volume of GPS systems in the last decade. These GPS systems are significantly more portable than all other systems, including the Transit Doppler system. The result of these developments is that the field of geodesy is now able to provide precise measurements over great distances spanning plate boundaries and stable plate interiors. These measurements are another tool that can be used to understand the deformation of the Earth.

During the late 1970's, a geodetic survey network was designed which encompassed most of the major tectonic features of the Papua New Guinea region. This network spans approximately 1000 km by 1000 km to the north

and east of Papua New Guinea. The network was designed to establish a high accuracy framework from which to measure the amounts of motion that are currently occurring in the region.

This network was first observed with TRANSIT Doppler in 1981. Although simulations showed that the accuracy of the Doppler was limited to approximately 0.5 m, it was envisaged that future observations of the network would utilise a more accurate and precise satellite system.

In 1990, most of this network was re-observed with GPS. Only the connection to the Pacific plate through the sites Nuguria and Carteret was not re-observed.

The 1991 GPS survey observed a dense network of sites in the vicinity of the Woodlark Spreading Centre. This was a reoccupation of part of a Doppler survey performed in 1975. However, the Doppler survey has not been processed for reasons discussed in Chapter 4, hence the 1991 survey is a first epoch determination for many of these sites.

In 1992, the connection to the Pacific plate was made with GPS. A subset of the 1990 survey was reoccupied to link the 1990 and 1992 surveys.

Stability analysis of the 1981 Doppler survey revealed that the existing data set is computationally unstable. For this reason, the Doppler survey has been discarded from this research. Without this as a base, many of the sites observed with GPS were left with only a single observation. Fortunately, additional surveys performed by the National Mapping Bureau of Papua New Guinea (NMB) were made available for this analysis by Peter Morgan of the University of Canberra (UC). These data spanned the period from 1990 to 1994 and materially added to the earlier GPS surveys.

1.4 The Aim of this Thesis

This research project was conceived with the aim of using Doppler and GPS data to determine the motion occurring across plate boundaries in the region, to answer some of the remaining questions about the location and motion of the tectonic plates surrounding Papua New Guinea. This evolved into a project in which multiple occupations of some sites with GPS were used for the same purpose.

In order to achieve this overall objective, this thesis has involved reducing all of the available GPS observations and combining the data from the various campaigns into a single, consistent solution within a modern reference frame: ITRF94.

1.5 Overview of this Thesis

Chapter 2 is a literature review of the tectonics. It is divided into two major sections; the first is a discussion of plate tectonic theory; the second is a review of the tectonic features and proposed models for the region. The tectonic theory has been applied to the features in the Papua New Guinea region where possible. This chapter provides the essential background for interpreting the GPS results.

Chapter 3 describes the Doppler and GPS systems. These descriptions are not intended to be comprehensive; other references give detailed accounts of the workings of both systems. Instead, this chapter describes the aspects of each system that were pertinent to this analysis, in particular, those parts of the models that needed special care and attention during processing to ensure that the aims of the thesis were met.

The Doppler and GPS surveys are described in Chapter 4. The reasons for discarding the 1975 Doppler survey are also discussed in this chapter. Discarding the Doppler had both positive and negative effects. The positive effect was that a "cleaner" solution, free from reference frame perturbation was possible. The negative effect was that it was no longer possible to confirm the GPS derived rates with GPS-Doppler rates spanning a longer time period. This also applies to the exclusion of 1981 Doppler data from this analysis.

Chapter 5 presents the stability analysis of the 1981 Doppler results. It has two major purposes. The first is to give the reader an understanding of the reasons for discarding the 1981 results from this analysis. Although it has been excluded from this research, it is possible that the 1981 Doppler data will be re-processed at some time in the future. The second purpose of this chapter is to give a thorough description of the processing options and the problems encountered so that the next researcher who approaches this data has some guidance to the pitfalls encountered in this analysis. As time passes, knowledge about the operation of the software inevitably diminishes. If these details are

not recorded now, they will be lost. Chapter 5 consists of two sets of tests. A "test" data set dating from 1974 was tested to establish how a stable solution should behave. The same tests were then applied to the 1981 data, to assess its stability. As a result of the findings in this chapter, the 1981 Doppler results were not used for comparisons with GPS in this analysis.

The GPS processing is described in Chapter 6, with particular reference to the problems associated with attaching the 1990 data to the ITRF94 reference frame. Early GPS data has not been successfully attached to the reference frame of later GPS data until now. The reasons for believing that this has now been achieved are discussed in detail.

Chapter 7 is the culmination of this research. It is the chapter in which the GPS results are applied to the tectonic problems of the region. The GPS results do resolve some of the tectonic issues of the region. Others remain unanswered.

The final chapter, Chapter 8, concludes this thesis. Recommendations for future survey work and interpretive work are given.

Chapter 2

Tectonics of the Papua New Guinea Region

2.1 A Brief History of the Development of the Plate Tectonic Theory

Plate tectonic theory is a unifying theory in geology and geophysics, that brings together many previously unrelated observations. It can explain the existence of mountain belts in some areas and the lack of them in others. The theory can also explain why earthquakes and volcanoes occur, and why these phenomena do not occur in an even distribution over the Earth. Geological similarities and similarities in fauna and flora on continents separated by large expanses of ocean can also be explained by this theory.

Several key discoveries and ideas led to the general acceptance of the plate tectonic theory, which are outlined below. The following development of the plate tectonic theory was adapted from Menard (1986), Weiner (1986) and Allegre (1988).

Plate tectonic theory began with the theory of Continental Drift, proposed by Wegener in 1912. During the nineteenth century, the theory of isostasy had been developed by Pratt, Dutton and Airy. Wegener suggested that if continents could undergo vertical movements, there was no reason why they could not also undergo horizontal movements. The similarity of coastlines on both sides of the Atlantic Ocean caused Wegener to propose that continents were able to drift. He proposed the existence of a super continent, Pangaea, that broke up during the Permian and formed Laurasia and Gondwanaland. He saw today's structure of continents as a result of these two super continents breaking up. Wegener proposed that the continents drifted across the ocean floor. As they drifted, large wrinkles formed on the leading edge of the continents, creating mountain ranges. In the wake of the continents, fragments of continental borders were left behind. These formed island chains. Wegener recognised three types of tectonic regions: compression zones, stretching

zones, and zones where continents move parallel to the faults. Towards the end of his life, after many revisions of his theory, Wegener also proposed that the mantle was capable of flow, and that convection of the mantle was the driving force of continental drift.

Unfortunately, Wegener's contemporaries in the scientific community largely dismissed his ideas, which were subsequently forgotten by all but a few scientists after his death in 1930.

During the 1960's, several key discoveries were made that linked together previously isolated fields of knowledge. This led to the reawakening and development of Wegener's theories into the plate tectonic theory used today.

Discoveries of the structure of the Earth began in the early 1900's in the field of seismology. In 1909, Mohorovicic showed that the speed of seismic waves changed abruptly at the inner edge of the Earth's crust, a boundary now known as the Mohorovicic Discontinuity, often abbreviated to Moho. In 1914, Gutenberg specified the location of the Earth's core at a depth of 2900 km. Thus, when Wegener was working on his continental drift theory, the major layers of the Earth were known: the core, mantle and crust. However, in 1926, Gutenberg made a very important discovery: there existed a "soft" layer inside the Earth, now known as the asthenosphere. Over the next decades, his successors studied this layer in detail and concluded it is less dense and more ductile than the layers above it.

During the 1930's, Wadati noticed that deep earthquakes only occur in restricted zones around the world, and that these earthquakes define an inclined plane. Fifteen years later, these findings were rediscovered by Benioff. Thus the Wadati-Benioff zones associated with oceanic trenches were discovered, although the link with trenches was not made at this time.

Until the 1940's, the ocean floor was largely unexplored. When exploration began, samples of sediment and rock were collected and measurements of the magnetic field were made. These explorations led to the discovery of five main types of submarine structures:

- continental slope which occurs between the shallow continental shelf and the abyssal plain. It has a slope of about 15%;
- abyssal plane, which has a depth of about 4000 m;

- oceanic ridges, which extend for many thousands of kilometres and attain a height above the abyssal plane of up to 3000 m;
- submarine trenches which can reach depths of 11000 m;
- volcanic islands which are strewn across the oceans, and are often aligned in specific directions.

The crustal samples collected on these exploratory journeys and geophysical measurements performed at sea also revealed that the oceanic crust has a different structure and thickness to the continental crust.

When rock is formed it contains certain radioactive isotopes which decay into non-radioactive by-products over time. In 1908, Rutherford suggested that this process could be used to determine the age of rock specimens. This technique was initially limited by the difficulty of measuring the tiny amounts of these isotopes present in rocks. However, after 1937, advances in spectro analysis technology largely removed these limitations. The ability to date rocks gave an absolute dimension to geology, which had previously only been able to work in relative time frames. This allowed the vast periods of time involved in forming geological structures to be quantified, and gave the first absolute determination of the age of the Earth.

Advancing technology also allowed petrologists to create rocks in laboratories. This led to an understanding of the conditions required for the formation of the rocks composing the Earth's crust.

Two additional factors important in the re-emergence of the Continental Drift theory involved magnetic data. The first of these factors was the increased understanding of the causes of the Earth's magnetism. The second factor was the discovery that when rocks form, they are magnetised in the direction of the current magnetic field. This field was first measured precisely by the Chinese in 1040. However, it was not until the late 1800's that magnetometers were developed in the West. The magnetic field varies with latitude, location and the composition of the underlying terrain. Measurements of magnetic anomalies (the difference between the measured and theoretical magnetic fields) revealed that the magnetic poles had wandered throughout history. The arcs defined by the magnetic fields in rocks did not coincide on different continents. However, by rotating continents to close the oceans, the arcs could be made coincident. This proposal was also met with scepticism by the scientists of the time. During

the 1960's, magnetic reversals were discovered on the ocean floor and a time scale for these reversals was developed. This time scale was found to be valid worldwide.

These apparently disparate observations began to be brought together during the 1960's. Hess postulated that the Earth's mantle was circulating in wide convection currents. The surface expression of the ascending portions of these currents are the oceanic ridges and the descending sections are represented by oceanic trenches. This theory explained several observed phenomena:

- the altitude of oceanic ridges;
- the very high levels of heat emitted at these ridges;
- the absence of very old rock on the ocean floor;
- the lack of sedimentary layers on the floor of the oceans of sufficient depth to have been accumulating since the Earth formed.

Dietz added to the theory when he realised that the crust alone could not be drifting. It did not have the necessary strength. A thicker layer was required, which he called the lithosphere.

Wilson also supported the theory with evidence showing that the oceanic islands are older the further they are located from oceanic ridges.

Three concepts were linked to add further evidence in support of seafloor spreading. These were: the discovery by Vacquier and Menard of bands of normal and reversed magnetic polarity on the ocean floor; the symmetry of these bands about oceanic ridges; and the time scale for magnetic reversals. Morley in Canada and Vine and Matthews in England combined the ideas of magnetic anomalies, the time scale of magnetic reversals and Hess' ideas about seafloor spreading. They proposed that basalt is continuously created at oceanic ridges and then drifts symmetrically away. This provides a continuous record of the fluctuations of the magnetic field. Thus their work supported the theories of Hess and Dietz.

Data from the Deep Sea Drilling Project confirmed that sediments overlying the basalt rocks of the ocean floor did increase in age further from the oceanic ridges. This provided additional evidence for the idea that the sea floor was spreading.

In 1965, Wilson and Coode independently developed the concept of transform faults. These can displace the linear patterns of magnetic anomalies. They linked transform faults and spreading centres with the idea that active spreading centres can be offset, but maintain their separation distance. Thus each section of the crust needs to be able to slide past the other. Wilson also showed that the same mechanism displaces oceanic trenches.

The zones of deep earthquakes identified by Wadati and Benioff were linked with oceanic trenches. Earthquakes were also shown to correspond with oceanic ridges.

The various pieces of evidence supporting sea floor spreading, oceanic trenches and transform faults were independently brought together into a unified theory of plate tectonics, firstly by Morgan and then by McKenzie and Parker. In April 1967, Morgan proposed that the surface of the Earth is composed of rigid plates. These can move over the Earth without changing shape. New material is added to the plates at sea floor spreading centres, and material is destroyed at oceanic trenches. Transform faults form small circles on the surface of the Earth which are centred around a point, called the pole of rotation. The movement of the ocean floor is described by the angular velocity about this pole. This idea was triggered by Menard's illustrations of fracture zones in the Pacific. In October 1967, McKenzie and Parker proposed a very similar model based on seismicity. Thus the theory of plate tectonics was developed.

2.2 Structure of the Earth

Determining the structure of the Earth was important for the acceptance of the theory of plate tectonics because it provided a plausible mechanism for the surface of the Earth to be moving. The layers of the Earth have different physical, chemical and therefore rheological (i.e. deformational) properties. The evidence for this layered structure came from two sources. The first was the acoustic waves generated by earthquakes. These waves are reflected and refracted by the different layers of the Earth. The pattern these waves then make on the surface of the Earth enabled seismologists to determine the nature and location of the boundaries between these layers. The second piece of evidence comes from the Earth's gravity field. If the density of the Earth was

uniformly the same as that of rocks on the surface, the force of gravity would be half what is observed (Cox and Hart, 1986).

2.2.1 The Core

The innermost layer is extremely dense. This is the inner core, and has a radius of approximately 1100 km. The layer surrounding this, the outer core, is primarily liquid iron. The Earth's magnetic field is generated in this layer. The radial width of the outer core is approximately 2400 km.

2.2.2 The Mantle

The mantle surrounds the core. It is divided into two layers: the upper and the lower mantle. The upper mantle consists of the layer above a depth of 670 km and is composed predominantly of ultramafic rocks. The upper mantle is not homogeneous. Seismic velocities of P (compressional) and S (shear) waves indicate that the upper mantle is more rigid under continental shields and oceanic basins, and less rigid under mountain belts, oceanic ridges and the concave side of island arcs, that is, in tectonically active regions (Spencer, 1988).

At a depth of 30 - 150 km, the upper mantle has a low velocity zone, called the asthenosphere. The depth of the asthenosphere differs from 30 - 50 km under oceanic regions to 150 km or more under continents. Few major earthquakes originate in the low velocity zone, except in oceanic trenches, which suggests that the rocks in the asthenosphere are less rigid than those above. This reduced rigidity allows the cool brittle crust and upper mantle above this zone to slide over the underlying portion of the mantle (Spencer, 1988).

The lower mantle extends from a depth of 700 km to the outer core. In the lower mantle, seismic velocities, density, rigidity and temperature all exhibit relatively uniform rates of change (Spencer, 1988).

2.2.3 The Crust

The outermost layer of the Earth is called the crust. The crustal material of the continental regions is structurally different to the oceanic crust. The average depth of the seafloor (3800 m) is nearly 5 km below the average elevation of

continental crust (840 m). Most of the surface of the Earth lies close to these two levels (Spencer, 1988). Continents and oceanic basins have different crustal thicknesses. The depth of the oceanic crust is approximately 5 - 10 km, whilst the average continental crust is 30 - 50 km thick (Cox and Hart, 1986, Spencer, 1988). As the crust tries to maintain isostatic equilibrium, the depth of crust under mountain belts increases to 65 - 70 km. Significant variations in the thickness of continental and oceanic crust occur in regions of island arcs, folded mountain belts and along ocean ridges, where no sharp Moho is observed. The Moho marks the distinct increase in P wave velocity from about 6.0 to 8.0 km/s (Spencer, 1988). The crust is generally weaker than the underlying upper part of the mantle, and unable to support the stresses involved with moving plates (Anderson, 1995). Thus the tectonic plates are thicker than the crust and include the upper part of the mantle. This layer is called the lithosphere and is discussed below.

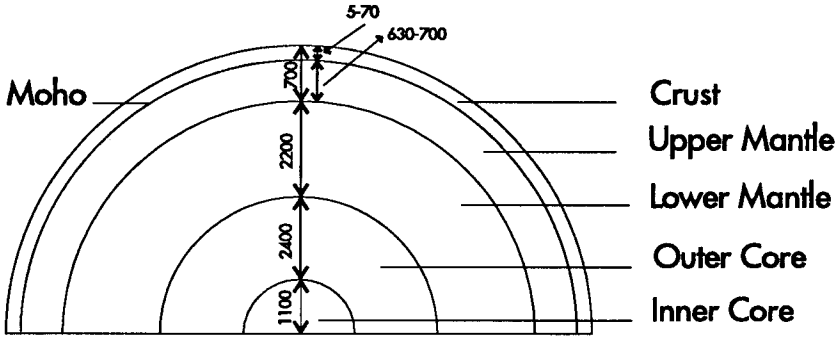

Figure 2.1 The structure of the Earth. The values shown are the radial widths of each layer in kilometres.

2.2.4 Lithosphere, Asthenosphere and Mesosphere

The outer layers of the Earth are the most important in explaining the presence of the variety of geological phenomena seen around the world. However, instead of referring to "crust", "upper mantle", and "lower mantle" in plate tectonic theory, these layers are regrouped into the lithosphere, asthenosphere and mesosphere. Expressed simply, the lithosphere is the strong outermost layer, consisting of the crust and part of the upper mantle. The asthenosphere underlies the lithosphere and is weaker due to its partially molten state. The mesosphere underlies the asthenosphere.

The mesosphere is the innermost layer of the mantle. The definition of its boundary with the asthenosphere is unclear, and its physical properties are not well known. The viscosity of the mesosphere appears to be somewhere between those of the asthenosphere and lithosphere (Cox and Hart, 1986).

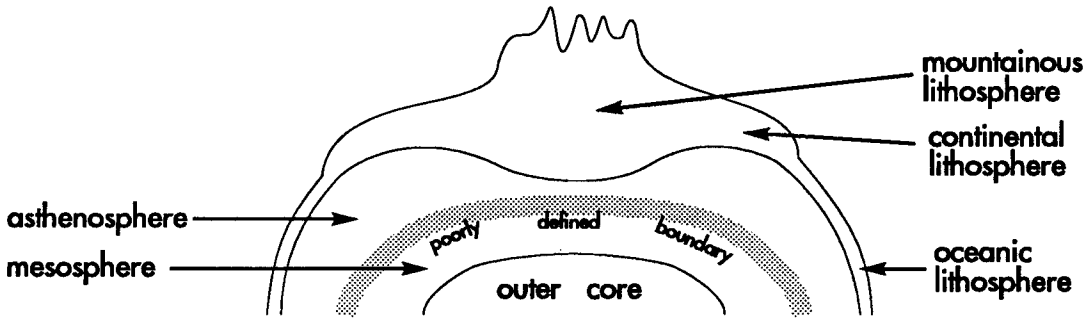

Figure 2.2 Lithosphere, asthenosphere and mesosphere are the layers referred to in plate tectonics. The lithosphere is the strong layer comprising the crust and upper section of the mantle. The asthenosphere is the ductile layer underlying the lithosphere. The mesosphere underlies the asthenosphere. Its properties and the boundary with the asthenosphere are currently not well defined.

Lithosphere/Asthenosphere Boundary

The lithosphere-asthenosphere boundary is defined by changes in rheology, density and therefore, temperature of the rock material (Anderson, 1995).

For example, earthquakes occur in the lithosphere when the amount of stress has accumulated to a critical level. Mantle material appears to be unable to store the stress required to cause earthquakes if it is hotter than about 650 °C (Anderson, 1995). This hotter region of the mantle corresponds to the asthenosphere. However, earthquakes do occur within the asthenosphere beneath ocean trenches, where the cool lithospheric slab penetrates the warmer asthenosphere, thus depressing the isotherms.

The velocity of seismic waves is higher in the lithosphere and lower in the asthenosphere. That is, the elastic seismic waves travel faster in the cooler, more rigid lithosphere. The transition between these velocity zones corresponds approximately to the 600 °C geotherm (Anderson, 1995).

The elastic thickness of a plate also corresponds to the 600 °C geotherm. The elastic thickness refers to the depth at which the thickness of a plate will duplicate the flexural shape of the lithosphere when deflected by a geological load (Anderson, 1995).

Although different criteria can define the depth of the transition between lithosphere and asthenosphere, they all indicate a definite zone at about the 650°C geotherm. This corresponds to a depth of approximately 100-150 km. This boundary is not fixed. It is transitional and constantly changing (Park, 1988).

The importance of this definition is that it distinguishes the two layers by their viscosity, or resistance to flow. The less viscous asthenosphere flows at a geologically significant rate, while the lithosphere is, to a first approximation, solid and does not flow. Plate tectonic theory is based on the premise that the lithosphere consists of a number of major blocks, or tectonic plates, which move on the surface of the Earth with little internal deformation. The majority of deformation occurs along the margins of these plates, where they are in collision with neighbouring plates.

Interactions Between Lithosphere, Asthenosphere and Mesosphere

The lithosphere, asthenosphere and mesosphere are constantly interacting. Material from the mesosphere rises up into the asthenosphere at sites of upwelling. It undergoes a rheological change and becomes less viscous asthenospheric material. Similarly, material from the asthenosphere can rise into the lithosphere where it cools and becomes more viscous.

The main exchange of asthenospheric into lithospheric material occurs at mid-ocean ridges. Material from the asthenosphere wells up into the ridge and moves laterally away as the plates continue to "grow". The material cools and turns into lithosphere material as it is transported away. The converse occurs when lithospheric material is converted into asthenospheric material in subduction zones. The slab descends into the asthenosphere, where it is heated. As it is heated, the material becomes less viscous and becomes part of the asthenosphere.

Properties of the Lithosphere and Asthenosphere

(i) Viscosity

The viscosity of the lithosphere is approximately 10^{25} Pa.s and greater. The viscosity of the asthenosphere is several orders of magnitude lower than this, being approximately 10^{21} - 10^{22} Pa.s, and varying on a local scale (Park, 1988). This difference in viscosity allows the lithosphere to move as a rigid body over the flowing asthenosphere.

(ii) Thermal Structure

Oceanic and continental lithosphere lose heat at about the same rate, approximately 1.5 Heat Flow Units (HFU), or 60 mWm^{-2}. Anomalous zones of high heat flow occur at ocean ridges, island arcs and continental rift zones, where material from the asthenosphere approaches the Earth's surface (Park, 1988).

It follows that as the newly created lithospheric material cools, its heat flow decreases. Thus the age of the lithosphere is linked to its temperature. Subduction zones, where generally old lithosphere is being destroyed, are regions of low heat flow.

Heat flow data is available for the Solomon Sea region. Joshima and Honza (1987) found the average heat flow of the Solomon Sea to be 2.08 HFU, or 87 mWm^{-2}. Their findings are discussed in more detail in Section 2.4.3.

(iii) Elasticity and Short term Strength

The study of seismic wave velocity gives information on short term (< 1 hour) lithospheric elasticity. The strength of the lithosphere determined by these methods is much greater than the strength of the lithosphere when it is subjected to forces over many millions of years. Anomalies in strength of the lithosphere occur in regions of active tectonics (Park, 1988).

The transmission of seismic waves through the lithosphere varies. The interiors of plates transmit seismic waves efficiently, whereas active zones transmit these waves inefficiently. This is due to the different temperature properties of

active and inactive regions. The P-wave velocities decrease at continental rift zones and ocean ridges, revealing zones of anomalously weak, warm material. S-waves are short wavelength shear waves, and so do not penetrate the low velocity zones of the P-waves. S-waves also reveal that active tectonic regions such as island arcs and ocean ridges are anomalous because they are regions of inefficient transmission of these waves. The dispersion of Rayleigh and Love waves (surface waves) can be used to estimate the rigidity of the lithosphere as a function of depth. These studies reveal that areas of weak material (ie asthenospheric material) underlie active volcanic regions (Park, 1988).

Besides seismic wave studies, electrical conductivity in the Earth reveals anomalies at island arcs and continental rift zones.

The combination of these studies implies that active tectonic regions display properties associated with the asthenosphere. By implication, the lithosphere in these regions must be thin. It follows, therefore, that the island arcs and spreading centres in the vicinity of Papua New Guinea are associated with a thin lithosphere under which asthenospheric material approaches the surface.

(iv) Long Term Strength

Park (1988) suggests that "the strength of the lithosphere controls both the initiation and subsequent evolution of major zones of deformation ... (and) is dependent on the vertical distribution of both ductile and brittle strengths." Brittle strength relates to the ability of the lithosphere to withstand stress without fracturing and is controlled by lithostatic pressure. It increases with depth. Ductile strength relates to the ability of the lithosphere to sustain large deformation without fracturing. It is controlled by temperature and decreases with depth. The brittle strength of the lithosphere allows the slab to descend to great depths in subduction zones, while the ductile strength allows the plate to bend as it enters the trench.

According to Park (1988), the balance between brittle and ductile strength determines the strength of the lithosphere and the occurrence of lithosphere failure. If a force is applied to tectonically stable lithosphere, the upper region will experience brittle deformation, and the lower region will undergo ductile deformation. Between the two regions is an elastic zone. This gives strength to the lithosphere. If the force continues to be applied over time, or is increased,

the brittle zone will extend downward, and the ductile zone will extend upwards until the elastic zone is reduced to zero, at which point whole-lithosphere failure will occur. This is the cause of intraplate tectonic activity.

Rocks are much stronger under compression than under extension, thus much greater stress levels or higher heat flow levels are required to cause compressional deformation. Park (1988) gives the example that for a heat flow of 80 mWm^{-2}, extensional stress of 20 MPa can cause deformation, whilst 40 MPa of stress is required to cause compressional deformation.

The crust is composed primarily of quartzo-feldspathic material. The mantle is composed mainly of olivine-rich material. The strength of the lithosphere depends on the relative proportions of these two materials. Oceanic lithosphere, which has a thin crust and is therefore composed mainly of olivine, is stronger than continental lithosphere. Typical ocean basins have heat flow rates of 40 - 50 mWm^{-2}, which, from Figure 2.3, require an unrealistically high amount of stress to cause deformation (Park, 1988).

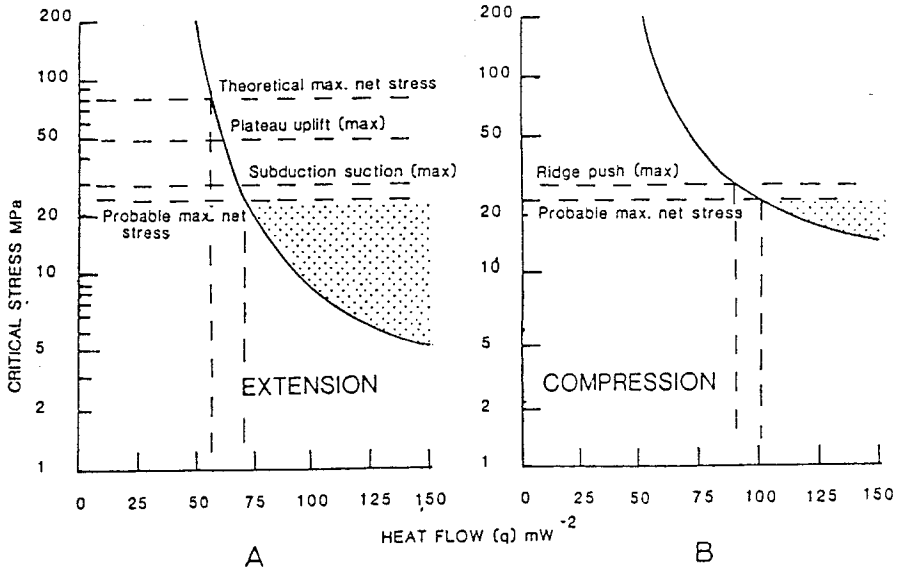

Figure 2.3 Curves of critical stress vs lithosphere heat flow for tensional stress (A) and compressional stress (B). The dotted areas represent potential deformation. © Reproduced with permission from Park (1988), Figure 2.27, page 46.

2.3 Plate Boundaries

There are three different types of interaction zones that can occur between tectonic plates:

- Destructive plate boundaries which, as the name implies, are regions where lithosphere is destroyed. These occur where two plates are moving towards each other.
- Constructive plate boundaries are regions in which new lithosphere is created by upwelling and cooling of asthenospheric material. This type of boundary occurs when two plates move away from each other.
- Conservative plate boundaries occur where two plates are moving past each other laterally along transform faults.

2.3.1 Destructive Boundaries

Two types of destructive boundaries that occur in the Papua New Guinea region will be discussed:

- subduction zones, and
- zones of collision between continents and island arcs.

Subduction Zones

Subduction zones have certain distinguishing features. They encompass the deepest sections of the ocean floor, and are associated with bands of volcanism and usually seismicity and negative gravity anomalies. There are many examples of subduction zones around the world. Despite their abundance and the study which has led to a refinement of the tectonic theory over the last two decades, the issues of how subduction is initiated and the fate of plates at great depth (> ~600 km) are still unresolved. Kincaid (1995) gives a summary of many of the different modelling techniques currently being investigated and the results. In this thesis, however, the causes of subduction are not being investigated: their presence in the Papua New Guinea region is. Subduction zones can occur where plates converge at approximately 2 to 15 cm/y, although well developed trenches and volcanic arcs do not occur when convergence rates are low, that is, in the range 2 to 4 cm/y (Kincaid, 1995).

Seismicity Associated with Subduction Zones

The piece of cold lithospheric material descending into the asthenosphere is called the slab. The slab remains colder and more brittle than the surrounding material of the asthenosphere. Earthquakes occur when the stresses associated with subduction accumulate to a critical level. The seismicity delineates a plane dipping away from the trench, known as either the Wadati-Benioff zone or the Benioff zone. The dip of this plane can vary from nearly horizontal to nearly vertical (Cox and Hart, 1986). It has been suggested by Park (1988) that the angle of dip depends upon the relative rate of convergence across the boundary, the absolute upper plate motion and the age of the subducted lithosphere. This is discussed shortly and will be applied to the Papua New Guinea region in Section 2.4.3. The Wadati-Benioff Zone is one of the most important pieces of evidence supporting the theory of subduction of oceanic lithosphere.

Examples of trenches in the Papua New Guinea region are the New Britain Trench, which is clearly active, and the Trobriand Trough, along which the presence or absence of active subduction is debated. These trenches are discussed in Section 2.4.3.

Mogi (1973) and Park (1988) suggest that earthquakes in a slab occur in a typical pattern. When the stress in the slab at the top of the trench reaches a critical level, a large earthquake will occur. However, before this large quake occurs, there will be numerous lower magnitude quakes in which small movements of sections of the slab occur. This movement propagates down the slab at a rate of approximately 50 km/y. When it reaches the end of the slab, a large earthquake occurs resulting in a sudden downward motion of the slab. This rapidly propagates back up the slab to trigger a large shallow earthquake. This may be either compressional (underthrust faulting) or extensional (normal faulting). Both types of fault have the desired effect of releasing the "stuck" portion of the slab and allowing it to move downwards.

The magnitude of the earthquakes that occur appears to depend upon two main factors:

- the age of the subducted lithosphere, and
- the degree of seismic coupling between the slab and the overlying lithosphere (Park, 1988).

Firstly, consider the age of the subducted lithosphere. As the lithosphere moves away from the spreading centre, it cools. Thus the age of the lithosphere affects its density, buoyancy and thickness. According to Park (1988) young warm lithosphere that is being subducted rapidly seems to be associated with the largest earthquakes. However, in the Solomon Sea where the Woodlark Spreading System is being rapidly subducted, there is an apparent gap in the seismicity. It has been suggested that this lack of seismicity occurs because the lithosphere is young and warm, and therefore remains sufficiently ductile to deform rather than rupture as it is being subducted. For this reason, it is quickly assimilated into the mantle (Weissel *et al.*, 1982). Subduction of the Woodlark Spreading Centre is discussed further in Section 2.4.3.

Secondly, consider the effects of seismic coupling. Seismic coupling results when stronger regions or obstacles on the slab cause an obstruction to further subduction. These obstructions need to be overcome before subduction can continue, and result in larger magnitude earthquakes.

Volcanism Associated with Subduction Zones

Volcanoes form above the slab, when the upper surface has descended to a depth of approximately 100 km. Fluids and volatiles from the crust that were carried down with the lithosphere migrate towards the surface. Thermal and mechanical perturbations of the asthenosphere above the subducted slab also cause upwellings of magma towards the surface (Cox and Hart, 1986). The spatial relationship between volcanoes and trenches will be discussed shortly.

Gravity Anomalies Associated with Subduction Zones

Trenches themselves are typically regions of negative gravity anomalies flanked by positive anomalies. The ocean floor is more dense than the water above it. A mass deficiency occurs where this is actively being dragged down by the dynamics of subduction, which causes the negative gravity anomaly (Cox and Hart, 1986; Park, 1988). On either side of the negative anomalies associated with the trench, are positive anomalies associated with the volcanic island arc on one side and the ocean floor on the other. The island arc has an excess of mass associated with the relatively dense volcanic rocks forming the arc. The lateral strength and continuity of the plate causes the sea floor just

preceding the trench to bend upwards prior to subduction (Park, 1988). These cause positive gravity anomalies around a trench.

Trench Depth

According to Kincaid (1995), there is a direct relationship between trench topography and subduction rate. Trench depth is directly correlated with slab pull force. This force is related to slab age, and intermediate slab dip angle. Kincaid states that numerical experiments indicate trench depth generally increases with fault dip, slab dip, slab length and the pre-subduction angle of the lithosphere.

Geometry of Subduction Zones

Park (1988) suggests that there are a number of factors controlling the geometry of subduction zones, none of which act in isolation. These factors include:

- the relative rate of plate convergence;
- the absolute velocity at which the upper plate is moving. Note that the "upper plate" is the plate above the subducting plate.;
- the age of the subducting oceanic lithosphere;
- the presence or absence of obstacles to subduction on the subducting plate.

(i) Relative Convergence Rate

Rates of convergence can range from approximately 2 - 15 cm/y. Kincaid (1995) states that well developed trenches and volcanic arcs occur when the rate of subduction is greater than about 4 cm/y.

A high relative convergence rate leads to a low angle of subduction. As stated previously, the volcanic arc forms when the top of the subducted slab has reached a depth of approximately 100 km. Therefore, a low angle of subduction will create a large arc-trench gap (150 - 600 km). High convergence rates also lead to depressed isotherms. As the plate rapidly subducts, it will retain its cool temperatures further into the asthenosphere. Thus the heat required to cause the necessary elements to rise to form the volcanic arc will not be acquired by the slab for a greater distance into the asthenosphere. This is another

contributing factor to the large arc-trench gap, and to the increased length of the Benioff zone associated with rapidly subducting trenches.

In contrast, short arc-trench gaps of 100 - 200 km and steeply dipping Benioff zones are the result of slow relative rates of convergence.

(ii) Absolute Upper Plate Motion

The absolute motion of the upper plate is important because the trench must move with it. Rapid motion of the upper plate may override the trench and reduce the influence of gravitational sinking on the slab (Park, 1988). The direction of motion of the upper plate is obviously important. If the upper plate is moving rapidly towards the trench, the result is a shallow angle of subduction and a long arc-trench gap. Thus the situations where the subducting plate moves quickly towards the trench or the overriding plate moves rapidly towards the trench have similar effects. However in the case of rapid upper plate motion towards the trench, the position of the island arc can be relocated 600-1000 km trench-ward of the old position.

If the upper plate has a slow upper plate motion, or is moving away from the trench, the angle of subduction is increased. This causes the trench to migrate seaward (Park, 1988).

(iii) Age of the Lithosphere

Several changes occur in the lithosphere as it ages. New lithosphere, at a mid-ocean ridge, is hot, thin and elevated from the sea floor. As it moves away from the ridge, it cools, thickens and becomes more dense. Thus the buoyancy of the lithosphere decreases away from the ridge. When less buoyant lithosphere is subducted, the dip of the slab tends to be steeper, potentially decreasing the arc-trench separation. However, when young, more buoyant lithosphere is subducted close to the ridge, the magma source is closer to the surface, which also tends to decrease the separation between the trench and arc.

In the Papua New Guinea region, the Solomon Sea is an interesting place to study this phenomenon. The age of the Solomon Sea lithosphere varies across the sea floor. Near the Woodlark Spreading Centre, the lithosphere is obviously very young. The spreading centre is being subducted to the northwest into the

New Britain Trench, thus the age of the subducted lithosphere must increase along the trench, away from the ridge. Subduction of the Woodlark Basin is discussed in Section 2.4.3.

(iv) The presence of Seamounts and Plateaux

Density of the lithosphere is reduced locally by the presence of seamounts or oceanic plateaux. These features, composed of less dense material than the surrounding oceanic lithosphere, increase the relative buoyancy of the slab and thereby reduce the angle of subduction. In some cases such obstacles will cause subduction to cease, and the motion must be accommodated on a new boundary. An example of this is the collision between the Ontong Java Plateau and the North Solomon Trench in the Miocene. It is generally thought by many authors (for example Herzig *et al.*, 1994) that the trench became blocked by the plateau, and a new trench formed to the south of New Britain to accommodate the continued convergence between the two plates.

In addition, the presence of an accretionary wedge on the subducting plate tends to flatten the slab inclination at shallow depths. This is caused by the weight of sediments depressing the lithosphere prior to subduction (Park, 1988).

Finally, subduction over long periods of time may thicken the upper plate because of the cumulative effects of accretion and depression of the isotherms (Park, 1988).

The trench geometry scenarios discussed here are applied to trenches in the Papua New Guinea region in Section 2.4.3.

Stress in the upper plate is controlled by all of the above factors. Steeply dipping slabs are associated with extensional stress in the upper plate, caused by the subduction suction force coupled with thermally induced isostatic uplift. In contrast, slabs dipping at a shallow angle are associated with compression forces in the upper plate because of the increased level of coupling of upper and lower plates. This allows horizontal compressional forces to be transmitted to the upper plate. The opposing causes of stress in a subduction zone (negative buoyancy causing extension and resistance causing compression)

tend to be approximately in balance. Some trenches exhibit net compression while others exhibit net extension (Park, 1988).

Zones of Collision between Continents and Island Arcs

Collision is the process in which the lithospheric material of the converging plates is overlapped, causing crustal thickening. The buoyancy of continental crust ensures that these collision zones exist, as continued subduction inevitably eliminates the seafloor separating continental material either side of a trench. There are two types of collision: continent-continent and continent-island arc. The latter occurs in Papua New Guinea. Many authors (for example Pigram and Davies, 1987; Abbott, 1995) postulate that the southern part of Papua New Guinea, part of the Australian craton, has collided with two island arcs in the last 40 Ma creating the current landmass. After the initial collision between continent and island arc lithosphere, subduction continues. This leads to the formation of mountain (or orogenic) ranges, crustal thickening and isostatic uplift (Park, 1988).

Active and recent mountain ranges are characterised by elevated topography (commonly 3-7 km) which is approximately isostatically compensated by a thick root of low density crustal material. According to Park (1988), this thickened crust is typically 1.5 to 2 times average thickness.

Initially, the crustal thickening which accompanies collision will lead to depression of the isotherms and reduced surface heat flow. However, over time, the lower section of the thickened crust heats up and undergoes prograde metamorphism and possibly melting. Thus the isotherms return to normal gradients and isostatic equilibrium is restored which causes uplift (Park, 1988).

It is possible in collision zones for part of the crust of one plate to become detached and override the other plate, while the remaining lithosphere continues to be subducted. This has been called flake tectonics. Sometimes the whole layer of the crust can become detached, which explains the presence of very high pressure metamorphic rocks within orogenic belts (Park, 1988).

It is also possible for oceanic crust to overthrust continental crust in ophiolite complexes. This process is called obduction. The presence of ophiolite complexes in collision zones can indicate the presence of a former subduction

zone. Typical ophiolite complexes can extend for several hundred kilometres in length, but never exceed 15 km in thickness (Park, 1988). Four major layers constitute the belt: pelagic sediments; pillow lavas; sheeted dykes; layered gabbros. These overlie ultrabasic mantle material. Examples of ophiolite complexes can be found along the Papuan Peninsula and New Guinea Highlands.

There are, however, significant differences between ophiolite belts and standard oceanic ridges which have been used to suggest that ophiolite belts are formed from anomalous oceanic lithosphere produced in back arc basins (Spray, 1983; Park, 1988).

2.3.2 Constructive Plate Boundaries

As explained in Section 2.2.4, the lithosphere is much stronger in compressional regimes than extensional regimes. A greater amount of stress is required to cause compressional deformation than extensional deformation. Therefore, there are many more extensional regimes on the surface of the Earth than compressional ones (Park, 1988).

Extensional regimes fall into the two main categories of

- divergent plate boundaries
- intraplate regimes

Intraplate regimes, such as continental rifts and extensional basins do not occur in the Papua New Guinea region. They are generally limited to the major plates. For this reason, they will not be discussed.

The types of divergent plate boundaries that occur in the Papua New Guinea region are:

- oceanic ridges
- back-arc spreading

Ocean Ridges

Oceanic ridges rise several kilometres in height above the abyssal plains, and can extend for many thousands of kilometres. The base of these mountain chains are typically several thousand kilometres wide. Oceanic ridges have several distinguishing features, including the occurrence of a narrow band

(~10 km) of moderate sized earthquakes near the crest of the ridge; unusually high heat flow; distinct magnetic lineations; and a gravity anomaly much smaller than would be expected from a mountain range of that size (Cox and Hart, 1986). According to Park (1988), the small gravity anomaly is explained by the large excess topographic mass of the ridge being almost exactly compensated by a mass deficiency caused by the less dense mantle material below the ridge.

Many of the properties of the asthenosphere occur at oceanic ridges, indicating that the lithosphere is very thin in these regions and the asthenosphere is much closer to the surface. For example, ridges are associated with:

- low electrical activity
- high attenuation of seismic waves
- high dispersion of surface waves
- inefficient propagation of S waves.

Park (1988) suggests that oblique spreading occurs at ridges where the spreading is asymmetrical. In Papua New Guinea, this can be seen along the Bismarck Sea Seismic Lineation. As discussed in Section 2.4.3, it is undergoing oblique extension, and has a rate of 7.4 cm/y to the north and 5.8 cm/y to the south. The Woodlark Spreading Centre is also spreading obliquely.

Backarc Spreading

Extensional tectonic regimes can occur at convergent plate boundaries. Under certain circumstances, tensional stresses are exerted on the upper and lower plates in subduction zones. As previously stated, shallow dipping slabs are associated with compressional stress, whereas steeply dipping slabs are associated with extensional stress (Park, 1988). The upper plate in a subduction zone experiences enhanced heat flow associated with volcanic arcs. From Figure 2.3, it is clear that this means much smaller extensional stress will be required for failure to occur. Extensional stresses are applied equally to the upper and lower plates, but the thermally weakened upper plate is the one that fails (Park, 1988). There have been several models proposed for the cause of back-arc spreading. Karig (1971) suggests spreading occurs because of the diapiric rise of hot mantle material released by the subduction process above the descending slab. Park (1988) gives an alternative view that back arc spreading is due to a secondary convective cell. Another suggestion is

that when the resultant of gradual seaward migration of the trench and the velocity of the upper plate has a component directed away from the trench, back-arc spreading occurs. Seaward migration of a trench can be explained by the gravitational pull of the descending slab, or a change in relative velocity of the converging plates which changes the profile of the descending slab (Park, 1988).

Back-arc spreading occurs on the upper plate in subduction zones on the concave side of the associated island arcs.

In Papua New Guinea, it has been suggested that the Bismarck Sea Seismic Lineation is an example of back-arc spreading. The tensional tectonics around the New Ireland Basin are probably also related to this.

2.3.3 Conservative Plate Boundaries

Conservative boundaries have already been mentioned as separating the segments of spreading centres. Much larger transform faults occur as major plate boundaries in their own right, for example the northeastern boundary of the Pacific plate. However, as no major strike-slip faults have been reported in the Papua New Guinea region, this type of boundary will not be discussed further.

2.3.4 Source of Plate Motion

The all encompassing answer to the question of what causes the surface of the Earth to move, is thermal energy. Heat is transferred from the Earth's core to the surface. However, the actual mechanisms causing plates to move are more controversial.

Convection

It seems certain that convection does occur in the mantle. The similarity over geological time scales of suites of igneous rocks supports this view. It indicates a well mixed source of these rocks, which suggests that the mantle is convecting (Park, 1988). However the extent of convection and its role in plate tectonics are uncertain. Current theories favour independent or only partially

coupled convection systems in the upper and lower mantle, with the convection systems being dominated by the location of descending slabs.

The presence of higher than average amounts of more dense material at trenches and less dense material at ridges means that major upwellings and downwellings in the mantle should cause distortions in the geoid. However, there is poor correlation between gravity anomalies and major tectonic features. This can possibly be explained by the transitory nature of the location of plate boundaries, requiring the convection system to lag behind (Park, 1988). The geoid does, however, reveal undulation wavelengths of several orders of magnitude which may be related to convection currents of several scales.

Park (1988) proposes that there are three levels of convection in the mantle, which can be related to the tectonic features as follows. Figure 2.4 shows the proposed levels of convection.

Geoid undulations reveal a long wave anomaly with a half wavelength of about 4000 km, which is approximately the size of the major plates. This scale of convection can be seen to return material from the trenches to the spreading centres. As the buoyancy of continental crust makes it nearly impossible for it to be subducted, the trenches will eventually subduct until they reach the margins of continents. Therefore, the location of continents must place some control on the location of subduction zones, and hence on the mantle flow patterns. However, as mentioned above, convective changes may lag behind continent migration due to the time taken for subducted material to heat up. This scale of convection is whole mantle convection.

The second scale of convection Park (1988) relates to upper mantle convection. This scale is proposed because it is thought that the change in physical and chemical properties which occurs at the upper and lower mantle boundary inhibits complete circulation. This implies that convection in the upper mantle is independent of, or only partially coupled with, convection in the lower mantle. An intermediate wavelength geoid undulation, with a half wavelength of about 1000 - 1500 km, has been associated with hotspots. It is thought that the hotspots are linked with an upper mantle convection system.

Finally, short wavelength gravity anomalies, with half wavelengths of 100 - 250 km, have been attributed to variations in the cooling pattern of a plate

as it moves away from a ridge. It is thought to be linked with small scale convection within the asthenosphere.

Plate Motion - Cause or Effect?

Accepting that convection occurs within the mantle leads to the question of driving forces. Does mantle convection drive plate tectonics, or does plate tectonic motion, in particular the location of descending slabs, drive the convection system?

Cox and Hart (1986) prefer the theory that plates are an active component in the convection system rather than the converse in which the convection system drives plate motion. Their arguments are summarised below.

In the passive plate theory, the plates are moved along the surface of the Earth by the action of the convection cells in the asthenosphere. Thus spreading centres mark the positions of the ascending limbs of the convection cell, and trenches mark the descending limbs. The distance between the ascending and descending limbs is determined by the length of the convection cell and would be expected to remain nearly constant during the lifetime of the cell (Cox and Hart, 1986).

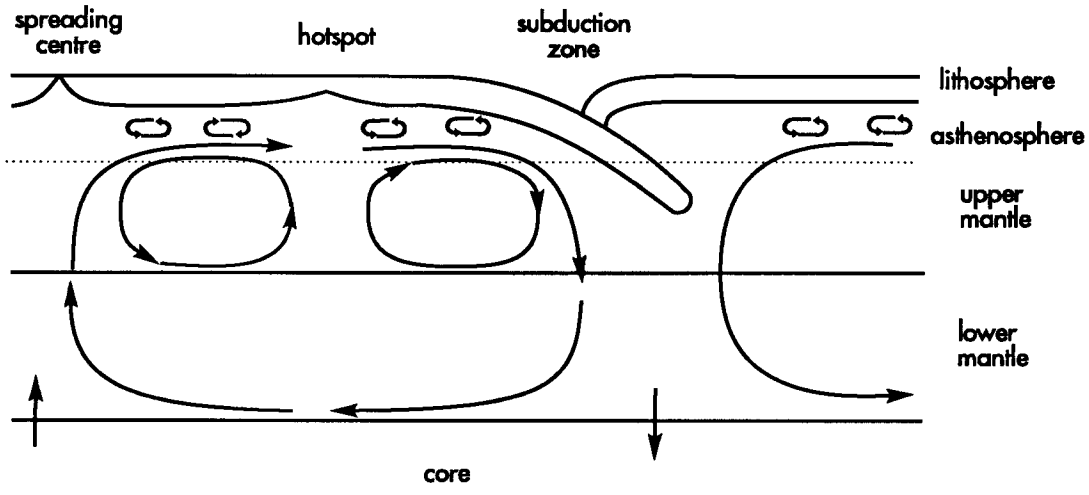

Figure 2.4 Convection patterns in the mantle. The large scale, whole mantle convection is linked to motion of the major plates. The upper mantle convection system is linked with hotspots. The small wavelength convection system is associated with patterns in the asthenosphere. Adapted from Park (1988).

The active plate theory uses the properties of the lithosphere and asthenosphere to explain why plates control convection. The lithosphere is colder, more viscous and more dense than the underlying asthenosphere. This greater density enables the lithosphere to sink into the asthenosphere. As it is cooler than the asthenosphere, it forms the descending limb of the convection cell. Ridges, under this theory, are simply cracks between diverging plates that have to be filled from local magma sources in the asthenosphere (Cox and Hart, 1986).

Evidence supporting the notion that plates are active components of the convection system is set out below.

Ridges consist of segments of spreading offset by transform faults. The passive plate theory requires these offsets to be mirrored by offsets in the convection cells. This is not unreasonable when the segments of spreading are about 1000 km long. Laboratory tests and simulations show that the ratio of width to depth in general convection cells is about 1. Therefore, a convection cell about 1000 km wide must be about 1000 km deep, which is consistent with a convection cell originating deep within the mantle. However, it is not uncommon for ridge segments to be as short as 10 km on the seafloor. This implies a convection cell of about 10 km deep using the width to depth ratio, which is inconsistent with whole mantle convection (Cox and Hart, 1986), but consistent with a system in which there is more than one scale of convection currents.

In contrast, the active plate theory explains ridges as cracks to be filled with magma from shallow sources in the asthenosphere nearby.

Ridges also sometimes jump to new positions, probably reflecting changes in the direction of plate motion, or propagate into new regions. The passive plate theory requires the ridge jumps to reflect jumps in the ascending limbs convection cells. The observation that ridges commonly jump at time intervals of only a few million years would require a physically implausible jerky mode of convection (Cox and Hart, 1986).

In contrast, the active plate theory explains this phenomenon as magma rising to fill a new crack created in the lithosphere as a result of a change in the direction of stresses caused by the shift in plate motion.

Ridges can also be subducted, either obliquely or parallel to a trench. In both the cases, the width to length ratio for convection cells becomes too small, based on values obtained by laboratory experiments and simulations (Cox and Hart, 1986).

Modelling the mantle convection patterns by Elder (1976) resulted in the following conclusions:

- subduction zones exert a major control on mantle convection
- continents cause small scale eddies which cause lateral forces and volcanic activity
- continental plates do not ride passively on a horizontal mantle convection system
- plates are not driven by mantle drag forces at the lithosphere-asthenosphere boundary
- plates are not driven by ridge push forces at spreading centres.

According to Kincaid (1995), the subduction of cool, chemically distinct oceanic lithosphere to depths of at least 670 km, drives plate tectonics and greatly contributes to the thermal and compositional evolution of the mantle. The recycling of crust and sediments through subduction zones ultimately contributes to the growth and evolution of continental crust and lithosphere.

Park (1988) concludes that no single force drives plate tectonics, but that all forces arise from the convective flow system itself.

2.3.5 Forces acting on a Plate

There are a number of forces thought to be acting on the tectonic plates. These are described below and illustrated in Figure 2.5.

Slab Pull

As mentioned previously, the oceanic lithosphere is cooler and more dense and therefore less buoyant than the underlying asthenosphere. Thus when a slab is being subducted, it exerts a pull force on the unsubducted portion of the plate. This is potentially the largest of the forces acting on a plate. It is counteracted to a certain extent by resistance forces (Park, 1988).

Subduction Suction

When a slab is being subducted, it has an extensional effect upon the over-riding plate. This force is called trench or subduction suction.

Ridge Push

Newly created lithosphere welling up from an ocean ridge moves laterally away from the ridge and cools. This movement exerts a pushing or compressional force on the plates on either side of the ridge.

Mantle Drag

Convection in the asthenosphere causes a drag effect on the base of the overlying lithosphere. This is considered to be a small force in comparison with the forces acting at the plate boundaries because of the relatively low viscosity of the asthenosphere. If, as suggested in Section 2.3.4 and Figure 2.4, the major plates overlie smaller convective cells, these would be expected to create drag forces in varying directions that would cancel each other out.

Resistance

Besides the resistance to subduction mentioned above, resistance forces are encountered at conservative plate boundaries. However, these forces are considered to be small in comparison with the forces exerted by slab pull and ridge push.

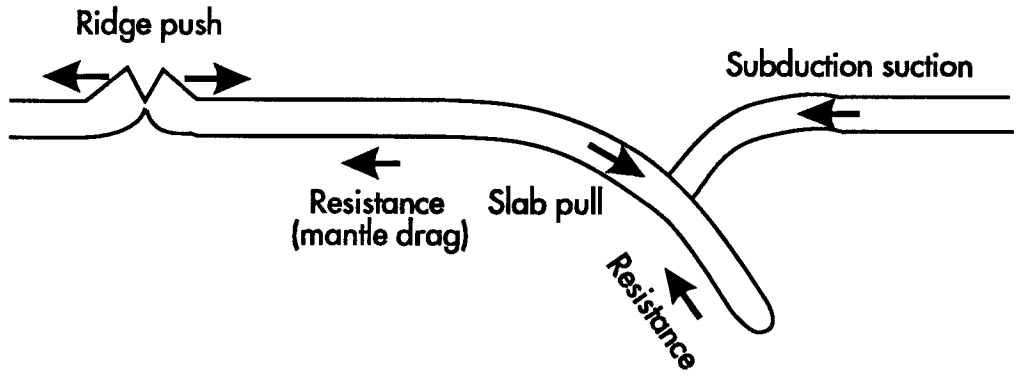

Figure 2.5 The forces acting on a lithospheric plate.

2.3.6 Life Cycle of a plate

Oceanic plates and continental plates have different life cycles (Cox & Hart, 1986). Continental plates undergo a complex cycle, with periods of rapid motion, when they are attached to a subducting slab, and periods of slow motion, when they are not. As continental lithosphere is buoyant, it resists subduction. When continental lithosphere reaches a trench, the subduction at the trench ceases, or is transferred elsewhere. The motion of the continent will then slow or stop. For this reason, continental plates will never truly disappear. If a trench is subsequently created on the other side of a continental plate, the continent will rapidly move towards the new trench, until it reaches it, when it will stop again.

Oceanic plates, on the other hand, generally do not have the buoyancy of continental plates. There are some exceptions to this generalisation, such as the Ontong Java Plateau on the Pacific plate. This is an oceanic plateau that has previously been mentioned because it is thought to have blocked subduction along the North Solomon Trench. Usually, however, oceanic plates can go on subducting until they completely disappear. An example of this is possibly occurring in the Solomon Sea. While an oceanic plate such as the Pacific plate is subducting on one side, new crust is being added to it on the other. Therefore, the lifespan of an oceanic plate is greater than the time it takes for a section of crust to move from the spreading centre to the trench, and can be hundreds of millions of years. For example, the Pacific plate has been in existence for at least 150 Ma, according to the age of the oldest magnetic stipes found on the plate. At its present rate, if spreading stopped now, it would take 80 Ma for the plate to disappear, giving the plate a lifespan of at least 230 Ma.

2.4 Tectonics of the Papua New Guinea Region

2.4.1 Regional Setting and History

The southwestern region of the Pacific is characterised by a complex tectonic regime. The area is rife with seismic and volcanic activity. This activity indicates the presence of major tectonic plate boundaries in the region. The southwest Pacific is in the collision zone between three large tectonic plates: the Eurasian, the Australian and the Pacific plates.

The landmass of Papua New Guinea and the surrounding islands have obviously not been constant throughout geological time periods. They are the result of the proposed collision in which the tip of the Australian continent has collided with island arcs and/or continental fragments. The collision is ongoing, with the New Britain arc currently colliding with Papua New Guinea (Abbott, 1995). A brief proposal of the history of the tectonic processes leading to today's configuration is given, based on the interpretation of Lee and Lawver (1995).

About sixty million years ago, during the Paleocene, India and Australia were travelling together on the same plate north eastwards towards the Eurasian continent. At this time, the continental margins of the Indo-Australian and Eurasian plates began to collide. India was moving at 123 mm/y and Australia at 12 mm/y. New Guinea, at this time, consisted only of the south-western section of today's island, which is part of the Australian craton. The Sepik Arc was located far to the east at approximately 165° longitude.

Ten million years later, during the Middle Eocene, the rotation of the continental margins coming into contact with Australia and India changed because India began to collide with Tibet. This collision is termed a hard collision, because it consisted of continental masses colliding. The velocity of India slowed to 96 mm/y while the velocity of Australia increased to 27 mm/y. There was some rotation of the Pacific plate bringing the Sepik Arc towards the Australian and New Guinea landmasses.

Forty million years ago, during the Late Eocene, the rotation of the Indo-Australian plate continued with Australia's velocity increasing to 55 mm/y and India's decreasing further to 46 mm/y. This illustrates very clearly, the

above statement that continents can have rapid or slow velocities depending on whether they are approaching landmasses or oceanic trenches. The rotation of the islands to the east continued, bringing the Sepik Arc and the Louisiade Islands closer to the Papua New Guinea/Australian landmass.

During the Oligocene, approximately 30 million years ago, Australia's velocity increased to 73 mm/y and India's to 52 mm/y. The Sepik Arc had almost collided with Papua New Guinea. The West Caroline Basin and the North New Guinea Arc, including the islands of New Britain and New Ireland, were being rotated towards the Southeast Asian conglomeration of islands.

The Late Oligocene saw the opening of an oceanic trench extending from the Philippines to south of the East New Guinea Composite Terrain. This is now the Papuan Peninsula, but at that time, it was located to the east at approximately 155°E. The Sepik Arc had collided with New Guinea and extended the landmass to the north, forming what is now known as the New Guinea Highlands. The North New Guinea Arc was approaching the trench separating it from New Guinea.

Fifteen million years ago, during the Miocene, the velocities of Australia and India had slowed to 66 mm/y and 45 mm/y respectively. The East New Guinea composite terrain had reached the trench it was approaching and caused a reversal in subduction, and relocation of the trench to the north of this block. New Guinea was now being subducted towards the trench.

Ten million years ago, the New Guinea landmass had reached the trench it had been approaching and stopped subduction there. The East New Guinea composite terrain had collided with the New Guinea landmass and formed the Papuan Peninsula. The remnants of this trench to the northeast of the Papuan Peninsula formed what is today the Trobriand Trough. To the east, the Ontong Java Plateau had reached the North Solomon Trench, and was stopping subduction in that trench. Subduction was accommodated at a new trench south of the New Britain and Solomon Islands: today's New Britain Trench. This collided with the Trobriand Trough in the northwest of the collision between the New Guinea mainland and the North New Guinea Arc.

During the last five million years, seafloor spreading has begun in the Bismarck Sea and the Woodlark Basin. The North New Guinea Arc has continued to collide with Papua New Guinea, creating the tectonic situation of today.

2.4.2 Motion of the Major Plates Surrounding the Papua New Guinea Region

Today, the Papua New Guinea region is tectonically surrounded by the Australian and Pacific plates. The Caroline plate may lie to the north (Weissel and Anderson, 1978), but evidence for its existence is equivocal. In absolute terms, the velocities of these plates are as follows. The Pacific plate is moving northwest at a rate of 10.2 cm/y; the Australian plate is moving north-northeast at a rate of 7 cm/y; and the Caroline plate, if it exists, is also moving northwest at a rate of 10.2 cm/y. That is, it is moving at the same rate and in the same direction as the Pacific plate (Circum- Pacific Council for Energy and Mineral Resources, 1982).

2.4.3 Tectonic Features of the Papua New Guinea Region

Papua New Guinea and Irian Jaya form one large island approximately 2500 km long and 600 km wide. Together, they form part of the northern edge of the Australian plate. The southern section of Papua New Guinea is part of the Australia craton, while the area from the centre of the island northwards is composed of island arcs and/or continental fragments accreted to the mainland over the last 20-30 million years.

The area encompassed by this study includes from the Irian Jaya border in the west to the Solomon Islands in the east, and from the Woodlark Spreading System in the south to Manus Island in the north (Figure 2.6).

This small region of the Earth, approximately 1000 km by 1000 km, contains some of the most complex tectonics. It has been actively studied for the last 30 years, which encompasses the full period since the plate tectonic theory was accepted by the scientific community.

The tectonic elements that make up this region are now described.

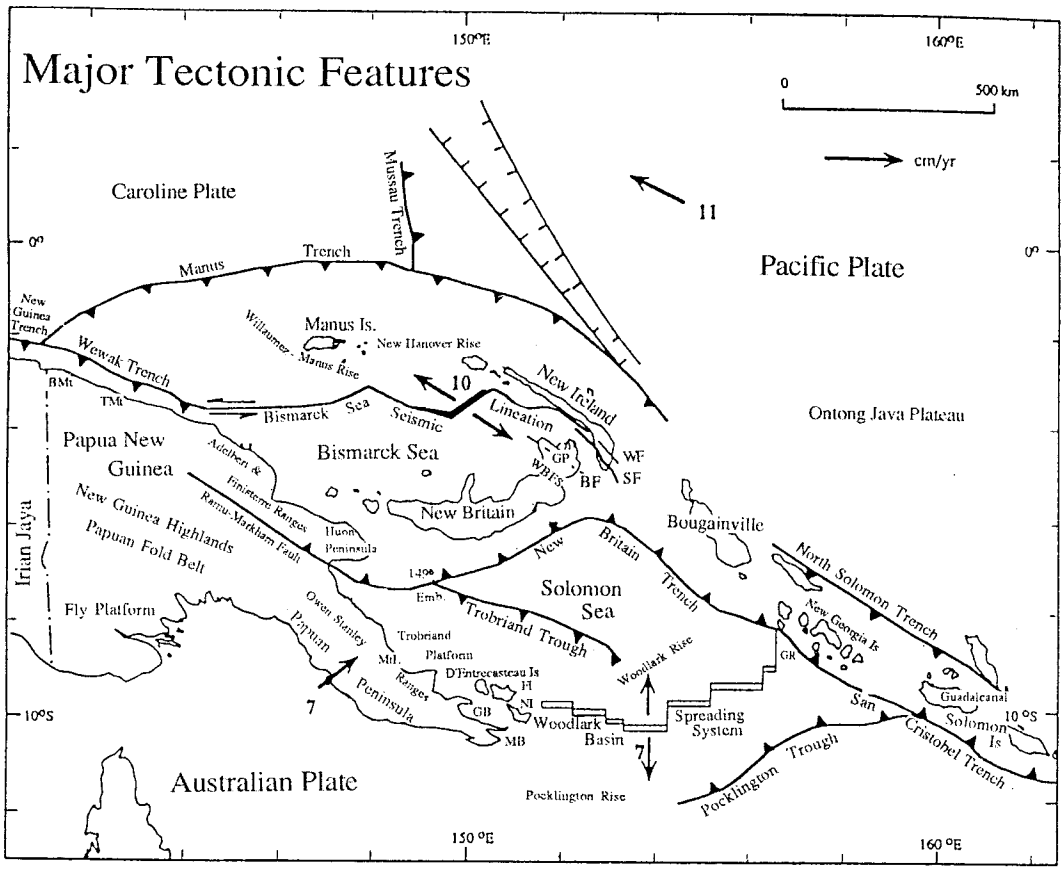

Figure 2.6a Tectonic elements of the Papua New Guinea region. The abbreviations are as follows: GP - Gazelle Peninsula; WF - Weitin Fault; BF - Baining Fault; SF - Sapom Fault; WBFS - Wide Bay Fault System; GR - Ghizo Ridge; GB - Goodenough Bay; MB - Milne Bay; NI - Normanby Island; FI - Fergusson Island. Plate velocities are from Circum-Pacific Council for Energy and Mineral Resources (1982).

Trenches

There are three trenches in the region of study. These are:

- the Trobriand Trough
- the New Britain Trench
- the Manus and North Solomon Trench system

Trobriand Trough

Whether the Trobriand Trough is an active or inactive subduction system is a widely debated issue in the literature. If active, many authors consider the Trobriand Trough to be the site of subduction of the Solomon Sea plate southwards under the Trobriand Platform and Papuan Peninsula.

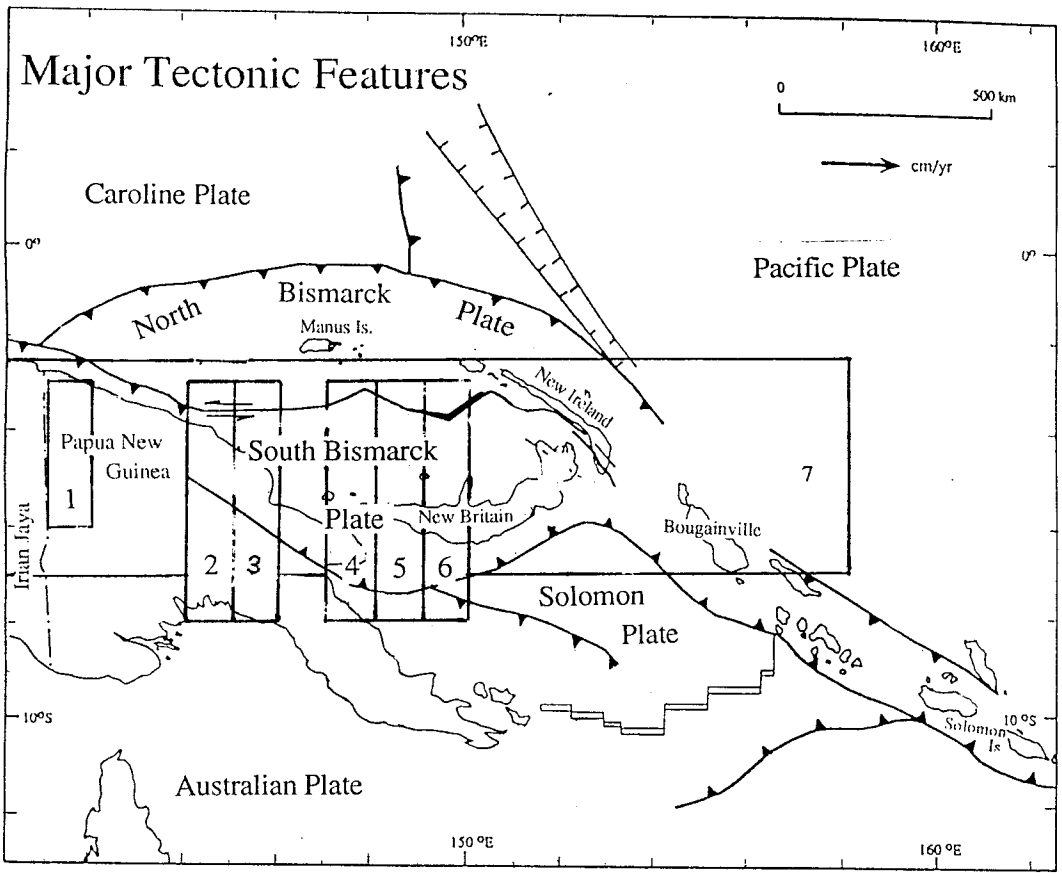

Figure 2.6b Proposed tectonic plates of the Papua New Guinea region. For a more detailed discussion of the models proposed by various authors, see Section 2.4.4 and Figure 2.14. The numbers 1-6 refer to the cross sections shown in Figure 2.8 and number 7 refers to the longitudinal section shown in Figure 2.9. The cross sections are: 1) 141°-142°; 2) 144°-145°; 3) 145°-146°; 4) 147°-148°; 5) 148°-149°; 6) 149°-150°.

Hamilton (1979) proposed that the Trobriand Trough is active or has only recently become inactive. He based this claim on two factors: the occurrence of Late Cenozoic andesite volcanism in southeast Papua New Guinea and the D'Entrecasteaux Islands; and the trench-like appearance of the northern margin of the Trobriand Platform. Only a few shallow earthquakes have been detected along the Trobriand Trough and there does not appear to be a clearly defined Wadati-Benioff zone associated with the trough (Abers and Roecker 1991). Figure 2.7 shows the seismicity associated with the Trobriand Trough and Papuan Peninsula. It is evident that seismicity is considerably less than that associated with the New Britain Trench. However, Ripper (1982) established the existence of a poorly defined Wadati-Benioff zone at intermediate depths dipping southwest beneath eastern Papua New Guinea. It does not extend further east than Mount Lamington, and can be detected between 148° and 149°E. In contrast to Hamilton's claim, Johnson (1979) and Smith (1982)

suggest that the few Quaternary volcanoes on the Papuan Peninsula that might form an associated volcanic arc are not related to subduction.

Davies *et al.* (1984) used seismic reflection profiles to show that there is an absence of sediment cover over the deformation front of the Trobriand Trough and active faulting along the strike of the trough. The sediment shows several stages of deformation: early thrusts on the inner wall and normal thrusts on the outer wall, and later faults that have elevated the outer trench margin. Also, thrust anticlines and slope basins are developed on the inner wall (Davies *et al.*, 1984, Lock *et al.*, 1987, Kirchoff-Stein *et al.,* 1992). On the basis of seismic reflection profiles, Lock *et al.* (1987) support Hamilton's proposal that the Trobriand Trough has been recently active. Davies *et al.* (1984) and Kirchoff-Stein *et al.* (1992) conclude that the Trobriand Trough is currently active, but that subduction is proceeding very slowly and aseismically. Kirchoff-Stein *et al.* (1992) estimate that the rate of subduction is 0.6 cm/y, but that it is not true oceanic subduction. Ripper (1982) believes that subduction ceased when the Trobriand Trough came into collision with the New Britain Trench.

The proposal that the Trobriand Trough is active, yet has very little seismic activity, and no clear Wadati-Benioff zone, is indirectly supported by the work of Kincaid (1995), who claims that subduction of less than approximately 4 cm/y does not produce a well developed trench and volcanic island arc structure.

Triple junction analysis of the South Bismarck, Solomon and Australian plates requires a motion of approximately 9 cm/y between the Australian and Solomon plates. This is discussed in Section 2.4.3. This is certainly not occurring on the Trobriand Trough. If it is active, it is not the main boundary between Australia and the Solomon Sea plate.

New Britain Trench

The New Britain Trench is undisputably a plate boundary. It separates the South Bismarck Sea from the Solomon Sea. To the west, the trench collides at an acute angle with the Trobriand Trough at the 149° Embayment (Tiffin *et al.,* 1987), where both trenches abruptly end. To the east, the New Britain Trench makes a sharp bend of about 72° between eastern New Britain Island and western Bougainville Island. From the bend, it continues in a

southeasterly direction to become the San Cristobel Trench opposite the Solomon Islands. The active volcanic arc associated with the New Britain Trench extends approximately 500 km further to the west than the trench itself, following the northern coast of Papua New Guinea.

It is generally thought that the small Solomon Sea and South Bismarck plates are in collision at the New Britain Trench, with the Solomon Sea plate subducting beneath New Britain in a northerly to north-northwest direction. Motion across the New Britain Trench is rapid. Johnson (1979) reviewed models proposed by Johnson and Molnar (1972), Curtis (1973), Krause (1973) and Taylor (1975). These models gave the rate of convergence as 6.2 cm/y in the west increasing to 12.5 cm/y eastwards. Krause (1973) and Curtis (1973) suggest that the rate of convergence increases along the trench to the northeast. The rate of convergence between the Solomon Sea plate and the Pacific plate east of the sharp bend in the New Britain Trench has been calculated from magnetic anomaly interpretations to be 14.5 cm/y at N45°E by Kroenke (1984).

The seismicity associated with the New Britain Trench is very intense, with a profusion of earthquakes in the 30 - 60 km depth range. The migration of earthquakes with depth in Figure 2.7, clearly illustrates the dip of the Wadati-Benioff zone to the northwest and northeast of the bend in the Trench at approximately 153°E. To a depth of 180 km, this northeastern migration of seismic activity with depth is apparent under Bougainville. Under New Britain, this pattern is clear to a depth of 350 km. Around the bend in the New Britain Trench, the earthquakes can be seen migrating along a Benioff zone to a depth of 500 km.

Earthquakes deeper than 500 km occur in two distinct zones, one northeast of Bougainville and the other in the Bismarck Sea. Cross sections of the seismicity at longitude 150°E show that these deep earthquakes appear in a linear trend with the shallower earthquakes, suggesting continuity of the slab. Profiles drawn along the meridians of longitude are seen in Figure 2.8. From Figures 2.7 and 2.8 it is clear that the slab generally descends to a depth of approximately 250 km. However, in two places, north of New Britain and north of Bougainville, earthquakes have been recorded at depths of 600 km and 500 km respectively.

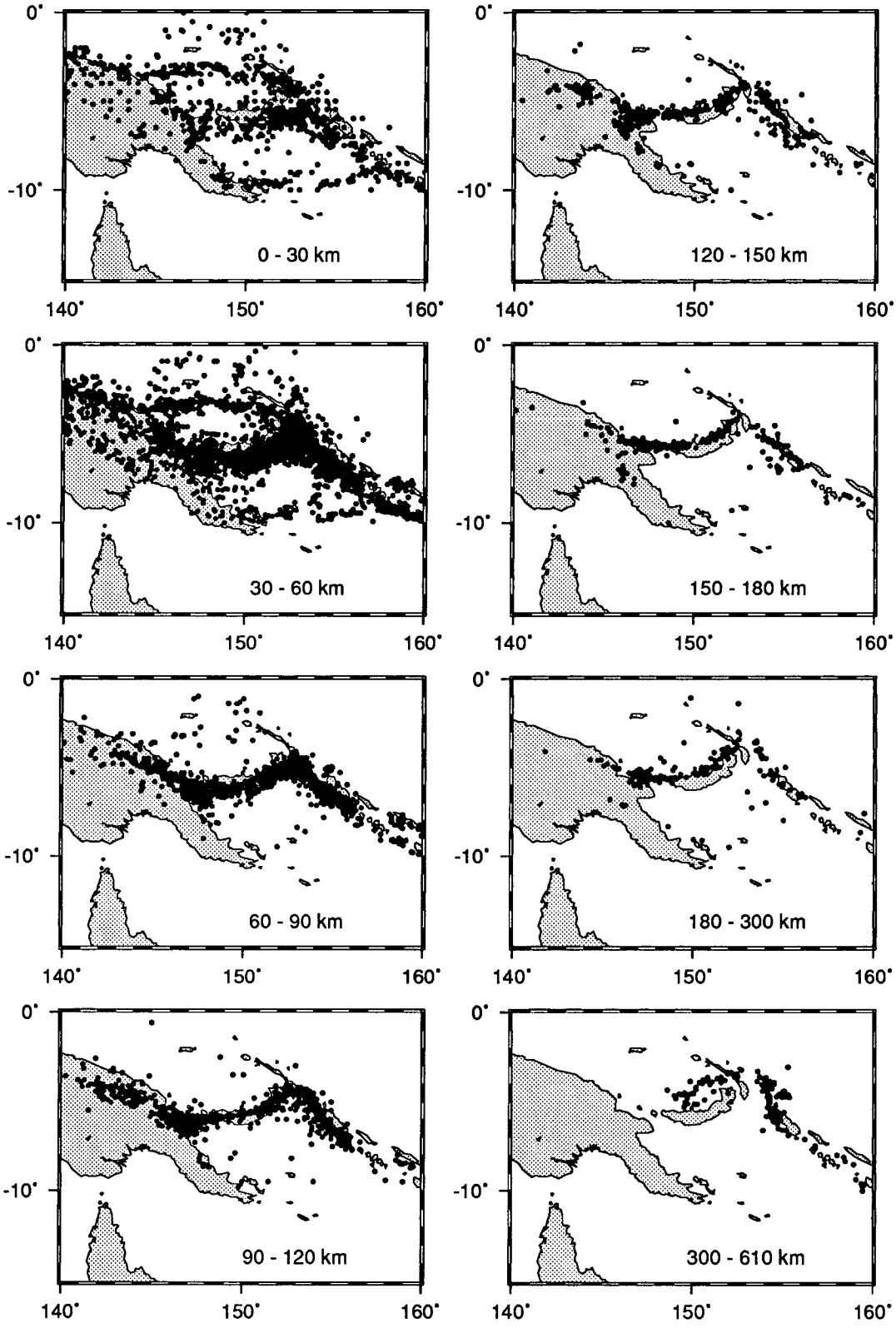

Figure 2.7 Seismicity of the Papua New Guinea region. Each diagram represents a different depth band.

Cross sections of the New Britain Trench shown in Figures 2.8 and 2.9 clearly illustrate the steep angle at which the slab is being subducted. The New Britain Trench extends along the coast of Bougainville and the New Georgia Islands. Subduction of the Solomon plate beneath Bougainville is accompanied by intense seismicity along a steeply dipping Wadati-Benioff zone (70-90° below 100 km) which extends to 200 - 250 km. Further south, subduction of the Australian plate beneath San Cristobel and Guadalcanal is also accompanied by intense seismicity along a steeply dipping Wadati-Benioff zone, extending to a depth of just over 100 km.

Between San Cristobel and Guadalcanal, the Woodlark Basin is being subducted. This provides an excellent site to study the effects of the lithosphere's age upon subduction patterns. Contrary to the expected effect of subduction of young lithosphere discussed in Section 2.3.1, there is very little seismicity associated with subduction of the spreading centre.

The tectonic features of this zone are unusual in several respects. Firstly, the seismicity is shallow (less than 80 km deep), diffuse and of low magnitude. There is no clearly defined Wadati-Benioff zone (Weissel *et al.*, 1982; Cooper and Taylor, 1987a). Secondly, the volcanism is unusually close to the trench. All volcanism in the New Georgia group occurs within 100 km of the trench axis, with active submarine volcanoes occurring on the trench wall, only 24-40 km from axis. The magma erupting from these volcanoes is chemically unusual. Finally, complex vertical motion is occurring on the Solomon Islands. This may also be due to the subduction of the Woodlark Spreading system (Weissel *et al.*, 1982).

An explanation for the trench characteristics specific to the site of subduction of the Woodlark Basin arises from the fact that the lithosphere is warm. It is therefore less rigid and deforms in a ductile manner rather than rupturing or underthrusting and sinking. Alternatively, the young warm lithosphere may rapidly reach thermal equilibrium with the surrounding asthenosphere, and be rapidly absorbed (Weissel *et al.*, 1982).

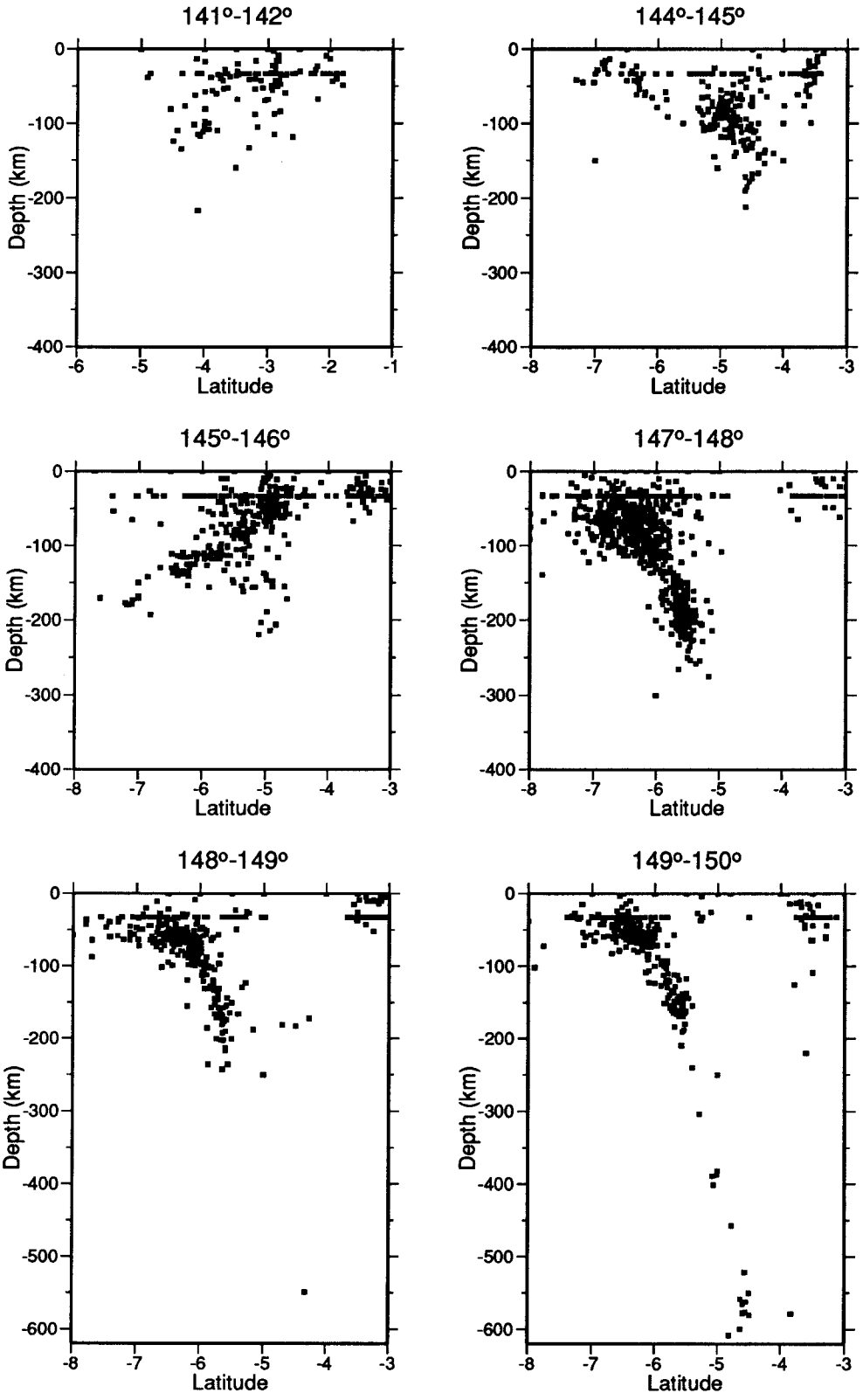

Figure 2.8 Cross sections of seismicity across Papua New Guinea and the western end of the New Britain Trench.

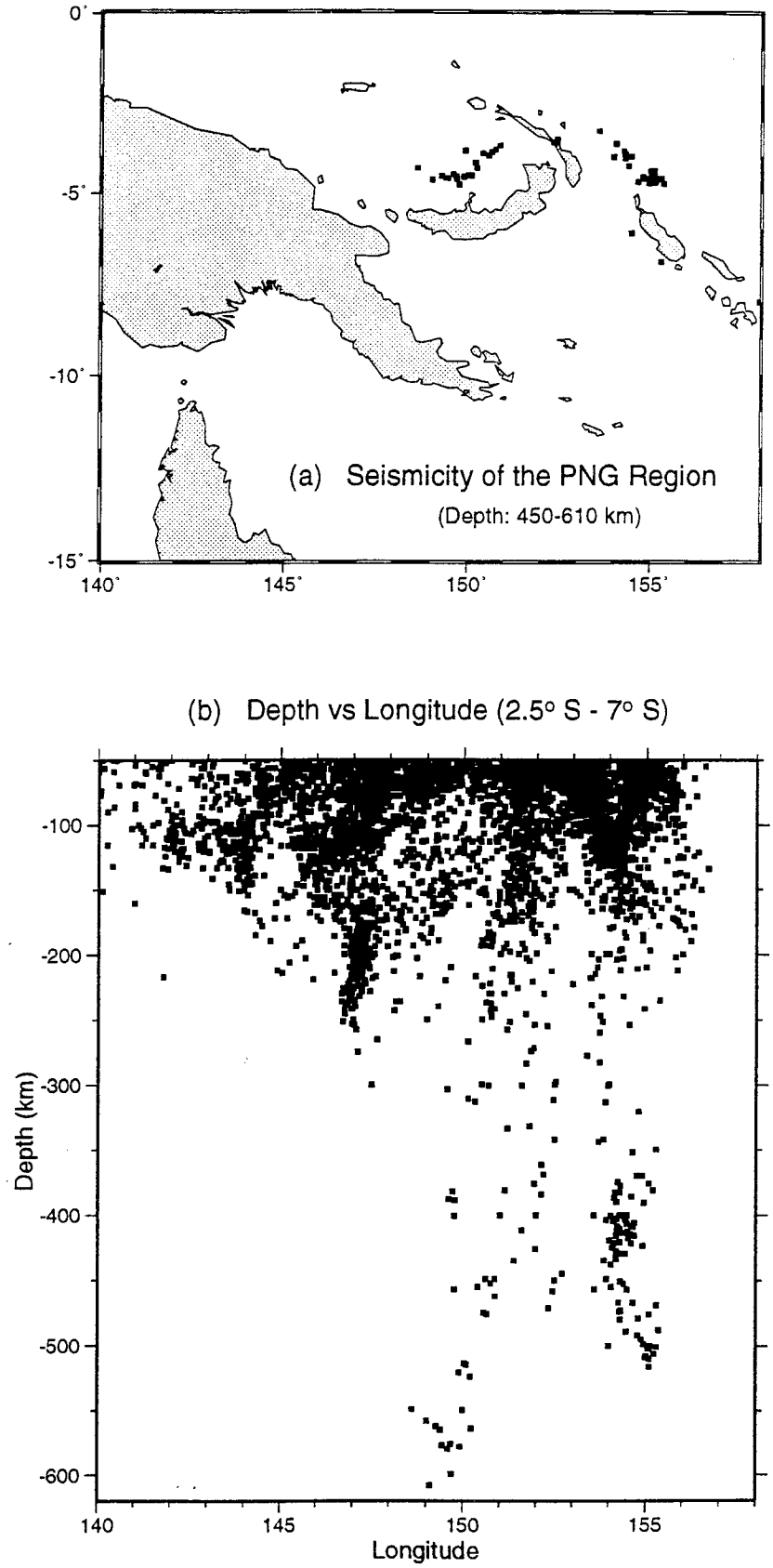

Figure 2.9 Deep seismicity associated with the New Britain Trench occurs in two distinct areas. This section, along the parallel of latitude shown, clearly shows the change in depth of seismic activity along the trench.

A southwest dipping Benioff zone is defined beneath the New Georgia Basin to a depth of 200 km. Cooper and Taylor (1987a) suggest that this indicates a remnant slab of Pacific lithosphere formerly subducted at the North Solomon Trench, before the subduction polarity reversed about 10 Ma ago with the arrival of the Ontong Java Plateau at the trench.

The geometry of subduction zones, discussed in Section 2.3.1, can be applied to the New Britain Trench, with the result that, in many ways, the New Britain Trench appears to be anomalous.

The New Britain Trench has a high relative rate of convergence, however, the angle of subduction is high, as seen in Figure 2.8. This is at variance with the expected low angle of subduction predicted by Park (1988) and discussed in Section 2.3.1.

The upper plate in the Solomon Sea/Bismarck Sea collision is the South Bismarck plate. The results of this analysis (Chapter 7) shows that Jacquinot Bay, on the South Bismarck plate, is moving rapidly to the southeast, or towards the trench, in an absolute sense. If this is representative of the motion of the South Bismarck plate, Park (1988) predicts that the subduction angle should be shallow. This is clearly not the case at the New Britain Trench. This could mean that the residual at Jacquinot Bay does not imply that the South Bismarck is simply moving southeast. A discussion of the possible motion of the South Bismarck plate is given in Chapter 7.

The age of subduction is also thought to affect trench geometry, as discussed in Section 2.3.1. The age of the Solomon Sea lithosphere is disputed in the literature. According to Davies *et al.* (1984), most of the marginal seas and small ocean basins around Papua New Guinea were formed by sea floor spreading in the Tertiary. The Solomon Sea probably fits in with this, although there is insufficient magnetic data over it to determine its age. Joshima and Honza (1987) used heat flow data and an age-depth relationship to determine that the Solomon Sea floor is about 30 Ma old. Karig (1972) also used heat flow data and determined that age to be mid-Tertiary, or about 30 Ma. Using a number of other published relationships, for example, between the length of the Wadati-Benioff zone, convergence rate and age, Davies *et al.* (1984) calculate an age of between 50 and 70 million years. However, they review many other estimates and conclude that the age of the Solomon Sea lies somewhere

between 40 and 60 Ma. Although the age is widely disputed, there is clearly an increase in the age of the lithosphere with distance from the Woodlark Spreading System. If we accept the conclusion of Davies *et al.* (1984) that the age is probably about 40-60 Ma, then it would be expected that the slab subducting under New Britain would be dipping steeply. From the seismicity profiles shown in Figure 2.8, it is clearly dipping steeply, and in this respect is in agreement with the model proposed by Park (1988).

Manus Trench - North Solomon Trench

The Manus Trench is an arcuate trench extending from the southern end of the Massau Trench, west to 142°E. It forms an arc with the North Solomon Trench which sweeps southeast along the northeastern side of Bougainville and the Solomon Islands.

Johnson and Molnar (1972) proposed that the Manus Trench forms the northern boundary of the North Bismarck plate, but recognise that the trench lacks significant seismicity and island arc volcanism associated with rapidly subducting plates. The trench does display the trench wall features associated with active subduction (Ryan and Marlow, 1988). According to Weissel and Anderson (1978), the Manus trench may be active at a very slow convergence rate, or may be a relic of an earlier active site of subduction. However, they place the boundary of the Caroline plate along the trench, thereby considering it active. Taylor (1979) rejected the possibility of this trench being active because of the low level of earthquake activity, thereby disputing the existence of the North Bismarck plate. According to Exon and Tiffin (1984), there is no North Bismarck plate: the northern part of the Bismarck Sea is part of the Pacific plate and is separated from the Caroline plate by the Manus Trough.

Thus opinion is divided about the activity or inactivity of the Manus Trench. As with the Trobriand Trough, it is possible that the trench is subducting at a rate of less than 4 cm/y, which, according to Kincaid (1995) would preclude the existence of a well-formed Wadati-Benioff zone and volcanic island arc.

The Papua New Guinea GPS survey networks extend only as far north as Manus Island and thus do not straddle the Manus Trench. It is not possible, then, to determine whether this trench is active or inactive in this thesis.

It appears to be generally accepted that the eastern extension of the Manus Trench, to the northeast of New Ireland and Bougainville, is inactive. Kroenke (1984) states that this trench system, including the Manus Trench, was probably activated in the Early Oligocene, and continued to be active throughout the Oligocene and early Miocene. Kroenke (1984) suggests that subduction ceased on this trench system when the Ontong Java Plateau collided with this trench system and the Eauripik Ridge collided with the Manus Trench north of Papua New Guinea.

Accreted Terrains

The southern part of Papua New Guinea, called the Fly Platform, is clearly part of the Australian plate. As seen in Figure 2.7, there is no seismic activity south of the Papuan Fold Belt, and no volcanic activity. The granite basement of this region is continuous with the Palaeozoic rocks of north Queensland, indicating that the Fly Platform has been part of the Australian continent since at least the Early Jurassic (Bain, 1973).

North and northeast of this stable region is a complex zone of faults and mountain ranges. Abbott (1995) and Bain (1973) divide Papua New Guinea into four major tectonic provinces:

- the Fly Platform, composed of undisturbed continental crust of the Australian Craton;
- the Papuan Fold Belt, to the north of the Fly Platform, is an active foreland fold and thrust belt composed of para-autochthonous continental crust;
- the New Guinea Highlands and Papuan Peninsula, north of the Papuan Fold Belt, are composed of a collage of allochthonous terrains sutured to the continent during the Oligocene and Miocene;
- the Adelbert and Finisterre Ranges, north of the Markham, Ramu, and Sepik river valleys, are a series of volcanic arc terrains, sutured to the continent during the Miocene and Pliocene.

The location of the boundary of the Australian plate in this complex tectonic structure is debated in the literature.

Northern Papua New Guinea consists of a number of accreted terrains. According to Pigram and Davies (1987) and Abbott (1995), the New Guinea Highlands and the Papuan Peninsula consist of at least 32 terrains that were sutured to the continent during the Oligocene and Miocene. A large proportion

of these terrains are of continental origin, which is unusual amongst orogens of the circum-Pacific region (Pigram and Davies, 1987). The terrains were fragments of Gondwana that were detached in the early Mesozoic and had independent histories before colliding with the Australian craton. The other terrains have the more common oceanic affinities. Davies *et al.* (1987) suggest that the Papuan Peninsula and the D'Entrecasteaux Islands have the same origin, which is consistent with them originally forming a continuous island arc. This arc collided with the Fly Platform along an extension of the Pocklington Trough, (named the Port Moresby Trough by Hamilton, 1979), which has been extinct since the early Pliocene (Hamilton, 1979). The presence of ophiolites in the Owen Stanley Ranges, which lie along the Papuan Peninsula, indicate that this was formerly a subduction zone. This ophiolite belt, the Papuan Ultramafic Belt, has been obducted southwest over the former northeast margin of the Papuan Peninsula (Abers and Roecker, 1991; Pigram and Davies, 1987). There is little or no seismic activity on the southern side of the Papuan Peninsula which suggests that the peninsula is part of the Australian plate.

Abers and Roecker (1991) suggest that the boundary between the Australian and Solomon plates might be in a weakly deforming zone to the northeast of the Papuan Peninsula. The motion across this boundary should be small and predominantly left-lateral slip at the Trobriand Trough.

Another island arc is thought to be currently colliding with Papua New Guinea. This consists of the Huon Peninsula, which has already collided, and the island arc which includes New Britain, New Ireland, Bougainville, Vanuatu, and the Solomon Islands. Davies *et al.* (1987) and Abbott (1995) show that these islands and the Huon Peninsula have the same origin: all were formed by island arc volcanism in the Cenozoic. Robinson (1974) named this the Outer Melanesian Arc. Falvey and Pritchard (1984) provide paleomagnetic evidence supporting this argument. Abbott (1995) and Cooper and Taylor (1987b) include the Adelbert and Finisterre Ranges as part of this collision.

Cooper and Taylor (1987b) discuss the collision and relate it to subduction reversal. Their paper proposes that there are four stages of collision in evidence:

- West of 144°E, the collision has progressed past suturing to full subduction polarity reversal, with the Pacific plate subducting to the southwest under the Australian plate;

- Between 144°E and 148°E, subduction reversal is in progress. Convergence between the Australian and Bismarck plates is accommodated by thrusting within the Adelbert and Finisterre Ranges and compression of the New Guinea Orogenic Belt. They propose that the Adelbert Block is sutured to the Australian plate and overthrusting the Bismarck Sea, whilst the Finisterre Block overthrusts the Papua New Guinea Orogenic Belt;
- West of the 149° Embayment, the Huon Peninsula has collided with the Australian margin and together they override a fold in the doubly subducted Solomon Sea lithosphere. The presence or absence of a doubly folded piece of lithosphere will be discussed further shortly.
- East of the 149° Embayment, the Solomon Sea plate is being subducted to the north into the New Britain Trench and southwest into the Trobriand Trough, bringing the island arc into collision with the Papua New Guinea landmass.

The dispute over the activity of the Trobriand Trough has already been discussed. It has obvious implications for this interpretation by Cooper and Taylor (1987b).

Whether there is still a piece of the slab remaining from earlier subduction along the Trobriand Trough is disputed. Cooper and Taylor (1987b) claim there is evidence from seismicity showing that there is a section of doubly subducted lithosphere. It has its axis parallel to the Ramu-Markham Fault and plunges to the west at an angle of 5° beneath the coastal ranges of northern Papua New Guinea. Figure 2.8 could be interpreted to support this proposal. However, Abers and Roecker (1991) could find no seismic evidence for this in their relocated hypocentres. Instead, they suggest that the seismicity shows a well defined north-dipping slab beneath northern New Guinea. They suggest this slab is flat at 100 km beneath the Huon-Finisterre Ranges and is nearly vertical from 150 km to 250 km in depth beneath the Bismarck volcanic arc to the north of Papua New Guinea. Whether it is Australian lithosphere, Bismarck lithosphere or some complex combination of the two above the flat slab is unclear. However, Abers and Roecker (1991) dispute the evidence suggesting a reversal in subduction direction in this region.

Cooper and Taylor (1987b) support the idea that subduction reversal is taking place currently, and that different stages of the process can be seen along the collision zone, as discussed above. Seno and Kaplan (1988) suggest that

subduction of the Caroline plate beneath the Australian plate is occurring between 140°E and 144°E. Further west, subduction is not occurring, and the oblique convergence of 11.1 cm/y at N65°E between the Caroline and Australian plates is being accommodated by two processes. These are, firstly left-lateral strike-slip motion along the Sorong and Tarera Faults in Irian Jaya. This region is beyond the scope of this study. Secondly, the convergence is accommodated by dip-slip thrusting representing internal deformation of the Australian plate to the west of 140°E, in the vicinity of the Medial Mountains. Seno and Kaplan (1988) also suggest that the South Bismarck plate may be underthrusting the New Guinea landmass near the junction between the New Guinea Trench and the Bismarck Sea Seismic Lineation. This supports the idea of Cooper and Taylor (1987b) that subduction reversal is taking place currently.

Puntodewo *et al.* (1994) concluded that convergence between the Australian and Pacific plates is highly partitioned between thrusting at the New Britain Trench, and in the Mamberambo Thrust Belt and strike-slip motion in the Highlands and at the Yapen Fault. This region is further west than the region encompassed by this study, but is relevant for continuity of tectonic motion west of Papua New Guinea, in Irian Jaya.

According to Abbot (1995), the Finisterre terrain, consisting of the Adelbert Block and the Finisterre Block, is currently colliding with Papua New Guinea and the collision has propagated from NW to SE through time. This collision has uplifted the Finisterre terrain to form the Adelbert and Finisterre Ranges. Tiffin *et al.*, (1987), suggest the Huon Peninsula (ie the Huon-Finisterre and Adelbert Blocks) is part of the Australian plate and has been since the Early Miocene. Davies *et al.*, (1987) interpret the diffuse zone of shallow earthquakes in the Ramu-Markham Valley, the Huon Peninsula and the Finisterre Range as an indication that north-dipping thrusts are still active and possibly include a component of transform motion. They suggest the Ramu-Markham Fault is the northern margin of the Australian plate, with the South Bismarck plate overriding the Australian plate. This is indicated by active emergence and convergent tectonism north of the Ramu-Markham Fault, and submergence and extensional tectonics south of it. Subsidence of the Morobe region could be investigated by future GPS surveys.

Kulig *et al.* (1994) suggest that the Huon Peninsula is being emplaced onto the Australian plate along a thrust fault dipping 25° to the north. This fault is 20 km

deep beneath Lae. They suggest that the Ramu-Markham Fault Zone may be accommodating little convergence at present.

It is clear from the above discussion that the location of the edge of the Australian plate is widely disputed. The geodetic results presented in later chapters can help to understand this problem, but cannot resolve it at present.

Transform Faults and Spreading Centres

There are two centres of spreading in the region:
- the Bismarck Sea Seismic Lineation
- the Woodlark Basin Spreading System.

Bismarck Sea Seismic Lineation

The water depth in the Bismarck Sea is about 2000 m, with moderate topography, except for the presence of two rises: the Willaumez Rise south and west of Manus Island; and the New Hanover - Manus Rise between New Hanover and Manus Island. Both of these rises have water depths of about 1000 m. Bouguer gravity values vary smoothly between +150 and +180 mGal and generally decrease towards the land. The only departures from this pattern are on the Willaumez and New Hanover - Manus Rises. On the Willaumez Rise, the Bouguer value decreases to +130 mGal, whilst on the New Hanover - Manus rise, the Bouguer value decreases to +100 mGal. There is an area across the centre of the Bismarck Sea which is sediment free. In the east this area has little topographic relief and is about 50 - 60 km wide. In the west it is narrower and more rugged. Sediment thickness increases towards land, reaching 2 km along the north Papua New Guinea coast (Connelly, 1976). This is the Bismarck Sea Seismic Lineation, named by Denham (1969). It is a system of spreading centres offset by left-lateral faults which crosses the floor of the Bismarck Sea (Taylor, 1979). It extends from the north west coast of Papua New Guinea to a point close to the north eastern tip of New Britain.

Focal mechanism solutions along the seismic lineation show left-lateral strike-slip motion. This led to Johnson and Molnar (1972), Curtis (1973) and Krause (1973) to interpret the zone as a broad, arcuate strike-slip fault. Connelly (1974, 1976) and Taylor (1975) noted that there are at least 4 discrete sections within the lineation, and agreed with Ripper (1975) that the epicentres were scattered too widely for a single strike-slip fault. Hamilton (1979) interpreted the zone as

an arcuate strike-slip system, with offsets along short, orthogonal spreading centres.

Connelly (1976) used magnetic data and sediment distribution to determine that the eastern half of the sea was the site of north-south extension at a rate of 8 cm/y. Taylor (1979) used bathymetric, focal mechanism and magnetic data to propose that the four sections composing the Bismarck Sea Seismic Lineation are: two transform faults, one spreading centre, and one leaky transform fault. Taylor (1979) determined that the best fitting pole of rotation between the Pacific and South Bismarck plates is at 18.5°S, 141°E and 4.0°/Ma in an anticlockwise direction.

The western-most section of the Seismic Lineation coincides with a chain of seamounts (Connelly, 1974). This trend continues west onto the Papua New Guinea landmass in a series of anastomosing faults that cut westward through the Toricelli and Bewani Mountains (Cooper and Taylor, 1987b). Taylor (1979) proposes that this section is a leaky transform fault, with chronologically distinct episodes of sinistral faulting and extensional intrusion.

The second section of the Seismic Lineation is a left-lateral transform fault, trending N60 - 65°W (Taylor, 1979; Exon and Tiffin, 1984; Eguchi *et al.*, 1989). It is marked by a prominent ridge and scarp (Taylor, 1979) and is less than 3 km wide (Eguchi *et al.*, 1989).

Taylor (1979) and Martinez and Taylor (1993), show that section three is actively spreading, as indicated by the coincidence of the first magnetic anomaly with the sediment free basement. However, all focal mechanisms for this section are strike-slip, indicating that the spreading centres are probably offset by small transform faults. Eguchi *et al.* (1987, 1989) show that this section is divided into several segments of earthquake activity, each trending west-northwest or east-southeast and narrower than 2 km. These represent several short transform faults offset by aseismic spreading segments which are not orthogonal to the opening direction, suggesting oblique spreading. Magnetic anomalies reveal that seafloor spreading has been asymmetric, with rates of 7.4 and 5.8 cm/y on the northern and southern sections respectively, giving a total extension rate of 13.2 cm/y (Taylor, 1979).

Taylor's (1979) fourth segment is also a left-lateral transform fault trending N60°W, which appears on the surface as transform faults on the Gazelle Peninsula and includes the Baining Fault, St Georges' Channel and the Sapom and Weitin Faults on southern New Ireland. It is probably at least partly responsible for the strongly linear shape of the south-west coast of New Ireland (Weibinger, 1973; Taylor, 1979; Exon and Tiffin, 1984; Exon *et al.*, 1986). Eguchi *et al.* (1989) divide this segment further into three strike-slip fault sections, and suggest that they could be separated by small spreading zones. Graben between New Ireland and New Britain suggest they are moving apart (Wiebenga, 1973; Brooks *et al.*, 1971), with New Ireland moving in a north-easterly direction. Lindley (1988) recognised the Wide Bay Fault System (separating the Gazelle Peninsula and the rest of New Britain) as a zone of anastomosing fractures trending north-northwesterly across the Wide Bay region and along the west coast of the Gazelle Peninsula. Movements along the Wide Bay Fault System have been both lateral and vertical, with left-lateral offsets along the fault of about 100 km. According to Lindley (1988), the Gazelle Peninsula experiences an extensional tectonic regime, directly related to the abrupt flexure of the New Britain Trench. The Solomon Sea plate has a relative northwestward direction of movement, and evidence from the Gazelle Peninsula indicates that the resultant stress response in the South Bismarck plate has been taken up by extensional and strike-slip tectonics. All major structural elements from the Gazelle Peninsula to east of New Ireland are extensional and/or strike-slip structures radial to the flexure of the New Britain Trench. The entire geological section from the western Gazelle Peninsula to the east coast of New Ireland, comprising many large, north-trending normal faults, represents a 150 km wide interval of extensional horst and graben tectonics (Lindley, 1988).

Molnar *et al.* (1975) give the relative pole of rotation between the Australian and Pacific plates to be 59.4°S and 175.7°W at -1.18°/Ma. Taylor (1979) uses this value to calculate the pole of rotation between the Australian and South Bismarck plates to be 4.3°S, 134°E at 3.39°/Ma in an anticlockwise direction.

Woodlark Spreading Centre

The Woodlark Spreading Centre is situated in the Woodlark Basin. The basin is bounded by the Woodlark Rise to the northwest, the Pocklington Trough to the southeast and the Pocklington Rise to the southwest. It extends as far as the Papuan Peninsula in the west and to the San Cristobel Trench in the east, where it forms a triple junction.

The Woodlark Spreading Centre has been defined by magnetic anomalies and seismological data (Weissel *et al.,* 1982). On the basis of magnetic lineations, Weissel *et al.,* (1982) showed that spreading in the Woodlark Basin was initiated sometime prior to 3.5 Ma ago. Taylor and Exon, (1987) used magnetic anomalies to show that the oldest preserved crust in the Woodlark Basin is 5 Ma old. The total opening rate has been approximately 6.0 cm/y for the last 1 Ma, and the spreading is asymmetrical, with 3.6 cm/y in the north direction and 2.4 cm/y in a southerly direction (Weissel *et al.*, 1982). The axial rift valley of the spreading centre is aligned in an east-northeast direction. The valley is about 10 km wide with relief of 500 to 1000 m (Taylor and Exon, 1987). Width and height of this valley decrease from east to west, with a width of about 7 km and 300 to 500 m of relief further west. In the eastern portion of the Woodlark Basin, the spreading centres are offset by north-south transform faults. According to Taylor and Exon (1987), the rate of spreading is approximately 7.2 cm/y in the east, decreasing to 5.6 cm/y in the west.

In the eastern portion of the Woodlark Basin, from about 151°E to its junction with the New Britain Trench, the spreading axis is clearly defined. Further west, the rift is less clear. A series of horst blocks and sediment filled graben occur between the Papuan Peninsula and the D'Entrecasteaux Islands. These indicate active extension. Between Normanby and Fergusson Islands, there is a westward trending zone of shallow earthquakes. Smith (1976) interpreted the eruption of mildly peralkaline rhyolites in the D'Entrecasteaux Islands as evidence that the rift is propagating westward into the Papuan Peninsula. The absence of older seafloor magnetic lineations in the western part of the basin also points to westward propagation of the rift (Benes *et al.*, 1994). Goodenough Bay and the Papuan Peninsula experience earthquakes which display mainly tensional focal mechanisms (Ripper 1982, Davies *et al.,* 1984). It is proposed that the rift is propagating into the Papuan Peninsula about a pole located 15° - 20° to the west (Weissel *et al.,* 1982) at a rate of about 14

cm/y (Taylor, 1987). The survey site at Alotau is located on the southern shore of Goudnough Bay. The motion of Alotau, located so close to the propagation of the spreading centre, is discussed in Section 7.4.

In the east, the Woodlark Spreading Centre is being subducted under the Solomon Islands at a rate of 12 cm/y. This is discussed further in Section 2.4.2.

The free-air gravity anomaly field in the eastern Woodlark Basin averages +30 to +40 mGal and is strongly correlated with topography. Bathymetric deeps along the rift axis, fracture zones and the edges of the basin are associated with relative gravity lows. The basement swells south of Ghizo Ridge are matched by gravity highs (Taylor, 1987).

Woodlark Rise

Earthquake activity forms a weakly defined seismic line along the northern flank of the Woodlark Rise. These shallow earthquakes include one with a right-lateral northeasterly strike-slip solution (Weissel *et al.,* 1982) and others with extensional and thrust solutions (Ripper, 1982). Weissel *et al.* (1982) interpret this seismicity to be a zone of partial decoupling of the Woodlark and Solomon Basins due to mechanical difficulties in subducting the young Woodlark lithosphere. They suggest that the Woodlark Basin is underthrusting the Pacific plate at a slower rate than the Solomon Sea Basin.

Solomon Sea Heat Flow Data

There is heat flow data available in the literature which, when combined with the work of Park (1988) on heat flow and deformation of the lithosphere, provide an interesting perspective on the tectonic activity of the Solomon Sea.

Joshima and Honza (1987) found the average heat flow of the Solomon Sea to be 2.08 HFU, or 87 mWm^{-2}. High values of 111 and 124 mWm^{-2} were measured along the Woodlark Rise. These values are sufficiently high that either extensional or compressional deformation could occur. The seismic focal mechanism solutions along the Woodlark Rise show strike-slip, extensional, and thrust faulting. The type of activity, therefore, is uncertain, but deformation appears to be occurring in this region. Along the Trobriand Trough, the heat flow was found to be 71-93 mWm^{-2}, whilst in the 149° Embayment, a value of

45 mWm^{-2} was measured. Values in the east of the Solomon Sea, offshore from the New Georgia Islands in the New Britain Trench, were 126 mWm^{-2} and 143 mWm^{-2} respectively (Weissel *et al.*, 1982). This is clearly associated with the subduction of the Woodlark Spreading Centre. Further north the rates show variability, from 27 to 99 mWm^{-2}.

Figure 2.3 shows that the high heat flow values in the region are sufficient to cause extensional deformation, and may be sufficiently high to cause compressional deformation. From this graph, Park (1988) estimated a heat flow of over 90 mWm^{-2} to cause compressional deformation. The average value for the Solomon Sea is very close to this, above the value required for extensional deformation. It is possible, therefore, that conditions exist in the Solomon Sea for deformation of the oceanic lithosphere to be occurring. If this is the case, the assumption of rigid plates may not be appropriate for this region.

Triple Junctions

Triple junctions, as their name suggests, occur where three tectonic plates intersect. Triple junctions may be stable, which means they maintain their shape through time, or unstable which means their shape evolves throughout time until it reaches a stable configuration. Thus unstable triple junctions are transient.

The kinematic behaviour and stability of triple junctions can be analysed by drawing appropriate vector triangles (Figure 2.10). The sum of the relative velocities of the vector triangle must be zero, provided that the plates are rigid (Park, 1988). Thus if $V_{B/A}$, $V_{C/B}$ and $V_{A/C}$ are the velocities of B relative to A, C relative to B and A relative to C respectively, then

$$V_{B/A} + V_{A/C} + V_{C/B} = 0$$

Three triple junctions will be discussed. These are:

- 149° Embayment (Solomon/Australian/South Bismarck triple junction);
- Solomon/Pacific/Australian triple junction;
- Solomon/South Bismarck/Pacific triple junction.

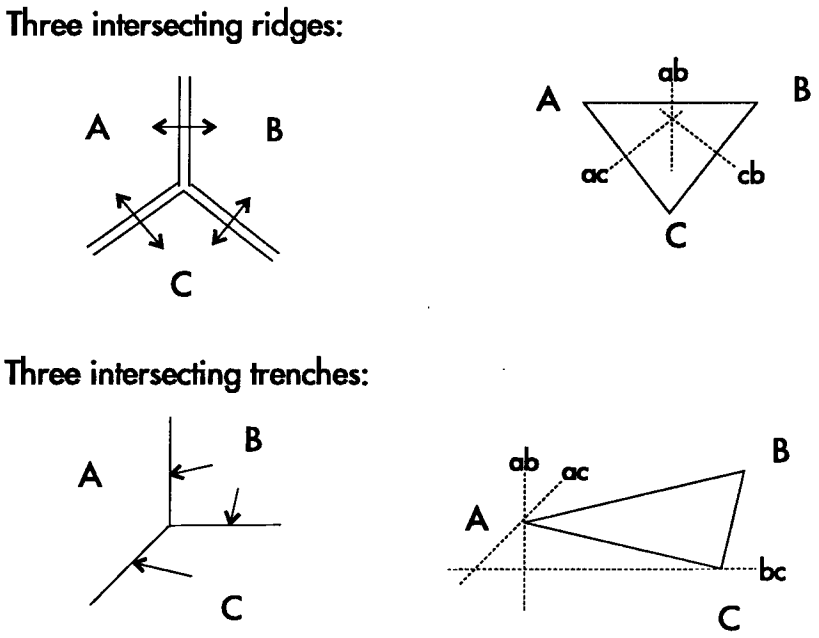

Figure 2.10 Stability of triple junctions determined by vector analysis. In the case of the ridge-ridge-ridge triple junction is stable. The trench-trench-trench triple junction is unstable. Adapted from Park (1988).

149° Embayment

The 149° Embayment marks the collision between the New Britain Trench and the Trobriand Trough. The collision between the Trobriand Trough and the New Britain Trench can be seen as an example of an unstable triple junction, as in the figure above. The position of the triple junction is migrating southeast through time.

Whether the Trobriand Trough is an active boundary or not is widely debated, as discussed earlier in this section. A triple junction analysis reveals that the Trobriand Trough is not accommodating the rate of motion required to close the vector diagram, shown below.

Clearly, the motions across the Australia-Bismarck and Solomon-Bismarck boundaries require motion of the order of approximately 9 cm/y to be occurring across the southwestern boundary between the Australian and Solomon plates. Clearly, this is not occurring along the Trobriand Trough. If it is subducting, it is generally accepted that the motion is slow. The implication of this is that the Trobriand Trough is not the boundary between the Solomon and Australian plates.

Using relative plate motions:

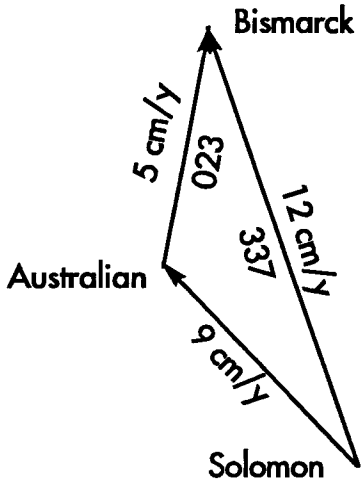

Figure 2.11 Vector diagram of the relative motions of the Bismarck, Solomon and Australian plates. Relative rates and azimuths are approximate, based on those given in Section 2.4.3 (New Britain Trench) and McClusky *et al.*, 1994.

The vector diagram above shows that the required boundary should be aligned approximately northwest-southeast, and accommodating motion of approximately 9 cm/y. The Papuan Peninsula is the other boundary, proposed in the literature. Although it is aligned in approximately the required direction, there are no reports of motion of this order of magnitude in the literature.

This raises two possibilities: the triple junction analysis is invalid because the motion is in the form of deformation, and the assumption of rigid plates is false; or there is no boundary between Australia and the Solomon Sea along the Trobriand Trough.

The first possibility should not be immediately discounted because it was shown in Section 2.2.4 that the heat flow reported for the Solomon Sea could be sufficiently high to allow deformation to occur. The GPS results discussed in Chapter 7 do not resolve this issue, but the possible location of such a boundary is discussed.

Solomon/Pacific/Australian

A triple junction is formed between the Pacific, Solomon and Australian plates. This triple junction has migrated back and forth as successive ridge and

transform sections have been subducted. Total migration in the last 3.5 million years is probably less than 200 km, implying the triple junction has remained adjacent to the volcanoes of the New Georgia Group (Weissel *et al.*, 1982). The Triple junction is currently a complex triangular zone bounded by the north trending Simbo Ridge and transform fault, the east trending Ghizo Ridge and a northwest trending ridge segment (Taylor and Exon, 1987). Magnetic lineations predict that there should be a spreading centre at the location of Ghizo Ridge. Taylor and Exon (1987) proposes that it is a spreading centre which has been altered by subduction choking and arc volcanism.

The vector diagram for the triple junction is given in Figure 2.12. It can be seen from this diagram, that the sum of the vectors is zero, which is the requirement for a triple junction. This is in contrast to the situation at the Australian-Solomon-Bismarck triple junction, discussed above.

Section 2.4.3 (New Britain Trench) quoted a Solomon-Pacific convergence rate of 14.5 cm/y at N45°E according to Kroenke (1984). Using this value in the above vector diagram increases the Australia-Solomon spreading rate to 7.1 cm/y and changes the azimuth of the vector to approximately 0°. This suggests that the triple junction is valid, and adds to the arguments in favour of the existence of the Solomon Sea plate. This section of the Solomon Sea plate is not moving with the Australian plate. If it was, a null result similar to the 149° Embayment analysis would be expected.

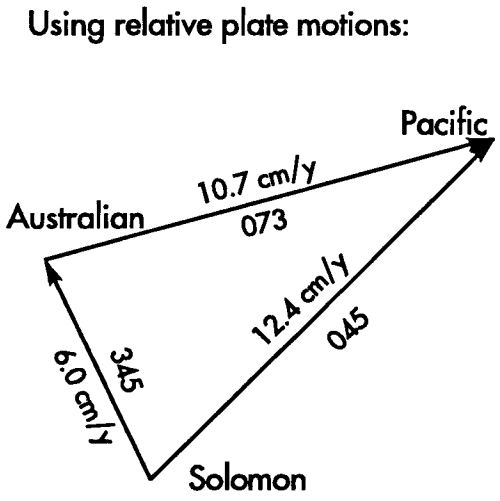

Figure 2.12 Vector diagram of the relative motions of the Australian, Pacific and Solomon plates. Values used are based on Weissel *et al.* (1982).

Solomon/South Bismarck/Pacific

The triple junction between the Solomon, South Bismarck and Pacific plates also presents problems. Figure 2.13 below shows that motion of approximately 13 cm/y is required between the Pacific and South Bismarck plates. This is a transform fault, for which there does not appear to be an estimate of relative motion in the literature. The Pacific plate is moving to the northwest at a rate of approximately 10 cm/y. The motion of the South Bismarck plate is uncertain, and is discussed further in Chapter 7. Hence this triple junction analysis is inconclusive.

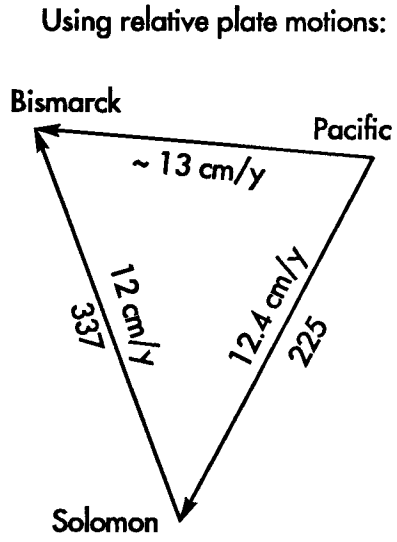

Figure 2.13. Vector diagram for the Solomon, Pacific, South Bismarck triple junction. Rates used are from the previous two figures.

2.4.4 Tectonic Models of the Region.

There have been several attempts to locate the boundaries of the region and form a complete picture of the tectonics of this area. These will be outlined below. In addition, many more detailed studies of single boundaries have been performed, from which the present level of understanding of the region, discussed above, has been gleaned. Models discussed in this section are shown in Figure 2.14.

Johnson and Molnar (1972)

Johnson and Molnar used earthquake focal mechanisms to determine the location and nature of the boundaries between the Australian and Pacific

plates. Their model proposes definitely two, and possibly three small plates in the region - the Solomon plate and the South Bismarck plate and possibly the North Bismarck plate.

The boundaries of the South Bismarck plate are given as the New Britain Trench to the south, in which the Solomon Sea plate is underthrusting the South Bismarck plate; an east-west belt of seismicity in the north defining a left-lateral strike-slip fault. The east and west boundaries are less clearly defined, but the western boundary lies in the belt of seismicity across northern New Guinea where Australia and the South Bismarck plates are probably converging. The eastern boundary is apparently defined by a left-lateral strike-slip boundary, which may be part of the Bismarck seismic zone or may be an extension of the faulting along the southwest coast of New Ireland.

The Solomon Sea plate is bounded to the west by eastern Papua New Guinea. To the east, "the active zone associated with the Solomon Islands" is the boundary. The southern boundary is not clearly defined, and coincides with a "diffuse belt of seismicity".

The North Bismarck plate is bounded by "a minor belt of activity" surrounding the northern part of the Bismarck Sea. This corresponds to the Manus Trench. "Active belts of seismicity" in northern Papua New Guinea form the southwestern boundary.

Curtis (1973)

Curtis proposed a model in 1973 which consisted of two definite small plates which he named the Solomon Sea and New Britain plates; and a third tentative plate to the north of the New Britain plate, which he called the Manus plate. This model was based on the study of earthquake focal mechanism solutions. As in all the proposed models, Curtis placed a boundary along the New Britain Trench, separating his Solomon Sea and New Britain plates, and recognised the New Britain Trench as a subduction zone, at which the Australian plate is underthrusting the Pacific plate adjacent to New Britain and Bougainville.

Curtis suggested the boundary of the Australian plate with each of the Manus plate, the New Britain plate and the Solomon Sea plate, lies along the Central Highlands Orogenic Belt and the Northern New Guinea Arc, the Owen Stanley

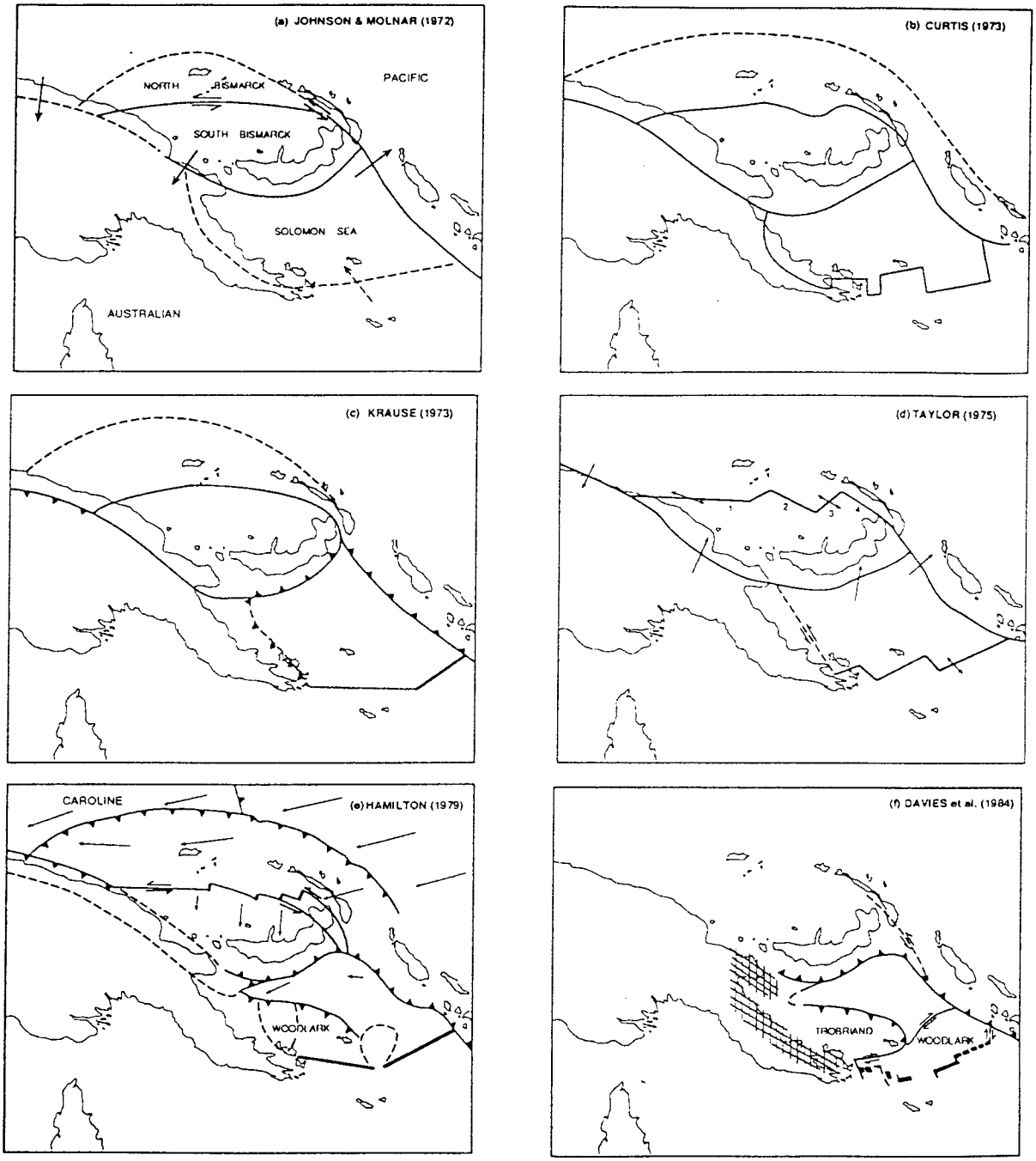

Figure 2.14 Interpretations of the plate boundary configurations for the region: (a) modified from Johnson and Molnar (1972), dashed arrow indicates spreading; (b) modified from Curtis (1973); (c) modified from Krause (1973); (d) modified from Taylor (1975); (e) modified from Hamilton (1979), arrows show direction of motion relative to the Australian plate; (f) modified from Davies *et al.* (1984), hatching denotes a zone of deformation that could be a transitional plate boundary.

Metamorphic Belt and the Papuan Ultramafic Belt. He pointed out that there was no clear pattern of focal mechanism solutions for this region from which he concluded that it must be a very complex deformation zone. The New Britain - Australian boundary is interpreted to be the zone lying between the Central Highlands Orogenic Belt and the Northern New Guinea Arc. Curtis interpreted the boundary between the Solomon and Australian plates to lie in the zone between the Papuan Ultramafic Belt and the Owen Stanley Metamorphic Belt. He suggested that this boundary is a normal fault with a strong left-lateral component.

As mentioned above, Curtis presented the Manus plate tentatively. Whether the Manus Trench is active or not is undecided (see Section 2.4.3 above), thus the presence of a microplate with this trench system as its northern and eastern boundary is unclear.

If the Manus plate does exist, then its southern boundary is the Bismarck Sea Seismic Lineation, which Curtis interpreted to be an east-west trending left-lateral strike-slip fault.

Curtis recognised the Woodlark Basin to be a zone of seafloor spreading, which he interpreted as the southern boundary of the Solomon Sea plate. He recognised the presence of five transform faults offsetting the sections of spreading.

The eastern boundary of the Solomon Sea plate is the New Britain Trench, which is where the Australian plate is underthrusting the Pacific plate.

Krause (1973)

Unlike Johnson and Molnar (1972), Krause proposed a model in which there are two small plates. He discounted the North Bismarck plate due to the lack of a clearly defined seismic zone along its northern boundary.

Taylor (1975)

The model proposed by Taylor in 1975 consisted of two small plates; the Solomon Sea plate and the South Bismarck plate. Taylor excluded the north

Bismarck plate from his model because of the discontinuous nature of the seismicity along the Manus trench.

The northern boundary of the South Bismarck plate is the Bismarck Sea Seismic Lineation, which he suggested was composed of four segments - two spreading segments and two transform faults. The northeastern boundary, he placed along the series of faults between northeastern New Britain and New Ireland.

As in all models, the New Britain Trench forms the northern and northeastern Boundary of the Solomon Sea plate. The southern boundary, he placed along the Woodlark Basin. The western boundary differs from that proposed in other models. He suggested it could be a (very speculative) transform fault offshore from the Papuan Peninsula.

Hamilton (1979)

The model proposed by Hamilton (1979) consists of four small plates between the Australian, Pacific and Caroline plates. These are the North Bismarck plate, the South Bismarck plate, the Solomon Sea plate and the Woodlark plate.

The north Bismarck plate is bounded by the Manus Trench to the north, the Bismarck Sea seismic lineation to the south. The southeastern boundary of this plate is unclear.

Hamilton placed the southwestern boundary of the South Bismarck plate along a zone of "subduction and crustal compression" along the north coast of Papua New Guinea, which includes the Adelbert and Finisterre Ranges, and the Huon Peninsula. The southeastern boundary is the New Britain Trench.

The Solomon Sea plate is defined by the Trobriand Trough (which Hamilton believes is active or only very recently become inactive) in the southwest. This merges into what Hamilton describes as an "oroclinal deformation" zone, which links the Trobriand Trough with the Woodlark Spreading Centre to form the southern and southeastern boundaries of this microplate. The northern and northeastern boundary is the New Britain Trench.

The smallest of the plates in this model is the Woodlark plate bounded by the western end of the Woodlark Spreading Centre to the south, and another zone of "oroclinal deformation" to the west.

Hamilton also computed relative poles of rotation for a number of pairs of plates in the region. They are as follows (approximate position, taken from Figure 154, Hamilton (1979)):

Woodlark plate and Australian plate	9° 30' S	150° 40' E
Solomon Sea plate and Australian plate	11° 50' S	151° 40' E
Solomon Sea plate and South Bismarck plate	6° 50' S	145° 30' E
North Bismarck plate and South Bismarck plate	13° 20' S	140° 0' E
South Bismarck plate and Australian plate	2° 50' S	143° 20' E
Pacific plate and North Bismarck plate	4° 20' S	155° 0' E
Caroline plate and North Bismarck plate	3° 20' N	159° 40' E

Davies et al. (1984)

Davies *et al.* (1984) , propose a model for the Solomon Sea area in which there are three small plates: the Solomon plate, the Woodlark plate and the Trobriand plate. This model takes into account the moderate level of shallow activity along the northern flank of the Woodlark Rise by interpreting this as the southeastern boundary of the Solomon plate. Davies *et al.* (1984) follow the work of Weissel *et al.* (1982) in defining this line of seismicity to be a right-lateral strike-slip fault, on the basis of a single fault plane solution. They suggest it may extend west southwest from a trench-transform-transform triple junction just east of Woodlark Island to intersect the Woodlark Basin ridge-transform system. The northern and northeastern boundaries of the Solomon plate are clearly defined as lying along the New Britain Trench. The southwestern boundary of the Solomon plate is thought to lie along the Trobriand Trough.

The Woodlark plate is defined by the Woodlark Spreading Centre to the south, the New Britain Trench to the northeast, with a transform fault linking the Woodlark Spreading Centre and the New Britain Trench.

The boundaries of the Trobriand plate are the Trobriand Trough and 149° Embayment in the northeast and north; a possible extension of the right-lateral strike-slip fault that forms the southern boundary of the Solomon plate; and a

diffuse band of seismicity along the Papuan Peninsula and Huon Peninsula. Davies *et al.* (1984) suggest that this diffuse boundary may be transitional, formed to accommodate a change from subduction along the Trobriand Trough to divergent or transform motion linked with the opening of the Woodlark Basin.

McClusky et al. (1994)

McClusky *et al.* (1994) used geodetic data (Doppler and GPS) to measure the rates of tectonic motion across many of the plate boundaries in the region. GPS to GPS comparisons found significant motion across the New Britain Trench (a decrease in baseline length at a rate of approximately 13±5 cm/y) and the Bismarck Sea Seismic Lineation (extension of approximately 10±4 cm/y). All other GPS-GPS comparisons showed no significant motion, with noise in the signal at the level of 10 cm swamping any tectonic motion.

Doppler to GPS comparisons were subject to lower levels of noise because of the time span of 10 years between the observation campaigns. The rates determined for the various baselines are shown in Figure 2.15. The main points to note are that significant motion, which agrees with geological estimates, occurs across:

- the New Britain Trench (15±1.5 cm/y to the northwest between the Solomon and Bismarck Seas and 12±3 cm/y to the northeast between the Solomon Sea and Pacific plate);
- the Bismarck Sea Seismic Lineation (15±4 cm/y); and
- the Woodlark Spreading Centre (9±3 cm/y),

Between Port Moresby, Morobe and Misima, there was no significant motion. Also, to the north of the Woodlark Spreading Centre, no significant motion occurred between Guasopa, Losuia, Morobe and Port Moresby. Likewise between Manus and Kavieng, both in the northern Bismarck Sea, no significant motion occurred. Between Witu and Jacquinot Bay, both in the South Bismarck Sea, no significant motion occurred. However, between Nuguria and Carteret, both of which are supposed to be located on the Pacific plate, motion of approximately 18±5 cm/y was detected. This result sparked an investigation of the Doppler results, which is discussed in Chapter 5.

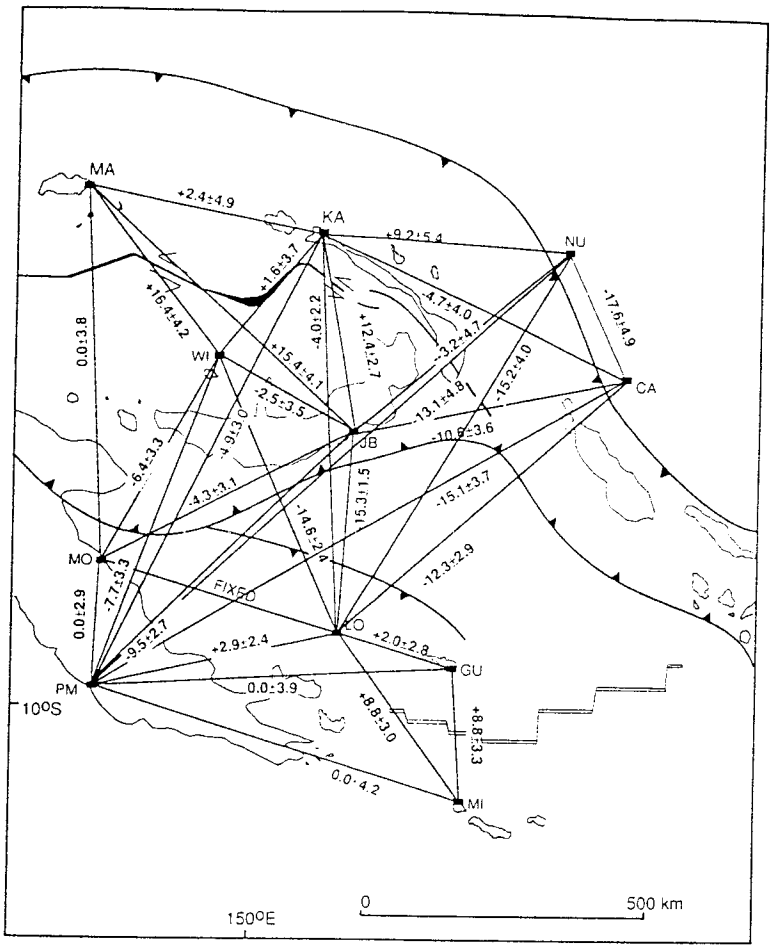

Figure 2.15 Rates of change of baseline lengths from the comparison between Doppler and GPS lengths. From McClusky et al. (1994).

As knowledge of the physical features of the region has increased, the models of the tectonic structure of the region have changed. It is clear from the preceding discussion that some boundaries are very clear, for example, the New Britain Trench, whilst others are uncertain, such as the boundary of the Australian plate in the complex region of faults and mountains in Papua New Guinea. It is questions such as these that this thesis aims to address by the use of geodetic observation, a tool only recently available for such a task.

Chapter 3

Satellite Systems and their use in Geodesy

3.1 Introduction

The development of Earth-orbiting satellite systems has had a large impact on surveying and geodesy. Such systems allow points on the surface of the Earth to be located with an accuracy and precision not possible by terrestrial survey methods. This has resulted in surveys extending over regional and global scales for the purpose of determining how the surface of the Earth is moving, traditionally the realm of Earth Sciences such as geology, seismology and geophysics.

One of the most productive satellite systems in use is the Global Positioning System (GPS). Other systems which have been used include the French DORIS system, the German PRARE system, the Russian GLONASS system, and Topex/Poseidon to name a few. Prior to the introduction of these systems, the most productive system was the U.S. Navy Navigation Satellite System (NNSS), or Transit Doppler System. Both the Transit Doppler system and the GPS system will be discussed in more detail shortly.

3.1.1 History of Satellite Geodesy

Before the advent of artificial satellites, geodesy was essentially four different disciplines: horizontal control; vertical control; astro-geodesy; physical geodesy. Each country initially had its own datum. By 1957, many of these had been linked by various methods, but long distance connections between datums were very inaccurate. Thus the major datums were of continental scale. The following history of satellite geodesy is condensed from the NASA report on the National Geodetic Satellite Program, 1977, parts 1 and 2.

With the launch of Sputnik-1 in 1957, geodesy entered a new era. The first new result was the derivation of the value of 1/298.3 for the Earth's flattening from observations of Explorer-1 and Sputnik-2. By 1964 a number of major developments had occurred:

- the Earth's flattening had been determined
- the major datums had been connected with errors of less than ±50 m (compared with ±100 - 200 m previously)
- the large features of the geoid were known over the oceans and unexplored or unknown continental interiors
- low frequency features of the gravitational potential were known.

There were a number of systems in use at the time, which can be grouped into two types:

- camera type tracking systems
- signal type tracking systems

Early Satellites Launched

The early satellites launched generally carried equipment to support both types of systems.

The initial Transit satellite, TRANSIT 1B (launched 1960) was purely a signal system using Doppler frequencies. It was launched to demonstrate feasibility of the Doppler navigation concept and to test various items of equipment involved in the Doppler navigation system.

The ANNA satellite, launched in 1962, was both a camera system and a signal system. It contained a transponder for the SECOR tracking system; a TRANSIT beacon emitting frequencies of 54 MHz and 216 MHz and a MINITRACK transmitter emitting 136 MHz. This was the first satellite launched specifically for geodesy, and provided data over a long period of time being fully operational until mid 1965 and offering limited service in 1972. This was the prototype for the GEOS series of satellites.

The Beacon Explorer satellites, launched in October 1964 and April 1965, also carried equipment for a variety of systems, including a TRANSIT type beacon emitting frequencies of 162 MHz and 324 MHz and a MINITRACK transmitter emitting 136 MHz; an array of corner cube reflectors to allow tests of the newly

developed laser-type distance measuring equipment. The major drawback of the Beacon satellites is that they were magnetically stabilised, and were therefore, upside down in the southern hemisphere.

The GEOS satellites, the first of which was launched in November 1965, contained flashing light for photogrammetric techniques; Doppler transmitters on frequencies 162 MHz, 324 MHz and 972 MHz allowing more sophisticated ionospheric corrections than the first order two frequency systems; SECOR transponder; GRARR transponder; MINITRACK transmitter at 136 MHz; range/range rate; and laser reflectors. The second GEOS satellite, launched in January 1968, carried similar beacons and transponders to the first. The major difference in the Doppler transponder was that timing marks were introduced on the 162- and 324-MHz frequencies.

Pageos (passive geodetic satellite) was a camera system, launched in June 1966. It was a balloon type satellite designed specifically for geometric satellite triangulation. It had a diameter of 30 m with a casing that specularly reflected sunlight.

3.1.2 Early Satellite Geodetic Techniques

Photogrammetric systems

Satellite triangulation is an optical method of determining the location of points on Earth by visually observing satellites. The world-wide satellite triangulation program using BC-4 cameras was used successfully in the 1960's to determine the relationships between the major world datums.

The method involved photographing special reflective satellites against a stellar background with a metric camera. The camera was fitted with a specially manufactured chopping shutter. The image that appeared on the photograph consisted of a series of dots depicting the path of each star and the satellite. The coordinates of selected dots were precisely measured using a photogrammetric comparator, and the associated spatial directions from the observing site to the satellite were then processed using an analytical photogrammetric model. Simultaneously photographing the same satellite from a neighbouring site and processing the data in an analogous way yields another set of spatial directions. Each pair of corresponding directions forms a

plane containing the observing points and the satellite, and the intersection of at least two planes results in the spatial direction between the observing sites. In the next step, these oriented directions were used to construct a global network with the scale being derived from several terrestrial traverses. An example is the European baseline running from Tromsφ in Norway to Catania on Sicily.

The major disadvantage of this system was that clear sky was required simultaneously at a minimum of two observing sites separated by some 4000 km. In addition, the equipment was massive and expensive. The system was further limited by the angular resolution of the photogrammetric technique. These disadvantages meant that optical direction measurement was soon supplanted by the electromagnetic ranging technique because of all-weather capability, greater accuracy, and lower cost.

Although there were no sites from the BC-4 photogrammetric satellite triangulation network located in Papua New Guinea, Thursday Island, on the northern tip of the Cape York Peninsula was part of this network. There were also sites at Culgoora, in northern NSW, and Perth. The lower precision of the technique has prohibited its use for the high precision geodetic problems such as detecting tectonic motion. The standard deviations of baselines by this technique are of the order of 1-4 m.

Geodetic SECOR System

SECOR (Sequential Collation of Range) operates on the principle that an electromagnetic wave propagated through space undergoes a phase shift proportional to the distance travelled. SECOR consists of four ground stations and an Earth-orbiting satellite. Each ground station contains a transmitter, a dual frequency receiver, data-processing equipment, and data display and recording equipment and is capable of acting as both a master station and a slave station. These terms will be explained shortly.

A ground station transmits a phase-modulated signal which is received by the satellite borne transponder and returned to the ground. The phase shift experienced by the signal during the round trip from ground to satellite and back to ground is measured by an electronic servo at the ground station, which provides as its output a digitised representation of range.

The master station is in control of the operation and its signal is modulated by frequencies additional to the ranging frequencies. One additional modulation gives commands to the satellite which activate and deactivate the transmission part of the satellite. The other additional modulation is relayed by the satellite to the slave stations to provide them with timing information. The slave stations transmit only range signals.

The modulation of the signal is determined by the requirements for accuracy and unambiguous measurements. For accuracy, since phase is compared, the shortest possible wavelength should be used. For unambiguous measurements, the longest wavelength compatible with the required range should be used. Unambiguous and accurate measurements are achieved by modulating with more than one frequency. Four modulation frequencies are included in the signals to provide adequate data on range. Ranges up to 524288 m can be measured unambiguously to an accuracy of 0.25 m.

SECOR can operate in three different modes. If the satellite is visible from all four stations, the stations can interrogate the satellite nearly simultaneously. Three ground stations are therefore placed in known locations, and the fourth station is put in an unknown location. This is illustrated in Figure 3.1. Range measurements from the three known stations determine the position of the satellite with respect to the known stations. Range measurements from the unknown station to at least three properly spaced locations of the satellite determine the location of the unknown station relative to the known stations.

If the unknown station is too far from the known stations, observation of the satellite simultaneously by all four ground stations is impossible, and another mode of operation may be used. This is also illustrated in Figure 3.1. This mode of operation is called the "orbital" mode. Again, three known stations simultaneously measure ranges to the satellite. These ranges are used to determine short arcs of the satellites orbit above the three ground stations. The short arcs can be extrapolated into the region above the unknown station. Interrogation of the satellite by this station provides the data for positioning the unknown station.

If the clocks of the stations can be synchronised, each station can observe independently of the other, which is the third mode of operation.

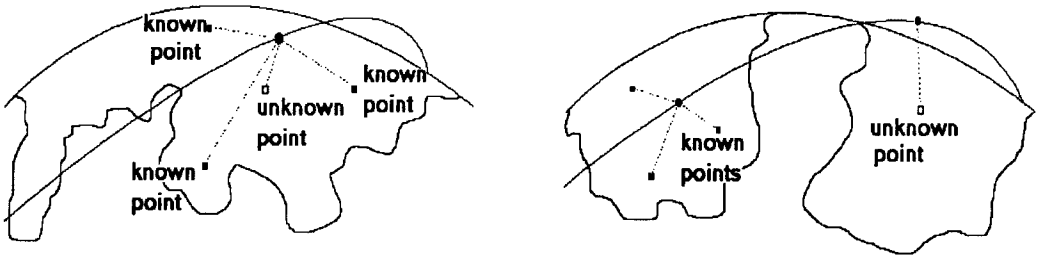

SECOR: simultanoeus mode of operation

SECOR: orbital mode of operation

Figure 3.1 Illustration of the simultaneous and orbital modes of operation for the SECOR system.

Because of the narrow bandwidth, the selection of the modulation frequencies and the small modulation index, the dispersive distortion of the SECOR signal along its propagation path is smaller than 1 part in 10^6 and the group velocity is practically constant within the bandwidth. Because of the altitude of the satellites, the signals travel through the ionosphere and experience a delay that must be considered in the calculation of distance. By using two frequencies, a correction for the ionospheric error in range is provided. In order to avoid overlapping of arriving signals at the satellites, the ground stations transmit the signals in sequentially arranged pulses.

The SECOR network included a site in Papua New Guinea, and several additional sites nearby. The site on Manus Island has subsequently been reoccupied by Doppler, in the 1981 survey, and by GPS in the 1990 and 1993 surveys. Other nearby sites which were observed by SECOR and subsequently with GPS are Darwin, and Guam. The SECOR coordinates of these sites, in terms of latitude, longitude and height from the solution WN14 are:

Manus	02°02'20.34"S	±0.11"	147°21'40.80"	±0.09"	82.38m	±2.38m
Darwin	12°27'15.12"S	±0.12"	130°48'58.51"	±0.10"	76.62m	±3.28m
Guam	13°26'22.08"N	±0.09"	144°38'05.87"	±0.08"	97.15m	±2.05m

The large standard deviations mean that this historical data is not sufficiently precise for tectonic analysis. A time span of approximately 80-100 years would be required before the tectonic motion at the fastest boundaries in the Papua New Guines region exceeded the 3σ precision of the measurements!

Laser Ranging Systems

Laser systems work on the principle that a beam of light is pointed at the satellite, from which it is reflected back to the ground. The two way travel time of the signal is recorded and used to calculate a range to the satellite. Accurate results require that the timing be measured accurately and corrections be applied for the bias introduced into the range from travelling through the atmosphere.

Monochromatic, high energy beams with a very low angle of divergence are used. These beams are emitted in sharply defined pulses. The high degree of collimation allowed the laser beam to hit the satellite with a significant amount of radiant energy. An array of corner cube reflectors on the satellite reflects the signal back to the ground. The monochromatic nature of the laser beam allows for efficient filtering to improve the signal to noise ratio. Timing systems of nanosecond precision are required.

The laser ranging system is mainly confined to observatories, although a few mobile systems have been built.

Transit Doppler System

The Transit Doppler System originated at the same time as the above mentioned techniques. It proved to be the more versatile of the systems, and was thus adopted as the primary geodetic satellite system for the Department of Defence (DoD). It was the system used for the initial survey of Papua New Guinea in 1981, and is therefore discussed in detail below.

In January, 1964, the NNSS became continuously operational. About this time, passive camera systems were replaced by the active signal systems, because of the greater flexibility, all-weather operation and greater accuracy of these techniques.

3.2 The Transit Doppler System

The Navy Navigation Satellite System, or Transit Doppler System, is described at length by McClusky (1993), Newton (1967), and Stansell (1971). A summary is included here, covering the aspects of the system relevant to the Doppler analysis performed as part of this research.

The Transit satellite system consisted of a small number of satellites (usually five) orbiting the Earth in polar, near circular orbits. Orbits were at an altitude of about 1000 km. Each orbit had a period of approximately 105 minutes. With this constellation, there was not a constant satellite coverage and only one satellite was generally visible at a time. The design goal of the system was to be able to get a position fix every 90 minutes, which was the nominal gap between satellite passes.

The system became continuously operational in January 1964. In 1967, commercial development of receivers for civilian purposes began. The region around Papua New Guinea was extensively surveyed with Doppler during the mid-1970's.

The satellites transmit messages on two stable carrier frequencies of approximately 150 MHz and 400 MHz. The signals are often combined in the receiver to determine the first order ionospheric effects. This can also be done later during the processing of the observations. The corrected 400 MHz carrier frequency is then used in the Integrated Doppler Measurements.

The messages carried on the above two frequencies contain the following information:

- the predicted ephemeris of the satellite
- timing signals derived from the structure of the broadcast message, the most important of which are the 2 minute and 4.6 second timing marks.

The broadcast message contains navigation information relating to the position of the satellite (orbital parameters and location of the satellite in the orbit) and additional useful information including the age of the broadcast message, the deviation of the satellite clock from the 400 MHz frequency and various timing marks.

The structure of the broadcast message is described by McClusky (1993). The broadcast message is a series of digital signals modulated onto the carrier frequencies. The signal consists of 6103 binary bits repeated every two minutes, hence the two minute timing signal mentioned above. The signal is divided into various combinations of words and bits. It transpires that six 39-bit words are transmitted every 4.600908 seconds. This timing interval is important for the reduction of the data in the 1981 Doppler campaign, discussed in Chapter 5. The so-called 30 second timing signal that was commonly used at the time was also derived from the 4.6 second interval. Six counts of the 4.6 second interval is approximately 27.6 seconds, and 7 counts is approximately 32.2 seconds. Three counts of 27.6 seconds plus one count of 36.8 seconds gives 119.6 seconds, which corresponds to the 2 minute timing mark. Thus the "30 second" timing marks actually varied from 6 to 7 counts of the 4.6 second timing mark, but the same pattern was repeated every two minutes.

3.2.1 Basic Principles of Doppler Operation

During a satellite pass, the range to the satellite decreases until the point of closest approach, and then increases until the satellite sets. The continually changing range affects the frequency at which the signal is received. This is known as the Doppler shift of the transmitted frequency and is the basis of the Transit Doppler system.

The receiver generates its own signal from an internal or external oscillator at approximately 400 MHz. The Doppler shifted received signal is beat with the receiver generated signal to obtain the Doppler measurement (Brown and Trotter, 1969).

The Doppler beat frequency is given by $(f_g - f_r)$. The integrated Doppler count is obtained by integrating the beat frequency with respect to time:

$$N = \int_{\tau=0}^{\tau} (f_g - f_r)dt \qquad (3.1)$$

where:

N is the integrated Doppler count from τ=0 to τ.

f_g, f_r are the receiver generated and received frequencies respectively

In Doppler positioning techniques, the range to the satellite at the time the signal is received is ambiguous by an integer number of wavelengths.

However, as the receiver maintains lock on the satellite, the change in phase of the signal is tracked. This quantity, N in equation 3.1, represents the cumulative count of the beat frequency. When multiplied by the signal wavelength, it gives the range to the satellite plus an unknown additive constant of integration. This is the ambiguity term, which is constant for a pass provided the signal is tracked continuously. Once continuity of tracking is lost, a new ambiguity is required. The orbital dynamics constrain the relative positions of the receiver and satellite. This, combined with the fact that the frequency at which the satellite transmits the signal is known, allows the coordinates of the site to be calculated from the integrated Doppler count (Hager et al, 1991).

3.2.2 Error sources

In reality, no system is error free, and Doppler positioning techniques are no exception. There are a number of error sources that need to be eliminated or modelled as part of the adjustment.

Ionospheric Delay

The ionospheric delay is an increase of the wavelength of the signal that occurs as it passes through the ionosphere. This increase occurs as the inverse proportion to the signal frequency. By observing two different frequencies, the effect of the ionosphere on each can be compared and the effects can then be eliminated to first order.

The JMR receivers used in the 1981 survey combine the 400 MHz and 150 MHz signals internally and record only the ionosphere free integrated Doppler count. This removes the first order ionospheric effects. Remaining effects are incorporated into a parameter in the range equation.

The effects of the ionosphere on the propagation of satellite signals is discussed more comprehensively in Section 3.3.3 in relation to the GPS system.

Tropospheric Refraction

The refraction of the signal as it passes through the troposphere cannot be simply removed, therefore it is usually modelled. The models incorporate temperature, pressure and relative humidity to estimate the effects on signals from satellites at different elevation angles observed at stations of different heights. These models usually consist of two components: a zenith delay model to determine the tropospheric delay at the observer's zenith and a mapping function to convert this value to the value at the elevation angle of the satellite. In the Short Arc Geodetic Adjustment (SAGA) software used in this analysis, the correction is of the form: (Brown and Trotter,1969)

$$\Delta r_t = -2\alpha f(E) \tag{3.2}$$

where the zenith delay term is

$$\alpha = (n_0 - 1)H_0 \tag{3.3}$$

and the mapping function is given by

$$f(E) = \frac{1}{\left[\mathrm{Sin}E + \sqrt{\mathrm{Sin}^2E + \frac{4H_0}{r_0}}\right]} \tag{3.4}$$

where:

n_0 is the index of refraction at the station;

r_0 is the radius of the Earth in metres;

H_0 is the scale height of the troposphere;

E is the elevation angle to the satellite.

The refractive index is computed using the atmospheric observations at the station or standard values by the equation

$$n_0 = 1 + 10^{-6}\left[103.49\left(\frac{P_0 - e_0}{T_0}\right) + \frac{86.26}{T_0}\left(1 + \frac{57.48}{T_0}\right)e_0\right] \tag{3.5}$$

where:

P_0 is the atmospheric pressure in millimetres of mercury;

e_0 is the water vapour pressure in millimetres of mercury;

T_0 is the temperature in degrees Kelvin; and

$H_0 \approx 29.2(T_0 - 30)$.

Propagation Delay

The propagation delay, or transmission delay, is the time taken for the signal to travel between the satellite and the receiver. As discussed above, the range is the product of the speed of light in a vacuum and the travel time of the signal. As the JMR receiver used in the 1981 observation campaign records its observation in the receiver time frame, the satellite time frame will be neglected to avoid confusion. The instant at which the receiver recognises a timing mark on the incoming signal, is necessarily not the time at which that timing mark was transmitted by the satellite. While the signal has travelled to the receiver, the satellite has moved forward in its orbit. Thus the position of the satellite given in the broadcast message does not represent the actual position of the satellite in the receiver time frame at the time the signal was received. The correction for propagation corrects the range from receiver to satellite to the actual position of the satellite at the time of reception of the signal. It is given by the equation:

$$\Delta r_p = \dot{r} \frac{r}{c} \tag{3.6}$$

Timing Errors

Errors or systematic trends in the receiver or satellite clocks are the largest source of error in the system. Both satellite and receiver clocks exhibit offsets from the nominal frequency and frequency drifts over extended periods of time. The satellite clocks were high precision crystal oscillators. These were steered to maintain accurate timing. The receiver clocks were quartz crystal oscillators, which were several orders of magnitude lower in precision than the satellite oscillators. If higher precision receiver timing was required, atomic oscillators with a low drift rate could be attached to the receivers. For example, the Doppler survey performed in the Papua New Guinea region in 1981 used a mixture of caesium and rubidium atomic oscillators on some sites and the standard crystal oscillators in the receivers at other sites. Other sources of error are caused by delays that occur in the circuitry of the receiver, for example in decoding the broadcast message. As a result, the ranges calculated to the satellite will be in error. In SAGA, the satellite and receiver clock errors are combined into a single error parameter because they are impossible to distinguish. The error is separated into two parts: an oscillator offset to the

required frequency that can be as large as 1000λ ms^{-1} and a drift rate which is of the order of 0.0002 ms^{-1}.

An additional timing error is associated with delays in the receiver circuitry which retard the recording of the Doppler signal. This delay is split into a systematic component (the receiver delay) and a random component (the timing jitter). The jitter is reduced by recording whole Doppler counts on the positive crossings of the beat frequency. The receiver delay must be removed (if it is known) or estimated in the adjustment process using an appropriate error model.

A further timing error is the inter-station timing bias which occurs when the receiver clock is not correctly synchronised to the satellite time frame (UTC). This error is usually estimated as part of the solution, with one bias estimated per station for each pass. This is discussed in more detail below.

The frequency transmitted by the satellite (f_s) and the frequency generated by the receiver (f_g) can be expressed as

$$f_s = f_\infty + \delta f_s + \dot{f}_s \tau \tag{3.7}$$

$$f_g = f'_\infty + \delta f_g + \dot{f}_g \tau \tag{3.8}$$

where:

f_∞, f'_∞ are the adopted values of the frequency transmitted by the satellite and the frequency generated by the receiver respectively;

$\delta f_s, \delta f_g$ are the bias terms in the adopted values of f_s and f_g respectively at $\tau = 0$.

$\dot{f}_s, \dot{f}_g$ are the drift rates of f_s and f_g respectively.

Each of these terms are treated as parameters in the solution.

Interstation Timing Bias

The inter-station timing bias is the result of the receiver timing errors mentioned above. Although each receiver is synchronised to the satellite, the errors inherent in each receiver are slightly different, resulting in slightly different synchronisation at each site for each pass. Therefore, for each station in each pass, an inter-station timing bias parameter is solved as part of the solution.

If the offset of the receiver clock with respect to a master clock at a reference epoch is τ_0, the offset at any epoch τ is given by

$$\delta\tau = \delta\tau_0 + \frac{\delta f_g}{f_\infty}\tau = \delta\tau_0 + \lambda_0 \frac{\delta f_g}{c}\tau \tag{3.9}$$

and the correction to the range difference is given by

$$\Delta r_\tau = \dot{r}\,\delta\tau = \dot{r}\,\delta\tau_0 + \lambda_0 \delta f_g \frac{\dot{r}}{c}\tau \tag{3.10}$$

Orbit Errors

The a priori orbit used in processing the 1981 survey is a broadcast orbit. These orbits are computed from tracking data observed at four sites - three of which are on the North American mainland, and the other on the atoll of Hawaii. The computed orbits are then extrapolated. It is these extrapolated orbits that are broadcast real time by the satellites. Extrapolated orbits are necessarily going to be erroneous due to inaccuracies in the models used to create them, and the use of different models and parameters in the solution. To overcome the orbit errors introduced into the solution, the orbit elements are estimated as part of the solution.

General Relativistic Correction

The general relativistic correction allows for the difference in gravitational potential between the satellite and the receiver. For nearly circular orbits, the altitude of the satellite is effectively constant over a satellite pass and the correction is proportional to time. Thus it can be absorbed by the clock offset error correction term.

3.2.3 Range Equations

Although the actual range to the satellite is unknown, equations expressing range difference as a function of signal travel time have been developed. These equations are taken directly from McClusky (1993), and are expressed in terms of two time frames: satellite and receiver time frames.

Satellite time frame:

$$(r_2 - r_1) = \lambda_g N_{1,2} - \lambda_g \left[f_g - f_t\right](t_2 - t_1) \tag{3.11}$$

Receiver time frame:

$$(r_2 - r_1) = \lambda_t N_{1,2} - \lambda_t \left[f_g - f_t\right](t_2' - t_1') \tag{3.12}$$

where:

r_1 , r_2 are ranges at times t_1 and t_2 or t_1' and t_2' respectively;
$N_{1,2}$ is the integrated Doppler count between times t_1 and t_2 or t_1' and t_2';
f_g, f_t are the frequencies generated by the receiver and received by the receiver respectively. Thus $(f_g - f_t)$ is the Doppler beat frequency;
t_1, t_2 are the times in the satellite time frame;
t_1', t_2' are the times in the receiver time frame;
λ_g , λ_t are the wavelengths of the receiver generated signal and the signal transmitted by the satellite respectively.

The Short Arc adjustment technique uses these range difference equations as a basis for developing the observation equations. A full development of the observation equations used can be found in McClusky (1993) and Brown and Trotter (1969).

The basic observation equation used for short arc adjustment is given as:

$$r^0 + a_0 + a_1\tau + a_2\tau^2 + a_3 r + \delta \dot{r}_s = \left[\left(X - X^c\right)^2 + \left(Y - Y^c\right)^2 + \left(Z - Z^c\right)^2\right] \tag{3.13}$$

where:

r^0 is the range difference from an arbitrary time τ to time $\tau = 0$;
a_0 is the unknown initial range, or ambiguity, called the zero set term. It has a nominal value of 1×10^7m;
a_1 is the combined satellite and receiver oscillator frequency offset error;
a_2 is the combined relative satellite and receiver drift error;
a_3 is the proportional frequency bias which is of the order of 1×10^{-6} or lower;
τ is any arbitrary time;

r is the range between satellite and receiver;
X, Y, Z are the satellite coordinates;
X^c, Y^c, Z^c are the receiver coordinates;
$a_0 + a_1\tau + a_2\tau^2 + a_3 r + \delta\dot{r}_s$ is the short arc error model.

In addition to the above equation, a few more error sources discussed in Section 3.2.2 need to be estimated. The correction to r^0 is given by the term Δr, where

$$\Delta r = \Delta r_I + \Delta r_T + \Delta r_p + \Delta r_\tau + \Delta r_G \qquad (3.14)$$

and
Δr_I is the correction for ionospheric refraction;
Δr_T is the correction for tropospheric refraction;
Δr_p is the correction for the propagation delay;
Δr_τ is the correction for the inter-station timing bias;
Δr_G is the general relativistic correction.

3.2.4 Short Arc Geodetic Adjustment (SAGA)

The Short Arc software used for this analysis was SAGA (Short Arc Geodetic Adjustment).

SAGA employs short arc orbital model in the adjustment of Doppler measurements from a tracking network in a simultaneous adjustment (McClusky 1993). The basic equations used in SAGA are given in Section 3.2.3.

SAGA is limited to 400 stations in the adjustment, with no more than 25 observed simultaneously. Any number of constraints may be applied to the a priori coordinates and to baselines in the form of azimuth, elevation and length constraints. The centre of mass of the Earth is also allowed to adjust. The terms of the error model incorporated into SAGA are given a priori constraints. This flexibility means that care needs to be exercised when constraints are applied. SAGA is inherently a rank deficient process, with a rank deficiency of six. This means that only six elements need to be constrained to establish the solution. Any more than six can introduce strain and distort the solution. This is discussed more fully in Chapter 5. Observations from all stations are adjusted simultaneously. An estimate of the covariance matrix of adjusted coordinates is

produced, but as the normal equations are not inverted, these estimates are not precise and only pertain to the diagonal elements.

3.3 Global Positioning System (GPS)

3.3.1 General Overview

The U.S. Department of Defence (DoD) developed the Global Positioning System (GPS) for military purposes. Primarily, it is a ranging system used to locate unknown points on or near the Earth from satellites of known position. DoD also promoted civilian use of the system. Civilian users are now a major user group.

The workings of GPS are described in detail by many authors (for example Hofmann-Wellenhof *et al*, 1994; Leick, 1995), so a full description of the system will not be given here. Instead, a general overview is given, in which the features that have particular relevance to this research are discussed in more detail.

GPS satellites emit signals on two microwave radio frequencies: 1575.42 MHz (the L1 frequency) and 1227.60 MHz (the L2 frequency). These frequencies are the carrier wave frequencies, which are modulated with various codes. Each satellite modulates the signals with unique pseudo random noise (PRN) codes, which are essentially timing signals used for determining travel time between the satellite and receiver. The time taken for the signal to travel to the receiver, multiplied by the velocity at which it travels, gives the range. Ranging to four satellites allows the user to solve for a three dimensional position and the receiver clock error.

When the signals leave the satellite, they travel through space at the speed of light until they reach the Earth's atmosphere. The outermost layer of the atmosphere, the ionosphere, changes the speed at which the signal is travelling. The ionospheric effects on the signal propagation are the largest natural source of error in GPS positioning (Klobuchar, 1991). Dual frequency observations eliminate most of the ionospheric effects, but in the equatorial regions, the effect of the ionosphere can be particularly severe (Wanninger, 1993). This is a significant source of error in the Papua New Guinea GPS surveys and is therefore discussed further in Section 3.3.3.

Between the ionosphere and the surface of the Earth lie the electrically neutral stratosphere and troposphere. The non-dispersive nature of these layers means that the velocity of a signal passing through them is independent of its frequency, hence the L1 and L2 GPS frequencies are affected equally. (Brunner and Welsch, 1993). The most effective means of dealing with the tropospheric delay is to model it. The errors caused by the troposphere and the model used in this analysis to correct the range are discussed in Section 3.3.3.

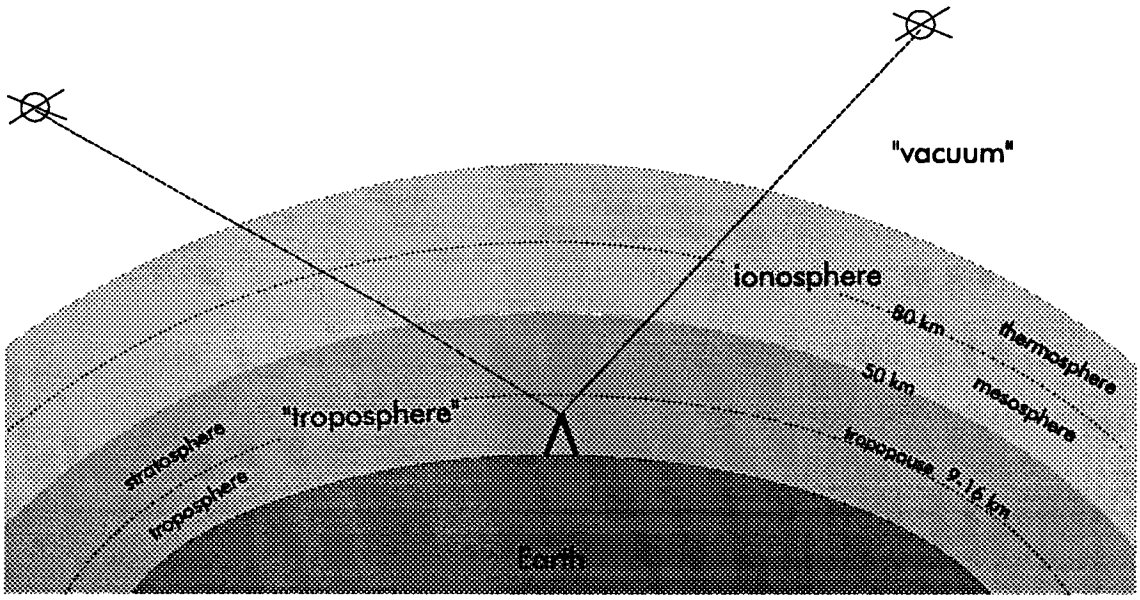

Figure 3.2 The layers of the Earth's atmosphere which affect the propagation of satellite signals.

The point on the antenna at which the signal is received is called the phase centre of the antenna, which usually differs from the physical centre of the antenna. The errors associated with the antenna are discussed in Section 3.3.4.

When the signal arrives at the receiver, it is mixed with an identical signal generated by the receiver. This allows the time delay between emission of the signal from the satellite and reception at the receiver site to be determined. Electrical delays in this process are small. When the code information and other information, such as satellite clock correction and orbit information, has been obtained, the codes are removed from the signal leaving the unmodulated carrier phase. This can then be used for phase measurements.

Point positioning with GPS, using the coded signals emitted from the satellites, gives accuracies in real time of 15-40 m, without Selected Availability (SA).

With SA implemented, point positioning is degraded to approximately 100 m. (Hofmann-Wellenhof *et al*, 1994). The effects of SA are discussed in more detail shortly. These levels of accuracy are insufficient for the accuracy requirements of many survey and geodetic applications. Instead, relative positioning is used and the phase of the carrier signal is measured to achieve precisions of a few centimetres.

3.3.2 Satellite Constellation

The fully operational GPS satellite constellation consists of 24 operational satellites in six orbital planes with an inclination of 55°. Each plane contains four satellites. An additional four active spare satellites are operational (Hofmann-Wellenhof *et al*, 1994).

There are a total of five types of satellites, either already in operation or planned for future use and currently under development (Hofmann-Wellenhof *et al*, 1994). These are:

- Block I. These were the prototype satellites launched between 1978 and 1985. They have now all been replaced with Block II satellites, but at the time of the Papua New Guinea crustal motion surveys, several Block I satellites were still in operation. The Block I satellites were in orbital planes of 63° inclination. Block I satellites did not have SA or Anti-Spoofing (AS) implemented. SA and AS are discussed shortly.
- Block II. The Block II satellites were the first in the 55° orbital planes. Access to the full positioning potential of the Block II satellites is denied to civilian users by the implementation of SA and AS. Block II satellites were launched between 1989 and 1990.
- Block IIA. These satellites were launched between 1990 and 1994. As far as this work is concerned, they are the same as the Block II satellites.
- Block IIR satellites will replace the Block II satellites. The first is scheduled to be launched this year (1996). These satellites are expected to have onboard hydrogen maser oscillators, which will be an order of magnitude more precise than the atomic clocks in the preceding satellites.
- Block IIF. These satellites are planned to be launched between 2001 and 2010.

The accuracy of the system is due to the atomic clocks which control all components of the signal. The Block II satellites each have four atomic clocks

on board: two rubidium and two caesium oscillators. These are stable to a few parts in 10^{-13} to 10^{-14} over a day (Hofmann-Wellenhof *et al*, 1994). The oscillators generate the fundamental frequency of 10.23 MHz, which is multiplied by 154 and 120 respectively to form the L1 and L2 frequencies:

$$L1 = 1575.42 \text{ MHz}$$
$$L2 = 1227.60 \text{ MHz}$$

The L1 carrier has a wavelength of approximately 19.0 cm and the L2 frequency has a wavelength of about 24.4 cm. Two frequencies are necessary for eliminating the major natural source of error, the ionosphere.

These carrier waves are modulated with PRN codes. The C/A code is modulated onto L1 only, and is available for civilian use. The wavelength of the C/A code is about 300m. The omission of the C/A code from L2 denies ordinary civilian users the full accuracy of the system because ionospheric corrections cannot be determined and must be modelled.

The P-code is modulated onto both the L1 and L2 carriers. It has a wavelength of about 30m. This code is known by non-military users. To deny non-authorised users access to dual frequency observations, a W-code is added to the P-code to create the encrypted Y-code, now that the system is fully operational. This process is called Anti-Spoofing and is discussed later in this section. Non-authorised users cannot decode this signal, although receivers have been developed that use various techniques to obtain L2 measurements without knowledge of the Y-code. These methods are discussed in Section 3.3.4

In addition to the PRN codes additional information, including satellite ephemerides, ionospheric modelling coefficients, status information, system time, satellite clock bias and drift are modulated onto the carrier frequencies in the form of the navigation message. The codes are all generated as multiples of the fundamental frequency (Hofmann-Wellenhof *et al*, 1994). The frequencies of these codes are:

Fundamental frequency	f_0	10.23 MHz
P-code	f_0	10.23 MHz
C/A-code	$f_0/10$	1.023 MHz
W-code	$f_0/20$	0.5115 MHz
Navigation message	$f_0/204600$	50 Hz

The carrier broadcast by the satellite is a broad spectrum signal that makes it less subject to jamming (Hofmann-Wellenhof *et al*, 1994).

Degradation of Accuracy - Selective Availability

Field tests showed that the accuracy of pseudo-ranges achieved from the C/A-code was significantly better than the expected 400m. Between 15 m and 40 m was achieved in position and less than a metre per second in velocity (Hofmann-Wellenhof *et al*, 1994). This lead the DoD to degrade the accuracy achievable by civilian users by implementing SA.

SA is achieved by two processes (Hofmann-Wellenhof *et al*, 1994). The first process is a dithering of the satellite clock. This is achieved by introducing errors of varying magnitude into the fundamental frequency of the satellite clock. Because the fundamental frequency and all harmonically related frequencies are controlled by the clocks, dithering affects the phase measurements and C/A- and P-code measurements. Thus the accuracy of ranges determined from both phase and code will be degraded. The second process involves degrading the quality of the broadcast ephemeris. This is achieved by truncating the ephemeris information transmitted to the users. Hence the satellite position cannot be accurately determined, and the computed position of the receiver will be inaccurate.

The result of SA is that for 95% of the time positions will be within error bounds of 100 m for horizontal position and 156 m for height. Velocities will be in error by up to 0.3 ms^{-1}. The time will be in error by up to 340 ns. At the 99.99% probability level, position errors will be within 300 m in the horizontal and 500 m in height (Hofmann-Wellenhof *et al*, 1994). According to Georgiadou and Doucet (1990), these values refer to the degradation applied when the constellation is fully operational, and that larger errors were to be expected at times prior to this.

SA is implemented on Block II and subsequent satellites. It was formally implemented on 25th March, 1990 (Hofmann-Wellenhof *et al*, 1994). At the time of the 1990 GPS survey in Papua New Guinea, SA was particularly severe. The problem of broadcast orbit inaccuracy was overcome by using precise ephemerides generated by a global network of tracking stations. Clock dithering can be eliminated by differencing if the receiver clocks are synchronised to observe simultaneously and are not separated by too great a distance. Problems arise when the receivers sample at different times, as was the case with the array of receivers, both global and local, used in the 1990 survey. The way it was dealt with will be discussed in Chapter 6.

Sandlin *et al* (1995) discuss a report jointly produced by the National Academy of Public Administration (NAPA) and the National Research Council (NRC) entitled "The Global Positioning System - Charting the Future". This report investigates the arguments for and against continued implementation of SA, and recommends SA be removed from all satellites. The arguments will not be discussed in detail, however they can be briefly stated thus:

- widespread DGPS networks and unrestricted GLONASS signals remove the security benefits of SA;
- present levels of degradation give adversaries a sufficient level of accuracy to inflict considerable damage;
- worldwide, civil users such as aviation, shipping, etc have come to depend on GPS and represent a strong lobby group against greater levels of degradation in times of conflict;
- more effective denial of access such as local signal jamming can easily be developed and would be much more effective;
- there are significant economic benefits arising from removing SA and keeping GPS as the primary global navigation system.

In March of this year (1996), the US government announced that it will be discontinuing the use of SA within the next decade, and that annual reviews of its use will be performed by the President of the USA beginning in the year 2000.

Informal statements from DoD have even suggested that an additional frequency signal should be provided to civilian users to improve removal of ionospheric effects! An additional frequency is currently being considered for implementation on Block IIF satellites.

Restriction of Access - Anti-Spoofing

Whilst SA degrades the accuracy that users can achieve with the signals available to them, Anti-Spoofing (AS) aims to deprive non-authorised users of the more accurate P-code, thus limiting accuracy. The means of achieving this is to use a secret W-code, which is added to the P-code. The result of the modulo-2 sum of the P-code and W-code is the Y-code, which is modulated onto both L1 and L2.

AS was first implemented on a full-time basis on 31st January, 1994, although it was switched on for trial periods prior to this, beginning of the weekend of the 1st August, 1992 (Hofmann-Wellenhof *et al*, 1994).

The frequency of the W-code is one twentieth the fundamental frequency, or 0.5115 MHz. This is important to the development of some receiver types, outlined in Section 3.3.4.

3.3.3 Signal Propagation

The following derivation is based on Hofmann-Wellenhoff *et al* (1994).

A signal propagating through space has a phase velocity of :

$$v_{ph} = \lambda f \tag{3.15}$$

This is the velocity at which the L1 and L2 carrier waves are propagating. The codes modulated onto these carrier waves have slightly different frequencies. Their combined velocity must be in terms of a group velocity, given by:

$$v_{gr} = -\frac{df}{d\lambda}\lambda^2 \tag{3.16}$$

A relationship between the phase and group velocity is given by:

$$v_{gr} = v_{ph} - \lambda\frac{dv_{ph}}{d\lambda} \tag{3.17}$$

In non-dispersive media, the phase and group velocities are both equal to the speed of light in a vacuum.

The propagation of a wave is dependent upon the refractive index of the medium through which it travels. This is expressed by the relationship:

$$v = \frac{c}{n} \tag{3.18}$$

where

c is the speed of light in a vacuum, and
n is the refractive index of the medium.

Using the above relationship, and using n_{ph} and n_{gr} to denote refractive indices for phase and group velocities respectively, it can be shown that the following relationship exists:

$$n_{gr} = n_{ph} - \lambda \frac{dn_{ph}}{d\lambda} \tag{3.19}$$

in terms of wavelength, or in terms of frequency:

$$n_{gr} = n_{ph} + f\frac{dn_{ph}}{df} \tag{3.20}$$

Propagation in the Ionosphere

The ionosphere is the outermost layer of the Earth's atmosphere, extending from approximately 50 km above the Earth to about 1000 km (Hofmann-Wellenhof *et al*, 1994; Brunner and Welsch, 1993). It consists of electrically charged particles: negatively charged electrons and positively charged ions. These are formed by the action of ultraviolet light on the atoms and molecules which comprise the upper part of the atmosphere. The ionosphere is dispersive for radio waves, which means that the velocity of a radio wave travelling through it depends upon its frequency.

The density of electrons in the ionosphere determines the velocity of the GPS radio signals as they pass through this layer as shown by equation 3.18 above. The refractive index of the ionosphere can be approximated by:

$$n_{ph} = 1 + \frac{c_2}{f^2} + \frac{c_3}{f^3} + \frac{c_4}{f^4} + \ldots\ldots \tag{3.21}$$

where the coefficients c_2, c_3, c_4, etc depend on the electron density, N_e (Seeber, 1993). This equation is usually truncated to the quadratic form:

$$n_{ph} = 1 + \frac{c_2}{f^2} \tag{3.22}$$

A measure of the density of electrons is the total electron content (TEC). This quantity is measured along the travel path of the signal. The TEC of the ionosphere at zenith is given by the TVEC. The TVEC is defined as the number of electrons in a vertical column with a cross-sectional area of one square metre. The TVEC is only useful for satellites at the zenith, so to express it as a value along the geometric path between satellite and receiver, the zenith angle must be taken into account:

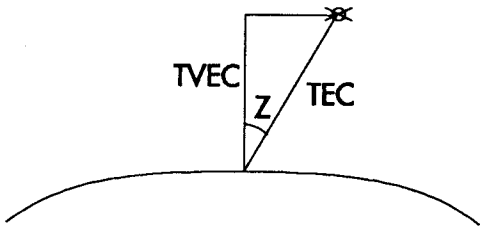

$$TEC = \frac{TVEC}{Cos\ Z}$$

The TEC can be found by:

$$TEC = \int N_e ds_0 \qquad (3.23)$$

in which

N_e is the electron density along the propagation path;

s_0 is the geometric range in a straight line between the satellite and receiver.

The TEC shows geographic and temporal variations. The mid latitude regions of the Earth are the most stable regions of the ionosphere. In these regions the diurnal behaviour of the TEC can be fairly accurately predicted. In contrast, the polar regions frequently experience major ionospheric disturbances. These are closely linked to magnetic activity. The worst affected regions, however, are the equatorial regions, within a band of ±30° of the Earth's magnetic equator. This equatorial activity is of particular relevance for the Papua New Guinea crustal motion studies, so it will be discussed further, after a description of the effects on the signal is given.

There are two effects on the signal. One effect, called phase advance of the signal, is the increased velocity of the sinusoidal carrier wave. The second effect is a delay in the group velocity of the multiple signals modulated onto the carrier phase. This is called the group delay. It has been found that the magnitude of the group delay is identical to the magnitude of the phase advance, but is opposite in sign (Klobuchar, 1991). Taking equation 3.22 above, differentiating and substituting into 3.20 results in the following equation for group refractive index:

$$n_{gr} = 1 - \frac{c_2}{f^2} \qquad (3.24)$$

Comparing equations 3.22 and 3.24 reveals that the refractive indices differ from unity by equal and opposite amounts. Seeber (1993) gives an estimate of c_2 to be:

$$c_2 = -40.3N_e$$

Using this value of c_2 and substituting into expressions for n_{gr} and n_{ph} shows that the group refractive index is greater than the phase refractive index. This

results in the phase velocity being greater than the group velocity derived from equation 3.18:

$$v_{gr} = \frac{c}{1+\frac{40.3N_e}{f^2}} \tag{3.25}$$

$$v_{ph} = \frac{c}{1-\frac{40.3N_e}{f^2}} \tag{3.26}$$

This effect can alternatively be shown by deriving formulae for the ionospheric refraction for phase and group signals. The ionospheric refraction is given by the difference between the measured range (s) and the geometric range (s_0) along the straight line between satellite and receiver:

$$\Delta l = s - s_0 \tag{3.27}$$

According to Fermat's principle, the measured range is defined as:

$$s = \int n ds \tag{3.28}$$

The geometric range can be considered to be a special case of the above integral in which n =1, giving:

$$s_0 = \int ds_0 \tag{3.29}$$

Thus the ionospheric refraction can be written in terms of refractive indices:

$$\Delta l_{ph} = \int n ds - \int ds_0 \tag{3.30}$$

With equations 3.22 and 3.24 above, the ionospheric refraction for both the carrier phase and group phase signals can be written:

$$\Delta l_{ph} = \int \left(1 + \frac{c_2}{f^2}\right) ds - \int ds_0 \tag{3.31}$$

$$\Delta l_{gr} = \int \left(1 - \frac{c_2}{f^2}\right) ds - \int ds_0 \tag{3.32}$$

If $\int 1 ds$ is substituted with $\int 1 ds_0$, the integration is performed along the geometric path rather than the actual path. Equations 3.31 and 3.32 above can be simplified:

$$\Delta l_{ph} = \int \frac{c_2}{f^2} ds_0 \tag{3.33}$$

$$\Delta l_{gr} = -\int \frac{c_2}{f^2} ds_0 \tag{3.34}$$

Thus it can be seen that the ionosphere has a positive effect upon the phase: the phase advance, discussed above; and a negative effect on the codes: the group delay, also discussed above. As the velocity of a signal propagating through the ionosphere depends upon the electron density, the effect of the ionosphere can be expressed in terms of TEC. TEC is defined above as (equation 3.23):

$$TEC = \int N_e ds_0$$

Using this, and the value of c_2 given above, equations 3.33 and 3.34 give the ionospheric effect on signal propagation (in units of length) as:

$$\Delta l_{ph} = -\frac{40.3}{f^2} TEC, \quad \text{or} \quad \Delta l_{ph} = -\frac{40.3}{f^2 \cos Z} TVEC \tag{3.35}$$

$$\Delta l_{gr} = \frac{40.3}{f^2} TEC, \quad \text{or} \quad \Delta l_{gr} = \frac{40.3}{f^2 \cos Z} TVEC \tag{3.36}$$

The group delay introduces a range error into the pseudo ranges measured with the P-code or C/A-code. This error can range from less than a metre to more than 100 m, depending on the severity of the ionospheric disturbances (Klobuchar, 1991). The phase advance and group delay are a result of the dispersive nature of the ionosphere. When the ionosphere is undisturbed, observing the dual frequency GPS signal allows most of this effect to be eliminated. It should be noted that the uncorrected P-code pseudo ranges are used in data cleaning and wide-lane ambiguity fixing.

Irregularities in the TEC ranging from a few metres to a few kilometres in extent can produce both refraction and diffraction effects on the GPS signal. Refraction causes a change in direction and velocity of the signal, whilst maintaining the phase of the wavefront. Diffraction does not preserve the wavefront, which results in temporal fluctuations in the amplitude and phase of the signal at the receiver (Wanninger, 1993). Fluctuations caused by either effect are called scintillations.

Within the equatorial band, the strongest effects are felt at approximately 10° north and south of the geomagnetic equator. There is a clear diurnal effect on the signal propagation, with scintillations occurring between sunset and midnight, local time, and sometimes continuing until dawn. On top of the diurnal variations, there is a seasonal variation. In the Pacific region, the strongest effects are felt between April and August, whilst the opposite part of the Earth, from America to India, experiences the strongest effects between September and March (Wanninger, 1993). In addition, there is an 11 year cycle that is dependent on the solar sunspot cycle. The number of scintillations increases with the amount of sunspot activity. According to Wanninger (1993) from 1989 to 1992, scintillation effects were particularly strong. This is supported by Klobuchar (1991) who reports that of the 22 sunspot cycles observed since the

early 1600s, the last two have been amongst the highest four levels of activity recorded.

The type of receiver used can also affect the impact that ionospheric activity has on the measurements (see Section 3.3.4 for a discussion of receivers). Amplitude scintillations (causing signal fading and enhancement) can cause the strength of the GPS signal to drop below the lock threshold of the receiver. According to Wanninger (1993), a code correlating receiver can maintain lock at lower signal levels than squaring or cross-correlation receivers. Thus data loss and cycle slip occurrence are greater for squaring receivers than code correlating receivers, and can reach 100 percent during severe amplitude scintillation activity. Phase scintillations (caused by sudden ionospheric refraction changes or diffraction) can change the phase of the L1 and L2 carrier waves by several cycles between two measurements separated by as little as 10 seconds (Wanninger, 1993). In addition to making the cycle slip repair process very difficult, these phase scintillations cause an apparent change in Doppler shift of greater than 1 Hz per second, which is beyond the tracking capability of many receivers. This results in a loss of lock.

It has been stated above that the effects of the ionosphere can be largely eliminated by performing dual frequency observations. The equations for carrier phase can be written:

$$\lambda_{L1}\Phi_{L1} = r' + c\Delta t_r + \lambda_{L1}N_{L1} - \Delta I_{L1} \tag{3.37}$$

$$\lambda_{L2}\Phi_{L2} = r' + c\Delta t_r + \lambda_{L2}N_{L2} - \Delta I_{L2} \tag{3.38}$$

or

$$\Phi_{L1} = r'\frac{1}{\lambda_{L1}} + f_{L1}\Delta t_r + N_{L1} - \frac{1}{\lambda_{L1}}\Delta I_{L1} \tag{3.39}$$

$$\Phi_{L2} = r'\frac{1}{\lambda_{L2}} + f_{L2}\Delta t_r + N_{L2} - \frac{1}{\lambda_{L2}}\Delta I_{L2} \tag{3.40}$$

in which:

$r' = c\Delta t_{rec-sat}$	is the first approximation of the pseudorange and includes receiver clock error. Satellite clock error has been corrected;
Δt_r	is the receiver clock error;
N_{L1}, N_{L2}	are the ambiguities in the L1 and L2 frequencies;
$\Delta I_{L1}, \Delta I_{L2}$	are the ionospheric delays for the L1 and L2 frequencies;
f_{L1}, f_{L2}	are the L1 and L2 frequencies.

These are linearly combined by:

$$\Phi_{L1,L2} = m_1\Phi_{L1} + m_2\Phi_{L2} \quad (3.41)$$

where m_1 and m_2 are constants to be determined. This gives:

$$\Phi_{L1,L2} = r'\left(\frac{m_1}{\lambda_{L1}} + \frac{m_2}{\lambda_{L2}}\right) + \Delta t_r\left(m_1 f_{L1} + m_2 f_{L2}\right) + m_1 N_{L1} + m_2 N_{L2} - \left(\frac{m_1}{\lambda_{L1}}\Delta I_{L1} + \frac{m_2}{\lambda_{L2}}\Delta I_{L2}\right) \quad .....(3.42)$$

in which the ionospheric term must be made to equal zero by appropriate selection of values for m_1 and m_2:

$$\frac{m_1}{\lambda_{L1}}\Delta I_{L1} + \frac{m_2}{\lambda_{L2}}\Delta I_{L2} = 0 \quad (3.43)$$

If m_1 is set to equal 1, then m_2 equals:

$$m_2 = -\frac{\lambda_{L2}\Delta I_{L1}}{\lambda_{L1}\Delta I_{L2}} \quad (3.44)$$

which can be written as:

$$m_2 = -\frac{f_{L2}}{f_{L1}} \quad (3.45)$$

when the expressions 3.34 and $c = \lambda f$ are substituted. This assumes travel along the geometric path.

Thus the linear combination for ionosphere-free phase is:

$$\Phi_{L1,L2} = \Phi_{L1} - \frac{f_{L2}}{f_{L1}}\Phi_{L2} \quad (3.46)$$

It should be noted that the approximations made in the derivation of this equation mean that the term "ionosphere-free" is not totally correct. For example, integration was performed along the geometric path rather than the travel path. In times of high ionospheric activity, described above, the differences between true travel path and the geometric path can become large, and the above equation will fail to remove all ionospheric effects from the data.

The Papua New Guinea GPS surveys in 1990, 1991 and May 1992 were all performed between May and August, with observations extending throughout the night. During data cleaning, particularly for the 1992 campaign, it was obvious when scintillations began to have an effect on the signal. There was not a particular problem with the receivers (squaring L2 receivers) losing lock, but cycle slips became a large problem. Double difference residuals oscillated between ±0.5 cycle, making repair very difficult. This is discussed further is Chapter 6.

Propagation in the Troposphere

Unlike the ionosphere, the stratosphere and troposphere are electrically neutral, which means they are non-dispersive for radio signals below 30 GHz (Brunner and Welsch, 1993). The troposphere is not a uniform layer: over the poles it extends to about 9 km in height; whilst in equatorial regions it can exceed 16 km in height. The stratosphere extends from the troposphere to a height of approximately 50 km. (Brunner and Welsh, 1993). Although not strictly correct, the troposphere and stratosphere are often collectively called the troposphere as this is the layer in which the bulk of the neutral atmosphere lies. Henceforth, "troposphere" will refer to both layers, for convenience.

The non-dispersive nature of the troposphere means that the velocity of a signal travelling through it is not dependent upon its frequency. This results in the delay of the carrier phase and the carrier modulation of both the L1 and L2 signals being equal. Therefore, the tropospheric delay cannot be determined and eliminated by observing two frequencies. Instead, it must be modelled.

The smallest error occurs where the signal travels the shortest distance through the troposphere: in the zenith direction. The signal delay in the zenith results in a range error of about 2.4 metres. This error increases with decreasing zenith angle to about 9.3 metres at a zenith angle of 75° (Brunner and Welsch, 1993). Reliable models are available for estimating the tropospheric delay. However, for high precision geodetic work, tropospheric modelling is a limiting factor in achievable accuracy, particularly in the height component. For example, an error of 1 cm in modelling the tropospheric zenith delay can cause an error of 3 cm in vertical position (Brunner and Welsch, 1993).

The tropospheric delay is defined as:

$$\Delta Trop = \int (n - 1) ds \tag{3.47}$$

where the integration is performed along the geometric path rather than the actual travel path. Instead of the refractive index, n, the refractivity N_T is used. It is defined by:

$$N_{Trop} = 10^6 (n - 1) \tag{3.48}$$

which means the tropospheric delay is:

$$\Delta Trop = 10^{-6} \int N_{Trop} ds \tag{3.49}$$

Saastamoinen (1973) determined the refractivity from gas laws. In his refined model, the tropospheric delay in metres is given by:

$$\Delta Trop = \frac{0.002277}{\cos z} \left[p + \left(\frac{1255}{T} + 0.05 \right) e - B \tan^2 z \right] + \delta R \tag{3.50}$$

where:

z is the zenith angle of the satellite;
p is the atmospheric pressure in millibars;
T is the temperature in Kelvin;
e is the partial pressure of water vapour in millibars;
B is a correction based on the height of the observation site;
δR is a correction based on the station height and zenith angle of the satellite.

The Saastamoinen model has an accuracy of 5 mm to a cut-off elevation angle of 15° (Brunner and Welsch, 1993).

3.3.4 Receivers and Antennas

There are a great variety of GPS receivers available for the multitude of applications to which GPS has been applied. The following description is limited to geodetic receivers with particular emphasis on the types of receivers used for the surveys in this analysis.

C/A-code carrier receivers

This type of receiver obtains code ranges and carrier phase from the L1 carrier frequency. The receiver uses a delay lock loop to perform the C/A code correlation and obtain code ranges. The PRN code is removed from the received signal, which is then filtered. The resultant Doppler shifted carrier wave is then passed to the phase lock loop where the phase measurement is performed. The result of this is the fractional phase offset between the received signal and the signal generated by the receiver (Hofmann-Wellenhof *et al*, 1994).

Measurements of the L2 carrier phase are also made using one of several codeless or quasi-codeless techniques described below. However, the use of codeless techniques decreases the signal to noise ratio (SNR) of the

measurements, which results in L2 signal dropouts necessitating cleaning. There are currently four methods of obtaining L2 measurements under AS: squaring; cross correlation; a combination of squaring and cross correlation; and "z-tracking".

1. Squaring Receivers

Squaring receivers mix, or multiply, the incoming signal with itself. As the modulations on the signal are created by shifting the signal by 180° (effectively changing the sign of the carrier phase), squaring the signal removes these modulations. The result is an unmodulated signal with half the wavelength of the original carrier phase.

This was the first codeless technique developed. It was first presented in Counselman (1981)

The advantage of this technique is that it requires no knowledge of either the P-code or the Y-code.

There are several disadvantages to using this technique. Firstly, it is more difficult to resolve ambiguities for signals with half the wavelength. Secondly, all information modulated onto the carrier wave is lost. This includes satellite clock and orbital information, but this is recoverable from the L1 signal. Finally, the SNR ratio is decreased. Compared with the code correlation technique, the SNR is reduced by 30 dB (Hofmann-Wellenhof *et al*, 1994).

2. Cross Correlation Receivers

The basis for the cross correlation technique is the fact that the unknown Y-code is the same on both the L1 and L2 carriers. This allows cross correlation of the L1 and L2 signals. As discussed previously, the propagation of the signal through the ionosphere is dependent on the frequency of the signal. This means that the Y-code propagation on L2 is slower than on L1. The time delay necessary to match the L1 signal with the L2 signal is the difference in travel time between the two signals. This delay is not constant, and must be adjusted to obtain maximum correlation between the signals. The resulting observables are a range difference, obtained from the time delay, and a phase difference of the two signals obtained from the carrier beat frequency

(Hofmann-Wellenhof *et al*, 1994). From these, the L2 code range and phase may be obtained thus:

$$R_{L2} = R_{L1,C/A} + (R_{L2,Y} - R_{L1,Y})$$

and

$$\Phi_{L2} = \Phi_{L1,C/A} + (\Phi_{L2} - \Phi_{L1})$$

where:

$R_{L1,C/A}$	is the range determined by correlation of the L1 C/A code;
$(R_{L2,Y} - R_{L1,Y})$	is the difference in range determined by cross correlation;
$\Phi_{L1,C/A}$	is the phase of the L1 carrier derived from the L1 C/A code;
$(\Phi_{L2} - \Phi_{L1})$	is the phase difference determined by cross correlation.

The advantages and disadvantages of this technique are the similar to those for a squaring receiver: no knowledge of the P- or Y- codes is required, but the information contained in the modulation is lost and there is a degradation in the SNR. However, a small improvement in the SNR (3 dB) is gained by this technique over the squaring technique. This means that compared with code correlation, a SNR degradation of 27 dB occurs (Hofmann-Wellenhof *et al*, 1994).

3. Code Correlation plus Squaring Receivers

This technique utilises the fact that the Y-code is generated by adding the W-code to the P-code. The W-code has a longer wavelength than the P-code so there remain sections of the Y-code which are identical to the P-code. The received Y-code is correlated with the receiver generated P-code. After this, a low-pass filter is applied by narrowing the bandwidth and the signal is then squared to remove the code (Hofmann-Wellenhof *et al*, 1994).

There are several advantages to this technique. It provides code range on the L2 signal. Also, correlation with the P-code provides better jamming immunity and an improvement in the multipath performance. Squaring in this technique results in a better SNR ratio than squaring L2 directly, because the SNR of a squared signal is inversely proportional to its bandwidth (Hofmann-Wellenhof *et al*, 1994).

Disadvantages of the technique are that a knowledge of the P-code is required; compared with code correlation, a SNR degradation of 17 dB occurs; and the squared L2 wavelength is half the original carrier phase, making ambiguity resolution more difficult.

4. Z-tracking Receivers

This technique also utilises the fact that the Y-code contains uncontaminated sections of P-code. The Y-code is correlated with the receiver generated P-code for both L1 and L2 separately. Since there is a separate correlation on L1 and L2, the W-code on each frequency is obtained. The encrypting signal is estimated for each frequency and is fed to the other frequency. This estimation is used to remove the encrypting code from the signal, leaving the same signal as would have been received if AS was not activated. Code ranges and full wavelength L1 and L2 carriers are obtained (Hofmann-Wellenhof *et al*, 1994).

Obtaining the full wavelength L2 signal and P-code ranges are clearly advantages of this technique. Of the four methods discussed, this one results in the best SNR ratio, with an improvement of 3 dB over the code correlation plus squaring technique discussed above.

However, when compared with the code correlation technique, a degradation of the SNR of 14 dB occurs.

In summary, none of the techniques developed for obtaining L2 measurements in an AS environment recover the signal as well as the code correlation technique. All four techniques discussed above result in a substantial degradation of the SNR. This has the problem that weaker signals are more sensitive to high ionospheric activity and jamming, which may cause loss of lock.

A variety of receivers have been used for the Papua New Guinea surveys. The initial surveys were performed using Trimble SSTs and SDTs. These are squaring receivers, thus the L2 data was available during periods of AS, but its signal to noise ratio was degraded. In the later surveys performed by the National Mapping Bureau (NMB), Ashtech LM-XII2 and LM-XII3 receivers were used. The problems associated with these receivers under AS conditions during the May 1993 survey are discussed in Section 4.2.5.

P-code receivers

These use knowledge of the P-code to lock onto both the L1 and L2 carriers. The P-code on the incoming signal is correlated against a receiver-generated replica of the P-code. When the signals are correlated, the code can be removed leaving the full wavelength carrier signal which is then used for carrier phase measurements.

The TI-4100 was one of the first P-code receivers developed. These were used as part of the global tracking network in 1990. TI-4100's measure the signal 920 ms before and after the GPS second. In general, the measurement before the GPS second was preserved and used. With the severe SA conditions and ionospheric effects of the 1990 survey, this timing difference caused problems which will be dealt with in a later section. These instruments were withdrawn from use with the arrival of the Trimbles, with their light weight, lower cost and increased reliability.

With the implementation of AS, the P-code is replaced with an unknown Y-code and the P-code receivers can no longer track the full wavelength L2 signal. However, these receivers have the option of operating in a codeless manner on the L2 frequency, as discussed above.

Y-code receivers

These receivers are limited to authorised users only because they require knowledge of the secret Y-code to decode the precise PRN code to overcome AS. They also correct the degradation imposed by SA (Hofmann-Wellenhof *et al*, 1994). This technique is generally only found on military hardware.

Antennas

According to Schupler and Clark (1991), the physical phase centre of an antenna generally does not coincide with the point at which the signal is received. The point to which the radio signal measurements are referred, called the phase centre, is the apparent electrical centre of the antenna. The phase centres for L1 and L2 are independent of each other, and will, therefore, only

be coincident by chance. The location of the phase centre varies from one receiver to another, but is generally the same for the same model of antenna.

For short and medium baselines observed with the same model of antenna at each end, with both antennas oriented in the same direction, the effects will tend to cancel out and the problem does not need to be considered. However, in our surveys, a number of different types of antennas were used in the global tracking network. How these antennas are aligned is unknown. As sites are separated by large distances, particularly large differences in longitude, even if they are aligned with respect to local north, the offset vectors will not be parallel, and the effects will not cancel (Schupler and Clark, 1991).

In addition to not being coincident with the physical centre of the antenna, the phase centre changes with the location of the incoming signal. Therefore, an antenna model must vary with both the azimuth and elevation of a satellite. Failing to model this effect will increase the noise level and therefore decrease the precision of the measurements.

The GAMIT software used in this analysis, includes an antenna model, however it was not used in the data analysis for reasons discussed in Chapter 6.

Multipath

Multipath occurs where a signal is received which has been reflected from a nearby surface and is not coming directly from the satellite. Signals which have been reflected in this way will have a longer travel path than unreflected rays.

Multipath is a well recognised problem, and antennas have been designed to try to minimise the effects of multipath. The gain of an antenna refers to its ability to receive weak signals. Antennas have been designed with non-uniform gain. The measure of change in gain with direction is called the gain pattern. If the gain is lower at lower elevation angles, less of the weaker multipath signals will be received. In addition, GPS signals have right-hand circular polarisation. A reflected signal becomes left-hand circularly polarised. Antennas which are insensitive to signals of the wrong polarisation also help reduce multipath effects. If a signal is reflected from two surfaces, it is of course right-hand

circularly polarised, and can then be received, but this is a more rare occurrence (Schupler and Clark, 1991).

Chapter 4

Doppler and GPS Surveys

4.1 Doppler Surveys

Two Doppler surveys were investigated as part of this research, with the intention of using them as first epoch observations of the GPS networks. These surveys were performed in 1975 and 1981.

4.1.1 1975 Doppler Survey

Between 4th October and 1st December, 1975 (days 277-335), the Royal Australian Survey Corps performed a Doppler survey of the south-western section of the Solomon Sea. Geoceivers were used. The survey consisted of 44 sites from the tip of the Papuan Peninsula to the Kiriwina (Trobriand) Islands in the north and Tagula Island in the south. The location of these sites is shown in Figure 4.1. The Army granted permission to process data from five of these sites for the Papua New Guinea crustal motion studies. These five sites (Wataluma, Urasi, Bunama, Haines and Wari) formed the basis of the 1991 GPS survey discussed in Section 4.2.2. The remaining sites were not available for use, and are therefore not named in Figure 4.1. Table 4.1 relates the reference numbers in this figure to the site names and summarises the survey information, including the days of observation and number of passes observed.

Only the two precise satellites were observed. Precise satellites had post-processed ephemerides computed from a global tracking network. These post-processed orbits were only computed for two of the Transit satellites. This gave a maximum of 8 passes per day: two passes with each satellite moving north, and two with each satellite is moving south.

Each site was occupied for approximately three days, resulting in an average of 16 passes per site. Table 4.1 shows the number of passes observed at each site for the entire survey. The observation schedule can be inferred from this table.

Table 4.1 - The number of passes observed at each site in the 1975 Doppler survey. In addition, the name of the sites is related to the reference number in Figure 4.1 for sites not observed with GPS.

Site	Map Reference	Observations (Day of Year)		No. of Passes	1991 GPS site name
		Start	End		
AA542	13	277	281	17	
AA541	12	277	279	14	
AA546	15	277	280	19	
AA545	14	278	281	18	
AA547	16	280	282	15	
AA549	17	283	286	14	
AA579	28	284	286	16	
AA551	18	284	286	12	
AA575	27	285	287	21	
AA555	21	287	290	17	
AA563	25	288	290	14	
AA524	3	288	291	15	
AA523	2	288	290	17	
AA552	19	289	291	15	
AA608	35	292	295	16	
AA557	22	292	294	14	
AA553	20	292	294	15	
AA561	23	295	297	13	
AA562	24	295	297	15	
AA518	1	298	301	21	
AA532	9	301	304	18	
AA525	4	303	306	18	
AA533	10	304	307	20	
AA534		305	307	16	Wari (east)
AA531		305	307	13	Wataluma
AA529	8	307	309	15	
QASCO 505	37	307	309	14	
7361C (ecce)	39	308	310	16	
QASCO 506		310	312	15	Urasi
AA522		311	313	16	Bunama
AA517		311	313	13	Haines
AA528	7	311	312	14	
AA526	5	313	316	16	
AA527	6	314	316	15	
1860T	38	314	317	15	
AA583	31	320	324	17	
AA584	32	321	326	20	
NOEL SODANO LT AMS 1963	36	326	328	15	
AA572	26	326	328	14	
AA585	33	327	329	14	
AA587	34	329	332	20	
AA539	11	330	332	14	
AA580	29	332	334	16	
AA581	30	333	335	13	

Clearly, the number of passes available for processing the five reoccupied sites ranged from 13 to 20. McClusky (1993) states that approximately 30-50 passes are required to determine coordinates to the sub 0.5 m level, and that less than 10 passes does not provide a reliable short arc solution. In addition, he found that approximately 50% of all raw observations were eliminated prior to the final solution. In view of the fact that this dataset contains fewer than 20 raw passes, it was decided not to proceed with processing the 1975 Doppler survey as the benefits were likely to be small for the amount of time required.

4.1.2 1981 Doppler Survey

During the late 1970's, the Australian Division of National Mapping (NATMAP) and the Australian Bureau of Mineral Resources (BMR) decided to establish a survey network for studying plate tectonic motion in the Papua New Guinea region. Transit Doppler techniques were to be used. The survey was performed in April 1981, after extensive planning and simulation to obtain the most efficient network design and observation schedule. The planning and performance of this survey are discussed in detail by Morgan (1981) and McClusky (1993).

The following brief description of the survey is summarised from McClusky (1993).

The survey was performed over thirty four days beginning on 23rd April, 1981. It was designed to straddle the major plate boundaries in the region. The various proposed boundaries have been discussed in Chapter 2. The survey was completed in three sections, each section being a complete entity in itself. Table 4.2 shows the stations observed in each of the three phases. Figure 4.1 corresponds to Table 4.2 , showing the sites observed. The first phase of the survey has stations located on all of the major plates: the Australian, Pacific, South Bismarck and Solomon plates. The second phase encompasses the boundaries between the Solomon plate, the South Bismarck plate and the Australian plate. The third and final section is concentrated around the boundary between the Solomon plate and the Australian plate.

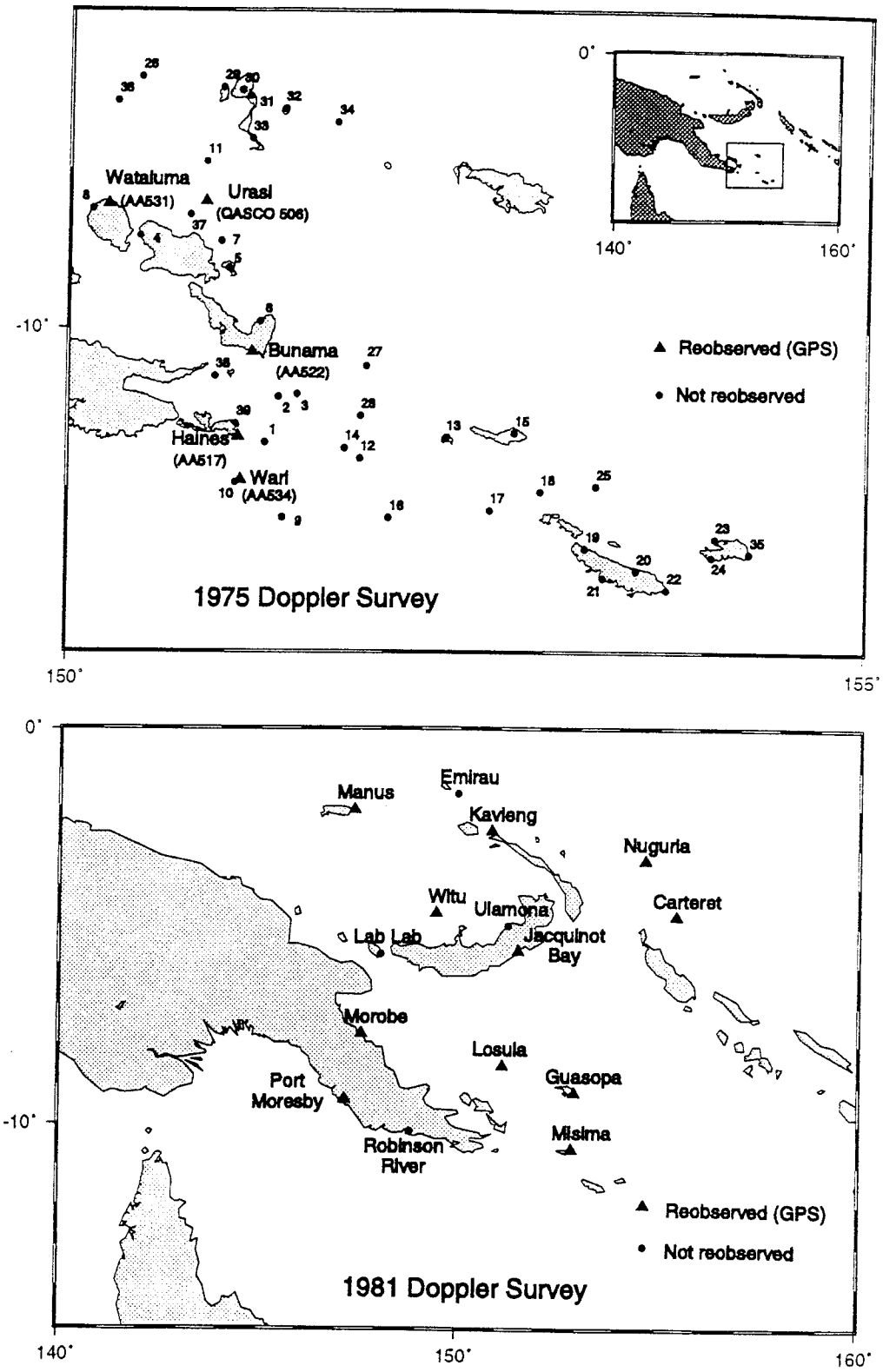

Figure 4.1 The 1975 and 1981 Doppler survey networks. Circles denote sites which have not been subsequently re-observed with GPS; triangles show those sites that have.

Table 4.2 Observation schedule for the 1981 Doppler survey. The three distinct phases of the survey are shown.

Phase 1															
Station	April								May						
	23	24	25	26	27	28	29	30	1	2	3	4	5	6	7
Losuia	•	•	•	•	•	•	•	•	•	•	•	•	•	•	•
Kavieng	•	•	•	•	•	•	•	•	•	•	•	•	•	•	
Emirau															•
Carteret	•	•	•	•	•	•	•	•	•	•	•	•	•	•	
Ulamona	•	•	•	•	•	•	•								
Nuguria								•	•	•	•				
Port Moresby														•	•
Jacquinot Bay	•	•	•	•											
Witu					•	•	•	•	•	•	•				
Morobe												•	•	•	•

Phase 2															
	May														
	8	9	10	11	12	13	14	15	16	17	18	19	20		
Losuia	•	•	•	•	•	•	•	•	•	•	•	•	•		
Emirau	•	•	•	•	•	•	•	•	•						
Lab Lab											•	•	•		
Manus			•	•	•	•	•	•	•	•	•	•	•		
Port Moresby	•	•	•	•	•	•	•	•	•	•	•	•	•		
Jacquinot Bay								•	•	•	•	•	•		
Witu				•	•	•	•								
Morobe	•	•	•												

Phase 3															
	May														
	21	22	23	24	25	26	27								
Losuia	•	•	•	•	•	•	•								
Misima		•	•	•	•	•									
Guasopa	•	•	•	•	•	•									
Port Moresby	•	•	•	•	•	•									
Robinson River					•	•									

Receiver malfunctions and unforeseen logistical problems delayed various parts of the survey, resulting in the third section of the survey being cut short. However, it was thought that although there was less data than planned, there was sufficient to obtain a reliable solution for those sites. Table 4.2 shows the number of days of observation at each site in the three phases of the survey.

The survey was processed in the SAGA (Short Arc Geodetic Adjustment) software package by McClusky (1993). The work of McClusky was continued as part of this thesis in the form of a stability analysis. The results of this are discussed in Chapter 5.

4.2 GPS Surveys

Between 1990 and 1992, three GPS surveys in the region of Papua New Guinea were performed by the University of New South Wales (UNSW) and the National Mapping Bureau (NMB) of Papua New Guinea, with assistance from other institutions. A full list of contributors to the surveys is given in the acknowledgments. The surveys were organised by geodesists from UNSW. The aim of the research was to use GPS to reoccupy and extend the 1975 and 1981 Doppler survey networks. This allowed the first geodetic determinations of plate motion to be made, and established a more precisely determined network of survey sites for future GPS surveys.

Four additional surveys have been included in this analysis. They were all performed by NMB. The observation periods were May 1992, May and August 1993 and July 1994. These surveys are discussed in Section 4.2.3 and shown in Figures 4.3 and 4.4.

4.2.1 The 1990 Survey

The first of the GPS surveys occurred from the 28th July to the 7th August (days 209-219) of 1990. Eleven sites were observed in total. Ten of these were reoccupations of the 1981 Doppler survey sites. As can be seen in Figure 4.2, the survey encompasses points on the Australian, Bismarck and Solomon plates. No sites were observed on the Pacific plate at this time. A new site was

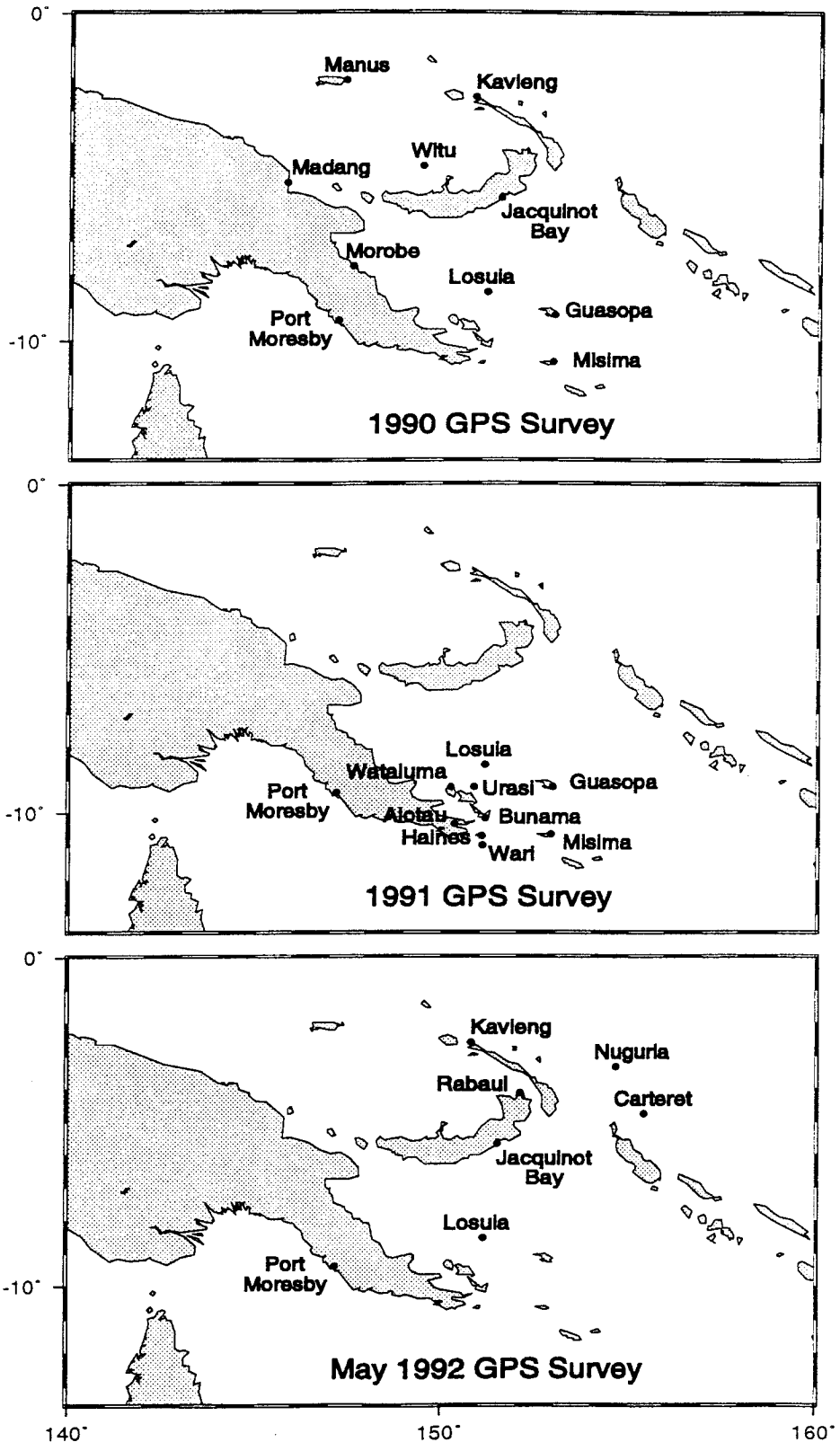

Figure 4.2 The survey networks observed with GPS in 1990, 1991 and 1992.

established at Alotau, however, it was only observed for a single session and was relocated in 1991 to a new position (discussed in Section 4.2.2). The 1990 Alotau data has not been processed by McClusky (1993) nor as part of this thesis.

The planning, execution and processing of this survey have been discussed in detail by McClusky (1993). McClusky processed the 1990 survey in the Bernese software (Version 3.3). It has been reprocessed in the GAMIT software as part of this thesis. The results of reprocessing are given in Chapter 6, and compared with the results of McClusky. A summary of the execution of the survey has been adapted from McClusky (1993) and McClusky *et al.,* (1994) for inclusion here.

Seven receivers were used in total: four Trimble SST receivers belonging to GPSCO[1] and three Trimble SDT receivers on loan to the NMB from Arman Larmer Surveys of Port Moresby. During the survey, there were five sites operating for at least nine of the eleven days. These were occupied by the four SST receivers and one of the SDT receivers. The other two SDT receivers occupied the remaining six sites. This observation schedule is illustrated in Table 4.3, in which the SST receivers are denoted by a dot and the SDT receivers are represented by a diamond. The occupations of both Alotau and Guasopa 9519 were weak, with only one day of observation each.

At three sites, the survey marks occupied in the 1981 Doppler campaign were not reoccupied. Eccentric observations were made due to security problems and operator error. At these sites connections have been established to tie the GPS and Doppler marks. Connections between the Misima sites (9195 and 9520) and the sites at Port Moresby (9518 and NMB GPS Tower) were directly observed with GPS later in 1990. With one receiver at Guasopa, the two sites (AA595 and 9519) were connected indirectly via the rest of the survey network. McClusky (1993) gives the following connections shown in Table 4.4.

[1] GPS Consortium comprising the School of Geomatic Engineering, UNSW (formerly School of Surveying); the Research School of Earth Sciences, ANU; Land Information Centre (LIC), NSW; and the NSW Department of Technical and Further Education (TAFE).

Table 4.3 The observation schedule of the 1990 GPS survey. The dots represent Trimble SST receivers and the diamonds denote Trimble SDT receivers. The site at Madang in the 1990 survey is a different site to that observed in August 1993. There is no connection between these sites.The site name abbreviations are shown for reference in later diagrams.

Station	Site Abbr.	July				August						
		28	29	30	31	1	2	3	4	5	6	7
Losuia	LOUS		●	●	●	●	●	●	●	●	●	●
Morobe	MORO	●	●	●	●	●	●	●	●	●	●	●
Jacquinot Bay	JACQ	●	●	●	●	●	●	●	●	●		
Witu	WITU	●	●	●	●	●	●	●	●	●	●	
Port Moresby	MORE	♦	♦	♦	♦	♦	♦	♦	♦	♦	♦	♦
Manus	MANU	♦	♦	♦	♦	♦						
Misima (9195)	MISI							♦	♦	♦	♦	♦
Kavieng	KAVI			♦	♦	♦	♦					
Guasopa (9519)	-							♦				
Guasopa (AA595)	GUAS								♦	♦	♦	
Madang	MADG	♦	♦									
Alotau	ALT2											♦

Table 4.4 Connections between 1990 GPS sites and 1981 Doppler sites in the WGS-84 reference frame. Values from McClusky (1993).

Station		ΔX	σX	ΔY	σY	ΔZ	σZ
From	To	(m)	(m)	(m)	(m)	(m)	(m)
Guasopa AA595	Guasopa 9519	-2.514	0.04	-3.460	0.04	4.590	0.04
Misima 9195	Misima 9520	-318.894	0.02	-603.650	0.02	76.988	0.02
Pt Moresby 9518	Pt Moresby GPS Tower	-1139.368	0.02	-2794.947	0.02	-3191.373	0.02

4.2.2 The 1991 Survey

A dense network of sites in the vicinity of the Woodlark Basin (Figure 4.2) was observed in 1991. The intention was to re-observe a subset of the 1975 Doppler network. This would allow detailed analysis of the Woodlark Spreading

Centre. The location of the sites is such that you would expect to see a greater rate of spreading to the east between Guasopa and Misima than further west, approaching the pole of rotation about which the spreading centre is opening. As has been discussed in Section 4.1.2, there were insufficient data in the 1975 survey to obtain a reliable solution. Therefore, many of the sites in the 1991 survey do not have a second occupation which makes this analysis less conclusive. However, the network has definite merit for such a study, and can be reoccupied at some time in the future with GPS.

The survey was performed between 7th and 21st August 1991 (days 219-233). A total of 10 sites were occupied. Table 4.6 shows the execution of the survey. The survey was performed with seven dual frequency Trimble SST receivers. Each day of observation consisted of 17 hours of tracking, beginning at approximately 3 pm. local time. An elevation cut off angle of 15° was used, and observations were made every 15 seconds. Meteorological data was also observed at each site. Temperature, pressure, relative humidity and wind speed were recorded with automatic logging equipment at five minute intervals at Alotau, Wataluma, Urasi and Misima. At all other sites temperature, pressure and relative humidity were measured manually approximately every hour. However, the meteorological observations were not used in the processing, as is standard practice today.

A few sites require more detailed discussion because of problems encountered with the survey marks or eccentric occupations requiring connections.

Urasi

The original Doppler survey mark consisted of 4 star pickets protruding from the ground, i.e. one picket as the survey mark and the remaining three as recovery marks. By 1991, the survey mark and one of the recovery marks had gone. Measurements between the two remaining star pickets agreed with the dimensions shown on recovery sketches. It was therefore assumed that the remaining marks were undisturbed. Recovery mark #2 was used as the site for the 1991 survey. Unfortunately, this star picket is bent to a significant angle with the ground. The GPS observations are referenced to the top of the star picket. The angle of the picket is such that any further small to medium changes in position will be difficult to detect, hence this is not a reliable site monument. It is suggested that any future surveys incorporating this site establish a new mark.

Wari

Two sites on Wari Island were observed in the 1975 Doppler survey. The main site was AA533 on the western side of the island. The reconnaissance found this site had been removed. However, AA534 on the eastern side of the island was found to be intact and was therefore observed in 1991.

Bunama

The survey mark AA522, observed in 1975, was found to be unstable at the time of the 1991 survey. Any future surveys involving this mark should therefore be wary in making comparisons with the results contained in this thesis for the Bunama site. If not already done, the mark should be stabilised before it is re-observed.

Alotau

The reconnaissance for the 1991 survey found that the mark at Alotau observed in the 1990 GPS survey (GS 9377) was of questionable quality. It is located in slippery clay soil on the side of a steep ridge. Its stability is, therefore, doubtful and a new site was selected for the 1991 survey. This was PSM 9538 located at Alotau airport, approximately 10 km from GS 9377.

A direct connection between the two marks was performed over two days in 1991. As the site GS 9377 was only observed for one day in 1990, it was not solved for in the 1990 solutions, as mentioned in Section 3.2.1. Any solution based on a single day of observation, with the limited 1990 global tracking station network and satellite coverage, is going to be weak. In addition, Alotau PSM 9538 was reobserved in August 1993. Any future surveys in the region would be advised to use the site PSM 9538 only.

Guasopa

In 1991, both of the 1990 sites were observed again at Guasopa. The tie was performed indirectly via the rest of the survey network. As only one receiver was available at this site, it was swapped from one site to the other on alternate days. Unfortunately the receiver malfunctioned for the first five days of the observation period. The receiver was replaced for the last three days of the

survey, but again malfunctioned on the final day. Thus 6 of the 8 days of observation were lost, resulting in only one day of observation per site. This is a very weak tie.

In the 1990 campaign, Guasopa AA 595 was solved for only one day. This is also a very weak determination of the site. Any future surveys using either site should perform a more reliable connection. However, any comparison based on one future reoccupation will be of limited use because of the weakness of prior solutions for this site.

Misima

Two sites were also observed at Misima in 1991. These were 9520 and 9195. The site 9520 was observed with Doppler in 1981. In 1990, 9195 was observed with GPS. Subsequent to the main GPS campaign in 1990, a direct tie with GPS was performed. The results of this tie are given in McClusky (1993) and reproduced in Section 4.2.1. In 1991, both marks were again occupied with GPS, but not simultaneously. The indirect tie from this campaign and that calculated by McClusky (1993) are shown in Table 4.5. Clearly, the two computations of the connection agree to within three standard deviations.

Table 4.5 The connection at Misima calculated in this analysis and calculated by McClusky (1993). The connection is computed (9195 - 9520).

X	σX	Y	σY	Z	σZ	Solution
318.832	0.019	603.703	0.015	-77.011	0.007	Chapter 6
318.894	0.02	603.650	0.02	-76.988	0.02	McClusky (1993)

In 1990, site 9195 was observed for five days. In 1991, site 9195 was observed for four days, and 9520 was observed for 8 days. Subsequent occupations of the Misima site in August 1992 and August 1993 observed the 9195 mark.

Throughout the survey, several sites experienced tracking problems. These problems fall into two groups. The first group consists of problems with PRN6 between the 7th and 12th of August at Urasi, Alotau, Port Moresby and Misima. The field notes for Haines also show that PRN 24 was declared unhealthy on the 11th. The second main group of problems occurred towards the end of the survey. PRN23 was difficult to track on the 20th at Wataluma, Alotau, Bunama

and Misima. PRN 2 also appears to have been causing problems on the 18th at Misima and Losuia. Other problems, for example PRN24 on the 18th at Wataluma, have only been noted at one site.

Table 4.6 Data collected during the 1991 GPS survey. Days in which all observations were lost due to receiver malfunctions are excluded from this table. All receivers used were Trimble SST instruments.

Station	Abbr.	August 1991														
		7	8	9	10	11	12	13	14	15	16	17	18	19	20	21
Alotau (9538)	ALT2	•	•	•	•	•	•	•	•	•	•	•	•	•	•	
Alotau (9377)	-	•	•													
Losuia	LOUS				•	•	•	•	•	•	•	•	•			
Port Moresby	MORE	•	•	•	•	•	•		•				•	•	•	•
Misima (9515)	MISI			•	•					•	•					
Misima (9520)	-					•	•	•	•			•	•	•	•	
Guasopa (AA 595)	GUAS														•	
Guasopa (9519)	-													•		
Haines	HAIN				•	•	•	•	•							
Urasi	URAS				•	•	•	•	•							
Wari	WARI									•	•	•	•	•	•	
Wataluma	WATA										•	•	•	•	•	
Bunama	BUNA										•	•	•	•	•	

4.2.3 The May 1992 Survey

The survey performed in May of 1992 was important because it linked the previous GPS surveys to the Pacific plate. In addition, a new site was established at the Rabaul Volcanological Observatory to serve as a reference for future surveys of the New Britain and New Ireland region.

The design of the survey allowed the sites of Port Moresby, Losuia, Kavieng and Jacquinot Bay to provide a link between this survey and the 1990 GPS survey. Nuguria and Carteret were observed for the first time with GPS, for the purpose of measuring the motion between the Pacific plate and the Bismarck, Solomon and Australian plates. This motion was to be determined by comparison with the 1981 Doppler results. However, as Chapter 5 reveals, the Doppler analysis is in doubt, thereby removing the primary value of this 1992

survey. The link between the Pacific plate and the Solomon and Bismarck plates has yet to be made with a second GPS occupation. Until it has been done, any analysis of the tectonics of the region will be incomplete.

As shown in Table 4.7, the survey was performed over a nine day period from 4th to 12th May (days 125-133), using seven codeless Trimble 4000SST receivers. Each observation period was approximately 12 hours duration, beginning at 7 pm local time. Observations were made at night to make use of the optimum satellite window. The data sampling rate was 15 seconds, and a cut off elevation of 15° was imposed. Once again, field operators made meteorological observations (pressure and wet and dry bulb temperature) every hour. These were discarded from the processing.

Table 4.7 The 1992 GPS survey as executed. All sites were observed with Trimble SST receivers.

Station	Abbr.	May 1992								
		04	05	06	07	08	09	10	11	12
Port Moresby	PORT	•	•						•	•
Losuia	LOUS			•	•	•	•	•	•	•
Jacquinot Bay	JACQ	•	•	•	•	•	•	•	•	•
Kavieng	KAVI	•	•	•	•	•	•	•	•	•
Nuguria	NUGU	•	•	•	•	•	•	•	•	
Carteret	CART	•	•	•	•	•	•	•	•	
Rabaul	RABL	•	•	•	•	•	•	•		
						Magnetic storm				

The receiver at Losuia malfunctioned on the first day of the survey. It was replaced by the receiver at Port Moresby after the second day of observation. For the last two days of the survey, the receiver from Rabaul was transferred to Port Moresby.

Several sites experienced tracking problems on some days of the survey. Jacquinot Bay experienced tracking problems on the 7th and 10th May. Losuia and Carteret experienced problems tracking the L2 signal from several satellites between the 6th and 10th May, inclusive. Other sites either did not experience or did not record significant tracking problems. A major magnetic storm occurred from 8th May (day 129) to 11th May (day 132), with particular

severity on 10th May. These dates and the dates of the tracking problems are not entirely coincident, therefore it cannot be clearly stated that this is the cause of the problem.

4.2.4 The August 1992 Survey

In addition to the above surveys, a further four GPS surveys of various regions were performed by NMB between 1992 and 1994. The 1992 and 1993 survey networks are shown in Figure 4.3. The 1994 network is shown in Figure 4.4. These data were initially reduced by Morgan *et al.* (1996) as part of the Zero Order Network for Australia. They have subsequently been reprocessed by the team at the UC with software and models consistent with this analysis. The resulting GAMIT h-files (containing the VCV information) were made available for this analysis by the UC team. These surveys were performed in August 1992, May 1993, August 1993 and July 1994.

The 1992 survey occurred between the 25th July and the 7th August. The observation schedule is illustrated in Table 4.8. Four sites were observed: Port Moresby and Misima (9195), which provided additional observations on sites already observed in earlier campaigns; and Vanimo and Aiambak which are located in the western regions of Papua New Guinea. These sites were not observed in earlier campaigns, and extend the area encompassed in the GPS analysis. Two receivers were used in the survey. An Ashtech P-code LM-XII3 receiver and an Ashtech LM-XII2. The Ashtech P-code receiver was stationed at Port Moresby for the entire survey while the Ashtech LM-XII2, observed the remaining three sites in turn.

Table 4.8 The data processed in the August 1992 survey. The receiver located at Port Moresby was an Ashtech P-code LM-XII3 receiver. The remaining sites were occupied by an Ashtech LM-XII2.

Station	Abbr	July							August						
		25	26	27	28	29	30	31	01	02	03	04	05	06	07
Port Moresby	PORT	•	•	•	•	•	•	•	•	•	•	•	•	•	•
Misima (9195)	MISI	•	•	•	•	•									
Aiambak	AIAM								•	•	•	•			
Vanimo	VANI												•	•	•

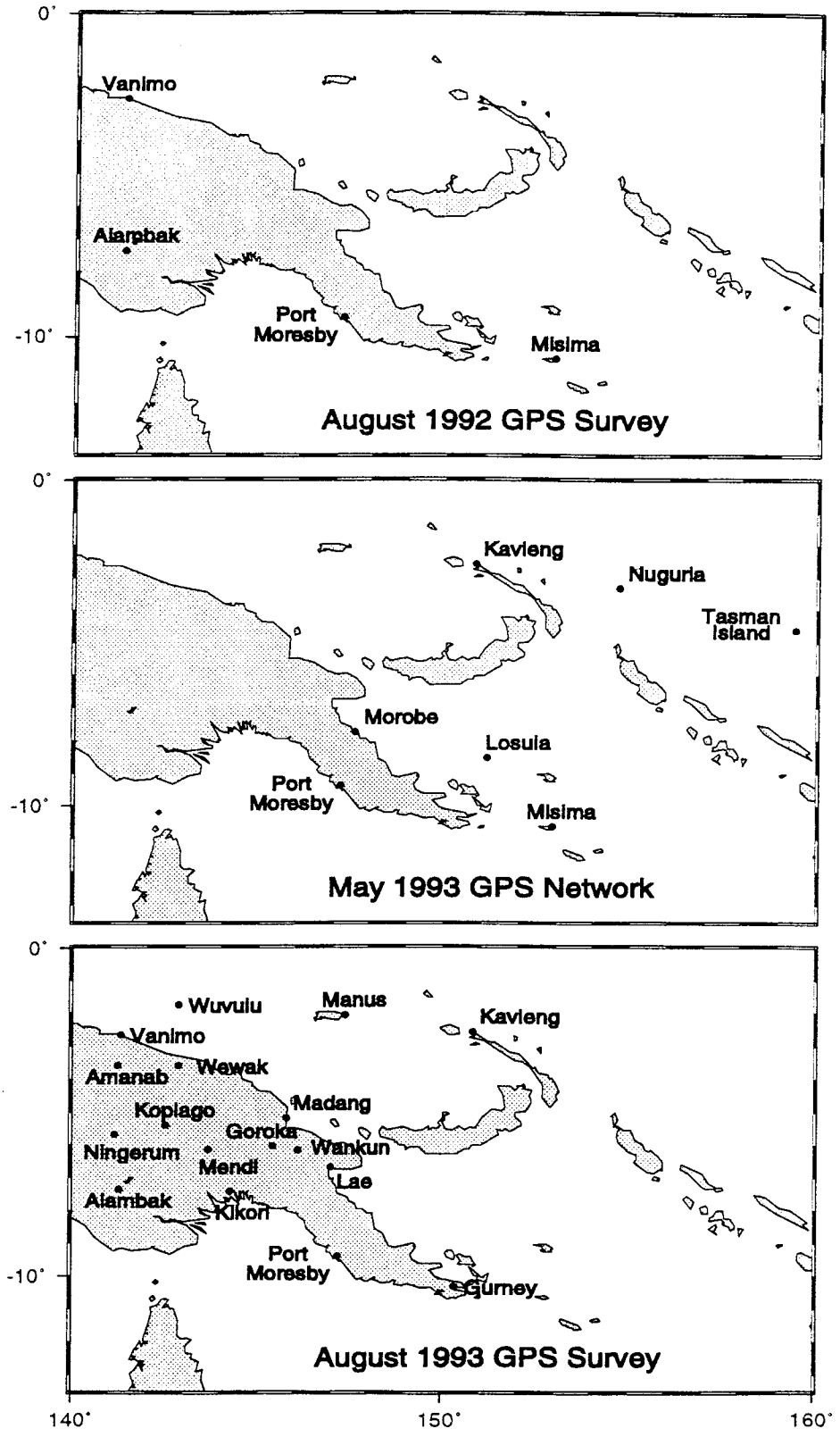

Figure 4.3 The networks surveyed with GPS in August 1992, May 1993 and August 1993 by the National Mapping Bureau of Papua New Guinea. Of the August 1993 survey, the observations from a number of sites shown in Table 4.10a-b have been processed. The site at Gurney is known as Alotau in our Doppler/GPS surveys.

4.2.5 The May-June 1993 Survey

Between the 14th May and 15th June 1993 (days 134-166), a survey was performed which involved observations at Port Moresby, Morobe, Losuia, Misima, Kavieng, Nuguria and Tasman Island. Of these sites, only Tasman Island had not been previously occupied with GPS. Figure 4.3 illustrates the survey network, and shows that Tasman Island is located on the Pacific Plate, further west than both Nuguria and Carteret. It provides an additional link between the complex tectonic region being studied and the Pacific plate. This survey was potentially important to the Papua New Guinea crustal motion study because it provided second GPS observations on two key sites: Nuguria and Morobe. Although McClusky (1993) determined the positions of these sites with Doppler from 1981, these results are doubtful. This is discussed fully in Chapter 5. Excluding the Doppler results leaves only a single occupation on several sites, including Witu, Morobe, Madang, Manus, Nuguria and Carteret. No velocities can be determined for these sites, thereby limiting the analysis possible from GPS observations alone. This survey was to provide an important velocity on one of the Pacific sites. Although the data on Nuguria was found to be incomplete (discussed shortly), the value of the survey was not entirely lost, because it provided a valuable second occupation of Morobe, which allows motion across the Papuan Peninsula to be measured.

Two receivers were used: an Ashtech P-code LM-XII3 and an Ashtech LM-XII2. The P-code receiver was stationed initially at Port Moresby, then relocated to Kavieng. The LM-XII2 receiver was used to observe the remaining sites, as shown in Table 4.9.

Unfortunately, on the 5th June, Anti-Spoofing was activated, and the LM-XII2 receiver, located on Nuguria at the time, was not switched into L2 squaring mode until three days later. The result of this was that for the three days of observations at Nuguria, no L2 data was tracked, rendering the data useless. As discussed above, this is particularly serious because it leaves the sites on the Pacific plate with only one occupation each.

Table 4.9 The observation schedule of the May 1993 survey. Diamonds represent full P-code receivers, whilst dots represent "half p-code" receivers. The significance of the receiver types lies in the fact that Anti-Spoofing was activated on 5th June, and all L2 data at Nuguria (small dots) was lost for the three days of its occupation.

Station	Abbr.	May 1993																
		14	15	16	17	18	19	20	21	22	23	24	25	26	27	28	29	30	31
Pt Moresby	PORT	♦	♦	♦	♦	♦	♦	♦	♦	♦	♦	♦	♦	♦	♦	•	•	•	•
Kavieng	KAVI																	♦	♦
Misima	MISI	•	•	•	•	•													
Losuia	LOUS					•	•	•	•										
Morobe	MORO											•	•	•					
Nuguria	NUGU																		
Tasman Isl.	TASP																		

Station	June 1993														
	01	02	03	04	05	06	07	08	09	10	11	12	13	14	15
Port Moresby	•	•	•											♦	♦
Kavieng	♦	♦	♦	♦	♦	♦	♦	♦	♦	♦	♦	♦			
Misima															
Losuia															
Morobe															
Nuguria					•	•	•								
Tasman Island										•	•	•	•	•	

4.2.6 The August-September 1993 Survey

In the period between the 15th August and the 10th September (days 227-253), 1993, an extensive GPS survey was performed on the mainland of Papua New Guinea. In addition, Kavieng, Manus and Wuvulu were surveyed. The network of sites is illustrated in Figure 4.3. Of this, the observations from the 28th August to the 5th September inclusive, have been processed by Morgan *et al.* (1996) as part of the Zero Order Network for Australia. The GAMIT h-files were made available for this analysis. The data from the 18th August to the 27th August was processed as part of this analysis. These two sections of the survey encompasses the sites shown in Table 4.10a-b below.

Table 4.10 a-b The observation schedule for the period 18th August to 5th September, 1993. Diamonds denote full P-code LM-XII3 receivers and dots represent "half P-code" LM-XII2 receivers. Table 4.10a represents the data reduced as part of this analysis; Table 4.10b represents data reduced by Morgan *et al.* (1996) for the Zero Order Network for Australia. Note: The 1990 and 1993 sites at Madang are different and unconnected.

(a)

Station	Abbr.	August							
		18	19	20	21	24	25	26	27
Port Moresby	MORE	♦	♦	♦	♦	♦	♦	♦	
Vanimo	VANI	•	•	•	•				
Aiambak	AIAM					•	•	•	•
Amanab	AMAN		♦	♦	♦				
Wewak	WEWA		♦	♦	♦	♦	♦		
Wuvulu	WUVU		♦	♦					
Kopiago	KOPI					♦	♦	♦	
Mendi	MEND							♦	♦

(b)

Station	Abbr.	August				September				
		28	29	30	31	01	02	03	04	05
Port Moresby	MORE	♦	♦	♦	♦	♦	♦	♦	♦	♦
Goroka	GORO	♦	♦	♦	♦					
Gurney	ALT2					♦	♦			
Kavieng	KAVI							♦	♦	♦
Kikori	KIKO	♦	♦	♦						
Madang	MADA	•	•	•	•	•	•			
Manus	MANU								•	•
Mendi	MEND	♦	♦							
Lae	UNIT				♦	♦	♦			
Wankun	WANK				♦	♦	♦			
Wuvulu	WUVU							♦	♦	♦

This survey is important to the Papua New Guinea crustal motion survey because it provides a second observation on Manus, allowing motion across the Bismarck Sea Seismic Lineation to be measured. It also includes the first of two observations at Lae and second observations at Vanimo and Aiambak. The motion of Lae, located on the southern section of the Huon Peninsula, will

provide an insight into the collision between Papua New Guinea and the New Britain Island Arc. The motion of Vanimo will provide an insight into the state of the collision and the nature of the boundary in the northwest of Papua New Guinea.

Five receivers were used for this survey. Four Ashtech full P-code LM-XII3 receivers and one half P-code LM-XII2. The observation schedule for the period 18th August to 5th September is shown in Table 4.10a,b.

4.2.7 The 1994 Survey

The final survey used in this analysis took place in July 1994. It involved two sites: Port Moresby and Lae. Port Moresby was observed for four days (27th-30th July) and Lae was observed for two days (27th-28th July), as shown in Table 4.11.

This survey provides a second observation of Lae, allowing a velocity for this site to be determined. The importance of this is stated above.

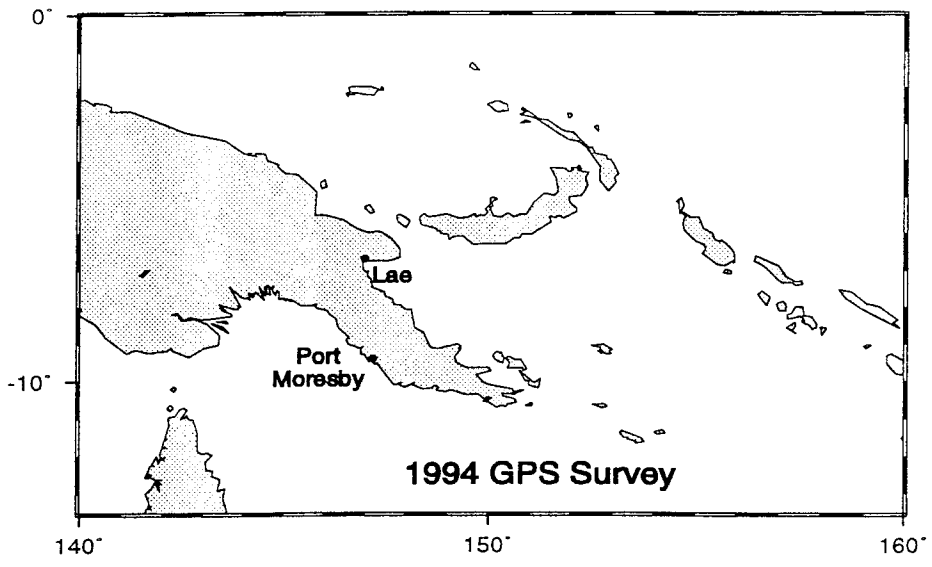

Figure 4.4 The location of the sites in the 1994 GPS survey.

Table 4.11 Observations in the 1994 GPS survey.

Station	Abbr.	July			
		27	28	29	30
Port Moresby	MORE	•	•	•	•
Lae	UNIT	•	•		

As mentioned in Section 4.2, the 1981 Doppler survey was processed by McClusky (1993). McClusky's work was continued as part of this research. The stability analysis performed on the Doppler dataset and the associated results and conclusions are discussed in Chapter 5.

The details of processing the GPS surveys and the associated results are presented in Chapter 6. The results are applied to the tectonics of the region in Chapter 7.

Chapter 5

Stability Analysis of the 1981 Doppler Survey

5.1 Introduction

The Short Arc Geodetic Adjustment (SAGA) software used by McClusky (1993) for his analysis uses full modelling for adjustments of regional or global extent. McClusky used a regional approach as public global data no longer existed. Indeed, global tracking data was generally the exclusive domain of groups such as the U.S Department of Defence (DoD) in 1981.

The JMR proprietary software, used by Morgan in his unpublished analysis (personal communication, 1995), uses incomplete models providing compensation, for the parameter adjustments.

Comparisons between preliminary GPS results and the Doppler results of McClusky (1993) revealed a discrepancy of approximately 1.7 m between the two Pacific sites: Nuguria and Carteret. This sparked a stability analysis of the Doppler results as this was the most likely source of the error, once the possibility of incorrect site occupation and erroneous site connections had been eliminated.

Attempts to duplicate McClusky's results to confirm the Nuguria and Carteret Doppler results were fruitless. These attempts were suspended when it became apparent that all solutions produced were unstable. The focus of the tests then shifted to understanding both the methodology used by McClusky and the data set thought to be used for his 1993 analysis.

Naturally, this change of emphasis altered the nature of the tests performed. In the first series of tests, the emphasis was how close each of the new solutions were to those of McClusky (1993). The most convenient way to test each trial solution was to compare baseline lengths.

The aim of the second series of tests was to achieve convergence. The most convenient way to examine the results of these solutions, was to observe changes in the coordinates, either from one iteration to the next within a solution, or between solutions.

5.2 Origin of Data and Software.

For the initial investigation, the data and software used by McClusky were recovered from the archives of the Computer Services Department (CSD) at UNSW. The instability of the results (discussed in detail below) caused some concern that the data had become corrupted in the intervening period between analyses. To ascertain whether this was the case, the half yearly backups held by the CSD were checked. The output files recovered in this search confirmed that the data itself had not been corrupted, although the number of satellite passes differed from the number used by McClusky (1993). McClusky used 306 passes, while this analysis used an input file consisting of 302 passes, of which only approximately 230 entered the solution. This raised concerns that perhaps McClusky's final input file had been on the system for less than six months and had therefore been missed by the CSD backup procedure which occurred at the end of June and December, each year.

To progress further with the analysis, additional information was required. The initial processing of the 1981 Doppler campaign was performed by Morgan (personal communication) at the University of Canberra using JMR proprietary software. Fortunately, the records of this processing were still intact and could be used to check the integrity of present dataset. This is discussed in Section 5.6.

As discussed by McClusky (1993), the planning of the 1981 survey was based on extensive tests performed by Morgan (1981). These tests involved a dataset from a survey performed in the northern hemisphere in 1974. This data set and the corresponding results were also recovered from computer backup tapes and in hard copy form. The exact origin of this data is unknown. However, it was processed in the SAGA software in 1974 and therefore provided an alternative data set with which to check that the software had not been corrupted at any time between 1974 and the present. The constraints and switches were also tested on this data set as a guide to which constraints

should have a large effect on a stable solution, and which should not. The details of this analysis will be discussed in Section 5.4.

5.3 Input Data and Solution Controls

Investigating the 1981 Doppler results inevitably required understanding all parts of the input to SAGA. The processing options are controlled by a number of switches contained in the input file. For this reason, a description of the input file and switches is included here. It should be noted that the nature of the input made detection of errors in the data difficult (Section 5.6). The following discussion also includes the results of testing these switches individually in various solutions using both the 1974 test data and the 1981 data.

The program SAGA originated in the late 1960's. In its original form, the input was in the form of punch cards. The current input file still reflects this, although it has been extensively updated to reflect modern file structures. It is divided into three sections:

5.3.1. "a - cards"

The "a-cards" contain the a priori site coordinates, reference frame constants, constraints for these parameters and various switches which control the processing.

Processing Switches

The following explains the purpose of each of the above-mentioned switches. The discussion of each switch is applied to the 1981 Doppler survey, and the results of testing the switch are given. For more information about either the structure of the input file or the nature of the switches, see Trotter (1972).

Clock Synchronisation

This switch controls whether the receiver clock is continually synchronised with the satellite clock (switch is on) or left to run at its own time (switch is off). For the 1981 data this switch should be off. The clocks are synchronised at the first two-minute marker, then left to run freely. This is supported by the testing of

this switch. If synchronisation is allowed, adjustment to the coordinates is up to 15 km and the solution diverges.

Transmission Timing Delay

The transmission timing delay, as discussed in Chapter 3, is the time taken between transmission of the signal from the satellite and reception of the signal by the receiver. Transmission and reception of the signal are not simultaneous. Section 3.2.3 showed that the range equations used in SAGA implicitly contain the travel time of the signal, so suppressing this delay will lead to errors in the range. As we do not want the timing delay suppressed, this switch should be on. However, test results on this switch are ambiguous because they show that it alters the results, but does not help the solution converge. This is interpreted to mean that errors greater than those introduced by suppressing the transmission delay are dominating the solution.

An example of a system that requires the transmission delay to be suppressed is the BEACON series. This system uses ground station timing marks which means that there is no transmission delay.

Processing Control

This switch gives three options:

- cycle count edit on, or;
- cycle count edit off, or;
- Intermittent Integrated Doppler (IID) adjustment.

The 1981 data should be clean. It should not be contaminated by cycle count errors because continuously integrated Doppler was used, in which no Doppler counts are lost. Therefore, it should not make any difference whether the "cycle count edit" option is on or off. This is supported by the tests performed.

The IID adjustment option allows point to point range difference reduction of data. It considers that Doppler counting is restarted at every data point, that is, the range bias (a_0 in equation 3.13) term is reinitialised at every epoch. For the 1981 analysis, continuously integrated Doppler counts were used. The fundamental observations were range rates, hence this option must be ignored.

Constraints

This switch controls whether minimum constraints are exercised or constraints are input from "cards" in the input file. The 1981 analysis required constraints to be read from the input file. SAGA is a rank deficient process that requires constraints on either the orbits or a central station. The compatibility of the orbit with the 1974 test data is unknown, whereas it is known that in the 1981 data the input orbit is incompatible. This means that the orbit cannot be used to impress scale and orientation onto the solution and the rank deficiencies must be removed by constraints on other parameters. The orbit is simply an a priori orbit and should be adjusted in the solution. However, for completeness, this option was also tested.

The 1981 data resulted in a diverging, computationally unstable solution. In contrast, the 1974 data set resulted in a significantly different solution, but the solution did converge. This implies that there are problems in the 1981 data set.

Frequency

This switch should only be used for 324 and 164 MHz range. As the JMR receivers used in the 1981 survey use frequencies of 400 MHz and 150 MHz this switch was ignored.

The constraints and switches discussed above are arranged into "schedules". If you know that a pass requires different constraints, for example, if different quality oscillators were used at different sites, different schedules of constraints can be applied. The schedules are selected by switches in the data section, or "b-cards", discussed in Section 5.3.2.

Reference Frame Constants

The 1981 Doppler coordinates are in the NWL-10D system (McClusky, 1993), therefore the reference frame constants used were:

Semi-Major axis of the Earth	6378145.0 m
Ellipsoid flattening (reciprocal)	298.25
Gravity constant ($/10^6$)	398601000 m^2s^{-3}
Rotation Rate of the Earth	0.000072921158 radians/s

A priori Coordinates and Coordinate Constraints

A priori coordinates are specified in latitude, longitude and height. The constraints for latitude and longitude are expressed in arc seconds, and the height constraint is in metres. For the 1981 analysis, one site (Losuia) was tightly constrained to ±0.01 m (which is equivalent to 0.0003" for latitude and longitude). Other sites were loosely constrainted at approximately 5 m. The importance of these constraints is discussed in Section 5.4.1.

5.3.2. "b - cards"

The "b-cards" comprise the bulk of the file and contain the range data from each site to each satellite and the state vector (orbit) for each pass. Each pass is preceded by the following header information:

- the time of initial state vector and/or time of desired epoch;
- the state vector, which is the X, Y, Z position and velocity of the satellite;
- a unique eight character pass identification number incorporating :
  - satellite number
  - last digit of the year (eg 1 for 1981)
  - day of the year
  - hour of the day
- the number of stations in the pass
- the clock correction for each station (not applicable for 1981)
- the number of zero sets for each station. A zero set is a block of data for which there was no loss of lock on the satellite. Multiple zero sets imply that the initial range to the satellite has to be reinitialised for each loss of lock on the satellite.
- the switches to select the various constraint schedules mentioned above.

The header is followed by the bulk of the data for that pass, arranged into zero sets. Note that the data section consists of station number and time of observation associated with each range rate observation. If any of these pieces of information, for example station numbers, were to be applied incorrectly, there would be no way of determining this from the range data itself. Extreme care and constant checking are required if this file is being constructed manually.

Each zero set is followed by weather information: pressure, temperature and relative humidity. These can be observed values or standard values. For 1981, standard values were used, as is common practice today.

5.3.3 "c - cards"

The "c-cards" contain baseline constraints that can be imposed on the network. These consist of azimuth, elevation and baseline length constraints. Azimuth and elevation constraints are equatorial values. They are described in Section 5.5.2. One baseline length constraint was applied by McClusky (1993) on the line Losuia - Morobe. This line was constrained to the value determined by the GPS analysis, with an a priori standard deviation of ±0.1 m, in order to impose the GPS scale onto the Doppler network.

The c-cards are necessary to remove the remaining rank deficiencies if only one station is tightly constrained.

5.4 Results of the Stability Tests on the 1974 Test Data

As mentioned previously, a "test" dataset comprising data and results from a survey in the northern hemisphere was used to provide answers to several questions:

- Was the software working correctly, or had it become corrupted?
- Was our understanding of the switches and constraints correct?
- Which constraints should a stable dataset be sensitive to?

The first question was answered very simply. The new solution generated using the 1974 dataset agreed with the historical results. Therefore, the software had not been corrupted in the intervening period between this work and that of McClusky (1993), or between the work of McClusky (1993) and its successful use in 1974.

The second question can be answered by saying that any initial misunderstandings about switches were clarified by a series of tests. The tests on constraints using the 1974 dataset confirmed expectations of how a stable dataset ought to behave when constraints are varied. The insights gained into the effects of switches and constraints were then applied to the 1981 survey data, which is detailed in Section 5.5.

The third question was also answered by testing the effects of different constraints on the 1974 dataset. Whilst the choice of the trial constraint values used in these tests might look quite arbitrary, they centred around the values used for the 1981 analysis. Where the constraints in the 1974 test data differed from those adopted in the 1981 Doppler processing, for example, the range-in-pass constraint, the 1981 value was the first trial value used.

For the purpose of these tests, a change of up to 0.5 m to the coordinate components of each site was considered to be insignificant, as this was the level of precision expected from the 1981 survey.

5.4.1 Fixed Coordinate Constraints

Although no sites in the SAGA processing are actually held fixed, the solution requires that one site have its coordinate elements tightly constrained (see text below). For convenience, this will be referred to as the "fixed" coordinate.

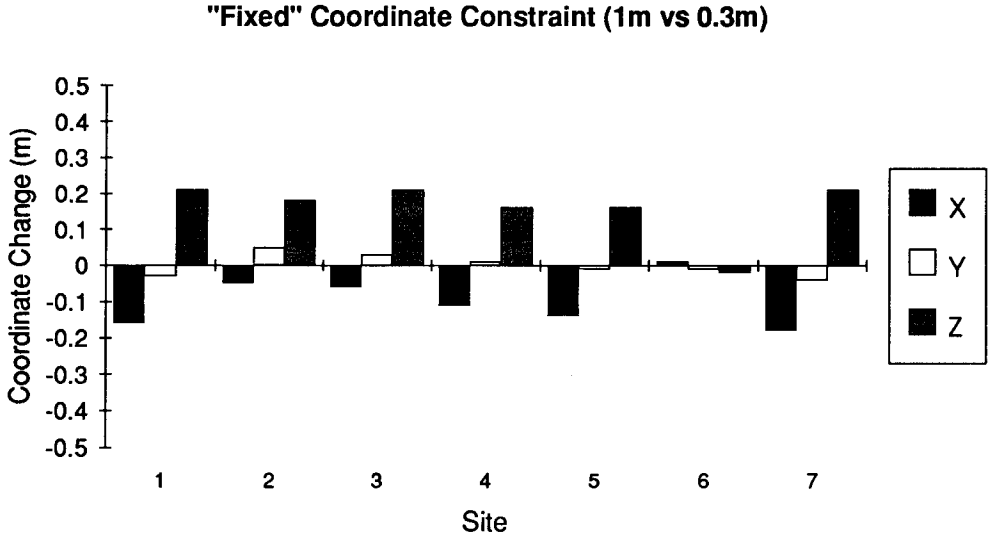

Figure 5.1 Effect on the final coordinates of changing the "fixed" coordinate constraint from ±0.3 m to ±1 m. The changes are less than 0.3 m, and are therefore insignificant.

The original solution, run to verify that the software had not become corrupted, used constraints of ±0.01", or approximately ±0.3 m, on the fixed coordinate. Figure 5.1 shows the changes to the final coordinate values when this constraint was altered to ±0.04", or approximately ±1 m. It is apparent that, although the coordinates change, the amounts by which they change are below the level of precision of the Doppler technique, and are therefore insignificant.

The graph showing the difference between the fixed coordinate constrained at ±3 m and ±0.3 m (Figure 5.2), clearly shows that the coordinate shifts introduced are above the 1 standard deviation precision of the Doppler technique, and are therefore considered to be significant.

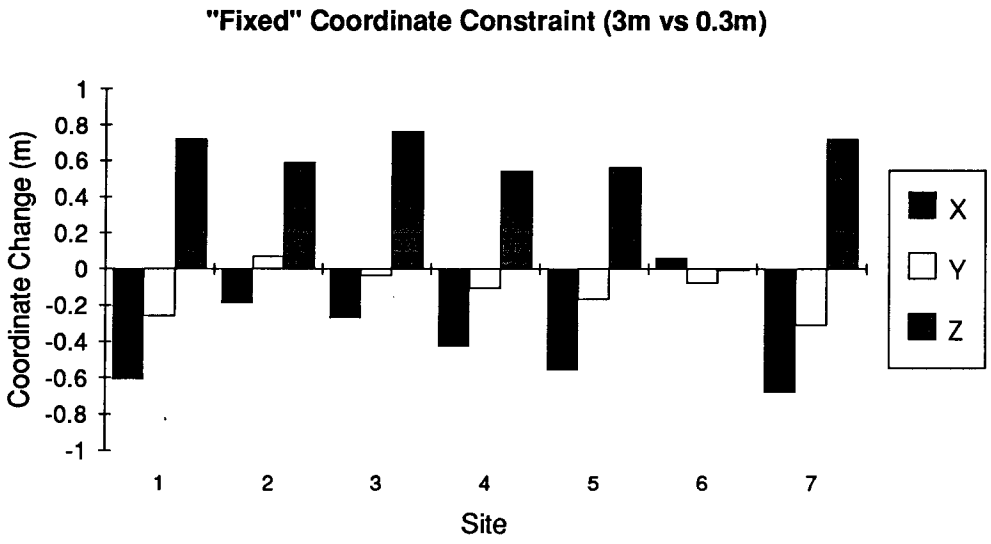

Figure 5.2 Effect on the final coordinates of loosening the "fixed" coordinate constraint from ±0.3 m to ±3 m. The changes are clearly greater than 0.5 m, and are therefore significant. Thus coordinate constraints of ±3 m no longer remove three of the rank deficiencies in the solution.

Both graphs clearly illustrate another very important point: that although the coordinates have changed, all sites have undergone approximately the same change, i.e. that there has been a block shift of the solution. This will be compared with the results of the 1981 tests on the fixed coordinate constraint in Section 5.5.1.

Further tests were performed in which the "fixed" coordinate was constrained at ±3 cm and ±1 cm (equal to 0.001" and 0.0003" respectively). As expected, the differences between these two solutions were negligible. The greatest difference between the two set of coordinates was 2 cm. In contrast, the 1981 solutions showed extreme sensitivity to this small change in constraints. The 1981 results are discussed in Section 5.5.1.

With constraints of approximately ±0.5 m (or 0.016") applied to the fixed coordinate, the final coordinates have changed by negligible amounts. Thus to

remove three of the rank deficiencies in the solution, the constraints on the coordinates must be equal to or tighter than ±0.5 m.

These tests conform to expectations of how a stable solution should behave given our understanding of the short arc adjustment technique. SAGA is a rank deficient process, with six rank deficiencies. This means that six elements need to be constrained for a defined solution. In practice, this can be done by tightly constraining the coordinates of two sites or constraining the coordinates of one site and the azimuth and elevation of another baseline. For 1981 and in this test data set, the latter approach was adopted. This was also the technique adopted by Morgan (1981) in designing the survey. The tests described above and summarised in Table 5.1, clearly show that constraints of ±3 m are insufficient to solve three of the rank deficiencies, and the solution is poorly defined. Constraints of ±0.5 m or tighter are sufficient to uniquely define the solution.

Table 5.1 Summary of the tests performed on the "fixed" coordinate constraints. Clearly, if the constraints on the fixed coordinate are greater than 0.5 m, the solution is not uniquely defined and three of the rank deficiencies in the solution are no longer removed.

Trial "Fixed" Coordinate Constraints		Effect upon the Solution
Seconds of Arc	Metres	
0.0003	0.01	Negligible
0.02	0.5	Negligible
0.04	1	Insignificant
0.1	3	Significant

5.4.2 Azimuth and Elevation Constraints

The effects of these constraints are dependent upon the value of the azimuth and/or elevation between the stations to which the constraints are being applied. The azimuth and elevation are equatorial values. Their calculation and the care required in determining the values to be applied are discussed in Section 5.5.2.

5.4.3 Orbit State Vector Constraints

Orbit constraints are applied to the X, Y, Z coordinates of the state vector and to the velocities associated with these quantities. In the region of our survey (longitude approximately 152°), X and Y components correspond approximately to radial and cross-track orbit components, respectively. The near polar orbits result in the Z coordinate representing the along-track orbit elements.

The orbit constraints used in the original 1974 analysis were ±100 m on the X, Y, Z components and ±1 ms^{-1} for each velocity component. Several tests were performed in which these constraints were relaxed, with the most extreme test using constraints of ±100,000 m and ±100 ms^{-1} on the X, Y, Z coordinates and velocities respectively. These tests clearly indicate that relaxing the orbit constraints does not alter the final coordinates of the sites. The maximum change in station coordinates was 3 cm.

In the next tests performed, the constraints were tightened. Constraints of ±50 m on the X, Y, Z coordinates and ±0.5 ms^{-1} on the velocity components did change the coordinates of the sites slightly. However, as the maximum change to any coordinate component was 11 cm, which is well below the level of precision obtainable by Doppler, the changes were deemed insignificant.

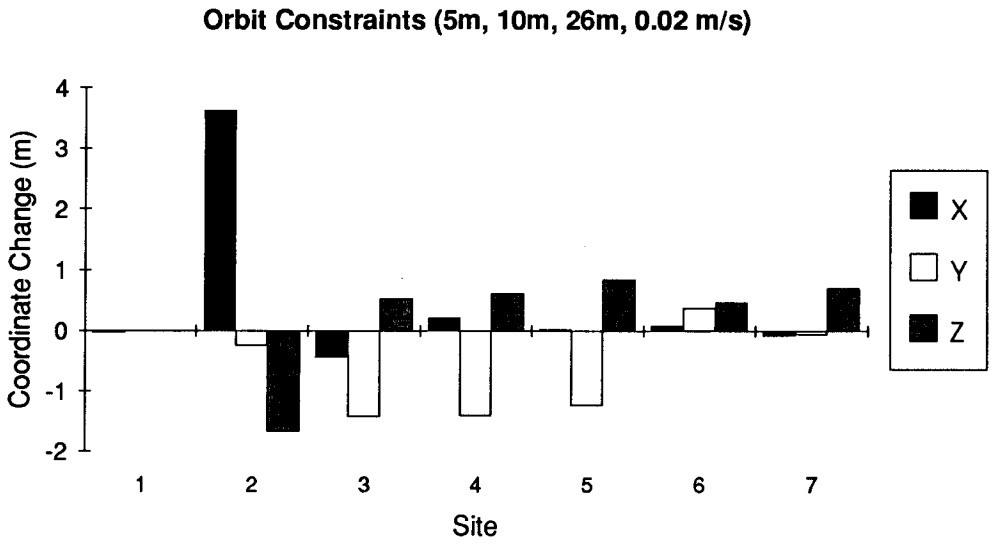

Figure 5.3 The effect on the site coordinates of tightening the orbit constraints to the recommended values for broadcast ephemerides (±26 m, ±10 m, ±5 m on along-track, cross-track and radial components respectively and ±0.02 ms^{-1} on the velocity components). These values were used by McClusky (1993) for his analysis. Clearly, these constraints have a significant effect on the site coordinates.

However, when the constraints were tightened to the values used by McClusky (1993), i.e. 5 m, 10 m, 26 m on X, Y, Z coordinates respectively and 0.02 ms^{-1} for the velocities, the solution was significantly affected, as shown by Figure 5.3. It is apparent that the coordinates are not affected equally, therefore the network was distorted.

Further tests indicated that the orbital constraints no longer had a significant effect on the coordinates when they were relaxed to ±25 m in X and Y, ±40 m in Z and ±0.5 ms^{-1} for the three velocity constraints. When constraints are tighter than this, any errors in the orbit are not allowed to fully adjust and are mapped into the coordinates. With loose constraints of the order of 1000 m, any incompatibility of reference frames alluded to in Section 5.3.1 are accommodated in the adjustment of the a priori orbit parameters. The satellite orbits are thought to be good to approximately 20 m. With constraints tighter than this, the reference frame of the orbits begins to be imposed on the coordinates. This is confirmed by the finding that the orbit constraints do not affect the solution when greater than or equal to ±25 m in X and Y, ±40 m in Z and ±0.5 ms^{-1} for velocities.

Table 5.2 Summary of the tests performed, showing the effect of changes of orbital constraints on the site coordinates.

Trial Orbital Constraints		Effect upon the Site Coordinates
X Y Z	X- Y- Z- velocity	
5m 10m 26m	0.02ms^{-1}	Significant
10m 15m 37m	0.02ms^{-1}	Significant
10m 15m 37m	0.5ms^{-1}	Significant
15m 20m 40m	0.5ms^{-1}	Significant
20m	0.2ms^{-1}	Significant
20m	0.5ms^{-1}	Significant
20m 20m 40m	0.5ms^{-1}	Significant
25m 25m 40m	0.5ms^{-1}	Insignificant
50m	0.5ms^{-1}	Insignificant
1000m	5ms^{-1}	Insignificant
100000m	10ms^{-1}	Insignificant

This series of tests confirms our understanding of the role of orbit constraints in the SAGA solution. With the application of constraints to the "fixed" site and to one azimuth and elevation, the rank deficiencies of the SAGA process are

removed. Therefore, the orbit does not need to be tightly constrained, but can be allowed to adjust freely. This is quite different from the situation we see in the 1981 tests, detailed in Section 5.5.3. Indeed, if the orbits are tightly constrained, distortions are introduced into the solution, and the site coordinates are adversely affected. The orbit should be totally free to adjust and the coordinates should determine the reference frame.

All tests performed on the orbit constraints are summarised in Table 5.2 above.

5.4.4 Error Model Constraints

The error model constraints comprise several elements. These were explained in Section 3.2.2. The error model terms used in the 1974 test data differ from those used by McClusky (1993) as shown in Table 5.3 below. Testing these parameters in the 1974 dataset consisted of applying McClusky's (1993) values and analysing the effects.

Table 5.3 Error Model constraints used in the 1981 and 1974 Doppler solutions.

Error Model Terms	1981		1974
	Atomic Oscillators	Crystal Oscillators	
initial range offset (m)	1×10^{7}	1×10^{7}	1×10^{7}
inter-station timing bias (s)	0.001	0.003	1×10^{-6}
frequency bias ratio	1×10^{-7}	1×10^{-7}	1×10^{-8}
oscillator offset (ms^{-1})	7.5	10	7.5
oscillator drift (ms^{-2})	0.002	0.004	0.0002
residual tropospheric delay (m)	0.3	0.3	0.04

McClusky (1993) gives the following guidelines:

initial range offset:	1×10^{6} m to 1×10^{7} m
frequency bias ratio	1×10^{-6} to 1×10^{-7}
inter-station timing bias:	50 μs to 500 μs
residual tropospheric delay:	0.2 m to 0.5 m

Each of the parameters were tested individually, with the following results.

Initial Range Offset

The constraint on the initial range offset is not critical to the solution. It was altered by two orders of magnitude from the 1974 a priori value, to 1 x 10^9 and 1 x 10^5 respectively. These changes resulted in negligible changes to coordinates, with all changes being below 2 cm.

Inter-station Timing Bias

The values used for the inter-station timing bias in both 1981 and 1974 differ from the values recommended by McClusky (1993). The value of 1 μs used in 1974 is significantly less, whilst the values of 1000 μs and 3000 μs used in 1981 are significantly greater than recommended values. The inter-station timing bias depends upon the type of oscillator used by the receiver. The clocks used in the 1974 survey are unknown. In 1981 both atomic and crystal oscillators were used, and the error model constraints applied accordingly.

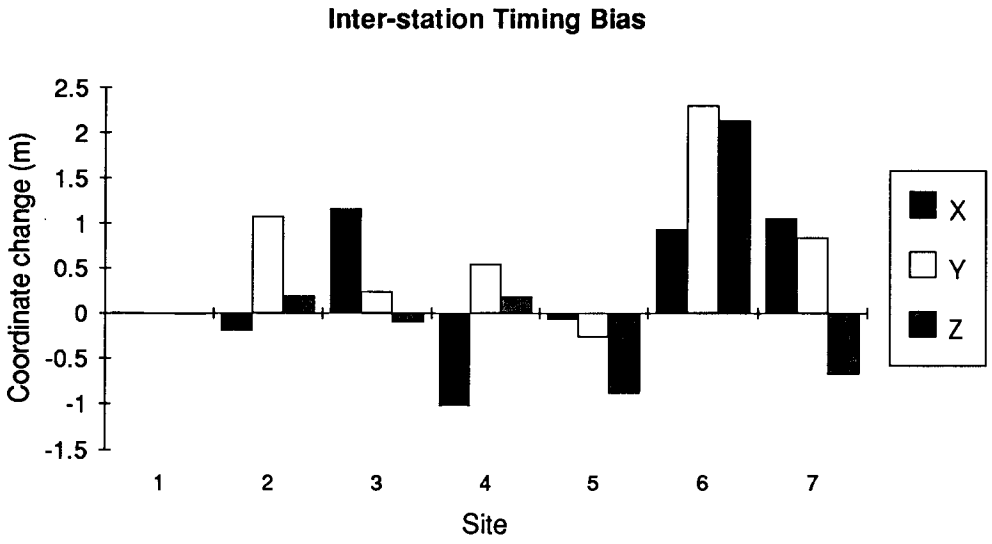

Figure 5.4 Effect of applying the 1981 atomic oscillator constraint (1000 μs) to the 1974 solution.

It is apparent from Figure 5.4 that the interstation timing bias is a critical constraint. Applying a constraint of 1000 μs in the solution changes the coordinates by up to 2.4 m. The coordinates changes are random.

Frequency Bias

The frequency bias constraint used in the 1974 solution is an order of magnitude smaller than that used in the 1981 analysis, and is outside the recommended limits. However, as mentioned above, the type of oscillators used in the 1974 survey are unknown.

Changing the constraint on the frequency bias by an order of magnitude, to the lower bound of the recommended values (1×10^{-7}) had an insignificant effect on the final coordinates. The maximum change was 0.11 m, which is below the level of precision of the technique.

Changing the constraint to the upper limit of the recommended values (1×10^{-6}) has a significant effect, as shown in Figure 5.5.

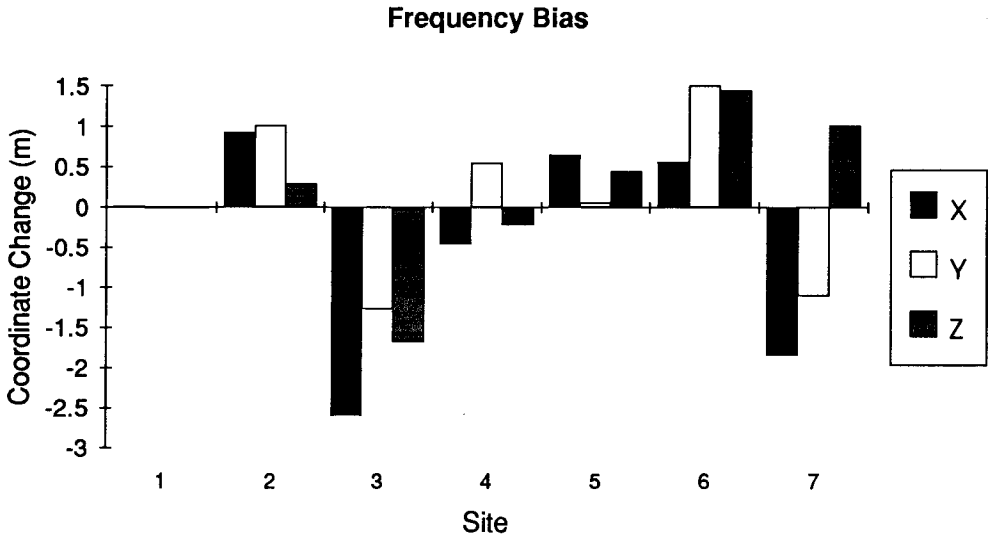

Figure 5.5 The effect on site coordinates of using 1×10^{-6} as the frequency bias constraint.

The tests above suggest that the magnitude of the constraint affects the magnitude of the coordinate changes. However, in view of the use of atomic frequency standards in the 1981 survey, it is difficult to evaluate how frequency biases of 0.1% can enter the system.

Oscillator Offset and Drift

The oscillator offset constraint used in the 1974 solutions was the same as that applied to the atomic oscillators used in the 1981 survey. Doubling the oscillator offset constraint from 7.5 ms^{-1} to 15 ms^{-1}, which is more relaxed than the constraint applied to the crystal oscillators in 1981, had an insignificant effect upon the solution. The maximum coordinate change was 14 cm, well below the precision of Doppler solutions.

The 1974 value of the oscillator drift constraint was an order of magnitude tighter than that applied to atomic oscillators in 1981. Changing the drift constraint to the 1981 value (0.002 ms^{-2}) also had an insignificant effect, changing coordinates by a maximum of 14 cm.

Residual Tropospheric Delay

The recommended values for residual tropospheric delay constraints are between 0.2 m and 0.5 m. The value used in the 1974 survey (0.04 m) is well below the recommended range. However, when this constraint was increased to the value used in the 1981 analysis, the effect on the site coordinates was insignificant. The largest coordinate change was 18 cm, which is below the limit of precision for Doppler.

Thus the solution is only sensitive to changes in two of the error model constraints: inter-station timing bias and frequency bias. The results are summarised in Table 5.4.

Table 5.4 Effects of altering the error model constraints.

Parameter	Experimental Value	Effect upon Site Coordinates
initial range offset/zero set	10^5-10^9	Insignificant
inter-station timing bias	0.001	Significant
scale term/frequency bias	10^{-7}	Insignificant
scale term/frequency bias	0.000001	Significant
sat/rec oscillator offset	15	Insignificant
sat/rec oscillator drift	0.002	Insignificant
residual tropospheric delay	0.3	Insignificant

5.4.5 Range-in-pass Constraint

The range-in-pass is also a critical constraint, as illustrated by Figure 5.6 below.

Figure 5.6 shows that changing the range-in-pass constraint from 10 cm to 7 cm makes up to 1.5 m change in coordinates. This is not consistent with knowledge of a change of this magnitude. The equivalent Doppler wavelength is 0.76 m. Only integer Doppler cycles are counted. Averaging is generally thought to occur as $\sqrt{n}$, n being the number of observations. The value used for

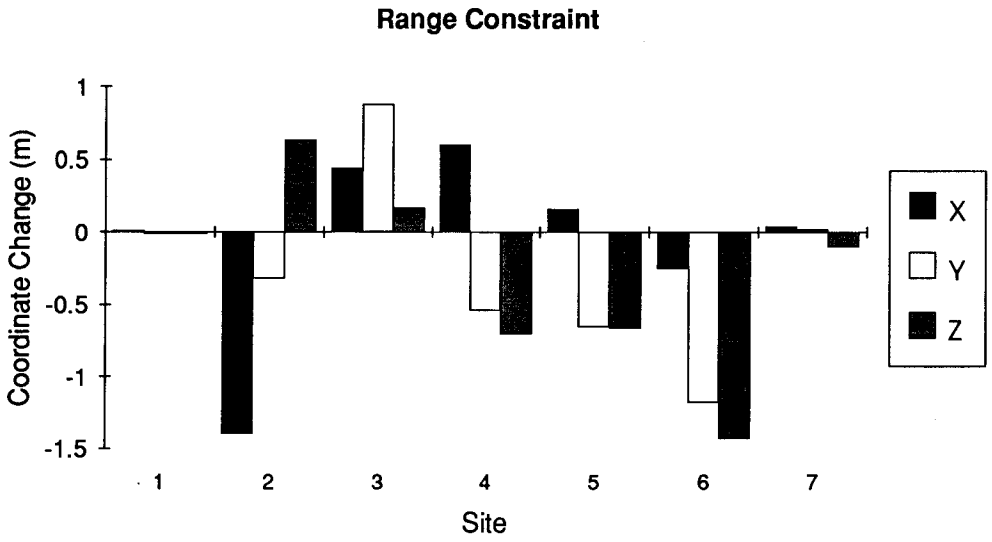

Figure 5.6 Effect on the station coordinates of changing the Range-in-pass constraint from 0.10 m to 0.07 m.

this constraint in the 1981 survey was determined by accepting that each minute of tracking produced 15 Doppler measurements and that at least 6 minutes of data were required to accept a pass. This makes a minimum of 90 observations. Using $\sqrt{n}$ gives $\sqrt{90}$, or approximately 10 cm. The sensitivity of the solution to a change from 0.10 m to 0.07 m in this constraint is not understood, unless the fact that this test data uses 30 second observations means that constraints of 0.10 m and 0.07 m are both too tight. However, 0.10 m was the constraint used when the original 1974 solution was recovered.

5.4.6 Centre of Mass Constraint

Whilst we believe that the centre of mass should be tightly constrained (0.01 m) in order to preserve the reference frame, if the rank deficiencies in the solution are removed with appropriate site and baseline constraints, it is not computationally necessary to do so. The position of the centre of mass is

implicit in the a priori site coordinates used. If these are not geocentric values, tight constraints on the centre of mass will force a geocentric reference frame onto the solution via the orbits. Loose centre of mass constraints allow for solutions to be in local, non-geocentric systems. Testing this constraint confirmed that when a priori site coordinates are in a geocentric frame, the constraints on the centre of mass will not affect the solution. The constraint was relaxed from 0.01 m to 5 m, with insignificant changes to results. The maximum coordinate change was 0.12 m, well below the limits of precision.

5.4.7 Summary of 1974 Test Data Stability Analysis

There are two important facts to note about the tests performed on the 1974 dataset. Firstly, the original solution was recovered with the current input file. The implication of this is that the software has not been corrupted. Secondly, all solutions did converge after one iteration, with the exception of the solution testing the operation of the clock synchronisation switch. This solution converged after two iterations.

In summary, the 1974 test data showed sensitivity to the following constraints:

- Range-in-pass constraint,
- Inter-station timing bias.

The solution was sensitive under certain conditions to the following constraints:

- Fixed coordinate constraint, only if it was relaxed to greater than ±3 m,
- Azimuth and Elevation constraints,
- Orbital constraints, only if they were tightened above 40 m in along-track, and 25 m in cross-track and radial components, 0.5 ms^{-1} velocity,
- Frequency Bias.

The fixed coordinate constraint, azimuth and elevation constraints and orbit constraints can all be used to eliminate the 6 rank deficiencies in the solution. The solutions were based on constraining the three coordinate elements and a geodetic azimuth and elevation to remove rank deficiencies. Therefore, it is not surprising that changing these constraints affects the solution. Where the azimuth and elevation constraints are not strong enough to prevent rotations of the system, the orbit constraints are required to control the system. However, where rotations are controlled by azimuth and elevation constraints, additional

constraints placed on the orbit can lead to distortions in the system, thus affecting the final coordinates.

The solution was insensitive to changes in other constraints.

5.5 1981 Stability Test

For the tests on the effects of constraints in the 1981 data, changes in coordinates became less important than achieving a convergent solution. It should be stated again that all test solutions performed on the 1974 dataset did converge within three iterations, and most after the first iteration.

Due to the data labelling errors in the input file, discussed in Section 5.6, both Manua and Emirau have been excluded from the stability tests.

5.5.1 Coordinate Constraints

As explained in Section 5.4.1, no coordinates are actually fixed in the SAGA adjustment. Once again, the one tightly constrained coordinate will be referred to as the "fixed" coordinate.

A stable solution should be sensitive to changes to the fixed coordinate constraint only when that constraint is relaxed to the point that it no longer removes three of the rank deficiencies in the system. This was clearly illustrated by the 1974 tests, in which it was found that the constraints could be relaxed to 1 m without significantly affecting the solution. In contrast, the 1981 dataset exhibited remarkable sensitivity to very small changes in the fixed coordinate constraint, even when that constraint was well below the level required to remove the rank deficiencies. Tightening this constraint from ±3 cm to ±1 cm changed the baseline lengths by up to 3 m. Note that all other site coordinates were constrained to ±5 m. This is illustrated in Figure 5.7. It was clearly shown in the 1974 tests that changing the fixed coordinate constraint from ±3 cm to ±1 cm should have a negligible effect on the solution.

Figure 5.7 also clearly shows that the coordinate corrections at different sites were not of the same magnitude. This means that the network experienced distortion rather than a block shift.

The 1981 dataset also does not behave in the same way as the 1974 dataset when loose constraints of 2 m are applied to the fixed site. The solution in this case is computationally unstable, indicated by negative standard errors in the results for all other loosely constrained (±5 m) sites. It has been stated above that it is important to have one coordinate tightly constrained. However, in view of the fact that McClusky (1993) initially performed an essentially free adjustment by loosely constraining all sites to ±25 m, it was expected that the solution would be weak with the loose coordinate constraints used in this test, but not to be computationally unstable and diverging. This expectation is enforced by the test data set in which there was a block shift of the coordinates when the ±2 m constraints were applied and the solution converged after one iteration.

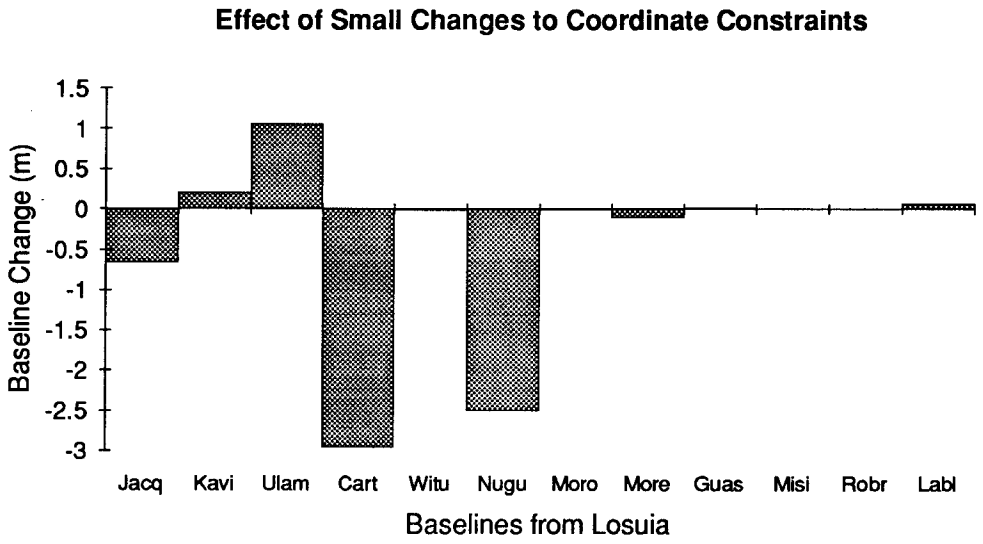

Figure 5.7 Differences in baseline lengths from two solutions:

1. constraints on Losuia ± 3 cm,
2. constraints on Losuia ± 1 cm.

In this solution, unconstrained sites were Jacquinot Bay (Jacq), Ulamona (Ulam), Robinson River (Robr), Lab Lab (Labl), Carteret (Cart) and Nuguria (Nugu). Other abbreviations stand for Kavieng (Kavi), Morobe (Moro), Port Moresby (More), Guasopa (Guas), Misima (Misi) and Witu.

It was thought that the sensitivity of the solution to changes in tight constraints implied a gross error in the coordinates. The coordinates were compared with those of McClusky (1993), which showed that the a priori coordinates for Losuia were indeed equal to their final values, and those of all other sites were within 2 m of the final values. The coordinate differences are shown in Table 5.5.

Thus the a priori coordinates were close to McClusky's (1993) final values, and the solution ought to have had the strength to adjust them. Clearly, it did not have this strength. If the solution was stable, only the coordinates for the "fixed" site (Losuia) would need to be good to the order of a centimetre.

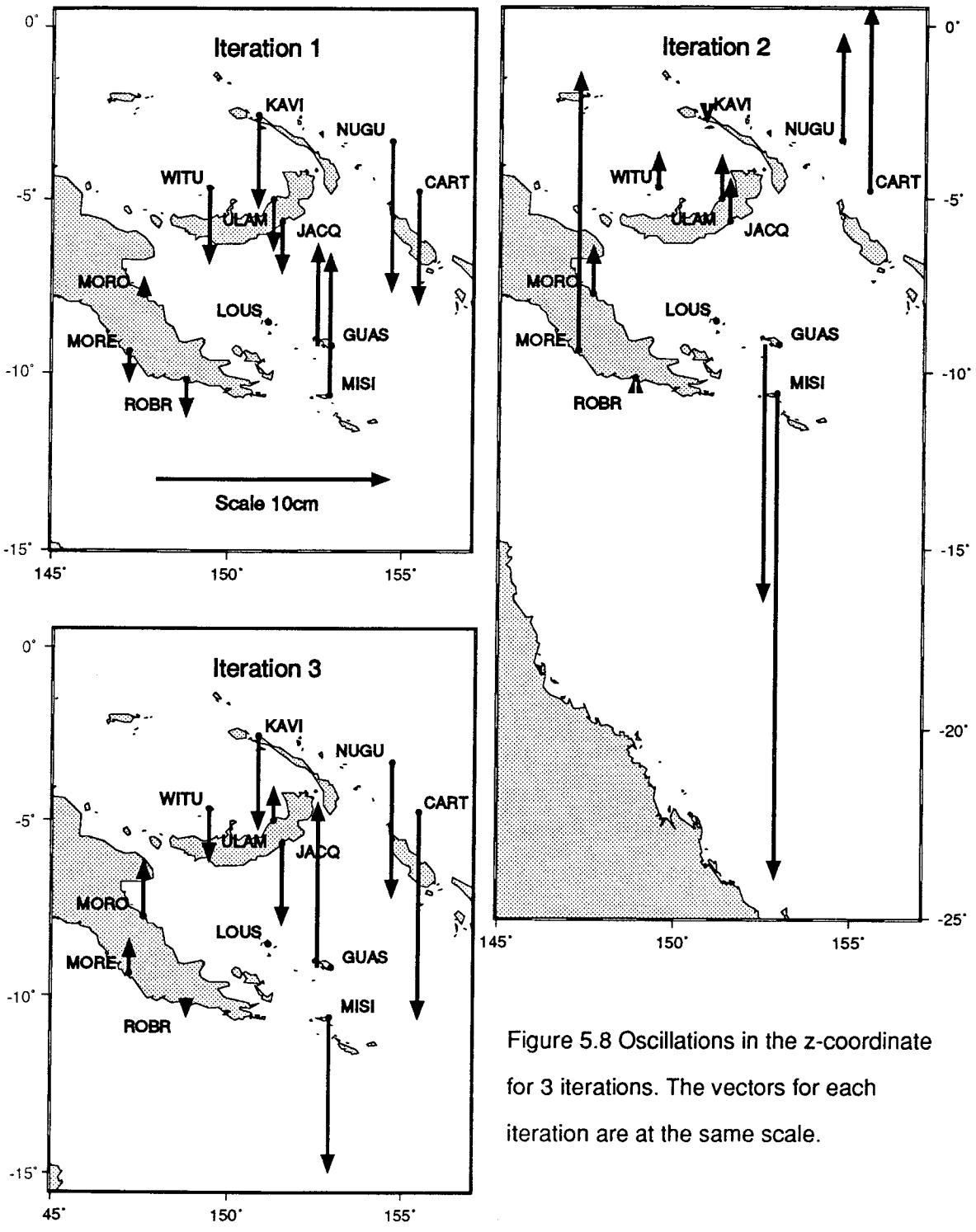

Figure 5.8 Oscillations in the z-coordinate for 3 iterations. The vectors for each iteration are at the same scale.

Table 5.5 shows the differences between a priori coordinates and the final coordinates of McClusky (1993).

Site	Coordinate Component	McClusky (1993)	a priori value	Δ (m)
Losuia	φ (° ' ")	-08 32 07.438	-08 32 07.438	0.00
	λ (° ' ")	151 07 30.251	151 07 30.251	0.00
	h (m)	91.23	91.2	0.03
Jacquinot Bay	φ	-05 38 42.898	-05 38 42.862	-1.11
	λ	151 30 19.006	151 30 18.995	+0.34
	h	158.64	158.3	+0.34
Kavieng	φ	-02 34 53.274	-02 34 53.203	-2.20
	λ	150 48 21.950	150 48 21.960	-0.31
	h	84.62	86.6	-1.98
Carteret	φ	-04 47 03.016	-04 47 03.016	0.00
	λ	155 27 48.504	155 27 48.507	-0.09
	h	80.35	80.3	+0.05
Ulamona	φ	-05 00 05.618	-05 00 05.618	0.00
	λ	151 14 50.133	151 14 50.132	+0.03
	h	92.57	92.6	-0.03
Witu	φ	-04 41 18.021	-04 41 17.975	-1.42
	λ	149 26 08.162	149 26 08.169	-0.22
	h	89.051	90.2	-1.15
Nuguria	φ	-03 20 07.676	-03 20 07.676	0.00
	λ	154 40 27.497	154 40 27.495	+0.06
	h	75.16	75.2	-0.04
Morobe	φ	-07 44 31.857	-07 44 31.804	-1.64
	λ	147 35 22.422	147 35 22.355	+2.07
	h	83.49	84.8	-1.31
Port Moresby	φ	-09 24 17.521	-09 24 17.487	-1.05
	λ	147 09 34.426	147 09 34.383	+1.33
	h	148.06	149.9	-1.84
Lab Lab	φ	-05 43 25.749	-05 43 25.749	0.00
	λ	148 03 44.028	148 03 44.027	+0.03
	h	100.56	100.5	+0.06
Guasopa	φ	-09 13 30.167	-09 13 30.201	+1.05
	λ	152 56 36.774	152 56 36.805	-0.96
	h	84.85	86.7	-1.85
Misima	φ	-10 41 17.514	-10 41 17.561	+1.45
	λ	152 50 20.826	152 50 20.839	-0.40
	h	88.51	88.6	-0.09
Robinson River	φ	-10 10 11.754	-10 10 11.754	0.00
	λ	148 49 28.121	148 49 28.121	0.00
	h	88.09	88.1	-0.01

When McClusky's (1993) final coordinates were entered into the solution as a priori values, the solution was significantly altered. Losuia was tightly constrained and all other sites had loose constraints of ±5 m applied. In view of the proximity of the previous a priori coordinates to the final coordinates of McClusky, (Table 5.5), the solution was not expected to change significantly. This is another indication of the instability of the solution.

In all of the tests discussed above, the coordinate corrections displayed a distinct trend. The Z coordinates experienced the largest corrections, ranging from zero on Losuia (because of its tight constraints) to approximately 10 - 15 m on some other sites. Not only were these coordinate corrections the largest of all coordinate components, but they also displayed a tilt across the network from southwest to northeast. Between iterations of the solution, several sites displayed large oscillations in the Z coordinate. This is clearly apparent in Figure 5.8. The corrections to the X and Y coordinates were smaller in magnitude than the Z corrections, generally being less than approximately 5 m.

A test was performed on a subset of data (days 113 - 118 inclusive) to try to curb the oscillations occurring in the Z coordinate. Sites observed on these days were Losuia, Jacquinot Bay, Kavieng, Carteret, Ulamona and Witu. Constraints of ±1 cm were applied to the latitudes of Kavieng, Carteret and Witu. Note that these sites form the outside boundary of the survey and leave the inner sites, Jacquinot Bay and Ulamona with ±5 m constraints, free to adjust. Losuia was also constrained to ±1 cm in all three components. The results of this test showed the outer sites with insignificant adjustments, and the loosely constrained sites with large corrections to the Z coordinates.

In all of the previous tests, and particularly the last discussed, one fact that stands out is that the sites to which constraints are applied, whether they are coordinate, baseline length, azimuth or elevation constraints, have significantly smaller adjustments and oscillations than the remaining loosely constrained sites. The value of azimuth and elevation constraints depends upon the baseline to which they are applied, as explained in Section 5.5.2. However, it is clearly shown that any constraint effectively applied, does benefit the site(s) to which it is applied but does not benefit any other sites. An extreme example of this is now discussed.

A solution was run in which the final coordinates of McClusky (1993) were all constrained to ±0.01 m. The coordinate corrections to the a priori values were all zero. The centre of mass term (loosely constrained at ±2 m on X and Y, ±5 m on Z) moved by -1.93 m in X; 1.24 m in Y; and 16.06 m in Z. The orbit corrections were realistic, ranging from close to 0 to 40 m in X, 55 m in Y and 118 m in Z. These values are at or below the tolerance levels set by McClusky (1993) for acceptance of a pass. Clearly, the orbits were not being unduly distorted. The change in the centre of mass position follows the general trend seen in all tests in which the changes in X and Y coordinates are significantly smaller than the change in Z coordinates. This result also enforces the finding that constraints affect the sites to which they are applied, be they coordinate, azimuth, elevation or baseline length constraints, but do not transmit their benefit to the remaining unconstrained sites (in this case, the centre of mass).

5.5.2 Azimuth and Elevation Constraints

In SAGA, azimuth and elevation are equatorial values. Azimuth and elevation constraints have different effects depending upon the baseline to which they are applied. Applying an elevation constraint to a N-S line may have very little effect, whilst applying the same constraint to an E-W line may be effective. It is important to establish which lines it will be worthwhile applying constraints to and what values should be applied.

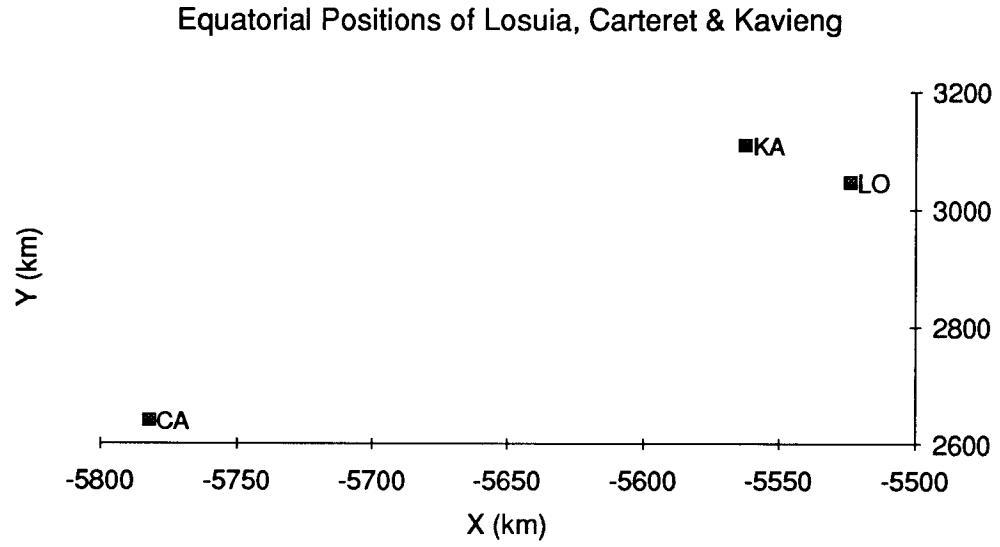

Figure 5.9 Plot of the X and Y coordinates of Losuia, Carteret and Kavieng projected onto the equatorial plane. Viewing the position on a map in terms of latitude and longitude can be deceiving when trying to visualise the coordinates in terms of X, Y and Z. Compare this with Figure 4.2

As the Papua New Guinea region is at approximately 150° longitude, changes in radius, longitude and latitude components are approximately equivalent to changes in X, Y, and Z respectively. To determine the azimuth of a line, it is projected onto the equatorial plane, as shown in Figures 5.9 and 5.10 (a). The azimuth is then given by the equations:

$$\text{SinA} = \frac{\Delta Y}{r} \text{ and } \text{CosA} = \frac{\Delta X}{r} \tag{5.1}$$

which give

$$\text{TanA} = \frac{\Delta Y}{\Delta X} \tag{5.2}$$

The elevation is shown in Figure 5.10 (b). It is calculated using the following equation:

$$\text{TanE} = \frac{\Delta Z}{r} \text{ and } \text{SinE} = \frac{\Delta Z}{R} \tag{5.3}$$

where

$$r = \sqrt{\Delta X^2 + \Delta Y^2}, \text{ and} \tag{5.4}$$

$$R = \sqrt{\Delta X^2 + \Delta Y^2 + \Delta Z^2} \tag{5.5}$$

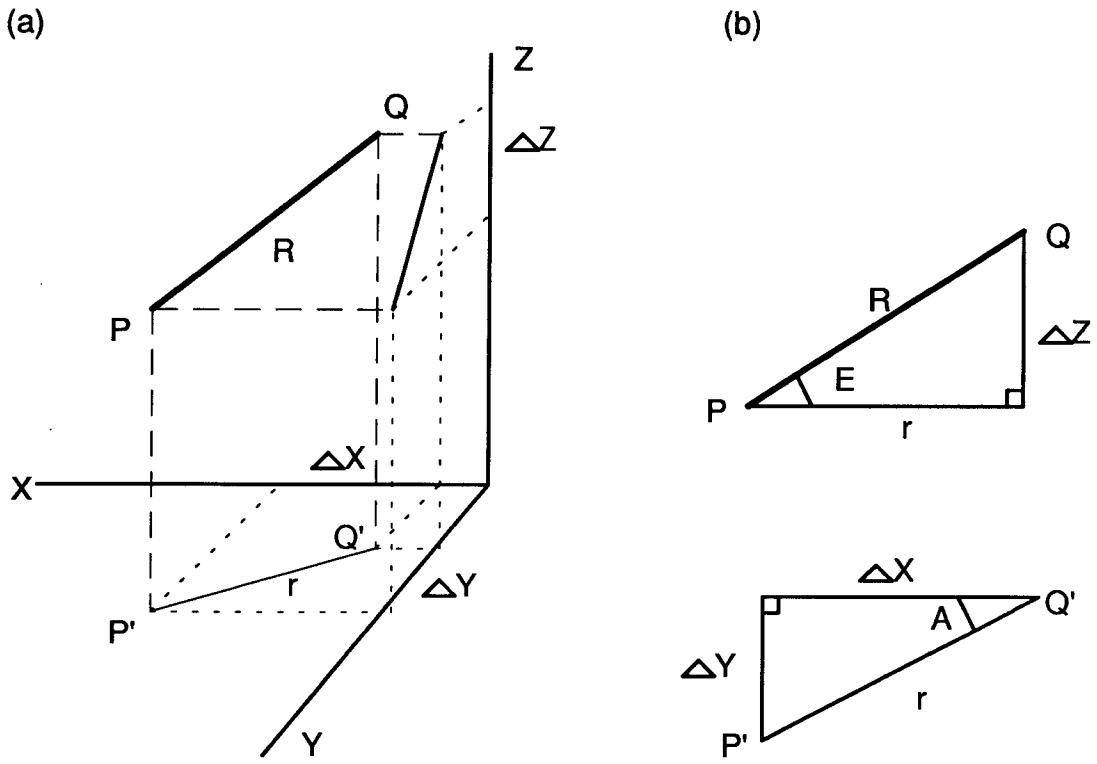

Figure 5.10 Equatorial azimuth and elevation of a line PQ.

As explained above, azimuth and elevation constraints need to be applied with care to ensure that the constraint is effective. The same constraint value applied to baselines of different azimuth and elevation will have different effects, due to the instability of the tangent ratio close to 90° and 270°. This is best illustrated with an example.

The baselines Losuia - Kavieng and Losuia - Carteret have very different elevation angles, as can be seen in the following calculations:

Losuia - Kavieng

DX = -38 601.22 m
DY = 61 795.57 m
DZ = 655 039.43 m

⇒ r = 72 861.146 m
E = 83°39' 10.74"

Changing E by 0.1" gives
E = 83°39' 10.84"
⇒ DZ = 655 042.29 m
Therefore applying a constraint of 0.1" is equivalent to approximately 2.9 m.

Changing E by 0.01" gives
E = 83°39' 10.75"
⇒ DZ = 655 039.69 m
Therefore applying a constraint of 0.01" is equivalent to approximately 0.29 m.

Losuia - Carteret

DX = -258 355.32 m
DY = -406 617.06 m
DZ = 411 981.21 m

⇒ r = 481 751.912 m
E = 40°32'10.20"

Changing E by 0.1" gives
E = 40°32'10.30"
⇒ DZ = 411 981.61 m
Therefore applying a constraint of 0.1" is equivalent to approximately 0.4 m

Changing E by 0.01" gives
E = 40°32'10.21"
⇒ DZ = 411 981.24 m
Therefore applying a constraint of 0.1" is equivalent to approximately 0.04 m

Thus the line Losuia - Kavieng with a high elevation angle, requires an apparently tighter elevation constraint to obtain the same actual level of constraint as the Losuia - Carteret line with a lower elevation angle. Similar care must be taken with azimuth constraints.

Having established this, tests on this 1981 data showed that the constraints curbed the oscillations on the stations to which they were applied, but did not improve the stability of the solution. This seems to be indicative of problems elsewhere, rather than the inherent ineffectiveness of baseline constraints.

5.5.3 Orbit State Vector Constraints

There are two main areas in which the tests on the 1981 orbit constraints are strikingly different from the 1974 orbit constraints:

- convergence of the solution,
- sensitivity to the constraints.

Figure 5.11 below shows the resulting corrections to a priori coordinates of Kavieng from the 4 iterations of a solution with orbit constraint values of 1000m for X, Y, Z and 10ms^{-1} for the X, Y, Z velocities. Note that the centre of mass constraints were loose (2m), which is why the CM term is also seen to be oscillating (Figure 5.12 a - d). However, if the solution is adequately constrained with one coordinate and azimuth and elevation constraints, there should be no remaining rank deficiencies and the solution should converge with loose centre of mass constraints, as shown in the tests on the 1974 dataset. Clearly, the coordinates for Kavieng are diverging. It should be emphasised that none of the tests on orbit constraints achieved convergence. The speed with which the solution turned from oscillating to diverging varied according to the level of constraints applied. Tight orbital constraints slowed the divergence of the solution, whilst loose orbital constraints brought the divergence forward several iterations. With the emphasis on coordinate changes, it should be noted that loose orbital constraints were also associated with large orbital corrections. For example, a solution with orbit constraints of ±50 m on X, Y, Z and ±0.5 ms^{-1} on the velocity components had orbit corrections of up to 1.5 km. A solution with orbit constraints of ±1000 m on X, Y, Z and ±10 ms^{-1} on the velocity components contained some orbit corrections of over 9999 km.

This is in stark contrast to the behaviour of the 1974 dataset, in which tight orbit constraints strained the solution, whilst changing loose orbit constraints had no effect on the solution at all.

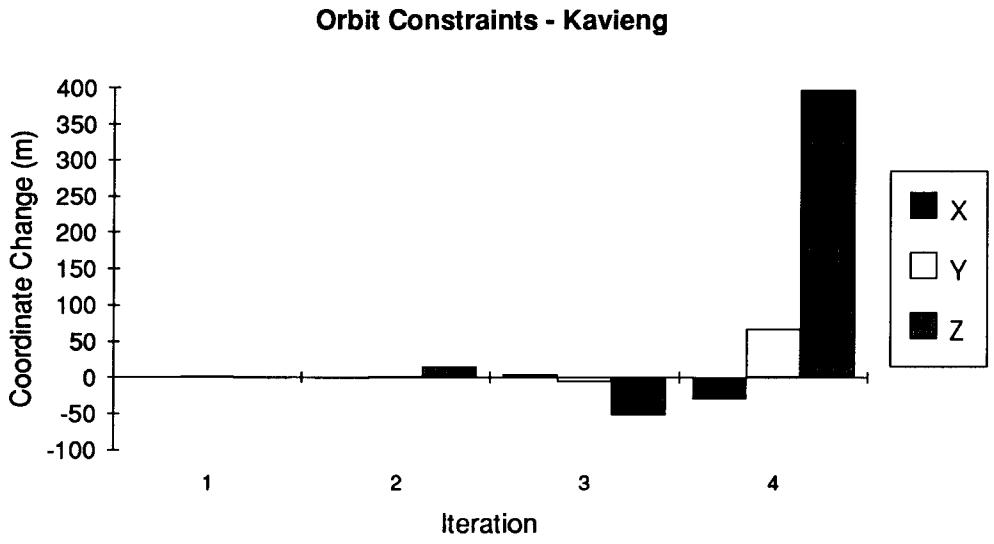

Figure 5.11 Four iterations of the solution at Kavieng, clearly showing divergence. Orbit constraints used in this solution were: X = 1000 m; Y = 1000 m; Z = 1000 m; velocity = 10 ms^{-1} for all three components.

Kavieng was selected for display in Figure 5.11 because it is one of the "better behaved" sites, illustrated in Figure 5.12 (a - d). All tests clearly show much larger oscillations at Carteret, Ulamona and Witu. Losuia is the "fixed" site in all of these tests, so its coordinates are not varying at all. The Losuia - Kavieng baseline was constrained with azimuth and elevation constraints, while the Losuia - Jacquinot Bay baseline was constrained in length. Other sites were unconstrained and show much greater sensitivity to changes in constraints, again confirming the finding that constraints curb the oscillations of the site to which they are applied but do not help achieve convergence of the solution.

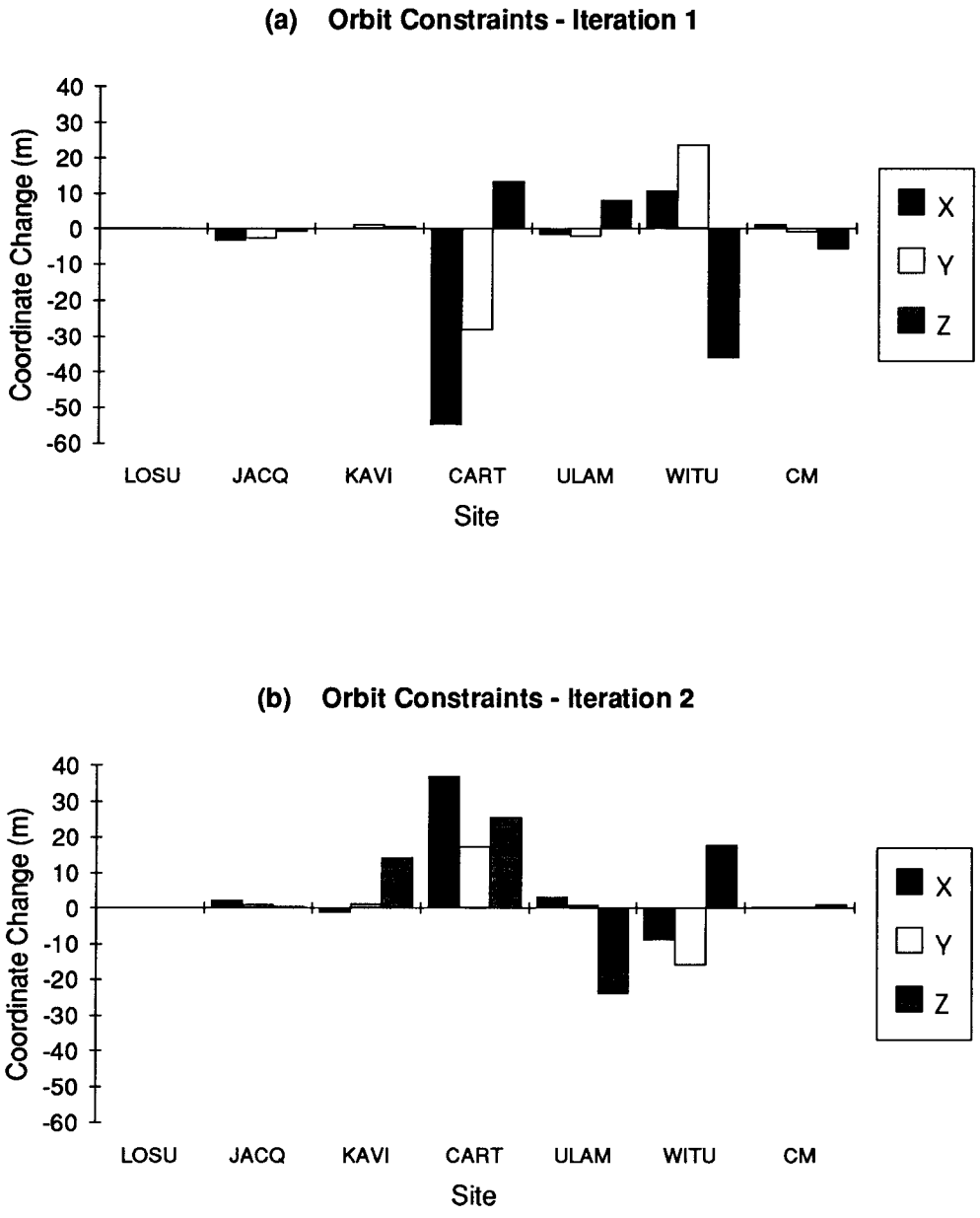

Figure 5.12 (a) - (b) Corrections to coordinates in the first four iterations of the solution. Constraints used were: X = 1000 m; Y = 1000 m; Z = 1000 m; velocity = 10 ms^{-1} for all three components. Clearly Carteret, Ulamona and Witu are oscillating wildly. Jacquinot Bay and Kaving are also oscillating, but to a lesser extent. Losuia is tightly constrained, therefore its coordinates remain unchanged.

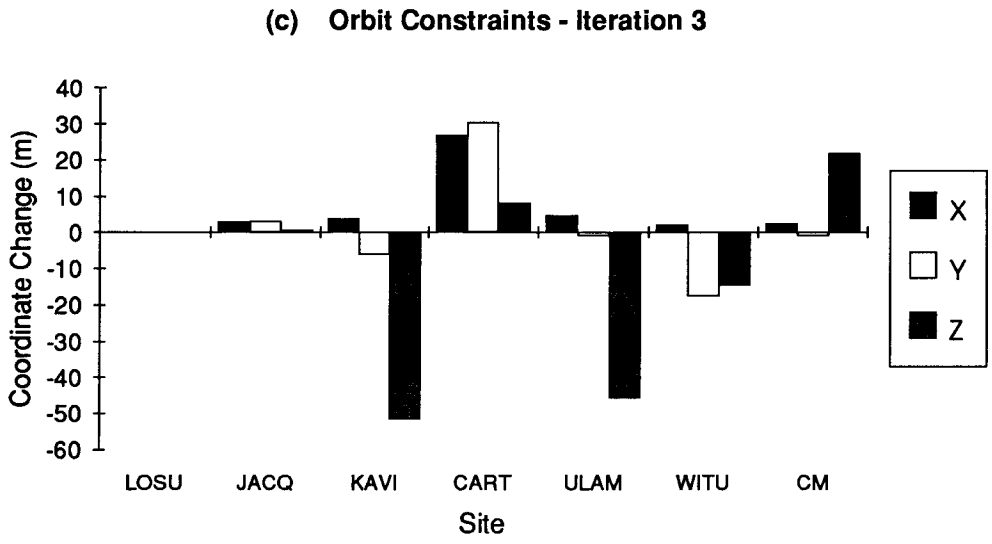

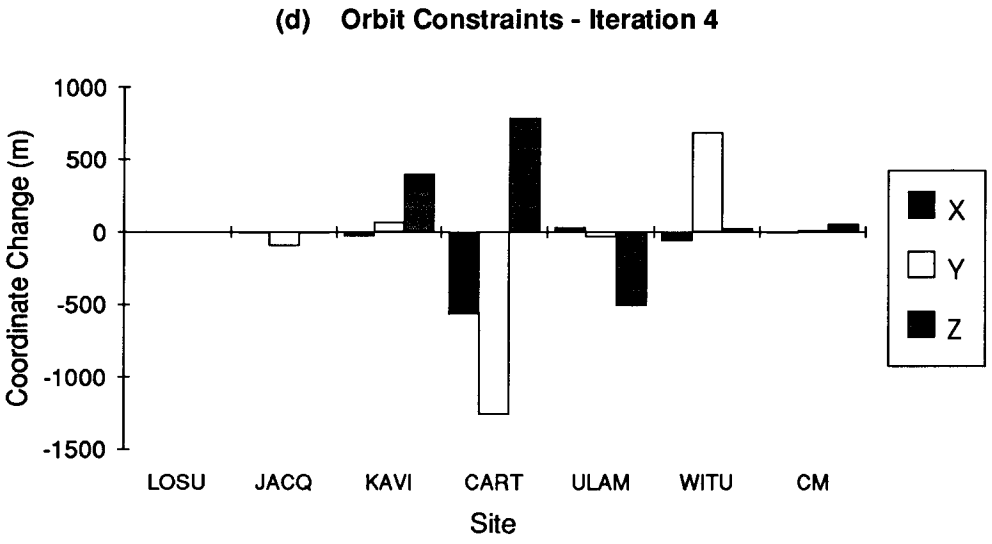

Figure 5.12 (c) - (d) Corrections to coordinates in the first four iterations of the solution. Constraints used were: X = 1000 m; Y = 1000 m; Z = 1000 m; velocity = 10 ms^{-1} for all three components. Clearly Carteret, Ulamona and Witu are oscillating wildly. Jacquinot Bay and Kaving are also oscillating, but to a lesser extent. Losuia is tightly constrained, therefore its coordinates remain unchanged.

It seems that the magnitude of the orbit constraints affects the magnitude of the oscillations of the site coordinates. This can be seen by comparing Figure 5.12 in which orbit constraints were ±1000 m on the X, Y, Z components and ±10 ms^{-1} for the velocity components, with Figure 5.13 (a - b) with X, Y, Z constraints of ±50 m and velocity constraints of ±0.5 ms^{-1}. Again, the result for Kavieng alone is displayed, but it is typical of other sites.

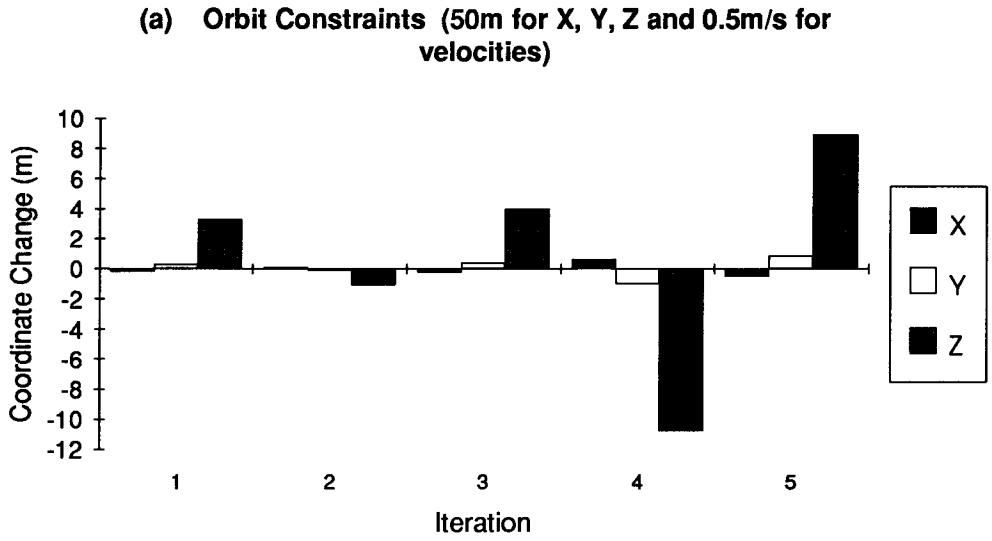

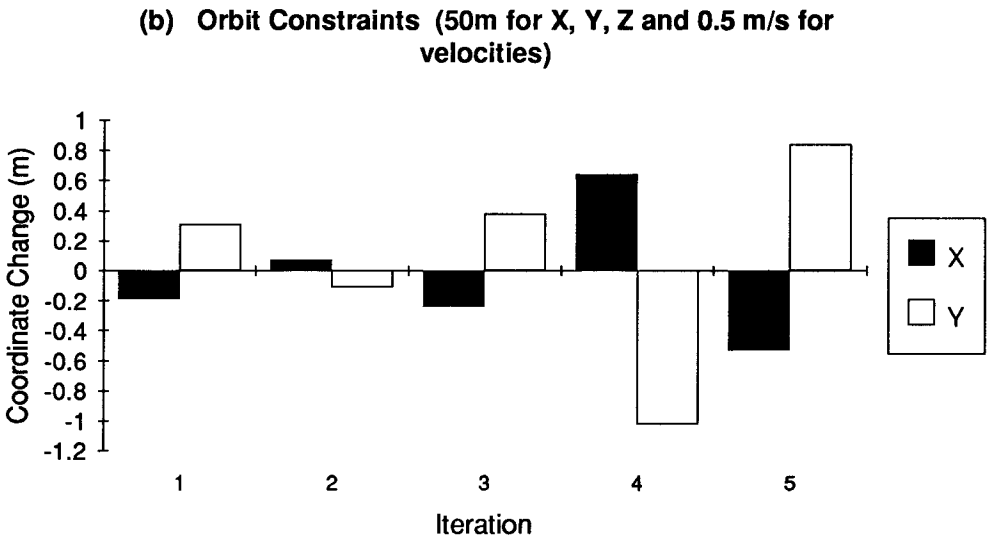

Figure 5.13 The corrections to a priori coordinates at Kavieng with orbit constraints of 50m for X, Y, Z and velocity constraints on X, Y, Z of $0.5ms^{-1}$. (a) clearly shows the major oscillations occur in the Z component, which corresponds to the along-track component of the orbit. The oscillations in Z dwarf the effects in X and Y at the scale of this graph, therefore (b) shows only the X and Y coordinate corrections. The X and Y oscillations are also significant, as seen in (b)

The sensitivity of the solutions to changes in orbital constraints is also markedly different to the results obtained in the 1974 tests.

Orbital constraints of 26m, 10m, 5m for the along-track, cross-track and radial components respectively, and $0.2ms^{-1}$ for all three components of the velocity are commonly accepted values (McClusky, 1993). However, Morgan

(unpublished report) states that in periods of high ionospheric activity, these constraints are too tight. The 1981 survey coincided with a period of high ionospheric activity. However, relaxing the orbital constraints, as discussed above, does not lead to a stable solution.

Small changes in the constraints applied should not affect the results of the solution. However, with this dataset the results were changed significantly for the totally unconstrained sites when small changes were made to the orbital constraints. McClusky (1993) used orbital constraints of 26m, 10m, 5m, and $0.02ms^{-1}$, therefore the coordinates from this solution were used as a base with which to compare the effects of small changes to constraints. Call this solution A. Another solution was run using orbital constraints of ±30m, ±15m, ±10m on the along-track, cross-track and radial components respectively, and $\pm 0.02ms^{-1}$ on the velocity components. This can be solution B. The graphs in Figure 5.14 below show the differences in the final coordinates between the two solutions A and B. Note that Carteret experienced an adjustment of approximately 20 m in the Z coordinate, which is much larger than expected.

The first conclusion to be reached from Figure 5.14 is that small changes to the applied constraints does indeed significantly affect the coordinates output from the solution. It should also be noted that the coordinates output from each of the three iterations in the solution displayed the large oscillations in the Z coordinate component similar to those seen in the graphs showing each iteration above. Oscillations were also present but smaller in X and Y components. This is the same effect as was seen in the tests on coordinate constraints. The Z component corresponds to the along-track component of the orbit.

Further observations that should be noted are that:

- the effects on the Z-coordinate are much greater than the effects on X and Y;
- Carteret and Witu show much greater changes than Jacquinot Bay and Kavieng, which were constrained;
- Ulamona also exhibits only small changes in X and Y. This anomaly could be explained by it's proximity to Jaquinot Bay (76 km), which was constrained.

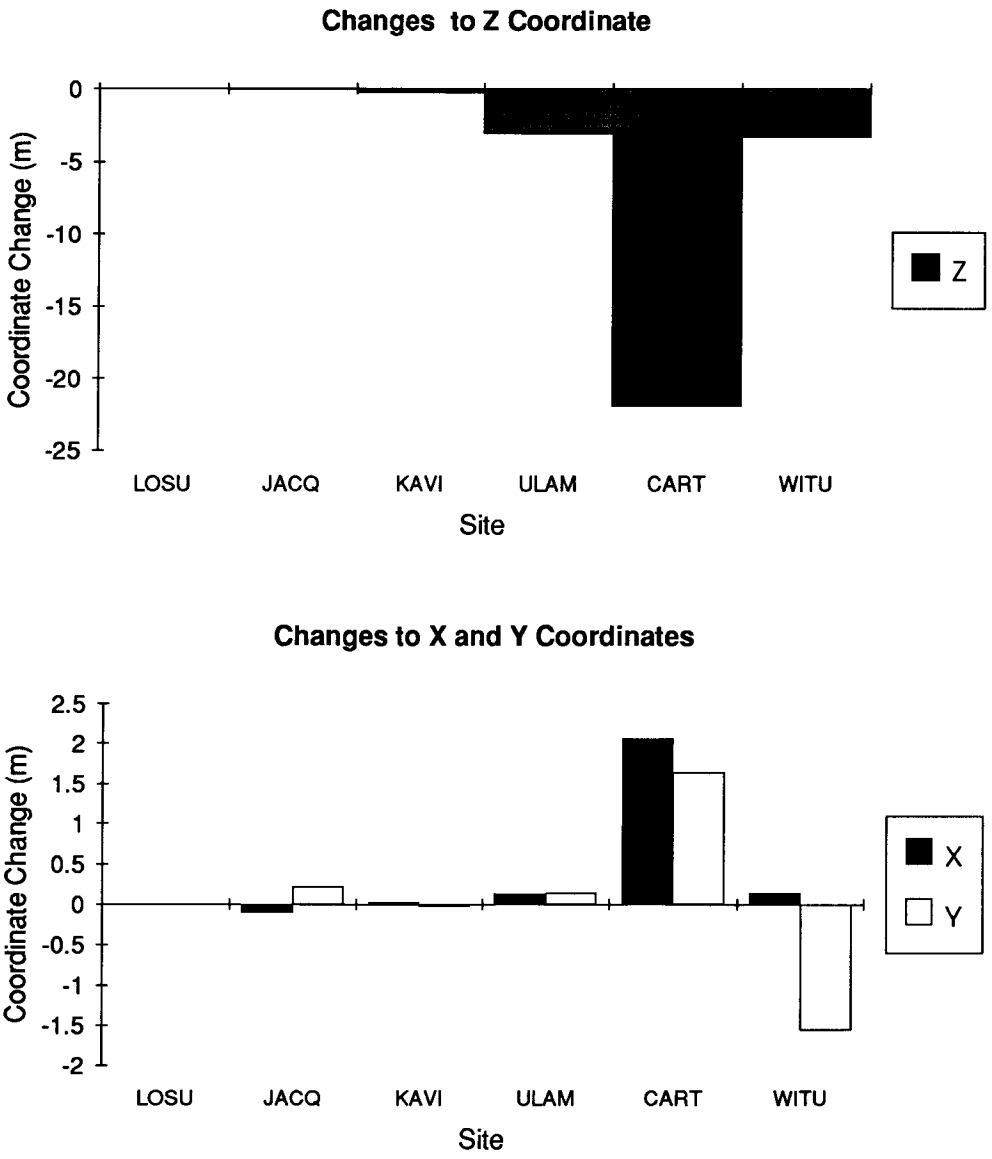

Figure 5.14 The differences in site coordinates from two solutions with small differences in orbit constraints:A - with orbital constraints of 5 m, 10 m, 26 m, and 0.02 ms^{-1}; B - with orbital constraints of 10 m, 15 m, 30 m, and 0.02 ms^{-1}.

Similarly, graphs for orbital constraints of 6 m, 11 m, 27 m and 0.02 ms^{-1} exhibit large coordinate changes as shown in Figure 5.15. Changes of up to 7 m in Z and 1.5 m in Y are obvious. Such small changes to orbit constraints should not have such pronounced effects upon the solution, unless both sets of constraints are too tight and are introducing strain into the solution. However, as explained above, relaxing the orbit constraints does not lead to a stable solution which makes this explanation unlikely.

(a) Small changes to Orbital Constraints - effect on Z coordinate

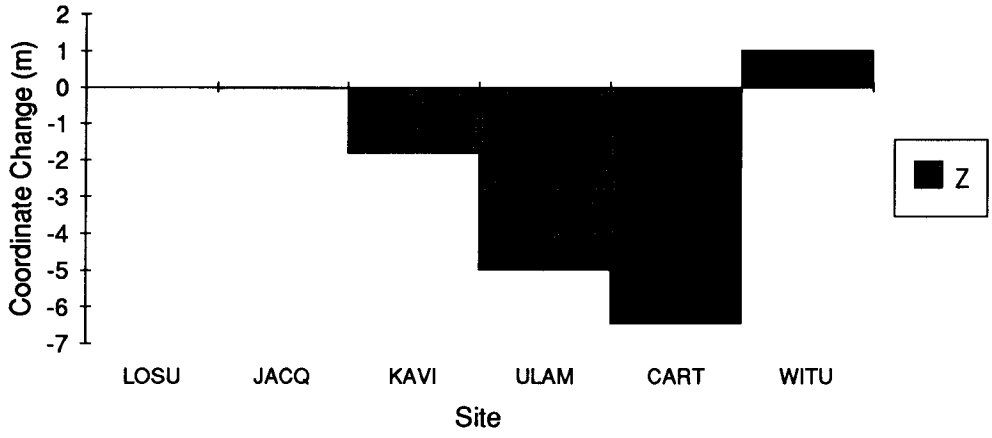

(b) Small changes in Orbital Constraints - effects on X and Y Coordinates

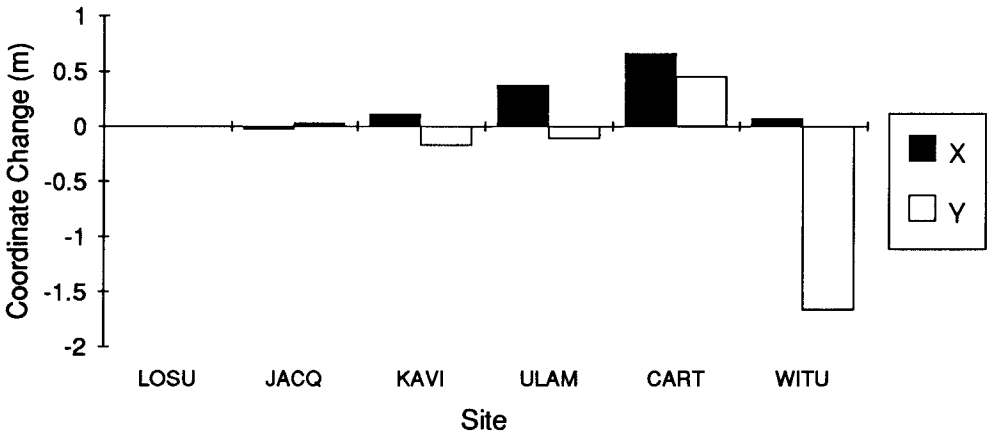

Figure 5.15 Differences in site coordinates from two solutions with orbital constraints of:

(1) 5 m, 10 m, 26 m, and 0.02 ms^{-1};

(2) 6 m, 11 m, 27 m and 0.02 ms^{-1}.

In summary, Table 5.6 shows the various orbit constraints tested and the results of those tests. None of the tests achieved convergence. The test in which constraints of ±7 m, ±12 m, ±28 m, in X, Y and Z, and ±0.02 ms^{-1} had not diverged after 3 iterations, was the closest to convergence of any of the tests! These constraints were therefore adopted as the best possible for the remaining tests.

Table 5.6 Summary of the tests performed on the orbit constraints.

Trial Orbit Constraints				Effect upon the Site Coordinates
X	Y	Z	velocity	
	(m)		(ms^{-1})	
1000	1000	1000	10	Diverge quickly
50	50	50	0.5	Oscillate then diverge
10	15	30	0.02	Oscillate. Slowly diverging
7	12	28	0.02	Had not diverged after 3 iterations.
7	12	28	0.03	Oscillate. Slowly diverging.
6	11	27	0.02	Oscillate. Slowly diverging
5	10	26	0.02	Oscillate then diverge

5.5.4 Error Model Constraints

McClusky (1993) was explicit in the values used for these constraints. However, due to the instability of the results, limited testing was also performed on these constraints. Three types of oscillators were used during the 1981 survey. These were caesium oscillators, rubidium oscillators and crystal (receiver) oscillators. In the processing, McClusky (1993) used two sets of constraints, one for the crystal oscillators and one for the caesium and rubidium oscillators. To test the effect of these constraints, the more relaxed constraints of the atomic oscillators were applied to the rubidium oscillator.

Figure 5.16 shows significant changes (>0.5 m) in baseline lengths to all unconstrained stations, some of which were not visited by the rubidium oscillator. Constrained sites which were visited by the rubidium oscillator appear to be unaffected by the change in constraints, with baseline length changes <0.1 m. The implication of this result is that the constraints on the sites, either applied to a priori coordinates or baseline components are the dominant force in the solution, and affect the results to a much larger degree than the oscillator constraints. Again, it is apparent that the site constraints affect only the stations to which they are applied and do not assist in stabilising the solution.

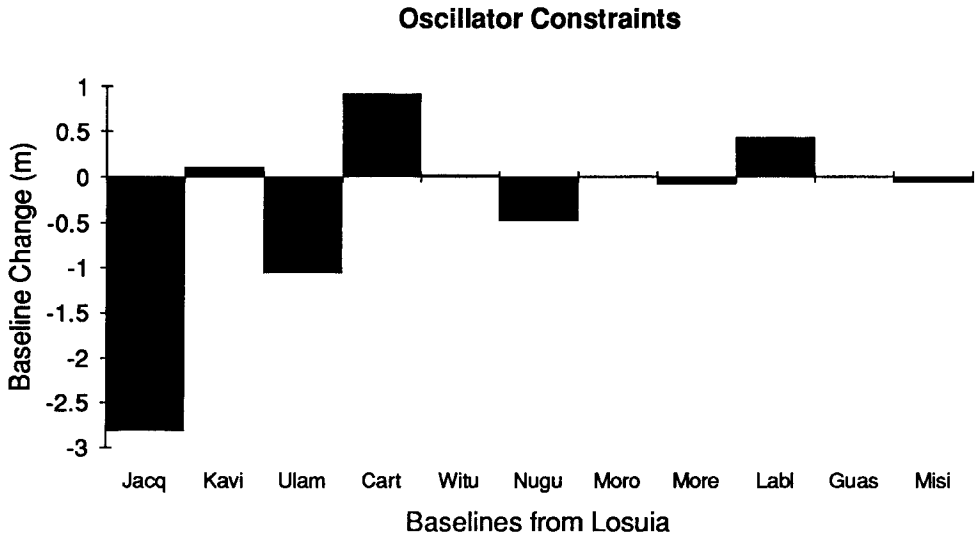

Figure 5.16 The effect of applying the atomic oscillator constraints to the rubidium oscillators, which usually have the same constraints as the caesium oscillators. In this solution, unconstrained sites were Jacquinot Bay (Jacq), Ulamona (Ulam), Lab Lab (Labl), Carteret (Cart) and Nuguria (Nugu). Other abbreviations stand for Kavieng (Kavi), Morobe (Moro), Port Moresby (More), Guasopa (Guas), Misima (Misi) and Witu. The rubidium oscillators were used at Jacquinot Bay, Witu, and Morobe.

5.5.5 Baseline Length Constraints

A baseline length constraint was applied to the 1981 Doppler solutions between the sites Losuia and Morobe. This line was constrained to the 1990 GPS length to ±0.10 m in order to force the GPS scale onto the Doppler network. Baseline constraints at the 1m level are ineffective. At the 0.5 m level, baseline constraints become effective, but only improve the stations involved. All tests involving baseline constraints showed that they were effective in constraining the positions of the sites to which they were applied, but these benefits were not passed on to the rest of the network.

5.5.6 Centre of Mass Constraints

The constraint on the centre of mass clearly affects the solution obtained for the 1981 dataset. Figure 5.17 illustrates the effect of tightening the constraints applied to the centre of mass from ±5 m to ±0.01 m. Once again, oscillations were present in the solution, which diverged after three iterations. The largest effects are in the Z coordinate, with changes of up to 16 m. X and Y coordinate changes were also significant. Note that the coordinate changes do not reflect a

block shift, implying that the relationship between the centre of mass and the coordinates of sites on the surface of the earth is weak.

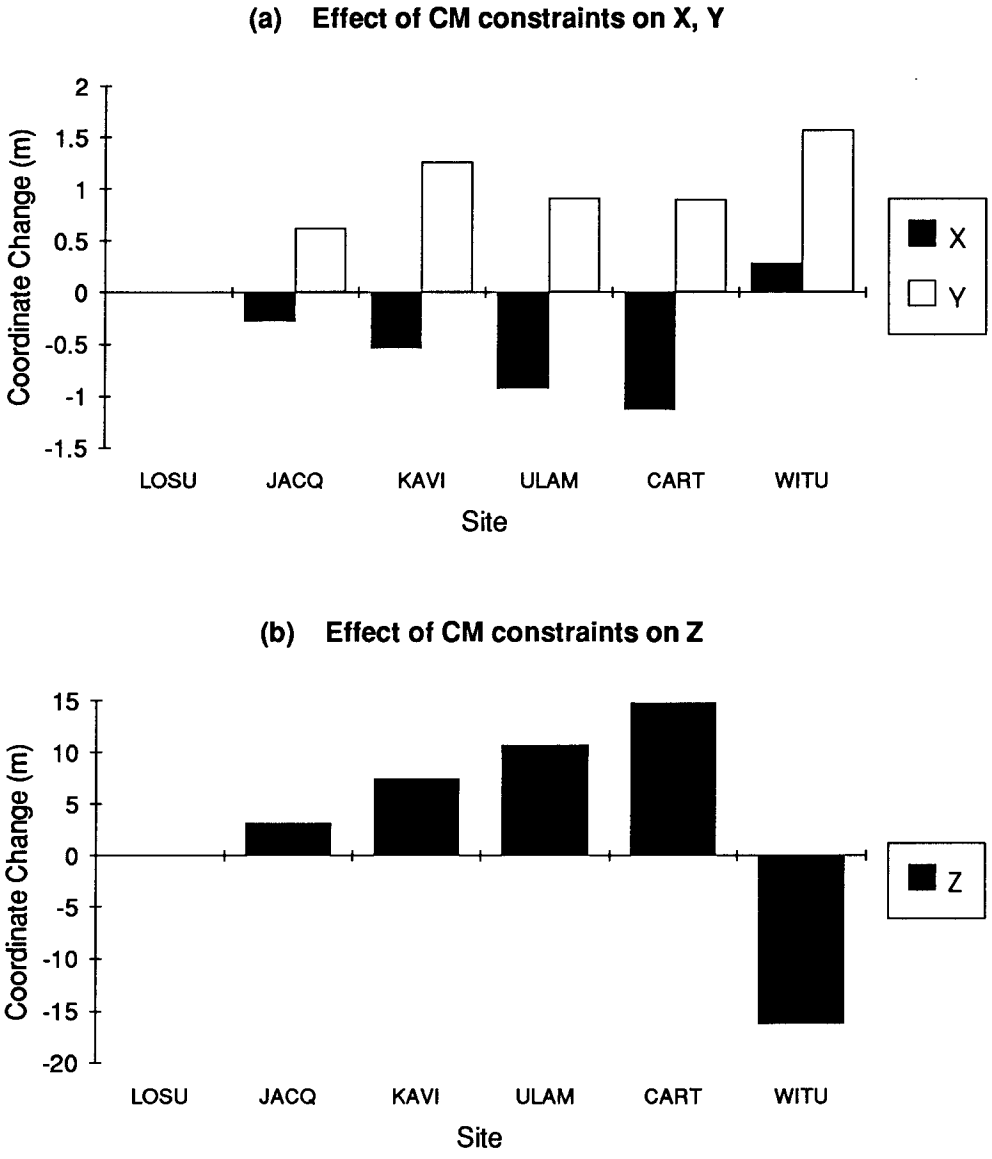

Figure 5.17 The effect upon the coordinates of changing the constraints on the centre of mass from ±5 m to ±0.01 m. (a) shows the effect on the X and Y coordinates. (b) shows the effect on the Z coordinates. Note that the scale on the varies between graphs.

The point to note is that the solution is definitely sensitive to CM constraints, in contrast to the 1974 test data.

5.5.7 Range-in-pass Constraint

The small change applied to the range-in-pass constraint (0.05 m) has clearly had a significant effect upon the solution. Figure 5.18 shows that changing the value of this constraint from 0.075 to 0.070 m has changed baseline lengths from Losuia to all unconstrained sites by up to 3 m. Baselines between other sites have changed by up to 6 m, consistent with movement of these sites of 1-6 m. The method used to calculate the value used for the constraint was outlined in Section 5.4.5. Although the 1974 results showed that the solution is indeed sensitive to this constraint, a value of 7 cm is a realistic constraint for the 1981 data. Changing that constraint by 5 mm has had a disproportionate effect upon the solution. Again, it is apparent that constrained sites have not experienced the same large motions as unconstrained sites.

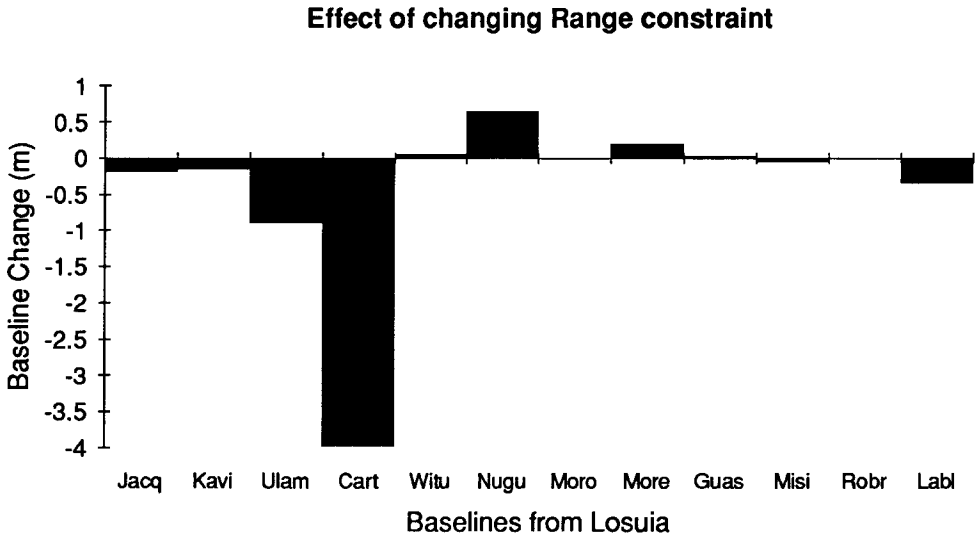

Figure 5.18 The effect of changing the range-in-pass constraint from ±0.075 m to ±0.07 m. Unconstrained sites were Jacquinot Bay (Jacq), Ulamona (Ulam), Robinson River (Robr), Lab Lab (Labl), Carteret (Cart) and Nuguria (Nugu). Other abbreviations stand for Kavieng (Kavi), Morobe (Moro), Port Moresby (More), Guasopa (Guas), Misima (Misi) and Witu.

5.5.8 Summary of 1981 Data Stability Analysis

In short, the 1981 Doppler data was sensitive to small changes in all constraints, and to small changes in a priori coordinate values.

5.6 Errors in the Input File and Their Effects

Comparison of input data used in this analysis with that of Morgan (unpublished analysis) revealed that two sections of data had been incorrectly labelled in the input for SAGA. The labels on Manus and Emirau had been swapped, and there was additional data from an unknown site labelled as Carteret. This obviously has serious consequences for the solution, because sections of the data are entering the solution with a priori coordinates in error by hundreds of kilometres with constraints on those coordinates of at most, a few metres.

However, this is not the cause of the solution instability. These errors will result in the affected passes having RMS values of thousands, and will therefore be deleted from the input as "bad" data. See McClusky (1993) for criteria for determining what constitutes bad data. Once removed or corrected, the solution should be stable.

The major problem caused by such errors is that large sections of otherwise good data are deleted, thereby weakening the solution. In addition, it was found that, although the input file physically contained 302 passes, the elevation cut-off angle excluded some of these from entering the solution. This left a total of 244 passes entering the adjustment, which is less than half the original number of 583 observed passes. This is at variance with McClusky (1993).

5.7 Conclusions

There is no doubt that the 1981 Doppler data is unstable in its present form. The cause of this instability has not been determined after extensive testing. As the data is sensitive to changes in all constraints, and the constraints appear only to benefit the sites to which they are applied, it is believed that there is more than one cause of the problem. These multiple causes are masking the effects of each other, making their location very dificult.

Two sections of data have been found to be incorrectly labelled. No other sections of data are displaying the symptoms of this error, but having found one instance of erroneous input, the possibility of other, perhaps more subtle errors cannot be ruled out. It is possible that something of this nature is causing the instability.

The fact that each section of the 1981 survey has been successfully processed in an independent software package implies that there is nothing inherently wrong with the data. The fact that the results from the 1974 test data were recovered implies that there is nothing inherently wrong with the SAGA software. From this, the only conclusion that can be drawn is that the cause of the instability lies with the data in the form used in this analysis.

Therefore, in the belief that the original data is stable, and the knowledge that the present SAGA dataset is incomplete and unstable, it is recommended that the raw observation data be recovered and the processing procedure be started again.

These tests clearly show that the data is totally unstable. Reprocessing from raw data is beyond the scope of this research due to constraints in both time and funding. For this reason, further tests were discontinued and the Doppler results of McClusky (1993) have not been used in comparisons with subsequent GPS reoccupations of the Doppler survey network.

Chapter 6

GPS Analysis and Results

Data processing was performed using the GAMIT/GLOBK software developed at the Massachusetts Institute of Technology (MIT). Processing is performed in two stages: in GAMIT, the data is cleaned and a weighted least squares algorithm is used to estimate the relative positions of the stations by fitting to doubly differenced phase observations. These solutions are generally performed on a daily basis. In GLOBK, the VCV matrices from the daily GAMIT solutions are combined into campaign solutions and multi-campaign solutions by a Kalman Filter, which estimates all of the global parameters such as station coordinates and velocities, orbital initial conditions and non-gravitational force parameters, and Earth rotation parameters. GLORG is a sub-program in the GLOBK software. Current practice is to run GLOBK with loose constraints and GLORG to apply tight constraints to site positions and velocities to define the reference frame. Various aspects of the processing will be discussed in this chapter.

6.1 Raw Data

The first stage in any data processing is obtaining the data. The data used in this research came from several sources in a variety of formats. The 1990, 1991 and May 1992 data (our surveys) were in the form of raw receiver files. These were converted to RINEX format (Gurtner & Mader, 1990) for input into GAMIT. The raw data for the May and August 1993, and the July 1994 surveys came from the National Mapping Bureau of Papua New Guinea via the University of Canberra (UC). It was also in RINEX format.

Global tracking data came from several sources, namely:

- Global data files were retrieved in the form of RINEX or GAMIT x-files from Scripps Institute of Oceanography (SIO), UCLA.
- Additional regional tracking data was retrieved in RINEX format from archives at UC.

- The 1990 global raw data files for the CIGNET sites came from the National Oceanic and Atmospheric Administration (NOAA) in ARGO format. This required conversion to FICA format, before it could be entered into GAMIT. The GAMIT manual (Version 9.40) gives a description of both ARGO and FICA formats.
- Additional 1990 global data files were obtained from Yehuda Bock at SIO.

In addition to data which was processed as part of this analysis, a considerable number of solutions extending from GIG91 to May 1996 were made available for the GLOBK/GLORG analysis by Peter Morgan of UC. These included the solutions used in the Zero Order Network for Australia (Morgan *et al.*, 1996).

In addition to GPS observations at each site, an orbit ephemeris is also required. In this analysis, the a priori orbits were obtained from SIO in the form of GAMIT g-files. On the few occasions when orbits were not available from SIO, the orbits from the previous or following day were integrated forward or back to form the a priori orbit.

6.2 GAMIT Processing Strategy

Morgan *et al.,* (1996) give a thorough description of processing in GAMIT. Such a detailed treatment will not be given here. The reader is referred to that document for details excluded from this account. Where possible, the processing strategy adopted for this work followed that used by Morgan as the surveys processed for this analysis were to be combined with additional campaigns processed by Morgan and his team at UC for the Zero Order Network for Australia. This gave repeat observations on some sites that would otherwise have had only a single occupation, and has therefore greatly enhanced this work.

With the exception of the 1992 PNG campaign, global and local sites were processed together, rather than using the hierarchical approach adopted by Morgan *et al.* (1996).

In 1990, a number of different receivers were in operation: Minimacs and TI4100s formed the basis of the global tracking network; Trimble SSTs and SDTs were used in the local network. Under the SA effects implemented at the time, the ideal method of processing the data would have involved solving the Minimacs and Trimble SSTs together, as they both observe on the GPS

second; processing the TI4100s together in a separate network as they observe at 920 ms before the GPS second; and finally, processing the Trimble SDTs together in another network as their sampling rate is variable up to 256 ms from the GPS second. This is the approach adopted by the team at MIT for their Mediterranean network (Morgan, personal communication, 1996). It was the approach used initially for this analysis. However, it was found that there were insufficient TI4100s available to form a global network. Whilst there were sufficient sites observed with Minimacs and Trimble SSTs to form a global network, it was a weak solution with some key sites, such as Kokee Park, excluded. The decision was therefore made to include all sites in a single solution despite the degradation caused by SA. That is, the decision was made to introduce some modelling errors in order to control other error sources and thereby obtain a stonger solution.

In 1992, the solution was separated into global and regional networks because the total number of sites observed exceeded the 25 site limit of GAMIT. Whilst this limit can be increased, computing resources did not allow it. The regional network included 5 of the global sites to act as a link between networks. These sites were: DS41, KOKR, TAIW, USUD, and YAR1. Additional fiducial sites (TAS1, TOWN, and WELL) were included in the regional solution. Initially, the global solution was taken directly from SIO, and the intention was to use the SIO orbit, and run a regional solution. This was to be combined in GLOBK with the SIO h-file. However, major changes in the GAMIT software meant that the global solutions also had to be re-run.

The global tracking networks available for the PNG90, PNG91, PNG92 and PNG93 (May) campaigns are shown in Figure 6.3a-d.

6.2.1 Clocks

Receiver clock models are contained in so-called i-files. The GAMIT manual suggests that these files are not required for processing. In general, they were not used. However, in 1990, with receivers sampling the GPS signal at different times in relation to the GPS second, and severe levels of SA implemented, the i-file was required to bring the observations to a common epoch. Figure 6.1a-b shows the effect of using the i-file to model the receiver clocks.

SA consists of two effects, discussed in Section 3.3.2. The effect of truncating the broadcast ephemeris has not affected this work, because post-processed a priori orbits were used, and then updated as part of the solution. However, the effect of dithering the satellite clocks was a serious issue, particularly for the 1990 survey. Dithering results in the a and b terms in Equation 6.1 no longer being constant. Clearly, bringing the observations from each site to a common epoch reduces the effects of SA through cancellation of the introduced errors, i.e. the $(t_{1,2}\text{-}t^0)$ terms in Equation 6.1 are minimised. Some error will remain because the distance between sites creates a time offset in the observation of the same part of the signal between distant sites, and the satellite clock terms then do not cancel. This can be seen in the equation for the double difference observable for stations 1 and 2 and satellites i and j (Morgan *et al.*, 1996):

$$\begin{aligned}\nabla\Delta\phi_{12}^{ij} = &-f_0\left[\tau_2^j - \tau_1^j - \tau_2^i + \tau_1^i\right] - \left[a^j + b^j\left(t_2 - t^0\right)\right]\left[\tau_2^j - \tau_1^j\right] \\ &+\left[a^i + b^i\left(t_1 - t^0\right)\right]\left[\tau_2^i - \tau_1^i\right] + \left(n_2^j - n_1^j - n_2^i + n_1^i\right) + \nabla\Delta\phi_{noise}\end{aligned} \tag{6.1}$$

where:

f_0 is the nominal frequency of the satellite clock;

$\tau_{1,2}^{i,j}$ are the propagation time delays which include the geometric delay and the delay caused by the ionosphere and troposphere;

$a^{i,j}$ are the current offsets of the respective satellite clocks from the nominal frequency;

$b^{i,j}$ are the linear drift terms of the respective satellite clocks;

$t_{1,2}$ are the epochs as recorded by the respective local receiver oscillators;

t^0 is the chosen reference epoch;

$n_{1,2}^{i,j}$ are the ambiguity terms of each station-satellite combination.

Figure 6.1a-b shows that the residuals are considerably flatter when the i-file has been used in modelling.

Satellite clocks are modelled in the j-file. J-files generated from the broadcast message were used in the analysis of each campaign, including 1990. GAMIT used to have the facility to solve for satellite clocks, thus removing the effects of SA. This feature is no longer operational but could have been restored with difficulty. The problem with the GAMIT approach of solving for satellite clocks from the c-files (which contain observed-computed residuals) is that precise coordinates of the stations are needed, as well as high quality clocks. Additionally, it is necessary to have the j-file corrected for the full orbit. Since only high quality atomic oscillators existed at the VLBI stations Kokee Park,

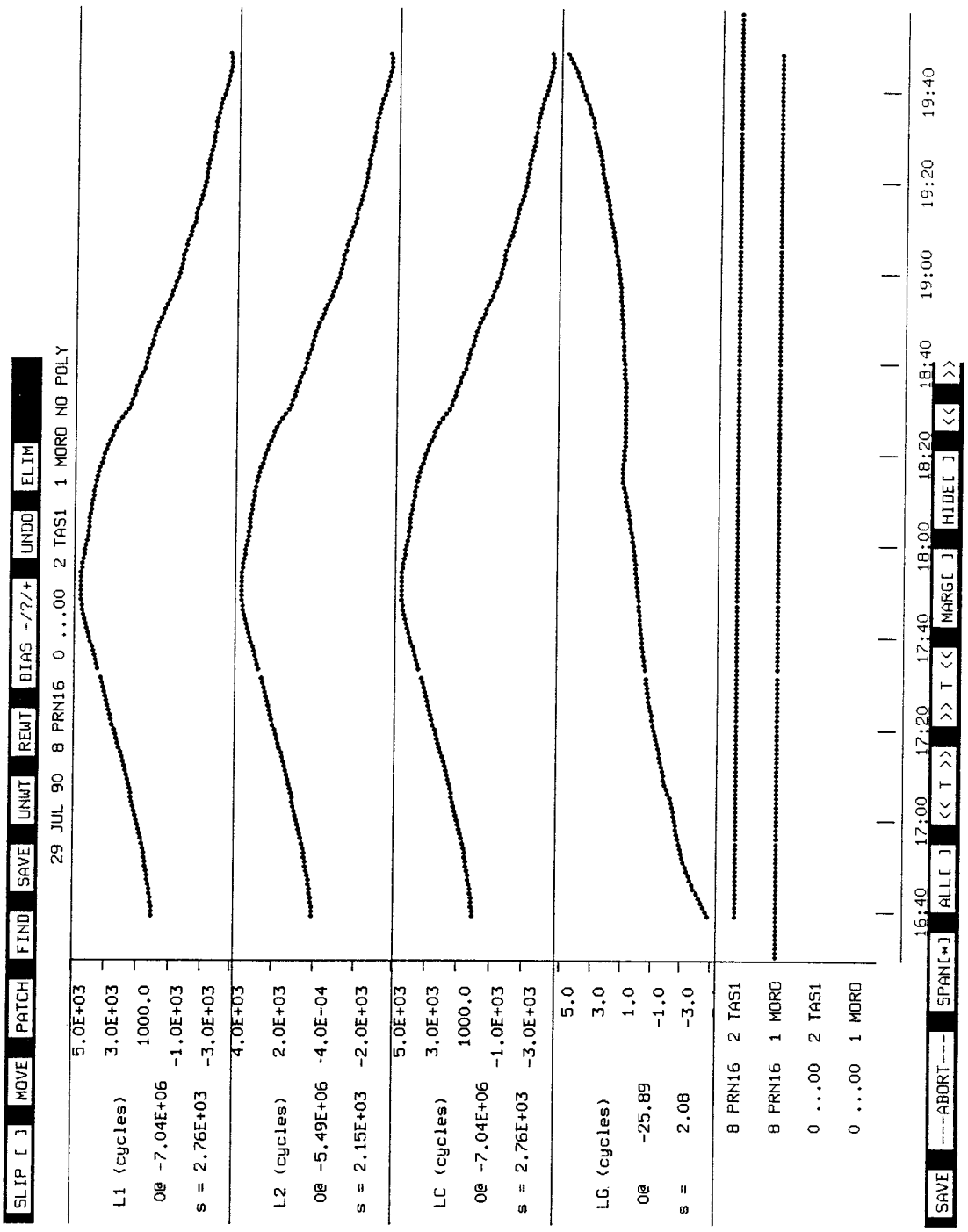

Figure 6.1 (a) Between station difference for satellite PRN16, sites Morobe and Tasmania. Modelling included using the i-file.

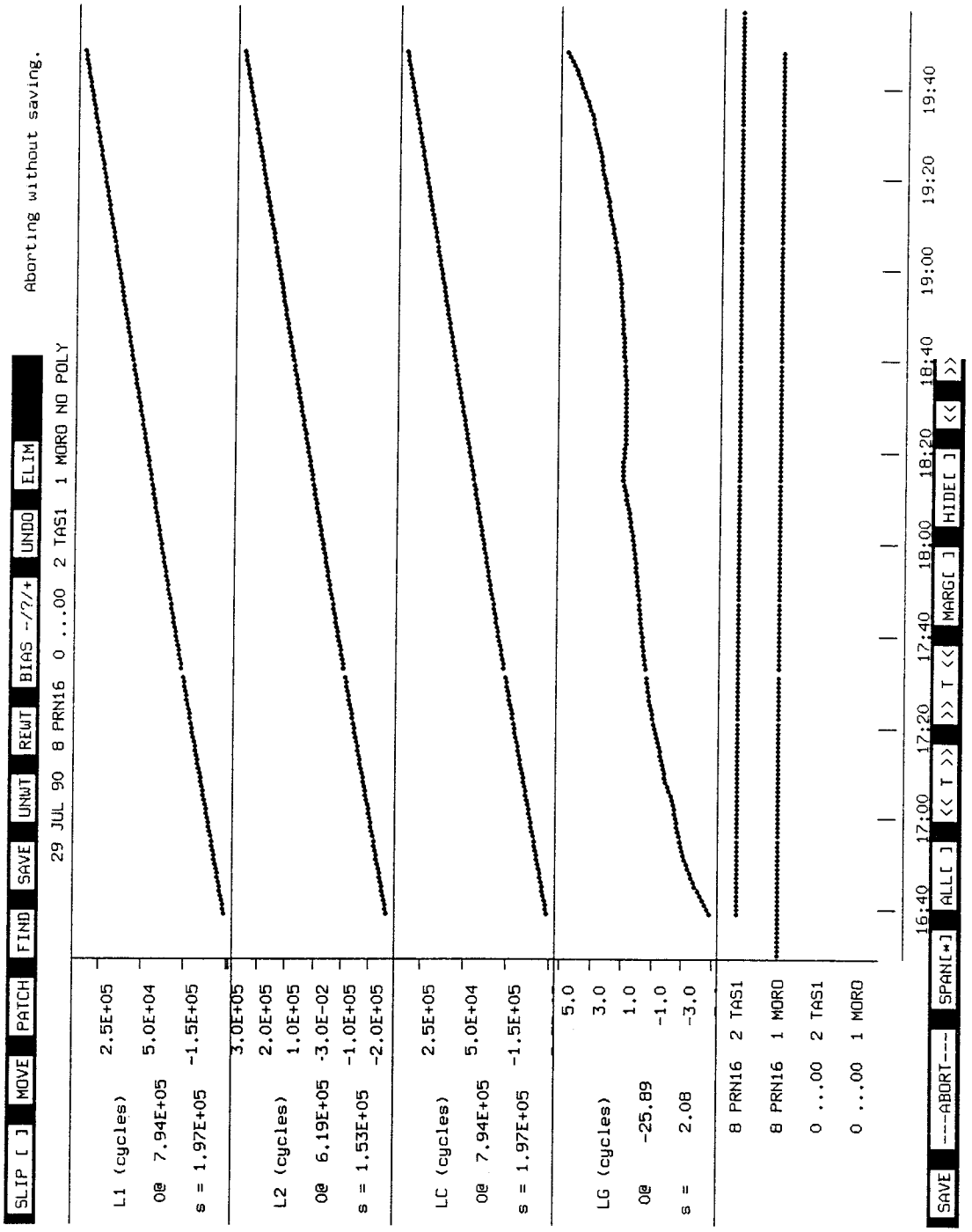

Figure 6.1 (b) Between station difference for satellite PRN16, sites Morobe and Tasmania. Modelling did not include using the i-file. Note the steeper slope when the i-file was not used.

6.2.2 Orbits

As stated above, orbits were estimated as part of the solution. The strategy used varied for some years, so each approach will be discussed.

Initially, the B1950 inertial reference frame was used for the orbits. However, with the release of GAMIT 9.40, J2000 was used. All data was subsequently reprocessed with orbits in the J2000 frame.

Orbit integration used the IGS/IERS 1992 standards. The Berne model was used for the radiation pressure modelling. Orbits were integrated with a 75 second step size and 900 second interval for the tabular ephemeris.

Not all earth orientation parameters were estimated: UT1 rate and pole position were estimated: UT1 and pole rate were not. As UT1 is highly correlated with the nodes of the satellite orbits, estimating UT1 with insufficient orbit and/or site constraints leads to high correlations between the X and Y position and velocity components of the orbits. To avoid this, only UT1 rate and pole position components were estimated.

Orbits were loosely constrained to allow free adjustment. The reference frame was determined by the global tracking network.

The orbital constraints used for the August 1993 campaign were: 10 ppm (about 200m) for the Keplerian elements; 10% on the direct and y-bias terms, 0.01% on the z-bias term and 0.1% on the remaining six radiation pressure terms. Seven of the 13 IGS core sites were constrained to ±0.02 m in east north and height components to be consistent with the constraints used to define the reference frame in GLORG.

The other campaigns were processed with the Keplerian elements constrained to 100 ppm, the direct and y-bias terms with 50% constraints, 0.01% on the z-bias term and 0.1% on the remaining six radiation pressure terms. The 13 IGS core sites were constrained to 0.10 m in east and north and 0.20 m in height.

All orbits were single day arcs, except the 1990 orbits, in which 3-day arcs were used to increase the strength of the solution by reducing the number of free parameters that needed to be estimated.

6.2.3 Modelling

As mentioned previously, the receiver clock files were generally not used in modelling. The 1990 data was an exception to this.

Yaw modelling was implemented. Although prior to June 1994, the yaw on the satellites is unpredictable and models are unavailable for the early data, implementing this option allows the removal of data during and/or after eclipse of the satellites.

Antenna modelling was not implemented as reliable models were only available for a small number of antennas at the time of processing.

Tide modelling was implemented with the frequency dependent and independent solid earth tides, and pole tides. This was implemented for consistency with current processing practices at UC, used to reprocess all data since the introduction of GAMIT Version 9.40.

6.2.4 Data cleaning

Data cleaning can be an arduous task. However, the use of automated cleaning routines has made the task much less time consuming. All data cleaning for this analysis was done with the routine AUTCLN. Postfit residuals were then checked in CVIEW and any residuals larger than 0.4 cycles were removed. Problematical data received greater attention, and an effort was made to remove segments of data with a standard deviation of greater than 0.2 cycles. The 1991-1993 surveys were initially run with default AUTCLN settings. These are contained in Appendix 6. However, an AUTCLN command file came with GAMIT, Version 9.40, and this was used for cleaning the 1990 data. These settings were too stringent and removed an unacceptably high proportion of the data (75-100%), therefore some parameters had to be changed.

Following is a brief description of the processes involved in the automatic cleaning procedure.

AUTCLN is an automatic data cleaning routine which flags gaps and jumps in the data which could represent cycle slips. Where possible, AUTCLN repairs cycle slips and removes the bias flags. When the data is unresolvable,

AUTCLN will unweight it so that it does not contaminate the solution. In order to achieve these cleaning outcomes, all combinations of available phase and pseudo range data are used.

The first process to be performed is the computation of error estimates for the satellite and receiver clocks using the range data. These estimates are then used as a priori values for the estimates of clock errors from phase data. Where large jumps are detected, a calculation is performed to determine the number of cycles required to make the range and phase estimates consistent. All jumps are flagged. The ionospheric delay estimates are also used in the detection of jumps. In polar and equatorial regions, the default values for ionospheric jump detection are too stringent. As Papua New Guinea lies close to the magnetic equator, parameters defining ionospheric jump detection criteria had to be relaxed, as discussed shortly.

Once clock jumps are flagged, all other gaps in the data of one epoch or greater are flagged, as it is more common for cycle slips to occur after gaps in the data than in sections of continuous data.

After scanning for gaps, the one-way phase data are scanned. Double differences are formed and scanned. When a slip is detected, the particular one way phase in which it occurred is determined by forming multiple double difference combinations.

There are obviously two very important factors affecting the quality of automated data cleaners: their ability to detect and flag problematical data, and their ability to resolve bias flags reliably.

The processes discussed above involve flagging problem areas in the data. The next stages involve trying to resolve those bias flags.

The number of slipped cycles at each flag in the one-way phase data are estimated. A decision then has to be made about whether the flag can be reliably removed or not. Firstly, data containing closely spaced bias flags is removed. When the flags are reasonably spaced, the continuity of LC, LG and wide-land combinations are analysed. However, flags are not removed in the one-way phase because this process is unreliable under AS as P-code is not

available. Instead, the reliability of flag removal is assessed in the double differences. If there are many gaps in the data, this process is unreliable.

The flag resolution loop is repeated four times as biases determined towards the end of the process may help resolve biases encountered in earlier stages of the process.

When the cleaning loop is complete, the one-way data is scanned again, and the segments of data containing slips too close to the end of the data are removed. Also, any data remaining in which the bias flags are too close together are removed.

When AUTCLN is run, it produces two output files: a complete log of the cleaning processes and a summary file. The log file is large and not very useful as a diagnostic tool. The summary file, however, contains the necessary detail for problem detection. An example of a summary file from 1990 in which most of the data was deleted is contained in Appendix 7.

For the PNG campaigns, the equatorial sites and the global tracking sites located in polar regions needed to have more relaxed ionospheric jump detection criteria applied, as mentioned above. These can be seen in the sample AUTCLN command file contained in Appendix 7. This was achieved by using the line:
ion_jump *site* 30 6 2 5
where *site* is each PNG site and other global tracking sites in polar or equatorial regions. The parameters controlling the ionospheric jump tolerance are:

max_gap: the maximum allowable gap in seconds over which an ionospheric jump can be applied
multiplier: a factor used to determine the tolerance, as explained below.
min dIon: the minimum allowable tolerance for detecting ionosphere jumps
max dIon: the maximum allowable tolerance for detecting ionosphere jumps

The tolerance for ionospheric jump detection will lie between the min-dIon and max-dIon values, with intermediate values computed by applying the multiplier to the change between the previous two data points.

For the equatorial and polar sites in these data sets, the parameter max_gap has been decreased from 240 s to 30 s, because of the more rapid fluctuations of the ionospheric activity in these regions. The multiplier has been increased

from 4 to 6 and the min_dlon term has been increased from 0.8 to 2 cycles. Both of these changes serve to increase the minimum threshold for detecting ionospheric jumps, which stops excess flagging of data.

Viewing the AUTCLN summary file for the 1990 data clearly reveals two problems. The first is that all data from Kwajalein is being removed. The table "editing report and site parameters" shows that the reason for this is that the signal to noise ratio is too low. To overcome this, the line:
site_params all 15 15 0 0
was inserted into the command file. The first two values represent the minimum elevation angles (i) to which data will be cleaned and (ii) to which the c-files are to be written. The final two values set the minimum SNR value to be used for L1 and L2 respectively. The default values vary according to receiver type. Setting them to zero allows all data into the solution, bypassing the signal to noise ratio check. Early RINEX files have a reputation for poorly set SNR flags (Tom Herring, personal communication, 1996), so it is best to ignore the flags and enter all data into AUTCLN.

The second problem involves large amounts of data being deleted because the bias flags are too close to the end of the data or too close together. The initial cleaning was performed on clean x-files from SIO to assess the viability of using AUTCLN to treat the conditions particular to the 1990 data. For this reason, the presence of large numbers of bias flags was disturbing. Large numbers of bias flags placed close together is generally an indication of poor a priori modelling. It is also a feature of the antenna radiation pattern at low elevation angles and near the zenith for the cross dipole antennas used with Minimac receivers. Poor modelling implies either poor coordinate values or poor orbits. However, in this case neither of these options were likely and the problem must involve the quality of the data itself. The answer to this problem was found in the tolerances for scanning double differences in the AUTCLN command file.

The dd_fit_tol sets the tolerances for inserting flags in the wide-lane and LC double differences. The scanning of each combination is controlled by three parameters:
Ratio : the allowable ratio of a jump compared with the local RMS
Min : the minimum jump that will be flagged
Max : the maximum value above which all jumps will be flagged.

The command file initially has the LC minimum value set at 0.1 cycles and the LC maximum value at 0.3 cycles. Whilst these may be acceptable values for recent data which suffers few cycle slips and generally lower noise levels than early data, they were clearly too stringent for the 1990 data. Values of 0.4 and 1.0 respectively were found to be acceptable. The minimum value of 0.4 cycles should allow jumps on the half-wavelength L2 data to be detected, without excessively flagging clean data. The default value of the ratio had to be decreased from 4 to 3 to allow for the increased levels of noise in the 1990 data.

These new settings resulted in 80-90% of the data being retained in the solution, whilst removing the majority of cycle slips. Scanning postfit residuals revealed only a few unflagged residuals above 0.4 cycles, which could be removed in CVIEW.

The AUTCLN command file used for the 1990 data was also successfully used to clean the August 1993 data. It was found that the default settings were too severe for data from Townsville, which was consistently being completely eliminated from the solution. The Townsville data was being deleted because bias flags were too close to the end of the data and too close together. These are the same symptoms displayed by the 1990 data, so it is not surprising to find that the AUTCLN command file used for the 1990 data left the data at Townsville available to enter the solution.

6.2.5 Ionospheric Effects on the Data

The effects on the GPS signal caused by propagation through the ionosphere have been discussed in Section 3.3. The 1990, 1991 and May 1992 surveys were all performed between May and August, with observations extending into the night, which is when the ionospheric scintillation effects are at their most severe. Although these effects did not cause particular problems in the 1990 and 1991 surveys, they were the cause of significant data loss during the May 1992 survey. It was clear from the data that the scintillations began to affect the signal approximately an hour after sunset. The observation session began at approximately 7pm, local time, each evening. Approximately the first hour of observations were trouble free. After this, the scintillations began to affect the signal propagation severely. Cycle jumps of ±1 cycle were common during this period. The CVIEW plot in Figure 6.2a gives an indication of both the sudden

start to the scintillation activity and the poor quality of data while this activity was occurring. It was found that the most effective way of dealing with data during this period was simply to delete it. Cycle slip repair was impossible because of the difficulty in distinguishing genuine cycle slips from fluctuations caused by ionospheric propagation.

Generally, the scintillation effects were apparent in the data for approximately four hours, and ended as abruptly as they had begun. From local midnight onwards, the data was generally problem free, and the ionosphere free linear combination ("LC" in GAMIT) was able to remove most of the long wavelength ionospheric effects. Figure 6.2b shows that these long wavelength ionospheric fluctuations are successfully removed by the LC combination. Day 128 was exceptionally troublesome, with the scintillation effects lasting throughout most of the night.

6.2.6 GAMIT Quality Assurance

The postfit NRMS of the daily solutions gives an indication of the quality of the solution. A value of about 0.3 indicates that there are probably no remaining cycle slips or systematic effects in the data (GAMIT Manual, Ver.9.40, 1995). Values for the various campaigns in this analysis were generally between 0.2 and 0.35. The higher values are most likely to be attributed to unmodelled SA effects and the different time marks of the receivers. There were a small number of exceptions, for example: day 214, 1990 had a value of 0.67 and day 230, 1993 had a value of 1.55. Where the NRMS was high, the solution was examined more closely. Experience has shown that when there are no other indications of problems (for example, the number of observations for the day and site/satellite corrections are similar to other days) a higher NRMS value may be acceptable if the data does not degrade the campaign solution. Day 230, 1993 was an example of this situation. In contrast, day 214, 1990 had an unusually high proportion of data deleted by AUTCLN, leaving approximately 50% of observations available for processing in the other days of 1990. Clearly, the high NRMS value in this case is indicative of problems. This was quickly confirmed when GLOBK formed the campaign solution. The whole day was subsequently rejected.

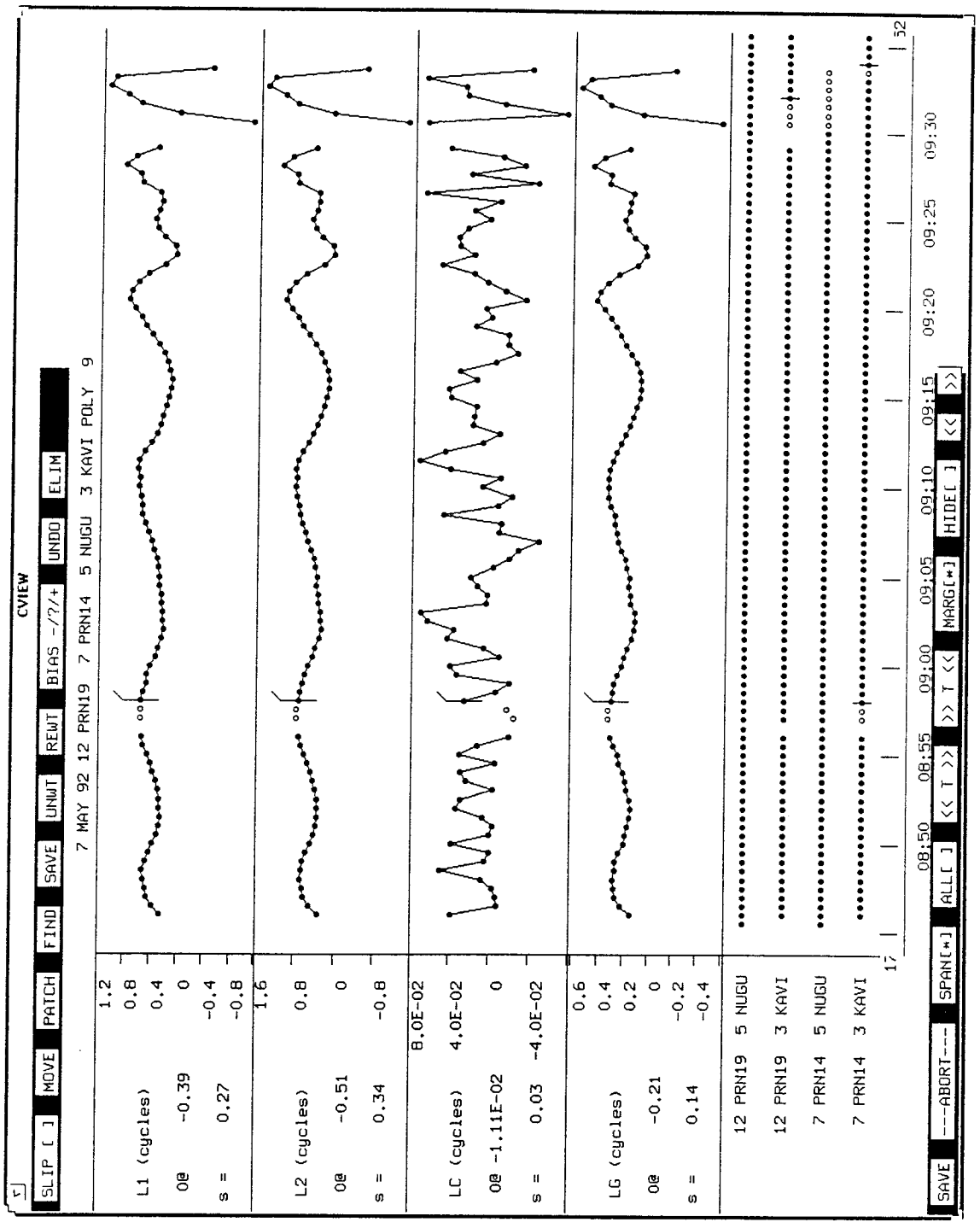

Figure 6.2 (a) The effect on the GPS signal of ionospheric scintillations. The ionosphere-free linear combination is unable to remove these short wavelength fluctuations, which are difficult to distinguish from genuine cycle slips.

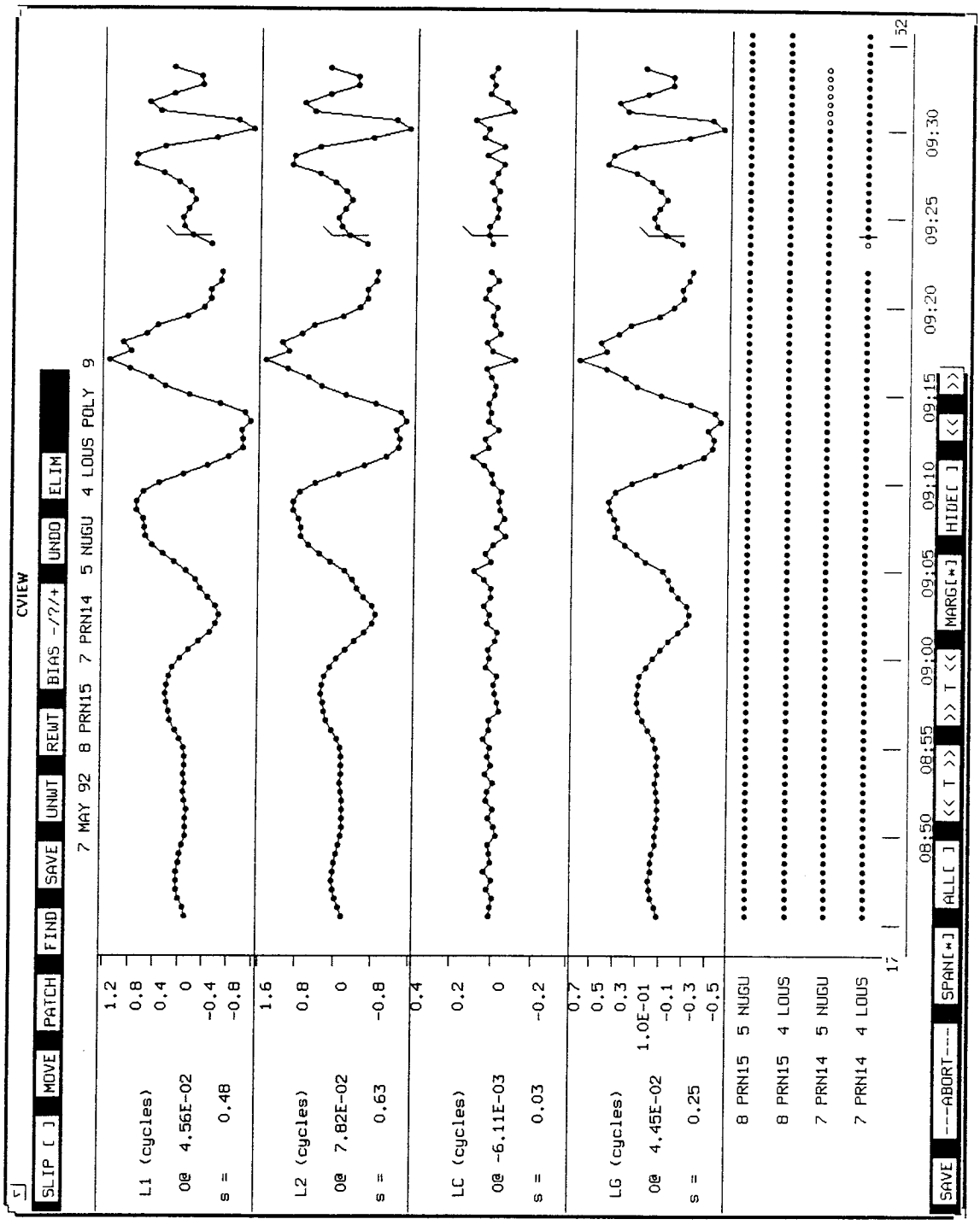

Figure 6.2 (b) The effect on the GPS signal of the long wavelength ionospheric fluctuations which occur at night. The ionosphere-free linear combination is able to remove these effects, which are NOT easily confused with cycle slips.

Table 6.1 Comparison of daily corrections to a standard set of a priori coordinates from the constrained GAMIT solutions for 1990. This forms part of the GAMIT quality assurance. Zeroes indicate the site was not observed on that day.

Site	Comp	Day 209	Day 210	Day 212	Day 213	Day 216	Day 217	Mean	S.D.
JACQ	ϕ (m)	-2.0091	-2.1069	-2.0965	-2.1370	-2.0246	-2.0698	-2.0740	0.0495
JACQ	λ (m)	0.8218	0.8861	0.8044	0.7774	0.6839	0.7001	0.7790	0.0764
JACQ	R (m)	-1.1702	-1.2726	-1.2781	-1.0761	-1.2994	-1.2040	-1.2167	0.0846
MADG	ϕ	0.2606	0.1780	0.0000	0.0000	0.0000	0.0000	0.2193	0.0584
MADG	λ	0.9139	0.8539	0.0000	0.0000	0.0000	0.0000	0.8839	0.0424
MADG	R	-1.5213	-1.6410	0.0000	0.0000	0.0000	0.0000	-1.5811	0.0846
MANU	ϕ	-0.0020	-0.0887	-0.0673	-0.1378	0.0000	0.0000	-0.0739	0.0563
MANU	λ	0.2162	0.2315	0.1891	0.1616	0.0000	0.0000	0.1996	0.0308
MANU	R	-0.2976	-0.4359	-0.3862	-0.2171	0.0000	0.0000	-0.3342	0.0968
MORE	ϕ	0.1140	0.0044	0.0336	-0.0174	0.0000	0.0457	0.0361	0.0501
MORE	λ	0.0916	0.0345	0.0194	0.0198	0.0000	-0.0386	0.0253	0.0464
MORE	R	0.3025	0.1697	0.1946	0.4278	0.0000	0.2997	0.2789	0.1027
MORO	ϕ	-0.1519	-0.2680	-0.2482	-0.2839	-0.1826	-0.2160	-0.2251	0.0511
MORO	λ	0.3386	0.3020	0.2695	0.2788	0.1487	0.2111	0.2581	0.0680
MORO	R	-0.2592	-0.4093	-0.3643	-0.1966	-0.3748	-0.2956	-0.3166	0.0805
TAS1	ϕ	0.0466	-0.0021	0.0251	0.0442	0.0462	0.2076	0.0613	0.0741
TAS1	λ	-0.1315	-0.0402	-0.0378	0.0411	-0.1134	-0.0273	-0.0515	0.0628
TAS1	R	0.1101	0.0666	-0.0071	0.3464	-0.0223	0.4968	0.1651	0.2099
WITU	ϕ	0.0253	-0.0823	-0.0680	-0.1321	-0.0044	-0.0507	-0.0520	0.0563
WITU	λ	-0.2858	-0.2820	-0.3246	-0.3975	-0.4736	-0.3898	-0.3589	0.0749
WITU	R	-0.2996	-0.4417	-0.3953	-0.1629	-0.3765	-0.3504	-0.3377	0.0978
LOUS	ϕ	0.0000	-0.0702	-0.0421	-0.0972	0.0137	-0.0197	-0.0431	0.0431
LOUS	λ	0.0000	0.0790	0.0445	0.0012	-0.0987	-0.0441	-0.0036	0.0704
LOUS	R	0.0000	-0.1742	-0.0973	0.0684	-0.1024	-0.0262	-0.0663	0.0917
KAVI	ϕ	0.0000	0.0000	0.4177	0.3834	0.0000	0.0000	0.4005	0.0243
KAVI	λ	0.0000	0.0000	-0.0571	-0.0702	0.0000	0.0000	-0.0637	0.0093
KAVI	R	0.0000	0.0000	-1.7377	-1.5332	0.0000	0.0000	-1.6355	0.1446
GUA2	ϕ	0.0000	0.0000	0.0000	0.0000	0.0000	-4.7509	-4.7509	0.0000
GUA2	λ	0.0000	0.0000	0.0000	0.0000	0.0000	-4.3117	-4.3117	0.0000
GUA2	R	0.0000	0.0000	0.0000	0.0000	0.0000	0.1980	0.1980	0.0000
MIS2	ϕ	0.0000	0.0000	0.0000	0.0000	0.0000	0.0735	0.0735	0.0000
MIS2	λ	0.0000	0.0000	0.0000	0.0000	0.0000	-0.0556	-0.0556	0.0000
MIS2	R	0.0000	0.0000	0.0000	0.0000	0.0000	0.0272	0.0272	0.0000

Two solutions are produced by GAMIT: a constrained solution and an unconstrained solution. Constrained solutions are examined during the cleaning/solving process. The unconstrained solution is used by GLOBK. A back solution from GLOBK determines long and short term repeatabilities of sites and baselines. Prior to this, an indication of the daily scatter can be obtained from the constrained GAMIT solutions. For this analysis, a single a priori coordinate file was used so that all days used the same a priori coordinates. Comparisons of the day to day corrections, therefore, gives an indication of daily repeatability of the adjusted coordinates. Table 6.1 shows the comparisons of corrections to coordinates for the 1990 Papua New Guinea sites. TAS1 is included as a typical example of the repeatability of the regional sites. Clearly, the repeatabilities for the Papua New Guinea in the constrained solution are of the order of 5cm in latitude, 7 cm in longitude and 10-15 cm in the radial component. A priori coordinates and velocities were iterated values from a GLOBK analysis of all subsequent data. Constraints were applied to MOJ1, ONSA, WELL, WES1, ORRO, BAKO, XMAS, LOUS and MORE at the level of 0.2 m for the horizontal components and 0.4 m for the height component. All other sites were constrained to ±100 m. Clearly, the corrections to the a priori coordinates do not exceed this.

With the rejected 1990 days included, the standard deviation about the daily mean increased to approximately 15 cm in latitude, 10 cm in longitude and remained in the range of 10-15 cm in radius. Day 214 was particularly problematical, with large corrections (of the order of 0.5 m) to the latitude component of the Papua New Guinea sites.

6.3 GLOBK Processing Strategy

6.3.1 A Consistent Reference Frame

Once the data is clean, it has to be combined into campaign and multi-campaign solutions which are in a consistent reference frame. For this analysis, the reference frame used was ITRF94, epoch 1993.0. The reference frame realisation is performed in GLOBK and GLORG.

The initial GLOBK analysis occurred during the GAMIT processing of each campaign. When sufficient days had been processed in GAMIT, they were also processed in GLOBK to check consistency within the campaign. Any days

which had large χ^2/f values (generally in excess of 10) were investigated further. See below for a description of the χ^2/f value.

However, the major GLOBK analysis occurred once all campaigns were complete. The task of combining all years data into a consistent reference frame was very important for enabling comparisons between different epochs necessary for the tectonic analysis to follow.

Problems were anticipated in attaching the 1990 data to the ITRF94 reference frame, based on the considerable changes that occurred in the global tracking network between 1990 and subsequent campaigns. The extent of the coverage and the number of available satellites can be seen in Figure 6.3 a-d and Figure 6.6. In addition, MIT and other worldwide institutions are also currently attempting to attach the early GPS data to the reference frame, with limited success. The problem is one which has not previously been solved. There were three major steps which led to successful attachment of the 1990 data to ITRF94. The first of these involved determining coordinates for all of the post-1991 sites. The second step involved determining coordinates for the 1990 global tracking sites, and the third involved finding the right combination of constraints to apply in GLORG.

Morgan *et al.* (1996) have produced a Zero Order Network for the Australasian region in the ITRF92 reference frame. All campaigns, from 1990 to 1993 had to be attached to the ITRF94 reference frame and combined with Morgan's data. Since computing that dataset, the UC group has re-analysed all of their data using the latest version of GAMIT, the J2000 celestial reference frame and the Berne orbit model, making their dataset directly comparable with ITRF94 and the work of this thesis. It was a standard procedure to combine the VCV information of this analysis with that of Morgan's analysis to produce a combined solution in ITRF94 from the PNG91 campaign to the latest 1996 solutions from Morgan and his team at the UC. For each successive solution, GLOBK generates a χ^2/f value which gives an indication of the consistency of the parameters in the newly introduced solution with the value of the same parameters accumulated from previous solutions entered into GLOBK. Values over 10 generally indicate that strain is being introduced by one or more of the parameters in the new solution. When the PNG91 to PNG93 data of this analysis was combined with Morgan's data, the χ^2/f values were below 10, indicating that this data did not conflict with Morgan's data.

However, combining the 1990 data proved to be more problematical because of the different global tracking network discussed above. To attach 1990 data to the same reference frame as subsequent years, the global tracking sites observed in 1990 had to be coordinated in ITRF94.

The starting point of the analysis involved trying to establish common sites between the 1990 and subsequent observation epochs. The CIGNET sites were incorporated into both the GIG91 and May 1992 campaigns. Comparisons with a combined VLBI/GPS coordinate list indicated that of all the CIGNET sites observed in 1990, only MOJ1, ONSA, WELL, ORRX, TAS1, and WTZX were possibly reoccupied in GIG91 and May 1992. An iterative procedure was then followed which involved solving in GLOBK, updating coordinates, and re-solving in GLOBK, with trial of constraints applied to different sites.

In hindsight, however, the problem revolved around determining the velocity terms and forcing them onto the 1990 data set, rather than performing a combined least squares solution of the coordinates and velocity terms together. The 1990 data were degraded by a number of factors, including the level of SA, the level of ionospheric scintillation activity, the number of satellites available and the global tracking network. These factors caused scatter in the 1990 solutions, and were initially being absorbed into the estimates of the velocity components. In addition, problems were being introduced by the use of the same site name in the solution for geographically different sites. These sites were able to be detected with the approach of forcing the velocity estimates onto 1990.

With the realisation that the velocity components were critical, GLOBK was run with the GIG91 to May 1996 data sets to transfer the velocity estimates from the modern data to the older data. These values were forced onto the older data. This was done for the sites TAS1, KOKE, MOJ1 and WES1. TSU1 was left to adjust freely to act as a test site. Forcing the velocity estimates from modern data in this way allowed the position of these sites to be determined at an epoch near 1991.8, which was propagated back to the 1990 epoch. This propagation over approximately one year minimised the detrimental effects of serious errors in the adopted velocity models, and allowed the transfer of coordinates for the global network to be transferred from the post-1992 period to the pre-1992 period. These a priori coordinates for the 1990 epoch allowed

the successful orbit improvement and adjustment required for a reliable solution.

Until coordinates were determined for the 1990 CIGNET sites, the strength of the 1990 solution was an issue which was temporarily resolved by combining the six days of 1990 observations into a single h-file. Figure 6.4 below clearly illustrates why combining the h-files improved the strength of the solution. All six days combined contain fewer observations than one day of 1996 data!

A side issue raised in Figure 6.4 concerns the lower number of observations per day for the 1991 campaign relative to the 1990 PNG campaign and GIG91. This is a result of not observing concurrently with a major global or regional campaign, as the PNG90 and GIG91 campaigns were. With current extensive coverage of global tracking stations, this is no longer an issue.

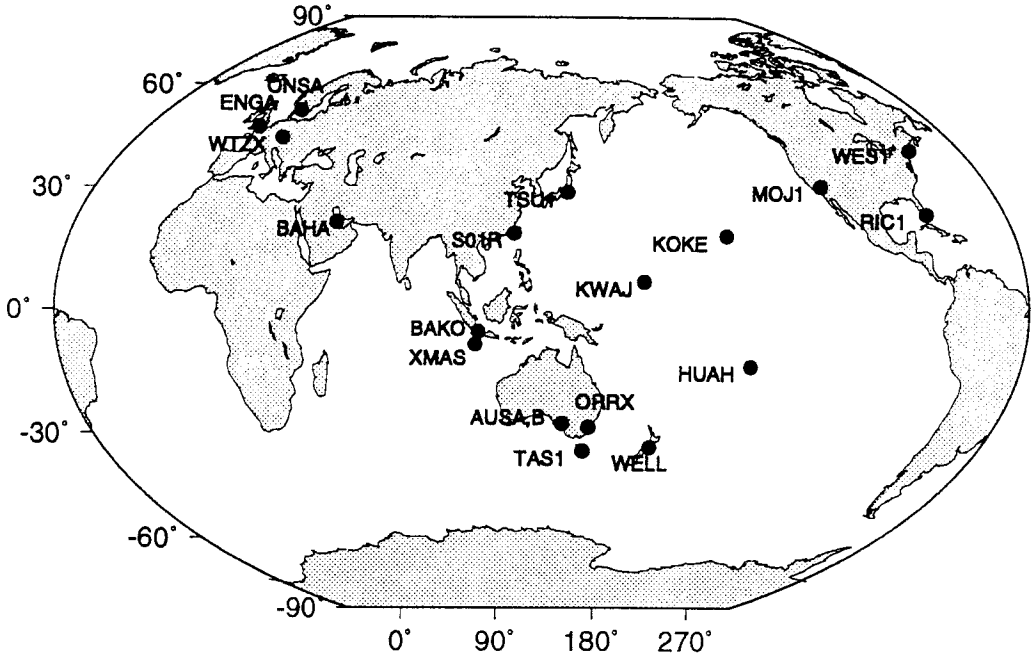

(a) 1990 Global Tracking Network

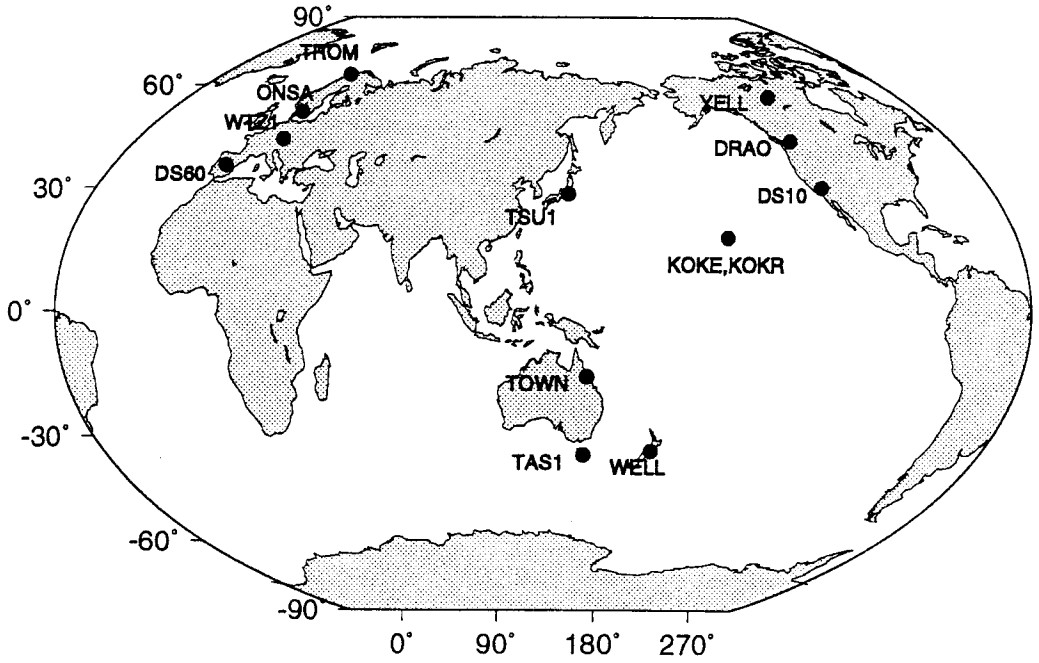

(b) 1991 Global Tracking Network

Figure 6.3 a-b The global tracking network available for processing in 1990, 1991, 1992, 1993.

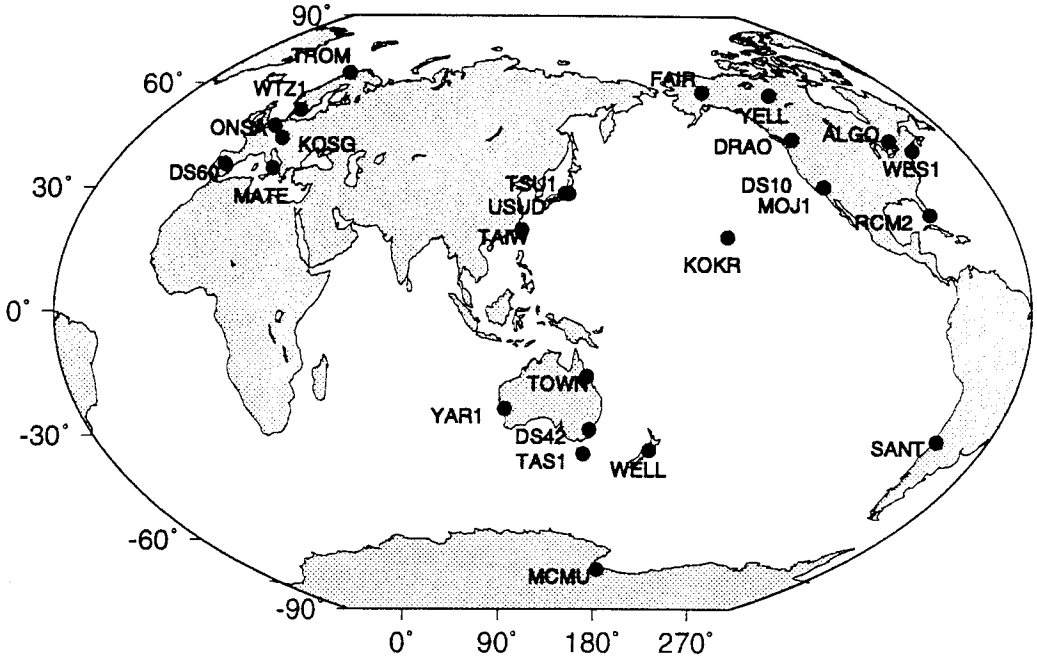

(c) 1992 Global Tracking Network

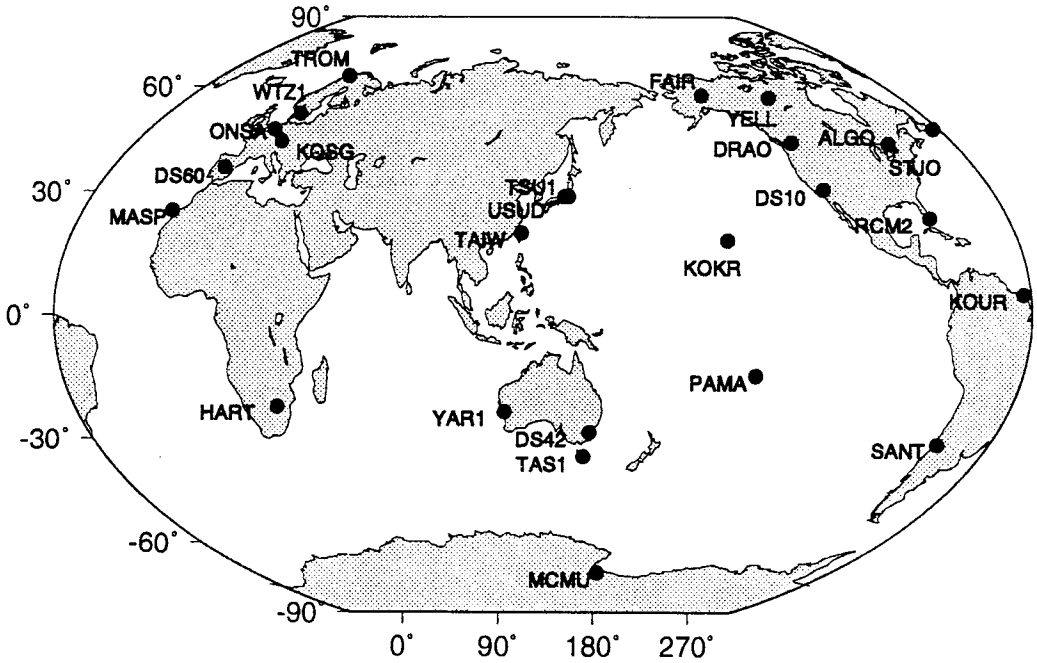

(d) 1993 Global Tracking Network

Figure 6.3 c-d The global tracking network available for processing in 1990, 1991, 1992, 1993.

Clearly, with the exception of PNG91, there is a steady increase in the number of observations available for processing with the passage of time because of the growth in the satellite constellation and available global tracking sites. Although PNG91 contained relatively fewer observations per day than the 1990 data set, the global tracking sites used were common with those used in the later campaigns. This can be seen in Figure 6.3a-d. In this regard, Figure 6.5 below is also misleading, because although 1990 has 18 global tracking sites, the fact that only KOKE, WES1, MOJ1 and TAS1 and TSU1 were able to be related to later tracking networks means that reference frame determination was not a straightforward procedure. In addition, data from Bahrain was extremely limited and the connection between the small European network and the Pacific network was weak.

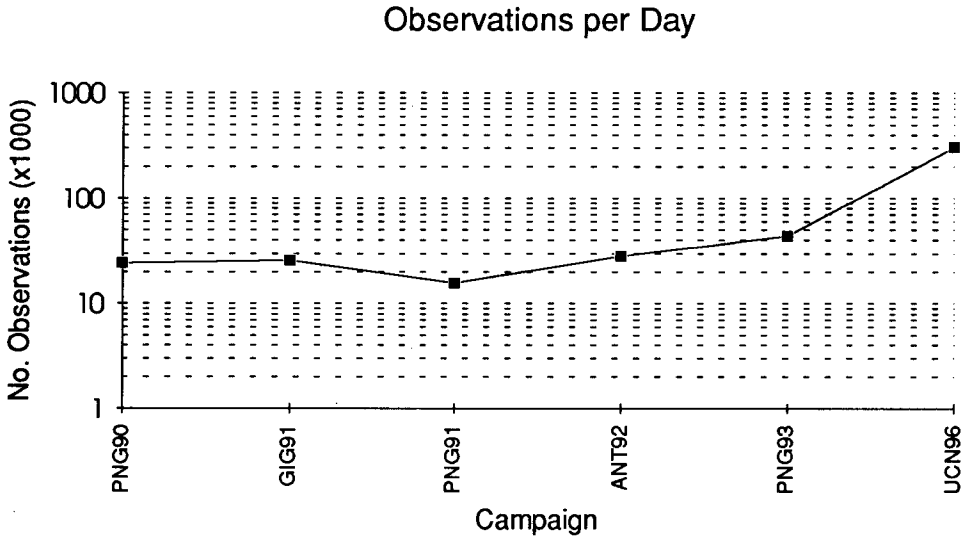

Figure 6.4 The mean number of observations per day from the 1990 campaign to the present. The low number of observations in 1991 is a result of not observing concurrently with a major global or regional campaign, as the PNG90 and GIG91 campaigns were.

However, once the reference frame had been correctly defined for the 1990 data, the data was entered into the final solution in separate daily h-files. The correctly defined reference frame gave sufficient strength to the solution to avoid the scatter of daily solutions, discussed shortly.

There were various indications that the reference frame issues for 1990 were unresolved, which dictated the approach taken in the solutions.

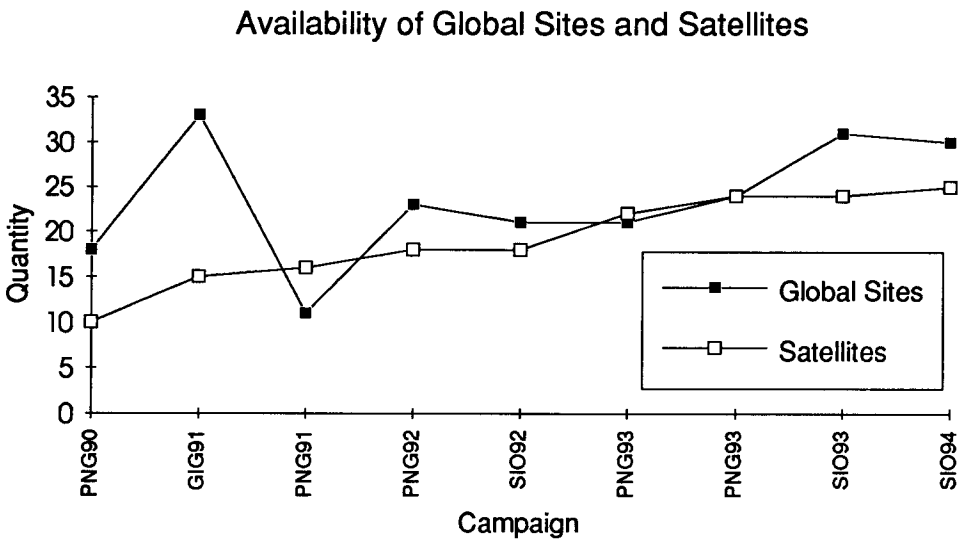

Figure 6.5 The availability of global tracking stations and satellites from 1990 to 1994. The relatively high number of global tracking sites available in 1990 is misleading because most of them did not form a part of subsequent global tracking network. Four sites in 1990 were able to be related to the reference frame from subsequent campaigns.

Firstly, high χ^2/f values in subsequent solutions indicated that there was strain being introduced by the reoccupied sites. The site(s) causing the problem had to be isolated. In this way, iterative solutions revealed that five of the CIGNET sites were able to be reliably coordinated. These were MOJ1, WES1, KOKE, TAS1 and TSU1. TSU1, as mentioned above, was used as a test site and allowed to adjust freely. In the final solution, this site behaved as expected, giving an additional indication that the reference frame issues had been correctly resolved.

Distortions introduced into the network also indicated reference frame problems. For example, the 1990 location of Losuia appeared to be 0.5 - 1 m in error in some solutions. Renaming the site in 1990 removed the strain with subsequent data but did not resolve the problem. Losuia is a well determined site with several subsequent reoccupations. Comparisons of baselines to Losuia, both the apparent 1990 position and the consistent 1991-1993 position, were made with the 1990 GPS baseline results of McClusky (1993). These revealed that the 1990 GLOBK estimate was incorrect. As a comparison between McClusky's results and those of a 1990-only GLOBK solution had revealed no discrepancies, the distortion was being introduced when 1990 data was fitted to the reference frame. Comparisons with McClusky's results are shown in Figure 6.6, and are discussed in more detail below.

The scatter of the daily solutions for 1990 was a further indication of problems in the solution. Clearly, if the constraints applied in GLOBK are insufficient, the daily solutions will vary considerably from day to day. This is indeed what was happening with the 1990 solutions. Repeatability plots from the back solution indicate variations of up to 2 m in position from day to day. Standard deviations were also large, particularly for the east component, ranging from approximately 0.3 m to 1 m. This problem was temporarily overcome by combining the six 1990 h-files into a single VCV matrix, as mentioned above. This step, however, did not solve the problem.

Initially, GLOBK was run with tight constraints on the CIGNET and IGS core sites. Although the reference frame was to be finally determined in GLORG, the iterative procedure of obtaining reliable coordinates for the 1990 sites required the reference frame to be defined in GLOBK. When the 1990 coordinates appeared to be resolved in the tight GLOBK solutions, a loose GLOBK solution was run which showed insignificant movement of the 1990 sites, thus the determined positions were correct. Table 6.5a-b gives the results of the two solutions for comparison.

As discussed above, the velocity terms were critical in transferring the reference frame to the pre-1992 data. Although GPS solutions are over-determined, the GLOBK analysis is not. Where there are two observations of a site, there are six data elements: coordinates for each occupation. For each site, a position and velocity in ITRF94 was being solved: 6 parameters. This leaves no redundancy. By equating the velocities, three of the parameters are removed, thus introducing redundancy into the system. The success of the procedure was verified in the final GLOBK solutions, in which the 1990 χ^2/f values for the 1990 data were no different from the 1992 and subsequent data.

The final solution was run with 296 experiments ranging from 1990 to May 1996. GLOBK was run with loose constraints applied. The constraints and a priori coordinates used are shown in Appendices 8 and 11 respectively. The 13 core IGS sites were entered with ITRF94 coordinates at epoch 1993.0. Sites which were to have their velocities forced in the GLORG run were entered with the same starting velocities as the sites to which they were to be forced. GLORG forces the corrections to be equal, thus if sites are to have the same output velocities, their a priori velocities must also be equal. The reference frame was determined in GLORG by tightly constraining seven of the 13 IGS

core sites to the ITRF94 position and forcing the velocities of these sites to the ITRF94 values. These sites were Yarragadee, Santiago and Tidbinbilla in the Southern Hemisphere and Kootwijk, Yellowknife, Kokee Rogue and Tromso in the Northern Hemisphere. Other sites had their velocities equated, which forces the corrections to the velocity components of the equated sites to be equal. This approach is used where one site is well determined, while a connected site is less well determined. For example, of the stations located at Richmond, RIC1 and RCM2 had their velocity components equated to those of RCM5, the better defined station. A full list of the equate commands applied is shown in the GLORG command file contained in Appendix 9.

6.3.2 Final Station Positions and Velocities with Formal Precisions

The cartesian positions and velocities for all sites are contained in Appendix 1. The epoch to which each coordinate refers is also shown. Appendix 2 shows the coordinates in the form of latitude, longitude and height. These refer to the same epoch as the coordinates shown in Appendix 1. Table 6.2 summarises the site positions and formal precisions of the sites in Papua New Guinea. Figure 7.1 shows the absolute velocities from the final GLOBK/GLORG solution. Appendix 3 shows the calculation of the velocity residuals.

6.3.3 Precision Indicators of the Final Results

The precision of the results should give an indication of the quality of the position and velocity estimates for each site. The precision estimates taken from the GLORG solution are formal uncertainties. These are well known for being notoriously optimistic! The problem, then, is to find a more realistic expression of the quality of the solution.

An alternative precision indicator can be obtained from a GLOBK back solution. In a back solution, parameters can be modelled as a random walk. To obtain the daily repeatability of the site positions, the coordinates are estimated as Markov parameters, and the quantity given to constrain the random walk is the power spectral density (PSD) of the white noise driving the random walk in units of m^2/y. The repeatability of the site coordinates for Port Moresby, Morobe and Losuia obtained from the back solutions run in this analysis can be seen in Figures 6.7, 6.8 and 6.9 respectively. The line of best fit through successive

Table 6.2 The geodetic coordinates of all sites in the Papua New Guinea surveys. The heights are based on the WGS84 ellipsoid. The standard deviations given are the formal uncertainties on the ENU components from the solution. The epoch for each site is the same as shown in Table 6.3.

Site	Latitude ° ' "	Longitude ° ' "	Ellipsoid Height	σLat (mm)	σLon (mm)	σHt (mm)
TASP	- 4 36 15.44585	159 26 46.70166	63.2587	1.9	5.6	9.9
CART	- 4 47 02.65480	155 27 50.07841	68.0663	1.4	4.2	7.5
NUGU	- 3 20 07.55530	154 40 28.13538	67.4168	1.4	3.9	6.3
GUA2	- 9 13 30.16594	152 56 37.21806	78.6605	29.7	109.6	227.3
GUA1	- 9 13 30.01113	152 56 37.35578	78.6344	4.2	12.3	27.9
MIS1	-10 41 17.39817	152 50 21.39955	81.1766	2.1	5.3	11.7
MISI	-10 41 19.90784	152 49 58.93701	87.4769	4.9	12.5	16.4
RABL	- 4 11 28.68904	152 09 44.86859	266.9281	1.5	4.4	7.4
JACQ	- 5 38 42.75860	151 30 19.60423	151.6128	6.0	19.7	28.3
BUNA	-10 09 07.78247	151 09 16.71222	131.2954	2.1	5.9	13.6
LOUS	- 8 32 07.26388	151 07 30.81578	85.1889	4.2	12.2	16.2
WARI	-10 57 20.60591	151 04 54.56236	174.3355	2.3	6.2	13.3
HAIN	-10 40 34.15318	151 03 43.92573	122.1557	2.2	6.2	13.8
URAS	- 9 12 20.15201	150 51 31.78907	145.0454	2.3	6.5	13.5
KAVI	- 2 34 53.06670	150 48 22.53604	78.8867	3.1	7.2	11.4
ALT1	-10 18 48.40946	150 27 26.83823	96.8747	5.7	14.6	35.9
ALT2	-10 18 37.51053	150 20 18.08942	94.8772	2.8	6.9	16.0
WATA	- 9 12 38.48661	150 14 33.02804	80.9149	2.1	5.7	12.7
WITU	- 4 41 17.84987	149 26 08.76090	84.2754	2.6	6.3	9.0
MORO	- 7 44 31.65491	147 35 22.96886	79.7353	4.2	11.9	21.4
MANU	- 2 03 02.29493	147 21 37.63659	129.8081	3.0	8.0	15.3
MORE	- 9 26 02.77100	147 11 12.19980	116.6390	1.7	3.1	5.2
UNIT	- 6 40 16.97028	146 59 52.37464	130.4139	2.7	6.7	15.4
WANK	- 6 08 52.07314	146 04 52.44181	510.0441	0.8	1.8	4.7
MADA	- 5 12 41.28939	145 46 56.19266	73.3383	0.7	1.4	3.7
MADG	- 5 09 43.80438	145 44 55.29454	460.9128	2.9	8.2	11.3
GOKA	- 6 04 53.07267	145 23 30.44603	1664.6260	0.7	1.5	4.0
KIKO	- 7 25 24.65412	144 14 55.76588	88.9980	0.8	1.9	4.6
WEWK	- 3 35 02.58477	143 40 00.14729	83.9543	0.7	1.7	3.2
MEND	- 6 08 36.73543	143 39 22.16528	1815.1874	0.7	1.6	3.8
WUVU	- 1 44 07.59585	142 50 10.07835	79.1020	0.8	1.6	3.7
KOPI	- 5 23 09.08504	142 29 42.19021	1412.8709	1.0	2.4	4.9
VANI	- 2 41 05.28331	141 18 15.65479	80.6111	3.3	8.6	18.8
AIAM	- 7 20 51.82090	141 16 01.44710	95.4951	3.1	8.1	18.3
AMAN	- 3 35 18.78215	141 12 54.33026	477.3260	0.8	2.3	4.3

Table 6.3 Final cartesian coordinates and formal uncertainties for the sites in the Papua New Guinea region.

Site	X (m)	Y (m)	Z (m)	Epoch	σX (mm)	σY (mm)	σZ (mm)
TASP	-5953042.278	2232112.211	-508584.358	1993.445	9.4	6.2	2.0
CART	-5782172.476	2639487.543	-528398.673	1992.348	7.0	4.8	1.6
NUGU	-5755507.864	2723752.869	-368612.803	1992.350	6.0	4.3	1.4
GUA2	-5607198.747	2863957.602	-1015751.287	1990.918	16.9	13.7	4.6
GUA1	-5607201.316	2863954.194	-1015746.588	1991.631	24.8	16.9	6.6
MIS1	-5577078.153	2861397.516	-1175144.143	1991.623	10.5	7.0	3.1
MISI	-5576759.293	2862001.148	-1175221.086	1992.565	3.6	2.5	1.2
RABL	-5625280.814	2970585.522	-463064.801	1992.346	7.1	5.0	1.6
JACQ	-5578632.258	3028263.693	-623240.731	1991.853	5.4	4.3	1.6
BUNA	-5499983.628	3029313.986	-1116842.453	1991.629	12.2	8.0	3.2
LOUS	-5523811.492	3046135.335	-940385.344	1992.154	4.8	3.7	1.5
WARI	-5481915.890	3028449.672	-1204231.327	1991.627	11.8	8.2	3.5
HAIN	-5485912.247	3033109.945	-1173846.013	1991.611	12.3	8.3	3.4
URAS	-5499656.374	3066247.540	-1013638.606	1991.611	12.4	8.1	3.3
KAVI	-5562412.947	3107930.006	-285346.189	1993.272	3.7	2.6	0.8
ALT1	-5459929.353	3094433.681	-1134392.547	1991.598	34.1	17.8	7.8
ALT2	-5453535.752	3105804.869	-1134062.724	1993.196	3.9	2.6	1.1
WATA	-5466222.433	3125151.861	-1014184.388	1991.627	11.4	7.6	3.0
WITU	-5473775.519	3232571.407	-517844.616	1990.579	8.2	7.2	2.7
MORO	-5335932.381	3387629.598	-853539.800	1992.132	5.8	5.0	1.8
MANU	-5367596.440	3437943.342	-226704.965	1993.109	5.1	3.7	1.0
MORE	-5288519.162	3409952.866	-1038574.347	1993.507	1.2	1.0	0.5
UNIT	-5313156.693	3450683.564	-736065.733	1994.007	2.7	2.1	0.9
MADA	-5252527.402	3571989.734	-575482.742	1993.662	2.9	2.3	0.8
MADG	-5251159.309	3575562.442	-570087.963	1990.572	10.0	9.5	3.1
WANK	-5262950.502	3539058.669	-678565.326	1993.666	4.0	2.9	1.0
GOKA	-5221573.462	3603226.563	-671387.071	1993.659	3.3	2.6	0.9
KIKO	-5133225.773	3695553.761	-818612.360	1993.657	4.0	3.0	1.0
WEWK	-5128211.338	3771635.400	-396055.907	1993.639	2.7	2.3	0.7
MEND	-5109574.920	3759378.933	-678236.519	1993.655	3.2	2.5	0.8
WUVU	-5080555.015	3851303.618	-191869.029	1993.651	3.1	2.6	0.8
KOPI	-5038707.359	3867027.412	-594810.727	1993.647	4.2	3.4	1.0
AMAN	-4962464.869	3987772.548	-396577.084	1993.631	3.7	3.2	0.9
VANI	-4972629.909	3983208.172	-296767.244	1993.321	2.5	2.2	0.7
AIAM	-4934886.487	3958248.627	-810301.129	1993.395	2.4	2.0	0.8

yearly estimates of the position can represent the velocity of the site if the a priori values are zero. The remaining site repeatability plots are contained in Appendix 4. It is believed that the estimates of precision obtained from these site repeatability values represent upper bounds of precision, and are therefore pessimistic values. The back solution was performed with standard PSD values applied to all sites estimated as Markov parameters. If these were to have been

optimised, it is felt that the repeatability estimates would have been more realistic estimates of the precision of the coordinates and velocity estimates.

With a lower bound on the precision from the formal uncertainties from the forward solution, and an upper bound from the daily repeatability from the back solution, some compromise had to be found. The scaling adopted, and the justification of it are discussed in Chapter 7.

6.3.4 GLOBK/GLORG Quality Assurance

Confidence in the 1990 results

The internal consistency of the 1990 data can be verified by two methods. Firstly, a GLOBK analysis on the six days used in this campaign showed that the campaign was internally consistent. χ^2/f values were below 5.

Also, comparison of the baseline lengths with those of McClusky (1993) showed differences of under 17 cm, with the majority of lines being different by less than 5 cm. These results are shown in Figure 6.6. The approximate 10 cm differences involved the site Guasopa. The 5-10 cm differences involved Madang. These were only observed for 1 and 2 days respectively in 1990 and are therefore weakly determined. Other comparisons were below 5 cm. Although from Figure 6.6 there appears to be a scale factor between the 1990-only GLOBK solution and the values computed by McClusky (1993), when calculated, the scale factor is -0.769 ± 1.069 parts in 10^7, which is not significantly different from zero.

The agreement between this analysis and McClusky (1993) gave confidence in the results because McClusky's results were obtained in Bernese Version 3.3, whilst those for this analysis were obtained in GAMIT 9.40. Thus independent packages had given the same results. Small differences were expected due to different modelling and editing techniques between the latest GAMIT package, and an old version (by today's standards) of Bernese.

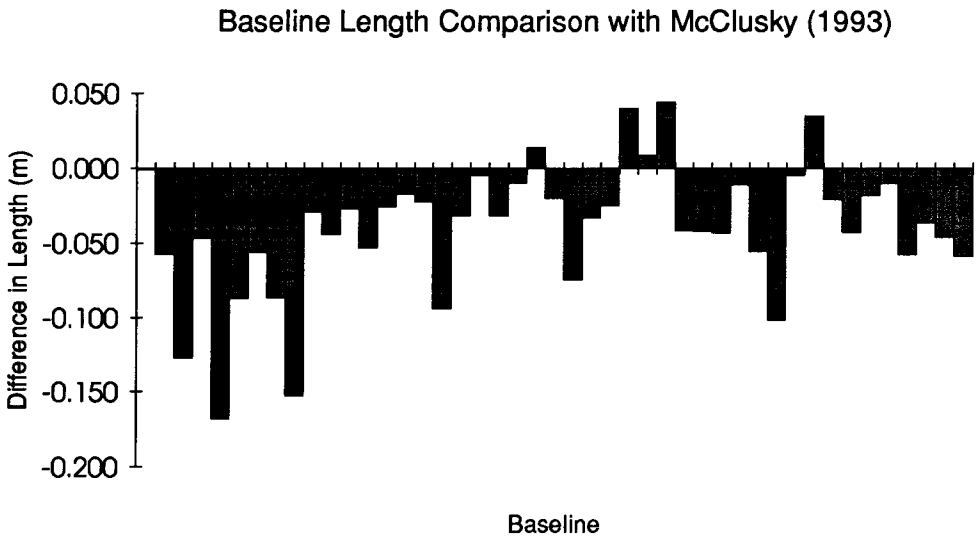

Figure 6.6 Shows the comparison between baseline lengths from McClusky (1993) and the GLOBK on the 1990 campaign.

The quality of the connection of the 1990 data to the reference frame is indicated by comparing solutions in which GLOBK is run with loose and tight constraints respectively. The constraints applied in each solution are shown in Table 6.4. The coordinates and standard deviations from each solution are shown in Table 6.5a-b. Clearly, the two sets of coordinates differ by less than 4 cm, which indicates the reference frame for the 1990 solutions alone is stable at the 5 cm level or better. To obtain this level of stability, the a priori coordinates and site velocities determined for the 1990 sites from the iterative solutions of the subsequent data must be correctly related to the reference frame. The good agreement between loosely and tightly constrained solutions suggests that the reference frame has been consistently defined in 1990 and later years.

There are several features to note about Tables 6.5 and 6.6. Comparing Tables 6.5a and 6.5b reveals that the greatest differences are in the precisions, rather than the coordinate values. The precisions for sites in the tight GLOBK solution are relatively uniform, and approximately 5 cm in magnitude. This indicates that the system is relatively well connected to the reference frame. In contrast, the precisions for the X and Y coordinates in the loosely constrained solution are up to approximately 0.5 m. This indicates that the system is weakly located about the Z-axis, which means that there is uncertainty in UT1. It was stated above that only the UT1 rate was solved for, and thus tighter station constraints

Table 6.4 Constraints applied to the GLOBK solution of the 1990 data in both the loosely constrained solution and the tightly constrained solution. Both solutions contain only 1990 data. The initial constraint applied to all sites is over-ridden by the constraints for individual sites.

Constraint type	Applied To	N	E	U	N rate	E rate	U rate
1990 Solution with Loose Constraints Applied:							
NEU	all	9.0	9.0	9.0	0.0	0.0	0.0
The CIGNET sites in PNG90							
NEU	KOKE	1.0	1.0	1.0	0.0	0.0	0.0
NEU	TAS1	1.0	1.0	1.0	0.0	0.0	0.0
NEU	MOJ1	1.0	1.0	1.0	0.0	0.0	0.0
NEU	WES1	1.0	1.0	1.0	0.0	0.0	0.0
NEU	WELL	1.0	1.0	1.0	0.0	0.0	0.0
NEU	MORE	1.0	1.0	1.0	0.0	0.0	0.0
NEU	LOUS	1.0	1.0	1.0	0.0	0.0	0.0
1990 Solution with Tight Constraints Applied:							
NEU	ALL	9.0	9.0	9.0	0.0	0.0	0.0
The CIGNET sites in PNG90							
NEU	KOKE	0.10	0.10	0.10	0.0	0.0	0.0
NEU	TAS1	0.10	0.10	0.10	0.0	0.0	0.0
NEU	MOJ1	0.10	0.10	0.10	0.0	0.0	0.0
NEU	WES1	0.10	0.10	0.10	0.0	0.0	0.0
NEU	WELL	0.10	0.10	0.10	0.0	0.0	0.0
NEU	MORE	0.20	0.20	0.20	0.0	0.0	0.0
NEU	LOUS	0.20	0.20	0.20	0.0	0.0	0.0

Table 6.5a Coordinates of the global sites from the 1990-only GLOBK solution with loose constraints applied to the CIGNET sites. Formal uncertainties are shown.

Site	X	Y	Z	σX (mm)	σY (mm)	σZ (mm)
1990 Solution with Loose Constraints Applied:						
ENGA	3981774.9269	-89252.1924	4965291.3558	63.4	326.2	132.8
WES1	1492233.1503	-4458088.5074	4296048.0863	360.3	131.3	128.4
RIC1	961309.5665	-5674075.8165	2740538.9952	456.6	95.6	127.8
MOJ1	-2356215.7894	-4646736.6931	3668456.2238	374.4	192.3	126.8
HUAH	-5345885.5086	-2958242.0025	-1824597.9407	242.8	427.9	126.9
KOKE	-5543818.0980	-2054583.0160	2387858.2780	172.5	443.3	125.9
WELL	-4780648.8390	436507.2020	-4185440.4839	64.5	383.1	129.4
KWAJ	-6160865.2304	1339912.1958	960841.9535	118.1	491.9	127.8
GUA2	-5607198.8464	2863957.7495	-1015751.3245	235.0	448.2	128.0
MISI	-5576759.3105	2862001.3546	-1175221.2019	234.9	445.8	128.1
JACQ	-5578632.3399	3028263.8445	-623240.6650	247.1	445.6	127.9
LOUS	-5523811.5242	3046135.4968	-940385.4574	248.6	441.3	127.9
KAVI	-5562413.0688	3107929.9643	-285346.2686	253.5	444.4	127.8
WITU	-5473775.6389	3232571.5546	-517844.6203	263.2	437.3	127.8
ORRX	-4446476.6280	2678104.9097	-3696261.9747	220.8	356.4	128.6
MORO	-5335932.4224	3387629.7636	-853539.8984	275.4	426.4	127.9
TAS1	-3950184.0408	2522364.6526	-4311588.6172	209.0	317.5	128.8
MANU	-5367596.5205	3437943.3075	-226705.0288	279.3	428.9	127.7
MORE	-5288519.2810	3409953.1452	-1038574.5372	277.2	422.6	127.9
MADG	-5251159.4280	3575562.5898	-570087.9623	290.2	419.7	127.8
TSU1	-3957193.7986	3310191.4560	3737733.3581	269.3	317.6	128.0
AUSA	-3942242.0621	3468859.6581	-3608197.2080	282.9	317.4	128.4
AUSB	-3942242.0299	3468859.5328	-3608197.1374	283.0	317.1	129.6
S01R	-2886619.1670	5082945.4657	2543377.6781	409.6	234.0	127.8
BAKO	-1836968.8064	6065617.4533	-716257.7429	488.2	154.1	126.8
XMAS	-1696462.9366	6039563.2606	-1149236.2820	486.1	143.1	126.8
BAHA	3633911.1658	4425278.0125	2799862.4337	382.3	307.4	143.4
WTZX	4075552.6433	931825.9144	4801589.1171	94.6	332.8	131.8
ONSA	3370658.9336	711877.1713	5349786.7703	82.1	277.8	132.9

Table 6.5 b Coordinates of the global sites from the 1990-only solution with tight constraints applied to the CIGNET sites. Formal uncertainties are shown.

Site	X	Y	Z	σX (mm)	σY (mm)	σZ (mm)
1990 Solution with Tight Constraints Applied:						
ENGA	3981774.9051	-89252.2055	4965291.3743	55.6	75.0	57.3
WES1	1492233.1167	-4458088.5052	4296048.1020	58.0	47.5	47.5
RIC1	961309.5289	-5674075.8102	2740539.0116	68.3	49.0	48.0
MOJ1	-2356215.8217	-4646736.6835	3668456.2429	57.0	41.5	46.6
HUAH	-5345885.5226	-2958242.0107	-1824597.9223	52.9	63.2	46.9
KOKE	-5543818.1141	-2054583.0095	2387858.2946	47.5	63.7	46.7
WELL	-4780648.8414	436507.1832	-4185440.4694	41.2	56.1	47.3
KWAJ	-6160865.2342	1339912.1923	960841.9661	42.9	66.7	46.7
GUA2	-5607198.8439	2863957.7390	-1015751.3126	54.6	63.2	46.7
MISI	-5576759.3077	2862001.3436	-1175221.1899	54.6	62.8	46.7
JACQ	-5578632.3377	3028263.8345	-623240.6534	52.9	61.1	46.5
LOUS	-5523811.5213	3046135.4858	-940385.4457	53.2	60.6	46.5
KAVI	-5562413.0669	3107929.9548	-285346.2572	54.4	61.7	46.5
WITU	-5473775.6363	3232571.5443	-517844.6088	54.6	60.4	46.4
ORRX	-4446476.6234	2678104.8904	-3696261.9616	51.9	53.5	47.0
MORO	-5335932.4190	3387629.7522	-853539.8869	55.9	59.2	46.5
TAS1	-3950184.0359	2522364.6302	-4311588.6033	51.1	50.9	47.0
MANU	-5367596.5180	3437943.2973	-226705.0176	56.6	60.0	46.5
MORE	-5288519.2772	3409953.1334	-1038574.5257	56.3	58.8	46.5
MADG	-5251159.4246	3575562.5787	-570087.9510	57.9	59.0	46.5
TSU1	-3957193.8044	3310191.4490	3737733.3694	58.1	52.0	47.6
AUSA	-3942242.0551	3468859.6374	-3608197.1954	59.5	54.9	47.7
AUSB	-3942242.0230	3468859.5117	-3608197.1244	60.4	53.2	49.9
S01R	-2886619.1672	5082945.4515	2543377.6887	74.1	47.6	47.4
BAKO	-1836968.7977	6065617.4345	-716257.7319	84.5	46.6	46.9
XMAS	-1696462.9273	6039563.2414	-1149236.2710	83.8	44.7	46.9
BAHA	3633911.1727	4425278.0015	2799862.4599	153.6	104.2	79.4
WTZX	4075552.6236	931825.9012	4801589.1365	53.1	72.8	54.7
ONSA	3370658.9135	711877.1587	5349786.7897	53.1	68.2	55.9

Table 6.6 Coordinates of the Papua New Guinea and regional sites from the 1990-only solution with both loose and tight constraints applied to the CIGNET sites in GLOBK. The reference frame has been enforced in GLORG, in the same way for both solutions, thus the differences are due to the different constraints applied in GLOBK. The differences at these sites are typical of the differences for all sites. Formal uncertainties are shown.

Site	X	Y	Z	σ_X	σ_Y	σ_Z
1990 Solution with Loose Constraints Applied in GLOBK						
WELL	-4780648.788	436507.058	-4185440.478	0.016	0.013	0.010
KWAJ	-6160865.222	1339912.150	960841.957	0.019	0.016	0.009
GUA2	-5607198.806	2863957.666	-1015751.332	0.023	0.022	0.010
MISI	-5576759.268	2862001.268	-1175221.209	0.022	0.021	0.010
JACQ	-5578632.306	3028263.768	-623240.674	0.015	0.016	0.009
LOUS	-5523811.486	3046135.414	-940385.466	0.015	0.016	0.009
KAVI	-5562413.040	3107929.892	-285346.278	0.019	0.018	0.010
WITU	-5473775.606	3232571.479	-517844.630	0.016	0.016	0.009
ORRX	-4446476.565	2678104.785	-3696261.982	0.013	0.012	0.012
MORO	-5335932.384	3387629.683	-853539.908	0.015	0.016	0.009
TAS1	-3950183.974	2522364.516	-4311588.624	0.011	0.008	0.013
MANU	-5367596.491	3437943.236	-226705.039	0.017	0.018	0.009
MORE	-5288519.240	3409953.062	-1038574.547	0.015	0.016	0.010
MADG	-5251159.393	3575562.513	-570087.973	0.017	0.018	0.010
1990 Solution with Tight Constraints Applied in GLOBK						
WELL	-4780648.792	436507.062	-4185440.481	0.015	0.013	0.013
KWAJ	-6160865.222	1339912.152	960841.956	0.019	0.016	0.009
GUA2	-5607198.807	2863957.668	-1015751.334	0.023	0.022	0.010
MISI	-5576759.268	2862001.270	-1175221.211	0.022	0.021	0.010
JACQ	-5578632.306	3028263.770	-623240.675	0.015	0.016	0.009
LOUS	-5523811.486	3046135.416	-940385.468	0.015	0.016	0.009
KAVI	-5562413.040	3107929.894	-285346.279	0.019	0.018	0.009
WITU	-5473775.606	3232571.481	-517844.631	0.016	0.016	0.009
ORRX	-4446476.567	2678104.787	-3696261.985	0.012	0.012	0.012
MORO	-5335932.384	3387629.685	-853539.910	0.015	0.016	0.009
TAS1	-3950183.977	2522364.518	-4311588.627	0.011	0.008	0.012
MANU	-5367596.490	3437943.238	-226705.040	0.017	0.018	0.009
MORE	-5288519.240	3409953.064	-1038574.548	0.015	0.016	0.010
MADG	-5251159.393	3575562.515	-570087.974	0.017	0.018	0.010

are required to specify the position of the system in the terrestrial reference frame.

Table 6.6 and Figure 6.7 clearly show that there is no significant difference between the loosely and tightly constrained GLOBK solutions once they have been attached to the ITRF94 reference frame by GLORG. That is, GLORG makes the two systems coincident by removing the rotation. The approach of applying loose constraints in GLOBK has the advantage that the stations can assume a natural, or unforced position in the GLOBK adjustment and GLORG can then be used to define the reference frame on these unforced positions.

Table 6.6 also shows that the internal consistency of the 1990 solution appears to be approximately 2 cm for each component. This is a significant advance on most other work in 1990 in which the internal precisions in a global reference frame are closer to 5 cm.

The transformation parameters from GLORG are shown for three solutions in Figure 6.7. These solutions are both of the 1990-only solutions (with tight and loose GLOBK constraints respectively), and the final combined 1990-1996 solution. Figure 6.7 shows several important features. Firstly, a comparison between the tight and loose 1990 solution transformation parameters reveals that they are not significantly different. This means that the reference frame is consistent between the 1990 solutions, and is not unduly influenced by the level of constraints applied in GLOBK. Secondly, the 1990-only solutions have transformation parameters consistent with the combined 1990-1996 solution, in translation, scale and X-rotation. Although the Y and Z rotations are statistically different, it must be remembered that the units are milliarcseconds, which confirms the statement above that the reference frame for the 1990-only solutions is stable to 5 cm or better.

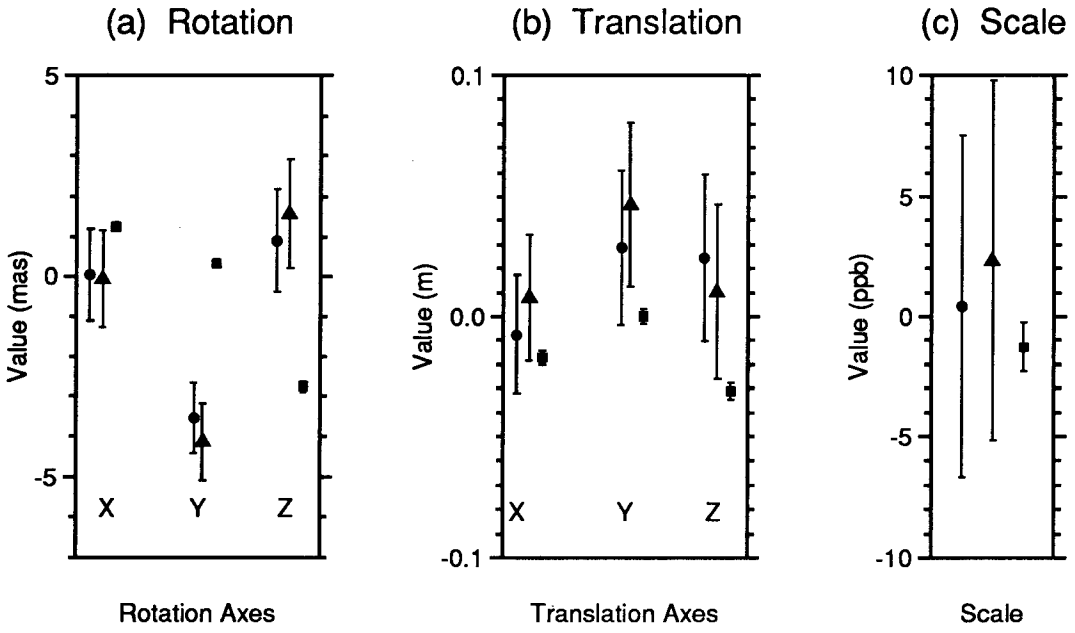

Figure 6.7 Graph showing the transformation parameters from GLORG for three solutions: 1. - 1990 tight GLOBK solution (circles)
2. - 1990 loose GLOBK solution (triangles)
3. - final combined 1990-1996 solution (squares)

Confidence in the final results

External consistency of the 1990 data with all subsequent data is indicated by several factors.

Firstly, the χ^2/f values indicate that there is no strain between any of the campaigns. All χ^2/f values were below 12.5, with 30% below 1.0 and 93% below 5.0.

The χ^2/f value for the total solution was 1.837.

The adjustments to the unconstrained global sites are shown in Table 6.7. The position corrections are generally under 10 mm. DS10 and ALGO are exceptions to this. DS10 is also exceptional in the corrections to the site velocity components. Velocity corrections to all other sites are generally under 5 mm/y. The adjustments to these test sites indicate that the reference frame is stable to the level of 10 mm.

Table 6.7 Adjustments to the unconstrained IGS Core site positions and velocities. Formal uncertainties are shown.

Site	Component	Units	Value	Adjustment	Std Dev.
DS60	X- coord.	(m)	4849202.4836	0.0002	0.0008
DS60	Y- coord.	(m)	-360329.1287	-0.0011	0.0006
DS60	Z- coord.	(m)	4114913.0932	0.0069	0.0007
DS60	X-rate	(m/yr)	-0.0082	-0.0020	0.0005
DS60	Y-rate	(m/yr)	0.0186	-0.0013	0.0003
DS60	Z-rate	(m/yr)	0.0102	-0.0025	0.0004
ALGO	X- coord.	(m)	918129.5287	0.0054	0.0005
ALGO	Y- coord.	(m)	-4346071.2259	0.0201	0.0006
ALGO	Z- coord.	(m)	4561977.8101	-0.0125	0.0006
ALGO	X-rate	(m/yr)	-0.0140	0.0018	0.0003
ALGO	Y-rate	(m/yr)	-0.0017	0.0034	0.0004
ALGO	Z-rate	(m/yr)	0.0008	-0.0027	0.0004
DS10	X- coord.	(m)	-2353614.1684	-0.0347	0.0007
DS10	Y- coord.	(m)	-4641385.4238	-0.0208	0.0008
DS10	Z- coord.	(m)	3676976.4813	0.0153	0.0007
DS10	X-rate	(m/yr)	-0.0213	-0.0067	0.0004
DS10	Y-rate	(m/yr)	-0.0083	-0.0113	0.0005
DS10	Z-rate	(m/yr)	0.0052	0.0109	0.0004
FAIR	X- coord.	(m)	-2281621.4064	0.0080	0.0005
FAIR	Y- coord.	(m)	-1453595.7949	-0.0005	0.0004
FAIR	Z- coord.	(m)	5756961.9341	0.0042	0.0008
FAIR	X-rate	(m/yr)	-0.0192	0.0016	0.0003
FAIR	Y-rate	(m/yr)	-0.0059	-0.0028	0.0003
FAIR	Z-rate	(m/yr)	-0.0099	0.0018	0.0005
HART	X- coord.	(m)	5084625.4542	0.0052	0.0024
HART	Y- coord.	(m)	2670366.5989	0.0032	0.0018
HART	Z- coord.	(m)	-2768493.9538	-0.0068	0.0014
HART	X-rate	(m/yr)	0.0082	0.0097	0.0014
HART	Y-rate	(m/yr)	0.0201	0.0037	0.0012
HART	Z-rate	(m/yr)	0.0116	-0.0064	0.0008
WTZ1	X- coord.	(m)	4075578.6039	0.0029	0.0005
WTZ1	Y- coord.	(m)	931852.6776	0.0019	0.0004
WTZ1	Z- coord.	(m)	4801570.0374	0.0167	0.0006
WTZ1	X-rate	(m/yr)	-0.0172	-0.0004	0.0001
WTZ1	Y-rate	(m/yr)	0.0175	0.0002	0.0001
WTZ1	Z-rate	(m/yr)	0.0059	0.0003	0.0001

Table 6.8 Coordinate adjustments to the seven sites constrained in GLORG. Velocities were forced to the ITRF94 values, and ITRF94 site coordinates were constrained to 0.001 m. The GLORG command file is given in Appendix 9. Formal uncertainties are shown.

Site	Component	Value (m)	Adjustment (m)	Std Dev. (m)
SANT	X- coord.	1769693.3344	0.0013	0.0004
SANT	Y- coord.	-5044574.1206	0.0154	0.0007
SANT	Z- coord.	-3468321.0582	0.0047	0.0005
YELL	X- coord.	-1224452.4709	0.0022	0.0003
YELL	Y- coord.	-2689216.1034	0.0076	0.0004
YELL	Z- coord.	5633638.2813	0.0013	0.0006
KOKR	X- coord.	-5543838.0888	0.0136	0.0008
KOKR	Y- coord.	-2054587.3024	0.0154	0.0005
KOKR	Z- coord.	2387809.6792	-0.0115	0.0004
DS42	X- coord.	-4460996.1098	-0.0037	0.0005
DS42	Y- coord.	2682557.0805	-0.0025	0.0004
DS42	Z- coord.	-3674443.7305	0.0030	0.0004
YAR1	X- coord.	-2389025.5121	-0.0053	0.0004
YAR1	Y- coord.	5043316.8786	-0.0058	0.0005
YAR1	Z- coord.	-3078530.7672	-0.0066	0.0004
TROM	X- coord.	2102940.3657	0.0101	0.0003
TROM	Y- coord.	721569.3770	-0.0107	0.0003
TROM	Z- coord.	5958192.1101	0.0141	0.0007
KOSG	X- coord.	3899225.2767	0.0104	0.0006
KOSG	Y- coord.	396731.8096	-0.0001	0.0004
KOSG	Z- coord.	5015078.3520	0.0203	0.0008

Some of the 1990 PNG sites were observed in three or four campaigns. This gives a well determined estimate of their position and velocity independent of the 1990 data. These sites (Port Moresby, Losuia, Kavieng and Misima) were constrained in the velocity components to ±5 mm of their post-1990 velocity estimates. By looking at whether/how much the 1990 data changes these estimates gives an idea of whether or not 1990 is causing strain in the solution. If it is not, then we can have more confidence in the velocity determinations which rely on 1990 data for a second occupation. Table 6.9 shows that introducing the 1990 data does not cause the site velocity corrections to exceed

the constraints. The corrections generally differ by under 5 mm. Exceptions are the east components of Losuia (6 mm) and Kavieng (11 mm). The site repeatability plots (Appendix 4) also show this effect. For example, Figure 6.9 illustrates that the 1990 data for Losuia is not significantly different from the line of best fit to the position estimates in the north and east components.

Table 6.9 The horizontal velocity components for three sites from two solutions: the first excluding the 1990 data and the second including the 1990 data. Formal uncertainties are shown.

Site	Comp.	GIG91-UCAN96 Solution		PNG90-UCAN96 Solution	
	N/E	Rate (m/y)	Std Dev.(m)	Rate (m/y)	Std Dev.(m)
Losuia	N	0.0681	0.0015	0.0712	0.0010
	E	0.0250	0.0046	0.0310	0.0028
Port Moresby	N	0.0596	0.0007	0.0598	0.0006
	E	0.0450	0.0012	0.0456	0.0011
Kavieng	N	0.0305	0.0015	0.0318	0.0010
	E	-0.0741	0.0046	-0.0635	0.0025

The transformation parameters output by GLORG for enforcing the reference frame on the loosely constrained GLOBK solution are state of the art values. They are shown in Table 6.10. It is to be noted that the scale is not significant. Tests indicated that this value can be changed, but not significantly, by adjusting the mix of the constrained stations in the GLORG run, in particular, by including ALGO and DS10.

Table 6.10 The transform parameters used to stabilise the reference frame in GLORG.

Position system stabilisation results	Value	Std Dev.
X Rotation (mas)	1.23832	0.10043
Y Rotation (mas)	0.32826	0.10222
Z Rotation (mas)	-2.76358	0.11748
X Translation (m)	-0.01718	0.00303
Y Translation (m)	0.00037	0.00303
Z Translation (m)	-0.03132	0.00338
Scale (ppb)	-1.27695	1.03253

The daily repeatability of the site position and baseline length between sites, gives another indication of the quality of the solution. Site and baseline repeatability information is obtained from a GLOBK back solution. However, back solutions require vast quantities of disk space and CPU time, so the solution had to be performed in two parts. A global set of experiments between 1990 and 1994 was common to both solutions. The 1992 local solutions were added to the first solution; the 1993 and 1994 local solutions were added to the second. Thus two solutions of about 98 experiments (individual GAMIT solutions) each were run. These solutions were then combined to plot the scatter diagrams.

The repeatability of each site from the scatter plots gives another indication of the quality of the site. For instance, the site repeatability plots of Port Moresby, shown in Figure 6.8, illustrate several features. Firstly, the scatter of the solutions in 1990 is within 10 cm. This indicates that the reference frame has been determined correctly for 1990. One of the early indications that there were reference frame problems was the scatter of several metres for 1990 solutions. Clearly this problem no longer exists. Secondly, there is an improvement in the scatter of the daily results as time progresses and the number of satellites and global tracking sites increases. This is also what we would expect to see. Thirdly, the figure shows that only two occupations of a site may not give a reliable velocity estimate for that site. Notice that if only 1990 and 1991 were used, the east velocity would be negative! Finally, a sufficient time period between observations is also important. If only the closely spaced observations within either 1992 or 1993 were to be used, the velocity estimates would differ. However, the velocities used for the analysis in Chapter 7 were not derived from the back solution results, but from the forward solution containing all available GPS data.

At UC, it is standard practice to use an earthquake file in the GLOBK solution to correct the heights for observations to different reference points, and different antenna types. The repeatability of the height component of Port Moresby indicates that there are height problems remaining in 1990, but these do not affect the estimates of horizontal position and velocity. This study is not interested in vertical motion of the sites, so these errors will not degrade the results.

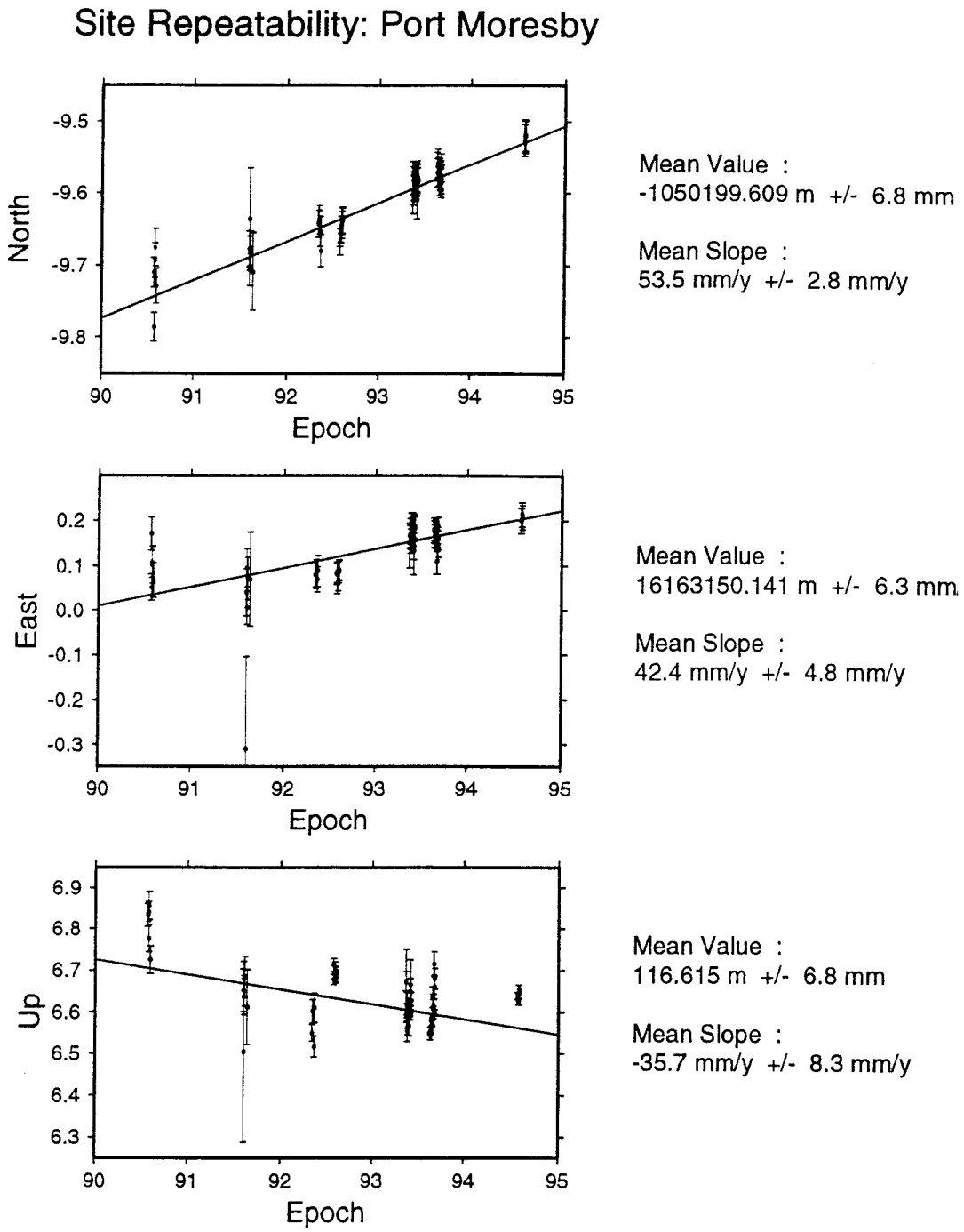

Figure 6.8 Repeatability of Port Moresby.

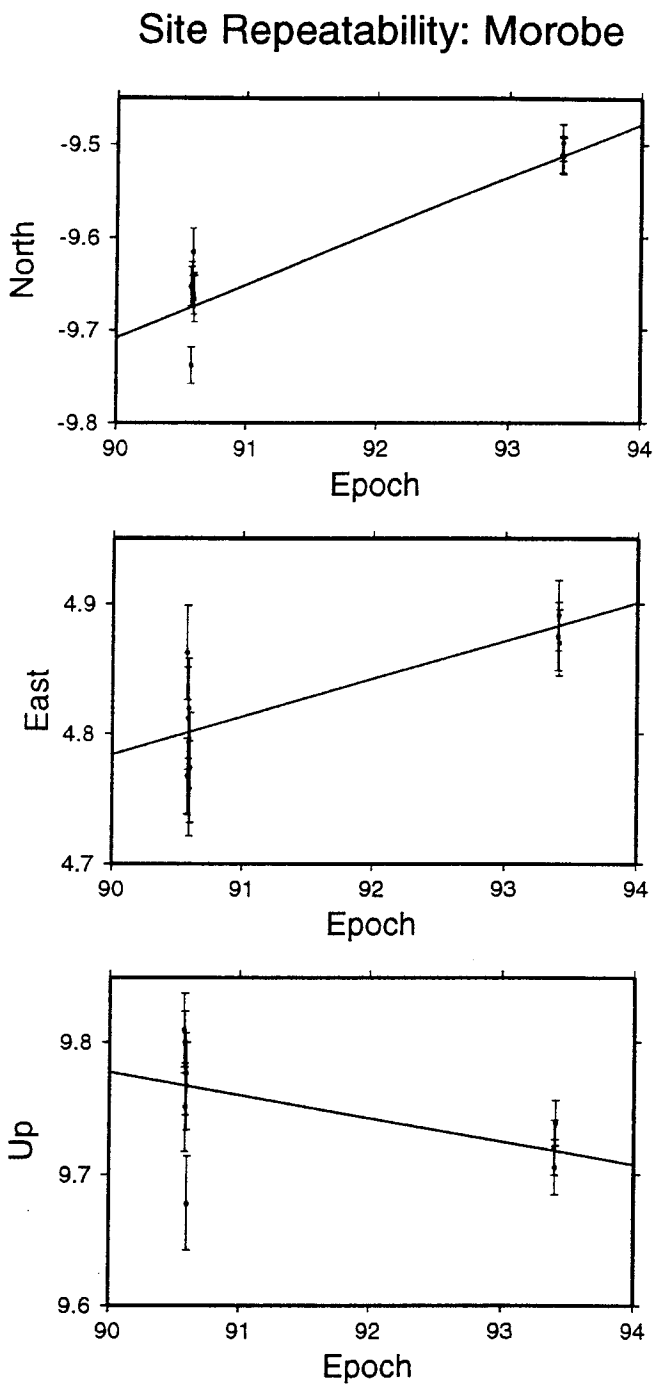

Mean Value :
-861849.604 m +/- 30.2 mm

Mean Slope :
57.7 mm/y +/- 8.4 mm/y

Mean Value :
16279894.836 m +/- 17.5 mm

Mean Slope :
29.3 mm/y +/- 7.5 mm/y

Mean Value :
79.746 m +/- 13.3 mm

Mean Slope :
-17.5 mm/y +/- 7.7 mm/y

Figure 6.9 Repeatability of Morobe.

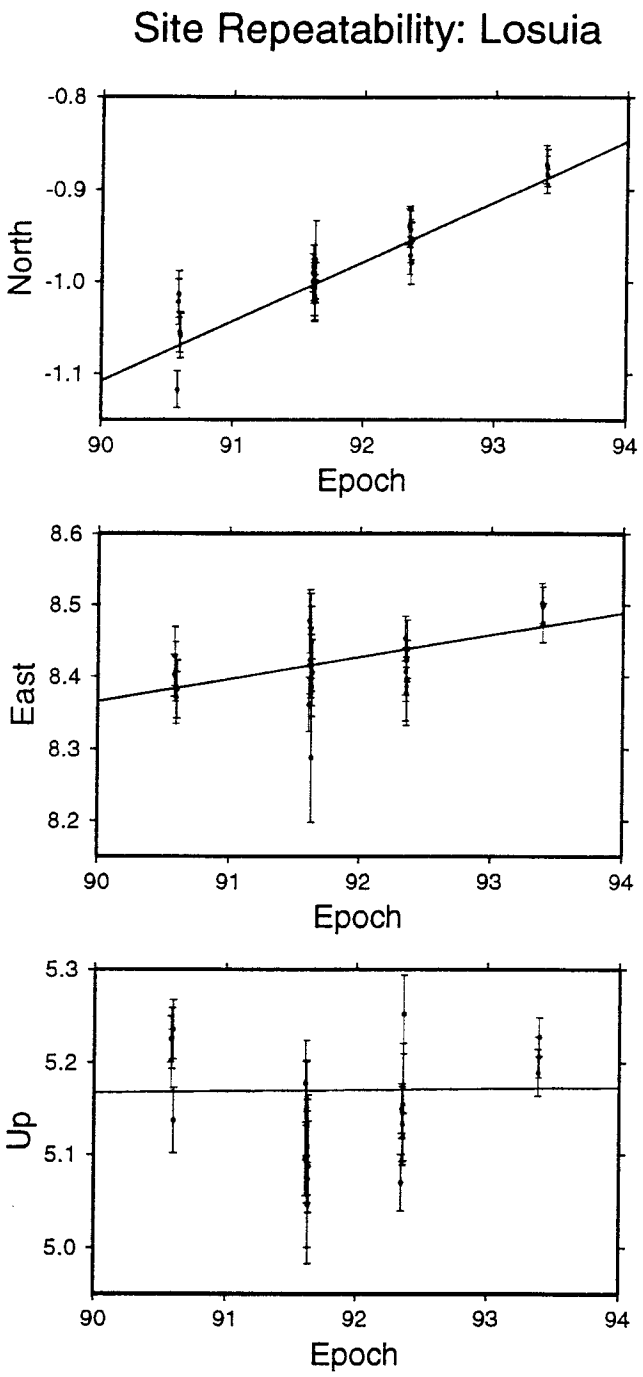

Mean Value :
-950150.978 m +/- 12.6 mm

Mean Slope :
65.0 mm/y +/- 5.2 mm/y

Mean Value :
16636898.427 m +/- 9.3 mm

Mean Slope :
30.8 mm/y +/- 7.8 mm/y

Mean Value :
85.170 m +/- 11.3 mm

Mean Slope :
1.2 mm/y +/- 11.2 mm/y

Figure 6.10 Repeatability of Losuia.

Table 6.11 Comparison between the rate for each site determined by the forward GLOBK solution, and the rate determined by the slope of the line of best fit determined by the GLOBK back solution.

Site	Comp. NEU	GLOBK/GLORG		Back Solution	
		Rate (mm/y)	Std Dev (mm/y)	Rate (mm/y)	Std Dev (mm/y)
MORE	N	59.8	0.6	53.5	2.8
	E	45.6	1.1	42.4	4.8
	U	-23.4	1.8	-35.7	8.3
TOWN	N	56.2	0.4	57.0	3.2
	E	37.5	0.8	40.6	4.9
	U	-1.0	1.7	-20.4	11.8
LOUS	N	71.2	1.0	65.0	5.2
	E	31.0	2.8	30.8	7.8
	U	39.4	3.5	1.2	11.2
AIAM	N	62.1	1.0	81.1	15.4
	E	68.3	2.7	101.8	19.5
	U	-63.7	6.2	-122.5	10.8
GUA2	N	84.3	5.6	70.6	50.6
	E	40.1	21.3	39.4	114.0
	U	17.5	40.8	26.9	85.4
MISI	N	54.9	1.3	53.8	7.2
	E	44.5	3.3	45.1	11.7
	U	-3.1	4.1	26.6	14.0
JACQ	N	-58.3	1.4	-76.4	8.0
	E	24.1	4.3	-2.0	10.6
	U	29.2	5.9	-57.8	13.0
KAVI	N	31.8	1.0	15.2	5.7
	E	-63.5	2.5	-64.9	9.9
	U	41.7	3.3	7.3	12.9
ALT2	N	57.6	0.9	54.3	7.7
	E	39.9	2.2	28.2	11.2
	U	16.4	4.8	40.1	8.1
MORO	N	65.1	1.0	57.7	8.4
	E	38.7	2.9	29.3	7.5
	U	28.2	4.5	-17.5	7.7
MANU	N	27.6	1.0	17.8	11.8
	E	-53.7	2.6	-67.3	8.5
	U	50.8	4.0	5.3	7.6
UNIT	N	55.0	1.1	51.9	21.8
	E	61.3	2.5	66.5	27.7
	U	-49.2	6.7	-42.3	27.1
VANI	N	30.6	1.1	46.2	15.0
	E	34.8	2.8	65.3	19.3
	U	32.3	6.1	-9.3	23.3

The repeatability plots of Morobe, shown in Figure 6.9, are typical of the sites with only two occupations. Clearly, again, the 1990 scatter is of an acceptable level. Clearly, also, the scatter of the 1993 results is smaller than that of 1990, as expected. Although only observed in two epochs, these epochs are separated by an interval of three years, which alleviates one of the possible problems mentioned above. The plot of the north component of Morobe highlights the importance of having several days of observation on a site. Although the majority of observations are clustered about 9.66 in 1990, the extreme values differ by just over 10 cm.

The slope of the line of best fit for each component of each site should give the velocity of the site in each component, if the a priori value is zero. These can be compared with the velocities output from the forward solution of GLOBK/GLORG. This comparison is shown in Table 6.11.

Clearly, the standard deviations from the daily repeatability statistics are much larger than the formal errors from GLORG. This is expected as it is well known that formal errors for GPS solutions are optimistic. This is primarily due to the large number of observations increasing the precision of the solution, coupled with unmodelled systematic effects reducing the accuracy of the solution.

Although there are some apparently large discrepancies between the two sets of rates, the standard deviations of the back solution estimates are large. It can be seen that the values agree within three standard deviations, the majority within one standard deviation. Exceptions are the height components for Aiambak, Jacquinot Bay, Morobe and Manus.

Clearly, the well determined sites, such as Port Moresby, Townsville and Losuia, have good agreement between solutions and have smaller standard deviations from the back solution than poorly determined sites, such as Guasopa.

From Table 6.11 above, it is clear that within the limits of the standard deviations, the rates from the full forward solution agree with the rates from the back solution. The implication of this is that the reference frame is well determined and does not significantly change when significant numbers of regional campaigns are excluded from the solution.

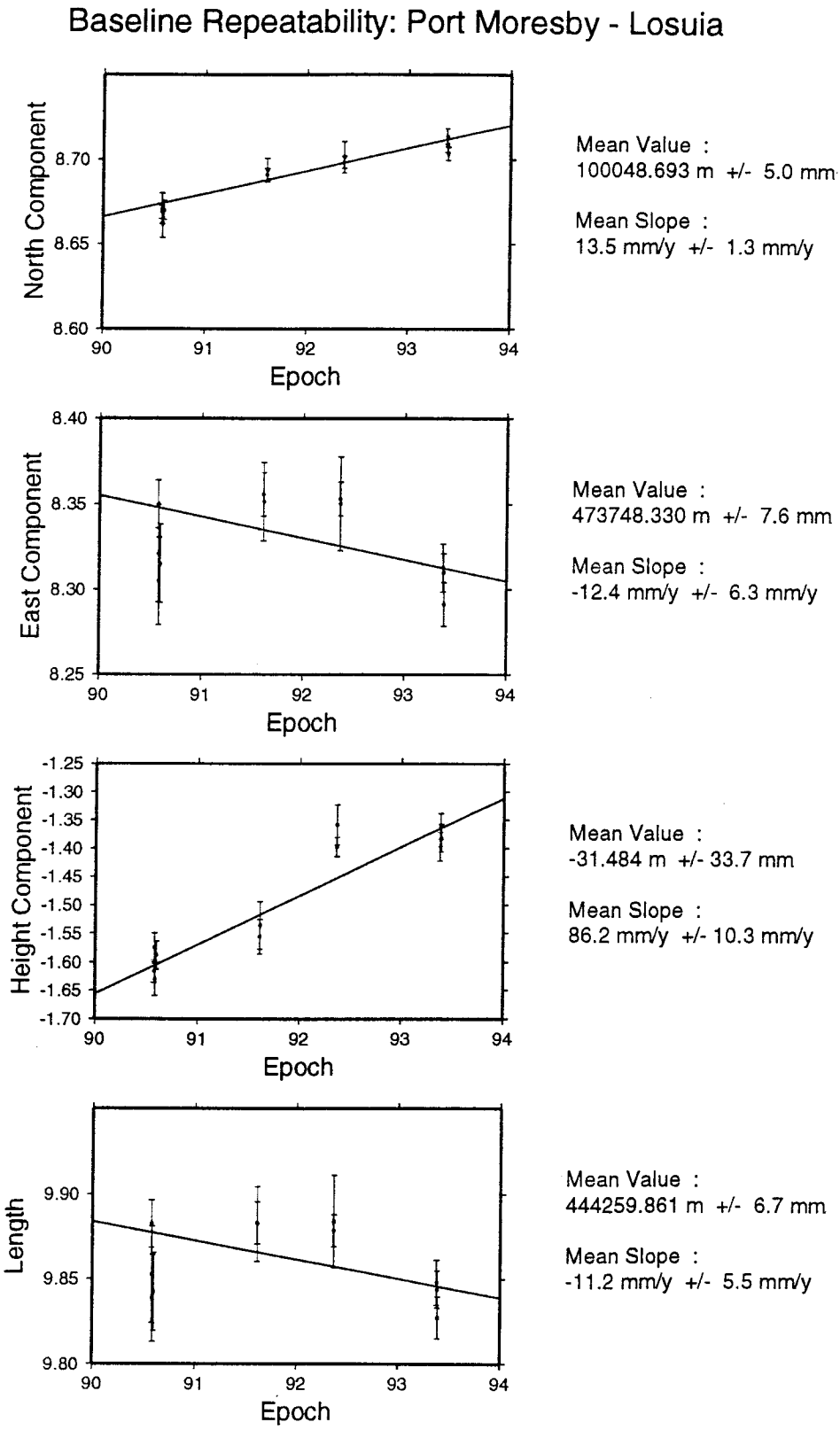

Figure 6.11 Baseline repeatability of Port Moresby to Losuia.

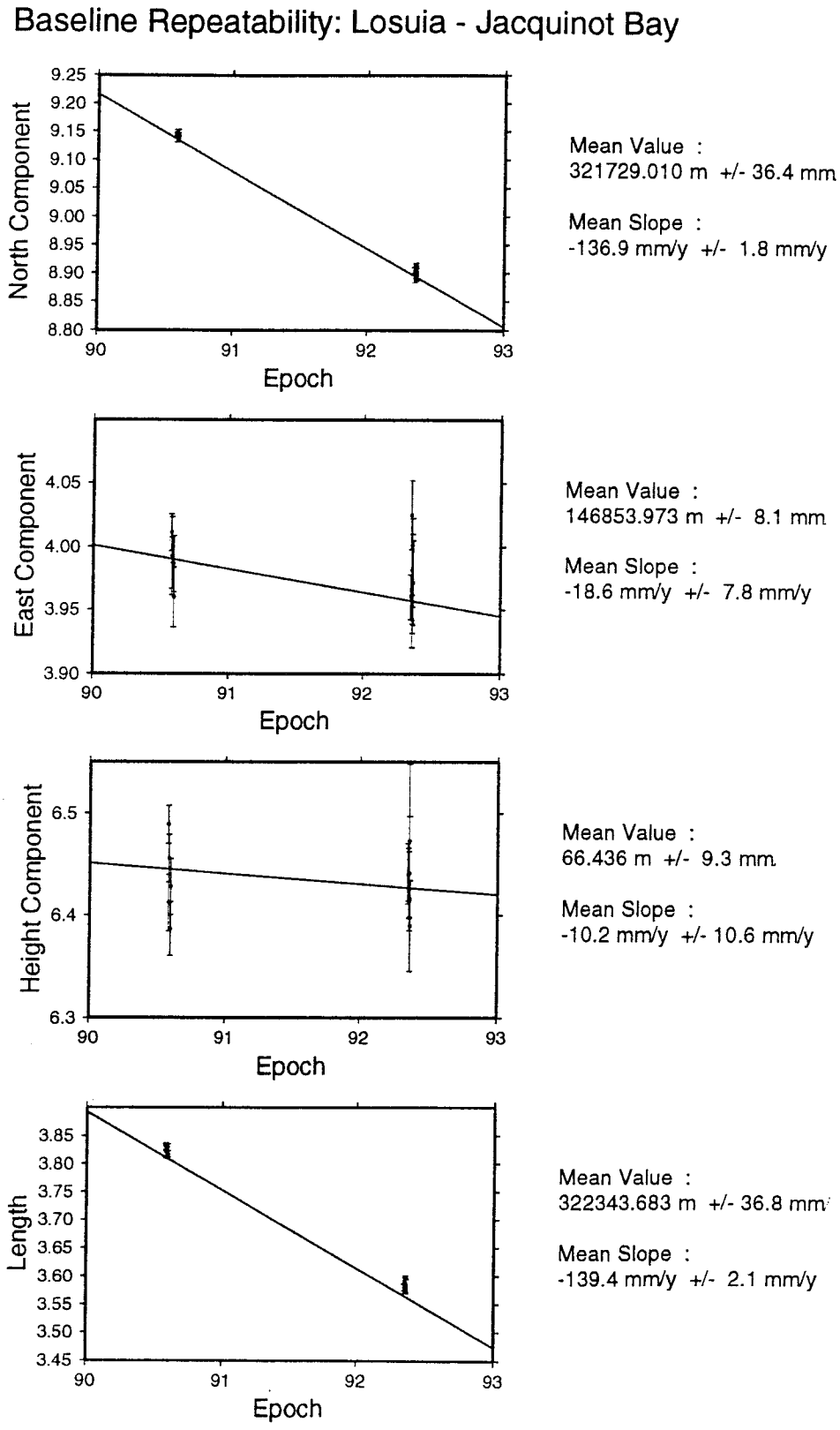

Figure 6.12 Baseline repeatability for Losuia to Jacquinot Bay.

Baseline repeatability plots have also been drawn. Figures 6.11 and 6.12 respectively, show the daily estimates of the baselines Port Moresby - Losuia and Losuia - Jacquinot Bay. Several aspects of these plots require comment. Firstly, notice that the baseline estimates are less scattered than the site estimates. Baselines are independent of the location of the origin and the orientation of the reference frame. Hence any small day to day variations in the reference frame definition will not affect baseline length.

In each figure, the north component is considerably less scattered than the east component. Clearly there is a height error at either Port Moresby or Losuia.

Again, the virtue in having more than two occupations of a site or baseline is highlighted in Figure 6.11. If any one of the observation epochs was omitted, the slope of the line of best fit would vary considerably, particularly in the east and length components.

6.3.5 Absolute Velocities and Velocity Residuals

The GLOBK/GLORG solution gives estimates of the position of each site and a velocity estimate for those sites with more than one observation period. These are absolute velocities in the reference frame of the solution, in this case, ITRF94. The positions and velocities are expressed as both cartesian and local NEU coordinates.

The velocity estimates from GLORG can be converted into velocity residuals with respect to a standard plate motion model. Velocity residuals are particularly useful for displaying differences between observed velocities and predicted velocities. The velocity residuals computed for this analysis were based on the NUVEL-1 plate motion model of DeMets *et al.* (1990). This is not the most recent model, which requires some explanation.

The NUVEL1 plate model is a global plate model based on 3 Ma-average global plate velocities (DeMets *et al.*, 1990). During the early 1990's, new evidence suggested that the geomagnetic reversal time scale was in error by up to 10% (DeMets, 1995). This resulted in the NUVEL-1 plate model being updated to the NUVEL-1A model. This updated model has angular velocities 4.38% slower than the original NUVEL-1 model (DeMets, 1995). However, Heki (1996) has found that the VLBI data from 16 global sites for the period

1979-1992, fit the global models better when the NUVEL1 model is corrected by increasing the angular velocities by 3.4 ± 1.2%.

This latest revision to the global plate model is not yet available in the form of poles of rotation and angular velocities necessary to implement the model. However, this is not going to have a significant effect on the majority of the results presented here. The revisions are less than 5%. When it is considered that the major plates in the PNG region have velocities of the order of 10 cm, this gives a change of the order of 0.5 mm. This is below the precision of the GPS results presented in this thesis, with the exception of Townsville and Port Moresby, which have greater precision due to the greater number of observation epochs on these sites.

Velocity residuals have, therefore, been calculated using the original NUVEL1 plate motion model. They are displayed in Figure 7.1(a-b). The precision of the residuals is critical for interpreting the GPS results, and is therefore discussed in detail in Chapter 7.

Chapter 7

Interpretation of the Results

7.1 Absolute Velocity Vectors and Velocity Residuals

The geodetic results presented in Chapter 6 are summarised in two figures, Figure 7.1a and Figure 7.1b. These figures show the velocity residuals at each site with respect to the Pacific (hatched) or Australian (black) plate. The residuals are shown in two figures for clarity, as the larger arrows and ellipses obscure the smaller ones. Error ellipses are at the same scale as the vectors, and are based on the scaled formal uncertainties of the rates from the GLORG output. The ellipses are shown at the 95% confidence level. The assumption is made that the predicted NUVEL1 velocities at each site are error free. The scaling factor applied to the formal uncertainties is discussed below. A comparison of the scaled 95% values with the GLOBK Markov values indicates that this scaling is not unrealistic. Figure 7.2 gives the absolute velocities of the survey sites. Error ellipses are at the same scale as the vectors, and scaled in the same way as the residual velocity error ellipses. Again, the ellipses are shown at the 95% confidence level.

Initially, the formal standard deviations were scaled by χ for the solution: a factor of 1.3. However, it was felt that the resultant velocity standard deviations were still too optimistic.

The alternative method, discussed more fully in Chapter 6, of determining the quality of a position and rate estimate involves extracting the daily repeatability information from the GLOBK back solution. This was also investigated, but it was felt that this gave an upper bound estimate of precision, and was therefore too pessimistic. The reason for believing the back solution gives a pessimistic estimate of repeatability is that it was performed with standard values entered for the Markov parameters for all sites. If instead, the Markov parameters had been optimised for each site, the daily repeatabilities obtained would probably have been more realistic. Additionally, it is well known that the level of the daily repeatability improves dramatically from the 1990 survey to the

(a)

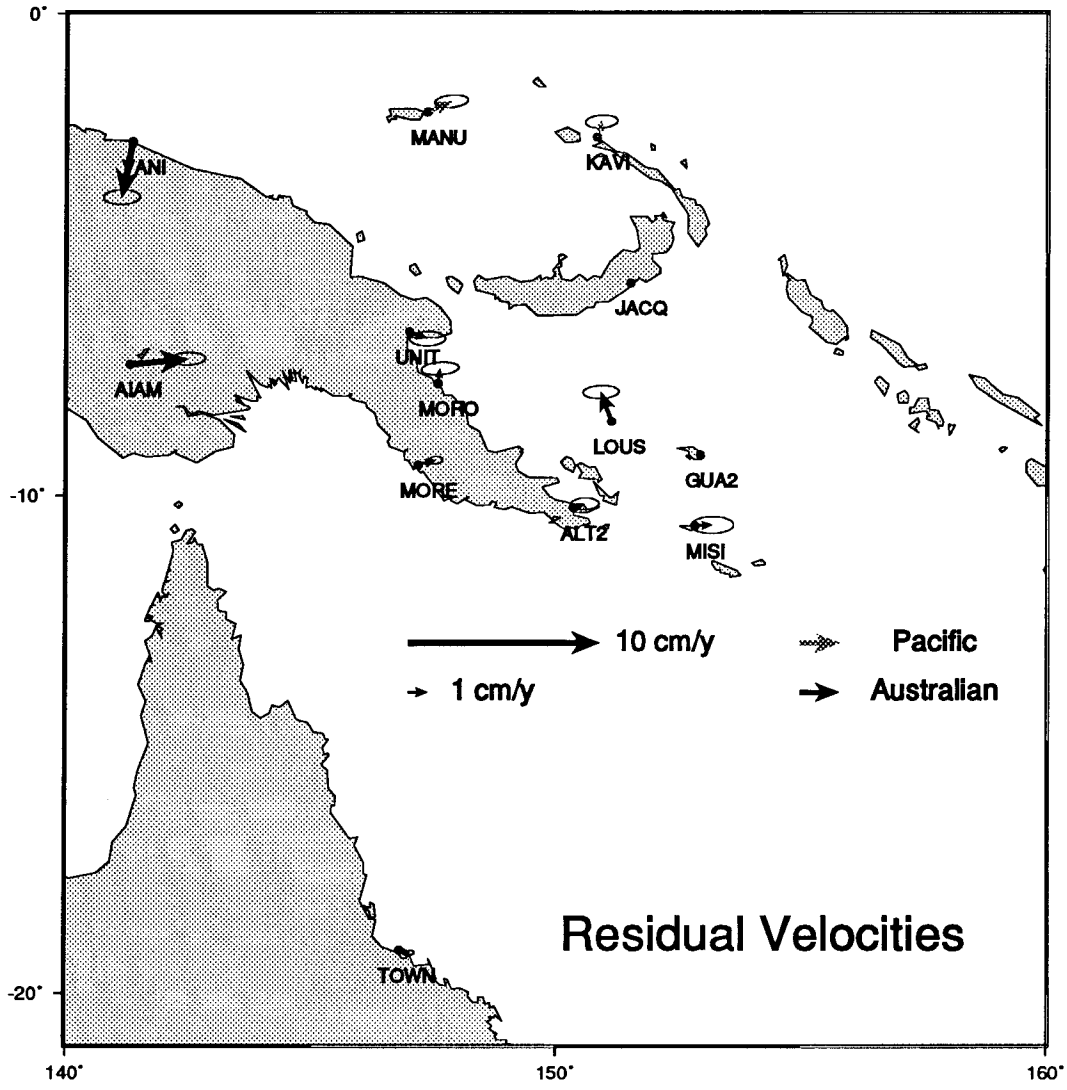

Figure 7.1(a) Velocity residuals with respect to the Australian plate (black) and the Pacific plate (hashed). Error ellipses are based on the scaled error estimates, and are at the same scale as the residuals. They are expressed at the 99.7% confidence level.

1994 surveys. This is primarily due to the combined effects of the growth of the global tracking network and the increase in the number of satellites. The estimates of precision obtained from the daily repeatability of the sites and baselines can be seen in Figures 6.10 - 6.13 and in Appendices 4 - 5.

(b)

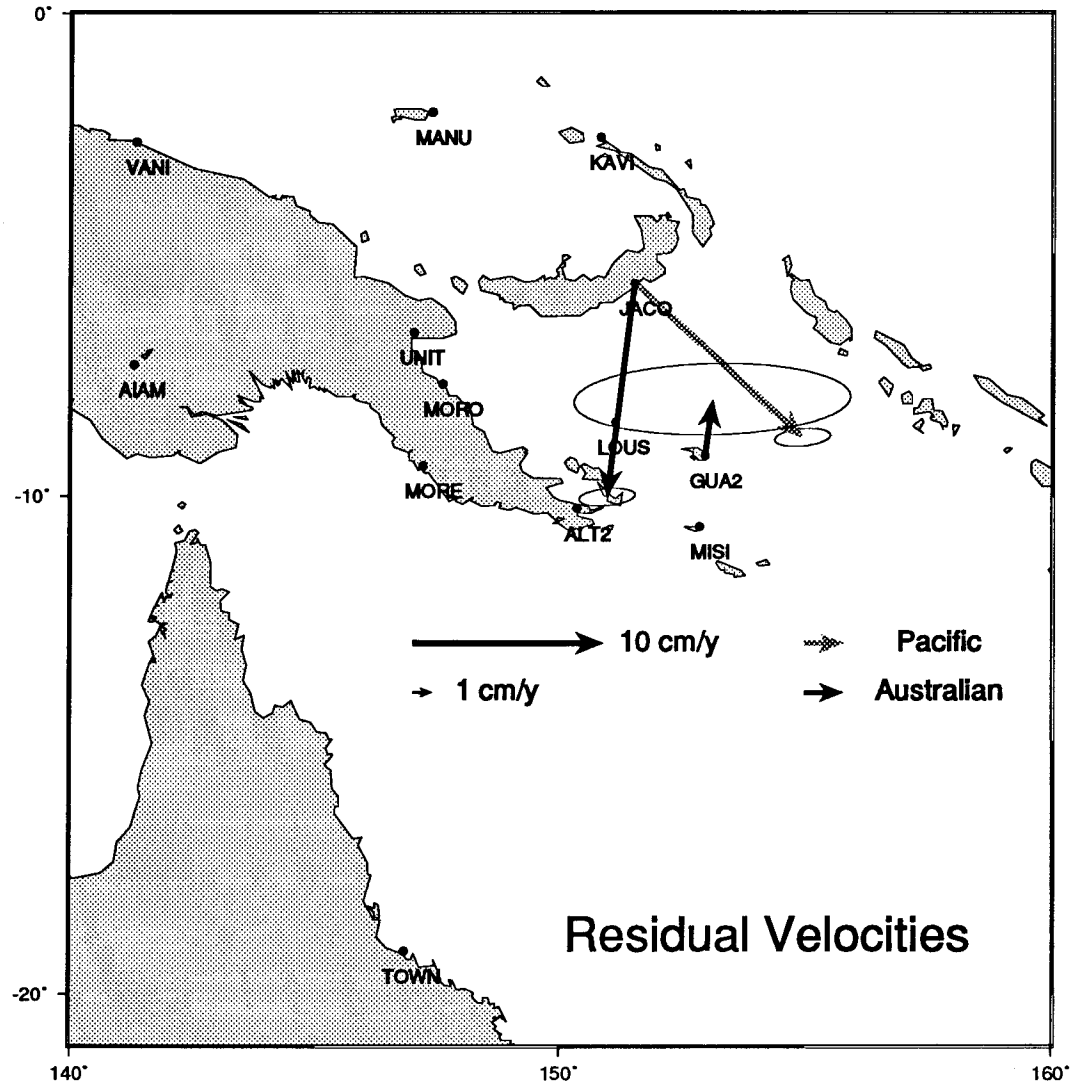

Figure 7.1(b) Velocity residuals with respect to the Australian plate (black) and the Pacific plate (hashed). Error ellipses are the scaled error estimates, and are at the same scale as the residuals. They are expressed at the 99.7% confidence level.

The standard deviation (error) had to lie between the formal values scaled by 1.3 and the larger values from the daily repeatability. For a sensible discussion, it is necessary to optimise the value of the error, so that formal errors, errors of dispersion, are most likely to cover the full space of the errors. In this discussion, the formal standard deviation of the baselines was multiplied by three to give a scaled error representing the 3σ estimate of uncertainty. For the error ellipses, since a two-dimensional space is being used, it must be remembered that the normal one sigma region of an error ellipse is only a 39%

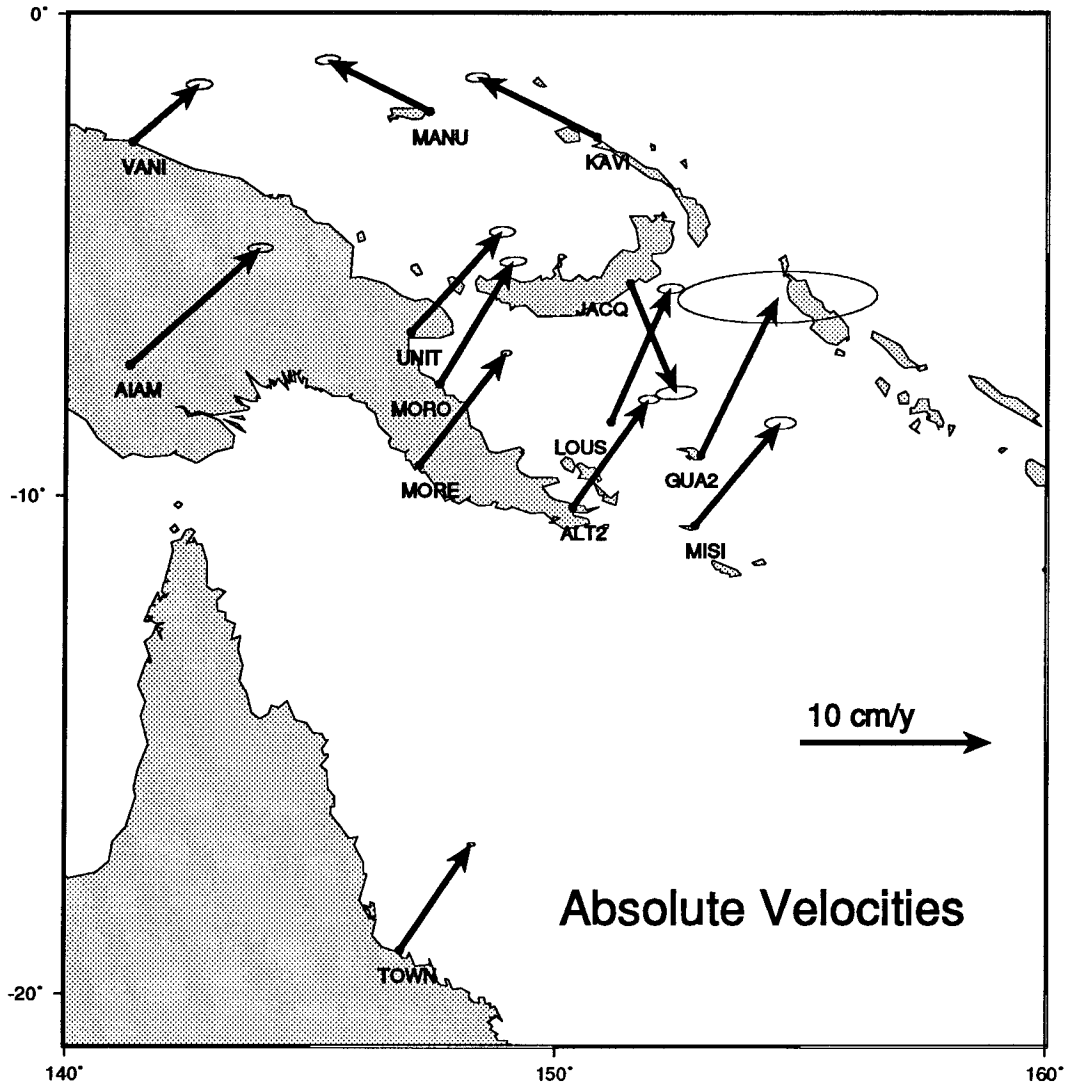

Figure 7.2 Absolute velocities of the survey sites. The error ellipses are at the same scale as the vectors. They are the scaled error estimates, explained in the text. Error ellipses are shown at the 99.7% confidence level.

probability space. To keep the uncertainties of the error ellipses consistent with the scaled baseline errors, a confidence interval of 99.74% was used. A 99.74% probability space, one in which dispersion errors have only a 0.26% probability of occurring, therefore, requires the basic ellipse to be scaled. This scaling factor is 3.42.

A significant issue in determining the correct scaling for the standard deviations is the lack of uniformity of their values due to time span, number of observations available and an unknown error in the applied NUVEL model. It is

clear that the NUVEL errors become important when the standard deviation of the determination is less than 5% of the NUVEL values. This occurs at Port Moresby and Townsville, whose precisions are near the mm/y level. Thus despite the apparent statistical significance of the ellipses for the velocity residuals at these two sites (Figure 7.1a), this study will assume that these differences are not significant due to the unknown error budget of the NUVEL model. The consistency of Townsville and Port Moresby with Australian plate velocities has been verified by Morgan *et al.* (1996) and Tregoning (1994), using shorter, less definitive spans of data.

It is useful, in addition to looking at the residual velocity of each site, to consider rates of change of baseline lengths to get an estimate of the motion occurring across plate boundaries. There are two principal methods of working with baselines. The first uses directly observed, or campaign derived baselines. These are compared between campaigns. This technique is the older technique, for while it is rotationally independent, it does not maximise the available information because of the limitation that the baselines must be either directly observed or campaign derived means.

The second technique, now generally preferred, uses point positions and velocity vectors. Using this approach allows the expansion/contraction along any baseline to be computed. The great advantage of this technique is that it allows the motion to be computed between sites which were not observed simultaneously, giving much greater possibilities for interpretation. Further, it allows the rate of change to be determined using the best possible site velocities from the solution. It is important to note that the velocity residuals must be used, i.e. the general rigid plate motion must be removed. The advantage of using velocity residuals instead of the absolute velocities from the GLORG output is that it removes the problem of the effects of plate rotations on the absolute velocity residuals. The major disadvantage of the method is the a priori knowledge of rigid plate motion. In the case of NUVEL, no precision estimates are available. Additionally, there is a recent series of revisions at the 5% level, as discussed in Chapter 6.

Using velocity residuals to compute baseline changes involves the transition from absolute values to relative values. In computing the error estimates of the baseline components, the covariance between sites must be taken into account.

The error estimates were computed by propagating the scaled formal variances of the site velocities, taking the covariances between sites into account, and assuming the NUVEL1 model to be error free in the computation of velocity residuals.

With care, comparisons can be made between estimates of baseline change computed from velocity residuals and estimates based on the daily repeatability of baselines between simultaneously observed sites. The limitations of the repeatability approach outlined above must be taken into account when selecting baselines for comparison. In addition, the daily repeatability estimates of baseline length include the height component, whereas the velocity residual estimates are horizontal. The height component becomes significant when a station is occupied by different antenna types in different campaigns. This is discussed by Morgan *et al.* (1996).

In the PNG surveys, Port Moresby was occupied for the duration of most of the surveys, and is, therefore, a good site for the comparison. Morobe, Alotau and Misima are also well determined sites with more simultaneous observations with Port Moresby than most other sites. Comparisons from these baselines are given in Table 7.1.

Table 7.1 Comparisons of the rate of baseline change between two methods: baseline repeatability and velocity residuals. The standard deviations of the velocity residual estimates are the scaled error values.

Baseline		Repeatability Estimate (mm/y)	Standard Deviation (mm/y)	Residual Velocity Estimate (mm/y)	Scaled Error (mm/y)
From	To				
MORE	MORO	+6.4	2.3	+9.7	8.0
MORE	ALOT	-1.8	3.6	-2.9	7.3
MORE	MISI	-2.3	10.8	-2.0	4.3

These estimates are in agreement at the one standard deviation level. Note also that the scaled error of the estimate of baseline change from the residual velocity is of a similar size to the estimate from the baseline repeatability estimate, i.e., up to about 10 mm/y. This implies that the scaling applied is of

the right magnitude, and re-emphasises that the solution is good to approximately 10 mm.

7.2 Interpretation of the Results

A significant issue for this interpretation is the correct scaling of the formal or repeatability estimates so that they encompass the variation of these estimates and variation of the estimated least squares parameters. The scaled error of the velocity residuals and baseline changes are discussed above and in Chapter 6. Throughout this interpretation, it has been found that the baseline rates of change computed from velocity residuals agree very well with the currently favoured interpretations of the tectonic and geological features of the region. Whether these baseline results and the results which appear to be emerging from them are significant or not, depends largely on their precision. Eisenhart (1963) treats this problem in detail. Since it is not possible to cut the data set into multiple slices and compare the estimated parameters (see McClusky (1993) and Morgan *et al.* (1996)), no estimate of variation of these values can be made and it is necessary to rely entirely on the commonly held belief that variations of an estimate are contained within 3σ of the estimate if the normal probability distribution applies.

7.2.1 Motion across the New Britain Trench

The velocity residuals with respect to the Australian plate for the sites about the New Britain Trench clearly indicate that significant motion is occurring across this boundary. The sites on the Australian plate have small residuals, which are within the bounds of their error ellipses. Apparent exceptions at Port Moresby and Townsville were discussed above. The residual at Losuia is also small (approximately 16 mm/y), but could have a significantly larger northward velocity than the NUVEL-1 model predicts if it is located on the Australian plate (discussed later). The residual at Jacquinot Bay, however, is approximately 120 mm/y, and is clearly significant.

The motion across this boundary can be computed from the velocity residuals, as discussed above. Several baselines cross this boundary from 147°E in the west to approximately 151°E in the east.

The baseline from Losuia to Jacquinot Bay is indicating a rate of -130±5 mm/y (scaled error). For comparison, the value calculated from the horizontal components of the baseline repeatability plots is -130±3 mm/y, which is very clearly in agreement. In Section 2.4.3, a value of 125 mm/y was quoted from the literature, which is not significantly different to the values from the GPS in this analysis. Estimates of motion exceed the noise in the solution by more than 10:1. The value also agrees with the rates determined from GPS measurements of -126±47 mm/y published by McClusky *et al.* (1994). However, it is a much more precise value by a factor of almost 10.

The line Losuia to Jacquinot Bay crosses the New Britain Trench at approximately 151°E at an oblique angle. The line from Guasopa to Jacquinot Bay, however, is approximately orthogonal to the trench. Hence, it would be expected that the motion across this line would be greater than that across the Losuia to Jacquinot Bay line. Unfortunately, the residual velocity at Guasopa is very poorly determined, which is clear from the size of its error ellipse in Figure 7.1b. However, it is interesting to note that the result of this computation gives a rate of 144 mm/y, which is larger than the rate of subduction along the previous line, as expected. Thus the uncertainty associated with this line and not the least squares estimate, is most likely to change as new data is added.

These two lines are the only lines which straddle only the New Britain Trench. Baselines from Unit (at Lae) and Morobe to Manus and Kavieng cross both the New Britain Trench at its western end, and the Bismarck Sea Seismic Lineation. The lines to Manus straddle the Lineation in a region which should correspond to the leaky left-lateral transform fault. According to Taylor (1979), the motion along this segment is predominantly left-lateral, with small periodic episodes of spreading. Assuming that currently it is undergoing transform motion, then this motion should not affect the length of baselines orthogonal to it. Similarly, the lines to Kavieng straddle the series of transform faults in Taylor's (1979) fourth segment of the Bismarck Sea Seismic Lineation. In both cases, the lines to Manus and Kavieng are approximately orthogonal to the transform faults (see Figure 7.3), and should be showing motion caused only by the New Britain Trench.

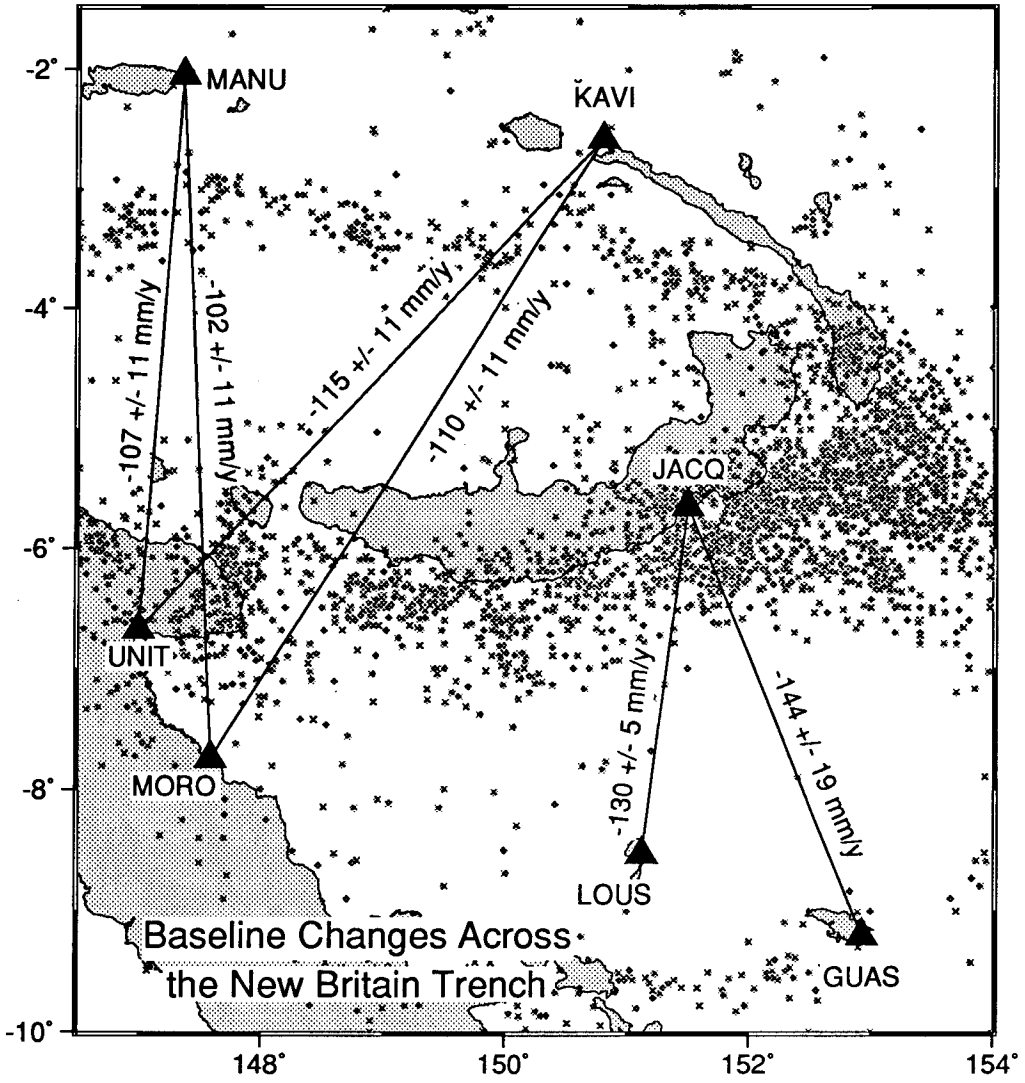

Figure 7.3 Rates of motion across the New Britain Trench along various baselines. Shallow seismicity (0-60 km) is shown to indicate the location of the trench. The scaled error is shown. It is to be noted that the signal to noise ratio is about 10:1 in all instances.

Calculating the rates across these baselines reveals the following:

- Unit to Manus is shortening at a rate of 107±11 mm/y;
- Morobe to Manus is shortening at a rate of 102±11 mm/y;
- Unit to Kavieng is shortening at a rate of 115±11 mm/y; and
- Morobe to Kavieng is shortening at a rate of 110±11 mm/y.

All uncertainties are scaled errors. The rates and scaled precisions are shown in Figure 7.3. Again, the signal to noise ratio in all cases is about 10:1.

Using scaled error estimates, these values are significantly higher than the published rate of convergence of 62 mm/y given in Section 2.4.3, and not significantly different to the rate between Jacquinot Bay and Losuia. This

seems to be implying that the subduction rate may decrease to the west along the New Britain Trench, but not to the extent published in the literature. Although contamination of the value across the Bismarck Sea Seismic Lineation could make these estimates erroneous, it should be noted that any effects which are being introduced would serve to decrease the rate estimate across the New Britain Trench. Additional GPS data will be helpful in determining if the small, currently insignificant, westerly decrease in subduction rate is real.

If the rate of convergence in the western regions of the New Britain Trench is higher than the published rates, the triple junction analysis performed in Section 2.4.3, and the conclusions drawn from it could be in error. However, the new estimates of motion above do not significantly change the result of the triple junction analysis. Using the rates above, and the azimuths as before (in Figure 2.12), gives a motion across the Trobriand Trough of 95 mm/y. This result does not change the conclusion that motion of this magnitude is not occurring along the Trobriand Trough. The triple junction, by these calculations, is invalid. One reason for this could be that the junction does not exist, which seems to imply that the Trobriand Trough is not an active boundary. This is discussed further in Section 7.3.3.

7.2.2 Motion across the Bismarck Sea Seismic Lineation.

There are two lines available for determining rates across the Bismarck Sea Seismic Lineation. These are from Jacquinot Bay to both Manus and Kavieng. The line Jacquinot Bay to Kavieng crosses the boundary in the east, obliquely crossing the transform faults to the south of New Ireland. The line from Jacquinot Bay to Manus obliquely straddles the central section of the boundary.

Using the rate of baseline change from the velocity residuals gives extension of:

- 127±11 mm/y between Jacquinot Bay and Kavieng; and
- 116±11 mm/y between Jacquinot Bay and Manus.

The uncertainties are scaled values. These rates are shown in Figure 7.4. The rate between Jacquinot Bay and Kavieng compares with an estimate of 103±44 mm/y determined by McClusky *et al.* (1994). It is to be noted again, that the estimates of this analysis have a signal to noise ratio of approximately 10:1, which is a significant improvement on the work of McClusky *et al.* (1994).

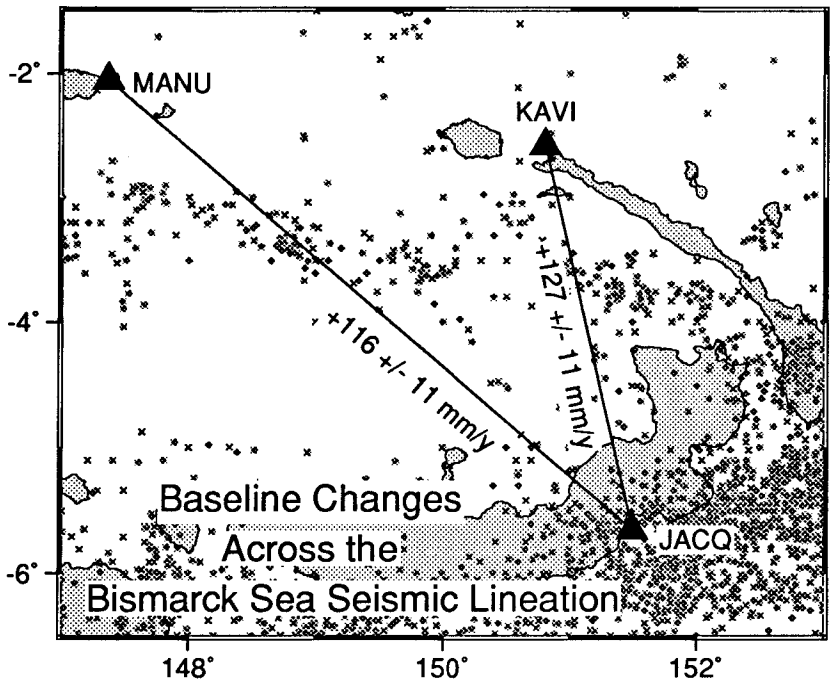

Figure 7.4 Rates of motion across the Bismarck Sea Seismic Lineation along various baselines. Shallow seismicity (0-60 km) is shown to indicate the location of the boundary. The errors are scaled estimates.

For comparison, the rate of change between Jacquinot Bay and Kavieng from the horizontal components of the baseline repeatability is 127 ± 18 mm/y. Once again, the agreement between the two estimates is very good. In this case, this is to be expected, with similar amounts of the data entering each technique. In this case, however, the standard deviation of the estimate from repeatabilities is higher than the scaled formal value which shows the east/west extent of the error ellipses (see Figure 7.1). It is interesting to note that the standard deviation on the length component of the line, which includes the height component, is 7 mm/y. This can be seen in Appendix 5.

The line from Jacquinot Bay to Manus was not directly observed, so there is no comparison to be made with a value from baseline repeatability.

Both estimates of motion across the different sections of the Bismarck Sea Seismic Lineation clearly agree with the values given in Section 2.4.3 of 132 mm/y.

The two rates from velocity residuals given above are not statistically different. Is there any tectonic reason to expect the estimates to be different? The line

from Jacquinot Bay to Manus is closer to being parallel to the direction of oblique spreading than the Jacquinot Bay - Kavieng line. As the spreading changes to left-lateral slip in the west, a cursory look at the tectonics would give rise to the expectation that the rate might decrease to the west. However, the situation appears to be more complex, and linked with the motion of the South Bismarck plate. This is discussed in more detail in Section 7.3.1.

7.2.3 Motion across the Woodlark Spreading Centre.

The velocity residuals, with their scaled errors, say very little about the Woodlark Spreading Centre. The large error ellipse on Guasopa excludes it from a serious role in the interpretation. The residual at Losuia has a northward component that is significant at the 95% confidence level. However, the magnitude of the residual is such that errors and uncertainties in the assumed NUVEL model may account for a significant portion of the residual. From this, the claim cannot be made that Losuia is moving significantly differently to the Australian plate, and hence motion across the Woodlark Spreading Centre is inconclusive. It is to be noted that the magnitude of the error estimate of lines not involving Guasopa are comparable with other estimates and hence the general level of precision of this work is near 12 mm/y. This gives a signal to noise ratio of approximately 2:1 for these baselines. Although this ratio is not sufficiently high to detect motion, it is interesting, to look at the baseline results, with scaled errors, to tenuously interpret motion across this boundary which will become clearer as higher signal to noise ratios are derived from additional data.

There are several baselines straddling the Woodlark Spreading Centre, from its western end in Goodenough Bay to approximately 152°E. These lines are from both Misima and Alotau to both Guasopa and Losuia, and are shown in Figure 7.5. Clearly, this network only encompasses a small section of the Woodlark Spreading Centre, and does not give an estimate of spreading rates towards the eastern end of the boundary.

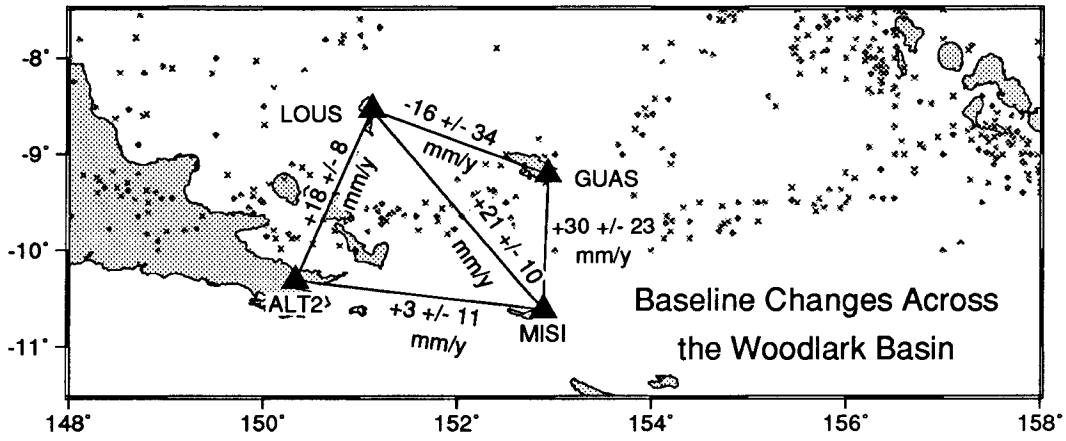

Figure 7.5 Rates of motion across the Woodlark Spreading Centre along various baselines. Shallow seismicity (0-60 km) is shown to indicate the location of the spreading centre. The scaled errors are shown.

From the velocity residuals, the rate between Losuia and Misima is 21±10 mm/y (scaled error). The line from Losuia to Misima is the only line which was directly observed. However, the baseline repeatability for this line uses only four observations for each site, which is a small subset of the total observations used to compute the velocity residuals. This highlights the advantage of using the velocity residuals for baseline computations. For comparison, the repeatability plots of the baseline Losuia-Misima shows that spreading is occurring across the Woodlark Spreading Centre at a horizontal rate of 22±16 mm/y. These plots are contained in Appendix 5. These two values are in agreement and the uncertainties are consistent which indicates the validity of the scaling applied.

Using the scaled error estimates, the spreading rates given above (approximately 20 mm/y) are significantly below the rate given by geological estimates (60 mm/y) in Section 2.4.3, and not significantly different to zero. While each line is not significant as an entity in itself, the spatial similarity of the results is striking. The similarity of these results clearly indicates that a 60 mm/y opening rate cannot be sustained at the 95% confidence level. Values near 20 mm/y appear to be more likely. With more precise values emerging after the addition of new data, it is not expected that the current least squares estimates of the rates will change.

As suggested in Section 2.4.3, the rate of opening decreases from east to west as the rift propagates into the Papuan Peninsula. The line from Losuia to

Misima crosses the Woodlark Spreading Centre at about 152°E. From Section 2.4.3, the rift is clearly defined to 151°E, hence the Losuia-Misima line crosses the rift towards its end and the spreading rate of 21 mm/y is not in conflict with geology.

It is interesting to compare the rate above with changes in baseline length for two additional baselines: Losuia-Alotau and Misima-Guasopa, although the latter is quite weak. The three lines cross the Woodlark Spreading Centre from the tip of the Papuan Peninsula, progressing to the east to about 152°E. The spreading rates are calculated to be 18±8 mm/y, 21±10 mm/y and 30±23 mm/y respectively. The scaled errors are given. The significance of these values depends on the standard deviations attributed to them. Looking at the rates alone reveals that there is indeed an increase in the spreading rate to the east, which is in agreement with the westward propagation of the rift, as discussed in Section 2.4.3. As stated above, this is below the published rate of 60 mm/y. However, the network does not extend beyond the western half of the spreading system, and the geological estimate of 60 mm/y motion cannot be confirmed or denied.

7.2.4 Sites on the Australian Plate.

There are five sites shown in Figure 7.1, which are generally accepted as being on the Australian plate. These are Townsville, Aiambak, Port Moresby, Alotau and Misima. Figure 7.8a-b shows that no seismic activity has occurred between these sites. The velocity residuals in Figure 7.1 show very clearly that these sites (with the exception of Aiambak) are moving with the Australian plate. The result at Aiambak is discussed more fully in Section 7.5, but it seems most likely that an unknown perturbing error, such as a centring error occurred in the antenna setup or reduction in one of the two occupations of this site. Without a third occupation, this is impossible to verify. If the rate of change of the baselines between the other four sites are computed, the results show striking cohesion, which can be seen in Figure 7.6. Port Moresby to Alotau is changing by -3±7 mm/y. Between Alotau and Misima, the rate of change is 3±11 mm/y. If

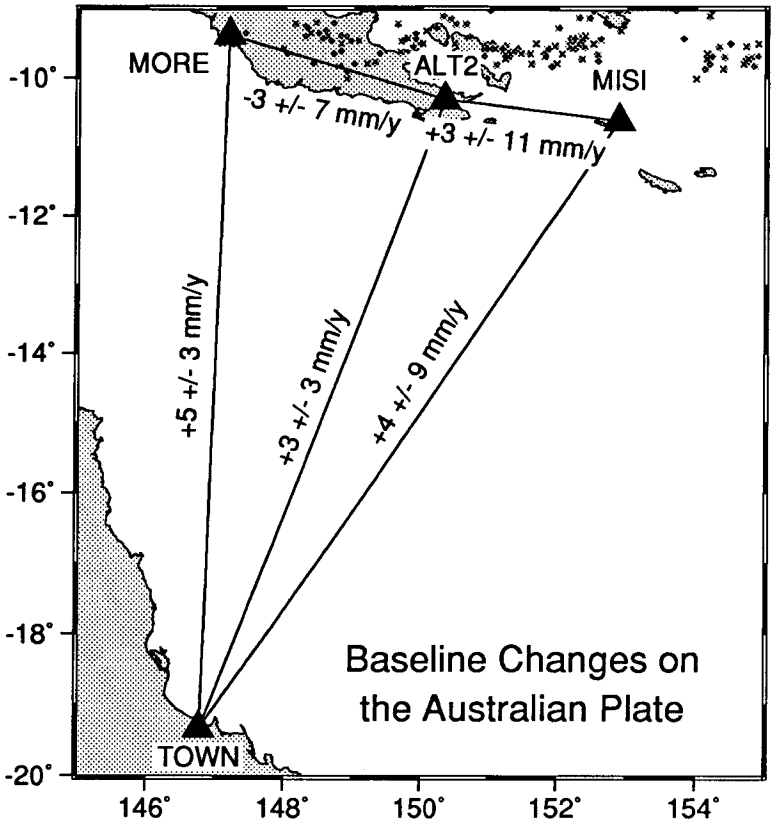

Figure 7.6 Rates of motion between four sites on the Australian plate with scaled errors. Shallow seismicity (0-60 km) is shown to indicate the location of the Woodlark Spreading Centre.

the network in increased to include Townsville, a similar pattern emerges. From Townsville, the rates of change to each of the following sites are: Port Moresby 5±3 mm/y; Alotau 4±3 mm/y; and Misima 4±11 mm/y. The scaled errors are given. In all cases, there is no statistically significant compression or extension occurring.

The velocity residuals and associated error ellipses for Morobe and Lae (UNIT), shown in Figure 7.1a-b are indicating that these sites are not significantly different from the Australian plate. The implications of this on the location of the Australian plate boundary with the proposed Solomon Sea plate are discussed in detail in Section 7.3.3. Again, it is interesting to look at the baseline rates of change and speculate on the possible implications.

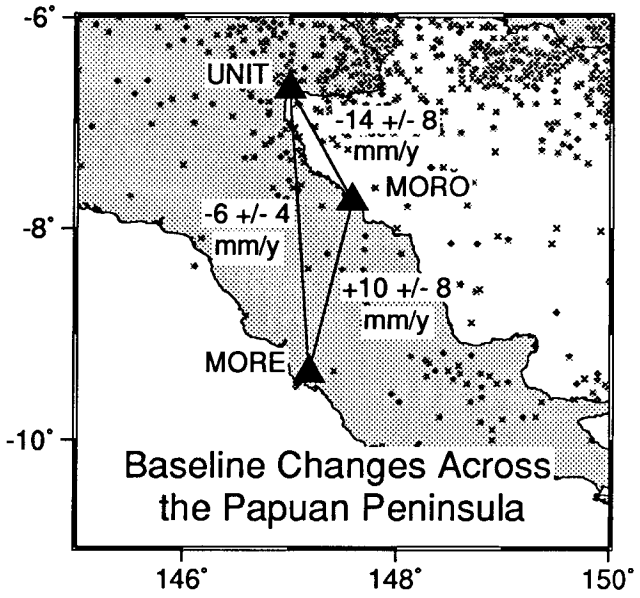

Figure 7.7 Rates of motion across the Papuan Peninsula from Morobe and Port Moresby to Lae (UNIT). Shallow seismicity (0-60 km) is also shown.

The lines from Port Moresby and Morobe to Unit are changing at a rate of -6±4 mm/y and -14±8 mm/y respectively, while Port Moresby to Morobe is changing at a rate of +10±8 mm/y. The scaled error estimates are given. The baseline results also support the notion that these sites are moving with the Australian plate. It is interesting to see that the rate of change between Port Moresby and Morobe is indicating extension. This is in conflict with the compression forces required to create the Owen Stanley Ranges. At 10 mm/y, however, it is not significantly different to zero. In this case, the signal to noise ratio is approximately 1:1. The results across the Owen Stanley ranges adds weight to the idea that these rates are good to about 10 mm/y and the insignificant motion of 10 mm/y between Port Moresby and Morobe could be a result of noise in the solution. These results imply that the Papuan Peninsula is now moving with the Australian plate. Since the seismic activity between these two sites is sparse, the geodetic results of no significant motion appear to be realistic. This is discussed further in Section 7.3.3.

7.3 Geodetic Results Applied to Unresolved Questions.

As discussed in Section 2.4.3, there are several unresolved questions about the number of microplates and the location of their boundaries in the Papua New Guinea region. These questions are as follows:

- Is there a South Bismarck Plate?

- Is there a North Bismarck Plate?
- Is there a Solomon Sea Plate?
- Is the Trobriand Trough active?
- Where is the south-western boundary between the Australian plate and proposed Solomon plate?
- Where is the south-western boundary between the Australian and proposed South Bismarck plate?
- Where is the boundary between the Australian and Caroline/Pacific plate to the north of New Guinea?

Answers to some of these questions are revealed in the geodetic results of this analysis.

7.3.1 Is there a South Bismarck plate?

The velocity residuals in Figure 7.1b clearly indicate that Jacquinot Bay is not moving with either the Pacific or Australian plates. The geodetic results do not reveal more than this fact. However, when this result is considered in light of the models proposed for the area and the distribution of seismic activity (Figures 2.7 and 7.8a-b), it seems to support the theory that there is a separate plate in the south Bismarck Sea. All models discussed in Section 2.4.3 agree on the existence of this microplate, and these results support this hypothesis.

Although this is the limit to the interpretation which can be performed with the current geodetic results, it is interesting to speculate further. If, as it seems, the South Bismarck plate does exist, how is it moving? The single velocity residual on this plate indicates that it is moving to the southeast. How does this fit in with the general tectonic picture? Figure 7.10 shows some absolute velocity vectors against the backdrop of shallow seismicity. This gives a clearer image of the motion of the plates and Jacquinot Bay on the South Bismarck plate relative to the tectonic features and plate boundaries. The Bismarck Sea Seismic Lineation, as the northern boundary of the South Bismarck plate, places some constraints on its motion. If the whole plate was moving to the southeast about some distant pole of rotation, the whole northern boundary should show spreading. The fact that it does not seems to imply that this is not how the plate is moving. With left-lateral, leaky transform motion in the west, and oblique, rapid spreading in the east, it appears as though the plate is rotating clockwise.

The left-lateral transform motion to the southwest of New Ireland could fit in with this scenario.

Of course, the type of boundaries depend upon the location of the pole of rotation of the plate, if indeed the South Bismarck plate is rotating. If it is rotating about its centre, in a similar way to the concentrically rotating bearing model proposed by DeMets (1995) for the Juan Fernandez microplate, the boundaries described above seem to fit.

This is, of course, pure conjecture. More than one site is required on a plate to determine a pole of rotation. Currently there is only one occupation of Witu, which is also on the South Bismarck plate. If this microplate is rotating about its centre, Witu should have a smaller absolute velocity than Jacquinot Bay, being located closer to the centre of the plate. Its velocity should have a greater west component than Jacquinot Bay. Madang and Rabaul could also be located on this plate. Additional occupations of these sites will be valuable in determining how the South Bismarck plate is moving, and relating it to the broad tectonic framework of collision between the Australian and Pacific plates.

7.3.2 Is there a North Bismarck plate?

Figure 7.1a reveals that the velocity residuals of Kavieng and Manus are not significantly different to the Pacific plate motion. There is no significant motion between these two sites, which conforms to the models shown in Figure 2.14, none of which show a boundary between these sites. This also agrees with the lack of seismic activity between these sites, shown in Figures 2.7 and 7.8a-b. The lack of a significant boundary, and the implication that the motion is the same as the Pacific plate seems to imply that the North Bismarck plate does not exist. This supports the work of Puntodewo *et al.* (1994) whose GPS results indicated that the Pacific plate extends as far west as Irian Jaya.

Puntodewo *et al.* (1994) assumed that the Caroline plate does not exist, which implies that the Manus Trench is not an active boundary. If the North Bismarck plate does not exist, as these results seem to indicate, the implication is that the Manus Trench is not a major plate boundary and activity along it is non-existent or very small. Seismicity along the Manus Trench is shallow and sparse, which also adds strength to the proposition that it is not a major plate boundary.

The rate of change of the baseline from Manus to Kavieng is -12±9 mm/y from the velocity residuals. The scaled error is given. The Kavieng - Manus baseline rate of change can also be estimated from the baseline repeatability plots because it was directly observed with GPS. Using only the horizontal components of the baseline repeatability gives an estimate of -7±9 mm/y. This is in agreement with the figure above, and not significantly different to zero. Whether there is some small amount of compression occurring between Kavieng and Manus cannot be determined from these results. It will be interesting to look at the results from future GPS surveys of these sites to see if this suggestion of minor compression is valid.

7.3.3 Is there a Solomon Sea plate?

This is a difficult question to answer and one which is not resolved by this research. Three boundaries of the proposed Solomon Sea plate are clearly defined: the New Britain Trench to the northwest and northeast; and the Woodlark Spreading Centre to the southeast. The location of the south-western boundary, between the Australian and Solomon Sea plates, is disputed in the literature. These results do not unambiguously define this plate. Morobe and Losuia appear to be moving with the Australian plate. Two sites, Losuia and Guasopa, could be located on either the proposed Solomon Sea plate, or the Australian plate, depending upon the location of this boundary.

This leads into the next important question: where is the south-western boundary between the Australian plate and proposed Solomon plate?

Indications from this research are that the Owen Stanley Ranges do not form the current boundary between the Australian and proposed Solomon Sea plates. Port Moresby and Morobe are both moving with the Australian plate, which means there is no active compression occurring along the Papuan Peninsula.

The residual at Losuia has a significant, but small, northward residual. The mainly northward residual velocity with respect to the Australian plate is realistic when it is considered that the Woodlark Spreading Centre is active to the south of Losuia. The small westward component of the residual is also realistic because the Woodlark Spreading Centre is opening at a more rapid rate to the east, which implies an anticlockwise rotation of the Solomon Sea. Weissel *et al*

(1982) suggest that the pole about which the spreading centre is opening is located approximately 15° to the west (see Section 2.4.3), which is consistent with lower rates of spreading in the west.

The residual at Guasopa also displays a predominantly northward component, but has a small eastward motion with respect to the Australian plate. However, the error ellipse is very large rendering this site useless for serious interpretation. It will be interesting to see how this site performs when it is reoccupied. However, its value will remain limited by the lack of a good pre-existing solution with which to compare it.

Figure 7.8a-b shows that there is sparse shallow seismicity between the Papuan Peninsula and Losuia. The majority of the seismic activity is confined to the region of the Woodlark Spreading Centre, so there is no obvious boundary occurring between the Papuan Peninsula and Losuia. Baseline changes computed from velocity residuals indicate a motion of -20±7 mm/y between Port Moresby and Losuia. Between Morobe and Losuia, a shortening of 10±9 mm/y is occurring. These are scaled error estimates. The rate between Morobe and Losuia is clearly insignificant. The rate between Port Moresby and Losuia is approaching a 3:1 signal to noise ratio, but at present is not significantly different to zero. This is another area in which new, more precise GPS solutions should be able to clarify the uncertainty in these results. Based on these results, there does not appear to be motion indicative of a plate boundary between the Papuan Peninsula and Losuia.

The triple junction analysis of the Solomon Sea/ Australian/ Bismarck triple junction shown in Section 2.4.3 revealed that the motion required along the Trobriand Trough if this junction is to exist, greatly exceeds all current estimates of motion, if indeed there is any. The implication of this is that the Trobriand Trough also does not form the boundary between the Solomon Sea plate and the Australian plate.

If the Owen Stanley Ranges and the Trobriand Trough do not form this boundary, then it is difficult to find an alternative location for it. Abers and Roecker (1991) suggested that the boundary might be a weakly deforming zone to the northeast of the Papuan Peninsula, but that motion should be small and predominantly left-lateral slip at the Trobriand Trough. Left-lateral motion is consistent with north-westward motion of the Solomon Sea due to the

increased rate of spreading to the east of the Woodlark Spreading Centre. Small motion will not satisfy the triple junction analysis discussed previously. The residual at Losuia is, however, consistent with left-lateral motion, but if left-lateral slip is occurring at the Trobriand Trough, it should not be evident at Losuia, which lies to the south of the Trough.

If there is no south-western boundary to the Solomon Sea plate, it is difficult to see how it can exist. If it does not exist, which seems to be indicated by these results, then the New Britain Trench must be accommodating all of the collision between the Australian plate and the Pacific plate. Where does this leave the Woodlark Basin Spreading Centre? Benes *et al.* (1994) have proposed that the Solomon Sea is being dragged away from the Australian plate by the action of the Pacific plate. Several authors (discussed in Section 2.4.3) have suggested that the Woodlark Spreading Centre is propagating into the Papuan Peninsula. If the Solomon Sea is being dragged away by the Pacific plate, then the Woodlark Basin represents a "tear" in the lithosphere. By the active plate theory discussed in Section 2.3.4, the Woodlark Spreading Centre represents a "gap" in the lithosphere, caused by the tearing action, which is being filled with material from the asthenosphere.

If this proposal is indeed what is happening in the Solomon Sea, there should be some evidence of an anticlockwise rotation. Could this explain the north-northwest residual at Losuia and the east-northeast residual at Guasopa? This speculation cannot be confirmed or denied by this research. Future observations on these two sites might provide evidence for or against a rotation of the Solomon Sea.

7.3.4 Is the Trobriand Trough Active?

This has been discussed above. The GPS data available cannot assist in answering this question, as there are no survey sites located to the northeast of the Trough. This was not an oversight in the planning, but a logistical constraint on the surveys due to lack of islands! Therefore, other means must be used to answer this question.

7.3.5 Where is the south-western boundary between the Australian and South Bismarck plates?

This question is also debated in the literature, as shown in Section 2.4.3. The residual for Lae (UNIT in Figure 7.1) helps to shed some light on this question. Lae lies within the Markham Valley. Its velocity residual is indicating that this site is moving with the Australian plate. This seems to imply that the Ramu-Markham Fault Zone is not the major boundary between these plates.

Motion between the Australian and Bismarck plates is compressional. Looking at the rate of change of the baseline between Morobe and Lae shows a small amount of compression, which may not be above the uncertainty of the solution. A rate of -14±8 mm/y (scaled error), is not statistically different to zero. It was suggested by Cooper and Taylor (1987b) that the Ramu-Markham Fault is a north dipping thrust which allows the Finisterre Block to over-ride the Australian plate. The insignificant rate above is clearly not accommodating the northeast motion of the Australian plate, required at such a boundary. Lae itself is located in the Markham Valley, and not in the numerous mountain ranges of the Huon Peninsula. As such, it may not be in a location which would show this process. The mountain ranges to the north of the Ramu-Markham Valley show intense seismic activity (Figure 7.8a-b) to a depth of about 150 km. Earthquakes occur at greater depth, to about 250 km, off the northern coast of Papua New Guinea, which seems to suggest a north-dipping Wadati-Benioff zone. However, with no sites located in the ranges or along the coast to the north of the Ramu-Markham Fault, this analysis cannot resolve this problem.

7.3.6 Where is the boundary between the Australian and Caroline/Pacific plate to the north of New Guinea?

The absolute velocities of the sites, shown in Figure 7.2, seem to be implying that all mainland PNG sites are moving with the Australian plate, including Vanimo. This site is certainly not displaying the motion of the Pacific plate. However, when the Australian plate velocity is subtracted, it becomes clear that Vanimo has a significant southward residual with respect to the Australian plate. This could be implying internal deformation of the Australian plate. An alternative possibility that cannot be refuted at this stage, is that the residual is a factor of the one year separation between observations, coupled with possible set-up errors.

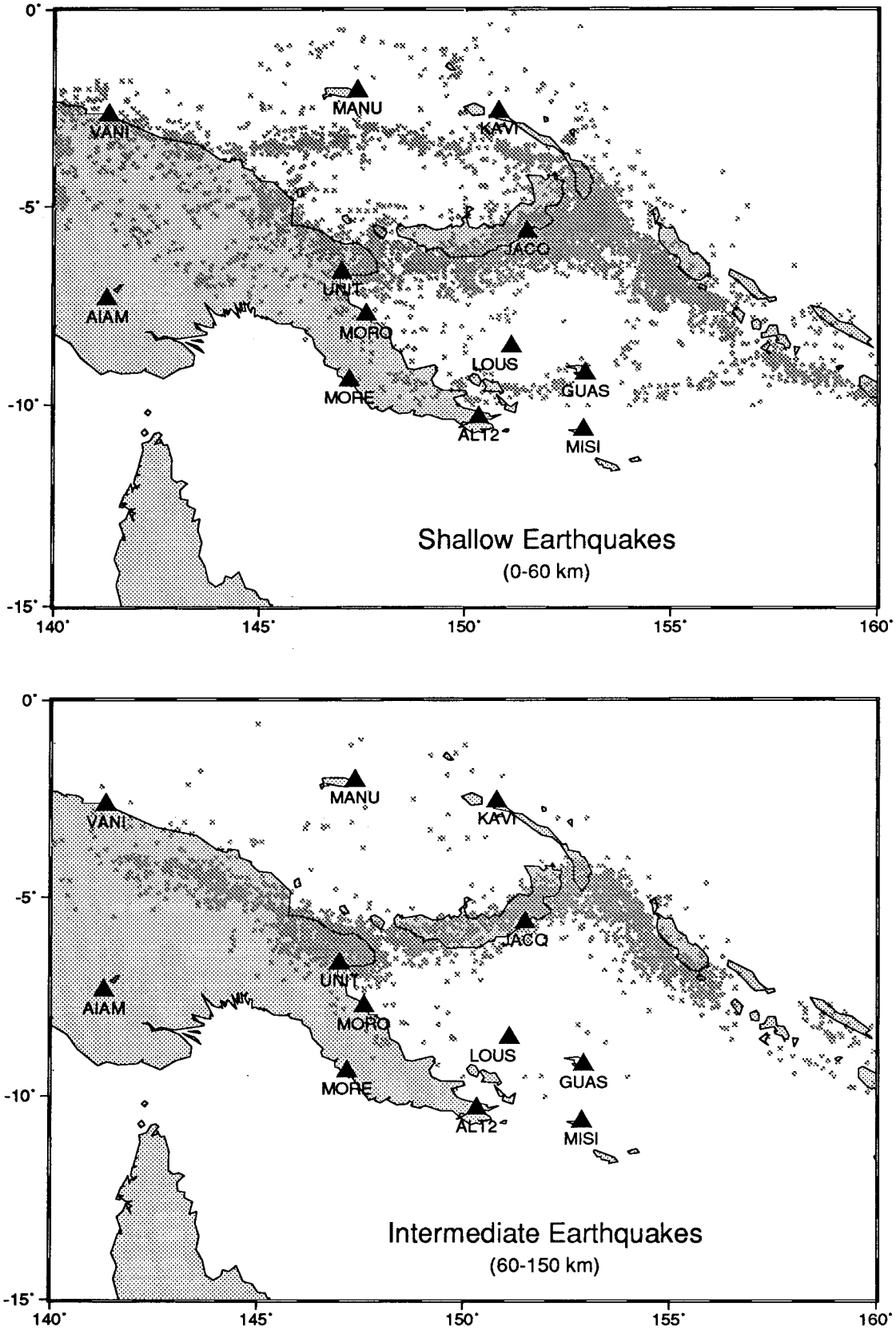

Figure 7.8a-b The location of the survey sites relative to the zones of:
(a) shallow seismicity, and (b) intermediate depth seismicity.

According to Cooper and Taylor (1987b), in the vicinity of Vanimo, the Pacific plate should be subducting beneath the Australian plate. Seno and Kaplan (1988) suggest that to the west of 140°E, the convergence between the two plates is accommodated by internal deformation of the Australian plate, and that between 140°E and 144°E the Bismarck plate is being subducted beneath the Australian plate. Vanimo is situated at approximately 141.3°E. Figure 7.8a-b show the location of the survey sites superimposed over the seismicity.

It is clear from Figure 7.3a that Vanimo is located in the midst of numerous shallow earthquakes. Figure 7.3b shows that Vanimo is located to the north of the tail end of the intermediate-depth earthquake activity. There is no deep earthquake activity around Vanimo, as shown in Figure 7.4. It is perhaps not surprising then to see a southward velocity residual. The geodetic results seem to support the proposal that internal deformation of the Australian plate is occurring, perhaps as far east as Vanimo.

7.4 The Localised effect of the Woodlark Spreading Centre.

The Woodlark Spreading Centre is propagating westward into the Papuan Peninsula in the vicinity of Normanby and Ferguson Islands. Alotau is situated only about 60 km to the south of this, on the southern shore of Goodenough Bay. Despite the proximity of this site to the propagating rift, it is showing no sign of deformation. The residual of this site with respect to the Australian plate is no more than a few millimetres and well within the noise of the solution.

Likewise, Misima is located less than 200 km from Guasopa with the Woodlark Spreading Centre in between. Misima is clearly moving with the Australian plate. The residual at Misima is well below the level of noise of the solution.

7.5 Eastward Motion of Aiambak

The eastward residual at Aiambak with respect to the Australian plate is a surprising result. At 29 mm/y, the residual is at the level of 3σ, which is generally considered to be the boundary between significance and insignificance of a result. However, there is no geological evidence to support such motion. Aiambak is located on the Fly Platform. Geological studies have shown that this part of Papua New Guinea is continuous with the Australian craton. There is no seismic activity in the vicinity to indicate a plate boundary or

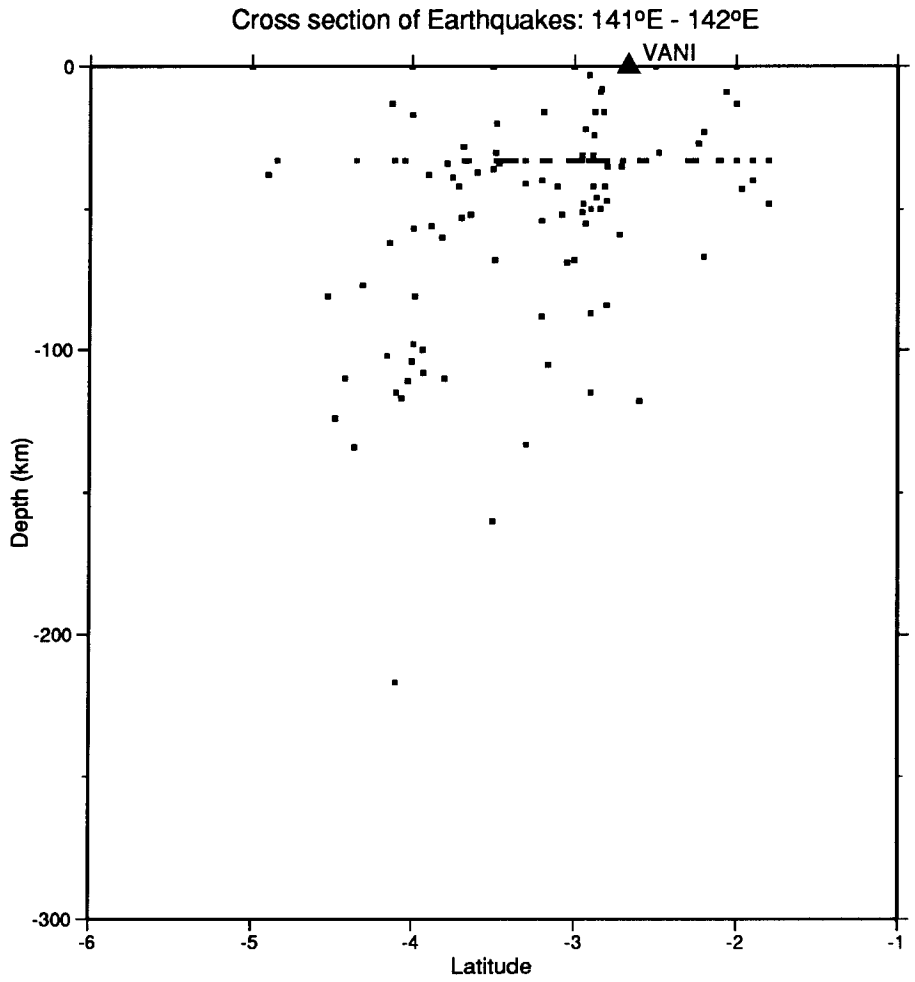

Figure 7.9 A cross section of seismicity at Vanimo.

internal deformation of the Australian plate (Figure 7.3). The solution for this site is clearly of the same standard as any of the other sites for which there were only two occupations, separated by only one year, such as Unit, Vanimo. However, the fact that the residual is clearly larger than the residuals at other sites which are expected to be on the Australian plate requires some consideration. The most likely cause of this anomalous motion at this stage is an erroneous occupation of the site at either of the observation periods. With a velocity residual of 29 mm/y and a span of one year between observations, it is a relatively small error to be investigating. It is quite possible that an antenna centring, or measurement error, or an error in the reduction of the antenna height could have occurred.

This highlights the point made above that two observation epochs are insufficient to obtain a reliable velocity estimate. If there was a third observation

on this site, it would reveal whether this is a genuine result, or a product of an erroneous site occupation.

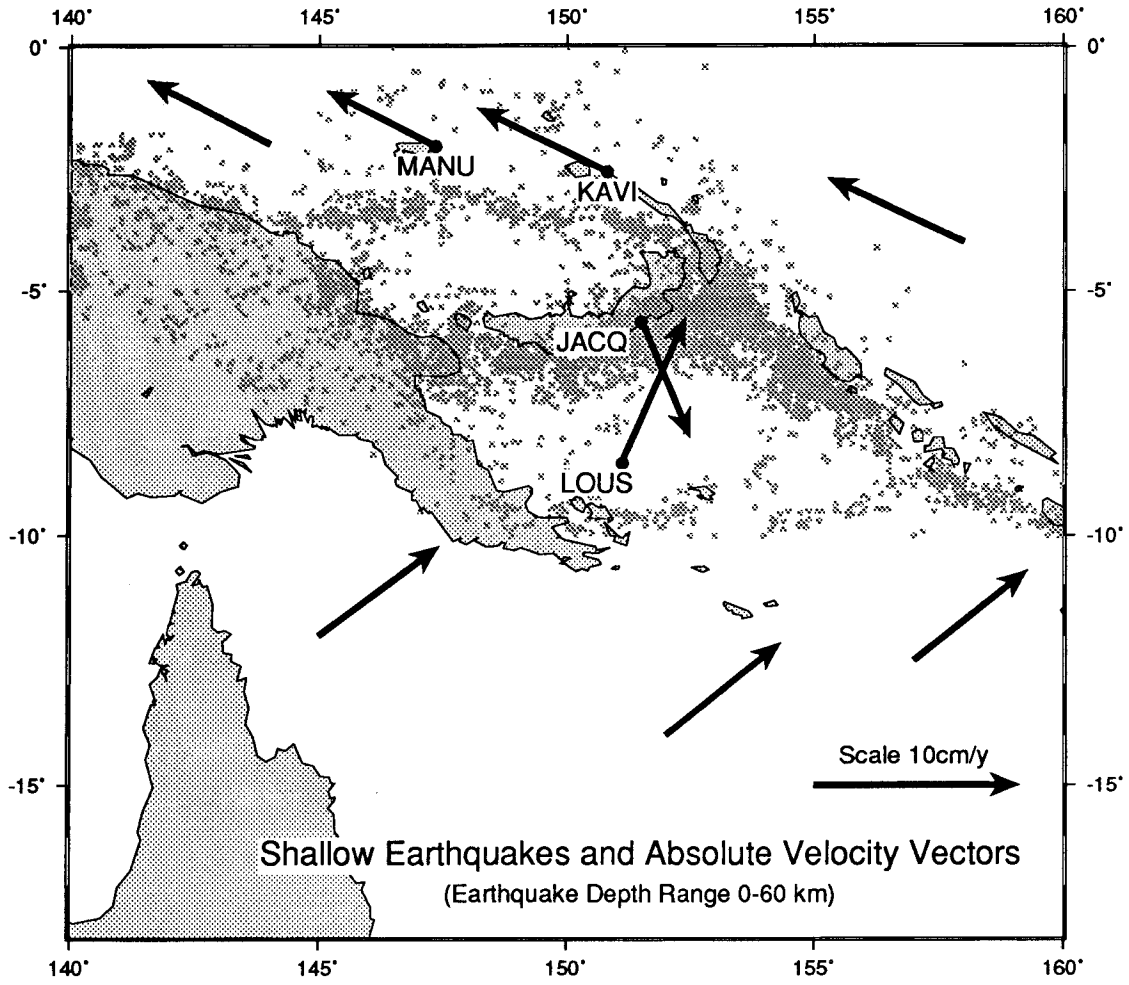

Figure 7.10 NUVEL-1 estimates of plate velocities for random points on the Australian and Pacific plates in relation to the tectonic features and boundaries associated with intense seismic activity.

Chapter 8

Conclusions and Recommendations

8.1 Summary of the Main Results

The aims of this thesis, as stated in Chapter 1, were to reduce the data from several GPS campaigns between 1990 and 1994; combine these results into a consistent ITRF94 reference frame; and to use the results to interpret the tectonics of the Papua New Guinea region. These aims have been met. As discussed in Chapter 6, the data have been successfully reduced and put into the ITRF94 reference frame at epoch 1993.0. The interpretation performed using these results has been discussed in Chapter 7.

A significant issue in this analysis was how to combine campaigns with significantly different global tracking networks into a consistent reference frame. There are several quality assurance indicators discussed in Chapter 6 that indicate that the reference frame is consistent at the level of 10-15 mm.

The main findings of this research are summarised below. The uncertainties shown here are scaled error estimates. A discussion of the precision of the results was given in Chapters 6 and 7. It should be emphasised that the scaled errors of the baseline results are consistent with the error ellipses shown in Figures 7.1 and 7.2. The precision of the results is the limiting factor in the interpretation of these results. The limitations of this research are highlighted, and areas in which additional data and analysis are required are outlined.

This analysis shows that the New Britain Trench is accommodating convergence of 130±5 mm/y between Losuia and Jacquinot Bay, which is in agreement with the geological estimates and the work of McClusky *et al.*, (1994). Towards the western end of the New Britain Trench, the convergence rate is found to be 107±11 mm/y and 102±11 mm/y for the lines Morobe - Manus and Lae - Manus respectively. These rates are not statistically different to the rate between Losuia and Jacquinot Bay at the 95% confidence

level, the normally accepted level. At the more lax 90% level, the difference is significant. This rate is significantly different to the geological estimate of approximately 60 mm/y discussed in Section 2.4.3. With a second occupation of Witu, and a third occupation on Jacquinot Bay, Morobe and Manus, the decrease in rate to the west, which is insignificant in this analysis, can be investigated further. The new data, even if no more precise, will be able to make use of a greater time span, which will improve the precision and thus noise will be lowered. It might, therefore, be able to determine if this is a significant decrease, or simply solution noise.

The rate of spreading across the Bismarck Sea Seismic Lineation from this analysis is 127±11 mm/y between Jacquinot Bay and Kavieng, and 116±11 mm/y between Jacquinot Bay and Manus. These values are not statistically different to the value published by McClusky *et al.* (1994) or the geological rate. Again, a second occupation of Witu, and a third on Jacquinot Bay and Manus will strengthen the geodetic estimate of motion.

Measurements across the western end of the Woodlark Spreading Centre show a rate of opening of 30±23 mm/y between Misima and Guasopa, decreasing to 18±8 mm/y between Alotau and Losuia. Although significantly less than the geological rate of approximately 60 mm/y, this estimate is for the western end of the Woodlark Spreading Centre. This result, therefore, supports the proposal of several authors, for example Weissel *et al.* (1982), that the rate of spreading decreases to the west. The acquisition of additional data will also improve these results and increase the signal to noise ratios, which will add significantly to the hypothesis of decreasing rates to the west.

Velocity residuals with respect to the Australian and/or Pacific plates present a remarkably simple picture of the region, with sites appearing to be located on one of only three plates. Port Moresby, Alotau and Misima are clearly moving with the Australian plate, as expected from geology and a lack of seismicity between these sites and the Australian mainland. The residual at Morobe is also indicating that this site is moving with the Australian plate. The implication of this result is that there is no significant compression occurring across the Owen Stanley Ranges, and the northern boundary of the Australian plate is not located here. Losuia and Guasopa have residuals that have a slightly higher north component than predicted by NUVEL1, but are not significantly different to the Australian plate motion, at the precision level of this analysis. Guasopa is

a weak result, and not very useful for interpretation. The implication of the result at Losuia is that the boundary between the Solomon Sea and Australian plates does not occur between Losuia and the Papuan Peninsula. Triple junction analysis of the Solomon, Australian and South Bismarck triple junction requires a high rate of motion along the Trobriand Trough in order to be valid. This does not appear to be occurring. One reason for a triple junction to be invalid is that the triple junction does not exist. This could mean that the Trobriand Trough also does not form the boundary of the Solomon/Australian plates. Without a clearly defined southwestern boundary, the existence of the Solomon Sea plate is questionable. Further field/survey work is required to resolve the situation here, although the scarcity of islands to the northeast of the Trobriand Trough makes direct GPS observations difficult. Analysis of this trench will have to rely on a combination of GPS and other sources of data, such as seismicity and heat flow.

The velocity residuals for Manus and Kavieng indicate that these sites are moving with the Pacific plate. This result tends to favour the models, for example, Taylor (1975), in which there is no North Bismarck plate. There is a hint of compression between these sites, which is currently below the precision of the data. It is not inconceivable that some compression could be occurring due to the proximity of these sites to the plate boundary. New data for these sites may clarify this. In addition, new data for Nuguria will provide more evidence, as this site is located well to the east of the boundary.

Jacquinot Bay is moving with neither the Australian nor the Pacific plates. The velocity residuals with respect to both plates are of the order of 100 mm/y. This, combined with the pattern of seismic activity, agrees with the models that propose the existence of a South Bismarck plate (see Figure 2.14). The way in which the South Bismarck plate is moving cannot be resolved on the result from one site.

Vanimo is showing a southward velocity residual with respect to the Australian plate. This could be evidence of deformation occurring in the Australian plate at its margin with the Pacific or Caroline plate. Alternatively, it could mean that Vanimo is not on the Australian plate at all. The absolute velocity vectors seem to imply that it is basically moving with Australia, but that the northward component is less than predicted by NUVEL1, possibly implying resistance to northward motion. Although there seems to be a valid geological basis for this

result, additional data on this site should indicate whether it is real, or a caused by an error in the geodic results. The result for Vanimo is of the same quality as other sites with similar observation patterns, given by the size of the error ellipse. There is, therefore, no reason to suspect the reduction of the observations. However, it is possible that the residual is the result of errors in the setup during either or both of the two epochs of observation. These comments also apply to Aiambak, discussed below.

Aiambak, which should be located firmly on the Australian plate according to geology and seismicity, is showing an eastward residual with respect to the Australian plate of approximately 30 mm/y. Geologically, there seems to be no basis for this result. It is felt, therefore, that the most likely cause of this residual is an error in either or both of the surveys. The observations for both Vanimo and Aiambak are separated by only one year, which means that errors of the order of 3 cm in either occupation of both sites could cause the velocity residuals. Such an error in the set up or reduction of the antenna is possible. Without a third occupation, there is no redundancy to allow for error detection. A future occupation of this site is highly recommended.

8.2 Suggested Future Research

The data used in this analysis was collected over a relatively short observation span. In addition, some of the sites used in this analysis have only been observed on two occasions. The dangers associated with double occupations were discussed in Chapter 6. Whilst these sites have greater uncertainties than those sites with multiple observation epochs, any errors that could easily have occurred in the occupation of these sites cannot be detected because there is no redundancy in the system. Errors will directly influence the velocity estimates for those sites. Therefore, the first recommendation is that this research is continued, with additional surveys to give a greater time span and multiple occupations of all sites.

This recommendation has been partially fulfilled recently. A major survey has been recently completed (August, 1996) in which the sites Port Moresby, Morobe, Alotau, Misima, Guasopa, Losuia, Witu, Jacquinot Bay, Kavieng, Manus, Nuguria, Carteret and Madang were reoccupied. This gives a six year time span of observations on most sites. New marks were observed at Rabaul

and Lae. The original mark at Rabaul was observed for a couple of days, but its stability is doubtful.

On some sites, this recent survey will give a third epoch of GPS data, which will strengthen the estimates of position and velocity on these sites considerably. These sites are Jacquinot Bay, Alotau, Morobe, Guasopa and Manus. The strength of the occupation of Guasopa is expected to give a good estimate of its position, but as stated in Chapters 6 and 7, Guasopa is very poorly determined in this analysis, which does not give a strong basis for comparisons. Additional future observations at Guasopa are highly recommended.

Other sites (Witu, Madang, Nuguria and Carteret) have been given a second epoch of measurements. Whilst these will now be available for interpretation of the tectonics, it must be remembered that these sites still lack redundancy, and any errors will be directly mapped into site velocity. Obtaining additional observations on these sites is still a high priority.

Mentioned above in the summary of the main findings were some areas in which this analysis is limited. This will now be elaborated upon.

8.2.1 The Bismarck Sea Region

From a geophysical viewpoint, understanding the motion of the Bismarck plate is important. As mentioned above, this research shows that Jacquinot Bay is moving with neither the Australian nor the Pacific plates. Although it is tempting to use this result to speculate about how the Bismarck plate is moving, a true understanding of the tectonic processes in action cannot be gleaned on the basis of one site. With a second occupation (and hopefully third, sometime in the future) on Witu and Madang, several unresolved questions may be answered. An important question to determine is whether there is any deformation occurring between these sites. That is, is the Bismarck Sea behaving as a rigid plate, as seismic activity suggests? The velocity vector for Jacquinot Bay seems to be implying that the plate is moving southeast. It is difficult to envisage the geometry of forces required to make a fragment between two northerly moving plates, move towards the south. Is there any evidence for a clockwise rotation of the Bismarck plate? A clockwise rotation, as proposed by Hamilton (1979), would best fit the left-lateral faulting at the

western end of the Bismarck Sea Seismic Lineation and the spreading component to the east. The recent second occupation on Witu, on the Bismarck plate, and Madang, possibly on the Bismarck plate, should clarify how this plate is moving.

8.2.2 The Solomon Sea Region

Another area that has not been resolved in this analysis is the Solomon Sea. This study seems to be indicating that the Solomon Sea is part of the Australian plate, but this result does need investigating further. Activity across the Trobriand Trough is difficult to measure directly because of the logistical constraint of requiring islands on which to locate stable GPS sites. However, triple junction analysis seems to demonstrate that current estimates of motion along this feature are insufficient to satisfy the geometry of a triple junction, suggesting it is not a major boundary. The motion of the Solomon Sea must, one would expect, display some differences to the Australian plate motion because of the action of the Woodlark Spreading Centre to the south. New GPS observations, with their higher precision, and a longer time span since the initial observations, should be able to show if there is evidence of an anti-clockwise rotation. With the opening rate greater in the east, this is where you would expect to see the greatest effect. Existing survey sites cover the western to central regions of the Woodlark Spreading Centre, and while the trend, if it exists, should also be apparent here, its effect will be smaller.

Although Guasopa has been recently reobserved, the observations used in this analysis were very poor. This analysis does not provide a well determined position or velocity for this site, which means that the recent reoccupation will be of limited value for tectonic analysis. A further reoccupation is required to obtain a reliable position and velocity estimate for Guasopa. Guasopa is an important site for studying the rate of Spreading of the Woodlark Spreading System. The dense survey network established in this area in 1991 has yet to be reoccupied. This analysis has given a tenuous indication that the spreading rate is decreasing to the west near the Papuan Peninsula. The dense network established in 1991 has definite merit for studying the spreading rate along the western portion of the spreading centre, and, with GPS precisions greatly improved with modern data, it may be possible to detect the small differences in motion that must be occurring in the western regions if indeed the rift is propagating into the Papuan Peninsula.

8.2.3 The Pacific Boundary Region

A significant limitation of this analysis is the lack of a connection to the Pacific plate. Second occupations on Nuguria, Carteret and Tasman Island will provide this important link. Although this analysis shows Kavieng and Manus to have motions of the Pacific plate, occupations on these sites will give short baselines along which to look for any signs of compression that could indicate remnant activity along the Manus/North Solomon Trench.

The transform motion along the northeastern boundary of the South Bismarck plate should also be discernible in comparisons between the South Bismarck sites and the Pacific sites.

Velocities for the Pacific sites will also allow the rate of subduction to the east along the New Britain Trench to be determined. This analysis was confined to looking at the central and western portions of the trench. A more complete picture should emerge with estimates of motion in the east.

8.2.4 Northern and Western Papua New Guinea

An area that has really been neglected in this analysis is the western region of Papua New Guinea. With the exception of Vanimo and Aiambak, the sites in western Papua New Guinea have only single occupations. The problem of the location of the boundary in this region could be elucidated by the establishment of a more dense survey network around the coast, including the volcanic islands to the north of the coastline, extending to the south, into the New Guinea Highlands and the Papuan Fold Belt. With such a survey network, the extent of the internal deformation of the Australian plate, if indeed that is what is occurring, could be analysed. Additional occupations on this and other sites in western Papua New Guinea, and ideally extending into Irian Jaya, will clarify the type of motion that is occurring along the northern boundary of the Australian plate. Is the collision being accommodated by internal deformation of the Australian plate as indications seem to suggest?

As mentioned above, extending the survey network to the volcanic islands off the northern coast of PNG will also help clarify the type of boundary in this region. Some unanswered questions include: Is there really a transition between active subduction and arc-continent collision? Is there any evidence to

support the proposal that the subduction polarity is reversing, following collision of the Bismarck Island Arc with the PNG landmass? Is there evidence to support the theory that the collision suture is healed to in the west of PNG and into Irian Jaya?

Studying this small region of PNG, whilst very interesting because of the diversity of tectonic features, only encompasses a very small section of the northern boundary of the Australian plate. Extending the study to the west to incorporate Irian Jaya could help to answer questions relating to, for example, the nature of the boundary and the existence of the Caroline plate.

Geodetic results should not, of course, be viewed in isolation. Combining the GPS results with other techniques currently used to study geophysics should give a more complete understanding of the tectonic processes in action at this major boundary.

References

Abbott L. D. (1995) Neogene tectonic reconstruction of the Adelbert-Finisterre-New Britain collision, northern Papua New Guinea. Journal of Southeast Asian Earth Science, 11(1): 33-51.

Abers G. A. Roecker S.W. (1991) Deep structure of an arc-continent collision: earthquake relocation and inversion for upper mantle P and S wave velocities beneath Papua New Guinea. Journal of Geophysical Research, 96(B4): 6379-6401.

Allegre C. (1988) The Behaviour of the Earth: Continental and Seafloor Mobility. Harvard University Press, Cambridge, Massachusetts and London, England, 272 pp, 1988.

Anderson D. L. (1995) Lithosphere, Asthenosphere, and Perisphere. Reviews of Geophysics, 33(1): 125-149.

Australian National Mapping Bureau (1983), PNG Crustal Motion Survey, Division of National Mapping, Canberra, Australia, Unpublished Report.

Bain J. H. C. (1973) A summary of the main structural elements of Papua New Guinea. The Western Pacific Island Arcs, Marginal Seas, Geochemistry., Editor P.J. Coleman.

Benes V., Scott S. D., Binns R. A. (1994) Tectonics of rift propagation into a continental margin: western Woodlark Basin, Papua New Guinea. Journal of Geophysical Research, 99(B3): 4439-4455.

Brooks J. A., Connelly J. B., Finlayson D. M., Wiebenga W. A. (1971) St George's Channel - Bismarck Sea Trough. Nature, 229: 205-207.

Brown D. C., Trotter J. E. (1969) SAGA, A Computer Program For Short Arc Geodetic Adjustment of Satellite Observations Report Number AFCRL-69-0800, Final Report for Contract Number F19628-69-C-0264 by DBA Systems Inc, P.O. Drawer 550 Melbourne, Florida 32901, to Air Force Cambridge Research Laboratories, Bedford Massachussetts,

Brunner F. K., Welsch W. M. (1993) Effect of the Troposphere on GPS Measurements. GPS World, 4(1) January 1993:42-51

Circum- Pacific Council for Energy and Mineral Resources, 1982. Plate Tectonics Map of the Circum-Pacific Region. Compiled by The Circum-Pacific Council for Energy and Mineral Resources. Published by The American Association of Petroleum Geologists. Tulsa, Oklahama, USA

Connelly J. B. (1974) A structural interpretation of magnetometer and seismic profiler records in the Bismarck Sea, Melanesian Archipelago. Geological Society of australia Journal, 21:459-469.

Connelly J. B. (1976) Tectonic development of the Bismarck Sea based on Gravity and magnetic modelling. Geophysical Journal of the Royal Astronomical Society, 46: 23-40.

Cooper P., Taylor B. (1987a) The spatial distribution of earthquakes, focal mechanisms and subducted lithosphere in the Solomon Islands. Circum-Pacific Council for Energy & Mineral Resources, 7: 67-88.

Cooper P., Taylor B. (1987b) Seismotectonics of New Guinea: a model for arc reversal following arc- continent collision. Tectonics, 6(1): 53-67.

Counselman C. C. (1981) Miniature interferometer terminals for Earth surveying - MITES. CSTG Bulletin, Vol. 3, International Activities, Technology and Mission Developments.

Cox A., Hart R. B. (1986) Plate Tectonics (How it Works). Blackwell Scientific Publications, 392pp.

Curtis J. W. (1973) Plate tectonics of the Papua New Guinea - Solomon Islands region. Journal of the Geological Society of Australia, 20 Pt.1: 21-36.

Davies H. L., Symonds P. A., Ripper I. D. (1984) Structure and evolution of the southern Solomon Sea region. BMR Journal of Australian Geology & Geophysics, 9: 49-68.

Davies H. L., Honza E., Tiffin D. L., Lock J., Okuda Y., Keene J.B., Murakami F., Kisimoto K. (1987) Regional setting and structure of the western Solomon Sea. Geo-Marine Letters, 7: 153-60.

DeMets C. (1995) Plate motions and crustal deformation. Reviews of Geophysics Supplement, July : 365-369.

DeMets C., Gordon R. G., Argus D. F., Stein S. (1990) Current plate motions. Geophysical Journal International, 101: 425-478.

Denham D. (1969) Distribution of earthquakes in the New Guinea - Solomon Islands region. Journal of Geophysical Research, 74(17): 4290-4299.

Eguchi T., Fujinawa Y., Ukawa M., Bibot L. (1987) Microearthquakes along the back-arc spreading system in the eastern Bismarck Sea. Geo-Marine Letters, 6: 235-40.

Eguchi T., Fujinawa Y., Ukawa M., Bibot L. (1989) Earthquakes associated with the back-arc opening in the eastern Bismarck Sea: activity, mechanisms, and tectonics. Physics of the Earth & Planetary Interiors, 56: 189-209.

Eisenhart C. (1963). Realistic Evaluation of the Precision and Accuracy of Instrument Calibration Systems. Journal of Research of the National Bureau of Standards, 67C(2):161-187.

Elder J. (1976) The Bowels of the Earth. Oxford University Press, Oxford, UK.

Exon N. F., Tiffin D.L. (1984) Geology and petroleum prospects of offshore New Ireland Basin in northern Papua New Guinea. Transactions of the 3rd Circum-Pacific Energy and Mineral Resources Conference, Honolulu 1982: 623-630.

Exon N. F., Stewart W. D., Sandy M. J., Tiffin D. L. (1986) Geology and offshore petroleum prospects of the eastern New Ireland Basin, northeastern Papua New Guinea. BMR Journal of Australian Geology and Geophysics, 10: 39-51.

Falvey D. A., Pritchard T. (1984) Preliminary paleomagnetic results from northern Papua New Guinea: evidence for large microplate rotations. in Watson S. T. (editor), Transactions of the 3rd Circum-Pacific Energy and Mineral Resources Conference, 22-28 August, 1982, Honolulu, Hawaii, p593-599.

GAMIT Manual (1995) Documentation for the GAMIT GPS Analysis Software, Release 9.40. Department of Earth, Atmosphere and Planetary Sciences, Massachusetts Institute of Technology; and Scripps Institute of Oceanography, University of California, San Diego, November 1995.

Georgiadou Y., Doucet K. D. (1990) The issue of Selective Availability. GPS World, Sept/Oct 1990: 53-56.

Gurtner W., Mader G. (1990) Receiver Independent Exchange Format Version 2. GPS Bulletin, 3(3):1-8.

Hager B. H., King R. W., Murray, M. H. (1991) Measurement of Crustal Deformation using the Global Positioning System. Annual Review of the Earth and Planetary Sciences, 19: 351-82.

Hamilton W. (1979) Tectonics of the Indonesian region. Geolical Survey Professional Paper, 1078: 288-307.

Heki K. (1996) Horizontal and Vertical Crustal Movements from Three-Dimensional Very Long Baseline Interferometry Kinematic Reference Frame:Implication from the Reversal Timescale Revision. Journal of Geophysical Research, 101(B2):3187-3198.

Herzig P., Hannington M., McInnes B., Stoffers P., Villinger H., Seifert R., (1994) Submarine volcanism and hydrothermal venting studied in Papua New Guinea. EOS 75 (44): 513.

Hoffmann-Wellenhof B., Lichtenegger H., Collins J. (1994) Global Positioning System Theory and Practice 3rd edition, Springer-Verlag, Wien.

Johnson R. W. (1979) Geotectonics and volcanism in Papua New Guinea: a review of the late Cainozoic. BMR Journal of Australian Geology and Geophysics, 4: 181-207.

Johnson T., Molnar P. (1972) Focal mechanisms and plate tectonics of the southwest Pacific. Journal of Geophysical Research, 77(26):5000-5031.

Joshima M., Honza E. (1987) Age estimation of the Solomon Sea based on heat flow data. Geo-Marine Letters, 6: 211-7.

Karig D. E. (1971) Origin and Development of marginal basins in the western Pacific. Journal of Geophysical Research, 76: 2542-2561.

Karig D. E. (1972) Remnant Arcs. Geological Society of America Bulletin, 83:1057-1068.

Kincaid C. (1995) Subduction Dynamics: From the trench to the core-mantly boundary. Reviews of Geophysics Supplement, July : 401-12.

Kirchoff-Stein K. S., Silver E. A., Bernstein-Taylor B. L., Mackay M. L. (1992) Active convergence at the Trobriand Trough system, southwestern Solomon Sea. EOS Transactions AGU, October 27: 536.

Klobuchar J. A. (1991) Ionospheric effects on GPS. GPS World, April 1991:48-51.

Krause D. C. 1973. Crustal Plates of the Bismarck and Solomon Seas. In Oceanography of the South Pacific, 1972. Compiled R. Fraser. New Zealand National Commission for UNESCO, Wellington, 1973. 271-280.

Kroenke L.W. (1984) Cenozoic tectonic development of the southwest Pacific. UN Economic & Social Commission for Asia & the Southwest Pacific, Technical Bulletin 6: 1-125.

Kroenke L.W. (1986) Tectonic Evolution of the southwest Pacific. Proceedings of the Pacific Marine Mineral Resources Tra. : 3-20.

Kulig C., McCaffrey R., Abers G. A., Letz H. (1994) Shallow seismicity of arc-continent collision near Lae, Papua New Guinea. Tectonophysics 227:81-93.

Lee T. Y., Lawver L A. (1995) Cenozoic plate reconstruction of Southeast Asia. Tectonophysics, 251(1-4): 85-138.

Leick A. GPS Satellite Surveying. 2nd Edition. John Wiley and Sons Inc., New York, USA, 560pp, 1995

Lindley D. (1988) Early Cainozoic stratigraphy and structure of the Gazelle Peninsula, east New Britain: an example of extensional tectonics in the New Britain arc-trench complex. Australian Journal of Earth Sciences, 35: 231-44.

Lock J., Davies H. L., Tiffin D. L., Murakami F., Kisimoto K. (1987) The Trobriand subduction system in the western Solomon Sea. Geo-Marine Letters, 7: 129-134.

Martinez F., Taylor B. (1993) Manus Basin, Bismarck Sea: an epitome of microplate deformation. EOS Transactions, AGU, October 26, 605.

McClusky S. (1993) First Epoch Determination of Crustal Motion in the Papua New Guinea Region: By Comparison of a 1981 Doppler Survey and a Repeat 1990 GPS Survey. Unpublished PhD Thesis, School of Geomatic Engineering, University of New-South-Wales.

McClusky S., Mobbs K., Stolz A., Barsby D., Loratung W., Lambeck K., Morgan P. (1994) The Papua New Guinea satellite crustal motion surveys. The Australian Surveyor, 39(3): 1-20.

Menard H. W. The Ocean of Truth: A Personal History of Global Tectonics. Princeton University Press, 353pp, 1986.

Mogi K. (1973) Relationship between shallow and deep seismicity in the western Pacific region. Tectonophysics, 17:1-22

Molnar P., Atwater T., Mammerick J., Smith S. M. (1975) Magnetic anomalies, bathymetry and the tectonic evolution of the south Pacific since the late Cretaceous. Royal Astronomical Society Geophysical Journal, 40: 381-420.

Morgan P. (1981) Simulation Studies for Crustal Motion Monitoring by Doppler in Papua New Guinea. Australian Journal of Geodesy and Photogrammetry, 35: 15-62.

Morgan P., Bock Y., Coleman R., Feng P., Garrard D., Johnston G., Luton G., McDowall B., Pearse M., Rizos C., Tiele, R. (1996) A Zero Order GPS Network for the Australian Region. University of Canberra, 1996.

NASA (1977) National Geodetic Satellite Program, Parts 1 & 2. NASA SP-365, Scientific and Technical Information Office, National Aeronautics and Space Administration, Washington DC, 1977. For sale by Superintendant of Documents, US Government Printing Office, Washington DC 20402, Stock No. 033-000-00625-0.

Newton R. R. (1967) The Navy Navigation Satellite System. Space Research VII(2):735-763.

Park R. G. Geological Structures and Moving Plates. Blackie Academic and Professional, Glasgow, U.K., 337pp, 1988.

Pigram C. J., and Davies H. L. (1987) Terranes and the accretion history of the New Guinea region . BMR Journal of Australian Geology and Geophysics, 10: 193-211.

Puntodewo S. S. O., McCaffrey R., Calais E., Bock Y., Rais J., Subarya C., Poewariardi R., Stevens C., Genrich J., Fauzi, Zwick P, Wdowinski S. (1994) GPS measurements of crustal deformation within the Pacific-

Australia plate boundary zone in Irian Jaya, Indonesia. Tectonophysics, 237: 141-153.

Ripper I. D. (1975) Seismicity and focal mechanisms in the New Guinea Solomon Islands region. Bull. Aust. Soc. Explor. Geophys., 6:80-81.

Ripper I. D. (1982) Seismicity of the Indo-Australian/Solomon Sea plate boundary in the southeast Papua region. Tectonophysics, 87: 355-369.

Robinson G. P. (1974) Geology of the Huon Peninsula. Geol. Survey of Papua New Guinea Mem. 3: 71pp.

Ryan H. F., Marlow M. S. (1988) Multichannel seismic-reflection data collected at the intersection of the Massau and Manus Trenches, Papua New Guinea. In Marlow M. S., Dadisman S. V., Exon N. F. (editors), 1988, Geology and offshore resources of Pacific island arcs - New Ireland and Manus region, Papua New Guinea, Circum-Pacific Council for Energy and Mineral Resources, Earth Science Series 9, Houston, Texas:201-208.

Saastamoinen J. (1973) Contribution to the theory of atmospheric refraction, Part 2, Refraction corrections in satellite geodesy. Bulletin Geodesique, 107: 13-34.

Sandlin A., McDonald K., Donahue A. (1995) Selective Availability: to be or not to be? GPS World, September 1995, 44-51.

Schupler, B.R., and Clark, T.A. (1991) How different antennas affect the GPS Observable. GPS World, 2(10) Nov/Dec 1991:32-36.

Seeber G. (1993) Satellite Geodesy. Walter de Gruyter, Berlin, 531pp.

Seno T., Kaplan D. E. (1988) Seismotectonics of western New Guinea. Journal Phys. Earth, 36: 107-124.

Smith I. E. M. (1976) Peralkaline rhyolitesfrom the D'Entrecasteaux Islands, Papua New Guinea. In R. W. Johnson (ed) Volcanism in Australasia. Elsevier, Amsterdam, pp275-285.

Smith I. E. M. (1982) Volcanic evolution in eastern Papua. Tectonophysics, 87:315-333.

Spencer E.W. Introduction to the Structure of the Earth. McGraw-Hill Book Company, 3rd Edition, 551pp, 1988.

Spray J. G. (1983) Lithosphere-asthenosphere decoupling at spreading centres and initiation of obduction. Nature, 304: 253-255.

Stansell T. H. (1971) Transit, the Navy Navigation Satellite System. Navigation, 18:93-109.

Taylor B. (1975) The tectonics of the Bismarck Sea region. Unpublished BSc. thesis, University of Sydney.

Taylor B. (1979) Bismarck Sea: evolution of a back-arc basin. Geology, 7: 171-174.

Taylor B. Exon N. F. (1987) An investigation of ridge subduction in the Woodlark - Solomons region: introduction and overview. Circum-Pacific Council for Energy & Mineral Resources, 7: 1-24.

Tiffin D. L., Davies H. L., Honza E., Lock J., Okuda Y. (1987) The New Britain Trench and 149° Embayment, western Solomon Sea. Geo-Marine Letters, 7: 135-142.

Tregoning, P. (1994) Global Positioning Measurements in the Australian and Indonesian Region. UNISURV 44, School of Geomatic Engineering, University of New South Wales.

Trotter, J. (1972) Input Instructions to the Modified Versions of SAGA. DBA Systems Inc., Florida, September 1972.

Wanninger L. (1993) Effects of the equatorial ionosphere on GPS. GPS World, July 1993: 48-54.

Weibinger W. A. (1973) Crustal structure of the New Britain - New Ireland region. In Coleman P. J. (editor) The western Pacific island arcs, marginal seas, geochemistry. University of Western Australia Press.

Weiner J., Planet Earth. Bantam Books Inc., 369pp, 1986.

Weissel J. K., and Anderson R. N. (1978) Is there a caroline plate?. Earth & Planetary Science Letters, 41: 143-58.

Weissel, J.K., Taylor, B., and Karner, G.D. (1982) The opening of the Woodlark Basin, subduction of the Woodlark spreading system, and the evolution of northern Melanesia since mid- pliocene time. Tectonophysics 87: 253-77.

Wiebenga, W.A. (1973) Crustal structure of the New Britain - New Ireland region. From: The Western Pacific Island arcs marginal seas geochemistry Editor: Coleman P.J University of Western Aust Press. : 163-77.

Final Solution Coordinates (Uncorrelated lines from GLORG output)

Site	X (m)	Y (m)	Z[2] (m)	Site velocities (X,Y,Z) (m/y)			Epoch[1]	σ_X (m)	σ_Y (m)	σ_Z (m)
ENGA_GPS	3981774.8134	-89252.3464	4965291.4422	-0.1567	-0.2369	0.2351	1990.580	0.0321	0.0247	0.0272
GRUN_GPS	1970765.6663	-98261.9381	-6046201.5929	0.0000	0.0000	0.0000	1992.010	0.0396	0.0204	0.0714
DS60_GPS	4849202.4925	-360329.1488	4114913.0821	-0.0082	0.0186	0.0102	1995.256	0.0006	0.0004	0.0006
STHL_GPS	6104823.7784	-605862.9883	-1740699.5508	0.0000	0.0000	0.0000	1992.570	0.0192	0.0150	0.0078
NEUL_GPS	2102610.2508	-309037.6796	-5993559.0515	0.0000	0.0000	0.0000	1991.064	0.0492	0.0338	0.0771
NEUM_GPS	2102610.0443	-309037.7237	-5993558.9301	0.0000	0.0000	0.0000	1991.067	0.0648	0.1713	0.2282
NEUN_GPS	2102610.6493	-309037.5694	-5993559.0490	0.0000	0.0000	0.0000	1991.067	0.0683	0.0572	0.0906
NEUO_GPS	2102610.5293	-309037.7564	-5993558.8920	0.0000	0.0000	0.0000	1991.070	0.0560	0.0575	0.1544
NEUP_GPS	2102611.0984	-309037.7029	-5993559.1994	0.0000	0.0000	0.0000	1991.070	0.0427	0.0452	0.0714
NEUQ_GPS	2102610.9130	-309037.6794	-5993558.7407	0.0000	0.0000	0.0000	1991.073	0.0623	0.0560	0.1856
NEUS_GPS	2102611.2213	-309039.6526	-5993556.5293	0.0000	0.0000	0.0000	1991.075	0.7071	2.2436	2.0498
NEUT_GPS	2102611.9816	-309037.7959	-5993558.9038	0.0000	0.0000	0.0000	1991.075	0.0385	0.0357	0.0656
MASP_GPS	5439189.1534	-1522054.8367	2953464.2281	-0.0069	0.0163	0.0137	1993.744	0.0014	0.0009	0.0009
ARNA_GPS	2587441.5967	-1042831.3204	5716573.5490	0.0000	0.0000	0.0000	1992.578	0.0184	0.0173	0.0228
FORT_GPS	4985386.6414	-3954998.5627	-428426.5092	-0.0141	0.0028	0.0119	1996.017	0.0009	0.0008	0.0004
BRAZ_GPS	4115014.1571	-4550641.6725	-1741444.1469	0.0001	-0.0003	-0.0002	1995.825	0.3126	0.8930	0.2097
BRAS_GPS	4114500.4672	-4551173.1351	-1741210.6568	0.0000	0.0000	0.0000	1992.593	0.0191	0.0178	0.0063
PARA_GPS	3763751.6128	-4365113.7585	-2724404.7799	0.0000	0.0000	0.0000	1992.590	0.0203	0.0210	0.0097
STJO_GPS	2612631.3079	-3426807.0145	4686757.7776	-0.0119	-0.0063	0.0167	1993.784	0.0008	0.0008	0.0009
KOUR_GPS	3839591.4387	-5059567.5211	579956.8790	0.0021	0.0006	0.0103	1993.814	0.0017	0.0018	0.0006
OHIG_GPS	1525877.0479	-2432481.5318	-5676145.2513	0.0400	-0.0413	-0.0858	1991.889	0.0091	0.0086	0.0130
OHI5_GPS	1525872.4678	-2432481.2867	-5676146.0931	0.0400	-0.0413	-0.0858	1996.087	0.0008	0.0009	0.0014
LPGS_GPS	2780102.9780	-4437418.8413	-3629404.6038	0.0188	-0.0344	-0.0071	1996.157	0.0006	0.0008	0.0006
DECE_GPS	1422140.8205	-2534034.2617	-5658736.1462	0.0000	0.0000	0.0000	1992.053	0.0599	0.0653	0.0558
BRMU_GPS	2304703.6403	-4874817.1731	3395186.8699	-0.0150	0.0055	-0.0010	1994.374	0.0017	0.0023	0.0016
RIOG_GPS	1429882.6805	-3495363.2139	-5122698.8524	0.0000	0.0000	0.0000	1992.029	0.0656	0.1033	0.1365
SANG_GPS	1769724.5459	-5044512.3232	-3468396.3914	0.0239	-0.0076	0.0150	1991.071	0.0228	0.0272	0.0184
SANT_GPS	1769693.3344	-5044574.1206	-3468321.0582	0.0225	-0.0066	0.0147	1996.338	0.0004	0.0007	0.0005
AREQ_GPS	1942826.7422	-5804070.2432	-1796893.9957	0.0118	0.0009	0.0130	1996.101	0.0005	0.0008	0.0004
WES1_GPS	1492233.0445	-4458088.4967	4296048.2338	-0.0060	-0.0068	0.0106	1996.338	0.0034	0.0047	0.0042
WES2_GPS	1492233.4359	-4458089.4837	4296046.0162	-0.0060	-0.0068	0.0106	1996.338	0.0091	0.0094	0.0095
BOGT_GPS	1744399.1388	-6116037.8177	512731.6140	0.1063	-0.0770	0.1882	1996.283	0.0008	0.0011	0.0003
ALGO_GPS	918129.5400	-4346071.2245	4561977.8095	-0.0140	-0.0017	0.0008	1995.528	0.0004	0.0005	0.0005
RCM5_GPS	961334.8024	-5674074.1855	2740535.1483	-0.0063	-0.0077	0.0050	1994.416	0.0013	0.0022	0.0012
RCM2_GPS	961318.9672	-5674090.9672	2740489.5953	-0.0063	-0.0077	0.0050	1993.342	0.0015	0.0023	0.0013
RIC1_GPS	961309.4485	-5674075.8293	2740539.0937	-0.0063	-0.0077	0.0050	1992.212	0.0031	0.0047	0.0027
RCM4_GPS	961242.8741	-5674021.6410	2740657.6438	0.0000	0.0000	0.0000	1993.636	0.0017	0.0028	0.0016

Site	X (m)	Y (m)	Z[2] (m)	Site velocities (X,Y,Z) (m/y)			Epoch[1]	σ_X (m)	σ_Y (m)	σ_Z (m)
GALA_GPS	42734.4392	-6377213.6741	-99580.9196	0.0000	0.0000	0.0000	1992.596	0.0095	0.0126	0.0041
INEG_GPS	-1260435.7926	-5788548.4870	2360340.6459	0.0000	0.0000	0.0000	1992.592	0.0070	0.0120	0.0053
PIE1_GPS	-1640916.7327	-5014781.1763	3575447.1457	-0.0109	-0.0073	0.0014	1993.994	0.0009	0.0012	0.0009
EISL_GPS	-1884951.7963	-5357595.8665	-2892890.5099	0.0727	-0.0189	-0.0100	1996.301	0.0009	0.0011	0.0007
EIS1_GPS	-1884997.7972	-5357589.7271	-2892871.0883	0.0727	-0.0189	-0.0100	1991.070	0.0233	0.0306	0.0190
SOCO_GPS	-2160812.3681	-5643009.7959	2034731.1690	0.0000	0.0000	0.0000	1992.591	0.0088	0.0158	0.0064
YELL_GPS	-1224452.4709	-2689216.1034	5633638.2813	-0.0204	-0.0042	-0.0027	1996.338	0.0003	0.0004	0.0006
BLYT_GPS	-2223206.5754	-4830299.8985	3510587.7601	0.0000	0.0000	0.0000	1994.149	0.0026	0.0040	0.0029
PIN2_GPS	-2369466.3702	-4761231.6771	3511396.5946	0.0360	0.0998	-0.0230	1993.099	0.0022	0.0031	0.0023
PIN1_GPS	-2369510.3897	-4761207.1832	3511396.1564	-0.0167	-0.0005	0.0402	1993.649	0.0012	0.0017	0.0013
ROCH_GPS	-2382183.1938	-4755085.1877	3511367.6167	0.0000	0.0000	0.0000	1992.039	0.0083	0.0130	0.0084
MOJ1_GPS	-2356215.9052	-4646736.6203	3668456.3252	-0.0200	-0.0011	-0.0037	1991.984	0.0027	0.0039	0.0029
DS10_GPS	-2353614.1488	-4641385.4162	3676976.4765	-0.0213	-0.0083	0.0052	1995.415	0.0006	0.0007	0.0006
GOL2_GPS	-2353614.1690	-4641385.4268	3676976.4829	-0.0192	-0.0080	0.0053	1996.338	0.0007	0.0009	0.0007
SIO3_GPS	-2455456.4243	-4767480.8029	3441383.6176	-0.0311	0.0138	0.0391	1993.769	0.0011	0.0015	0.0011
SIO1_GPS	-2455521.6469	-4767213.4039	3441654.8935	-0.0370	0.0051	0.0424	1991.738	0.0039	0.0064	0.0045
SIO2_GPS	-2455539.2531	-4767224.0910	3441628.9052	-0.0356	0.0058	0.0421	1993.438	0.0050	0.0061	0.0047
MATH_GPS	-2443215.2748	-4706037.5796	3533477.5832	-0.0243	0.0006	0.0318	1993.753	0.0011	0.0014	0.0010
JPL1_GPS	-2493304.1033	-4655215.5061	3565497.3520	-0.0325	0.0114	0.0161	1993.898	0.0011	0.0014	0.0011
PVEP_GPS	-2525523.0938	-4670030.8265	3522843.0606	-0.0090	0.0317	0.0370	1993.736	0.0011	0.0014	0.0010
BYRD_GPS	-547611.0940	-965498.3335	-6261279.3666	-1.9731	11.3331	-1.6454	1992.038	0.0055	0.0055	0.0117
DRAO_GPS	-2059164.6200	-3621108.3860	4814432.4041	-0.0104	0.0002	-0.0074	1993.659	0.0007	0.0008	0.0009
VNDP_GPS	-2678089.8157	-4525437.7596	3597431.5078	-0.0750	-0.0603	0.0961	1993.744	0.0012	0.0016	0.0013
QUIN_GPS	-2517230.9285	-4198595.1798	4076531.2636	-0.0170	-0.0124	0.0073	1993.722	0.0012	0.0014	0.0013
PGC0_GPS	-2327188.0127	-3522528.9308	4764832.3063	0.0000	0.0000	0.0000	1991.071	0.0059	0.0085	0.0093
ALBH_GPS	-2341332.8333	-3539049.4967	4745791.3847	0.0015	0.0094	-0.0121	1992.820	0.0034	0.0042	0.0047
FAIR_GPS	-2281621.3896	-1453595.7896	5756961.9428	-0.0192	-0.0059	-0.0099	1995.461	0.0004	0.0004	0.0007
FAI2_GPS	-2281615.1723	-1453627.8904	5756960.8762	-0.0206	-0.0079	-0.0039	1996.301	0.0006	0.0005	0.0012
PAMA_GPS	-5245194.8964	-3080472.0197	-1912825.2849	0.1452	0.1465	0.0982	1995.739	0.0011	0.0009	0.0005
HUAH_GPS	-5345885.4666	-2958241.9888	-1824597.8969	-0.0072	0.0589	0.0318	1990.582	0.0238	0.0245	0.0099
KOKE_GPS	-5543818.1424	-2054582.7411	2387858.5697	-0.0072	0.0589	0.0318	1996.338	0.0063	0.0033	0.0030
KOKR_GPS	-5543838.0888	-2054587.3024	2387809.6792	-0.0070	0.0600	0.0305	1996.338	0.0008	0.0005	0.0004
WSAM_GPS	-6134394.6693	-860418.5413	-1514829.5003	0.0000	0.0000	0.0000	1991.069	0.0198	0.0172	0.0081
CHAT_GPS	-4590670.8901	-275483.0189	-4404596.7976	-0.0192	0.0107	0.0328	1996.177	0.0006	0.0005	0.0005
VITI_GPS	-6073527.4868	276502.1773	-1921630.4543	0.0000	0.0000	0.0000	1992.590	0.0094	0.0055	0.0039
AUCK_GPS	-5105680.9833	461564.0532	-3782181.7780	-0.0162	-0.0233	0.0387	1996.182	0.0006	0.0005	0.0004
WELL_GPS	-4780648.7916	436507.1461	-4185440.4159	0.0229	-0.0023	0.0458	1992.604	0.0021	0.0013	0.0018
OUSD_GPS	-4387888.5808	733420.8817	-4555178.6246	-0.0724	0.0569	-0.0335	1996.338	0.0006	0.0005	0.0005

Site	X (m)	Y (m)	Z[2] (m)	Site velocities (X,Y,Z) (m/y)			Epoch[1]	σ_X (m)	σ_Y (m)	σ_Z (m)
OTA1_GPS	-4387888.1966	733420.7244	-4555178.3302	-0.0724	0.0569	-0.0335	1993.669	0.0037	0.0020	0.0036
OTAG_GPS	-4388296.9982	733507.1872	-4554771.7461	-0.0684	0.0531	-0.0322	1993.079	0.0020	0.0012	0.0019
KWJ1_GPS	-6160881.0062	1339882.9055	960810.4394	0.0000	0.0000	0.0000	1996.294	0.0024	0.0011	0.0005
KWAJ_GPS	-6160865.1399	1339912.0945	960841.9679	0.0000	0.0000	0.0000	1990.578	0.0135	0.0098	0.0048
MCMU_GPS	-1310695.1961	310468.8068	-6213363.4754	0.0064	-0.0248	-0.0026	1996.338	0.0013	0.0012	0.0026
MCM0_GPS	-1310856.3562	310431.4580	-6213347.7638	0.0064	-0.0248	-0.0026	1996.338	0.0249	0.0260	0.0469
MCM1_GPS	-1310621.7499	310414.1181	-6213400.3587	0.0064	-0.0248	-0.0026	1996.338	0.0015	0.0013	0.0035
MCM4_GPS	-1311703.2780	310815.1222	-6213255.2032	0.0064	-0.0248	-0.0026	1996.338	0.0005	0.0004	0.0009
TNO1_GPS	-1623858.5224	462478.2419	-6130048.8843	0.0000	0.0000	0.0000	1992.033	0.0230	0.0202	0.0554
TASP_GPS	-5953042.2779	2232112.2108	-508584.3577	0.0000	0.0000	0.0000	1993.445	0.0094	0.0062	0.0020
MAC1_GPS	-3464038.4464	1334172.7348	-5169224.2954	-0.0045	0.0048	0.0447	1995.792	0.0008	0.0006	0.0010
CART_GPS	-5782172.4758	2639487.5426	-528398.6732	0.0000	0.0000	0.0000	1992.348	0.0070	0.0048	0.0016
NUGU_GPS	-5755507.8638	2723752.8691	-368612.8034	0.0000	0.0000	0.0000	1992.350	0.0060	0.0043	0.0014
BRUN_GPS	-5020720.5779	2499067.3736	-3027805.1905	-0.0604	-0.0135	0.0522	1992.599	0.0048	0.0031	0.0030
QUT1_GPS	-5046767.5303	2568457.2276	-2925288.0735	-0.0604	-0.0135	0.0522	1992.575	0.0063	0.0039	0.0037
GUA2_GPS	-5607198.7473	2863957.6025	-1015751.2868	-0.0457	-0.0217	0.0804	1990.918	0.0169	0.0137	0.0046
GUA1_GPS	-5607201.3158	2863954.1936	-1015746.5877	-0.0446	-0.0200	0.0803	1991.631	0.0248	0.0169	0.0066
MIS1_GPS	-5577078.1531	2861397.5158	-1175144.1433	-0.0154	-0.0442	0.0581	1991.623	0.0105	0.0070	0.0031
MISI_GPS	-5576759.2933	2862001.1476	-1175221.0864	-0.0267	-0.0363	0.0545	1992.565	0.0036	0.0025	0.0012
CROW_GPS	-4821560.4337	2482901.7555	-3345746.3203	-0.0445	-0.0026	0.0448	1992.599	0.0040	0.0024	0.0027
SUGA_GPS	-5126895.1110	2689409.6909	-2667603.4123	-0.0484	-0.0124	0.0477	1993.438	0.0081	0.0064	0.0054
RABL_GPS	-5625280.8140	2970585.5216	-463064.8013	0.0000	0.0000	0.0000	1992.346	0.0071	0.0050	0.0016
JACQ_GPS	-5578632.2582	3028263.6928	-623240.7313	-0.0320	-0.0100	-0.0609	1991.853	0.0054	0.0043	0.0016
EC19_GPS	-4644354.4300	2549989.7015	-3539040.9542	0.0000	0.0000	0.0000	1994.148	0.0051	0.0035	0.0037
TEXA_GPS	-4899985.6157	2692597.6070	-3060138.9269	-0.0604	-0.0135	0.0522	1992.583	0.0035	0.0023	0.0022
BUNA_GPS	-5499983.6278	3029313.9863	-1116842.4526	0.0000	0.0000	0.0000	1991.629	0.0122	0.0080	0.0032
LOUS_GPS	-5523811.4915	3046135.3349	-940385.3442	-0.0583	-0.0033	0.0646	1992.154	0.0048	0.0037	0.0015
WARI_GPS	-5481915.8898	3028449.6717	-1204231.3267	0.0000	0.0000	0.0000	1991.627	0.0118	0.0082	0.0035
HAIN_GPS	-5485912.2474	3033109.9450	-1173846.0129	0.0000	0.0000	0.0000	1991.611	0.0123	0.0083	0.0034
URAS_GPS	-5499656.3736	3066247.5396	-1013638.6057	0.0000	0.0000	0.0000	1991.611	0.0124	0.0081	0.0033
FLAG_GPS	-4597580.5207	2564076.0674	-3589225.0128	-0.0417	0.0007	0.0434	1992.570	0.0033	0.0022	0.0025
KAVI_GPS	-5562412.9466	3107930.0059	-285346.1891	-0.0066	0.0764	0.0299	1993.272	0.0037	0.0026	0.0008
MULA_GPS	-5115154.9604	2872883.2230	-2494381.9559	-0.0484	-0.0124	0.0477	1993.437	0.0095	0.0074	0.0062
OAKS_GPS	-5113582.8900	2874686.8564	-2495475.0617	-0.0608	-0.0261	0.0699	1992.680	0.0037	0.0026	0.0021
ALT1_GPS	-5459929.3527	3094433.6813	-1134392.5472	-0.0167	-0.0429	0.0629	1991.598	0.0341	0.0178	0.0078
ALT2_GPS	-5453535.7525	3105804.8694	-1134062.7244	-0.0428	-0.0216	0.0537	1993.196	0.0039	0.0026	0.0011
WATA_GPS	-5466222.4332	3125151.8607	-1014184.3879	0.0000	0.0000	0.0000	1991.627	0.0114	0.0076	0.0030
EDEN_GPS	-4408335.5806	2554608.9857	-3823983.7847	-0.0390	0.0040	0.0420	1992.570	0.0030	0.0020	0.0024

Site	X (m)	Y (m)	Z[2] (m)	Site velocities (m/y)			Epoch[1]	σ_X (m)	σ_Y (m)	σ_Z (m)
BATH_GPS	-4594786.6335	2699295.8889	-3494244.2627	-0.0468	0.0028	0.0389	1993.533	0.0010	0.0007	0.0007
WITU_GPS	-5473775.5187	3232571.4073	-517844.6159	-0.0950	-0.1186	-0.2276	1990.579	0.0082	0.0072	0.0027
BASS_GPS	-5113385.1952	3047287.0018	-2283502.2527	-0.0484	-0.0124	0.0477	1993.438	0.0099	0.0080	0.0066
DS40_GPS	-4460988.1328	2682362.2666	-3674626.2624	-0.0366	-0.0030	0.0442	1996.338	0.0063	0.0047	0.0046
DS41_GPS	-4460979.7030	2682380.7284	-3674623.9478	-0.0366	-0.0030	0.0442	1996.338	0.0030	0.0024	0.0023
DS42_GPS	-4460996.1098	2682557.0805	-3674443.7305	-0.0366	-0.0030	0.0442	1996.338	0.0005	0.0004	0.0004
TID2_GPS	-4460996.1098	2682557.0801	-3674443.7298	-0.0366	-0.0030	0.0442	1996.338	0.0007	0.0006	0.0006
ORRO_GPS	-4446478.9122	2678112.6058	-3696270.2774	-0.0297	0.0011	0.0473	1992.549	0.0016	0.0011	0.0012
ORRX_GPS	-4446476.5740	2678104.8058	-3696261.9847	-0.0323	0.0018	0.0532	1990.581	0.0088	0.0096	0.0077
MUCK_GPS	-4860804.9926	2991738.3526	-2837860.7549	-0.0484	-0.0124	0.0477	1992.572	0.0039	0.0026	0.0023
CHAR_GPS	-4101998.2633	2566148.1742	-4141759.1591	-0.0287	-0.0033	0.0581	1993.659	0.0021	0.0015	0.0019
TRIA_GPS	-3990830.5155	2501499.2685	-4286339.1156	-0.0287	-0.0033	0.0581	1992.570	0.0027	0.0021	0.0025
MORO_GPS	-5335932.3808	3387629.5980	-853539.8005	-0.0517	-0.0130	0.0607	1992.132	0.0058	0.0050	0.0018
TAS1_GPS	-3950184.1579	2522364.5663	-4311588.5193	-0.0469	0.0071	0.0349	1993.810	0.0015	0.0010	0.0013
HOB1_GPS	-3950183.9907	2522364.4517	-4311588.3011	-0.0469	0.0071	0.0349	1994.296	0.0008	0.0006	0.0007
HOBA_GPS	-3950071.3378	2522415.2033	-4311638.4705	-0.0469	0.0071	0.0349	1995.381	0.0005	0.0005	0.0005
MANU_GPS	-5367596.4398	3437943.3421	-226704.9652	-0.0146	0.0731	0.0258	1993.109	0.0051	0.0037	0.0010
MORE_GPS	-5288519.1621	3409952.8658	-1038574.3471	-0.0135	-0.0455	0.0628	1993.507	0.0012	0.0010	0.0005
UNIT_GPS	-5313156.6928	3450683.5645	-736065.7332	0.0022	-0.0746	0.0603	1994.007	0.0027	0.0021	0.0009
TOWN_GPS	-5041024.9642	3296980.3042	-2090553.3248	-0.0352	-0.0217	0.0533	1993.368	0.0012	0.0009	0.0006
TOWA_GPS	-5036492.1784	3298900.0720	-2099859.7238	-0.0352	-0.0217	0.0534	1993.492	0.0012	0.0010	0.0006
WANK_GPS	-5262950.5025	3539058.6689	-678565.3264	0.0346	-0.0790	0.0556	1993.666	0.0040	0.0029	0.0010
GILG_GPS	-4470744.2680	3016577.4537	-3394500.1834	-0.0631	-0.0029	0.0342	1994.273	0.0020	0.0015	0.0014
SPM9_GPS	-3989108.2357	2699944.0164	-4166666.7871	-0.0287	-0.0033	0.0581	1992.568	0.0043	0.0030	0.0038
MADA_GPS	-5252527.4020	3571989.7342	-575482.7425	0.0000	0.0000	0.0000	1993.662	0.0029	0.0023	0.0008
MADG_GPS	-5251159.3091	3575562.4422	-570087.9633	0.0000	0.0000	0.0000	1990.572	0.0100	0.0095	0.0031
BANZ_GPS	-4610424.0351	3148699.7608	-3073895.9555	-0.0984	0.0176	0.0149	1994.105	0.0020	0.0016	0.0013
BULL_GPS	-4271156.6629	2929587.3195	-3710093.7113	-0.0519	0.0047	0.0314	1993.811	0.0017	0.0013	0.0013
GOKA_GPS	-5221573.4620	3603226.5634	-671387.0714	0.0346	-0.0790	0.0556	1993.659	0.0033	0.0026	0.0009
BARC_GPS	-4808764.0902	3330247.5096	-2535054.5643	-0.0585	-0.0084	0.0398	1992.586	0.0039	0.0028	0.0021
PIEB_GPS	-5045675.8723	3522171.1489	-1674322.7092	-0.0460	-0.0160	0.0486	1992.600	0.0075	0.0051	0.0034
GUAM_GPS	-5071312.7866	3568363.4786	1488904.3091	0.0086	-0.0237	-0.0140	1996.158	0.0007	0.0007	0.0003
CAMW_GPS	-3942894.7325	2790759.3334	-4151125.7013	-0.0409	0.0014	0.0464	1993.659	0.0020	0.0016	0.0018
ATKI_GPS	-4119867.9165	2918876.3694	-3884282.4874	-0.0554	0.0017	0.0320	1993.843	0.0013	0.0010	0.0011
EMUU_GPS	-4867427.0212	3487912.8213	-2191805.1310	-0.0460	-0.0160	0.0486	1992.592	0.0046	0.0033	0.0022
KIKO_GPS	-5133225.7731	3695553.7607	-818612.3603	0.0178	-0.0698	0.0590	1993.657	0.0040	0.0030	0.0010
BENW_GPS	-4040118.6962	2944818.5920	-3948080.7579	-0.0531	0.0060	0.0347	1992.568	0.0028	0.0022	0.0024
WEWK_GPS	-5128211.3377	3771635.4000	-396055.9068	0.0000	0.0000	0.0000	1993.639	0.0027	0.0023	0.0007

Site	X (m)	Y (m)	Z[2] (m)	Site velocities (m/y)			Epoch[1]	σ_X (m)	σ_Y (m)	σ_Z (m)
MEND_GPS	-5109574.9201	3759378.9329	-678236.5192	0.0346	-0.0790	0.0556	1993.655	0.0032	0.0025	0.0008
WUVU_GPS	-5080555.0150	3851303.6178	-191869.0292	0.0346	-0.0790	0.0556	1993.651	0.0031	0.0026	0.0008
SAKL_GPS	-3465323.0390	2638268.1715	4644082.7142	0.0000	0.0000	0.0000	1992.594	0.0052	0.0046	0.0043
KOPI_GPS	-5038707.3590	3867027.4118	-594810.7271	0.0000	0.0000	0.0000	1993.647	0.0042	0.0034	0.0010
HOWI_GPS	-4523298.6707	3485332.7803	-2832259.2180	-0.0734	0.0027	0.0299	1994.571	0.0022	0.0019	0.0014
GREN_GPS	-4955371.4958	3842257.5709	-1163835.2380	0.0178	-0.0698	0.0590	1992.600	0.0170	0.0129	0.0052
OLVE_GPS	-4384863.2576	3448388.9012	-3082582.1339	-0.0711	-0.0010	0.0341	1994.027	0.0016	0.0013	0.0011
PORT_GPS	-3922962.0057	3117568.4776	-3932953.7883	-0.0475	0.0084	0.0363	1993.887	0.0015	0.0013	0.0013
SUND_GPS	-4239032.1532	3377934.9074	-3351167.8823	-0.0725	0.0049	0.0292	1994.353	0.0019	0.0016	0.0014
VANI_GPS	-4972629.9089	3983208.1720	-296767.2436	-0.0480	-0.0061	0.0290	1993.321	0.0025	0.0022	0.0007
AIAM_GPS	-4934886.4874	3958248.6270	-810301.1286	0.0004	-0.0879	0.0696	1993.395	0.0024	0.0020	0.0008
AMAN_GPS	-4962464.8689	3987772.5483	-396577.0841	0.0000	0.0000	0.0000	1993.631	0.0037	0.0032	0.0009
NORM_GPS	-4730119.9985	3818318.6457	-1924292.9970	-0.0134	-0.0424	0.0707	1992.600	0.0065	0.0045	0.0031
LLTR_GPS	-4117215.8062	3333728.2371	-3539972.5894	-0.0638	0.0016	0.0362	1993.896	0.0014	0.0012	0.0011
TSU1_GPS	-3957193.8029	3310191.2957	3737733.3636	0.0164	-0.0478	-0.0353	1991.046	0.0113	0.0085	0.0069
TSKB_GPS	-3957199.2246	3310199.6580	3737711.7130	0.0164	-0.0478	-0.0353	1995.938	0.0009	0.0008	0.0007
BREA_GPS	-4451878.7604	3786508.9291	-2546090.4414	-0.0434	-0.0198	0.0503	1992.591	0.0046	0.0034	0.0027
AMUN_GPS	-245.0618	210.0265	-6359570.0122	7.5676	-6.4434	0.2939	1992.037	0.0046	0.0047	0.0105
BRDV_GPS	-4355678.9243	3740239.8581	-2769201.3813	-0.0715	0.0014	0.0339	1993.661	0.0019	0.0017	0.0012
WILF_GPS	-4529722.3453	3909094.1968	-2203537.5223	-0.0405	-0.0054	0.0506	1993.313	0.0025	0.0020	0.0014
AUSA_GPS	-3942241.9996	3468859.5353	-3608197.2261	0.0000	0.0000	0.0000	1990.580	0.0166	0.0233	0.0117
AUSB_GPS	-3942241.9613	3468859.3863	-3608197.1315	0.0000	0.0000	0.0000	1990.581	0.0193	0.0197	0.0181
STAN_GPS	-3916469.8792	3455298.5083	-3649242.6969	-0.0310	-0.0034	0.0472	1993.200	0.0017	0.0015	0.0014
HWKR_GPS	-4055042.3531	3597135.1139	-3350585.2445	-0.0566	0.0046	0.0386	1993.659	0.0021	0.0017	0.0015
USUD_GPS	-3855262.5919	3427432.2010	3741020.9376	0.0326	0.0408	0.1393	1992.340	0.0052	0.0051	0.0040
USU5_GPS	-3855262.9786	3427432.5102	3741020.3621	-0.0022	-0.0061	-0.0102	1995.786	0.0006	0.0006	0.0005
WOLL_GPS	-4523681.4612	4083441.9579	-1876187.2123	-0.0134	-0.0424	0.0707	1993.666	0.0033	0.0028	0.0016
ELDO_GPS	-4543818.3639	4263716.3091	-1358180.7760	-0.0455	-0.0325	0.0585	1993.666	0.0037	0.0033	0.0015
GROO_GPS	-4489874.8134	4265802.3251	-1519918.0035	-0.0455	-0.0325	0.0585	1993.666	0.0035	0.0031	0.0015
ALYA_GPS	-4487413.8174	4269234.1113	-1517520.5619	-0.0455	-0.0325	0.0585	1993.666	0.0034	0.0030	0.0015
CLIF_GPS	-4018348.2129	3874926.6160	-3075181.8808	-0.0716	0.0290	0.0303	1993.659	0.0021	0.0019	0.0015
ROPE_GPS	-4365327.2730	4355926.9779	-1623109.8123	-0.0455	-0.0325	0.0585	1993.667	0.0033	0.0030	0.0014
SHAM_GPS	-4189540.2728	4309929.8857	-2127995.3827	-0.0372	-0.0117	0.0569	1993.667	0.0026	0.0025	0.0014
ALIC_GPS	-4052051.7346	4212836.1818	-2545106.0538	-0.0324	-0.0231	0.0629	1993.491	0.0010	0.0010	0.0006
CEDU_GPS	-3753472.0998	3912740.9855	-3347961.0181	-0.0563	0.0156	0.0381	1993.846	0.0011	0.0010	0.0008
THEV_GPS	-3739792.0437	3911197.3952	-3364706.8851	-0.0384	0.0072	0.0485	1992.571	0.0029	0.0028	0.0022
JOHN_GPS	-3929600.8284	4183187.8467	-2774030.9654	-0.0903	0.0260	0.0277	1993.386	0.0017	0.0016	0.0011
JUNC_GPS	-3733309.5946	4184347.9290	-3029196.8377	-0.0716	0.0290	0.0303	1993.659	0.0022	0.0021	0.0015

Site	X (m)	Y (m)	Z[2] (m)	Site velocities (m/y)			(X,Y,Z)	Epoch[1]	σ_X (m)	σ_Y (m)	σ_Z (m)
DARW_GPS	-4091358.7171	4684606.8367	-1408580.6928	-0.0440	-0.0402		0.0662	1993.399	0.0013	0.0014	0.0006
KDMN_GPS	-4017368.6766	4629016.3611	-1759073.4440	-0.0455	-0.0325		0.0585	1993.667	0.0029	0.0030	0.0014
WINN_GPS	-4077253.7554	4710296.8293	-1363184.1571	-0.0455	-0.0325		0.0585	1992.570	0.0031	0.0033	0.0014
PILL_GPS	-4073402.3538	4712253.6462	-1367883.5083	-0.0455	-0.0325		0.0585	1992.569	0.0031	0.0033	0.0014
KILI_GPS	-3777444.0094	4668166.2870	-2143627.2203	-0.0167	0.0010		0.0540	1993.670	0.0021	0.0023	0.0012
DEAK_GPS	-3448618.5217	4265479.9544	-3244110.0592	-0.0384	0.0072		0.0485	1993.666	0.0017	0.0018	0.0013
RAWL_GPS	-3586428.2238	4539145.8365	-2678896.4724	-0.0501	0.0296		0.0379	1993.554	0.0015	0.0016	0.0010
PIVT_GPS	-3806295.3673	4823694.5669	-1704766.5239	-0.0455	-0.0325		0.0585	1993.670	0.0024	0.0027	0.0013
TAEJ_GPS	-3120422.9153	4086355.4796	3761769.6545	-0.0256	-0.0264		-0.0379	1996.338	0.0006	0.0006	0.0005
CAIG_GPS	-3137868.6930	4393013.3246	-3385234.1121	-0.0140	0.0474		0.0484	1993.675	0.0021	0.0026	0.0018
GIBS_GPS	-3365970.1127	4763630.4874	-2572813.4574	-0.0657	0.0499		0.0236	1993.675	0.0022	0.0026	0.0015
BATE_GPS	-3124556.0170	4828049.6079	-2750068.6274	-0.0657	0.0499		0.0236	1993.675	0.0019	0.0025	0.0015
BROO_GPS	-3241494.8177	5134037.2837	-1946745.5480	0.0614	-0.0400		0.0891	1993.564	0.0027	0.0035	0.0016
ESPE_GPS	-2800864.6647	4500724.6573	-3534886.5770	-0.0407	0.0734		0.0175	1993.609	0.0021	0.0027	0.0020
TAIW_GPS	-3024781.9133	4928936.8422	2681234.4772	-0.0275	-0.0277		-0.0102	1995.265	0.0009	0.0010	0.0006
KALG_GPS	-2853510.9287	4665806.3622	-3271380.8360	-0.0140	0.0474		0.0484	1993.675	0.0019	0.0025	0.0017
SHAO_GPS	-2831733.2355	4675666.0484	3275369.5315	-0.0435	-0.0148		-0.0111	1996.150	0.0006	0.0006	0.0004
MANL_GPS	-3184192.3989	5291065.8472	1590599.1856	0.0000	0.0000		0.0000	1992.596	0.0064	0.0074	0.0027
RATH_GPS	-2979541.6636	5090380.4691	-2420393.9256	-0.0216	0.0013		0.0593	1993.675	0.0021	0.0028	0.0016
S01R_GPS	-2886619.1356	5082945.2630	2543377.6586	-0.5989	0.0924		-0.1842	1990.579	0.0144	0.0142	0.0079
COOL_GPS	-2711522.9681	5098133.3218	-2700765.2620	-0.0333	0.0046		0.0561	1993.675	0.0020	0.0029	0.0017
TORB_GPS	-2422745.3955	4630068.1596	-3645119.6329	-0.0294	0.0309		0.0482	1993.675	0.0021	0.0028	0.0020
KARR_GPS	-2713832.1358	5303935.1495	-2269515.2349	-0.0209	-0.0183		0.0679	1993.470	0.0009	0.0013	0.0007
CAVE_GPS	-2375390.5607	4875553.8560	-3345387.2380	-0.0372	0.0226		0.0480	1993.665	0.0016	0.0024	0.0016
PERT_GPS	-2368686.9178	4881316.5187	-3341796.2258	-0.0445	0.0038		0.0534	1995.815	0.0004	0.0005	0.0004
PER2_GPS	-2368701.4127	4881361.6696	-3341721.0536	-0.0272	-0.0142		0.0689	1993.355	0.0011	0.0016	0.0011
YAR1_GPS	-2389025.5121	5043316.8786	-3078530.7672	-0.0488	0.0121		0.0493	1996.338	0.0004	0.0005	0.0004
TIMB_GPS	-2702792.8894	5747549.3100	583412.7370	0.0000	0.0000		0.0000	1993.659	0.0057	0.0065	0.0014
CARN_GPS	-2325633.2558	5290021.8669	-2690511.0657	-0.0450	0.0080		0.0530	1993.675	0.0021	0.0033	0.0018
CASE_GPS	-902599.1548	2409535.2542	-5816536.7381	0.0030	-0.0140		0.0040	1996.338	0.0055	0.0063	0.0110
CAS1_GPS	-901776.1665	2409383.4318	-5816748.4119	0.0030	-0.0140		0.0040	1996.338	0.0005	0.0006	0.0011
KAYA_GPS	-2119512.9123	6015103.2935	89809.9796	0.0000	0.0000		0.0000	1992.597	0.0141	0.0173	0.0032
BAKO_GPS	-1836968.8728	6065617.2582	-716257.7693	-0.0196	0.0071		0.0010	1993.344	0.0021	0.0031	0.0009
XMAS_GPS	-1696463.0742	6039563.0637	-1149236.1839	-0.0696	0.0104		0.0616	1992.592	0.0020	0.0030	0.0012
CHUL_GPS	-1132728.2633	6092488.5501	1504562.1179	0.0000	0.0000		0.0000	1996.271	0.0021	0.0036	0.0011
COCO_GPS	-741949.8513	6190961.6614	-1337768.7948	-0.0571	-0.0475		0.0754	1993.223	0.0013	0.0023	0.0009
LHAS_GPS	-106937.6139	5549269.6010	3139215.7437	0.0439	-0.3668		-0.1810	1995.848	0.0011	0.0015	0.0009
COLB_GPS	1113302.9670	6233645.2587	760258.5096	0.0000	0.0000		0.0000	1992.599	0.0049	0.0068	0.0021

Site	X (m)	Y (m)	Z[2] (m)	Site velocities (X,Y,Z) (m/y)			Epoch[1]	σ_X (m)	σ_Y (m)	σ_Z (m)
DAV1_GPS	486854.5351	2285099.3186	-5914955.6826	0.0045	-0.0071	0.0026	1995.896	0.0007	0.0007	0.0014
IISC_GPS	1337936.8523	6070317.1154	1427876.4908	-0.0378	0.0098	0.0218	1996.163	0.0007	0.0008	0.0004
MLTG_GPS	1803857.4418	6099996.0010	462747.3388	0.0000	0.0000	0.0000	1996.303	0.0072	0.0113	0.0019
MALE_GPS	1805486.5351	6099592.4127	461710.8446	0.0000	0.0000	0.0000	1996.300	0.0021	0.0035	0.0007
GAN1_GPS	1847796.0417	6104033.8007	-76520.6265	0.0000	0.0000	0.0000	1996.259	0.0043	0.0067	0.0011
KERG_GPS	1406274.0056	3918195.7503	-4816159.6182	-0.0109	0.0066	-0.0058	1992.037	0.0112	0.0187	0.0203
KER5_GPS	1406337.3338	3918161.1150	-4816167.3602	-0.0082	0.0077	-0.0076	1996.175	0.0006	0.0008	0.0008
KIT3_GPS	1944945.3829	4556652.1830	4004325.9657	-0.0161	-0.0099	-0.0074	1996.157	0.0006	0.0006	0.0006
DOVE_GPS	885318.3533	1974376.4618	-5980930.2444	0.0000	0.0000	0.0000	1991.072	0.0165	0.0213	0.0327
MAW1_GPS	1111287.1333	2168911.2883	-5874493.5674	0.0137	0.0106	-0.0172	1993.718	0.0022	0.0025	0.0046
REUN_GPS	3364095.5845	4907945.1180	-2293468.6342	0.0000	0.0000	0.0000	1992.591	0.0066	0.0070	0.0035
SEY1_GPS	3602870.8279	5238174.3039	-516275.5355	0.2205	-0.0923	-0.0246	1996.027	0.0031	0.0033	0.0008
BAHA_GPS	3633911.1587	4425277.8412	2799862.5408	0.0087	0.0153	-0.0227	1990.585	0.1380	0.0824	0.0601
DJIB_GPS	4583088.5550	4250979.1218	1266241.2975	0.0000	0.0000	0.0000	1992.597	0.0061	0.0063	0.0024
MALI_GPS	4865366.4831	4110737.4345	-331121.7275	-0.0466	-0.0358	0.0234	1996.273	0.0014	0.0012	0.0005
SYOW_GPS	1766182.5331	1460336.7562	-5932285.4258	0.0000	0.0000	0.0000	1992.037	0.0052	0.0054	0.0095
HART_GPS	5084625.4456	2670366.5776	-2768493.9661	0.0082	0.0201	0.0116	1995.276	0.0018	0.0015	0.0011
METS_GPS	2892571.0113	1311843.2713	5512634.0195	-0.0164	0.0135	0.0091	1992.695	0.0028	0.0020	0.0045
TROM_GPS	2102940.3657	721569.3770	5958192.1101	-0.0193	0.0107	0.0051	1996.338	0.0003	0.0003	0.0007
MATG_GPS	4641950.8939	1393056.7550	4133280.3204	-0.0275	0.0139	0.0060	1991.070	0.0132	0.0081	0.0113
MATE_GPS	4641949.8206	1393045.2000	4133287.2936	-0.0240	0.0037	0.0051	1992.616	0.0037	0.0023	0.0032
GRAZ_GPS	4194424.0467	1162702.4830	4647245.3024	-0.0166	0.0184	0.0098	1993.437	0.0077	0.0062	0.0086
WTZ1_GPS	4075578.6039	931852.6776	4801570.0374	-0.0172	0.0175	0.0059	1996.338	0.0005	0.0004	0.0006
WTZX_GPS	4075552.5072	931825.7113	4801589.1956	-0.0181	0.0206	0.0087	1990.580	0.0180	0.0103	0.0159
WETB_GPS	4075579.2760	931807.2458	4801570.9788	-0.0185	0.0208	0.0090	1996.338	0.0089	0.0048	0.0096
ONSA_GPS	3370658.7357	711876.9828	5349786.8597	-0.0127	0.0159	0.0146	1993.547	0.0006	0.0004	0.0009
NALL_GPS	1202430.6776	252626.6439	6237767.5146	-0.0179	0.0074	0.0012	1996.037	0.0004	0.0003	0.0014
NAL1_GPS	1202431.3831	252626.7317	6237770.7162	-0.0182	0.0084	0.0028	1991.072	0.0105	0.0086	0.0291
FORS_GPS	2061367.6132	432558.4284	-6000283.7490	0.0000	0.0000	0.0000	1992.037	0.0138	0.0097	0.0265
HONE_GPS	3132539.0314	566401.7266	5508609.8524	0.0000	0.0000	0.0000	1991.070	0.0090	0.0053	0.0129
ARLT_GPS	5991291.5795	773713.6019	2040608.5620	0.0000	0.0000	0.0000	1992.599	0.0068	0.0039	0.0030
KOSG_GPS	3899225.2767	396731.8096	5015078.3520	-0.0146	0.0173	0.0089	1996.338	0.0006	0.0004	0.0008
HERS_GPS	4033470.2989	23672.6804	4924301.1864	-0.0178	0.0049	-0.0031	1992.543	0.0048	0.0027	0.0054

1 The epoch at which the position estimate would be independent of the rate estimate.
2 The position estimate is at the average uncorrelated epoch
Where a site velocity is not estimated, the a priori velocity is listed.

ITRF94 Geodetic coordinates from the final solution expressed in latitude, longitude and height on the WGS84 ellipsoid.

Site	Latitude (° ' ")	Longitude (° ' ")	Ellipsoid Height (m)
ENGA	51 27 13.64994	-1 17 2.69628	167.4550
GRUN	-72 2 19.59930	-2 51 15.80782	1240.0118
DS60	40 25 44.97740	-4 14 58.77982	829.4718
STHL	-15 56 31.80384	-5 40 3.59289	452.0059
NEUL	-70 35 50.57943	-8 21 40.89381	54.2363
NEUM	-70 35 50.58415	-8 21 40.90096	54.0561
NEUN	-70 35 50.56789	-8 21 40.87760	54.3596
NEUO	-70 35 50.56899	-8 21 40.89725	54.1811
NEUP	-70 35 50.55539	-8 21 40.88408	54.6555
NEUQ	-70 35 50.55616	-8 21 40.88444	54.1608
NEUS	-70 35 50.51444	-8 21 41.06957	52.2716
NEUT	-70 35 50.52521	-8 21 40.88055	54.6715
MASP	27 45 49.78559	-15 37 59.79989	198.7528
ARNA	64 8 20.40964	-21 57 4.29889	91.7969
FORT	-3 52 38.80685	-38 25 32.20354	19.4652
BRAZ	-15 56 50.91398	-47 52 40.32932	1106.1901
BRAS	-15 56 43.16736	-47 53 5.12250	1089.8295
PARA	-25 26 54.13020	-49 13 51.43733	925.7479
STJO	47 35 42.85866	-52 40 39.88949	152.8427
KOUR	5 15 7.84730	-52 48 21.45264	-25.7798
OHIG	-63 19 14.51690	-57 54 0.95783	31.1019
OHI5	-63 19 14.60533	-57 54 1.22717	30.6681
LPGS	-34 54 24.28686	-57 55 56.27723	29.8563
DECE	-62 58 30.26961	-60 41 53.36940	22.2627
BRMU	32 22 13.43209	-64 41 46.57746	-11.6073
RIOG	-53 47 7.74874	-67 45 5.46784	31.1781
SANG	-33 9 3.94139	-70 40 4.87525	724.0610
SANT	-33 9 1.04277	-70 40 6.80090	723.0369
AREQ	-16 27 55.85191	-71 29 34.04949	2488.9334
WES1	42 36 48.08280	-71 29 35.97163	85.7623
WES2	42 36 48.00664	-71 29 35.96909	85.0411
BOGT	4 38 24.25790	-74 4 51.38161	2577.0433
ALGO	45 57 20.88042	-78 4 16.91720	200.8731
RCM5	25 36 49.60542	-80 23 2.14970	-15.5916
RCM2	25 36 48.07531	-80 23 2.80975	-22.7494
RIC1	25 36 49.75776	-80 23 3.05549	-16.2435
RCM4	25 36 54.13840	-80 23 5.08368	-23.1966
GALA	0 54 2.21553	-89 36 57.81660	2.5146
INEG	21 51 22.15533	-102 17 3.12552	1889.3232
PIE1	34 18 5.42405	-108 7 8.13142	2347.6911
EISL	-27 8 53.55206	-109 22 59.86344	114.5497
EIS1	-27 8 52.85012	-109 23 1.51337	114.1196
SOCO	18 43 36.35468	-110 57 9.94771	5.5941
YELL	62 28 51.22116	-114 28 50.51434	180.8529
BLYT	33 36 37.49779	-114 42 53.45636	86.0256
PIN2	33 36 43.72870	-116 27 27.41097	1258.3378
PIN1	33 36 43.75846	-116 27 29.36268	1256.1665
ROCH	33 36 39.67951	-116 36 35.16032	1393.7174
MOJ1	35 19 53.43587	-116 53 17.34506	904.5222
DS10	35 25 30.56297	-116 53 21.29277	986.6874
GOL2	35 25 30.56279	-116 53 21.29330	986.7062
SIO3	32 51 52.92382	-117 15 1.45202	34.9088
SIO1	32 52 3.98176	-117 15 8.39183	7.5397

Site	Latitude (° ' ")			Longitude (° ' ")			Ellipsoid Height (m)
SIO2	32	52	2.96380	-117	15	8.80563	8.1873
MATH	33	51	24.06292	-117	26	12.51728	396.9135
JPL1	34	12	17.34722	-118	10	23.59746	423.9724
PVEP	33	44	35.83557	-118	24	15.27087	69.4202
BYRD	-80	0	47.19738	-119	33	39.70458	1505.1734
DRAO	49	19	21.43230	-119	37	29.92850	541.8661
VNDP	34	33	22.71053	-120	36	59.19897	-11.5013
QUIN	39	58	28.39706	-120	56	39.93031	1105.7703
PGC0	48	38	54.96236	-123	27	3.87670	1.6002
ALBH	48	23	23.21563	-123	29	14.88905	31.7373
FAIR	64	58	40.80590	-147	29	57.25707	319.0031
FAI2	64	58	40.44011	-147	29	54.93819	323.1142
PAMA	-17	34	0.26176	-149	34	28.32650	337.4078
HUAH	-16	43	59.71847	-151	2	28.54117	50.9274
KOKE	22	7	36.25694	-159	39	53.62867	1166.9616
KOKR	22	7	34.53641	-159	39	53.72128	1167.3411
WSAM	-13	49	51.07898	-172	0	56.53135	51.7314
CHAT	-43	57	20.83642	-176	33	57.01608	57.9871
VITI	-17	39	3.32715	177	23	36.10981	86.8549
AUCK	-36	36	10.24502	174	50	3.78708	132.7092
WELL	-41	16	29.61998	174	46	58.63784	37.8201
OUSD	-45	52	10.20926	170	30	39.31944	26.2407
OTA1	-45	52	10.21203	170	30	39.32370	25.7475
OTAG	-45	51	51.33777	170	30	38.49455	24.6229
KWJ1	8	43	19.93658	167	43	48.88202	38.2287
KWAJ	8	43	20.99686	167	43	47.83860	33.8167
MCMU	-77	50	52.22687	166	40	25.57843	-19.4490
MCM0	-77	50	47.44810	166	40	36.83091	-3.6065
MCM1	-77	50	55.12746	166	40	31.13554	-1.0898
MCM4	-77	50	18.05412	166	40	9.56838	98.0931
TNO1	-74	41	55.69503	164	6	10.57717	72.1925
TASP	-4	36	15.44585	159	26	46.70166	63.2587
MAC1	-54	29	58.31876	158	56	9.00227	-6.8243
CART	-4	47	2.65480	155	27	50.07841	68.0663
NUGU	-3	20	7.55530	154	40	28.13538	67.4168
BRUN	-28	31	29.59306	153	32	17.30444	135.5599
QUT1	-27	28	38.51283	153	1	37.34039	92.8852
GUA2	-9	13	30.16594	152	56	37.21806	78.6605
GUA1	-9	13	30.01113	152	56	37.35578	78.6344
MIS1	-10	41	17.39817	152	50	21.39955	81.1766
MISI	-10	41	19.90784	152	49	58.93701	87.4769
CROW	-31	50	36.58732	152	45	12.34292	84.1966
SUGA	-24	53	7.18255	152	19	11.61905	110.7279
RABL	-4	11	28.68904	152	9	44.86859	266.9281
JACQ	-5	38	42.75860	151	30	19.60423	151.6128
EC19	-33	55	8.39933	151	13	51.41001	83.4600
TEXA	-28	51	19.62627	151	12	38.54480	538.2138
BUNA	-10	9	7.78247	151	9	16.71222	131.2954
LOUS	-8	32	7.26388	151	7	30.81578	85.1889
WARI	-10	57	20.60591	151	4	54.56236	174.3355
HAIN	-10	40	34.15318	151	3	43.92573	122.1557
URAS	-9	12	20.15201	150	51	31.78907	145.0454
FLAG	-34	27	57.58124	150	51	5.54595	75.1083
KAVI	-2	34	53.06670	150	48	22.53604	78.8867
MULA	-23	10	22.49917	150	40	46.65558	118.3723

Site	Latitude (° ' ")	Longitude (° ' ")	Ellipsoid Height (m)
OAKS	-23 11 1.39436	150 39 24.29305	100.9325
ALT1	-10 18 48.40946	150 27 26.83823	96.8747
ALT2	-10 18 37.51053	150 20 18.08942	94.8772
WATA	-9 12 38.48661	150 14 33.02804	80.9149
EDEN	-37 4 27.40374	149 54 28.50170	17.2817
BATH	-33 25 46.83273	149 34 1.46547	756.5697
WITU	-4 41 17.84987	149 26 8.76090	84.2754
BASS	-21 7 0.30680	149 12 26.85760	122.1983
DS40	-35 24 3.99499	148 58 54.43997	683.6910
DS41	-35 24 3.89075	148 58 53.64089	684.2162
DS42	-35 23 57.15243	148 58 47.98724	665.3581
TID2	-35 23 57.15242	148 58 47.98725	665.3575
ORRO	-35 38 11.11908	148 56 22.05616	1356.2329
ORRX	-35 38 11.01437	148 56 22.27373	1346.5027
MUCK	-26 35 24.70093	148 23 18.41148	393.4002
CHAR	-40 45 12.62898	147 58 13.88778	51.1964
TRIA	-42 29 43.20868	147 55 12.11805	9.4702
MORO	-7 44 31.65491	147 35 22.96886	79.7353
TAS1	-42 48 14.30174	147 26 23.98801	56.9597
HOB1	-42 48 14.30101	147 26 23.98830	56.6628
HOBA	-42 48 16.98308	147 26 19.43753	41.1324
MANU	-2 3 2.29493	147 21 37.63659	129.8081
MORE	-9 26 2.77100	147 11 12.19980	116.6390
UNIT	-6 40 16.97028	146 59 52.37464	130.4139
TOWN	-19 15 35.33206	146 48 50.83183	97.7833
TOWA	-19 20 50.42958	146 46 30.79037	587.0468
WANK	-6 8 52.07314	146 4 52.44181	510.0441
GILG	-32 21 35.60347	145 59 27.58433	544.3221
SPM9	-41 3 1.97107	145 54 31.39137	13.1424
MADA	-5 12 41.28939	145 46 56.19266	73.3383
MADG	-5 9 43.80438	145 44 55.29454	460.9128
BANZ	-28 59 56.69550	145 40 7.63349	172.7274
BULL	-35 47 51.10268	145 33 13.55397	171.6888
GOKA	-6 4 53.07267	145 23 30.44603	1664.6260
BARC	-23 34 20.05894	145 17 45.46407	308.8507
PIEB	-15 19 9.27979	145 4 57.89862	482.2016
GUAM	13 35 21.58474	144 52 6.10271	201.9076
CAMW	-40 51 50.61486	144 42 33.65522	164.6596
ATKI	-37 45 26.78917	144 40 58.40993	145.0725
EMUU	-20 13 42.56726	144 22 31.00954	1029.3043
KIKO	-7 25 24.65412	144 14 55.76588	88.9980
BENW	-38 29 8.02252	143 54 42.89074	491.3782
WEWK	-3 35 2.58477	143 40 0.14729	83.9543
MEND	-6 8 36.73543	143 39 22.16528	1815.1874
WUVU	-1 44 7.59585	142 50 10.07835	79.1020
SAKL	47 1 46.96389	142 43 0.29761	89.9503
KOPI	-5 23 9.08504	142 29 42.19021	1412.8709
HOWI	-26 32 3.93017	142 23 4.94172	227.0508
GREN	-10 35 2.60985	142 12 39.57445	130.0772
OLVE	-29 5 16.66844	141 49 2.71311	323.7820
PORT	-38 18 53.46618	141 31 33.30711	47.3979
SUND	-31 53 57.29394	141 26 59.62962	408.7493
VANI	-2 41 5.28331	141 18 15.65479	80.6111
AIAM	-7 20 51.82090	141 16 1.44710	95.4951
AMAN	-3 35 18,78215	141 12 54.33026	477.3260

Site	Latitude (° ' ")	Longitude (° ' ")	Ellipsoid Height (m)
NORM	-17 40 34.45011	141 5 17.93547	64.2725
LLTR	-33 55 45.90883	141 0 9.90606	34.4306
TSU1	36 6 21.19907	140 5 15.10592	72.3088
TSKB	36 6 20.44948	140 5 14.98856	67.2453
BREA	-23 40 53.17999	139 37 2.80778	196.5482
AMUN	-89 59 49.60211	139 24 8.18407	2817.7062
BRDV	-25 54 2.59173	139 20 49.82808	67.3319
WILF	-20 20 34.96913	139 12 22.37104	554.1561
AUSA	-34 40 26.16394	138 39 17.24431	35.7229
AUSB	-34 40 26.16377	138 39 17.24771	35.5645
STAN	-35 7 23.98373	138 34 46.95140	306.5177
HWKR	-31 53 36.62798	138 25 28.21024	328.9205
USUD	36 7 59.22463	138 21 43.35581	1508.5402
USU5	36 7 59.20009	138 21 43.35685	1508.6002
WOLL	-17 13 13.78053	137 55 40.90296	106.7864
ELDO	-12 22 36.51234	136 49 17.53648	158.1363
GROO	-13 52 41.31306	136 27 57.51100	88.8575
ALYA	-13 51 21.04729	136 25 38.20883	78.3699
CLIF	-29 0 44.70690	136 2 27.43989	158.5668
ROPE	-14 50 26.71032	135 3 42.32459	140.3703
SHAM	-19 37 2.26738	134 11 18.58499	469.7680
ALIC	-23 40 12.44735	133 53 7.84758	603.3264
CEDU	-31 52 0.01728	133 48 35.37599	144.7465
THEV	-32 2 43.03133	133 42 59.81605	33.6747
JOHN	-25 56 49.10696	133 12 34.73757	571.9952
JUNC	-28 32 18.44242	131 44 22.57710	282.9210
DARW	-12 50 37.36018	131 7 57.84786	125.1852
KDMN	-16 6 56.74960	130 57 13.03645	125.8366
WINN	-12 25 23.75763	130 52 46.59090	82.9006
PILL	-12 28 0.38050	130 50 27.75176	80.3530
KILI	-19 46 1.84390	128 58 46.25812	496.3863
DEAK	-30 46 13.00712	128 57 19.29734	143.7689
RAWL	-24 59 41.11546	128 18 45.52128	825.1608
PIVT	-15 36 20.45689	128 16 34.93443	86.0169
TAEJ	36 22 27.91901	127 21 57.88247	77.4886
CAIG	-32 15 48.94316	125 32 15.70324	93.8055
GIBS	-23 56 39.45347	125 14 41.77563	413.5886
BATE	-25 42 25.55038	122 54 34.65096	480.1622
BROO	-17 53 21.77892	122 16 2.01598	27.8668
ESPE	-33 52 27.14875	121 53 40.52002	28.9513
TAIW	25 1 16.79491	121 32 11.54463	43.9608
KALG	-31 3 19.19953	121 26 56.74479	446.4449
SHAO	31 5 58.71693	121 12 1.58875	22.0650
MANL	14 32 13.81862	121 2 23.13342	69.2981
RATH	-22 26 47.68308	120 20 29.86386	532.7141
S01R	23 39 18.99449	119 35 32.51990	49.9215
COOL	-25 12 51.30781	118 0 25.14955	468.5158
TORB	-35 4 42.02442	117 37 17.10491	237.9648
KARR	-20 58 53.17169	117 5 49.87255	109.2211
CAVE	-31 50 24.69471	115 58 31.94621	-6.5978
PERT	-31 48 7.09417	115 53 6.88942	12.7749
PER2	-31 48 4.21672	115 53 6.63582	13.0616
YAR1	-29 2 47.61305	115 20 49.10402	241.3103
TIMB	5 17 0.41016	115 11 7.15045	113.2914
CARN	-25 6 50.40038	113 43 53.60941	-7.3800

Site	Latitude (° ' ")	Longitude (° ' ")	Ellipsoid Height (m)
CASE	-66 16 44.61006	110 32 8.46208	1.9337
CAS1	-66 17 0.09100	110 31 10.94032	22.4507
KAYA	0 48 44.01981	109 24 38.45744	101.2213
BAKO	-6 29 27.79434	106 50 56.06832	158.2268
XMAS	-10 26 58.57216	105 41 22.60059	260.4125
CHUL	13 44 7.61108	100 31 56.25758	-13.9611
COCO	-12 11 18.07060	96 50 2.27111	-35.2084
LHAS	29 39 26.42170	91 6 14.34942	3624.6562
COLB	6 53 30.85563	79 52 26.30707	-75.7634
DAV1	-68 34 38.36114	77 58 21.41079	44.4076
IISC	13 1 16.18719	77 34 13.34042	843.7213
MLTG	4 11 19.18737	73 31 34.63011	-94.1053
MALE	4 10 45.35460	73 30 40.26339	-94.7565
GAN1	0 41 31.40014	73 9 28.91943	-90.7693
KERG	-49 21 4.84131	70 15 23.41069	74.4600
KER5	-49 21 5.27976	70 15 19.87762	73.0344
KIT3	39 8 5.15899	66 53 7.59281	622.5034
DOVE	-70 14 1.18214	65 50 54.03778	1088.5269
MAW1	-67 36 17.15888	62 52 14.58009	59.1099
REUN	-21 12 29.68347	55 34 18.30542	1557.6470
SEY1	-4 40 25.39248	55 28 45.84623	537.2247
BAHA	26 12 32.89239	50 36 29.31163	-13.6781
DJIB	11 31 34.58237	42 50 49.29605	710.5366
MALI	-2 59 45.28495	40 11 39.81628	-23.3446
SYOW	-69 0 24.60164	39 35 6.14975	42.1617
HART	-25 53 13.57184	27 42 27.93630	1555.3920
METS	60 13 2.89422	24 23 43.13683	94.5788
TROM	69 39 45.89047	18 56 17.97518	132.4571
MATG	40 38 56.60253	16 42 16.49934	534.4393
MATE	40 38 56.86587	16 42 16.04144	535.6819
GRAZ	47 4 1.66156	15 29 36.51640	538.3214
WTZ1	49 8 39.20734	12 52 44.04272	666.0600
WTZX	49 8 40.38293	12 52 43.03273	659.9768
WETB	49 8 39.45914	12 52 41.85026	660.5765
ONSA	57 23 43.07011	11 55 31.85099	45.5849
NALL	78 55 46.50055	11 51 54.29575	78.4379
NAL1	78 55 46.49795	11 51 54.28582	81.7159
FORS	-70 46 38.97706	11 51 3.69587	137.6779
HONE	60 8 36.73792	10 14 56.58196	177.5927
ARLT	18 46 53.32839	7 21 30.36412	448.4758
KOSG	52 10 42.33137	5 48 34.71057	96.8724
HERS	50 52 2.32228	0 20 10.56669	76.5093

GUA2 AUST -5607198.748 2863957.603 -1015751.286
****

Nuvel NNR model estimates of movement, (X,Y,Z) for 1.0 years.				-0.0243	-0.0285	0.0535
GLOBK/GLORG model estim. of movement, (X,Y,Z) for 1.0 years.				-0.0454	-0.0222	0.0802
Difference GLOBK/GLORG - NUVEL				-0.0211	0.0063	0.0267
Nuvel NNR estimates in NEU.	0.0542	0.0364	-0.0001			
GLOBK rate estimates in NEU.	0.0840	0.0404	0.0171			
Diffs. GLOBK/GLORG - NUVEL in NEU	0.0298	0.0040	0.0171			

polar coordinates degrees from north & decimeters

POLAR NUVEL NNR estimates bearing/length.	33.877	0.653
POLAR GLOBK estimates bearing/length.	25.695	0.932
POLAR residual estimates bearing/length.	7.679	0.301

MISI AUST -5576759.293 2862001.148 -1175221.086
****

Nuvel NNR model estimates of movement, (X,Y,Z) for 1.0 years.				-0.0251	-0.0270	0.0534
GLOBK/GLORG model estim. of movement, (X,Y,Z) for 1.0 years.				-0.0266	-0.0365	0.0543
Difference GLOBK/GLORG - NUVEL				-0.0015	-0.0095	0.0009
Nuvel NNR estimates in NEU.	0.0543	0.0355	-0.0001			
GLOBK rate estimates in NEU.	0.0547	0.0446	-0.0032			
Diffs. GLOBK/GLORG - NUVEL in NEU	0.0004	0.0092	-0.0031			

polar coordinates degrees from north & decimeters

POLAR NUVEL NNR estimates bearing/length.	33.159	0.648
POLAR GLOBK estimates bearing/length.	39.224	0.706
POLAR residual estimates bearing/length.	87.637	0.092

JACQ AUST -5578632.259 3028263.693 -623240.731
****

Nuvel NNR model estimates of movement, (X,Y,Z) for 1.0 years.				-0.0232	-0.0315	0.0547
GLOBK/GLORG model estim. of movement, (X,Y,Z) for 1.0 years.				-0.0318	-0.0107	-0.0612
Difference GLOBK/GLORG - NUVEL				-0.0086	0.0208	-0.1159
Nuvel NNR estimates in NEU.	0.0550	0.0388	0.0000			
GLOBK rate estimates in NEU.	-0.0587	0.0246	0.0288			
Diffs. GLOBK/GLORG - NUVEL in NEU	-0.1137	-0.0142	0.0288			

polar coordinates degrees from north & decimeters

POLAR NUVEL NNR estimates bearing/length.	35.195	0.673
POLAR GLOBK estimates bearing/length.	157.275	0.636
POLAR residual estimates bearing/length.	-172.875	1.145

JACQ PCFC -5578632.259 3028263.693 -623240.731
****

Nuvel NNR model estimates of movement, (X,Y,Z) for 1.0 years.				0.0284	0.0572	0.0235
GLOBK/GLORG model estim. of movement, (X,Y,Z) for 1.0 years.				-0.0318	-0.0107	-0.0612
Difference GLOBK/GLORG - NUVEL				-0.0602	-0.0679	-0.0847
Nuvel NNR estimates in NEU.	0.0236	-0.0638	0.0000			
GLOBK rate estimates in NEU.	-0.0587	0.0246	0.0288			
Diffs. GLOBK/GLORG - NUVEL in NEU	-0.0822	0.0884	0.0288			

polar coordinates degrees from north & decimeters

POLAR NUVEL NNR estimates bearing/length.	-69.730	0.680
POLAR GLOBK estimates bearing/length.	157.275	0.636
POLAR residual estimates bearing/length.	132.934	1.208

LOUS AUST -5523811.492 3046135.335 -940385.344
****

Nuvel NNR model estimates of movement, (X,Y,Z) for 1.0 years.				-0.0250	-0.0286	0.0546
GLOBK/GLORG model estim. of movement, (X,Y,Z) for 1.0 years.				-0.0582	-0.0037	0.0643
Difference GLOBK/GLORG - NUVEL				-0.0332	0.0249	0.0097
Nuvel NNR estimates in NEU.	0.0552	0.0371	-0.0001			
GLOBK rate estimates in NEU.	0.0708	0.0313	0.0391			
Diffs. GLOBK/GLORG - NUVEL in NEU	0.0157	-0.0058	0.0391			

polar coordinates degrees from north & decimeters

POLAR NUVEL NNR estimates bearing/length.	33.918	0.665
POLAR GLOBK estimates bearing/length.	23.866	0.775
POLAR residual estimates bearing/length.	-20.188	0.167

KAVI PCFC -5562412.947 3107930.005 -285346.189
****

Nuvel NNR model estimates of movement, (X,Y,Z) for 1.0 years.				0.0310	0.0576	0.0233
GLOBK/GLORG model estim. of movement, (X,Y,Z) for 1.0 years.				-0.0065	0.0758	0.0297
Difference GLOBK/GLORG - NUVEL				-0.0375	0.0182	0.0064
Nuvel NNR estimates in NEU.	0.0233	-0.0654	0.0000			
GLOBK rate estimates in NEU.	0.0316	-0.0630	0.0413			
Diffs. GLOBK/GLORG - NUVEL in NEU	0.0083	0.0024	0.0413			

polar coordinates degrees from north & decimeters

POLAR NUVEL NNR estimates bearing/length.	-70.397	0.694
POLAR GLOBK estimates bearing/length.	-63.379	0.705
POLAR residual estimates bearing/length.	15.857	0.086

ALT2 AUST -5453535.756 3105804.867 -1134062.725
****

Nuvel NNR model estimates of movement, (X,Y,Z) for 1.0 years.				-0.0265	-0.0265	0.0547
GLOBK/GLORG model estim. of movement, (X,Y,Z) for 1.0 years.				-0.0449	-0.0232	0.0534
Difference GLOBK/GLORG - NUVEL				-0.0184	0.0033	-0.0013
Nuvel NNR estimates in NEU.	0.0556	0.0361	-0.0001			
GLOBK rate estimates in NEU.	0.0574	0.0424	0.0175			
Diffs. GLOBK/GLORG - NUVEL in NEU	0.0019	0.0062	0.0176			

polar coordinates degrees from north & decimeters		
POLAR NUVEL NNR estimates bearing/length.	33.036	0.663
POLAR GLOBK estimates bearing/length.	36.418	0.714
POLAR residual estimates bearing/length.	73.319	0.065

MORO AUST -5335932.381 3387629.598 -853539.800
****

Nuvel NNR model estimates of movement, (X,Y,Z) for 1.0 years.				-0.0268	-0.0280	0.0564
GLOBK/GLORG model estim. of movement, (X,Y,Z) for 1.0 years.				-0.0515	-0.0136	0.0604
Difference GLOBK/GLORG - NUVEL				-0.0247	0.0144	0.0040
Nuvel NNR estimates in NEU.	0.0569	0.0380	-0.0001			
GLOBK rate estimates in NEU.	0.0647	0.0391	0.0277			
Diffs. GLOBK/GLORG - NUVEL in NEU	0.0078	0.0010	0.0278			

polar coordinates degrees from north & decimeters		
POLAR NUVEL NNR estimates bearing/length.	33.779	0.684
POLAR GLOBK estimates bearing/length.	31.136	0.756
POLAR residual estimates bearing/length.	7.552	0.079

MANU AUST -5367596.440 3437943.341 -226704.965
****

Nuvel NNR model estimates of movement, (X,Y,Z) for 1.0 years.				-0.0238	-0.0334	0.0570
GLOBK/GLORG model estim. of movement, (X,Y,Z) for 1.0 years.				-0.0142	0.0722	0.0255
Difference GLOBK/GLORG - NUVEL				0.0096	0.1056	-0.0315

Nuvel NNR estimates in NEU.	0.0570	0.0409	0.0000
GLOBK rate estimates in NEU.	0.0273	-0.0531	0.0500
Diffs. GLOBK/GLORG - NUVEL in NEU	-0.0297	-0.0941	0.0500

polar coordinates degrees from north & decimeters

POLAR NUVEL NNR estimates bearing/length.	35.697	0.702
POLAR GLOBK estimates bearing/length.	-62.815	0.597
POLAR residual estimates bearing/length.	-107.516	0.987

MORE AUST -5288519.162 3409952.865 -1038574.347
****

Nuvel NNR model estimates of movement, (X,Y,Z) for 1.0 years.				-0.0280	-0.0262	0.0563
GLOBK/GLORG model estim. of movement, (X,Y,Z) for 1.0 years.				-0.0133	-0.0465	0.0626
Difference GLOBK/GLORG - NUVEL				0.0147	-0.0203	0.0063

Nuvel NNR estimates in NEU.	0.0571	0.0372	-0.0001
GLOBK rate estimates in NEU.	0.0595	0.0463	-0.0241
Diffs. GLOBK/GLORG - NUVEL in NEU	0.0024	0.0091	-0.0240

polar coordinates degrees from north & decimeters

POLAR NUVEL NNR estimates bearing/length.	33.090	0.681
POLAR GLOBK estimates bearing/length.	37.890	0.754
POLAR residual estimates bearing/length.	75.104	0.094

UNIT AUST -5313156.701 3450683.560 -736065.733
****

Nuvel NNR model estimates of movement, (X,Y,Z) for 1.0 years.				-0.0266	-0.0289	0.0568
GLOBK/GLORG model estim. of movement, (X,Y,Z) for 1.0 years.				0.0166	-0.0682	0.0598
Difference GLOBK/GLORG - NUVEL				0.0432	-0.0393	0.0030
Nuvel NNR estimates in NEU.	0.0571	0.0387	0.0000			
GLOBK rate estimates in NEU.	0.0535	0.0482	-0.0577			
Diffs. GLOBK/GLORG - NUVEL in NEU	-0.0036	0.0095	-0.0576			

polar coordinates degrees from north & decimeters

POLAR NUVEL NNR estimates bearing/length.	34.099	0.690
POLAR GLOBK estimates bearing/length.	41.986	0.720
POLAR residual estimates bearing/length.	111.024	0.101

TOWN AUST -5041024.962 3296980.305 -2090553.325
****

Nuvel NNR model estimates of movement, (X,Y,Z) for 1.0 years.				-0.0329	-0.0160	0.0540
GLOBK/GLORG model estim. of movement, (X,Y,Z) for 1.0 years.				-0.0341	-0.0217	0.0532
Difference GLOBK/GLORG - NUVEL				-0.0012	-0.0057	-0.0008
Nuvel NNR estimates in NEU.	0.0572	0.0313	-0.0001			
GLOBK rate estimates in NEU.	0.0557	0.0368	-0.0018			
Diffs. GLOBK/GLORG - NUVEL in NEU	-0.0015	0.0055	-0.0017			

polar coordinates degrees from north & decimeters

POLAR NUVEL NNR estimates bearing/length.	28.722	0.652
POLAR GLOBK estimates bearing/length.	33.460	0.668
POLAR residual estimates bearing/length.	105.174	0.057

VANI AUST -4972629.909 3983208.172 -296767.243
****

Nuvel NNR model estimates of movement, (X,Y,Z) for 1.0 years.				-0.0277	-0.0302	0.0593
GLOBK/GLORG model estim. of movement, (X,Y,Z) for 1.0 years.				-0.0479	-0.0069	0.0285
Difference GLOBK/GLORG - NUVEL				-0.0202	0.0233	-0.0308
Nuvel NNR estimates in NEU.	0.0594	0.0409	0.0000			
GLOBK rate estimates in NEU.	0.0300	0.0353	0.0317			
Diffs. GLOBK/GLORG - NUVEL in NEU	-0.0294	-0.0056	0.0317			

polar coordinates degrees from north & decimeters

POLAR NUVEL NNR estimates bearing/length.	34.585	0.721
POLAR GLOBK estimates bearing/length.	49.658	0.464
POLAR residual estimates bearing/length.	-169.204	0.299

AIAM AUST -4934886.488 3958248.628 -810301.129
****

Nuvel NNR model estimates of movement, (X,Y,Z) for 1.0 years.				-0.0303	-0.0258	0.0589
GLOBK/GLORG model estim. of movement, (X,Y,Z) for 1.0 years.				0.0034	-0.0916	0.0705
Difference GLOBK/GLORG - NUVEL				0.0337	-0.0658	0.0116
Nuvel NNR estimates in NEU.	0.0594	0.0391	-0.0001			
GLOBK rate estimates in NEU.	0.0623	0.0693	-0.0685			
Diffs. GLOBK/GLORG - NUVEL in NEU	0.0029	0.0303	-0.0684			

polar coordinates degrees from north & decimeters

POLAR NUVEL NNR estimates bearing/length.	33.350	0.711
POLAR GLOBK estimates bearing/length.	48.051	0.932
POLAR residual estimates bearing/length.	84.458	0.304

Site Repeatability: Vanimo

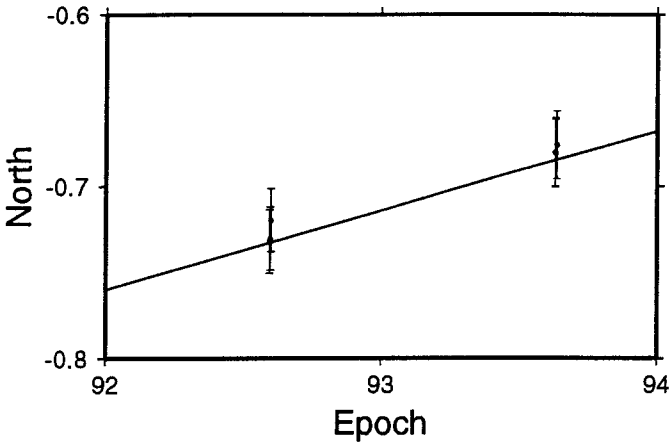

Mean Value :
-298870.705 m +/- 10.8 mm

Mean Slope :
46.2 mm/y +/- 15.0 mm/y

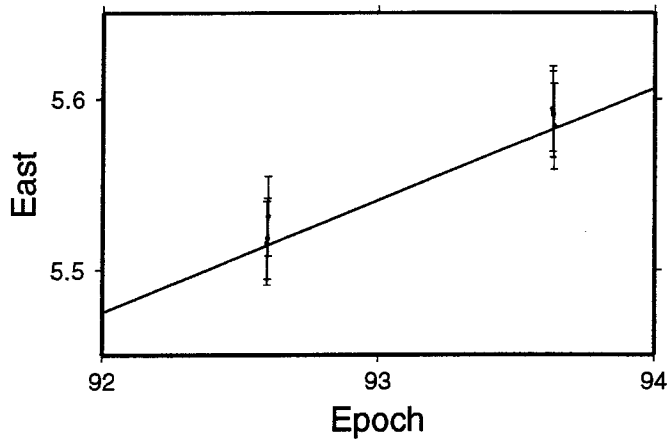

Mean Value :
15712665.554 m +/- 15.3 mm

Mean Slope :
65.3 mm/y +/- 19.3 mm/y

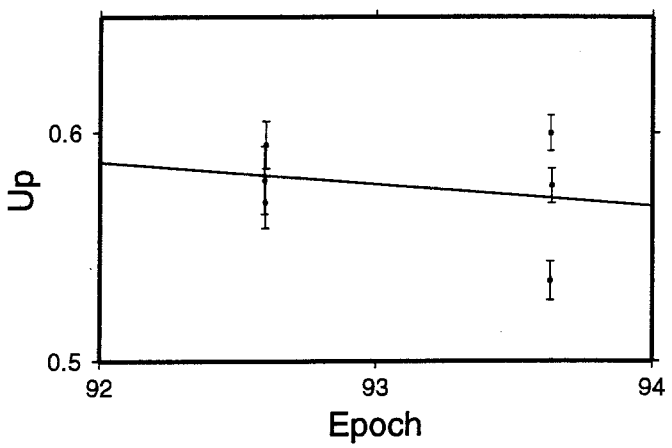

Mean Value :
80.576 m +/- 10.2 mm

Mean Slope :
-9.3 mm/y +/- 23.3 mm/y

Site Repeatability: Lae

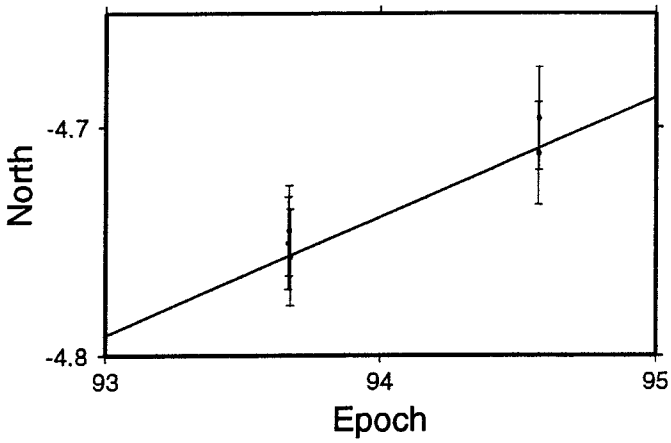

Mean Value :
-742654.734 m +/- 11.6 mm

Mean Slope :
51.9 mm/y +/- 21.8 mm/y

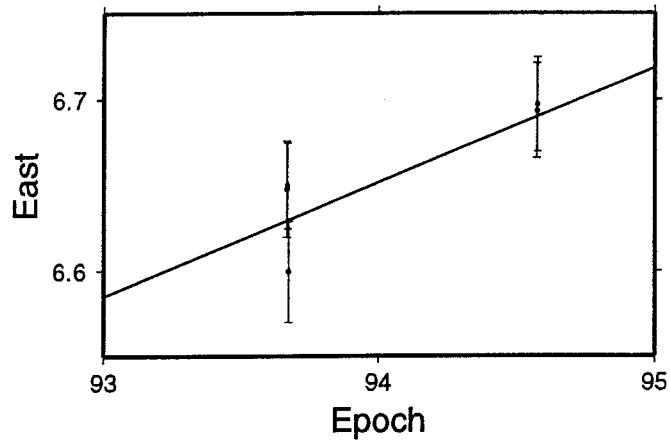

Mean Value :
16252896.659 m +/- 17.0 mm

Mean Slope :
66.5 mm/y +/- 27.7 mm/y

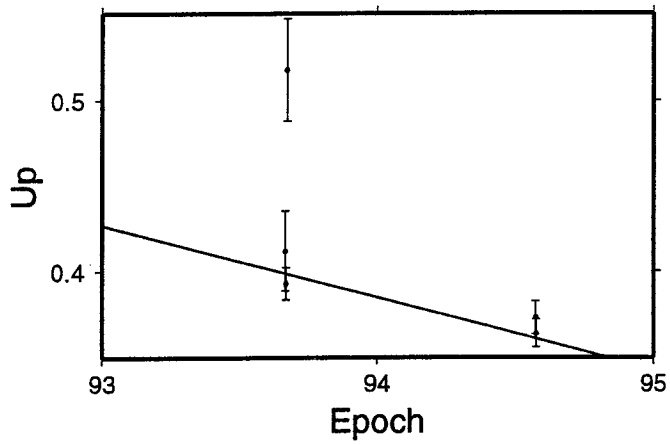

Mean Value :
130.381 m +/- 13.5 mm

Mean Slope :
-42.3 mm/y +/- 27.1 mm/y

Site Repeatability: Townsville

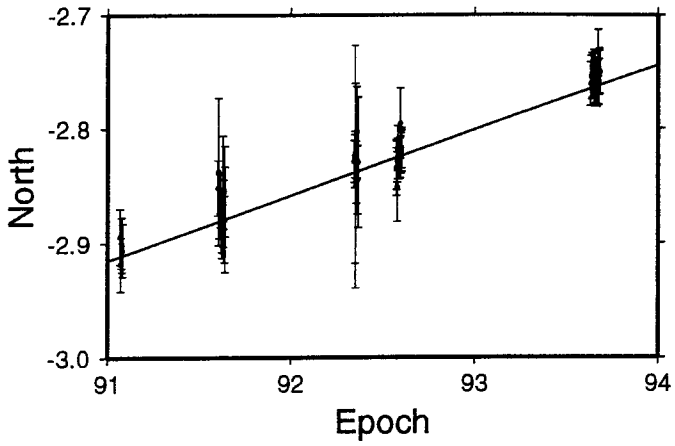

Mean Value :
-2143992.813 m +/- 6.8 mm

Mean Slope :
57.0 mm/y +/- 3.2 mm/y

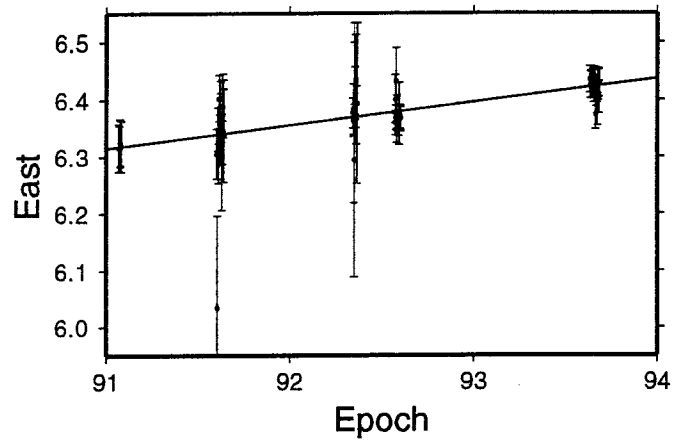

Mean Value :
15428546.388 m +/- 5.1 mm

Mean Slope :
40.6 mm/y +/- 4.9 mm/y

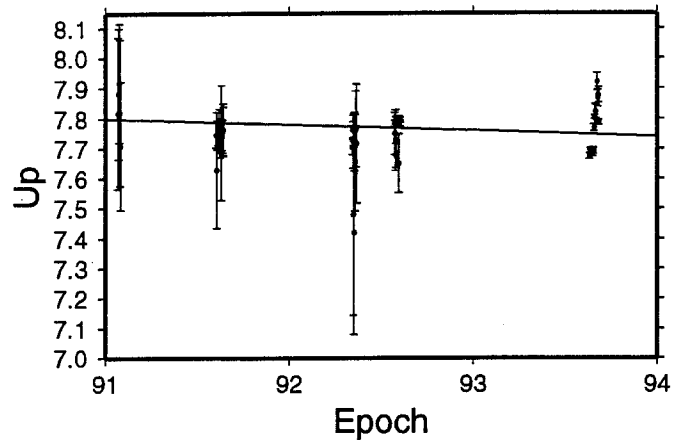

Mean Value :
97.763 m +/- 6.6 mm

Mean Slope :
-20.4 mm/y +/- 11.8 mm/y

Site Repeatability: Morobe

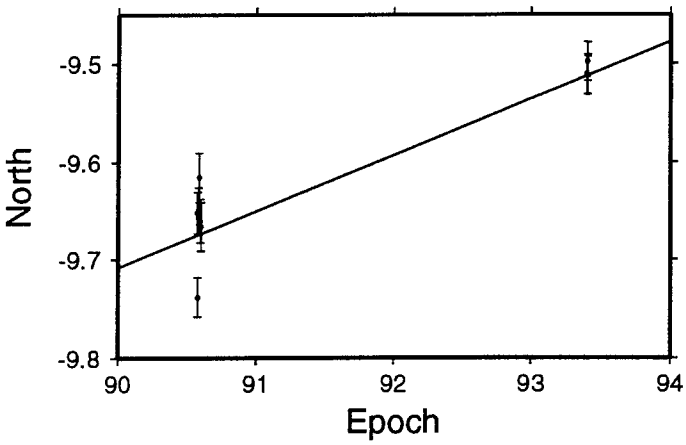

Mean Value :
-861849.604 m +/- 30.2 mm

Mean Slope :
57.7 mm/y +/- 8.4 mm/y

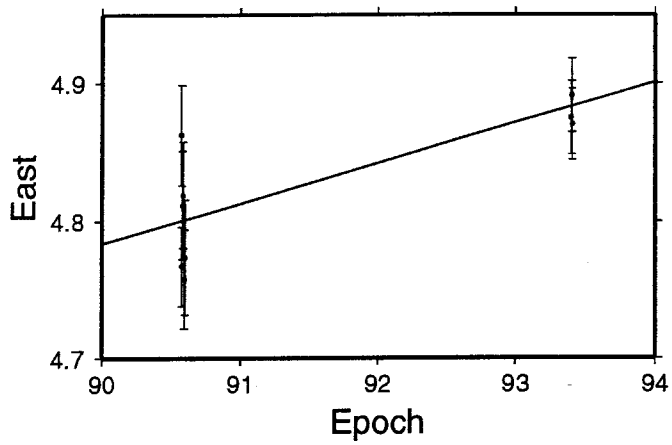

Mean Value :
16279894.836 m +/- 17.5 mm

Mean Slope :
29.3 mm/y +/- 7.5 mm/y

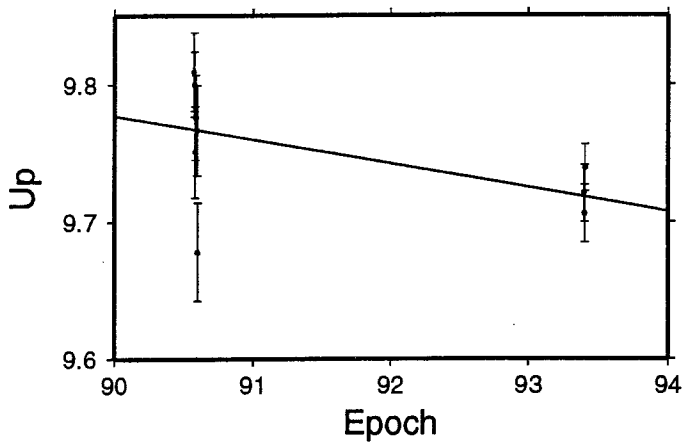

Mean Value :
79.746 m +/- 13.3 mm

Mean Slope :
-17.5 mm/y +/- 7.7 mm/y

Site Repeatability: Port Moresby

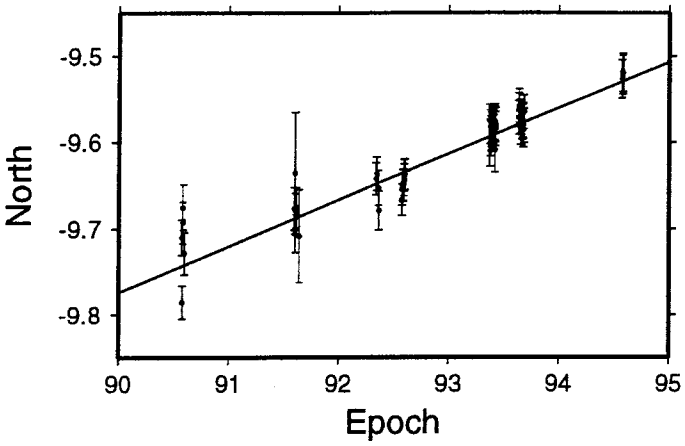

Mean Value :
-1050199.609 m +/- 6.8 mm

Mean Slope :
53.5 mm/y +/- 2.8 mm/y

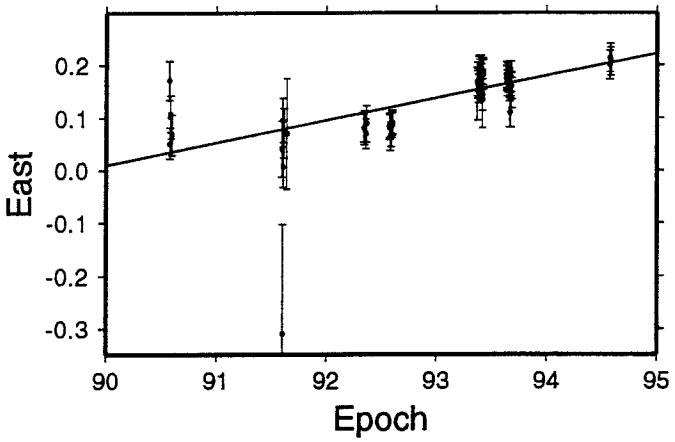

Mean Value :
16163150.141 m +/- 6.3 mm

Mean Slope :
42.4 mm/y +/- 4.8 mm/y

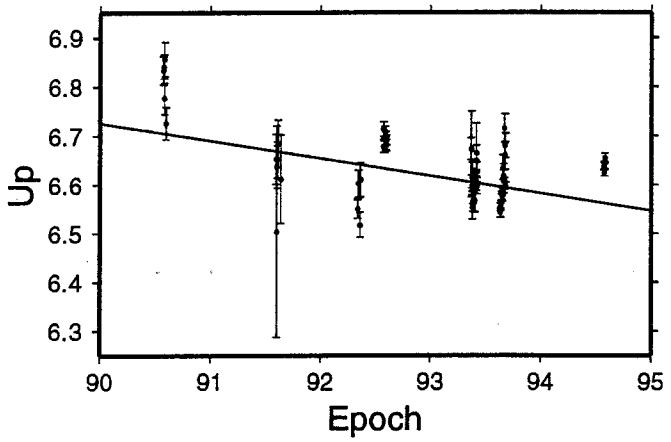

Mean Value :
116.615 m +/- 6.8 mm

Mean Slope :
-35.7 mm/y +/- 8.3 mm/y

Site Repeatability: Misima

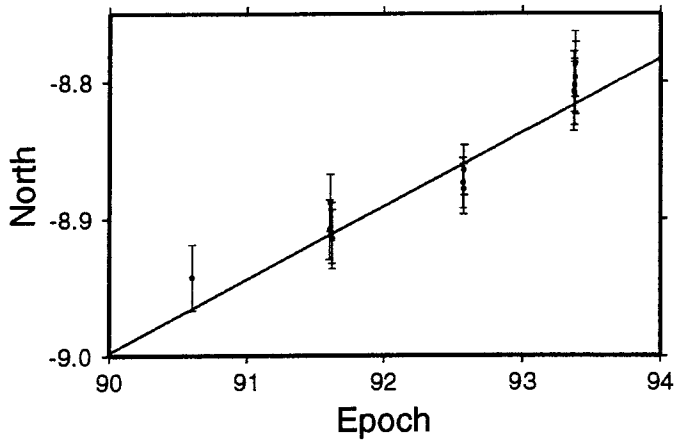

Mean Value :
-1189878.863 m +/- 13.6 mm

Mean Slope :
53.8 mm/y +/- 7.2 mm/y

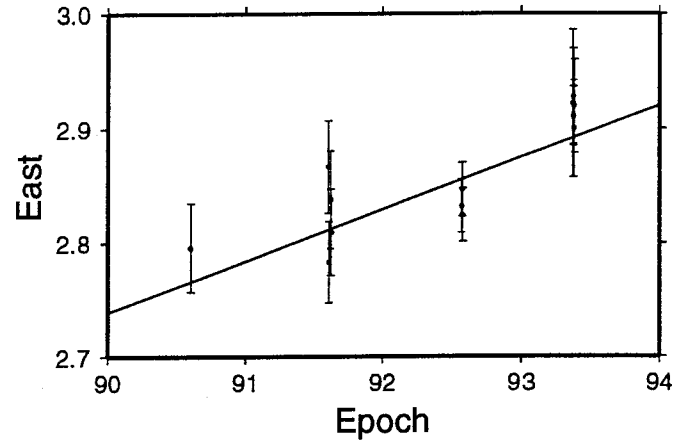

Mean Value :
16718102.852 m +/- 12.5 mm

Mean Slope :
45.1 mm/y +/- 11.7 mm/y

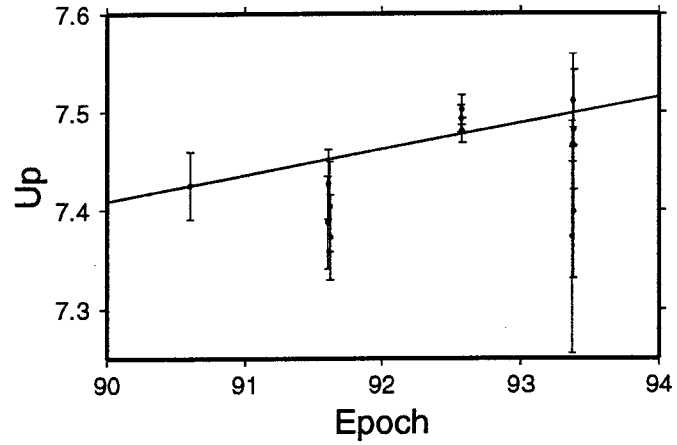

Mean Value :
87.475 m +/- 9.1 mm

Mean Slope :
26.6 mm/y +/- 14.0 mm/y

Site Repeatability: Manus

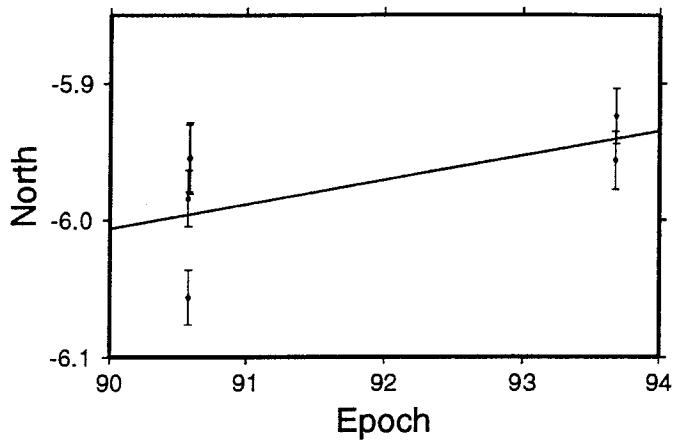

Mean Value :
-228275.974 m +/- 19.9 mm

Mean Slope :
17.8 mm/y +/- 11.8 mm/y

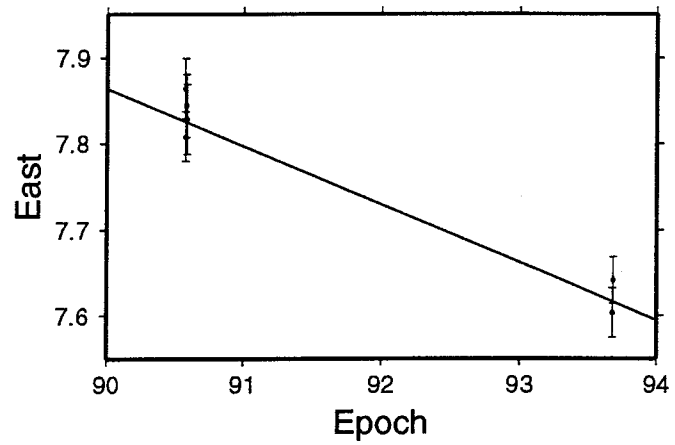

Mean Value :
16393577.743 m +/- 47.2 mm

Mean Slope :
-67.3 mm/y +/- 8.5 mm/y

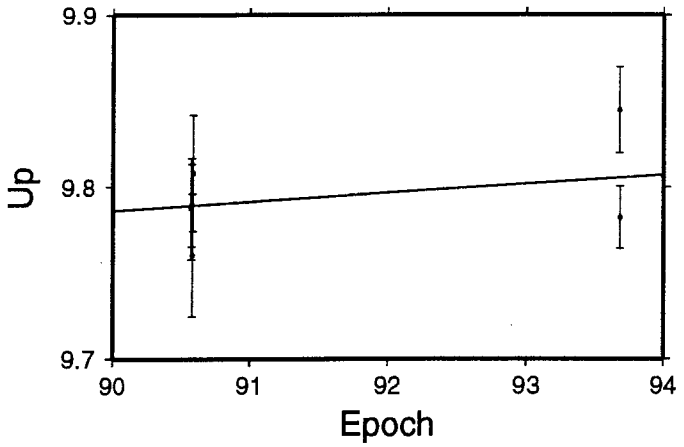

Mean Value :
129.796 m +/- 11.2 mm

Mean Slope :
5.3 mm/y +/- 7.6 mm/y

Site Repeatability: Losuia

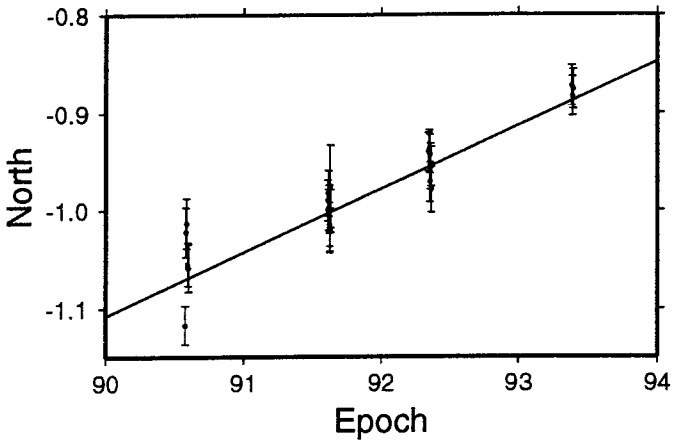

Mean Value :
-950150.978 m +/- 12.6 mm

Mean Slope :
65.0 mm/y +/- 5.2 mm/y

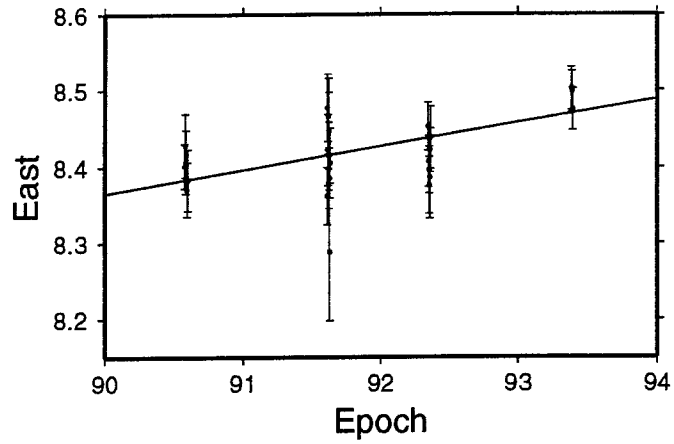

Mean Value :
16636898.427 m +/- 9.3 mm

Mean Slope :
30.8 mm/y +/- 7.8 mm/y

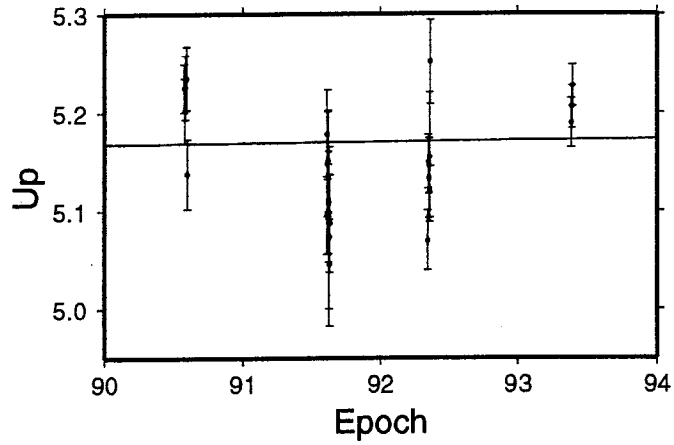

Mean Value :
85.170 m +/- 11.3 mm

Mean Slope :
1.2 mm/y +/- 11.2 mm/y

Site Repeatability: Kavieng

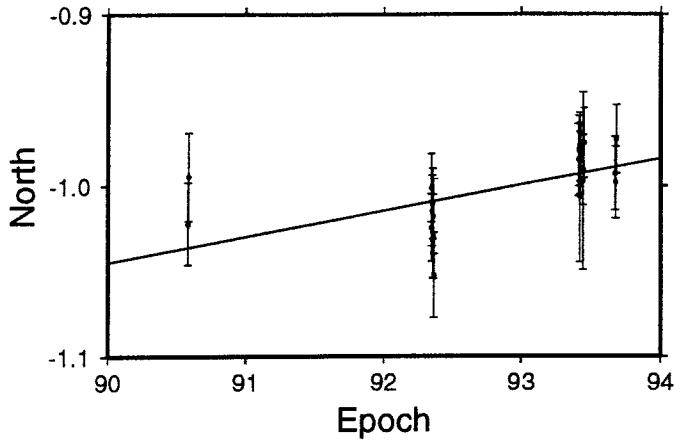

Mean Value :
-287361.001 m +/- 4.9 mm

Mean Slope :
15.2 mm/y +/- 5.7 mm/y

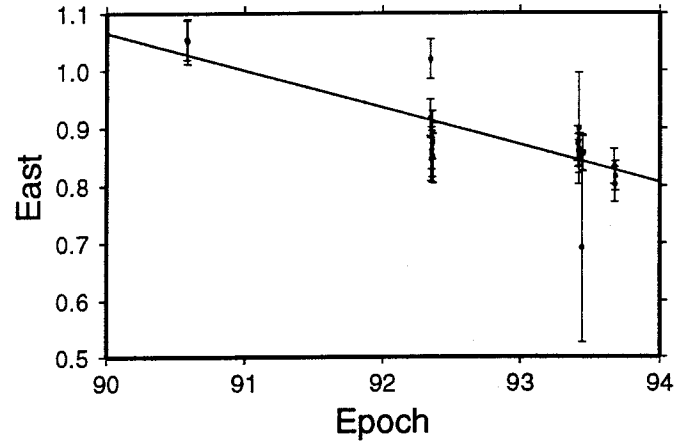

Mean Value :
16770640.877 m +/- 15.3 mm

Mean Slope :
-64.9 mm/y +/- 9.9 mm/y

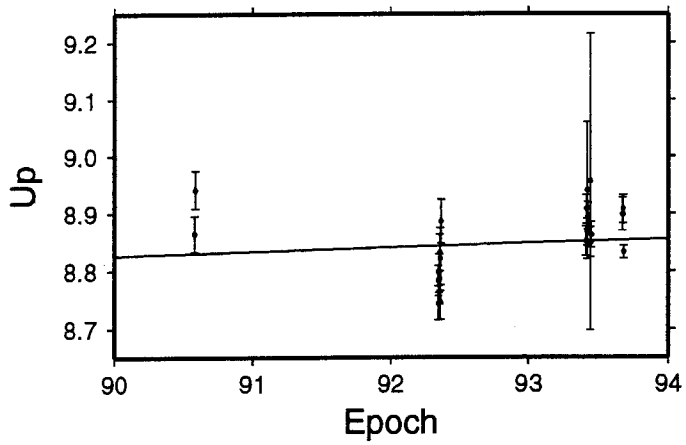

Mean Value :
78.847 m +/- 10.6 mm

Mean Slope :
7.3 mm/y +/- 12.9 mm/y

Site Repeatability: Jacquinot Bay

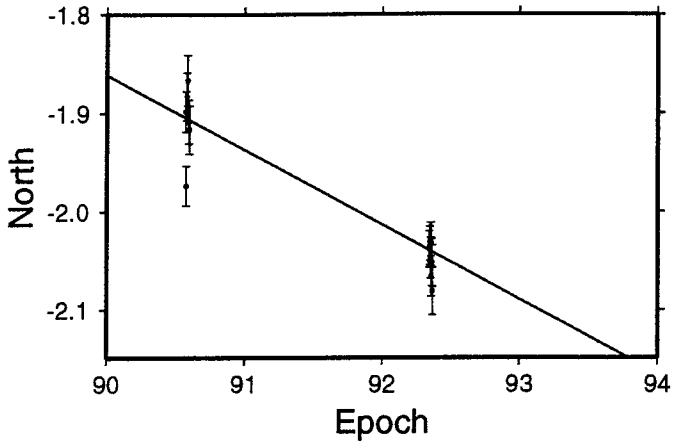

Mean Value :
-628421.998 m +/- 18.5 mm

Mean Slope :
-76.4 mm/y +/- 8.0 mm/y

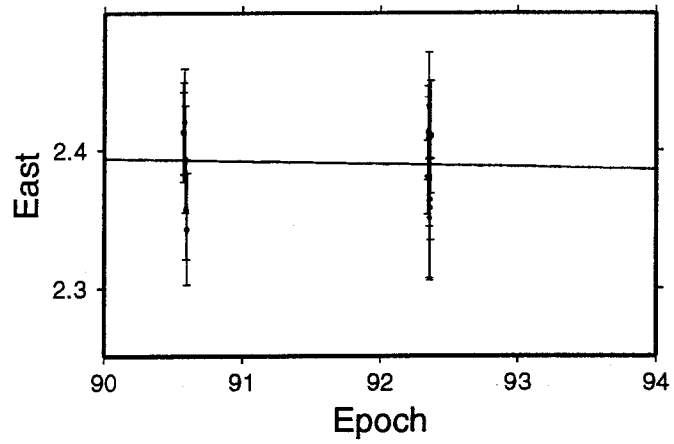

Mean Value :
16783752.391 m +/- 9.0 mm

Mean Slope :
-2.0 mm/y +/- 10.6 mm/y

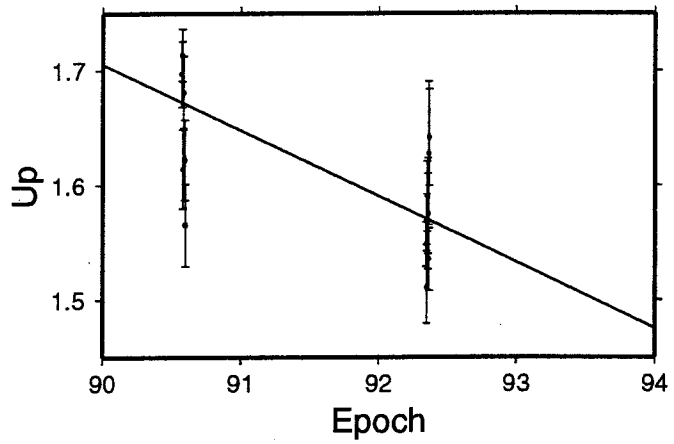

Mean Value :
151.602 m +/- 17.2 mm

Mean Slope :
-57.8 mm/y +/- 13.0 mm/y

Site Repeatability: Guasopa

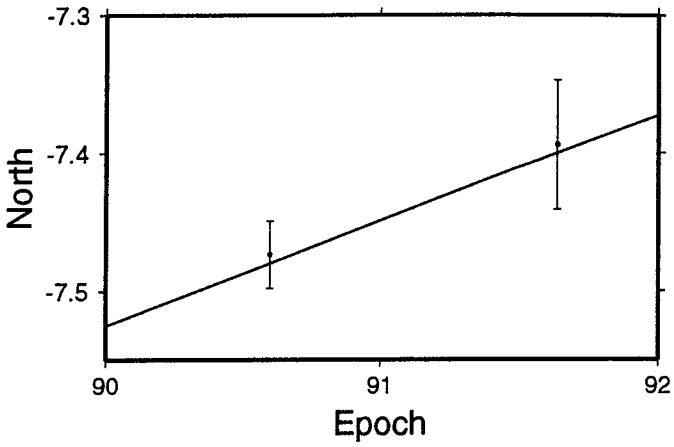

Mean Value :
-1026927.456 m +/- 32.5 mm

Mean Slope :
76.0 mm/y +/- 50.6 mm/y

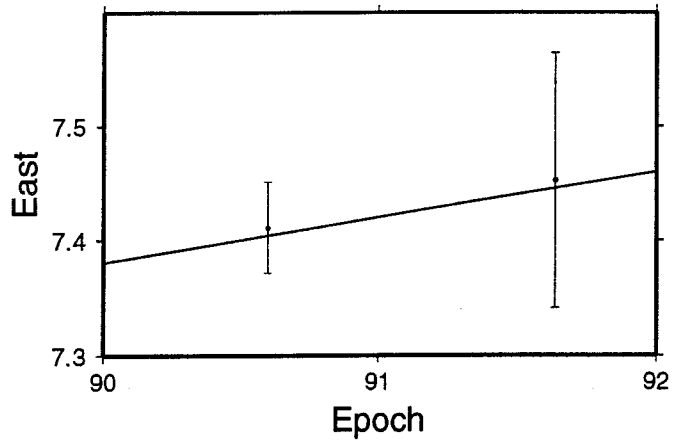

Mean Value :
16805417.416 m +/- 37.7 mm

Mean Slope :
39.4 mm/y +/- 114.0 mm/y

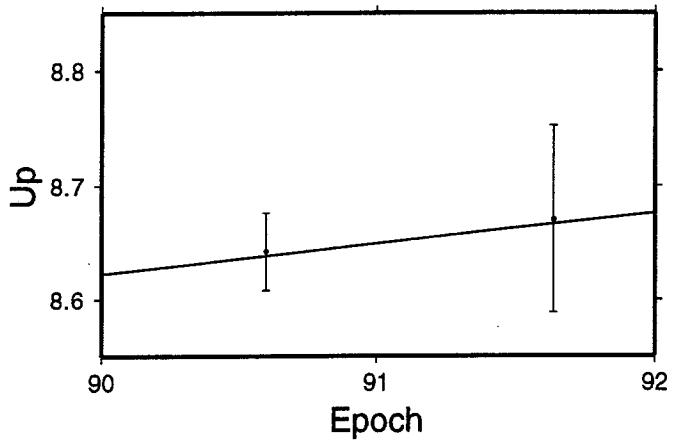

Mean Value :
78.646 m +/- 31.5 mm

Mean Slope :
26.9 mm/y +/- 85.4 mm/y

Site Repeatability: Alotau

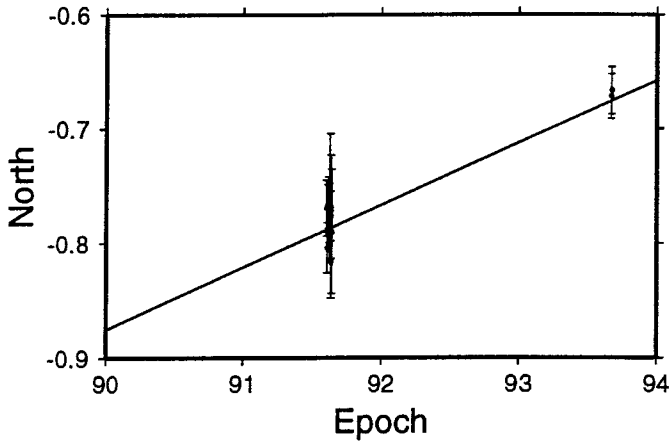

Mean Value :
-1147750.761 m +/- 11.6 mm

Mean Slope :
54.3 mm/y +/- 7.7 mm/y

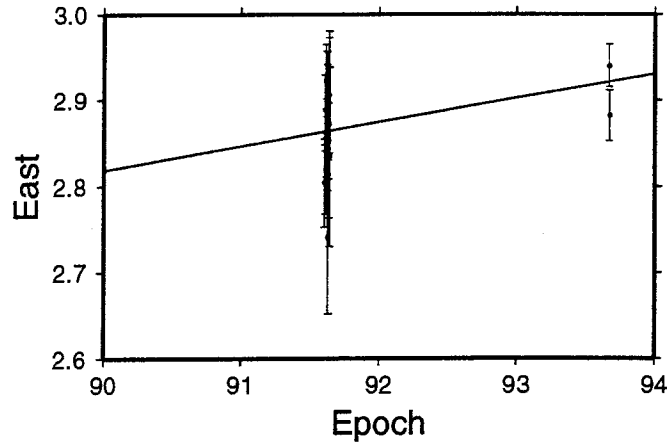

Mean Value :
16465342.877 m +/- 12.1 mm

Mean Slope :
28.2 mm/y +/- 11.2 mm/y

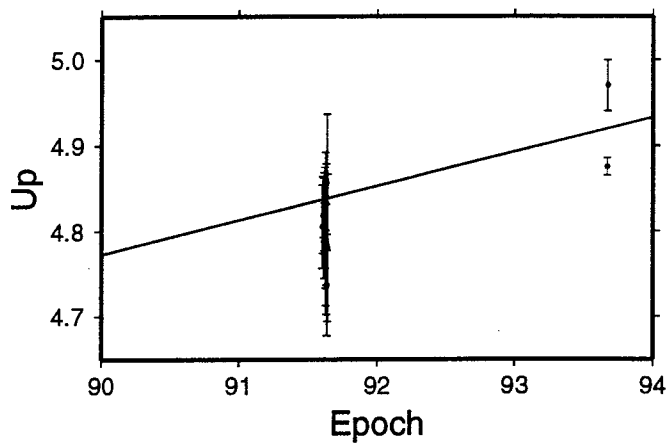

Mean Value :
94.857 m +/- 12.6 mm

Mean Slope :
40.1 mm/y +/- 8.1 mm/y

Site Repeatability: Aiambak

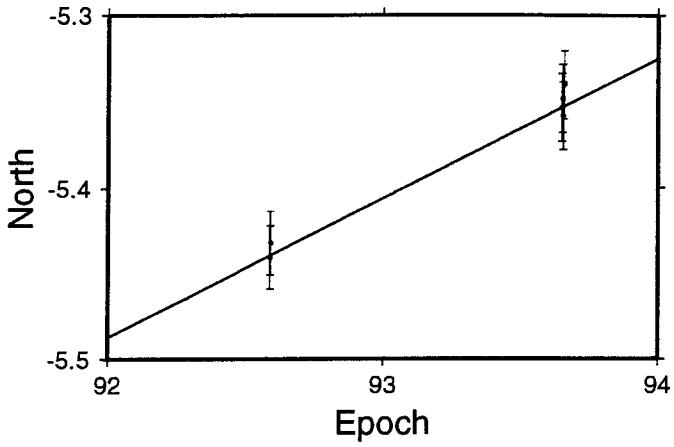

Mean Value :
-817945.382 m +/- 18.7 mm

Mean Slope :
81.1 mm/y +/- 15.4 mm/y

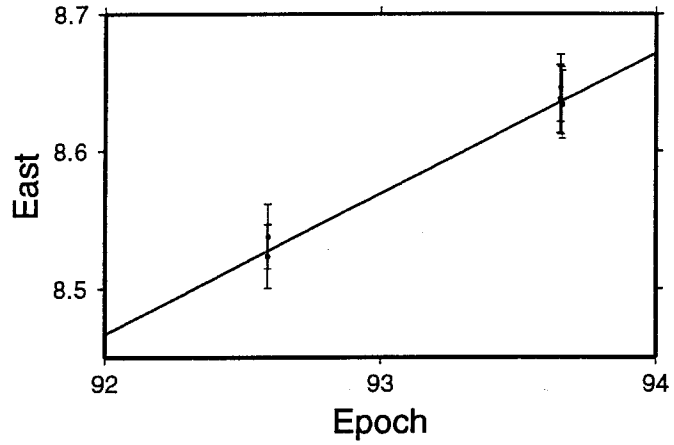

Mean Value :
15596618.600 m +/- 23.3 mm

Mean Slope :
101.8 mm/y +/- 19.5 mm/y

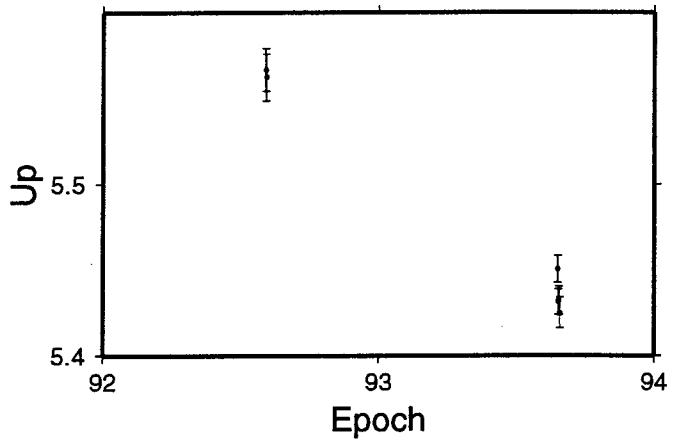

Mean Value :
95.456 m +/- 21.6 mm

Mean Slope :
-122.5 mm/y +/- 10.8 mm/y

Baseline Repeatability: Port Moresby - Morobe

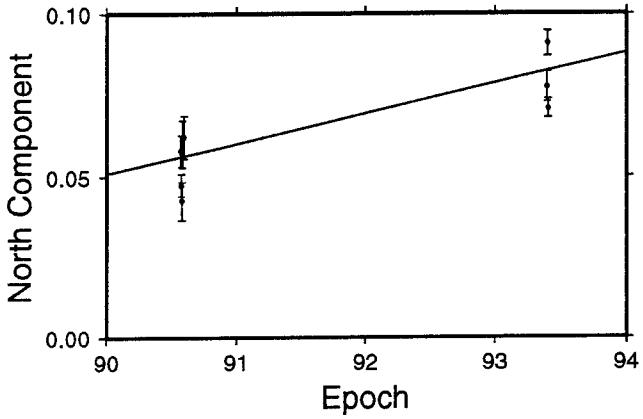

Mean Value :
188350.066 m +/- 5.7 mm

Mean Slope :
9.2 mm/y +/- 2.3 mm/y

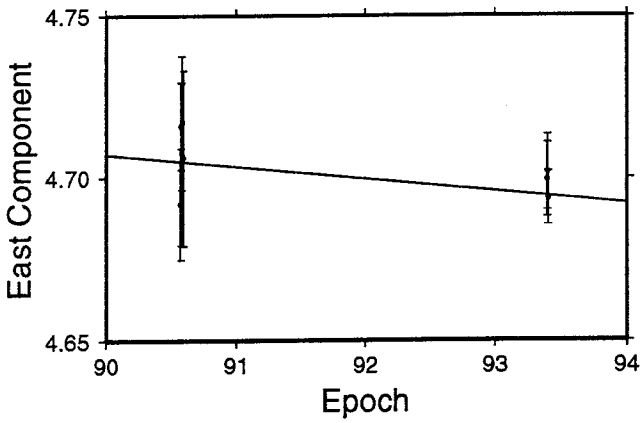

Mean Value :
116744.701 m +/- 4.7 mm

Mean Slope :
-3.9 mm/y +/- 3.6 mm/y

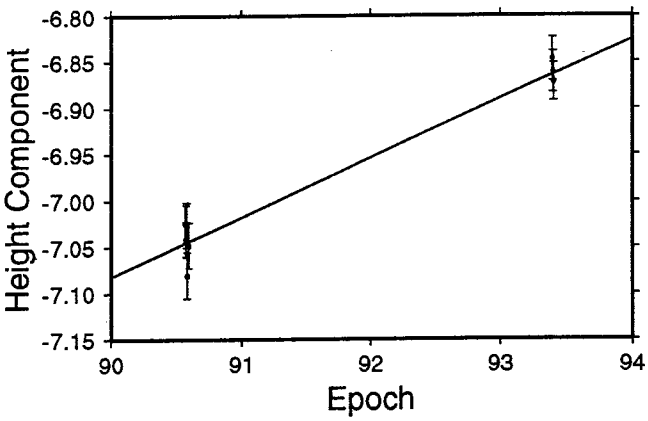

Mean Value :
-36.973 m +/- 33.6 mm

Mean Slope :
63.9 mm/y +/- 5.7 mm/y

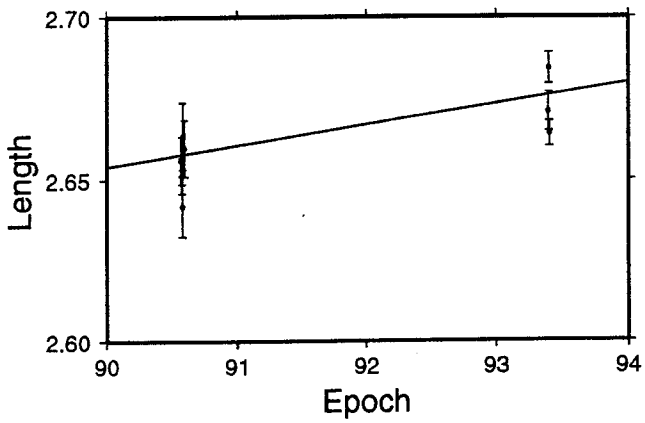

Mean Value :
192312.665 m +/- 4.5 mm

Mean Slope :
6.4 mm/y +/- 2.3 mm/y

Baseline Repeatability: Port Moresby - Lae

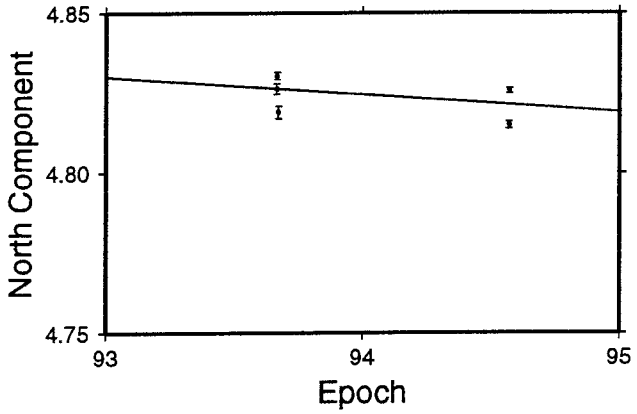

Mean Value :
307544.824 m +/- 2.7 mm

Mean Slope :
-5.6 mm/y +/- 6.5 mm/y

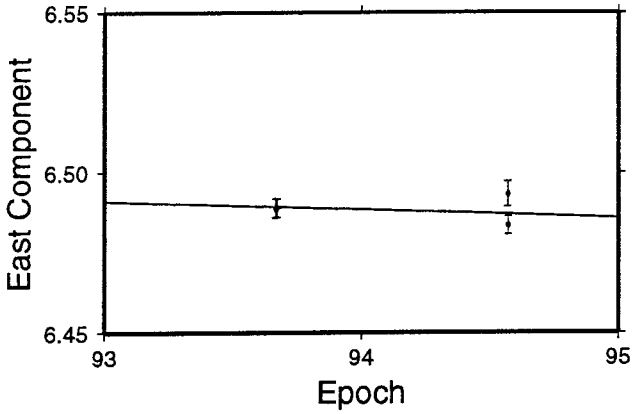

Mean Value :
89746.488 m +/- 1.5 mm

Mean Slope :
-2.3 mm/y +/- 3.7 mm/y

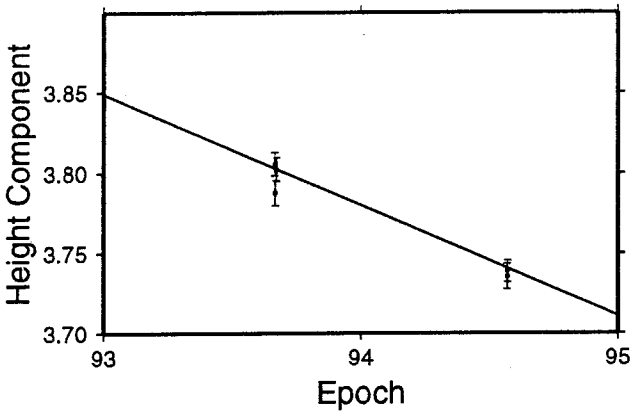

Mean Value :
13.773 m +/- 15.6 mm

Mean Slope :
-68.8 mm/y +/- 7.6 mm/y

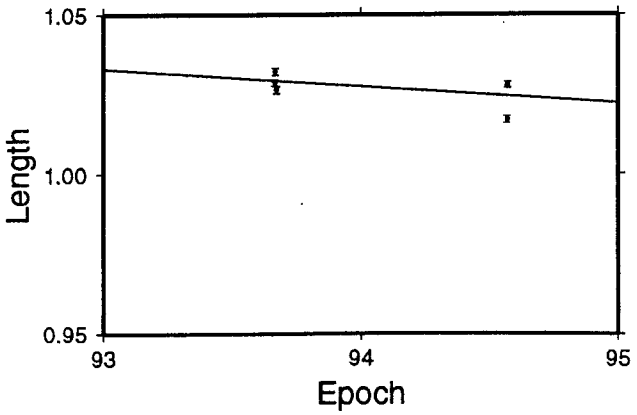

Mean Value :
306231.027 m +/- 2.3 mm

Mean Slope :
-5.6 mm/y +/- 5.1 mm/y

Baseline Repeatability: Port Moresby - Misima

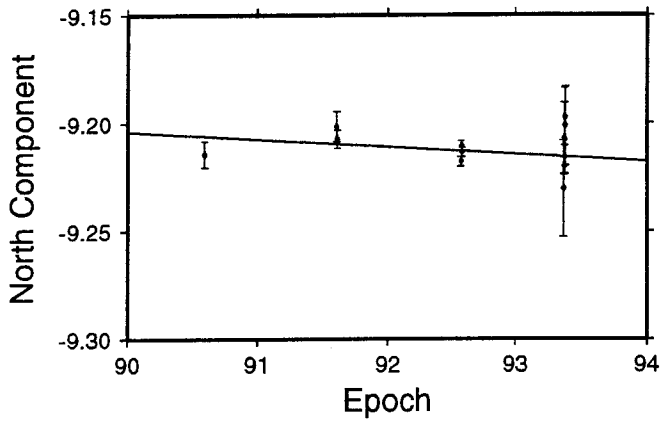

Mean Value :
-139679.214 m +/- 1.4 mm

Mean Slope :
-3.5 mm/y +/- 2.5 mm/y

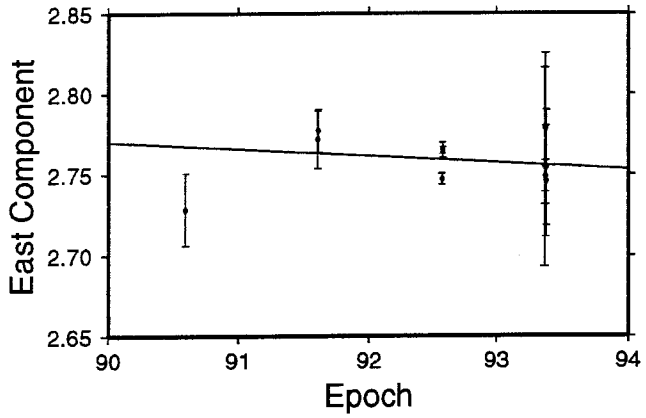

Mean Value :
554952.759 m +/- 2.9 mm

Mean Slope :
-4.2 mm/y +/- 10.5 mm/y

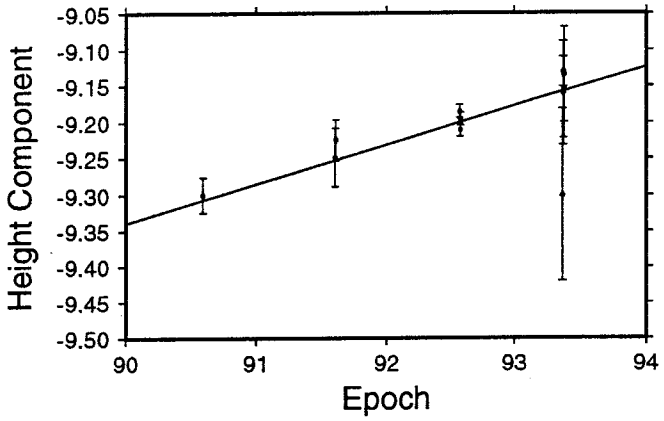

Mean Value :
-29.199 m +/- 9.0 mm

Mean Slope :
53.7 mm/y +/- 9.9 mm/y

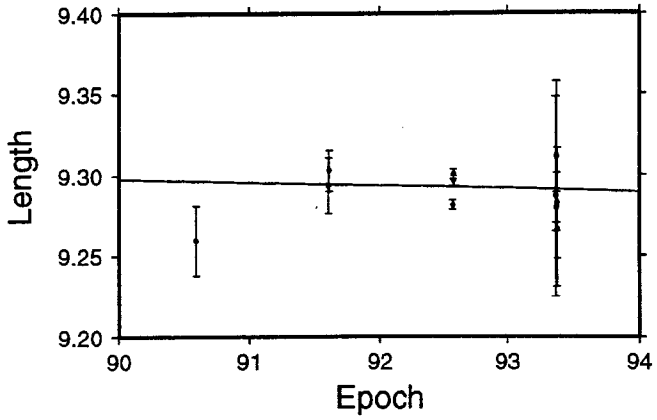

Mean Value :
634039.292 m +/- 2.8 mm

Mean Slope :
-2.3 mm/y +/- 10.8 mm/y

Baseline Repeatability: Port Moresby - Losuia

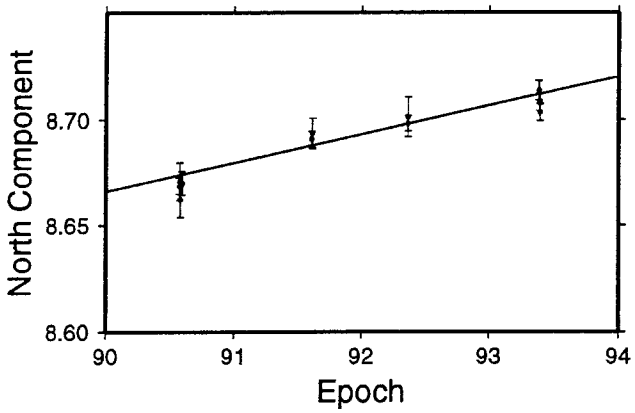

Mean Value :
100048.693 m +/- 5.0 mm

Mean Slope :
13.5 mm/y +/- 1.3 mm/y

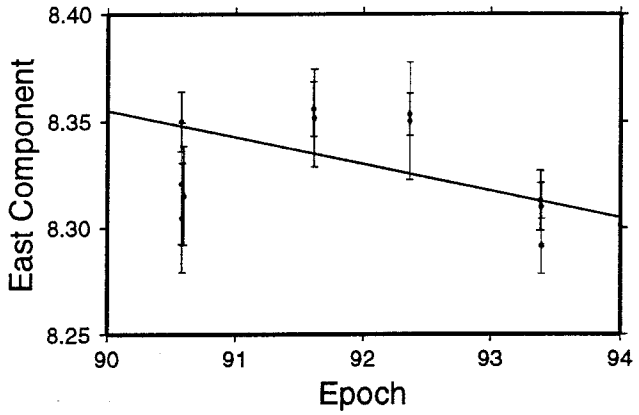

Mean Value :
473748.330 m +/- 7.6 mm

Mean Slope :
-12.4 mm/y +/- 6.3 mm/y

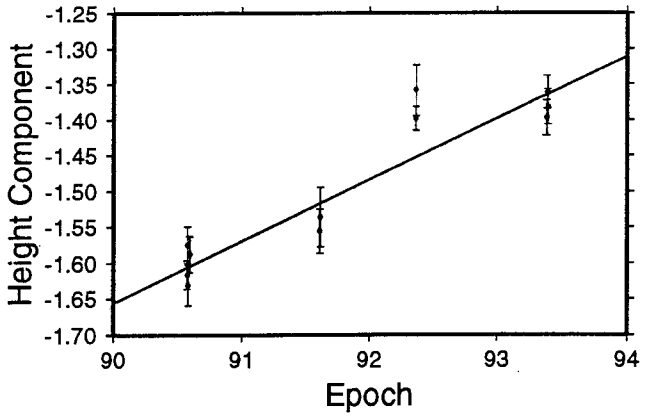

Mean Value :
-31.484 m +/- 33.7 mm

Mean Slope :
86.2 mm/y +/- 10.3 mm/y

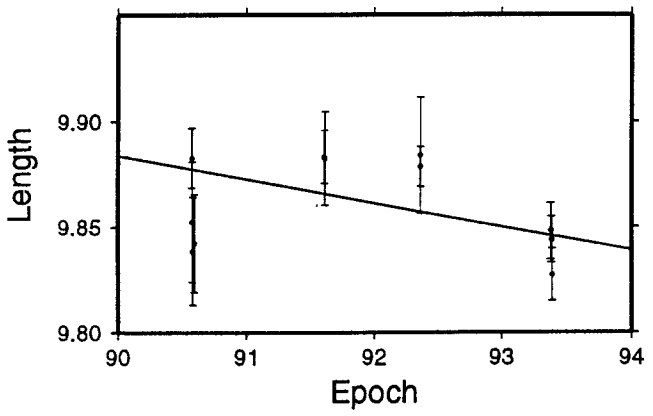

Mean Value :
444259.861 m +/- 6.7 mm

Mean Slope :
-11.2 mm/y +/- 5.5 mm/y

Baseline Repeatability: Port Moresby - Kavieng

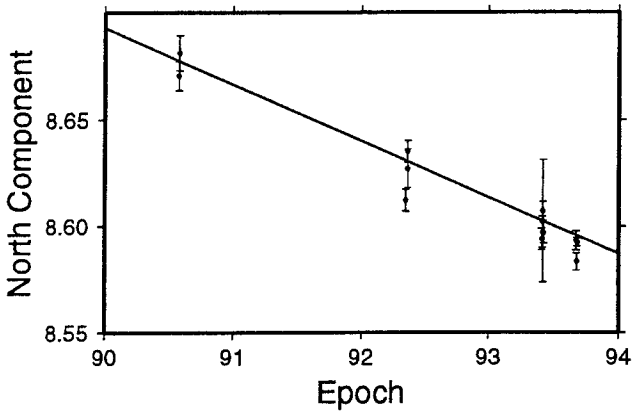

Mean Value :
762838.603 m +/- 6.4 mm

Mean Slope :
-26.5 mm/y +/- 2.2 mm/y

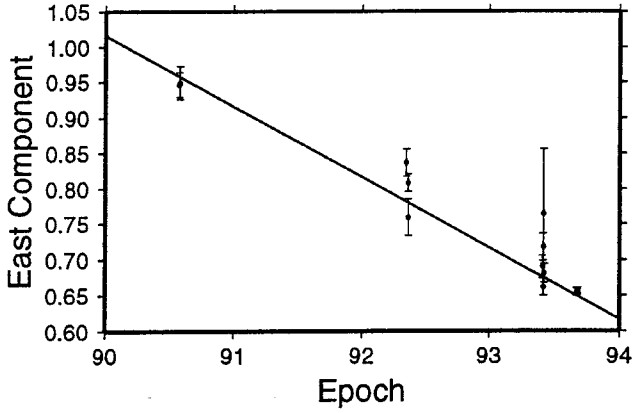

Mean Value :
607490.677 m +/- 17.5 mm

Mean Slope :
-99.7 mm/y +/- 5.2 mm/y

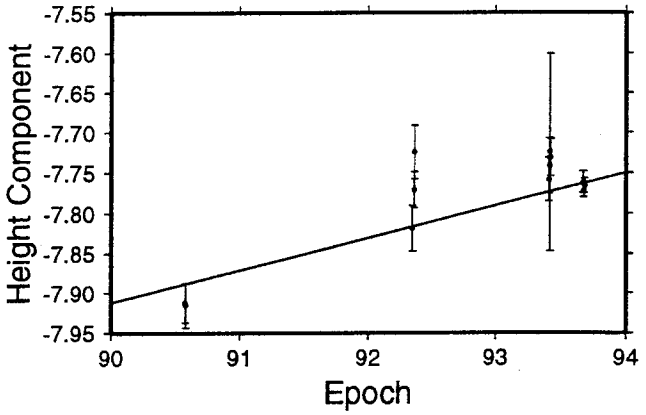

Mean Value :
-37.774 m +/- 11.4 mm

Mean Slope :
40.5 mm/y +/- 8.3 mm/y

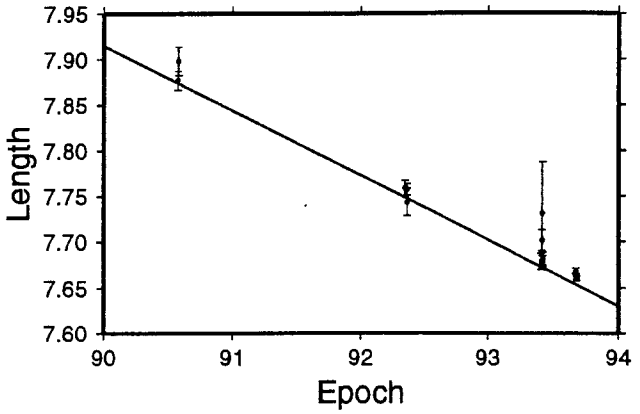

Mean Value :
856497.673 m +/- 10.3 mm

Mean Slope :
-71.1 mm/y +/- 2.5 mm/y

Baseline Repeatability: Losuia - Jacquinot Bay

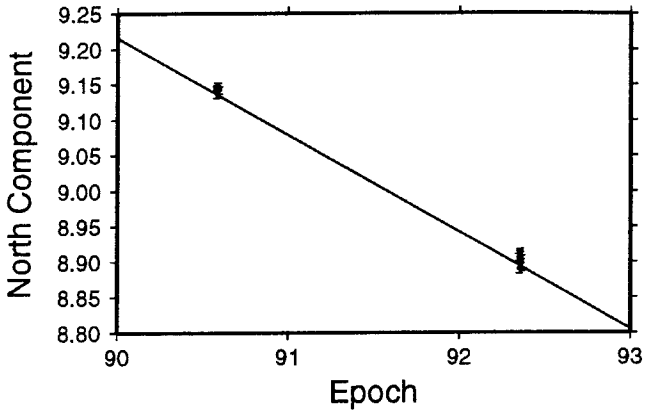

Mean Value :
321729.010 m +/- 36.4 mm

Mean Slope :
-136.9 mm/y +/- 1.8 mm/y

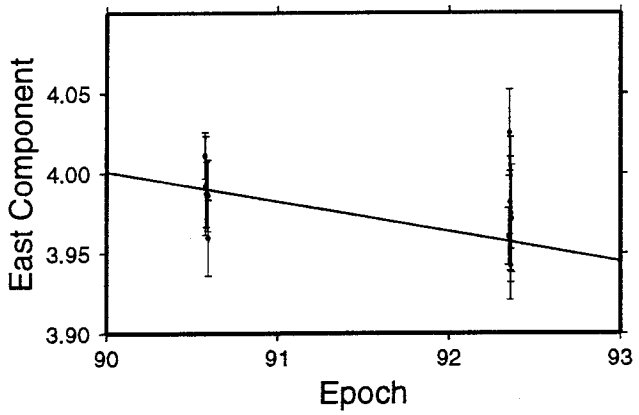

Mean Value :
146853.973 m +/- 8.1 mm

Mean Slope :
-18.6 mm/y +/- 7.8 mm/y

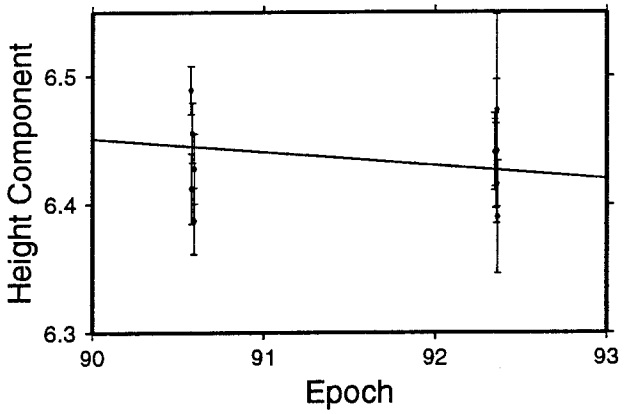

Mean Value :
66.436 m +/- 9.3 mm

Mean Slope :
-10.2 mm/y +/- 10.6 mm/y

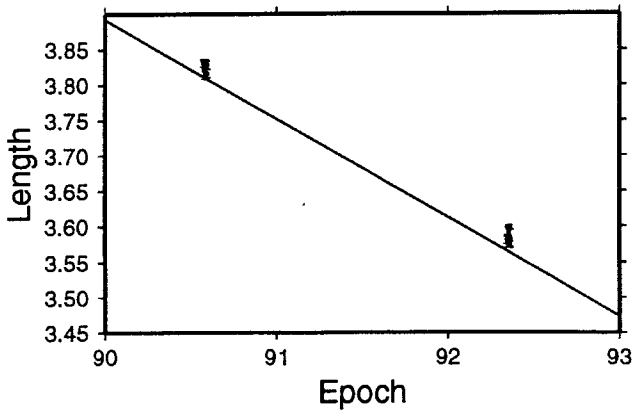

Mean Value :
322343.683 m +/- 36.8 mm

Mean Slope :
-139.4 mm/y +/- 2.1 mm/y

Baseline Repeatability: Port Moresby - Jacquinot Bay

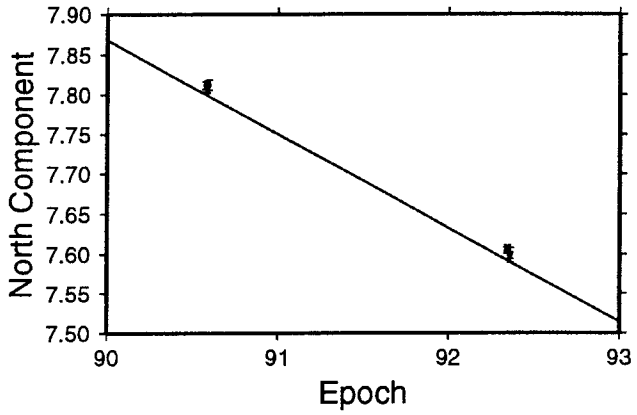

Mean Value :
421777.691 m +/- 36.5 mm

Mean Slope :
-118.1 mm/y +/- 2.0 mm/y

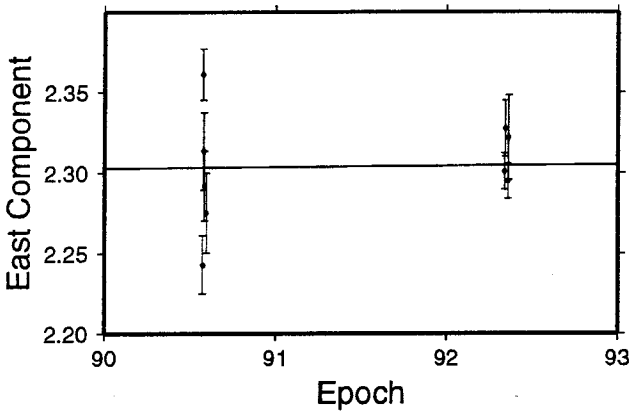

Mean Value :
620602.304 m +/- 10.4 mm

Mean Slope :
0.7 mm/y +/- 13.0 mm/y

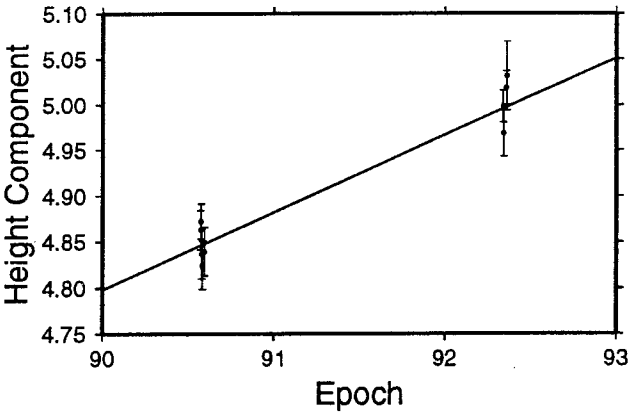

Mean Value :
34.925 m +/- 27.2 mm

Mean Slope :
84.4 mm/y +/- 8.5 mm/y

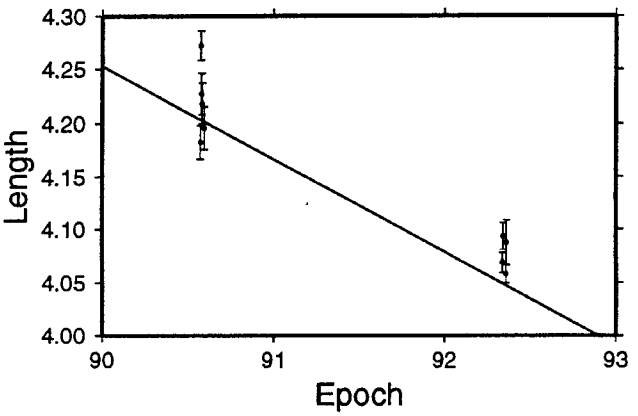

Mean Value :
634314.122 m +/- 27.1 mm

Mean Slope :
-87.2 mm/y +/- 10.4 mm/y

Baseline Repeatability: Port Moresby - Alotau

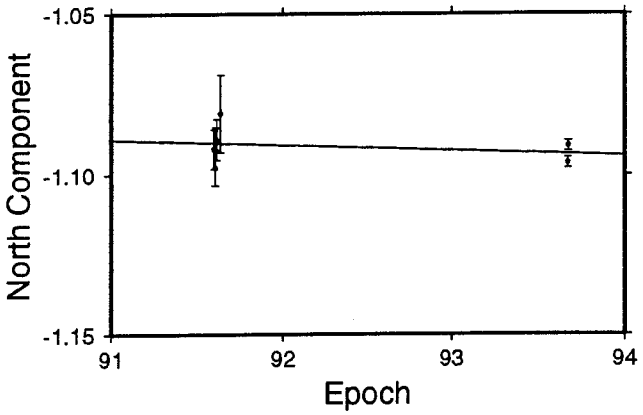

Mean Value :
-97551.093 m +/- 1.3 mm

Mean Slope :
-1.5 mm/y +/- 1.6 mm/y

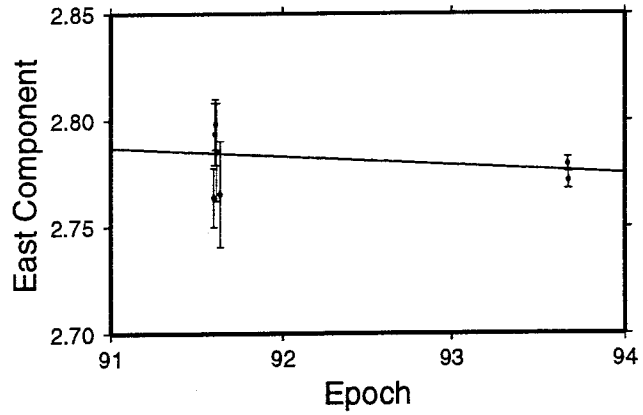

Mean Value :
302192.777 m +/- 2.7 mm

Mean Slope :
-4.1 mm/y +/- 4.2 mm/y

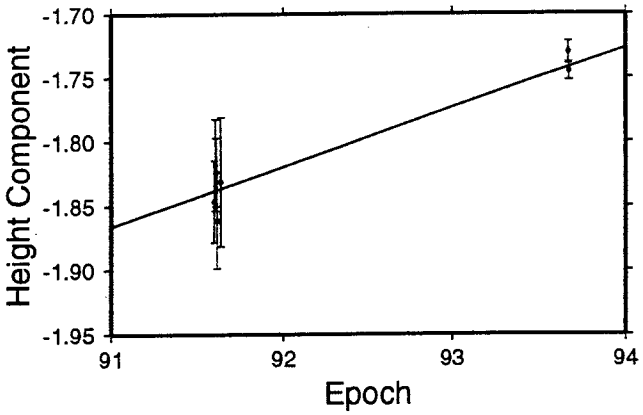

Mean Value :
-21.750 m +/- 13.1 mm

Mean Slope :
46.4 mm/y +/- 7.9 mm/y

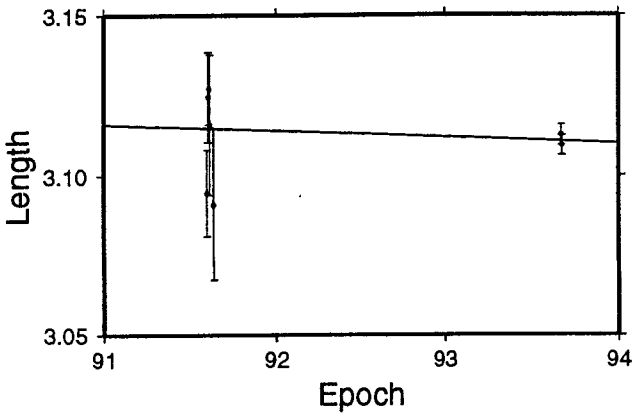

Mean Value :
358963.111 m +/- 2.1 mm

Mean Slope :
-1.8 mm/y +/- 3.6 mm/y

Baseline Repeatability: Port Moresby - Aiambak

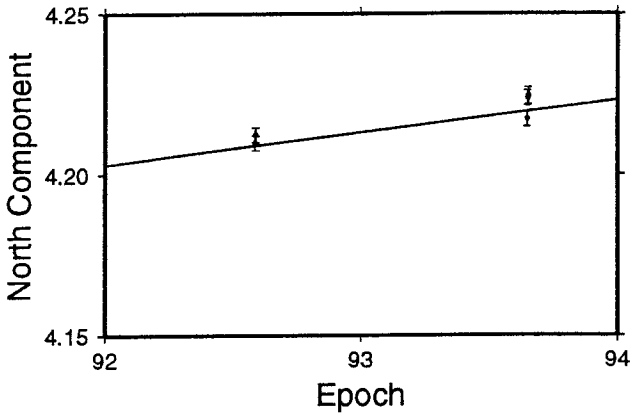

Mean Value :
232254.217 m +/- 2.9 mm

Mean Slope :
9.9 mm/y +/- 2.9 mm/y

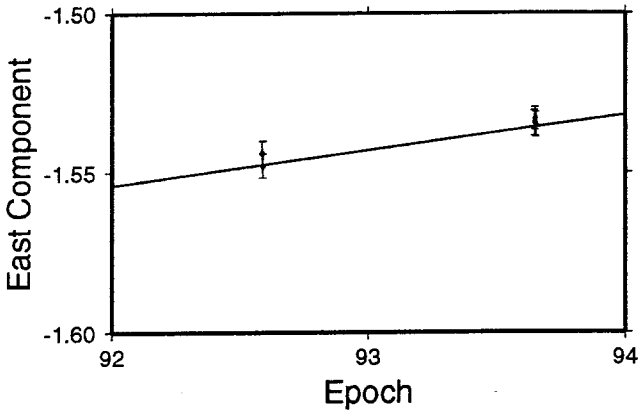

Mean Value :
-566531.539 m +/- 2.9 mm

Mean Slope :
11.0 mm/y +/- 3.3 mm/y

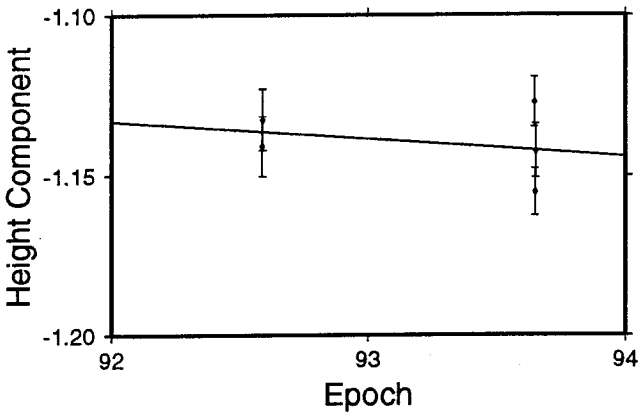

Mean Value :
-21.140 m +/- 5.2 mm

Mean Slope :
-5.2 mm/y +/- 11.9 mm/y

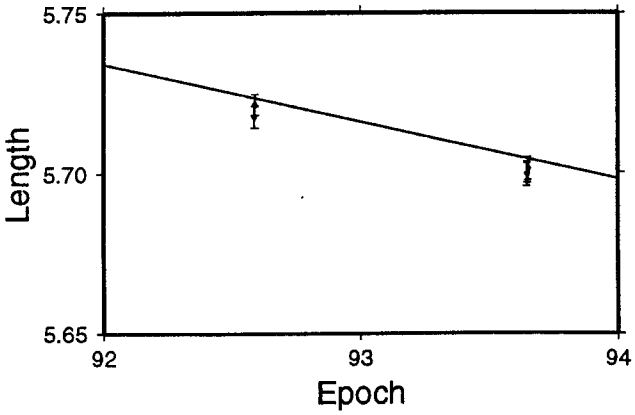

Mean Value :
691225.708 m +/- 4.8 mm

Mean Slope :
-18.2 mm/y +/- 2.9 mm/y

Baseline Repeatability: Losuia - Misima

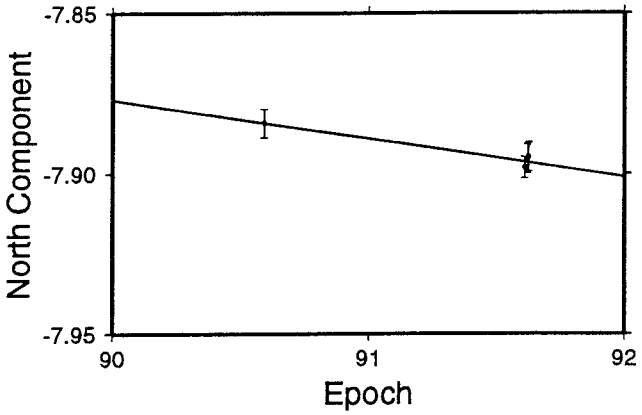

Mean Value :
-239727.894 m +/- 3.0 mm

Mean Slope :
-12.1 mm/y +/- 4.9 mm/y

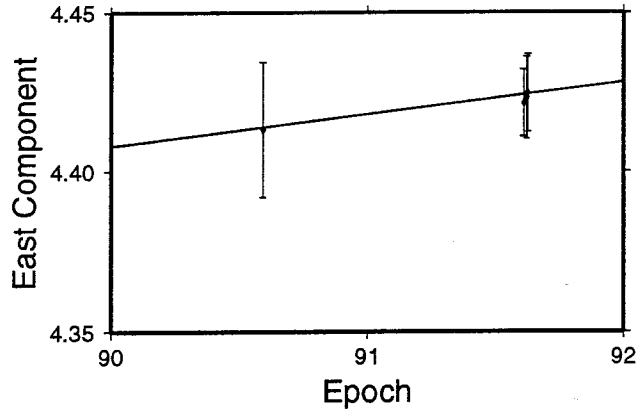

Mean Value :
81204.422 m +/- 6.5 mm

Mean Slope :
9.7 mm/y +/- 21.9 mm/y

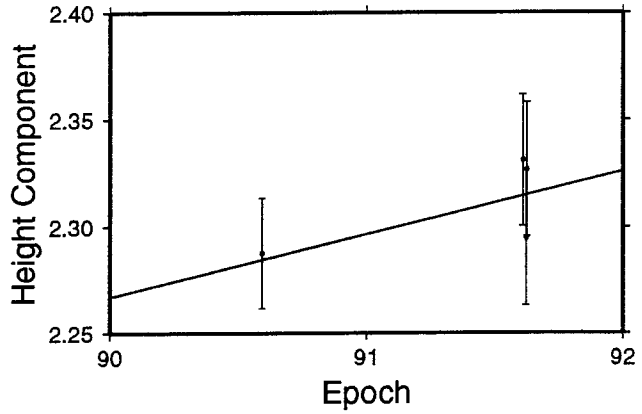

Mean Value :
2.308 m +/- 14.8 mm

Mean Slope :
29.6 mm/y +/- 30.9 mm/y

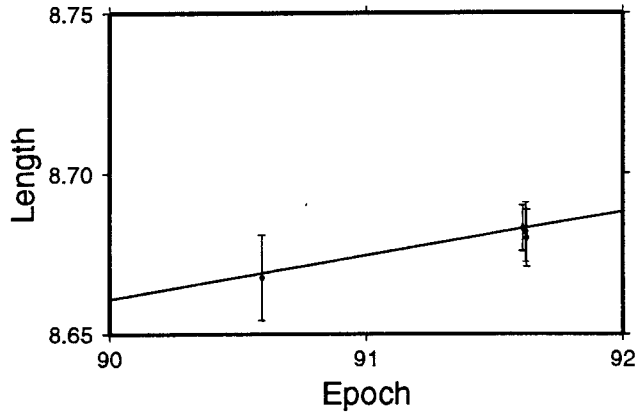

Mean Value :
303078.680 m +/- 4.5 mm

Mean Slope :
13.6 mm/y +/- 13.7 mm/y

Baseline Repeatability: Kavieng - Manus

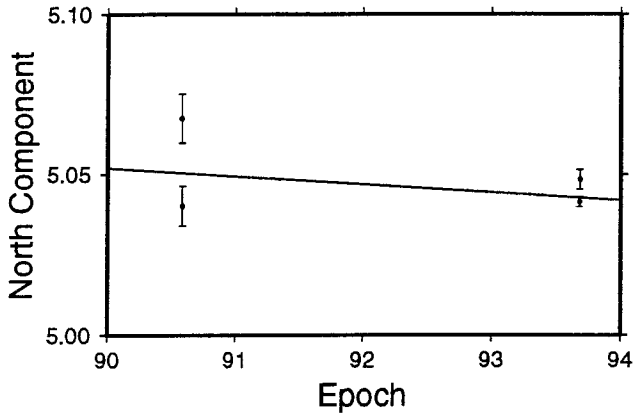

Mean Value :
59085.043 m +/- 2.9 mm

Mean Slope :
-2.6 mm/y +/- 3.9 mm/y

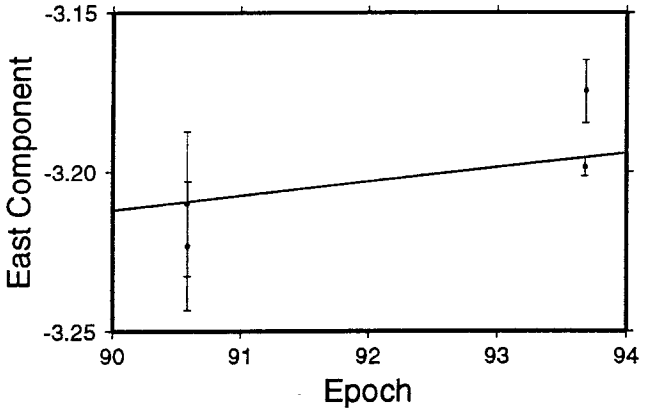

Mean Value :
-377063.197 m +/- 4.3 mm

Mean Slope :
6.7 mm/y +/- 8.2 mm/y

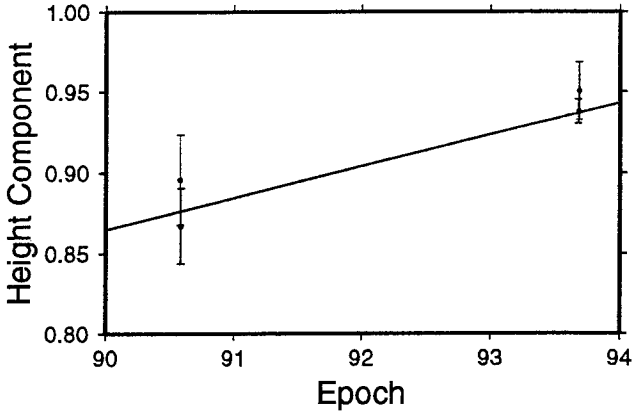

Mean Value :
50.931 m +/- 12.4 mm

Mean Slope :
19.6 mm/y +/- 6.2 mm/y

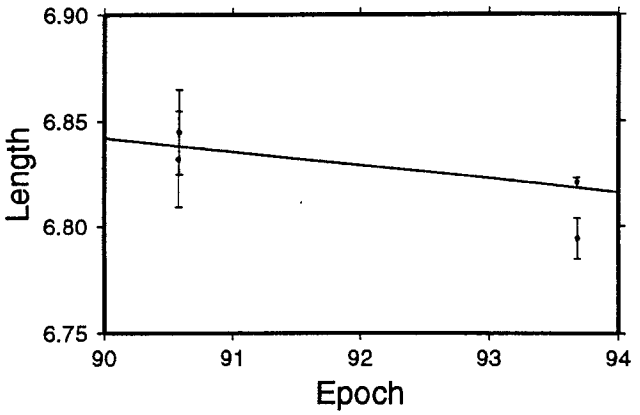

Mean Value :
387686.820 m +/- 3.8 mm

Mean Slope :
-6.5 mm/y +/- 9.2 mm/y

Baseline Repeatability: Kavieng - Jacquinot Bay

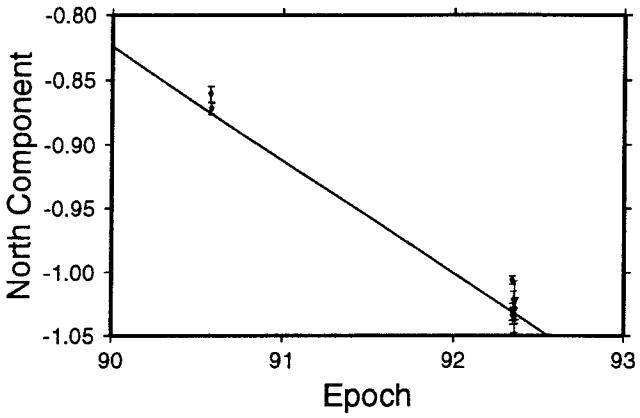

Mean Value :
-341060.992 m +/- 21.6 mm

Mean Slope :
-88.6 mm/y +/- 5.7 mm/y

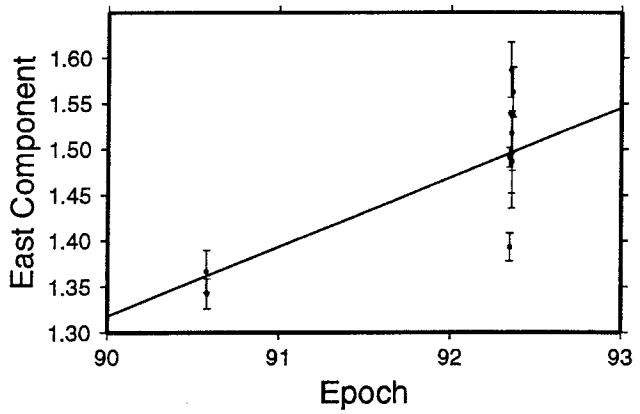

Mean Value :
13111.461 m +/- 21.7 mm

Mean Slope :
75.5 mm/y +/- 22.2 mm/y

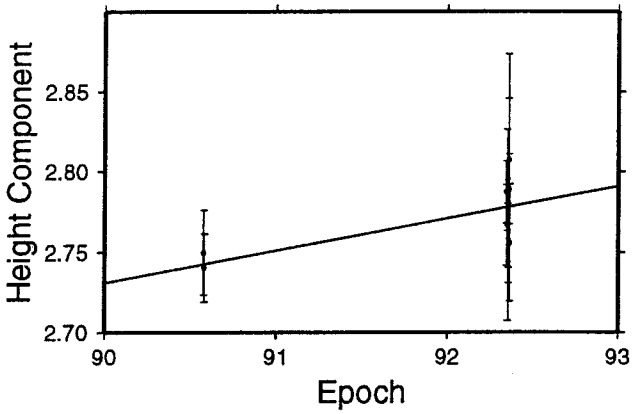

Mean Value :
72.769 m +/- 8.7 mm

Mean Slope :
20.0 mm/y +/- 11.0 mm/y

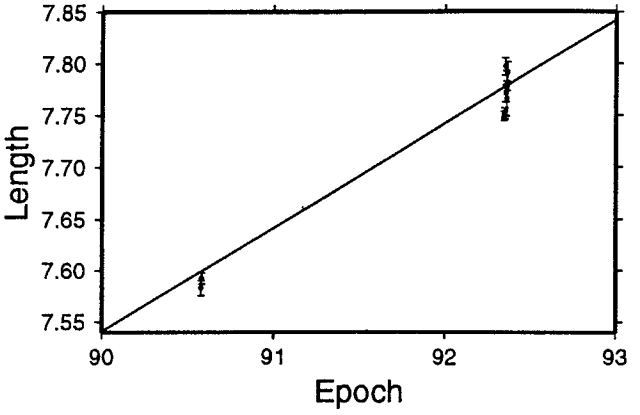

Mean Value :
347537.732 m +/- 24.0 mm

Mean Slope :
100.3 mm/y +/- 6.7 mm/y

```
++++++++++++++++++++++++++++++++
 AUTCLN  Defaults   Version 2.17
++++++++++++++++++++++++++++++++

 CURRENTS DEFAULTS ARE:
++++++++++++++++++++++++++++++++++++++++++++++++++
 AUTCLN  Version 2.17 Run parameter status
 COMMAND FILE:                defaults
 SUMMARY FILE:                autcln.sum
 RANGE CLOCK ROOT:
 PHASE CLOCK ROOT:
 PHASE RESIDUAL ROOT:
 SINGLE DIFFERENCE ROOT:
 DOUBLE DIFFERENCE REPORT:

 INPUT CFILES:
  1. DEF              Default settings
 OUTPUT CFILE SERIES

 EDITING AND JUMP PARAMETERS
 Range-clock tolerances       100.00 n-allan sd    0.95 usec
 Millisec clock reset         100.00 usec
 Bad-rage tolerances           30.00 n-range sd  190.29 m
 Relative clock weight         10.00
 Minimum epochs for gaps
 SITE Sze  SITE Sze  SITE Sze  SITE Sze  SITE Sze  SITE Sze  SITE Sze  SITE Sze  SITE Sze  SITE Sze
 DEF    1

 BIAS DETECTION AND FIXING PARAMETERS
 One-way mean and max differences for range clock  2000.00  1000.00, for phase clock    200.00   100.00
 Double differnce: Ratio   10.00 Min Chi**2     3.00 Max separation  1800.0 secs, Gap factor 5.00
 Max. data returns: WL  100 DD LC   50 DD LG   10. Max gap for one-way fix   10 secs
 Double difference slip detection:
 WL: Scale  5.00 Min (cyc)  2.00 Max (cyc)10.00
 LC: Scale  3.00 Min (cyc)  0.35 Max (cyc) 0.80
 One-way triming: Min. time between bias flags   120.0 secs, min number epochs    8
                  Min. fraction to last bias     0.100     , min number epochs   24
 Ionospheric jump detector (first and values) which differ
 Site  MaxGap (sec) dIon scale MIN dIon (cyc) MAX dIon (cyc)
 DEF       240.00        4.000        0.800        5.000
```

```
MISCELLANEOUS PARAMETERS
GAMIT Elev. cutoff used
CVIEW Editing not used
DATA GAPS  not ignored
One bias or gap  not allowed in single differences
Data in AUTCLN   Cleaned to  0.00 deg, saved to  0.00 deg
```

```
++++++++++++++++++++++++++++++++++++++
   1990 AUTCLN Command File
++++++++++++++++++++++++++++++++++++++

   rng_jump_tol 100 0.1
 * clk_reset_tol [jump difference (usec)]
   clk_reset_tol 600
   rng_resid_tol 300 300
   ion_jump_tol all  30  4   2.0  6
   ion_jump_tol yell  30 5.0 3.0 10
 * rng_noise [reciever code/all] [noise (mm)]
   max_rclk_ 3
 * rel_clk_weight [weight]
 * rng_clk_root [range clock root of file names]
 * phs_clk_root [phase clock root of file names]
 * phs_res_root [phase residual root of file names]
 * sng_diff_root [single difference file root]
 * residual_site [list of four character codes/all/none]
 * summary_file [name of summary file/6]
   rcv_allan_sd ds10  10.0
 *_ remove_bias_cond 10.0 3.0 1800.0
   remove_bias     30   4.0 3600 4
   allow_one_bg yes
 *_ use_gamit_elev yes
   summary    autcln.rapid.sum
   use_gamit   no
   min_elev   15
   use_cview_edit yes
 * use_mm_range [yes/no]
 * ignore_gaps [yes/no]
 * flag_gaps [yes/no]
 * remove_ms_jump [yes/no]
   remove_first_bia yes
 * edit_site_sv [site code] [prn] [start epoch] [stop epoch]
 * edit ssss pn epci epcf
 * cutoff(micro) = 1.000000 gap(epoch) = 5.000000
 * cutoff(micro) = 1.000000 gap(epoch) = 5.000000
 * cutoff(micro) = 1.000000 gap(epoch) = 5.000000
 * cutoff(micro) = 1.000000 gap(epoch) = 5.000000
 * cutoff(micro) = 1.000000 gap(epoch) = 5.000000
 * cutoff(micro) = 1.000000 gap(epoch) = 5.0000000
 * phs_fit_tol 1000 1000 1000 1000
```

```
  phs_fit_tol 5000 4999  500  499
* status_report all -clk_jmp_proc -PASS2_SLIPS +PASS1 -DD_est
  status +dd_scan +dd2scan
* dd_report [dd report file name] [option]
* min_elevation [min elevation (deg)]
* trim_oneway_tol [min_dtl_bias] [min_good_bias] [min_dtr_end] [min_good_end]
* dd_return_size [max wl] [max lc] [max lg]
*- dd_fit_tol     4.0   0.5   4.0   0.4   2.0
   dd_fit_tol       3     0.8   3.0   3     0.4   1.0
   scan_sites all
* site dependent ion parameters
   ion_jump  ALT1 30 6  2  5
   ion_jump  ALT2 30 6  2  5
   ion_jump  CART 30 6  2  5
   ion_jump  cas1   30  6 2 5
   ion_jump  dav1   30  6 2 5
   ion_jump  darw   30  6 2 5
   ion_jump  FAIR 30 6  2  5
   ion_jump  GUA1 30 6  2  5
   ion_jump  GUA2 30 6  2  5
   ion_jump  JACQ 30 6  2  5
   ion_jump  KAVI 30 6  2  5
   ion_jump  KOUR 30 6  2  5
   ion_jump  LOUS 30 6  2  5
   ion_jump  MADG 30 6  2  5
   ion_jump  MADA 30 6  2  5
   ion_jump  MANU 30 6  2  5
   ion_jump  MCMU 30 6  2  5
   ion_jump  mcm4   30  6 2 5
   ion_jump  MIS1 30 6  2  5
   ion_jump  MIS2 30 6  2  5
   ion_jump  MISI 30 6  2  5
   ion_jump  MORO 30 6  2  5
   ion_jump  MORE 30 6  2  5
   ion_jump  nall   30  6 2 5
   ion_jump  NUGU 30 6  2  5
   ion_jump  RABL 30 6  2  5
   ion_jump  tiru   30  6 2 5
   ion_jump  TROM 30 6  2  5
   ion_jump  TRMT 30 6  2  5
   ion_jump  WATA 30 6  2  5
   ion_jump  WARI 30 6  2  5
```

```
  ion_jump  WITU 30 6  2  5
  ion_jump  YELL 30 6  2  5
  ion_jump  YKN1 30 6  2  5
# Bad range and clock edits: cutoff(micro) = 1.000000 gap(epoch) = 5.000000
## START OF ECLIPSE DATA EDITS ##
 edit_site_sv  all  2  1218  1278
 edit_site_sv  all  2  2656  2716
 edit_site_sv  all 14  1032  1092
 edit_site_sv  all 14  2472  2532
 edit_site_sv  all 16    94   154
 edit_site_sv  all 16  1534  1594
 edit_site_sv  all 20   322   382
 edit_site_sv  all 20  1762  1822
 edit_site_sv  all 21   596   656
 edit_site_sv  all 21  2034  2094
 edit_site_sv  all 22   658   718
 edit_site_sv  all 22  2098  2158
 edit_site_sv  all 23   486   546
 edit_site_sv  all 23  1926  1986
## FINISH OF ECLIPSE DATA EDITS ##
```

++
Summary of Cleaning with Stringent Settings (1990)
++
AUTCLN SUMMARY FILE: Version 2.17

Clock and Range noise statistics at iteration 3

Site/PRN	Allan SD@100 sec (ppb)	#	Range rms (mm)	#	
AUSA	0.171996	1095	190.3	2467	COR
ENGA	0.898999	774	1113.2	1492	COR
MOJ1	0.001000	0	4757.3	0	MIN
S01R	100.000000	738	4616.0	2757	TRM
WES1	0.001000	0	4757.3	0	MIN
AUSB	0.175047	1086	190.3	2231	COR
HUAH	100.000000	530	3365.4	2252	TRM
ONSA	0.142550	784	1622.5	1764	COR
TAS1	0.001000	0	4757.3	0	MIN
WTZM	0.001000	0	4757.3	0	MIN
BAHA	0.337716	643	197.7	1281	COR
KOKE	0.057832	907	190.3	2143	COR
ORRO	100.000000	1063	3102.2	3262	TRM
TSU1	0.001000	0	4757.3	0	MIN
XMAS	100.000000	654	4810.7	2750	TRM
BAKO	100.000000	658	3513.7	2722	TRM
KWAJ	30.000000	0	190.3	1	TRM
RIC1	0.001000	0	4757.3	0	MIN
WELL	100.000000	1395	2951.6	3749	TRM
PRN_02	0.286788	1151			
PRN_03	1.000000	566			
PRN_06	0.113208	1203			
PRN_09	0.115445	1242			
PRN_12	0.124343	951			
PRN_13	0.158941	938			
PRN_14	0.301202	1096			
PRN_16	0.762532	1047			
PRN_17	0.170809	781			
PRN_18	0.203071	1051			
PRN_20	0.175012	620			

DDScan bias flags added report for pass 1

SITE	PN02	03	06	09	12	13	14	16	17	18	20
AUSA	98	3	88	33	38	3	56	87	0	21	59
ENGA	22	12	47	32	1	25	0	36	5	22	0
MOJ1	53	5	35	14	7	18	27	13	2	12	12
S01R	2	15	12	22	7	28	28	7	37	6	27
WES1	29	5	35	28	15	52	56	6	5	5	1
AUSB	36	76	2	36	0	38	0	10	79	96	77
HUAH	22	21	17	16	5	26	26	33	20	45	8
ONSA	31	2	31	25	10	58	54	36	18	0	0
TAS1	49	69	16	30	15	11	21	24	42	66	51
WTZM	47	11	59	18	4	83	78	43	12	33	1
BAHA	60	11	60	1	0	0	18	3	11	32	0
KOKE	68	4	67	37	17	16	58	0	0	0	0
ORRO	31	41	32	54	25	37	12	30	22	40	32
TSU1	58	3	7	10	9	24	88	6	2	10	4
XMAS	4	5	11	14	4	2	1	4	2	9	5
BAKO	11	9	20	39	11	23	9	18	2	20	6
KWAJ	0	0	0	0	0	0	0	0	0	0	0
RIC1	12	1	12	12	4	32	32	1	5	0	2
WELL	38	42	53	38	30	31	38	56	47	55	58

DATA AMOUNTS (Good: # good data; Gap: # deleted in gaps; BF: # bias flags 2*max separation)

SITE	PRN	Good	Gap	BF	PRN	Good	Gap	BF	PRN	Good	Gap	BF	PRN	Good	Gap	BF
AUSA	PN02	0	322	0	PN03	0	0	0	PN06	90	266	2	PN09	120	195	3
	PN12	47	203	1	PN13	0	0	0	PN14	81	122	0	PN16	86	293	1
	PN17	88	0	0	PN18	88	60	0	PN20	0	243	0				
ENGA	PN02	112	88	1	PN03	0	34	0	PN06	0	217	0	PN09	100	136	2
	PN12	0	0	0	PN13	56	86	1	PN14	48	0	0	PN16	42	136	0
	PN17	83	22	0	PN18	0	98	0	PN20	0	0	0				
MOJ1	PN02	142	192	3	PN03	314	20	2	PN06	137	135	2	PN09	163	97	2
	PN12	213	30	4	PN13	198	80	6	PN14	166	67	1	PN16	216	43	1
	PN17	358	10	2	PN18	198	46	0	PN20	260	14	4				
S01R	PN02	213	16	4	PN03	66	63	1	PN06	274	57	2	PN09	228	118	4
	PN12	222	45	3	PN13	46	91	0	PN14	123	58	3	PN16	242	31	4
	PN17	99	123	1	PN18	267	48	7	PN20	0	81	0				

DATA AMOUNTS (Good: # good data; Gap: # deleted in gaps; BF: # bias flags 2*max separation)

SITE	PRN	Good	Gap	BF	PRN	Good	Gap	BF	PRN	Good	Gap	BF	PRN	Good	Gap	BF
WES1	PN02	204	132	0	PN03	289	15	3	PN06	177	167	3	PN09	211	135	5
	PN12	221	102	2	PN13	0	110	0	PN14	136	150	3	PN16	268	10	3
	PN17	162	44	2	PN18	249	5	1	PN20	312	11	0				
AUSB	PN02	74	69	0	PN03	45	298	1	PN06	0	0	0	PN09	52	166	0
	PN12	0	0	0	PN13	134	179	4	PN14	207	0	0	PN16	0	12	0
	PN17	113	260	1	PN18	0	261	0	PN20	0	209	0				
HUAH	PN02	0	60	0	PN03	85	134	3	PN06	72	111	2	PN09	132	138	2
	PN12	88	28	1	PN13	150	137	4	PN14	87	54	1	PN16	253	146	7
	PN17	26	83	0	PN18	125	195	3	PN20	0	9	0				
ONSA	PN02	99	151	1	PN03	0	12	0	PN06	121	141	3	PN09	0	147	0
	PN12	90	61	2	PN13	0	135	0	PN14	71	118	0	PN16	121	112	2
	PN17	159	55	2	PN18	0	0	0	PN20	0	0	0				
TAS1	PN02	149	77	0	PN03	96	221	3	PN06	141	77	4	PN09	139	95	2
	PN12	72	112	1	PN13	213	73	4	PN14	201	33	1	PN16	46	84	1
	PN17	155	166	2	PN18	80	200	1	PN20	59	178	1				
WTZM	PN02	188	162	3	PN03	247	28	2	PN06	30	209	0	PN09	218	63	5
	PN12	324	12	3	PN13	182	189	4	PN14	195	136	1	PN16	172	115	4
	PN17	237	36	2	PN18	196	97	2	PN20	315	0	1				
BAHA	PN02	173	170	5	PN03	0	31	0	PN06	124	196	1	PN09	0	0	0
	PN12	0	0	0	PN13	0	0	0	PN14	145	41	1	PN16	0	0	0
	PN17	147	51	1	PN18	47	128	0	PN20	0	0	0				
KOKE	PN02	0	185	0	PN03	114	9	1	PN06	48	285	0	PN09	267	160	5
	PN12	186	74	4	PN13	128	103	4	PN14	228	118	1	PN16	0	0	0
	PN17	150	0	0	PN18	0	0	0	PN20	0	0	0				
ORRO	PN02	167	166	6	PN03	179	180	4	PN06	209	132	4	PN09	0	212	0
	PN12	113	135	2	PN13	67	216	1	PN14	85	54	1	PN16	150	89	4
	PN17	185	117	4	PN18	117	215	2	PN20	0	170	0				
TSU1	PN02	183	89	1	PN03	346	5	3	PN06	272	39	2	PN09	198	33	2
	PN12	292	15	4	PN13	204	67	1	PN14	137	146	0	PN16	345	17	5
	PN17	338	5	2	PN18	327	41	4	PN20	249	13	1				
XMAS	PN02	219	6	4	PN03	120	2	3	PN06	239	52	3	PN09	317	133	6
	PN12	210	79	6	PN13	205	25	5	PN14	195	1	3	PN16	194	36	2
	PN17	49	0	0	PN18	263	57	4	PN20	248	26	3				

DATA AMOUNTS (Good: # good data; Gap: # deleted in gaps; BF: # bias flags 2*max separation)

SITE	PRN	Good	Gap	BF	PRN	Good	Gap	BF	PRN	Good	Gap	BF	PRN	Good	Gap	BF
BAKO	PN02	127	53	2	PN03	44	76	1	PN06	161	115	5	PN09	251	231	7
	PN12	173	65	3	PN13	150	96	4	PN14	136	44	3	PN16	159	78	3
	PN17	58	3	0	PN18	215	94	4	PN20	211	72	3				
KWAJ	PN02	0	0	0	PN03	0	0	0	PN06	0	0	0	PN09	0	0	0
	PN12	0	0	0	PN13	0	0	0	PN14	0	0	0	PN16	0	0	0
	PN17	0	0	0	PN18	0	1	0	PN20	0	0	0				
RIC1	PN02	318	58	3	PN03	89	18	1	PN06	161	50	3	PN09	154	109	2
	PN12	222	29	3	PN13	211	92	4	PN14	77	167	1	PN16	310	18	2
	PN17	209	23	5	PN18	182	8	1	PN20	245	10	0				
WELL	PN02	237	123	3	PN03	59	207	1	PN06	77	172	2	PN09	176	195	3
	PN12	271	142	1	PN13	139	203	4	PN14	283	116	3	PN16	0	226	0
	PN17	98	179	1	PN18	133	212	2	PN20	150	214	1				

ELEVATION ANGLE HISTOGRAM

SITE	0- 5	5-10	10-15	15-20	20-25	25-30	30-35	35-40	40-45	45-50	50-55	55-60	60-65	65-70	70-75	75-80	80-85	85-90	Min (dg)
AUSA	0	0	0	44	76	48	23	37	47	76	40	68	17	24	27	73	0	0	15.03
ENGA	0	0	0	50	68	71	65	60	29	24	25	23	8	0	8	10	0	0	15.05
MOJ1	0	0	0	16	109	189	241	276	200	190	205	250	311	191	120	32	18	17	18.13
S01R	0	0	0	81	138	169	217	169	198	196	197	112	93	76	74	60	0	0	15.32
WES1	0	0	0	30	303	302	221	214	267	248	146	133	117	68	87	70	23	0	17.73
AUSB	0	0	0	50	47	57	37	28	48	48	41	34	48	51	53	60	10	13	15.02
HUAH	0	0	0	50	76	122	115	134	149	162	83	61	36	30	0	0	0	0	15.09
ONSA	0	0	0	35	47	55	29	34	46	86	86	70	39	45	60	19	10	0	15.14
TAS1	0	0	0	0	18	56	86	106	96	109	149	163	146	165	93	60	65	39	21.38
WTZM	0	0	0	29	193	250	188	164	203	211	200	199	142	149	155	124	83	14	17.00
BAHA	0	0	0	25	72	75	60	64	70	57	57	9	10	26	36	51	11	13	15.23
KOKE	0	0	0	42	57	151	191	188	124	81	60	91	124	12	0	0	0	0	15.04
ORRO	0	0	0	31	66	88	159	109	95	145	84	207	110	91	49	15	23	0	15.22
TSU1	0	0	0	28	224	314	369	296	281	209	196	218	189	223	161	123	60	0	18.17
XMAS	0	0	0	70	147	327	474	232	177	227	322	100	39	43	56	16	12	17	15.20
BAKO	0	0	0	61	172	346	255	135	149	213	254	36	19	24	21	0	0	0	15.11
KWAJ	0	0	0	0	0	0	0	0	0	0	0	0	0	0	0	0	0	0	90.00
RIC1	0	0	0	0	145	367	326	255	192	278	153	122	82	111	59	56	32	0	20.80
WELL	0	0	0	108	187	256	168	169	205	111	89	90	54	44	59	38	43	2	15.15

BIAS FLAG REPORT: Types

ORG-Original JMP-Big Jump ION-Ion Jump GAP-Data Gap DDS-DD scan WLS-Wide Lane DDC-DD cleaning

SITE	# Flagged							# Remaining								# Edited								# with jump							
	ORG	JMP	ION	GAP	DDS	WLS	DDC	ORG	JMP	ION	GAP	DDS	WLS	DDC	ORG	JMP	ION	GAP	DDS	WLS	DDC	ORG	JMP	ION	GAP	DDS	WLS	DDC
AUSA	1	0	0	0	479	4	0	0	0	0	0	8	0	0	1	0	0	0	467	4	0	0	0	0	0	4	0	0
ENGA	7	0	0	15	206	5	0	1	0	0	0	3	0	0	6	0	0	15	201	5	0	0	0	0	0	2	0	0
MOJ1	5	0	0	9	207	0	6	2	0	0	2	23	0	1	3	0	0	7	178	0	2	0	0	0	0	5	0	2
S01R	3	0	0	53	196	0	4	0	0	0	9	15	0	2	2	0	0	39	167	0	2	1	0	0	3	3	0	0
WES1	10	0	0	18	241	0	4	3	0	0	5	16	0	2	7	0	0	12	218	0	1	0	0	0	1	1	0	0
AUSB	1	0	0	4	443	2	0	0	0	0	1	5	0	0	1	0	0	2	435	2	0	0	0	0	1	3	0	0
HUAH	2	0	0	63	240	0	0	0	0	0	7	15	0	0	2	0	0	53	223	0	0	0	0	0	3	2	0	0
ONSA	4	0	0	27	267	2	0	0	0	0	3	6	0	0	4	0	0	24	256	2	0	0	0	0	0	4	0	0
TAS1	2	0	0	9	416	0	2	0	0	0	2	15	0	0	2	0	0	7	392	0	2	0	0	0	0	8	0	0
WTZM	3	0	0	9	395	0	0	2	0	0	3	23	0	0	1	0	0	6	366	0	0	0	0	0	0	4	0	0
BAHA	0	0	0	6	192	2	0	0	0	0	1	8	0	0	0	0	0	5	182	2	0	0	0	0	0	2	0	0
KOKE	0	0	0	14	268	1	0	0	0	0	2	12	0	0	0	0	0	11	252	1	0	0	0	0	1	4	0	0
ORRO	5	0	0	65	357	0	2	0	0	0	4	21	0	1	5	0	0	59	329	0	1	0	0	0	2	6	0	0
TSU1	3	0	0	4	230	0	5	3	0	0	1	21	0	2	0	0	0	0	202	0	1	0	0	0	3	3	0	0
XMAS	1	0	0	58	68	0	4	1	0	0	15	20	0	3	0	0	0	43	39	0	1	0	0	0	0	4	0	0
BAKO	3	0	0	41	169	0	0	1	0	0	5	26	0	0	2	0	0	32	128	0	0	0	0	0	3	6	0	0
KWAJ	3	0	0	0	0	0	0	0	0	0	0	0	0	0	3	0	0	0	0	0	0	0	0	0	0	0	0	0
RIC1	9	0	0	30	122	0	6	5	0	0	8	15	0	2	3	0	0	20	106	0	1	1	0	0	1	1	0	2
WELL	10	0	0	52	492	0	0	0	0	0	8	19	0	0	8	0	0	43	467	0	0	2	0	0	1	4	0	0

EDITING REPORT AND SITE PARAMS

SITE	MnCLN (deg)	MnOUT (deg)	SNR L1	SNR L2	LSNR	GF03	RCLK	GF02	BEND	BCLS	NPED	GF-1	GF04	DDSC	INTR	GFUN	BDL2	NODD	ELEV	EDIT	MMRG	ELCL	Good
AUSA	15.00	15.00	2	2	0	0	0	0	163	1753	0	82	416	0	0	0	0	0	422	0	0	422	600
ENGA	15.00	15.00	2	2	0	0	0	1	234	931	0	102	578	0	0	0	0	0	586	248	0	586	441
MOJ1	15.00	15.00	2	2	262	537	0	0	122	735	0	148	1	0	0	0	48	0	176	0	3907	176	2365
S01R	15.00	15.00	2	2	43	0	0	0	246	737	0	168	2	0	0	0	43	0	8	86	0	8	1780
WES1	15.00	15.00	2	2	237	574	0	0	104	1052	0	368	0	0	0	0	50	0	192	0	4156	192	2229
AUSB	15.00	15.00	2	2	0	0	0	0	152	1476	0	19	262	0	0	0	0	0	265	0	0	265	625
HUAH	15.00	15.00	2	2	122	0	0	0	139	1179	0	31	262	0	0	0	121	0	273	0	0	273	1018
ONSA	15.00	15.00	2	2	0	0	0	0	171	998	0	66	55	0	0	0	0	0	59	52	0	59	661
TAS1	15.00	15.00	2	2	317	644	0	0	256	1410	0	366	0	0	0	0	8	0	193	0	3933	193	1351
WTZM	15.00	15.00	2	2	249	542	0	0	93	1126	0	45	0	0	0	0	24	0	180	0	4031	180	2304
BAHA	15.00	15.00	2	2	0	0	0	0	28	617	0	17	145	0	0	0	0	0	149	0	0	149	636
KOKE	15.00	15.00	2	2	0	0	0	0	88	934	0	29	52	0	0	0	0	0	53	0	0	53	1121
ORRO	15.00	15.00	2	2	273	0	0	0	304	1727	0	139	348	0	0	0	268	0	360	0	0	360	1272
TSU1	15.00	15.00	2	2	246	538	0	0	84	530	0	75	0	0	0	0	20	0	179	0	4058	179	2891
XMAS	15.00	15.00	2	2	81	0	0	0	74	425	0	131	0	0	0	0	81	0	4	87	0	4	2259
BAKO	15.00	15.00	2	2	58	0	0	0	110	946	0	104	1	0	0	0	56	0	4	76	0	4	1685
KWAJ	15.00	15.00	2	2	3934	0	0	0	0	1	0	89	1	0	0	0	3934	0	5	0	0	5	0
RIC1	15.00	15.00	2	2	451	814	0	0	48	711	0	442	0	0	0	0	81	0	154	0	4064	154	2178
WELL	15.00	15.00	2	2	174	0	0	0	137	2121	0	241	471	0	0	0	174	0	491	0	0	491	1623

```
++++++++++++++++++++++++++++++++++++++++++++++++++
AUTCLN  Version 2.17 Run parameter status
COMMAND FILE:                autcln.cmd
SUMMARY FILE:                autcln.rapid.sum
RANGE CLOCK ROOT:
PHASE CLOCK ROOT:
PHASE RESIDUAL ROOT:
SINGLE DIFFERENCE ROOT:
DOUBLE DIFFERENCE REPORT:

INPUT CFILES:.
 1. AUSA  COR   causa0.209
 2. ENGA  COR   cenga0.209
 3. MOJ1  MIN   cmoj10.209
 4. S01R  TRM   cs01r0.209
 5. WES1  MIN   cwes10.209
 6. AUSB  COR   causb0.209
 7. HUAH  TRM   chuah0.209
 8. ONSA  COR   consa0.209
 9. TAS1  MIN   ctas10.209
10. WTZM  MIN   cwtzm0.209
11. BAHA  COR   cbaha0.209
12. KOKE  COR   ckoke0.209
13. ORRO  TRM   corro0.209
14. TSU1  MIN   ctsu10.209
15. XMAS  TRM   cxmas0.209
16. BAKO  TRM   cbako0.209
17. KWAJ  TRM   ckwaj0.209
18. RIC1  MIN   cric10.209
19. WELL  TRM   cwell0.209
OUTPUT CFILE SERIES +

EDITING AND JUMP PARAMETERS
Range-clock tolerances       100.00 n-allan sd    0.10 usec
Millisec clock reset         600.00 usec
Bad-rage tolerances          300.00 n-range sd  300.00 m
Relative clock weight         10.00
```

```
Data pre-editing for  16 cases
   # SITE   PRN  Start  Stop Epoch
  1 BAKO     3    814   890
  2 ENGA     0      2    61
  3 ENGA     3     62    94
  4 ENGA     3    108   116
  5 ENGA    14     62    94
  6 ENGA    16    149   151
  7 ENGA    18    236   239
  8 ENGA    18    252   253
  9 ONSA     3    807   815
 10 ONSA     3    822   824
 11 ONSA    16    127   167
 12 S01R     3    764   837
 13 S01R     3    843   843
 14 S01R     3    849   860
 15 S01R     3    908   909
 16 XMAS     3    803   889
Minimum epochs for gaps
SITE Sze  SITE Sze  SITE Sze  SITE Sze  SITE Sze  SITE Sze  SITE Sze  SITE Sze  SITE Sze  SITE Sze
AUSA   1  ENGA   1  MOJ1   1  S01R   1  WES1   1  AUSB   1  HUAH   1  ONSA   1  TAS1   1  WTZM   1
BAHA   1  KOKE   1  ORRO   1  TSU1   1  XMAS   1  BAKO   1  KWAJ   1  RIC1   1  WELL   1

BIAS DETECTION AND FIXING PARAMETERS
One-way mean and max differences for range clock  5000.00  4999.00, for phase clock    500.00   499.00
Double differnce: Ratio   30.00 Min Chi**2    4.00 Max separation  3600.0 secs, Gap factor 4.00
Max. data returns: WL  100 DD LC   25 DD LG    5. Max gap for one-way fix   10 secs
Double difference slip detection:
WL: Scale  3.00 Min (cyc)  0.80 Max (cyc) 3.00
LC: Scale  3.00 Min (cyc)  0.10 Max (cyc) 0.30
One-way triming: Min. time between bias flags   120.0 secs, min number epochs    8
                 Min. fraction to last bias     0.100     , min number epochs   24
Ionospheric jump detector (first and values) which differ
Site  MaxGap (sec) dIon scale MIN dIon (cyc) MAX dIon (cyc)
AUSA       30.00        4.000        2.000        6.000
```

```
MISCELLANEOUS PARAMETERS
GAMIT Elev. cutoff not used
CVIEW Editing used
DATA GAPS  not ignored
One bias or gap  allowed in single differences
```

```
This is the command file for a globk run
This file is resident in the soln directory from where globk's
are run.
*=============================================
Here comes the part essential to make a-priori orbits from
combined solution
H-file instead of using pre-made sv.apr which were produced
from individual
days solutions

 make_svs  /data7/gps/tables/png90_ucan6_sv.apr

*=============================================
Here comes the part to correct Heights for Antennae changes by
using
the RENAME facility within the EarthQuake command
DONT FORGET that the eq_file format is the same as this cmd
file
*i.e  BLANK first column

 eq_file /data7/gps/solns/ds42_fixer
*=============================================
The first com_file contains the globk common blocks. writing
this file in the
soln directory is normal
The second file, srt_file contains direct access time ordered
lists. Writing this file to the soln
directory is normal
The third file, sol_file, is a scratch file containing the
variance/covariance
matrix for the solution. Care this can become large. You need a
large chunk of free disk

 com_file png90uc96com.bin
 srt_file png90uc96srt.bin
 sol_file png90uc96sol.bin
*=============================================

Now setup the a-priori information files. There are two of
them.
The first is the station coordinates. the second the satellite
ephemerides.

 apr_file /data8/gps/solns/glorg_sites.apr
 svs_file /data7/gps/tables/png90-ucan6_sv.apr
*=========================

Setup the bak solution file, necessary for stochastic solutions
Otherwise not generally needed unless markov elements are being
used.
* bak_file ann92-94_backsol.prt
* descript global back solution
* bak_opt 2
*=========================
* OUT_GLB
* produces a combined binary hfile for all experiments within
this solution
*
 out_glb png90_ucan6.pjm_loose.GLX
*=========================
* PRINT Commands
 prt_opt   16
 crt_opt   16
```

```
*=========================
consistent with the tightest site.
 apr_neu   all    99.0    99.0    99.0   0.50    0.50    0.50
*The Southern hemisphere
 apr_neu  yar1    10.0    10.0    10.0   0.20    0.20    0.20
 apr_neu  sant    10.0    10.0    10.0   0.20    0.20    0.20
 apr_neu  hart    10.0    10.0    10.0   0.20    0.20    0.20
 apr_neu  ds42    10.0    10.0    10.0   0.20    0.20    0.20
*The Northern hemisphere
 apr_neu  algo    10.0    10.0    10.0   0.20    0.20    0.20
 apr_neu  ds10    10.0    10.0    10.0   0.20    0.20    0.20
 apr_neu  ds60    10.0    10.0    10.0   0.20    0.20    0.20
 apr_neu  fair    10.0    10.0    10.0   0.20    0.20    0.20
 apr_neu  kokr    10.0    10.0    10.0   0.20    0.20    0.20
 apr_neu  kosg    10.0    10.0    10.0   0.20    0.20    0.20
 apr_neu  trom    10.0    10.0    10.0   0.20    0.20    0.20
 apr_neu  wtz1    10.0    10.0    10.0   0.20    0.20    0.20
 apr_neu  yell    10.0    10.0    10.0   0.20    0.20    0.20
*ARN sites
* USE THE GLOBAL COMMAND TO SPECIFY THE FOLLOWING AUSTRALIAN
SITES
* apr_neu  alic    5.00    5.00    5.00   0.20    0.20    0.20
* apr_neu  bako    5.00    5.00    5.00   0.20    0.20    0.20
* apr_neu  bath    5.00    5.00    5.00   0.20    0.20    0.20
* apr_neu  coco    5.00    5.00    5.00   0.20    0.20    0.20
* apr_neu  darw    5.00    5.00    5.00   0.20    0.20    0.20
* apr_neu  hoba    5.00    5.00    5.00   0.20    0.20    0.20
* apr_neu  karr    5.00    5.00    5.00   0.20    0.20    0.20
* apr_neu  otag    5.00    5.00    5.00   0.20    0.20    0.20
* apr_neu  towa    5.00    5.00    5.00   0.20    0.20    0.20
* apr_neu  town    5.00    5.00    5.00   0.20    0.20    0.20
* apr_neu  well    5.00    5.00    5.00   0.20    0.20    0.20
*ANTARCTIC Sites for which  velocity is to be determined
* USE GLOBAL DEFAULTS FOR ALL SITES EXCEPT BYRD AND AMUNDSEN
* apr_neu  cas1    5.00    5.00    5.00   0.20    0.20    0.20
* apr_neu  dav1    5.00    5.00    5.00   0.20    0.20    0.20
* apr_neu  mac1    5.00    5.00    5.00   0.20    0.20    0.20
* apr_neu  maw1    5.00    5.00    5.00   0.20    0.20    0.20
* apr_neu  ohi5    5.00    5.00    5.00   0.20    0.20    0.20
* apr_neu  ohig    99.0    99.0    99.0   0.0001  0.0001  0.0001
 apr_neu  byrd   99.00   99.00   99.00   10.00   10.00    0.20
 apr_neu  amun   99.00   99.00   99.00   10.00   10.00    0.20
* apr_neu  mcmu    5.00    5.00    5.00   0.20    0.20    0.20
* apr_neu  mcm4    5.00    5.00    5.00   0.20    0.20    0.20
* apr_neu  kerg5   5.00    5.00    5.00   0.20    0.20    0.20
* ANTARCTIC Sites for which NO velocity is to be determined
* ZERO VELOCITY DERIVED BY SETTING constraints on velocity to
* mm or less level
 apr_neu  neul   99.0    99.0    99.0   0.0001    0.0001    0.0001
 apr_neu  neum   99.0    99.0    99.0   0.0001    0.0001    0.0001
 apr_neu  neun   99.0    99.0    99.0   0.0001    0.0001    0.0001
 apr_neu  neuo   99.0    99.0    99.0   0.0001    0.0001    0.0001
 apr_neu  neup   99.0    99.0    99.0   0.0001    0.0001    0.0001
 apr_neu  neuq   99.0    99.0    99.0   0.0001    0.0001    0.0001
 apr_neu  neur   99.0    99.0    99.0   0.0001    0.0001    0.0001
 apr_neu  neus   99.0    99.0    99.0   0.0001    0.0001    0.0001
 apr_neu  neut   99.0    99.0    99.0   0.0001    0.0001    0.0001
 apr_neu  case   99.0    99.0    99.0   0.0001    0.0001    0.0001
 apr_neu  davi   99.0    99.0    99.0   0.0001    0.0001    0.0001
 apr_neu  dece   99.0    99.0    99.0   0.0001    0.0001    0.0001
 apr_neu  fors   99.0    99.0    99.0   0.0001    0.0001    0.0001
 apr_neu  grun   99.0    99.0    99.0   0.0001    0.0001    0.0001
 apr_neu  kerg   99.0    99.0    99.0   0.0001    0.0001    0.0001
```

```
 apr_neu  mcmg   99.0   99.0   99.0  0.0001    0.0001    0.0001
 apr_neu  mcm0   99.0   99.0   99.0  0.0001    0.0001    0.0001
 apr_neu  riog   99.0   99.0   99.0  0.0001    0.0001    0.0001
 apr_neu  syow   99.0   99.0   99.0  0.0001    0.0001    0.0001
 apr_neu  tno1   99.0   99.0   99.0  0.0001    0.0001    0.0001
 apr_neu  dove   99.0   99.0   99.0  0.0001    0.0001    0.0001
*Common 92/93/94 sites
* HANDLE WITH THE all command
* apr_neu  atki    5.00   5.00   5.00  0.20    0.20    0.20
* apr_neu  banz    5.00   5.00   5.00  0.20    0.20    0.20
* apr_neu  broo    5.00   5.00   5.00  0.20    0.20    0.20
* apr_neu  bull    5.00   5.00   5.00  0.20    0.20    0.20
* apr_neu  cedu    5.00   5.00   5.00  0.20    0.20    0.20
* apr_neu  espe    5.00   5.00   5.00  0.20    0.20    0.20
* apr_neu  gilg    5.00   5.00   5.00  0.20    0.20    0.20
* apr_neu  hob1    5.00   5.00   5.00  0.20    0.20    0.20
* apr_neu  hob2    5.00   5.00   5.00  0.20    0.20    0.20
* apr_neu  john    5.00   5.00   5.00  0.20    0.20    0.20
* apr_neu  lltr    5.00   5.00   5.00  0.20    0.20    0.20
* apr_neu  olve    5.00   5.00   5.00  0.20    0.20    0.20
* apr_neu  per2    5.00   5.00   5.00  0.20    0.20    0.20
* apr_neu  pert    5.00   5.00   5.00  0.20    0.20    0.20
* apr_neu  port    5.00   5.00   5.00  0.20    0.20    0.20
* apr_neu  rawl    5.00   5.00   5.00  0.20    0.20    0.20
* apr_neu  stan    5.00   5.00   5.00  0.20    0.20    0.20
* apr_neu  sund    5.00   5.00   5.00  0.20    0.20    0.20
* apr_neu  unit    5.00   5.00   5.00  0.20    0.20    0.20
* apr_neu  wilf    5.00   5.00   5.00  0.20    0.20    0.20
* apr_neu  xmas   99.00  99.00  99.00  0.0001  0.0001  0.0001
*Australasian Sites for which no velocity determination is to
*be attempted
 apr_neu  alya   99.00  99.00  99.00  0.0001  0.0001  0.0001
 apr_neu  barc   99.00  99.00  99.00  0.0001  0.0001  0.0001
 apr_neu  bass   99.00  99.00  99.00  0.0001  0.0001  0.0001
 apr_neu  bate   99.00  99.00  99.00  0.0001  0.0001  0.0001
 apr_neu  benw   99.00  99.00  99.00  0.0001  0.0001  0.0001
 apr_neu  bm45   99.00  99.00  99.00  0.0001  0.0001  0.0001
 apr_neu  bm46   99.00  99.00  99.00  0.0001  0.0001  0.0001
 apr_neu  bm55   99.00  99.00  99.00  0.0001  0.0001  0.0001
 apr_neu  brdv   99.00  99.00  99.00  0.0001  0.0001  0.0001
 apr_neu  brea   99.00  99.00  99.00  0.0001  0.0001  0.0001
 apr_neu  brun   99.00  99.00  99.00  0.0001  0.0001  0.0001
 apr_neu  caig   99.00  99.00  99.00  0.0001  0.0001  0.0001
 apr_neu  camw   99.00  99.00  99.00  0.0001  0.0001  0.0001
 apr_neu  carn   99.00  99.00  99.00  0.0001  0.0001  0.0001
 apr_neu  cave   99.00  99.00  99.00  0.0001  0.0001  0.0001
 apr_neu  char   99.00  99.00  99.00  0.0001  0.0001  0.0001
 apr_neu  clif   99.00  99.00  99.00  0.0001  0.0001  0.0001
 apr_neu  cool   99.00  99.00  99.00  0.0001  0.0001  0.0001
 apr_neu  crow   99.00  99.00  99.00  0.0001  0.0001  0.0001
 apr_neu  deak   99.00  99.00  99.00  0.0001  0.0001  0.0001
 apr_neu  dill   99.00  99.00  99.00  0.0001  0.0001  0.0001
 apr_neu  ec19   99.00  99.00  99.00  0.0001  0.0001  0.0001
 apr_neu  eden   99.00  99.00  99.00  0.0001  0.0001  0.0001
 apr_neu  eldo   99.00  99.00  99.00  0.0001  0.0001  0.0001
 apr_neu  emuu   99.00  99.00  99.00  0.0001  0.0001  0.0001
 apr_neu  flag   99.00  99.00  99.00  0.0001  0.0001  0.0001
 apr_neu  gibs   99.00  99.00  99.00  0.0001  0.0001  0.0001
 apr_neu  gren   99.00  99.00  99.00  0.0001  0.0001  0.0001
 apr_neu  groo   99.00  99.00  99.00  0.0001  0.0001  0.0001
 apr_neu  howi   99.00  99.00  99.00  0.0001  0.0001  0.0001
 apr_neu  hwkr   99.00  99.00  99.00  0.0001  0.0001  0.0001
 apr_neu  junc   99.00  99.00  99.00  0.0001  0.0001  0.0001
```

```
 apr_neu  kalg    99.00  99.00  99.00  0.0001  0.0001  0.0001
 apr_neu  kdmn    99.00  99.00  99.00  0.0001  0.0001  0.0001
 apr_neu  kili    99.00  99.00  99.00  0.0001  0.0001  0.0001
 apr_neu  muck    99.00  99.00  99.00  0.0001  0.0001  0.0001
 apr_neu  mula    99.00  99.00  99.00  0.0001  0.0001  0.0001
 apr_neu  norm    99.00  99.00  99.00  0.0001  0.0001  0.0001
 apr_neu  otal    99.00  99.00  99.00  0.0001  0.0001  0.0001
 apr_neu  per3    99.00  99.00  99.00  0.0001  0.0001  0.0001
 apr_neu  pieb    99.00  99.00  99.00  0.0001  0.0001  0.0001
 apr_neu  pill    99.00  99.00  99.00  0.0001  0.0001  0.0001
 apr_neu  pivt    99.00  99.00  99.00  0.0001  0.0001  0.0001
 apr_neu  qut1    99.00  99.00  99.00  0.0001  0.0001  0.0001
 apr_neu  rath    99.00  99.00  99.00  0.0001  0.0001  0.0001
 apr_neu  rope    99.00  99.00  99.00  0.0001  0.0001  0.0001
 apr_neu  sham    99.00  99.00  99.00  0.0001  0.0001  0.0001
 apr_neu  spm9    99.00  99.00  99.00  0.0001  0.0001  0.0001
 apr_neu  suga    99.00  99.00  99.00  0.0001  0.0001  0.0001
 apr_neu  texa    99.00  99.00  99.00  0.0001  0.0001  0.0001
 apr_neu  thev    99.00  99.00  99.00  0.0001  0.0001  0.0001
 apr_neu  torb    99.00  99.00  99.00  0.0001  0.0001  0.0001
 apr_neu  tria    99.00  99.00  99.00  0.0001  0.0001  0.0001
 apr_neu  winn    99.00  99.00  99.00  0.0001  0.0001  0.0001
 apr_neu  woll    99.00  99.00  99.00  0.0001  0.0001  0.0001
*PNG Sites for which NO velocity is to be determined
 apr_neu   alt1   99.0   99.0   99.0  0.0001   0.0001    0.0001
 apr_neu   aman   99.0   99.0   99.0  0.0001   0.0001    0.0001
 apr_neu   buna   99.0   99.0   99.0  0.0001   0.0001    0.0001
 apr_neu   cart   99.0   99.0   99.0  0.0001   0.0001    0.0001
 apr_neu   goka   99.00  99.00  99.0  0.0001   0.0001    0.0001
 apr_neu   gua1   99.0   99.0   99.0  0.0001   0.0001    0.0001
 apr_neu   hain   99.0   99.0   99.0  0.0001   0.0001    0.0001
 apr_neu   kiko   99.00  99.00  99.00 0.0001   0.0001    0.0001
 apr_neu   kopi   99.00  99.00  99.00 0.0001   0.0001    0.0001
 apr_neu   mada   99.00  99.00  99.00 0.0001   0.0001    0.0001
 apr_neu   madg   99.00  99.00  99.00 0.0001   0.0001    0.0001
 apr_neu   mend   99.00  99.00  99.00 0.0001   0.0001    0.0001
 apr_neu   mis1   99.0   99.0   99.0  0.0001   0.0001    0.0001
 apr_neu  mis2    99.0   99.0   99.0  0.0001   0.0001    0.0001
 apr_neu  nugu    99.0   99.0   99.0  0.0001   0.0001    0.0001
 apr_neu  rabl    99.0   99.0   99.0  0.0001   0.0001    0.0001
 apr_neu  tasp    99.0   99.0   99.0  0.0001   0.0001    0.0001
 apr_neu  uras    99.0   99.0   99.0  0.0001   0.0001    0.0001
 apr_neu  wank    99.00  99.00  99.00 0.0001   0.0001    0.0001
 apr_neu  wari    99.0   99.0   99.0  0.0001   0.0001    0.0001
 apr_neu  wata    99.0   99.0   99.0  0.0001   0.0001    0.0001
 apr_neu  wewk    99.0   99.0   99.0  0.0001   0.0001    0.0001
 apr_neu  witu    99.00  99.00  99.00 0.0001   0.0001    0.0001
 apr_neu  wuvu    99.00  99.00  99.00 0.0001   0.0001    0.0001
*PNG SITES TO BE SPECIALLY CONTROLLED
*This special control relates to the velocities which are 5mm
* constraints
 apr_neu  more  50.00  50.00  50.00  0.005  0.005  0.005
 apr_neu  misi  50.00  50.00  50.00  0.005  0.005  0.005
 apr_neu  kavi  50.00  50.00  50.00  0.005  0.005  0.005
 apr_neu  lous  50.00  50.00  50.00  0.005  0.005  0.005
*GLOBAL Sites for which NO velocity is to be determined
 apr_neu  blyt    99.0   99.0   99.0  0.0001   0.0001    0.0001
 apr_neu  ds41    99.0   99.0   99.0  0.0001   0.0001    0.0001
 apr_neu  graz    99.0   99.0   99.0  0.0001   0.0001    0.0001
 apr_neu  gumr    99.0   99.0   99.0  0.0001   0.0001    0.0001
 apr_neu  jplb    99.0   99.0   99.0  0.0001   0.0001    0.0001
 apr_neu  kaya    99.0   99.0   99.0  0.0001   0.0001    0.0001
 apr_neu  male    99.0   99.0   99.0  0.0001   0.0001    0.0001
```

```
 apr_neu  rich    99.0   99.0   99.0  0.0001   0.0001    0.0001
 apr_neu  roch    99.0   99.0   99.0  0.0001   0.0001    0.0001
 apr_neu  sio2    99.0   99.0   99.0  0.0001   0.0001    0.0001
 apr_neu  timb    99.0   99.0   99.0  0.0001   0.0001    0.0001
 apr_neu  viti    99.0   99.0   99.0  0.0001   0.0001    0.0001
 apr_neu  vndb    99.0   99.0   99.0  0.0001   0.0001    0.0001
 apr_neu  wes2    99.0   99.0   99.0  0.0001   0.0001    0.0001
 apr_neu  tid2    99.0   99.0   99.0  0.0001   0.0001    0.0001
 apr_neu  wsam    99.0   99.0   99.0  0.0001   0.0001    0.0001
 apr_neu  huah    99.0   99.0   99.0  0.0001   0.0001    0.0001
 apr_neu  orrx    99.0   99.0   99.0  0.0001   0.0001    0.0001
 apr_neu  enga    99.0   99.0   99.0  0.0001   0.0001    0.0001
 apr_neu  bogt    99.0   99.0   99.0  0.0001   0.0001    0.0001
 apr_neu  rcm4    99.0   99.0   99.0  0.0001   0.0001    0.0001
 apr_neu  gol2    99.0   99.0   99.0  0.0001   0.0001    0.0001
 apr_neu  fai2    99.0   99.0   99.0  0.0001   0.0001    0.0001
 apr_neu  ousd    99.0   99.0   99.0  0.0001   0.0001    0.0001
 apr_neu  kwaj    99.0   99.0   99.0  0.0001   0.0001    0.0001
 apr_neu  kwj1    99.0   99.0   99.0  0.0001   0.0001    0.0001
 apr_neu  mcm1    99.0   99.0   99.0  0.0001   0.0001    0.0001
 apr_neu  ausa    99.0   99.0   99.0  0.0001   0.0001    0.0001
 apr_neu  ausb    99.0   99.0   99.0  0.0001   0.0001    0.0001
 apr_neu  taej    99.0   99.0   99.0  0.0001   0.0001    0.0001
 apr_neu  s01r    99.0   99.0   99.0  0.0001   0.0001    0.0001
 apr_neu  chul    99.0   99.0   99.0  0.0001   0.0001    0.0001
 apr_neu  lhas    99.0   99.0   99.0  0.0001   0.0001    0.0001
 apr_neu  mltg    99.0   99.0   99.0  0.0001   0.0001    0.0001
 apr_neu  gan1    99.0   99.0   99.0  0.0001   0.0001    0.0001
 apr_neu  sey1    99.0   99.0   99.0  0.0001   0.0001    0.0001
 apr_neu  baha    99.0   99.0   99.0  0.0001   0.0001    0.0001
 apr_neu  mali    99.0   99.0   99.0  0.0001   0.0001    0.0001
 apr_neu  wtzx    99.0   99.0   99.0  0.0001   0.0001    0.0001
*NEW ZEALAND sites no velocities to be determined
* These are DORIS sites no velocities to be determined
 apr_neu  arlt    99.00  99.00  99.00  0.0001  0.0001  0.0001
 apr_neu  arna    99.00  99.00  99.00  0.0001  0.0001  0.0001
 apr_neu  bras    99.00  99.00  99.00  0.0001  0.0001  0.0001
 apr_neu  colb    99.00  99.00  99.00  0.0001  0.0001  0.0001
 apr_neu  djib    99.00  99.00  99.00  0.0001  0.0001  0.0001
 apr_neu  gala    99.00  99.00  99.00  0.0001  0.0001  0.0001
 apr_neu  ineg    99.00  99.00  99.00  0.0001  0.0001  0.0001
 apr_neu  manl    99.00  99.00  99.00  0.0001  0.0001  0.0001
 apr_neu  para    99.00  99.00  99.00  0.0001  0.0001  0.0001
 apr_neu  reun    99.00  99.00  99.00  0.0001  0.0001  0.0001
 apr_neu  sakl    99.00  99.00  99.00  0.0001  0.0001  0.0001
 apr_neu  soco    99.00  99.00  99.00  0.0001  0.0001  0.0001
 apr_neu  sthl    99.00  99.00  99.00  0.0001  0.0001  0.0001
* These are GIG 91  and other sites no velocities to be
* determined
 apr_neu  sang    99.00  99.00  99.00 0.0001   0.0001    0.0001
 apr_neu  aron    99.00  99.00  99.00 0.0001   0.0001    0.0001
 apr_neu  braz    99.00  99.00  99.00 0.0001   0.0001    0.0001
 apr_neu  eis1    99.00  99.00  99.00 0.0001   0.0001    0.0001
 apr_neu  eis1    99.00  99.00  99.00 0.0001   0.0001    0.0001
 apr_neu  pgc0    99.00  99.00  99.00 0.0001   0.0001    0.0001
 apr_neu  wsam    99.00  99.00  99.00 0.0001   0.0001    0.0001
 apr_neu  matg    99.00  99.00  99.00 0.0001   0.0001    0.0001
 apr_neu  wetb    99.00  99.00  99.00 0.0001   0.0001    0.0001
 apr_neu  nal0    99.00  99.00  99.00 0.0001   0.0001    0.0001
 apr_neu  nal1    99.00  99.00  99.00 0.0001   0.0001    0.0001
 apr_neu  hone    99.00  99.00  99.00 0.0001   0.0001    0.0001
*============================
*The Southern hemisphere
```

```
*The Northern hemisphere
 apr_svs    all     1000     1000    1000    100    100    100
 apr_rad    all     1. 1. 0 .02 0 .02 .02 .02 .02 .02 .02
*============================
* now try for a consistent set of earth orientation parameters
- Tom's UT1
* rotation stopper. This runs out during the process but is
* good at the start where it is
* needed
*
*  in_pmu /data5/gps/tables/vlbi_84.1_94.04.apr
* apr_wob     100    100  10  10     0    0    0    0
* apr_ut1     100     10   0   0     0    0    0    0
*
*this ends the command file
```

```
C
C=============================================================
C GLORG COMMAND FILE
C=============================================================
C The new apr_file made from ITRF94 @ 1993.0 for fiducial sites
C It is this file that sets the a-prioris
  apr_file /data8/gps/solns/glorg_sites.apr
C
C=============================================================
C The essence of this GLORG file is a CONSTRAINED solution.
C This means that we can look at corrections etc at the constrained and
C free sites and know what is happening to these sites.
C There are 13, actually more now, high quality core GPS sites
C The debate is a relatively minimum set or a well overdetermined set.
C We need a minimum of three sites and some velocities. Note we are
C doing a 7 parameter solution with some rates and hence the minimum set is
C three stations. We do not have a hugely overdependant set at 6 to 8 stations.
C Using all 13 could be construed as overdetermined.
C The follwing 8 station model is considered midrange. YAR1 and KOSG are
C SLR stations in the global network while DS42, HART, ALGO, FAIR
C are VLBI stations.
C
  use_site clear  YAR1 SANT DS42 KOSG TROM YELL KOKR
C
C other excellent sites are KOKR, YELL and WTZ1
C use the DSN sites DS10 and DS60 to complete the 13
C
C An interesting sequence of tests might be to put in all 13 stations at 0.02 and
C then progressively remove those stations that have
C  the biggest adjustments or residuals.
C Only the front page of the results should be needed and the quality of the fit
C should increase as these stations are excluded.
C
C Use the local N,E,U coordinate system
C
 LOCAL_EQ

C Southern Hemisphere ITRF Sites all constrained to 1 centimeter
C  and ITRF Velocities held


  constra 0.001 sant_gps npos
  constra 0.001 sant_gps epos
  constra 0.001 sant_gps upos
  force sant_gps ndot 0.000
  force sant_gps edot 0.000
  force sant_gps udot 0.000
```

```
constra 0.001 yar1_gps npos
constra 0.001 yar1_gps epos
constra 0.001 yar1_gps upos
force yar1_gps ndot 0.000
force yar1_gps edot 0.000
force yar1_gps udot 0.000

constra 0.001 ds42_gps npos
constra 0.001 ds42_gps epos
constra 0.001 ds42_gps upos
force ds42_gps ndot 0.000
force ds42_gps edot 0.000
force ds42_gps udot 0.000

C Northern Hemisphere ITRF Sites all constrained to 1 centimetre

constra 0.001 trom_gps npos
constra 0.001 trom_gps epos
constra 0.001 trom_gps upos
force trom_gps ndot 0.000
force trom_gps edot 0.000
force trom_gps udot 0.000

constra 0.001 kosg_gps npos
constra 0.001 kosg_gps epos
constra 0.001 kosg_gps upos
force kosg_gps ndot 0.000
force kosg_gps edot 0.000
force kosg_gps udot 0.000

constra 0.001 kokr_gps npos
constra 0.001 kokr_gps epos
constra 0.001 kokr_gps upos
force kokr_gps ndot 0.000
force kokr_gps edot 0.000
force kokr_gps udot 0.000

constra 0.001 yell_gps npos
constra 0.001 yell_gps epos
constra 0.001 yell_gps upos
force yell_gps ndot 0.000
force yell_gps edot 0.000
force yell_gps udot 0.000

C CIGNET SITES for which the plate velocities are TO BE EQUATED include
C Richmond, Westford, Kokee Park,  Hobart, Townsville, Tsukuba, Wetzell.
C Information may become available at Mojave latter
C This equation is needed to backwards extend the reference frame.
```

```
C at Richmond use modern  to define CIGNET values
C The precisions on the solutions are similar, all 0.001m or less with up largest
C between RCM5 and RCM2. Rate variations donot exceed 0.001 in any
C component. this indicates solutions have similar rates. With small rates and
C differences any errors in this site are not expected to propagate. RIC1 is less
C well defined, but not dissimilar, and clearly should take the value of RCM5.
  equate RCM5 ndot RCM2 ndot
  equate RCM5 edot RCM2 edot
  equate RCM5 udot RCM2 udot

  equate RCM5 ndot RIC1 ndot
  equate RCM5 edot RIC1 edot
  equate RCM5 udot RIC1 udot

C at Townsville use the CIGNET value since only two years at AFN site
C at Townsville CIGNET from GIG91 to 1993, AFN oly 1992,1993 and 1994 as
C of July 1996.The solutions are very similar with almost identical precisions.
C Major differences are a sinking at TOWN and a rise at TOWA. These are
C near 1 cm per year. This means that the up rates should not be equated.
C Since the difference is of the order of 5mm/yr no differences will be detected.
  equate TOWN ndot TOWA  ndot
  equate TOWN edot TOWA  edot
  equate TOWN udot TOWA  udot

C at Tsukuba use the modern rogue value, TSKB. There is an order of
C magnitude in precision on the rates between TSKB and TSU1. The latter has
C rates in the 0.1 m/yr range as well compared to the 0.001m/yr range for
C TSU1. This is a clear case of using TSkb to replace TSU1 rates. The mean
C epoch of TSU1 is 1991.4 so no large errors will be introduced by replacing
C  the values.
  equate TSKB ndot TSU1  ndot
  equate TSKB edot TSU1  edot
  equate TSKB udot TSU1  udot

C at Westford Massachusetts use old CIGNET WES1 values.
C Since WES2 has no velocity in its own right this is the only method
C WES1 is well determined.
 equate WES1 ndot WES2  ndot
 equate WES1 edot WES2  edot
 equate WES1 udot WES2  udot

C at Hobart use the new AFN location HOBA, also called HOB2
C a difficult situation with the up rates varying. At TAS1 the up rate is -0.0509
C while at HOBA it is 0.0013. This appears to be antennae/system related. Will
C enforce the HOBA value. This could be a problem with TAS1 having an
C epoch of 1992.5 and need to get to 1990.5. Rates at HOB1 and HOBA
C are very similar and no side effects from equating should be experienced.
C This uniformity adds weight to the transfer of the up rate to the TAS1 point.
 equate HOBA ndot TAS1 ndot
 equate HOBA edot TAS1 edot
```

```
 equate HOBA udot TAS1 udot

  equate HOBA ndot HOB1 ndot
  equate HOBA edot HOB1 edot
  equate HOBA udot HOB1 udot

C at Kokee Park, Hawaii use the rogue location. Only KOKR is determined.
C It is well determined. all components at the few mm/yr
  equate KOKR ndot KOKE ndot
  equate KOKR edot KOKE edot
  equate KOKR udot KOKE udot

C at Wetzell use the WTZ1 site to define earlier values. The long term
C mm/yr precision of WTZ1 should be transfered through to WTZB.
  equate WTZ1 ndot WETB ndot
  equate WTZ1 edot WETB edot
  equate WTZ1 udot WETB udot
C
C END CIGNET LIST
C ******************************************************
C now do some ANTARCTIC Sites

C at O'Higgins use the current site OHIG. Some concern at
C high settling rate, 0.1m/yr. Clear need to transfer through the corrections.
  equate ohig edot ohi5 edot
  equate ohig ndot ohi5 ndot
  equate ohig udot ohi5 udot

C At CASEY use the permanent station CAS1. CASE had no velocity
C and hence this equation is correct. CAS1 is a high quality solution.
 equate CAS1 ndot CASE ndot
 equate CAS1 edot CASE edot
 equate CAS1 udot CASE udot

C at McMurdo use the current location MCM4. The precision on MCM4
C is clearly superior to the other determinations being in the mm/yr region.
C MCM0 was a no rate solution and hence must be equated. MCMU is very
C similar to MCM4 and differences are small. precisions slightly worse.
C No harm done in the equation. MCM1 has cm/yr precisions and is
C less well determined. Rates of right sign but higher.
  equate MCM4 ndot MCMU ndot
  equate MCM4 edot MCMU edot
  equate MCM4 udot MCMU udot

  equate MCM4 ndot MCM0 ndot
  equate MCM4 edot MCM0 edot
  equate MCM4 udot MCM0 udot

  equate MCM4 ndot MCM1 ndot
  equate MCM4 edot MCM1 edot
```

```
  equate MCM4 udot MCM1 udot
C
C END ANTARCTIC  LIST
C ******************************************************
C now do some other AUSTRALIAN  Sites

C at TIDBINBILLA use DS42. DS42 is the highest precision solution.
C DS40 is a cm/yr precision on rates compared to mm/yr at DS42.
C Equation is correct. DS41 was not a rate solution and hence equation
C is correct. TID2 is less well determined at this instant.
  equate DS42 ndot DS40 ndot
  equate DS42 edot DS40 edot
  equate DS42 udot DS40 udot

  equate DS42 ndot DS41 ndot
  equate DS42 edot DS41 edot
  equate DS42 udot DS41 udot

  equate DS42 ndot TID2 ndot
  equate DS42 edot TID2 edot
  equate DS42 udot TID2 udot
C
C END AUSTRALIAN  LIST
C ******************************************************
C END EQUATE SECTION
C ******************************************************


C
C set the parameters to be determined in setting the origin.
C standard 7 parameter model is used.
C
 pos_org  xrot yrot zrot xtran ytran ztran scale
C
C lower the influence of heights on the transformation process
C by a factor of 10
 cnd_hgtv  10
```

```
* PNG _ KIMM site renames
*
  rename are1_gps areq_gps
  rename car1_gps cart_gps
  rename mis2_gps misi_gps
  rename guny_gps alt2_gps
  rename orro_gps orrx_gps 90 1  1 0 0 91 1  1 0 0
  rename wtzm_gps wtzx_gps 90 1  1 0 0 91 1  1 0 0
*******************************************************************
* ANT 93 SYOW height correction
  rename syow_gps syow_gps 93 1 15 0 0 93 1 23 0 0 0.0 0.0 -1.369 NEU
*******************************************************************
* ANT 92 MAWS / MAW1 connection
  rename maws_gps maw1_gps 91 1  1 0 0 93 1  1 0 0 -235.055 -154.248
10.749 NEU
*******************************************************************
* ANT 94 MCMU name correction
  rename mcmu_gps mcm0_gps 90 1  1 0 0 91 2  1 0 0
  rename mcmg_gps mcmu_gps
*******************************************************************
* ANT 92 DAVI / DAV1 connection
  rename davi_gps dav1_gps 91 1  1 0 0 93 1  1 0 0 0.0 0.0 -0.013 NEU
*******************************************************************
* ANT 91/92  DS40 / TIDB name correction
  rename tidb_gps ds40_gps 92 1  1 0 0 92 3  1 0 0
* AUS 94/day211   TIDB / DS42 name correction
  rename tidb_gps ds42_gps 94 7 29 0 0 96 5 31 0 0
* ARN 92,93 DS42 height correction
  rename ds42_gps ds42_gps 92 7 25 0 0 94 8  1 0 0 0.0 0.0 -0.092 NEU
*******************************************************************
*******************************************************************
*  GLOBAL ITRF sites
*******************************************************************
* GIG 91 fixers
  rename ykn1_gps yell_gps 91 1 23 0 0 91 1 30 0 0
  rename jplm_gps jpl1_gps 91 1 23 0 0 91 1 30 0 0
  rename nall_gps nal1_gps 91 1 23 0 0 91 1 30 0 0
  rename aron_gps algo_gps 91 1 23 0 0 91 1 30 0 0
  rename eisl_gps eis1_gps 91 1 23 0 0 91 1 30 0 0
  rename gold_gps ds10_gps
  rename madr_gps ds60_gps
  rename kokb_gps kokr_gps
  rename wett_gps wtz1_gps
  rename rich_gps ric1_gps
  rename usud_gps usu5_gps 95 9 1 0 0 96 5 31 0 0
  rename usu3_gps usu5_gps
  rename nyal_gps nal1_gps 91 2 1 0 0 96 5 31 0 0
  rename ohig_gps ohi5_gps 95 9 1 0 0 96 5 31 0 0
  rename kerg_gps ker5_gps 95 9 1 0 0 96 5 31 0 0
* These are attempts to resolve site changes between IGS93 and ANT94
  rename sio2_gps siox_gps 94 1  1 0 0 95 1  1
*******************************************************************
*   AUSTRALIAN sites
*******************************************************************
* Gnangara Trimble site ARN 92,93
  rename pert_gps per2_gps 92 7 24 0 0 93 1  1 0 0
  rename perx_gps pert_gps 93 1  1 0 0 95 1  1 0 0
  rename perr_gps pert_gps 93 1  1 0 0 95 1  1 0 0
* Hobart AFN site
  rename hoba_gps hoba_gps 93 8 25 0 0 94 1  1 0 0 0.0 0.0 -0.032 NEU
  rename hob2_gps hoba_gps 91 1  1 0 0 96 5 31 0 0 0.0 0.0  0.0648 NEU
* Height corrections for AFN sites
  rename alic_gps alic_gps 94 7 26 0 0 94 7 31 0 0 0.0 0.0 -0.032 NEU
  rename towa_gps towa_gps 94 7 26 0 0 94 7 31 0 0 0.0 0.0 -0.038 NEU
  rename cedu_gps cedu_gps 93 8 25 0 0 94 1  1 0 0 0.0 0.0 -0.032 NEU
  rename cedu_gps cedu_gps 94 7 26 0 0 94 7 31 0 0 0.0 0.0 -0.038 NEU
  rename darw_gps darw_gps 94 7 26 0 0 94 7 31 0 0 0.0 0.0 -0.032 NEU
  rename karr_gps karr_gps 94 7 26 0 0 94 7 31 0 0 0.0 0.0 -0.034 NEU
```

```
*********************************************************************
* New Zealand session two sites
  rename E072_GPS  D072_GPS
  rename E078_GPS  D078_GPS
  rename E100_GPS  D100_GPS
  rename E105_GPS  D105_GPS
  rename E131_GPS  D131_GPS
  rename E143_GPS  D143_GPS
  rename E158_GPS  D158_GPS
  rename E191_GPS  D191_GPS
  rename E212_GPS  D212_GPS
  rename E253_GPS  D253_GPS
  rename E309_GPS  D309_GPS
  rename E320_GPS  D320_GPS
  rename E338_GPS  D338_GPS
  rename E425_GPS  D425_GPS
  rename E431_GPS  D431_GPS
  rename E452_GPS  D452_GPS
  rename E469_GPS  D469_GPS
  rename E473_GPS  D473_GPS
  rename E482_GPS  D482_GPS
  rename E483_GPS  D483_GPS
  rename MCMR_GPS  MCMU_GPS
```

Apriori coordinate file used for the final solution.

```
  ENGA_GPS  3981774.8240   -89252.3535  4965291.4425 -0.1567 -0.2369  0.2351 1990.580  0.0322  0.0248  0.0273
  GRUN_GPS  1970765.6678   -98261.9403 -6046201.5978  0.0000  0.0000  0.0000 1992.010  0.0397  0.0206  0.0715
  DS60_GPS  4849202.5040  -360329.1940  4114913.0440 -0.0062  0.0199  0.0127 1993.0000  ITRF94A  13407S012 MADRID
  NEUL_GPS  2102610.2885  -309037.7312 -5993559.0533  0.0000  0.0000  0.0000 1991.064  0.0514  0.0386  0.0783
  NEUM_GPS  2102610.0828  -309037.7613 -5993558.9469  0.0000  0.0000  0.0000 1991.067  0.0682  0.1739  0.2285
  NEUN_GPS  2102610.6813  -309037.6261 -5993559.0543  0.0000  0.0000  0.0000 1991.067  0.0694  0.0612  0.0927
  NEUO_GPS  2102610.5669  -309037.7974 -5993558.9090  0.0000  0.0000  0.0000 1991.070  0.0587  0.0610  0.1564
  NEUP_GPS  2102611.1302  -309037.7582 -5993559.1993  0.0000  0.0000  0.0000 1991.070  0.0456  0.0489  0.0727
  NEUQ_GPS  2102610.9588  -309037.7220 -5993558.7658  0.0000  0.0000  0.0000 1991.073  0.0665  0.0606  0.1885
  NEUS_GPS  2102611.2620  -309039.6953 -5993556.5649  0.0000  0.0000  0.0000 1991.075  0.7082  2.2473  2.0524
  NEUT_GPS  2102612.0128  -309037.8414 -5993558.9002  0.0000  0.0000  0.0000 1991.075  0.0404  0.0395  0.0669
  MASP_GPS  5439189.1524 -1522054.8399  2953464.2212 -0.0062  0.0185  0.0167 1993.802  0.0017  0.0011  0.0011
  FORT_GPS  4985386.6460 -3954998.5625  -428426.5112 -0.0129  0.0055  0.0146 1995.858  0.0011  0.0011  0.0005
  BRAZ_GPS  4115014.1601 -4550641.6715 -1741444.1474  0.0001 -0.0003 -0.0002 1995.825  0.3126  0.8930  0.2097
  BRAS_GPS  4114500.3184 -4551173.1804 -1741210.6522  0.0000  0.0000  0.0000 1996.338  0.0203  0.0190  0.0075
  STJO_GPS  2612631.3047 -3426807.0160  4686757.7734 -0.0095 -0.0044  0.0191 1993.847  0.0010  0.0010  0.0011
  KOUR_GPS  3839591.4364 -5059567.5216   579956.8745  0.0049 -0.0002  0.0132 1993.874  0.0020  0.0022  0.0007
  OHIG_GPS  1525877.0529 -2432481.5377 -5676145.2662  0.0370 -0.0399 -0.0987 1992.036  0.0099  0.0094  0.0146
  OHI5_GPS  1525872.4649 -2432481.2822 -5676146.0823  0.0370 -0.0399 -0.0987 1995.968  0.0011  0.0012  0.0019
  LPGS_GPS  2780102.9802 -4437418.8393 -3629404.6038  0.0229 -0.0366 -0.0099 1996.107  0.0008  0.0010  0.0008
  DECE_GPS  1422140.8226 -2534034.2559 -5658736.1491  0.0000  0.0000  0.0000 1992.053  0.0600  0.0653  0.0561
  BRMU_GPS  2304703.6383 -4874817.1734  3395186.8665 -0.0067  0.0042  0.0047 1994.375  0.0018  0.0023  0.0016
  RIOG_GPS  1429882.6827 -3495363.2133 -5122698.8550  0.0000  0.0000  0.0000 1992.029  0.0657  0.1033  0.1366
  SANG_GPS  1769724.5696 -5044512.3731 -3468396.3913  0.0239 -0.0076  0.0150 1991.070  0.0277  0.0348  0.0195
  SANT_GPS  1769693.2580 -5044574.1140 -3468321.1120  0.0225 -0.0066  0.0147 1993.0000  ITRF94B  41705M003 SANTIAGO
  AREQ_GPS  1942826.7426 -5804070.2429 -1796893.9969  0.0109  0.0030  0.0149 1995.991  0.0007  0.0010  0.0005
  WES1_GPS  1492233.0659 -4458088.4749  4296048.1849 -0.0060 -0.0068  0.0106 1991.813  0.0036  0.0048  0.0043
  WES2_GPS  1492233.4480 -4458089.4648  4296045.9798 -0.0060 -0.0068  0.0106 1993.437  0.0092  0.0096  0.0097
  BOGT_GPS  1744399.1401 -6116037.8080   512731.6136  0.1063 -0.0770  0.1882 1996.269  0.0011  0.0016  0.0005
  ALGO_GPS   918129.5760 -4346071.2290  4561977.8110 -0.0158 -0.0051  0.0035 1993.0000  ITRF94B  40104M002 ALGONQUIN
  RCM5_GPS   961334.8001 -5674074.1852  2740535.1457  0.0135 -0.0218  0.0173 1994.416  0.0014  0.0022  0.0012
  RCM2_GPS   961318.9611 -5674090.9669  2740489.5899  0.0135 -0.0218  0.0173 1993.339  0.0017  0.0024  0.0013
  RIC1_GPS   961309.4419 -5674075.8526  2740539.1005  0.0135 -0.0218  0.0173 1992.078  0.0035  0.0056  0.0032
  PIE1_GPS -1640916.7366 -5014781.1749  3575447.1431 -0.0084 -0.0066  0.0019 1994.001  0.0010  0.0013  0.0010
  EISL_GPS -1884951.7975 -5357595.8687 -2892890.5109  0.0727 -0.0189 -0.0100 1996.274  0.0012  0.0015  0.0009
  EIS1_GPS -1884997.7898 -5357589.7642 -2892871.0876  0.0727 -0.0189 -0.0100 1991.070  0.0263  0.0358  0.0197
  YELL_GPS -1224452.4050 -2689216.0970  5633638.2890 -0.0204 -0.0042 -0.0027 1993.0000  ITRF94B  40127M003
YELLOWKNIFE
  BLYT_GPS -2223206.5793 -4830299.8965  3510587.7576  0.0000  0.0000  0.0000 1994.149  0.0026  0.0040  0.0029
```

```
  PIN2_GPS -2369466.3762 -4761231.6750  3511396.5917 -0.0147 -0.0003  0.0406 1993.101  0.0023  0.0031  0.0024
  PIN1_GPS -2369510.3948 -4761207.1814  3511396.1544 -0.0147 -0.0003  0.0406 1993.663  0.0013  0.0017  0.0013
  ROCH_GPS -2382183.2017 -4755085.1851  3511367.6127  0.0000  0.0000  0.0000 1992.039  0.0083  0.0130  0.0084
  MOJ1_GPS -2356215.9124 -4646736.6189  3668456.3217 -0.0190 -0.0008 -0.0034 1991.994  0.0028  0.0040  0.0029
  DS10_GPS -2353614.0850 -4641385.4130  3676976.4850 -0.0146  0.0030 -0.0057 1993.0000  ITRF94A  40405S028 GOLDSTONE
  GOL2_GPS -2353614.1673 -4641385.4247  3676976.4817 -0.0192 -0.0080  0.0053 1996.255  0.0010  0.0013  0.0010
  SIO3_GPS -2455456.4289 -4767480.8009  3441383.6151 -0.0356  0.0058  0.0421 1993.770  0.0012  0.0015  0.0011
  SIO1_GPS -2455521.6555 -4767213.4018  3441654.8899 -0.0356  0.0058  0.0421 1991.741  0.0039  0.0064  0.0045
  SIO2_GPS -2455539.2586 -4767224.0890  3441628.9024 -0.0356  0.0058  0.0421 1993.438  0.0050  0.0061  0.0047
  MATH_GPS -2443215.2794 -4706037.5777  3533477.5807 -0.0226  0.0009  0.0321 1993.754  0.0011  0.0014  0.0011
  JPL1_GPS -2493304.1079 -4655215.5040  3565497.3497 -0.0304  0.0118  0.0163 1993.911  0.0011  0.0014  0.0011
  PVEP_GPS -2525523.0984 -4670030.8244  3522843.0581 -0.0072  0.0319  0.0374 1993.738  0.0011  0.0014  0.0011
  BYRD_GPS  -547611.0941  -965498.3340 -6261279.3726 -1.9579 11.3371 -1.6699 1992.038  0.0060  0.0060  0.0119
  DRAO_GPS -2059164.6236 -3621108.3841  4814432.4003 -0.0089  0.0000 -0.0065 1993.677  0.0007  0.0008  0.0009
  VNDP_GPS -2678089.8203 -4525437.7574  3597431.5052 -0.0735 -0.0606  0.0968 1993.745  0.0013  0.0017  0.0013
  QUIN_GPS -2517230.9327 -4198595.1777  4076531.2606 -0.0153 -0.0118  0.0077 1993.724  0.0012  0.0015  0.0013
  PGC0_GPS -2327188.0203 -3522528.9280  4764832.3004  0.0000  0.0000  0.0000 1991.071  0.0059  0.0086  0.0094
  ALBH_GPS -2341332.8390 -3539049.4965  4745791.3843  0.0041  0.0118 -0.0157 1992.824  0.0035  0.0043  0.0048
  FAIR_GPS -2281621.3450 -1453595.7840  5756961.9690 -0.0208 -0.0031 -0.0117 1993.0000  ITRF94B  40408M001 FAIRBANKS
  FAI2_GPS -2281615.1718 -1453627.8897  5756960.8753 -0.0206 -0.0079 -0.0039 1996.222  0.0009  0.0008  0.0019
  PAMA_GPS -5245194.9284 -3080472.0408 -1912825.2989 -0.0072  0.0589  0.0318 1995.672  0.0015  0.0013  0.0006
  HUAH_GPS -5345885.4695 -2958241.9883 -1824597.9039 -0.0072  0.0589  0.0318 1990.582  0.0239  0.0248  0.0100
  KOKE_GPS -5543818.1244 -2054582.9200  2387858.4620 -0.0072  0.0589  0.0318 1993.162  0.0063  0.0033  0.0030
  KOKR_GPS -5543838.0790 -2054587.5180  2387809.5890 -0.007   0.0600  0.0305 1993.0000  ITRF94B  40424M004
KOKEE_PARK
  WSAM_GPS -6134394.6626  -860418.5457 -1514829.5043  0.0000  0.0000  0.0000 1991.069  0.0201  0.0176  0.0082
  CHAT_GPS -4590670.8891  -275483.0205 -4404596.7972 -0.0221  0.0065  0.0386 1996.133  0.0008  0.0006  0.0006
  VITI_GPS -6073527.5010   276502.1796 -1921630.4602  0.0000  0.0000  0.0000 1992.590  0.0096  0.0057  0.0040
  AUCK_GPS -5105680.9816   461564.0525 -3782181.7780 -0.0152 -0.0300  0.0454 1996.138  0.0008  0.0007  0.0006
  WELL_GPS -4780648.7908   436507.1450 -4185440.4152  0.0250  0.0030  0.0504 1992.622  0.0023  0.0015  0.0019
  OUSD_GPS -4387888.5706   733420.8726 -4555178.6184 -0.0724  0.0569 -0.0335 1996.228  0.0009  0.0007  0.0008
  OTA1_GPS -4387888.1952   733420.7286 -4555178.3281 -0.0724  0.0569 -0.0335 1993.669  0.0038  0.0021  0.0036
  OTAG_GPS -4388296.9988   733507.1885 -4554771.7465 -0.0724  0.0569 -0.0335 1993.093  0.0021  0.0013  0.0020
  KWJ1_GPS -6160881.0101  1339882.9032   960810.4425  0.0000  0.0000  0.0000 1996.303  0.0031  0.0015  0.0007
  KWAJ_GPS -6160865.1377  1339912.0899   960841.9681  0.0000  0.0000  0.0000 1990.578  0.0143  0.0108  0.0051
  MCMU_GPS -1310695.2134   310468.8840 -6213363.4645  0.0064 -0.0248 -0.0026 1993.502  0.0018  0.0016  0.0038
  MCM0_GPS -1310856.3649   310431.5574 -6213347.7479  0.0064 -0.0248 -0.0026 1991.072  0.0266  0.0273  0.0475
  MCM1_GPS -1310621.7607   310414.1624 -6213400.3597  0.0064 -0.0248 -0.0026 1994.537  0.0017  0.0016  0.0036
  MCM4_GPS -1311703.2795   310815.1269 -6213255.2029  0.0064 -0.0248 -0.0026 1996.124  0.0006  0.0006  0.0012
  TNO1_GPS -1623858.5211   462478.2392 -6130048.8877  0.0000  0.0000  0.0000 1992.033  0.0231  0.0203  0.0555
  TASP_GPS -5953042.2830  2232112.2220  -508584.3646  0.0000  0.0000  0.0000 1993.445  0.0095  0.0064  0.0021
  MAC1_GPS -3464038.4451  1334172.7336 -5169224.3014 -0.0036  0.0034  0.0475 1995.668  0.0009  0.0007  0.0011
```

```
  CART_GPS -5782172.4805  2639487.5491  -528398.6785  0.0000  0.0000  0.0000 1992.348  0.0071  0.0049  0.0016
  NUGU_GPS -5755507.8686  2723752.8758  -368612.8086  0.0000  0.0000  0.0000 1992.350  0.0061  0.0044  0.0015
  GUA2_GPS -5607198.7510  2863957.6067 -1015751.2927 -0.0446 -0.0200  0.0803 1990.921  0.0170  0.0137  0.0046
  GUA1_GPS -5607201.3187  2863954.1987 -1015746.5938 -0.0446 -0.0200  0.0803 1991.631  0.0249  0.0170  0.0067
  MIS1_GPS -5577078.1555  2861397.5202 -1175144.1491 -0.0154 -0.0442  0.0581 1991.623  0.0106  0.0071  0.0031
  MISI_GPS -5576759.2988  2862001.1547 -1175221.0917 -0.0154 -0.0442  0.0581 1992.575  0.0038  0.0027  0.0013
  RABL_GPS -5625280.8183  2970585.5280  -463064.8066  0.0000  0.0000  0.0000 1992.346  0.0071  0.0050  0.0017
  JACQ_GPS -5578632.2621  3028263.6972  -623240.7391 -0.0357 -0.0072 -0.0616 1991.897  0.0056  0.0045  0.0017
  EC19_GPS -4644354.4306  2549989.7035 -3539040.9586  0.0000  0.0000  0.0000 1994.148  0.0051  0.0035  0.0038
  BUNA_GPS -5499983.6305  3029313.9915 -1116842.4590  0.0000  0.0000  0.0000 1991.629  0.0123  0.0081  0.0033
  LOUS_GPS -5523811.4973  3046135.3406  -940385.3470 -0.0617  0.0002  0.0643 1992.196  0.0049  0.0038  0.0016
  WARI_GPS -5481915.8937  3028449.6774 -1204231.3333  0.0000  0.0000  0.0000 1991.627  0.0119  0.0083  0.0036
  HAIN_GPS -5485912.2503  3033109.9496 -1173846.0187  0.0000  0.0000  0.0000 1991.611  0.0124  0.0084  0.0035
  URAS_GPS -5499656.3765  3066247.5445 -1013638.6114  0.0000  0.0000  0.0000 1991.611  0.0125  0.0081  0.0034
  KAVI_GPS -5562412.9607  3107930.0163  -285346.1998 -0.0145  0.0853  0.0271 1993.192  0.0040  0.0029  0.0010
  ALT1_GPS -5459929.3566  3094433.6861 -1134392.5520 -0.0167 -0.0429  0.0629 1991.598  0.0341  0.0178  0.0078
  ALT2_GPS -5453535.6886  3105804.9091 -1134062.8156 -0.0167 -0.0429  0.0629 1991.616  0.0078  0.0054  0.0024
  GUNY_GPS -5453535.7910  3105804.8722 -1134062.7064 -0.0167 -0.0429  0.0629 1993.668  0.0046  0.0031  0.0014
  WATA_GPS -5466222.4365  3125151.8665 -1014184.3943  0.0000  0.0000  0.0000 1991.627  0.0115  0.0077  0.0031
  BATH_GPS -4594786.6392  2699295.8921 -3494244.2618 -0.0506  0.0056  0.0369 1993.650  0.0011  0.0009  0.0009
  WITU_GPS -5473775.5158  3232571.4092  -517844.6205 -0.0950 -0.1186 -0.2276 1990.579  0.0086  0.0076  0.0029
  DS40_GPS -4460987.9714  2682362.2723 -3674626.4674 -0.0366 -0.0030  0.0442 1991.814  0.0066  0.0050  0.0048
  DS41_GPS -4460979.5548  2682380.7399 -3674624.1279 -0.0366 -0.0030  0.0442 1992.350  0.0030  0.0025  0.0023
  DS42_GPS -4460995.9840  2682557.0930 -3674443.8810 -0.0366 -0.0030  0.0442 1993.0000  ITRF94B  50103M108
TIDBINBILLA
  TID2_GPS -4460996.1081  2682557.0792 -3674443.7331 -0.0366 -0.0030  0.0442 1996.256  0.0010  0.0008  0.0008
  ORRO_GPS -4446478.9106  2678112.6064 -3696270.2805 -0.0323  0.0018  0.0532 1992.554  0.0017  0.0012  0.0013
  ORRX_GPS -4446476.5737  2678104.7940 -3696261.9977 -0.0323  0.0018  0.0532 1990.581  0.0104  0.0111  0.0083
  MORO_GPS -5335932.3843  3387629.6008  -853539.8014 -0.0537 -0.0115  0.0613 1992.192  0.0059  0.0051  0.0019
  TAS1_GPS -3950184.0919  2522364.5552 -4311588.5673 -0.0467  0.0064  0.0366 1992.482  0.0016  0.0012  0.0015
  HOB1_GPS -3950183.9819  2522364.4557 -4311588.3242 -0.0467  0.0064  0.0366 1993.970  0.0009  0.0008  0.0008
  HOBA_GPS -3950071.3272  2522415.2011 -4311638.4775 -0.0467  0.0064  0.0366 1995.182  0.0006  0.0006  0.0006
  MANU_GPS -5367596.4553  3437943.3559  -226704.9770 -0.0235  0.0795  0.0233 1993.045  0.0055  0.0041  0.0012
  MORE_GPS -5288519.1741  3409952.8797 -1038574.3551 -0.0167 -0.0429  0.0629 1993.486  0.0015  0.0013  0.0008
  UNIT_GPS -5313156.7119  3450683.5737  -736065.7389  0.0232 -0.0749  0.0626 1994.016  0.0030  0.0023  0.0011
  TOWN_GPS -5041024.9688  3296980.3187 -2090553.3411 -0.0438 -0.0124  0.0496 1993.223  0.0014  0.0012  0.0008
  TOWA_GPS -5036492.1820  3298900.0791 -2099859.7311 -0.0438 -0.0124  0.0496 1993.471  0.0014  0.0011  0.0008
  WANK_GPS -5262950.5217  3539058.6821  -678565.3335  0.0346 -0.0790  0.0556 1993.666  0.0041  0.0031  0.0012
  GILG_GPS -4470744.2890  3016577.4568 -3394500.1781  0.1983  0.1294 -0.2296 1994.571  0.0022  0.0018  0.0016
  MADA_GPS -5252527.4277  3571989.7495  -575482.7500  0.0000  0.0000  0.0000 1993.662  0.0033  0.0026  0.0010
  MADG_GPS -5251159.3043  3575562.4469  -570087.9687  0.0000  0.0000  0.0000 1990.572  0.0104  0.0099  0.0033
  BANZ_GPS -4610424.0837  3148699.7735 -3073895.9536 -0.1193  0.1563 -0.2487 1994.571  0.0023  0.0020  0.0016
```

EDEN_GPS	-4408335.7292	2554609.1269	-3823983.5617	-0.0390	0.0040	0.0420	1996.338	0.0056	0.0060	0.0039
BASS_GPS	-5113385.3253	3047287.1073	-2283502.0725	-0.0484	-0.0124	0.0477	1996.338	0.0074	0.0073	0.0045
MUCK_GPS	-4860805.1677	2991738.4397	-2837860.5103	-0.0484	-0.0124	0.0477	1996.338	0.0061	0.0064	0.0037
CHAR_GPS	-4101998.3469	2566148.2558	-4141758.9629	-0.0287	-0.0033	0.0581	1996.338	0.0039	0.0041	0.0029
TRIA_GPS	-3990830.6303	2501499.3752	-4286338.8347	-0.0287	-0.0033	0.0581	1996.338	0.0054	0.0058	0.0040
SPM9_GPS	-3989108.3459	2699944.1226	-4166666.5055	-0.0287	-0.0033	0.0581	1996.338	0.0065	0.0062	0.0050
BARC_GPS	-4808764.2970	3330247.6110	-2535054.3511	-0.0585	-0.0084	0.0398	1996.338	0.0063	0.0064	0.0036
PIEB_GPS	-5045676.0272	3522171.2256	-1674322.4635	-0.0460	-0.0160	0.0486	1996.338	0.0089	0.0077	0.0044
CAMW_GPS	-3942894.8463	2790759.4251	-4151125.5367	-0.0409	0.0014	0.0464	1996.338	0.0040	0.0041	0.0029
EMUU_GPS	-4867427.1781	3487912.8957	-2191804.8852	-0.0460	-0.0160	0.0486	1996.338	0.0068	0.0066	0.0036
BENW_GPS	-4040118.8950	2944818.7337	-3948080.5654	-0.0531	0.0060	0.0347	1996.338	0.0057	0.0058	0.0039
SAKL_GPS	-3465323.0382	2638268.2694	4644082.7583	0.0000	0.0000	0.0000	1996.338	0.0068	0.0065	0.0052
GREN_GPS	-4955371.4066	3842257.4447	-1163834.9545	0.0178	-0.0698	0.0590	1996.338	0.0178	0.0141	0.0059
NORM_GPS	-4730120.0262	3818318.6172	-1924292.6696	-0.0134	-0.0424	0.0707	1996.338	0.0083	0.0072	0.0042
BREA_GPS	-4451878.9022	3786508.9807	-2546090.1906	-0.0434	-0.0198	0.0503	1996.338	0.0070	0.0064	0.0039
BRDV_GPS	-4355679.0994	3740239.9507	-2769201.2481	-0.0715	0.0014	0.0339	1996.338	0.0044	0.0043	0.0026
WILF_GPS	-4529722.3346	3909094.2768	-2203537.4617	-0.0445	-0.0536	0.0364	1993.538	0.0050	0.0049	0.0028
STAN_GPS	-3916469.8887	3455298.5910	-3649242.6335	-0.0343	-0.0316	0.0291	1993.696	0.0044	0.0042	0.0029
HWKR_GPS	-4055042.4958	3597135.2127	-3350585.1005	-0.0566	0.0046	0.0386	1996.338	0.0044	0.0042	0.0027
WOLL_GPS	-4523681.4784	4083441.9145	-1876186.9764	-0.0134	-0.0424	0.0707	1996.338	0.0054	0.0051	0.0029
ELDO_GPS	-4543818.4675	4263716.2870	-1358180.5723	-0.0455	-0.0325	0.0585	1996.338	0.0059	0.0055	0.0029
GROO_GPS	-4489874.9182	4265802.3060	-1519917.8012	-0.0455	-0.0325	0.0585	1996.338	0.0057	0.0053	0.0029
ALYA_GPS	-4487413.9212	4269234.0920	-1517520.3593	-0.0455	-0.0325	0.0585	1996.338	0.0057	0.0053	0.0029
CLIF_GPS	-4018348.3914	3874926.7788	-3075181.7591	-0.0716	0.0290	0.0303	1996.338	0.0045	0.0042	0.0027
ROPE_GPS	-4365327.3734	4355926.9587	-1623109.6101	-0.0455	-0.0325	0.0585	1996.338	0.0055	0.0051	0.0028
SHAM_GPS	-4189540.3522	4309929.9300	-2127995.1875	-0.0372	-0.0117	0.0569	1996.338	0.0050	0.0046	0.0027
THEV_GPS	-3739792.1718	3911197.5348	-3364706.6433	-0.0384	0.0072	0.0485	1996.338	0.0064	0.0057	0.0038
JUNC_GPS	-3733309.7691	4184348.0876	-3029196.7164	-0.0716	0.0290	0.0303	1996.338	0.0047	0.0041	0.0028
KDMN_GPS	-4017368.7778	4629016.3429	-1759073.2448	-0.0455	-0.0325	0.0585	1996.338	0.0055	0.0048	0.0027
WINN_GPS	-4077253.8946	4710296.8256	-1363183.8786	-0.0455	-0.0325	0.0585	1996.338	0.0069	0.0058	0.0032
PILL_GPS	-4073402.4929	4712253.6424	-1367883.2297	-0.0455	-0.0325	0.0585	1996.338	0.0069	0.0059	0.0032
KILI_GPS	-3777444.0347	4668166.3648	-2143627.0372	-0.0167	0.0010	0.0540	1996.338	0.0050	0.0042	0.0026
DEAK_GPS	-3448618.6085	4265480.0509	-3244109.8904	-0.0384	0.0072	0.0485	1996.338	0.0046	0.0039	0.0026
PIVT_GPS	-3806295.4663	4823694.5488	-1704766.3267	-0.0455	-0.0325	0.0585	1996.338	0.0053	0.0045	0.0027
CAIG_GPS	-3137868.7150	4393013.5234	-3385233.9446	-0.0140	0.0474	0.0484	1996.338	0.0049	0.0041	0.0029
GIBS_GPS	-3365970.2660	4763630.6926	-2572813.3551	-0.0657	0.0499	0.0236	1996.338	0.0051	0.0042	0.0028
BATE_GPS	-3124556.1700	4828049.8102	-2750068.5252	-0.0657	0.0499	0.0236	1996.338	0.0050	0.0040	0.0027
BROO_GPS	-3241494.7860	5134037.3505	-1946745.5016	-0.0524	-0.0707	0.0749	1993.633	0.0056	0.0048	0.0029
ESPE_GPS	-2800864.6514	4500724.7298	-3534886.5371	-0.0470	0.0487	0.0021	1993.670	0.0050	0.0042	0.0030
KALG_GPS	-2853510.9473	4665806.5560	-3271380.6683	-0.0140	0.0474	0.0484	1996.338	0.0050	0.0040	0.0028
MANL_GPS	-3184192.3529	5291065.9505	1590599.2384	0.0000	0.0000	0.0000	1996.338	0.0093	0.0085	0.0039
RATH_GPS	-2979541.6955	5090380.5385	-2420393.7283	-0.0216	0.0013	0.0593	1996.338	0.0053	0.0042	0.0028

```
  BULL_GPS -4271156.7041  2929587.3267 -3710093.6924   0.0273   0.1349 -0.3788 1994.571   0.0021   0.0018   0.0017
  GOKA_GPS -5221573.4822  3603226.5800  -671387.0791   0.0346  -0.0790  0.0556 1993.659   0.0036   0.0028   0.0011
  GUAM_GPS -5071312.7873  3568363.4797  1488904.3113   0.0158  -0.0342 -0.0113 1996.098   0.0010   0.0009   0.0004
  ATKI_GPS -4119867.9261  2918876.3739 -3884282.4911  -0.0557   0.0027  0.0322 1993.948   0.0017   0.0014   0.0014
  KIKO_GPS -5133225.7918  3695553.7772  -818612.3683   0.0178  -0.0698  0.0590 1993.657   0.0042   0.0032   0.0012
  MEND_GPS -5109574.9481  3759378.9571  -678236.5283   0.0346  -0.0790  0.0556 1993.657   0.0042   0.0033   0.0012
  WUVU_GPS -5080555.0399  3851303.6390  -191869.0438   0.0346  -0.0790  0.0556 1993.675   0.0051   0.0042   0.0013
  HOWI_GPS -4523298.6736  3485332.7852 -2832259.2231  -0.0734   0.0027  0.0299 1994.571   0.0023   0.0020   0.0015
  OLVE_GPS -4384863.3008  3448388.9052 -3082582.1218   0.1094   0.0172 -0.1945 1994.571   0.0022   0.0019   0.0015
  PORT_GPS -3922962.0394  3117568.4867 -3932953.7683   0.5333   0.5290 -0.0336 1994.571   0.0019   0.0017   0.0017
  SUND_GPS -4239032.1711  3377934.9127 -3351167.8809   0.1526   0.5472 -0.0685 1994.571   0.0021   0.0018   0.0016
  VANI_GPS -4972629.8775  3983208.1827  -296767.2703   0.0178  -0.0698  0.0590 1992.599   0.0046   0.0040   0.0013
  AIAM_GPS -4934886.4885  3958248.7039  -810301.1902   0.0178  -0.0698  0.0590 1992.591   0.0052   0.0041   0.0015
  LLTR_GPS -4117215.8538  3333728.2429 -3539972.5711  -0.1070   0.2038 -0.0878 1994.571   0.0020   0.0018   0.0016
  TSU1_GPS -3957193.8056  3310191.2984  3737733.3633   0.0245  -0.0525 -0.0404 1991.092   0.0115   0.0089   0.0071
  TSKB_GPS -3957199.2275  3310199.6613  3737711.7153   0.0245  -0.0525 -0.0404 1995.900   0.0010   0.0009   0.0008
  AMUN_GPS     -245.0602      210.0243 -6359570.0182   7.5781  -6.4423  0.2114 1992.037   0.0051   0.0053   0.0106
  AUSA_GPS -3942241.9987  3468859.5304 -3608197.2401   0.0000   0.0000  0.0000 1990.580   0.0176   0.0241   0.0122
  AUSB_GPS -3942241.9512  3468859.3689 -3608197.1409   0.0000   0.0000  0.0000 1990.581   0.0199   0.0205   0.0182
  USUD_GPS -3855262.5872  3427432.2038  3741020.9326  -0.0029  -0.0038 -0.0082 1992.340   0.0053   0.0052   0.0040
  USU5_GPS -3855262.9816  3427432.5123  3741020.3640  -0.0029  -0.0038 -0.0082 1995.740   0.0008   0.0008   0.0006
  ALIC_GPS -4052051.7338  4212836.1844 -2545106.0598  -0.0333  -0.0225  0.0633 1993.464   0.0011   0.0011   0.0008
  CEDU_GPS -3753472.0992  3912740.9884 -3347961.0224  -0.0591   0.0175  0.0373 1993.845   0.0011   0.0011   0.0009
  JOHN_GPS -3929600.7538  4183187.8276 -2774030.9923   0.1549   0.1980 -0.3614 1992.575   0.0033   0.0032   0.0021
  DARW_GPS -4091358.7192  4684606.8438 -1408580.6980  -0.0429  -0.0384  0.0664 1993.410   0.0015   0.0016   0.0008
  RAWL_GPS -3586428.1744  4539145.8112 -2678896.5133  -0.0657   0.0499  0.0236 1992.601   0.0045   0.0047   0.0030
  TAEJ_GPS -3120422.9156  4086355.4845  3761769.6601  -0.0256  -0.0264 -0.0379 1996.239   0.0009   0.0009   0.0007
  TAIW_GPS -3024781.9190  4928936.8397  2681234.4762  -0.0316  -0.0269 -0.0081 1995.432   0.0011   0.0012   0.0007
  SHAO_GPS -2831733.2358  4675666.0512  3275369.5336  -0.0451  -0.0102 -0.0067 1996.096   0.0008   0.0009   0.0006
  S01R_GPS -2886619.0939  5082945.2672  2543377.6466  -0.5989   0.0924 -0.1842 1990.579   0.0168   0.0167   0.0082
  KARR_GPS -2713832.1352  5303935.1531 -2269515.2378  -0.0239  -0.0164  0.0675 1993.481   0.0010   0.0014   0.0008
  CAVE_GPS -2375390.5587  4875553.8556 -3345387.2399  -0.0372   0.0226  0.0480 1993.665   0.0017   0.0024   0.0016
  PERT_GPS -2368686.9095  4881316.5196 -3341796.2370  -0.0453   0.0038  0.0548 1995.621   0.0005   0.0007   0.0005
  PER2_GPS -2368701.4200  4881361.6650 -3341721.0339  -0.0453   0.0038  0.0548 1993.674   0.0013   0.0019   0.0013
  YAR1_GPS -2389025.3440  5043316.8440 -3078530.9250  -0.0488   0.0121  0.0493 1993.0000  ITRF94B  50107M004
YARRAGADEE
  TIMB_GPS -2702792.8972  5747549.3250   583412.7352   0.0000   0.0000  0.0000 1993.659   0.0059   0.0067   0.0015
  CASE_GPS  -902599.1652  2409535.3124 -5816536.7596   0.0030  -0.0140  0.0040 1992.036   0.0057   0.0066   0.0110
  CAS1_GPS  -901776.1679  2409383.4394 -5816748.4129   0.0030  -0.0140  0.0040 1995.791   0.0007   0.0008   0.0014
  KAYA_GPS -2119512.9088  6015103.3014    89809.9756   0.0000   0.0000  0.0000 1992.597   0.0143   0.0176   0.0033
  BAKO_GPS -1836968.8692  6065617.2611  -716257.7715  -0.0218  -0.0084  0.0053 1993.217   0.0025   0.0039   0.0011
  XMAS_GPS -1696463.3032  6039562.8656 -1149235.8728  -0.0624  -0.0534  0.0836 1996.338   0.0022   0.0033   0.0013
```

```
  COCO_GPS   -741949.8494   6190961.6628 -1337768.7942 -0.0626 -0.0482  0.0757 1993.231  0.0015  0.0025  0.0011
  LHAS_GPS   -106937.6152   5549269.6011  3139215.7440  0.0439 -0.3668 -0.1810 1995.848  0.0012  0.0015  0.0009
  COLB_GPS   1113302.9813   6233645.2637   760258.5122  0.0000  0.0000  0.0000 1992.601  0.0058  0.0092  0.0025
  DAV1_GPS    486854.5342   2285099.3194 -5914955.6820  0.0035 -0.0074  0.0052 1995.755  0.0008  0.0010  0.0018
  IISC_GPS   1337936.8520   6070317.1151  1427876.4894 -0.0422  0.0127  0.0195 1996.115  0.0010  0.0011  0.0006
  MALE_GPS   1805486.5352   6099592.4141   461710.8528  0.0000  0.0000  0.0000 1996.308  0.0090  0.0190  0.0046
  KERG_GPS   1406274.0099   3918195.7498 -4816159.6258 -0.0109  0.0066 -0.0058 1992.037  0.0113  0.0188  0.0204
  KER5_GPS   1406337.3329   3918161.1147 -4816167.3589 -0.0109  0.0066 -0.0058 1996.125  0.0008  0.0010  0.0011
  KIT3_GPS   1944945.3821   4556652.1841  4004325.9654 -0.0215 -0.0087 -0.0097 1996.101  0.0008  0.0008  0.0007
  DOVE_GPS    885318.3810   1974376.4281 -5980930.2440  0.0000  0.0000  0.0000 1991.072  0.0181  0.0243  0.0334
  MAW1_GPS   1111287.1356   2168911.2885 -5874493.5720  0.0124  0.0114 -0.0156 1993.779  0.0025  0.0029  0.0047
  SEY1_GPS   3602870.7948   5238174.3183  -516275.5317  0.2205 -0.0923 -0.0246 1995.875  0.0032  0.0033  0.0009
  BAHA_GPS   3633911.1692   4425277.8384  2799862.5282  0.0087  0.0153 -0.0227 1990.585  0.1382  0.0826  0.0603
  DJIB_GPS   4583088.5611   4250979.1225  1266241.2945  0.0000  0.0000  0.0000 1992.601  0.0077  0.0078  0.0031
  MALI_GPS   4865366.4853   4110737.4386  -331121.7285 -0.0466 -0.0358  0.0234 1996.241  0.0020  0.0017  0.0007
  SYOW_GPS   1766182.5364   1460336.7548 -5932285.4331  0.0000  0.0000  0.0000 1992.037  0.0056  0.0060  0.0096
  HART_GPS   5084625.4540   2670366.5410 -2768494.0070 -0.0015  0.0164  0.0180 1993.0000  ITRF94B  30302M002
HARTEBEESTHOEK
  METS_GPS   2892571.0135   1311843.2659  5512634.0101 -0.0211  0.0163  0.0076 1992.694  0.0028  0.0021  0.0046
  TROM_GPS   2102940.4200    721569.3520  5958192.0790 -0.0193  0.0107  0.0051 1993.0000  ITRF94B  10302M003 TROMSO
  MATG_GPS   4641950.8975   1393056.7462  4133280.3058 -0.0275  0.0139  0.0060 1991.070  0.0133  0.0082  0.0114
  MATE_GPS   4641949.8239   1393045.1929  4133287.2830 -0.0275  0.0139  0.0060 1992.611  0.0038  0.0025  0.0034
  GRAZ_GPS   4194424.0454   1162702.4810  4647245.2920 -0.0166  0.0184  0.0098 1993.437  0.0079  0.0064  0.0088
  WTZ1_GPS   4075578.6570    931852.6180  4801570.0020 -0.0168  0.0173  0.0056 1993.0000  ITRF94A  14201M009 WETTZELL
  WTZX_GPS   4075552.5227    931825.7010  4801589.1929 -0.0181  0.0206  0.0087 1990.581  0.0181  0.0104  0.0160
  WETB_GPS   4075579.3753    931807.1285  4801570.9183 -0.0181  0.0206  0.0087 1991.070  0.0090  0.0048  0.0096
  ONSA_GPS   3370658.7354    711876.9779  5349786.8505 -0.0139  0.0175  0.0159 1993.563  0.0008  0.0005  0.0011
  NALL_GPS   1202430.6795    252626.6438  6237767.5137 -0.0182  0.0084  0.0028 1995.902  0.0005  0.0005  0.0017
  NAL1_GPS   1202431.3817    252626.7265  6237770.7089 -0.0182  0.0084  0.0028 1991.072  0.0106  0.0087  0.0292
  FORS_GPS   2061367.6155    432558.4267 -6000283.7561  0.0000  0.0000  0.0000 1992.037  0.0140  0.0101  0.0265
  HONE_GPS   3132539.0317    566401.7196  5508609.8413  0.0000  0.0000  0.0000 1991.070  0.0091  0.0053  0.0130
  ARLT_GPS   5991291.5793    773713.5942  2040608.5530  0.0000  0.0000  0.0000 1992.601  0.0082  0.0042  0.0036
  KOSG_GPS   3899225.3150    396731.7520  5015078.3020 -0.0146  0.0173  0.0089 1993.0000  ITRF94A  13504M003 KOOTWIJK
  HERS_GPS   4033470.2995     23672.6730  4924301.1765 -0.0167  0.0057  0.0002 1992.539  0.0048  0.0027  0.0055
  BRUN_GPS  -5020720.8050   2499067.4599 -3027804.9295 -0.0604 -0.0135  0.0522 1996.338  0.0065  0.0068  0.0042
  QUT1_GPS  -5046767.7575   2568457.3143 -2925287.8111 -0.0604 -0.0135  0.0522 1996.338  0.0077  0.0073  0.0047
  CROW_GPS  -4821560.6016   2482901.8786 -3345746.0870 -0.0445 -0.0026  0.0448 1996.338  0.0060  0.0064  0.0041
  SUGA_GPS  -5126895.2428   2689409.7899 -2667603.2274 -0.0484 -0.0124  0.0477 1996.338  0.0065  0.0067  0.0041
  TEXA_GPS  -4899985.8402   2692597.6907 -3060138.6653 -0.0604 -0.0135  0.0522 1996.338  0.0057  0.0064  0.0037
  FLAG_GPS  -4597580.6812   2564076.1986 -3589224.7858 -0.0417  0.0007  0.0434 1996.338  0.0057  0.0062  0.0039
  MULA_GPS  -5115155.0915   2872883.3239 -2494381.7732 -0.0484 -0.0124  0.0477 1996.338  0.0078  0.0074  0.0047
  OAKS_GPS  -5113583.0638   2874686.9454 -2495474.8256 -0.0484 -0.0124  0.0477 1996.338  0.0057  0.0065  0.0036
```

```
COOL_GPS -2711523.0317  5098133.3967 -2700765.0733 -0.0333  0.0046  0.0561 1996.338  0.0053  0.0041  0.0029
TORB_GPS -2422745.4570  4630068.3046 -3645119.4663 -0.0294  0.0309  0.0482 1996.338  0.0050  0.0041  0.0031
CARN_GPS -2325633.3485  5290021.9455 -2690510.8855 -0.0450  0.0080  0.0530 1996.338  0.0054  0.0043  0.0030
REUN_GPS  3364095.6243  4907945.1039 -2293468.6093  0.0000  0.0000  0.0000 1996.338  0.0093  0.0094  0.0051
RCM4_GPS   961242.9076 -5674021.6597  2740657.6478  0.0000  0.0000  0.0000 1993.653  0.0109  0.0075  0.0112
WEWK_GPS -5128211.2716  3771635.3775  -396055.9126  0.0000  0.0000  0.0000 1993.653  0.0091  0.0099  0.0109
KOPI_GPS -5038707.2909  3867027.3896  -594810.7328  0.0000  0.0000  0.0000 1993.653  0.0097  0.0101  0.0109
AMAN_GPS -4962464.8032  3987772.5273  -396577.0892  0.0000  0.0000  0.0000 1993.653  0.0096  0.0100  0.0110
CHUL_GPS -1132728.2647  6092488.5472  1504562.1217  0.0000  0.0000  0.0000 1996.311  0.0034  0.0063  0.0019
MLTG_GPS  1803857.4413  6099996.0020   462747.3470  0.0000  0.0000  0.0000 1996.311  0.0073  0.0113  0.0021
MALE_GPS  1805486.5043  6099592.3858   461710.8545  0.0000  0.0000  0.0000 1996.311  0.0023  0.0036  0.0011
GAN1_GPS  1847796.0399  6104033.8009   -76520.6176  0.0000  0.0000  0.0000 1996.311  0.0045  0.0068  0.0014
```

Publications from

THE SCHOOL OF GEOMATIC ENGINEERING

(Formerly School of Surveying)

THE UNIVERSITY OF NEW SOUTH WALES

All prices include postage by surface mail. Air mail rates on application. (Effective August 1997)

To order, write to Publications Officer, School of Geomatic Engineering
The University of New South Wales, Sydney 2052, AUSTRALIA

NOTE: ALL ORDERS MUST BE PREPAID

UNISURV REPORTS - S SERIES

S8 - S20	Price (including postage) :		$10.00
S29 onwards	Price (including postage) :	Individuals	$25.00
		Institutions	$30.00

S8 A. Stolz, "Three-D Cartesian co-ordinates of part of the Australian geodetic network by the use of local astronomic vector systems", Unisurv Rep. S8, 182 pp, 1972.

S10 A.J. Robinson, "Study of zero error & ground swing of the model MRA101 tellurometer", Unisurv Rep. S10, 200 pp, 1973.

S12. G.J.F. Holden, "An evaluation of orthophotography in an integrated mapping system", Unisurv Rep. S12, 232 pp, 1974.

S14. Edward G. Anderson, "The Effect of Topography on Solutions of Stokes` Problem", Unisurv Rep. S14, 252 pp, 1976.

S16. K. Bretreger, "Earth Tide Effects on Geodetic Observations", Unisurv S16, 173 pp, 1978.

S17. C. Rizos, "The role of the gravity field in sea surface topography studies", Unisurv S17, 299 pp, 1980.

S18. B.C. Forster, "Some measures of urban residential quality from LANDSAT multi-spectral data", Unisurv S18, 223 pp, 1981.

S19. Richard Coleman, "A Geodetic Basis for recovering Ocean Dynamic Information from Satellite Altimetry", Unisurv S19,332 pp, 1981.

S20. Douglas R. Larden, "Monitoring the Earth's Rotation by Lunar Laser Ranging", Unisurv Report S20, 280 pp, 1982.

S29 Gary S Chisholm, "Integration of GPS into hydrographic survey operations", Unisurv S29, 190 pp, 1987.

S30. Gary Alan Jeffress, "An investigation of Doppler satellite positioning multi-station software", Unisurv S30, 118 pp, 1987.

S31. Jahja Soetandi, "A model for a cadastral land information system for Indonesia", Unisurv S31, 168 pp, 1988.

S33. R. D. Holloway, "The integration of GPS heights into the Australian Height Datum", Unisurv S33, 151 pp.,1988.

S34. Robin C. Mullin, "Data update in a Land Information Network", Unisurv S34, 168 pp. 1988.

S35. Bertrand Merminod, "The use of Kalman filters in GPS Navigation", Unisurv S35, 203 pp., 1989.

S36. Andrew R. Marshall, "Network design and optimisation in close range Photogrammetry", Unisurv S36, 249 pp., 1989.

S37. Wattana Jaroondhampinij, "A model of Computerised parcel-based Land Information System for the Department of Lands, Thailand," Unisurv S37, 281 pp., 1989.

S38. C. Rizos (Ed.), D.B. Grant, A. Stolz, B. Merminod, C.C. Mazur "Contributions to GPS Studies", Unisurv S38, 204 pp., 1990.

S39. C. Bosloper, "Multipath and GPS short periodic components of the time variation of the differential dispersive delay", Unisurv S39, 214 pp., 1990.

S40. John Michael Nolan, "Development of a Navigational System utilizing the Global Positioning System in a real time, differential mode", Unisurv S40, 163 pp., 1990.

S41. Roderick T. Macleod, "The resolution of Mean Sea Level anomalies along the NSW coastline using the Global Positioning System", 278 pp., 1990.

S42. Douglas A. Kinlyside, "Densification Surveys in New South Wales - coping with distortions", 209 pp., 1992.

S43. A. H. W. Kearsley (ed.), Z. Ahmad, B. R. Harvey and A. Kasenda, "Contributions to Geoid Evaluations and GPS Heighting", 209 pp., 1993.

S44. Paul Tregoning, "GPS Measurements in the Australian and Indonesian Regions (1989-1993)", 134 + xiii pp, 1996.

S45. Wan-Xuan Fu, "A study of GPS and other navigation systems for high precision navigation and attitude determinations", 332pp, 1996.

S46. Peter Morgan et al, "A zero order GPS network for the Australia region", 187 + xii pp, 1996.

S47. Yongru Huang, "A digital photogrammetry system for industrial monitoring", 145 + xiv pp, 1997.

S48. Kim Mobbs, "Tectonic interpretation of the Papua New Guine Region from repeat satellite measurements", 256 + xc pp, 1997.

S49. Shaowei Han, "Carrier phase-based long-range GPS kinematic positioning", 185 + xi pp, 1997.

S50. Mustafa D Subari, "Low-cost GPS systems for intermediate surveying and mapping accuracy applications", 179 + xiii pp, 1997.

MONOGRAPHS

Prices include postage by surface mail

		Price
M1.	R.S. Mather, "The theory and geodetic use of some common projections", (2nd edition), 125 pp., 1978.	$15.00
M2.	R.S. Mather, "The analysis of the earth's gravity field", 172 pp., 1971.	$8.00
M3.	G.G. Bennett, "Tables for prediction of daylight stars", 24 pp.,1974.	$5.00
M4.	G.G. Bennett, J.G. Freislich & M. Maughan, "Star prediction tables for the fixing of position", 200 pp., 1974.	$8.00
M8.	A.H.W. Kearsley, "Geodetic Surveying", 96 pp, (revised) 1988.	$12.00
M11.	W.F. Caspary, "Concepts of Network and Deformation Analysis",183 pp., 1988.	$25.00
M12.	F.K. Brunner, "Atmospheric Effects on Geodetic Space Measurements", 110 pp., 1988.	$16.00
M13.	Bruce R. Harvey, "Practical Least Squares and Statistics for Surveyors", (2nd edition), 319 pp., 1994.	$30.00
M14.	Ewan G. Masters & John R. Pollard (Ed.), "Land Information Management", 269 pp., 1991. (Proceedings LIM Conference, July 1991).	$20.00
M15/1	Ewan G. Masters & John R. Pollard (Ed.), "Land Information Management - Geographic Information Systems - Advance Remote Sensing Vol 1" 295 pp., 1993 (Proceedings of LIM & GIS Conference, July 1993).	$30.00
M15/2	Ewan G. Masters & John R. Pollard (Ed.), "Land Information Management - Geographic Information Systems - Advance Remote Sensing Vol 2" 376 pp., 1993 (Proceedings of Advanced Remote Sensing Conference, July 1993).	$30.00
M16.	A. Stolz, "An Introduction to Geodesy", 112 pp., 1994.	$20.00
M17	Chris Rizos, "Principles and Practice of GPS Surveying", 565 pp., 1997.	$50.00